MINISTERUL CERCETĂRII ŞI INOVĂRII

Aerospace Europe
CEAS 2017 Conference

European Aerospace "Quo Vadis?"

(6th CEAS Air & Space Conference)

Palace of the Parliament - Bucharest, ROMANIA

16th-20th October 2017

ADDENDUM

Organized by:

COMOTI
ROMANIAN RESEARCH & DEVELOPMENT INSTITUTE FOR GAS TURBINES

AAAR
Asociatia Aeronautica si Astronautica a Romaniei

Romanian Research and Development Institute for Gas Turbines COMOTI

Coordinator: Ionuț PORUMBEL

PROCEEDINGS

of the 6th CEAS Air and Space Conference

Aerospace Europe 2017

ADDENDUM

Not peer reviewed material presented at the conference

Editor: George Bogdan GHERMAN

Bucharest, 2017

Section I

Keynote addresses

Presentation 1

Aerospace Europe & CEAS: strengthening collaboration & knowledge dissemination

Christophe Hermans
CEAS president, Deputy Director of the German Dutch Wind tunnels DNW, NLR CTA, NVvL president

Aerospace Europe & CEAS: strengthening collaboration & knowledge dissemination

by Christophe Hermans, CEAS president, Deputy Director of the German Dutch Wind tunnels DNW, NLR CTA, NVvL president (christophe.hermans@dnw.aero)

Europe has a strong aeronautical sector with:

- an excellent aviation education system attracting the best students (higher education represented at European level by PEGASUS)
- a strong research community pooling knowledge and infrastructure (university research represented at European level by EASN, research establishments represented at European level by EREA)
- and a competitive industry base, with Airbus as the no. 1 global civil airframe manufacture, major engine OEMs (like RR, SAFRAN) and their supply chains.

It is therefore equally important to provide at a European level a platform of well recognized global conferences, networking opportunities for professionals, thematic events and high ranked journals to publish peer-reviewed papers.

This is what we as CEAS, the Council of European Aeronautical Societies, are offering, but we do not do this on our own. CEAS has 13 national member societies representing roughly 35.000 individual aeronautical professionals all over Europe and we are proud to closely collaborate

COUNCIL OF EUROPEAN AEROSPACE SOCIETIES

Aerospace Europe & CEAS: strengthening collaboration & knowledge dissemination

by Christophe Hermans, CEAS president, Deputy Director of the German Dutch Wind tunnels DNW, NLR CTA, NVvL president (christophe.hermans@dnw.aero)

with our corporate members EASA, ESA, Eurocontrol, students association EUROAVIA, LAETA (our friends from Portugal) and MoU partners like EASN, EREA, AAE, ICAS and AIAA.

It is our mission to support knowledge transfer and provide networking opportunities through a structure of Technical Committees, high level specialist conferences and a biennial Aerospace Europe conference, our Journals and open access paper publications that can be found on the Aerospace Europe platform, a new initiative recently launched by our partnering societies in Europe with EU support.

CEAS is celebrating its 25^{th} anniversary this year. As the European aerospace industry grew closer together in the mid-eighties of the previous century through a series of collaborative projects and the formation of more permanent cross-border industrial entities, it was evident that a closer cooperation between European aerospace scientists and engineers would be beneficial. The various national European aeronautical societies had served the aerospace community well for decades, realized that a closer, more permanent relationship would help to increase the research leverage through the creation of a pan European network of researchers. 4 Founding fathers established CEAS at the 1992 Farnborough Air Show, within 2 years 4 more national societies joined the new council (at that time). The history of CEAS has been described in a publication that will be officially presented at the conference.

Aerospace Europe & CEAS: strengthening collaboration & knowledge dissemination

by Christophe Hermans, CEAS president, Deputy Director of the German Dutch Wind tunnels DNW, NLR CTA, NVvL president (christophe.hermans@dnw.aero)

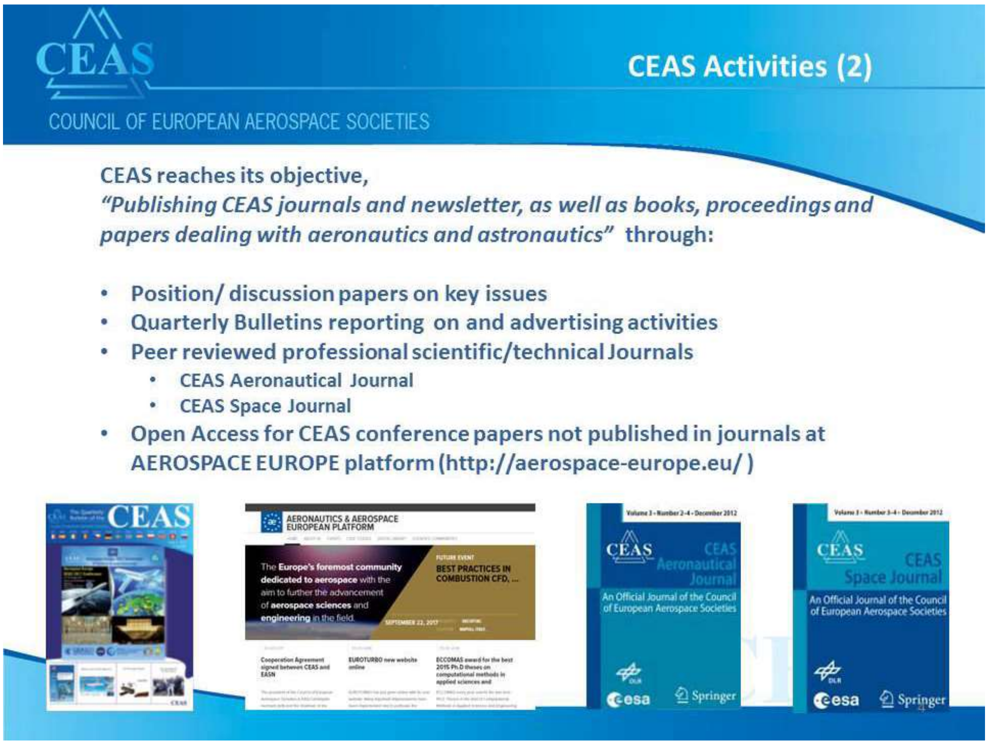

Knowledge dissemination is supported by our two scientific CEAS Journals, that we publish with significant editorial support of DLR and ESA (80.000 full articles downloads in 5 years, or 250 per article). Open access paper publications of our thematic and global events can be found on the Aerospace Europe platform, a new initiative recently launched by our partnering societies like ECCOMAS, ERCOFTAC, EUROTURBO, EUCASS and EUROMECH in Europe with EU support in the framework of ECAero-2. The platform also contains a calendar of aeronautical events and working environment for use cases in aerodynamics (www.aeropsace-europe.eu.

Presentation 18

New Trends in Open Innovation Strategies

Florin Paun
Group Innovation Director
AKKA TECHOLOGIES

AKKA TECHNOLOGIES

New Trends in Open Innovation Strategies

Dr. Florin Paun

Group Innovation Director

PASSION FOR TECHNOLOGIES

What is the INNOVATION?
→ INNOVATION = CREATIVITY + VALUE

« Successful Exploitation of a New Idea » E. von Hippel, Harvard, MIT

What means VALUE ?

Dynamic Capabilities- A. Sen

→ Commercial, Capital, Access to Resources (Capacities), Human Capital

TM rights Know-how

Direct- see RyanAir
Non direct- see electric cars plug

→ Material vs Intangible Assets (IP?,... Information?, Stress Avoidance?,...)

What means Entrepreneur?

- Assuming Risks ?
- Solution oriented ?
- Independent ?
- Dreamer? Fool? Selfish ? Nerd ? Jerk ? → Guilty or not ? Does he realize ?
- (his) Project Convicted → Non Empathic over-Passionate “Autism” ?

What complementary features to succeed ?
- Charismatic, Leader, Manager, Promoter, Planner, Creative, Non-Conformist…
- Empathic, Ethic, Trustful, Fast Learner, Resilient, …
- Technical? Human Science?

→ Not a single person posses all this characteristics
→ Need to know how to be surrounded and mentored with the right persons

Build the right → Entrepreneurial Team (as a state of mind) to get into
→ Entrepreneurship (as a day to day activity)

Innovation Paradigm : Positioning on the TRL
Hybrid Humans Entrepreneurially minded

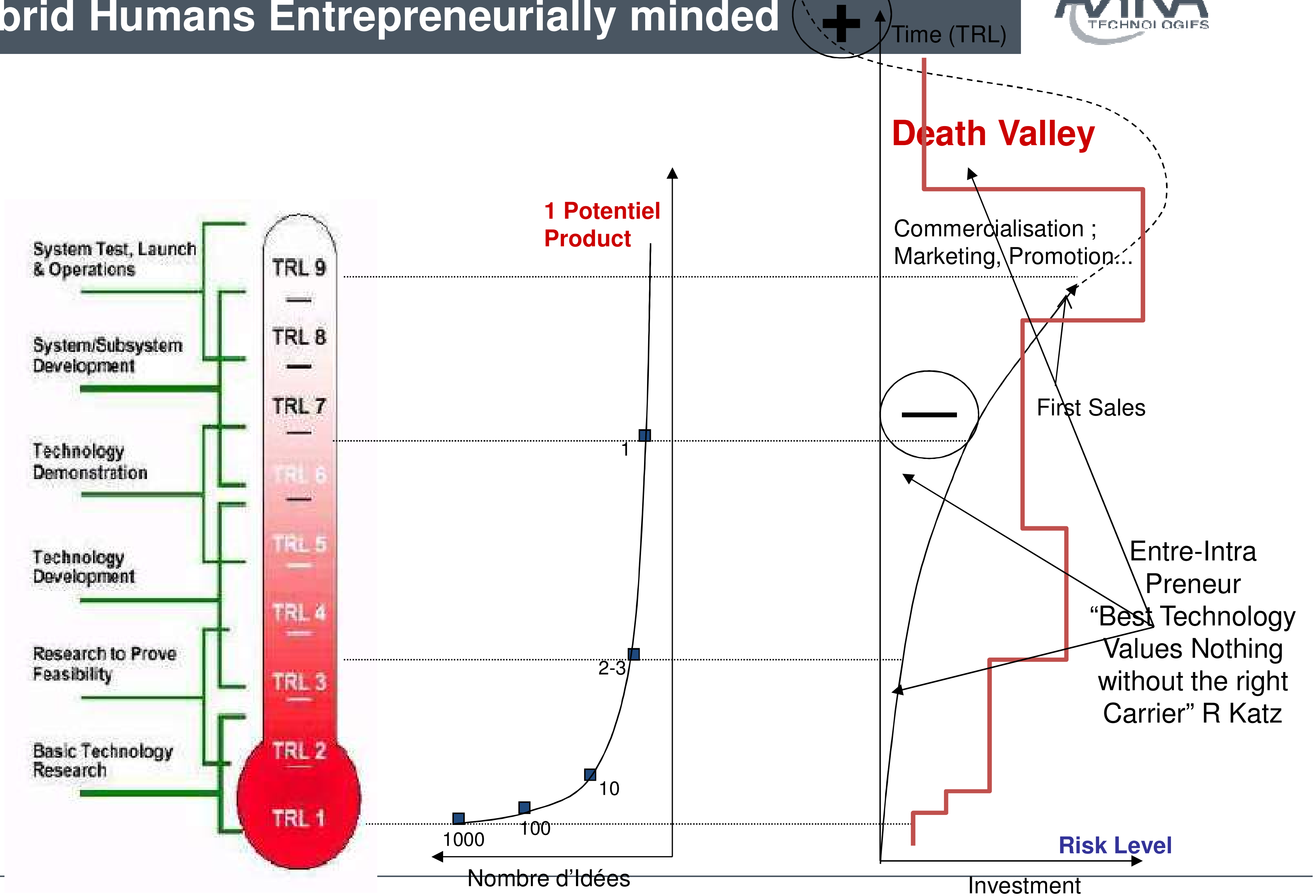

Value Distribution Channel

Study case – Commercial Aircraft

historically

Passenger	*ß Value input (100)*
Airline	*Air France, Lufthansa…*
Aircraft Manufacturer	*Airbus, Boeing,… (<7)*
Development Office	*Deciders for Technology* *(System architect)*
Corporate Research Center	*Technology providers*
R&D Centers (Applied R&D)	*Onera, DLR, Universities*
Universities (Basic R&D)	

Vertical competition
Horizontal competition

Critical - **Strategic Partnership (IP exclusivity)**
Competitive Advantages (quality, costs, time, **IP exclusivity**)

Concomitancy and Innovation Occurrence

Fondamentals – from Value Distribution Channel

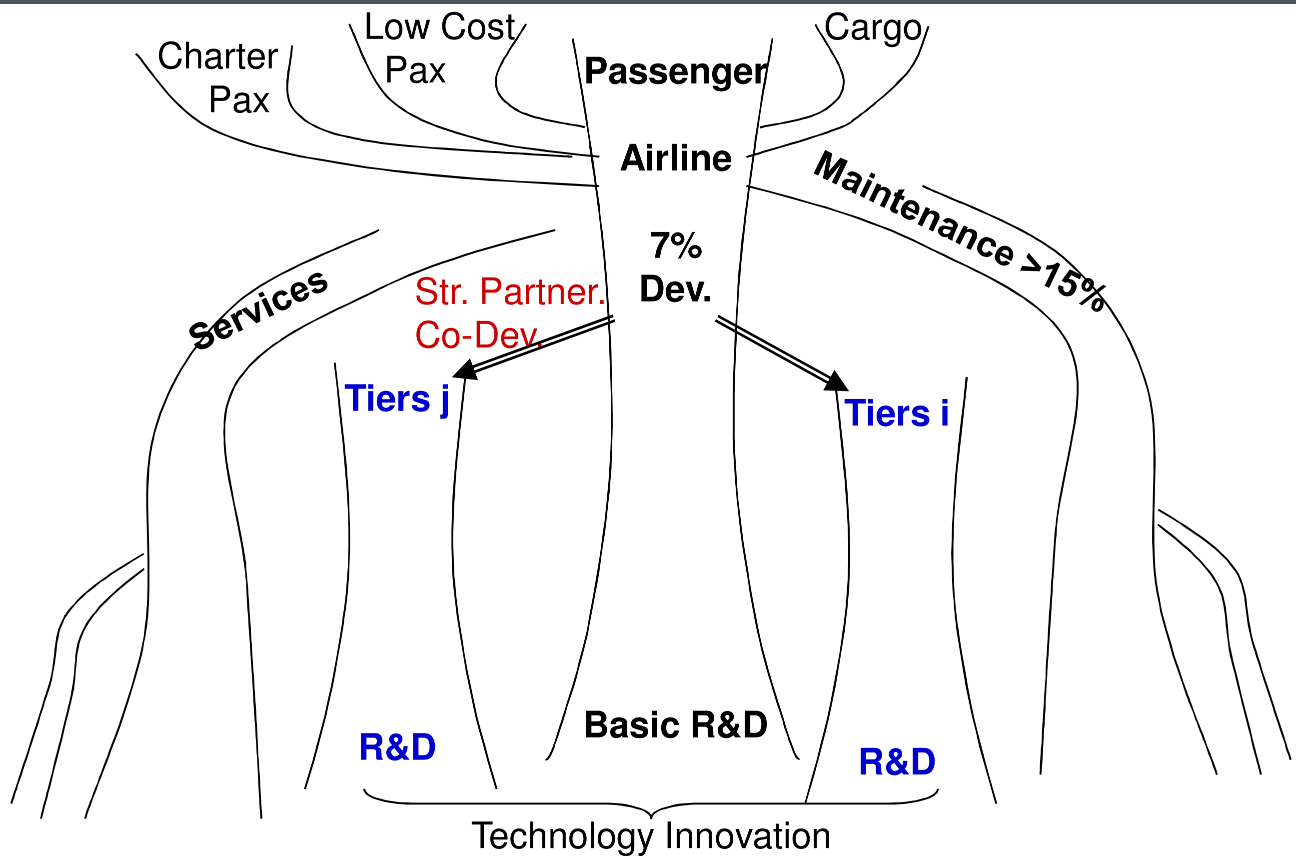

→ To Value Distribution Tree – this perception induce Business Model Innovation

- **See Ryan Air reducing maintenance by using brand new aircraft**
- **additional to Create discomfort → pay for Stress Avoidance**
- **additional to the use of secondary Airports… Create Low Cost**

In Practice : How to proceed and with whom? How and What to Deal?

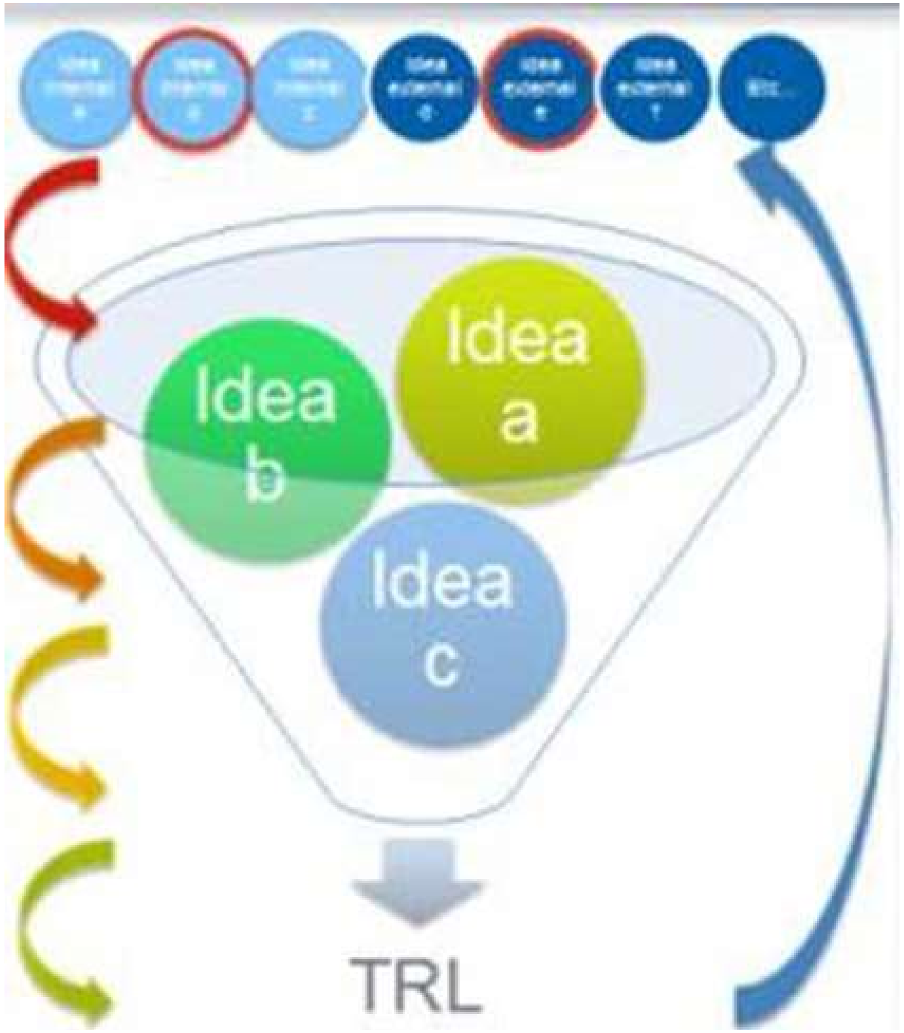

Prof Henry Chesbrough UC Berkeley. Open Innovation :
Renewing Groth From Industrial R & D, 10th Annual Innovation
Convergence, Minneapolis Sept 27, 2004

Page 14

In Practice : How to proceed and with whom? How and What to Deal?

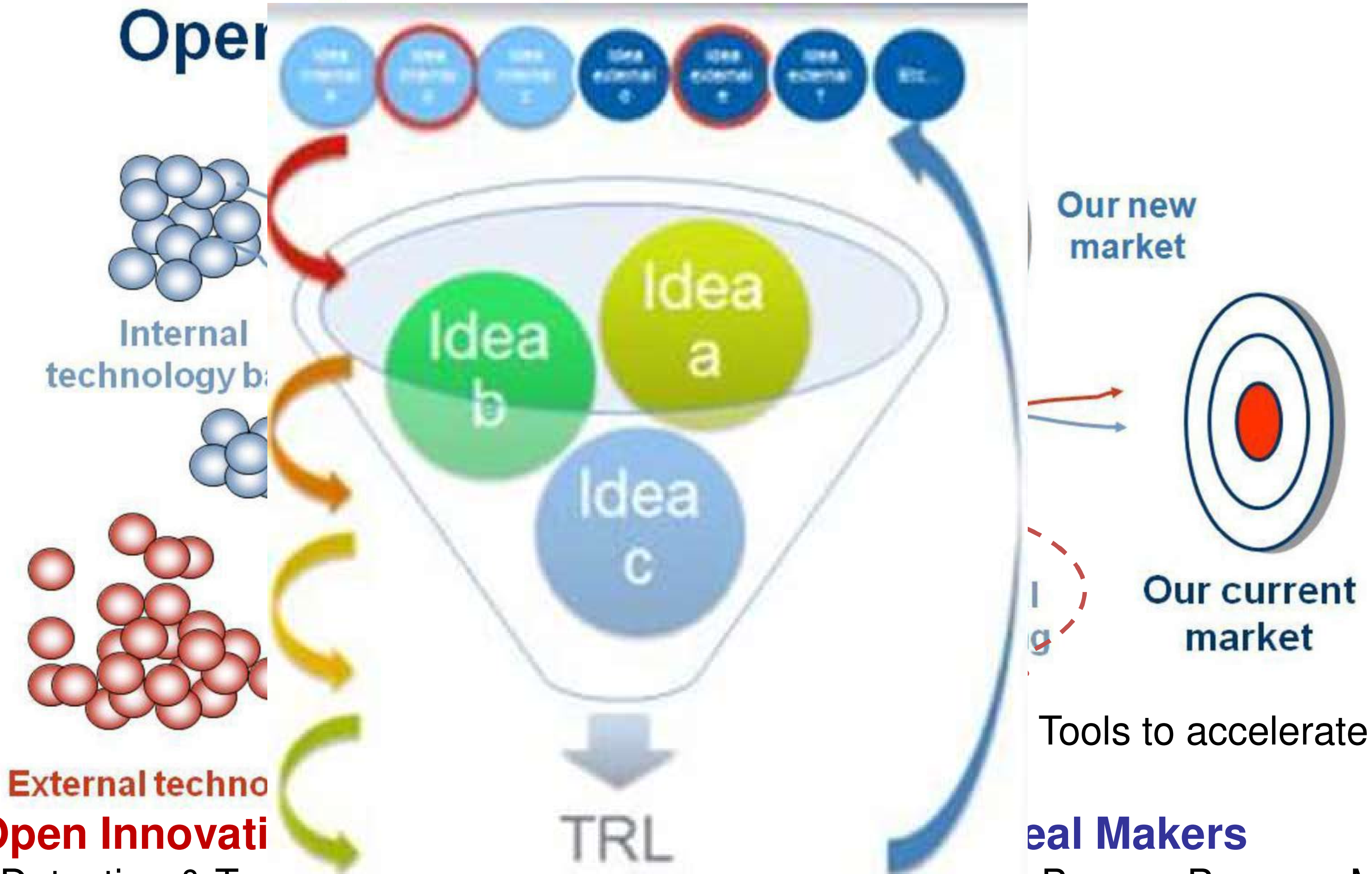

Open Innovati **eal Makers**

- Detecting & Transactionning the IP ; Tech Scouters, legals, Buyers, Program Managers

Prof Henry Chesbrough UC Berkeley. Open Innovation : Renewing Groth From Industrial R & D, 10th Annual Innovation Convergence, Minneapolis Sept 27, 2004

Page 15

Concomitancy and Innovation Occurrence Challenges

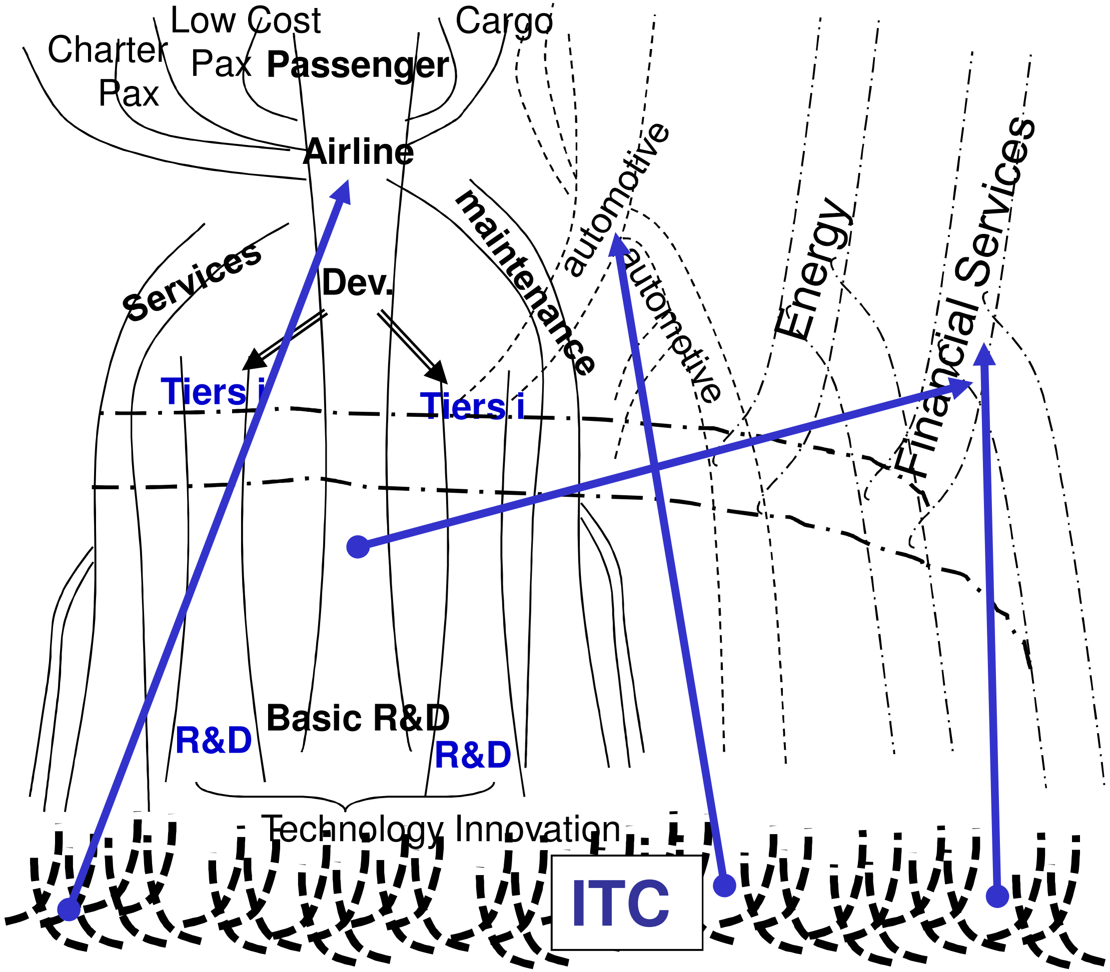

Examples of Direct Impact on Disrupting the Business Model

1) Dynamic pricing for Airlines
2) Onboard connected Pads
   → democratize "BlaBlaCar"
3) Financial Predictions based on Big Data Analysis (Quant Cube)
4) + ongoing developments for Satellite imaging use

…

→ To Value Distribution Tree

→ To Value Distribution Interconnected "Mangrove Forest"

Life in Mangrove Forest

- How to see beyond your « radar » the emergent technologies impacting your business core faster then your own product/service development time?
→ Detecting and Closing deals 10x faster
→ "Sentinels vs Predators" – TechScouting vs Emmerging Technology

- How to distribute the created Value
→ Track and Deal the related IP
→ With whom? Hybrid Humans!

- **What activity and what to incentivize to create agility?**
→ Agile Tech Demonstrator ← Hard Tendency

Production = Rowing Team
→ Demos Adoption Speed

Demonstration = Rafting Team
→ Fail fast, Fail cheap, Try again

Exploration = Treasure Hunters
→ Fast environment/tools learners

How to… survive? Being Agile ?

Life in Mangrove Forest

- **How to see beyond your « radar » the emergent technologies impacting your business core faster then your own product/service development time?**
  → **Detecting and Closing deals 10x faster**
  → **"Sentinels vs Predators"**

- **How to distribute the created Value**
  → **Track and Deal the related IP**

- **With whom? Hybrid Humans!**

- **What activity and what to incentivize to create agility?**

Demonstration = Rafting Team
→ Fail fast, Fail cheap, Try again

How to… survive? Being Agile ?

Life in Mangrove Forest

- How to see beyond your « radar » the emergent technologies impacting your business core faster then your own product/service development time?

→ Detecting and Closing deals 10x faster

→ "Sentinels vs Predators"

- How to distribute the created Value

→ Track and Deal the related IP

- **With whom? Hybrid Humans!**

- **What activity and what to incentivize to create agility?**

Exploration = Treasure Hunters
→ Fast environment/tools learners

Actors Positioning - Asymmetries !!!

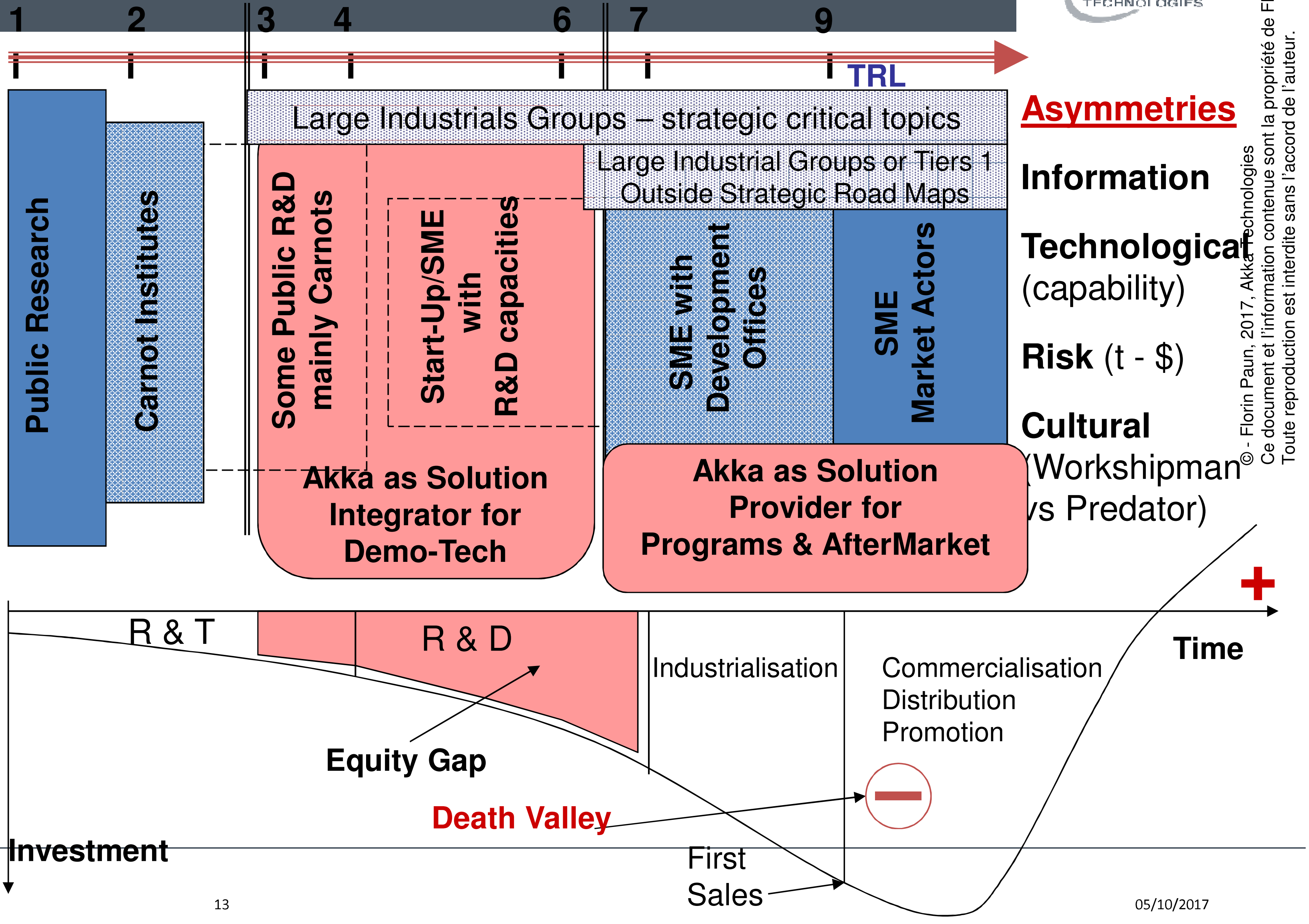

Akka's Position in the Mangrove Forest

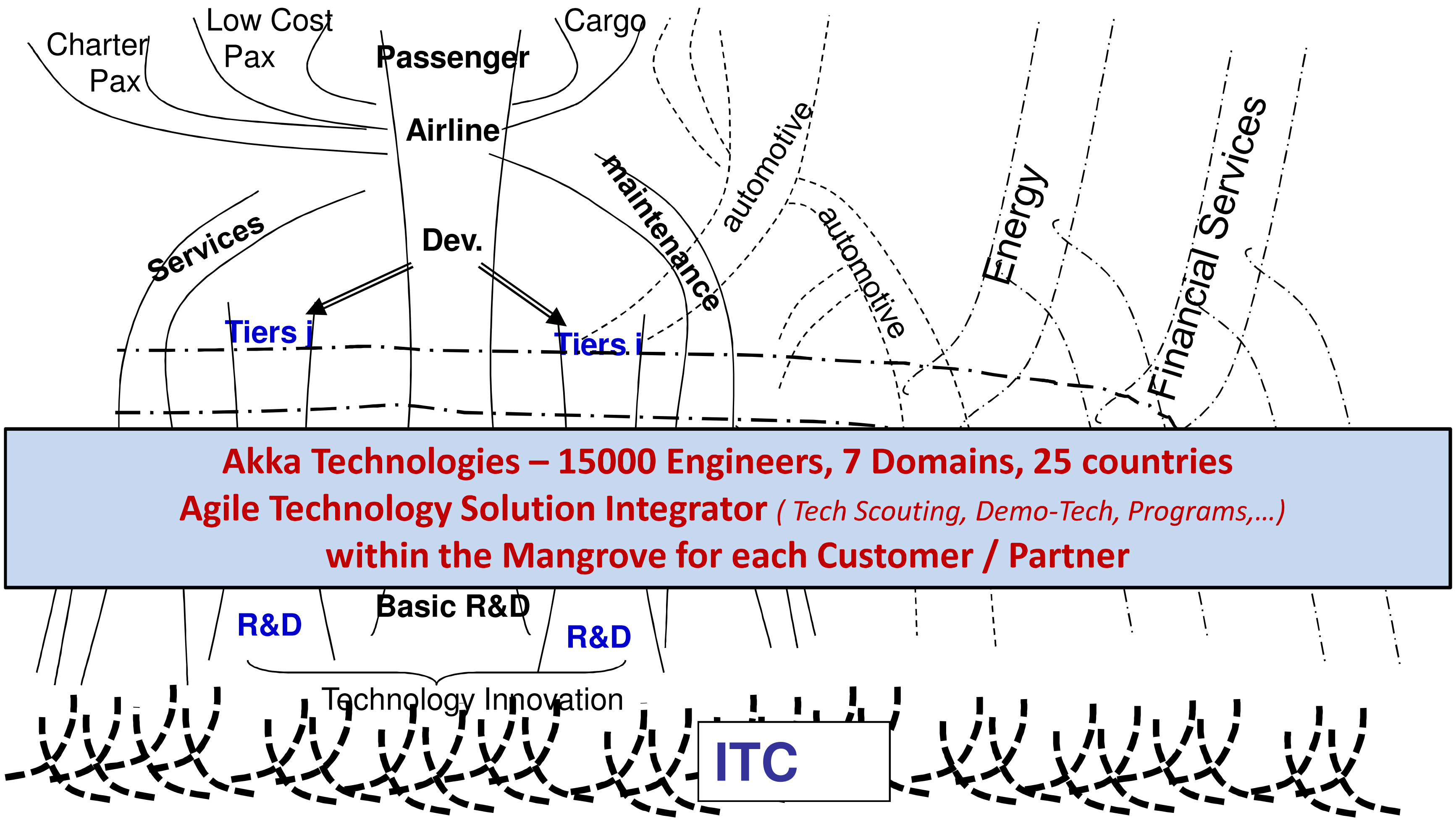

A MULTI-SPECIALIST GROUP

A WORLDWILDE **MULTI-SPECIALIST**

REVENUE BY BUSINESS SEGMENT (2016)

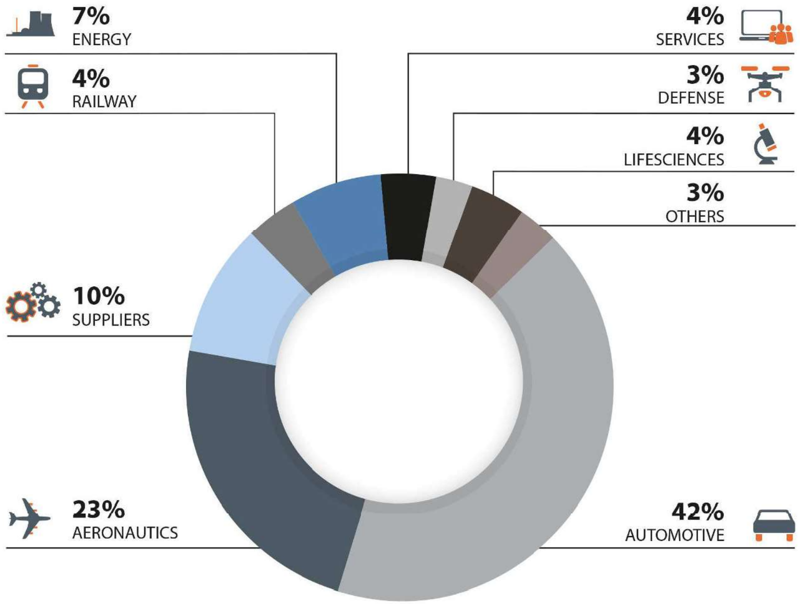

REVENUE BY BUSINESS UNIT (2016)

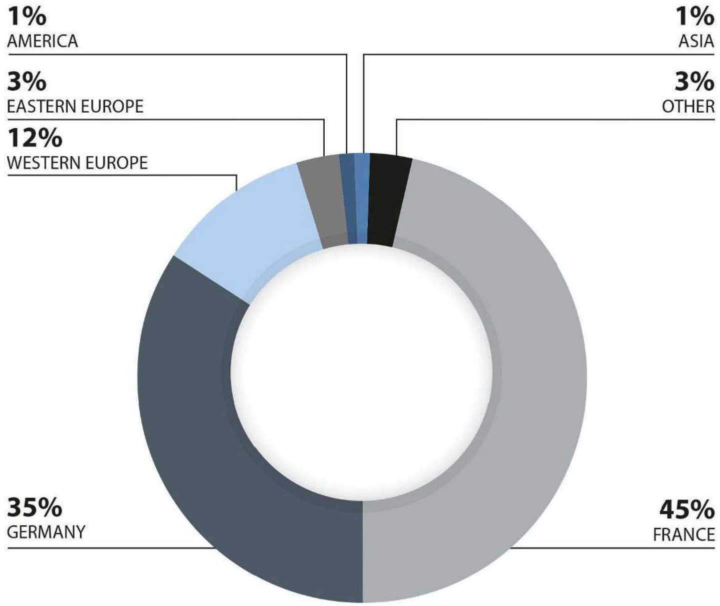

Page 23

ADDED VALUE **FOR A GLOBAL OFFER**

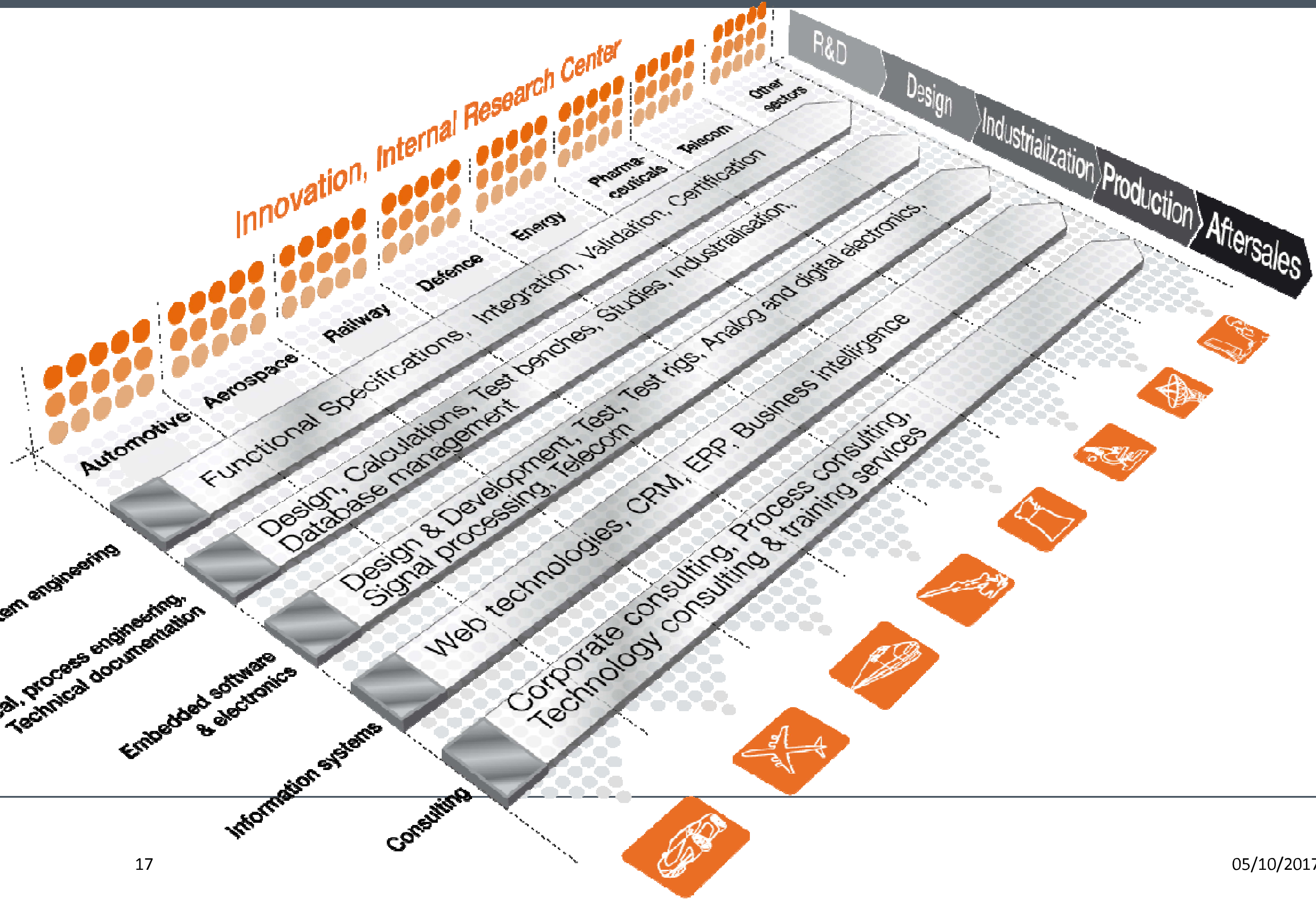

Page 24

AKKA, A WORLDWIDE COMPANY

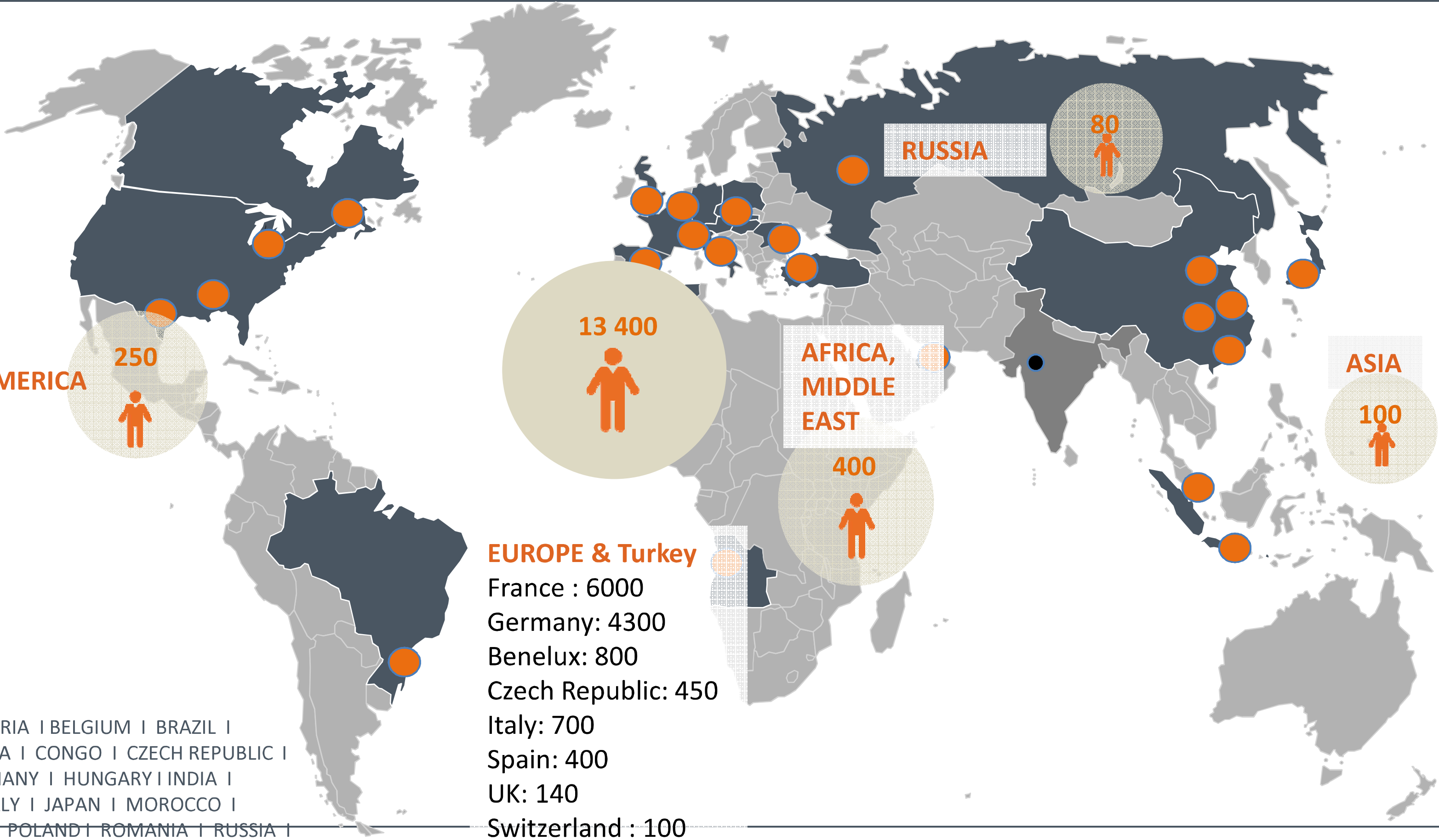

EUROPE & Turkey
France : 6000
Germany: 4300
Benelux: 800
Czech Republic: 450
Italy: 700
Spain: 400
UK: 140
Switzerland : 100
Turkey: 70
Romania: 450

ALGERIA I AUSTRIA I BELGIUM I BRAZIL I CANADA I CHINA I CONGO I CZECH REPUBLIC I FRANCE I GERMANY I HUNGARY I INDIA I INDONESIA I ITALY I JAPAN I MOROCCO I NETHERLANDS I POLAND I ROMANIA I RUSSIA I SINGAPORE I SPAIN I SLOVAKIA I SWITZERLAND I TURKEY I UNITED ARAB EMIRATES I UNITED KINGDOM I UNITED STATES I

AKKA INNOVATION TOOLS & Projects…

KATALYST AKKA STARTUPS ACCELERATOR

Win-win partnerships set up between selected Startups and AKKA in 4 domains Connectivity, Cybersecurity, Big Data & AI, visualization technologies.

LINK & GO by **AKKA Research**

Automated, safe, urban and social, Link & GO is a dual-mode (manual or automatic drive) concept car. The innovations it incorporates will help drive the design changes for future urban vehicles.

- Embedded technologies allow for the autonomous driving
- Motor Directive suspension (MSD)
- Drive by wire
- 48 volt electrical architecture
- Interfacial multi-modal graphics

AIRCOBOT **by AKKA Research**

The aim of the project «Air-COBOT» (Aircraft enhanced Inspection by smaRt &Collaborative rOBOT) is to design and setup a collaborative mobile robot for aircraft inspection. The robot is capable to ensure safe travel and trajectories, do Non Destructive Testing -NDT- (IR-3D-Visible…) and have communication with information system maintenance of the aircraft.

PLUME PROJECT by **AKKA Research**

Develop an ECONOMICAL, INNOVATIVE and ULTRALIGHT Aircraft SEAT.
Technological transfer from automotive to aeronautic
TECHNOLOGIES
Thermoplastics (2nd composites generation), assembly by welding, automatized manufacturing processes

OUR AUTOMOTIVE

01- VEHICLE ARCHITECTURE

05-STYLING & DESIGN
Sketching, Clay-modelling, surface development, model making…

02-CHASSIS/SUSPENSION SYSTEM
Chassis & Suspension, power steering, braking,…

03- BODY & CLOSURE
Tank, Doors & hatches, lightweight…

04-INTERIOR/EXTERIOR
Window lifts, seats, lighting, dashboard, A/C…

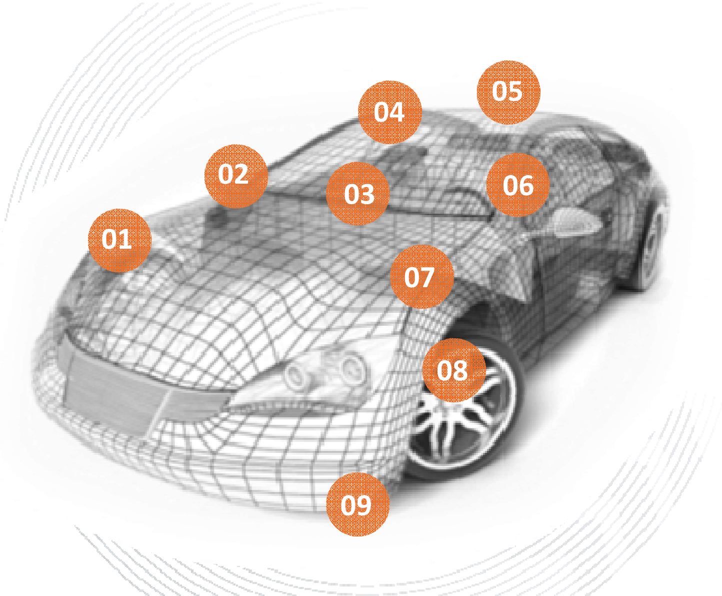

06-EMBEDDED SOFTWARE
Connectivity, App, Multimedia/Infotainment, diagnosis, HMI, security…

07-ELECTRICAL / ELECTRONIC SYSTEMS
ECUs, E/E Architecture, wiring harness, ADAS

08-POWERTRAIN
Traditional & alternative powertrain systems, incl. Hybrid & e-Drive, energy management…

09-CALCULATION & SIMULATION
NVH, passive safety, crash and flow simulation…

PARTS, TEST BENCHES AND TOOLS PROTOTYPING

TESTING, INTEGRATION AND VALIDATION

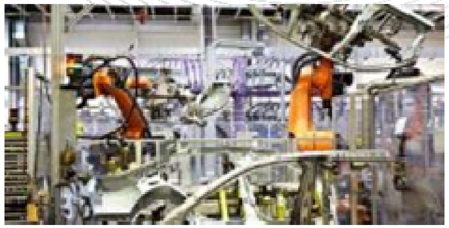

INDUTRIALIZATION, PROCESS ENGINEERING AND AFTER SALES

TECHNOLOGY AND MANAGEMENT CONSULTING

OUR AERONAUTICS

01-COCKPIT ERGONOMICS

02-EMBEDDED SOFTWARE

03-SYSTEM CONCEPTION AND INTEGRATION & INSTALLATION
Hydro-electric, avionic, …

04-AEROSTRUCTURE
Metal, Composite,
Static calculation,
Stress/Non linear, Cinematic

05-FLIGHT PHYSICS AND AERODYNAMICS

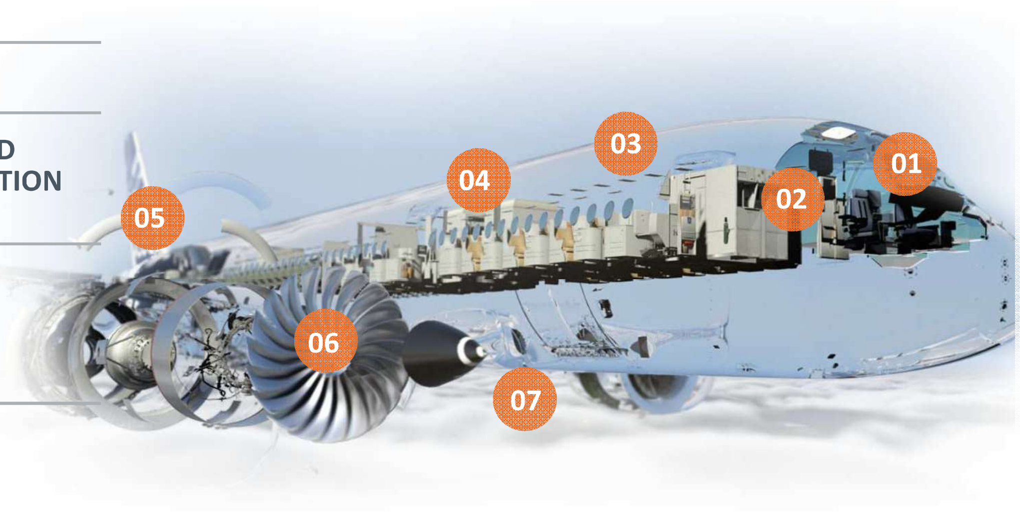

06-FLIGHT OPERATIONS AND MAINTENANCE

07-AIRCRAFT MODIFICATIONS

3D TOOLS
Virtual Maintenance, Digital mockup, Viewer 3D Real Time…

GROUND/FLIGHT TESTS

TECHNICAL PUBLICATIONS MAINTENANCE, SERVICE BULLETIN, ELECTRICAL SCHEMATICS…

PARTS & TOOLS PROTOTYPING

TESTING AND VALIDATION

INDUTRIALIZATION AND PROCESS ENGINEERING

MANAGEMENT CONSULTING

OUR RAILWAYS

01-SIGNALLING
ERTMS, TVM, ETCS…

02-CONTROL/ COMMAND
TCMS, networks…

03-PASSENGER INFORMATION SYSTEM
Communication, sound, video…

04-INTERIOR FITTINGS
Cladding, , seating, lighting…

05-CALCULATIONS AND SIMULATIONS
RDM, crash, fatigue, thermal…

06-MECHANICAL STRUCTURE STUDIES
Shell, bogies, bodywork…

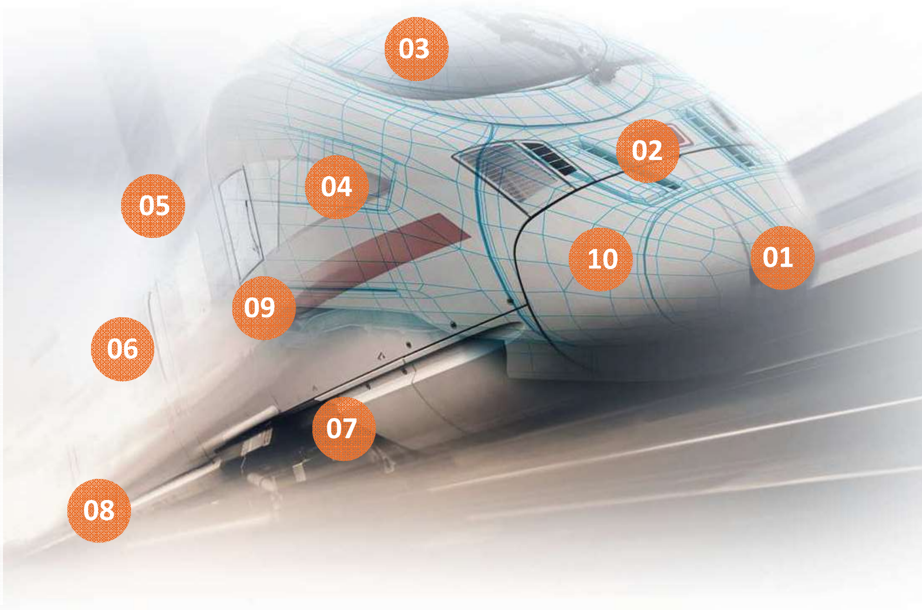

07-EQUIPMENT INSTALLATION
Electrical, mechanical, pneumatic

08-OPERATIONAL SECURITY
Reliability, safety…

09-ARCHITECTURE AND TECHNICAL SPECIFICATIONS OF TRAIN FUNCTIONS
Traction/braking, temperature control, doors, high/low voltage

10-POWERTRAIN CALCULATORS
Capacity sizing, engine steering

Page 29

OUR INFRASTRUCTURE

01-STATION
Train, Tram, Metro ...

02-PASSENGER FACILITIES

03-RAILROAD
Ballast ...

04-ENGINEERING STRUCTURE
Bridge ...

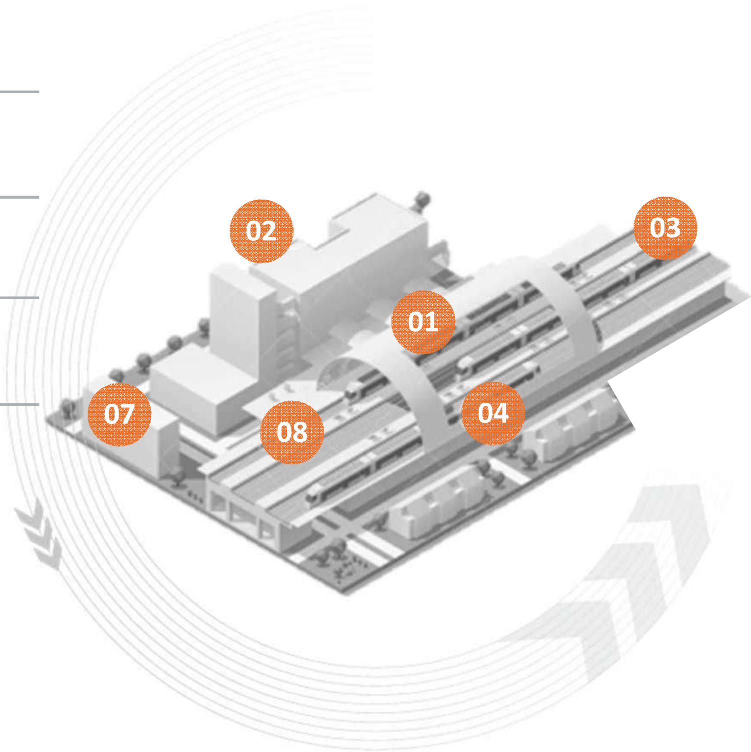

07-UNDERGROUND FACILITIES

08-CATENARIES

Page 30

OUR LIFESCIENCES

« AKKA intervenes at all stages of the life cycle of the medicine »

DEVELOPMENT

- Research
- Clinical studies
- Industrial and pharmaceutical development

AUTHORISATION

QUALITY ASSURANCE

ENGINEERING

- New Build
- Process Engineering

SYSTEM & INFORMATIQUE

- Realization and maintenance of applications for management of chemical libraries
- Development of a Web application for the management of Quality and Conformity (QMS))
- Realization of a data flow management application
- Organization, planning and monitoring of projects and resources for the integration of marketing tools in the client's information system
- Back-Office applications (marketing management, electronic customer document management)

ENGINEERING

- Project owner support for the construction of a development laboratory on a biotechnology centre
- Validation and optimisation of the scale-up of formulation and the dose packaging of a vaccine
- Stability studies in relation to the submission of NDA dossiers to the FDA
- Installation of a new production line for powdered culture media
- Management of the cleaning of a freeze-dryer and managing the Performance Qualification of the manual cleaning of the spreading parts and fasteningsz
- Set-up of the CMMS/Monitoring of the Plant Maintenance SAP module migration project

OUR ENERGY

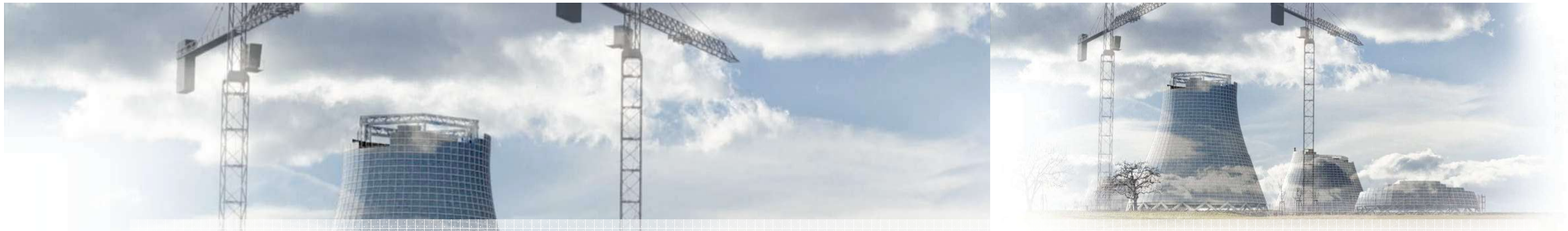

NEW FUEL CYCLE PROJECTS

NEW REACTOR PROJECTS

EXTRACTION | **TRANSFORMATION**

Supplier quality, inspection

Offshore, onshore, subsea

PRODUCTION
- Renewables
- Thermal
- Nuclear
- Integrated logistics support, Support engineering

DISTRIBUTION
- Trading, optimisation upstream-downstream

DEMOLITION
- Impact studies, demolition scenarios
- Storage treatment, waste disposal

OPERATING SAFETY, RISK MANAGEMENT

INSTRUMENTATION & CONTROL

CLIENT/PROJECT MANAGEMENT SUPPORT

PROCUREMENT, TENDERING, EXPEDITING

INFORMATION SYSTEMS

Page 32

OUR TELECOM

PROJECT MANAGEMENT AND COORDINATION:
- Radio deployment / swap
- FTTH deployment
- Services platforms (SMS, MMS, SVA

CONFIGURATION/PARAMETER SETTING AND ADMINISTRATION:
- Routers and network switches
- Telecoms equipment

CAPACITY PLANNING:
- Radio access networks (2G, 3G)
- Core networks
- Fixed access networks (ADSL, FTTH, DSLAM)

SYSTEMS INTEGRATION / VALIDATION, SUPPORT LEVELS 3 AND 4
- Radio access networks (2G, 3G, 4G)
- Transmission networks (optical and wireless)
- Data (IP) and voice (VoIP) networks

THANK YOU FOR YOUR ATTENTION

florin.paun@akka.eu

PASSION FOR TECHNOLOGIES

Section II

EREA – Future Sky

Presentation 2301

FUTURE SKY

Aviation Research for Tomorrow and Beyond

Josef Kaspar
EREA Vice Chairman and Future Sky Coordinator

EREA
Association of
European Research Establishments in Aeronautics

FUTURE SKY

Aviation Research for Tomorrow and Beyond

Josef Kaspar

EREA Vice Chairman

and Future Sky Coordinator

Association of European Research Establishments in Aeronautics

EREA in numbers

> 5.000

Employees in aeronautics

~ 180

Number of PhD Thesis

~ € 0,5 Bln

Annual spend on research in aeronautics

> 6.000

Number of Publications

The role of EREA

Research

Development & Integration of technologies

Transfer to industry

Production & commercialisation

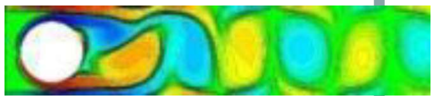

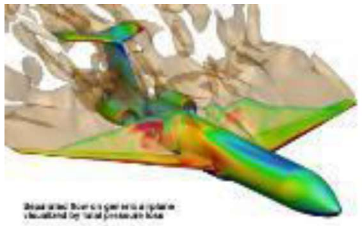

EREA

Universities

Industrial partners, Spin-offs, Start-ups

Looking back to the future

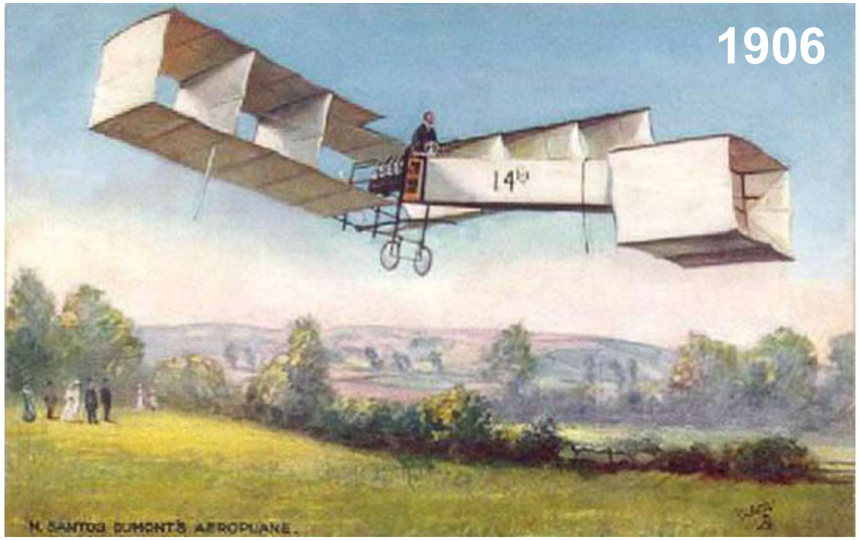

Convergence of concepts

Looking back to the future

THF, Berlin-Tempelhof 1923

FRA, Frankfurt Airport 2006

Persistent growth of air traffic

CHALLENGES

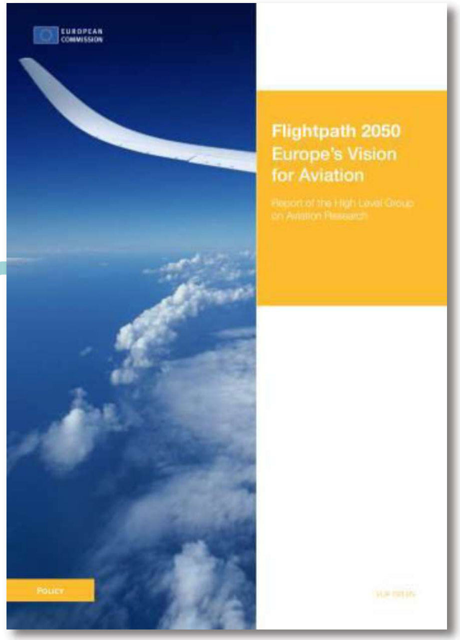

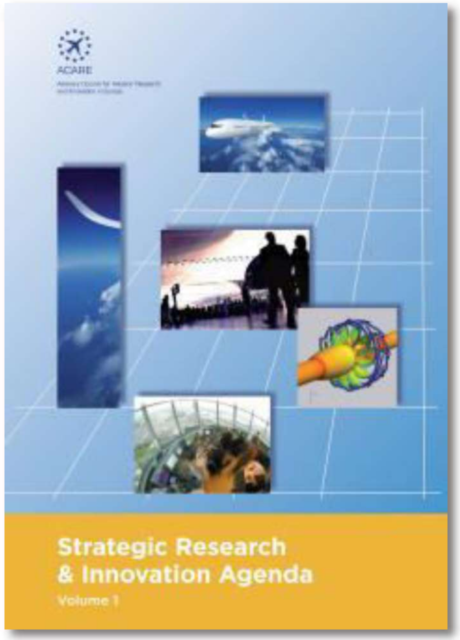

- Meeting Societal and Market Needs
- Maintaining and Extending Industrial Leadership
- Protecting the Environment and the Energy Supply
- Ensuring Safety and Security
- Prioritizing Research, Testing Capabilities and Education

How to get there?

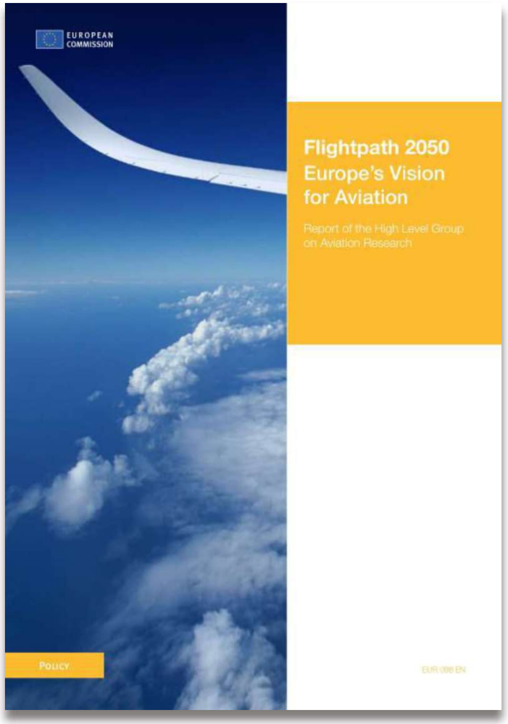

+ national aerospace strategies

How to get there?

By Opening Up New Perspectives in Joint Research

N+1

Joint Undertaking

N+2

Joint Research Initiative

ATS Generation

FUTURE SKY PARTNERS

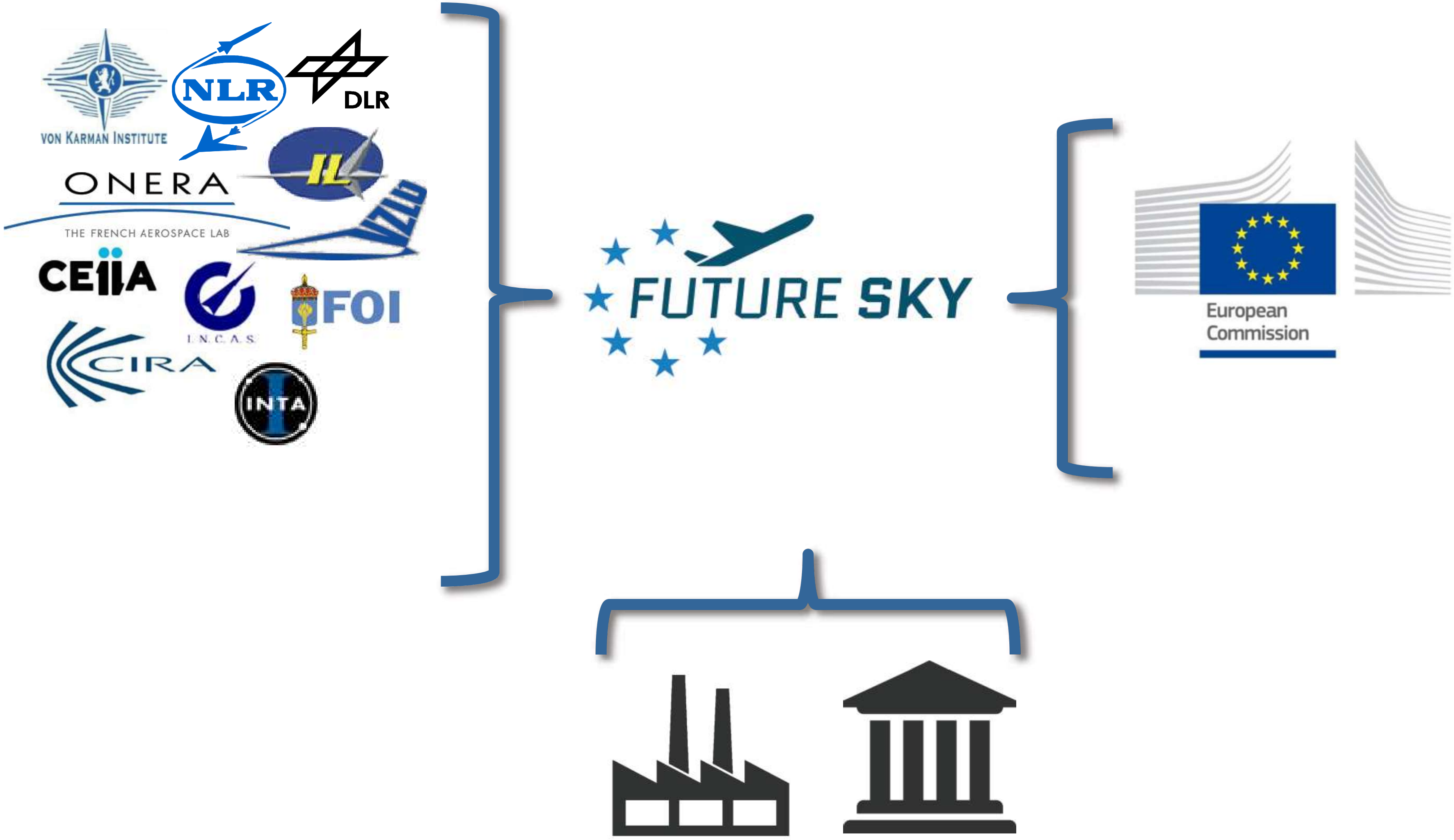

FUTURE SKY ADDED VALUE

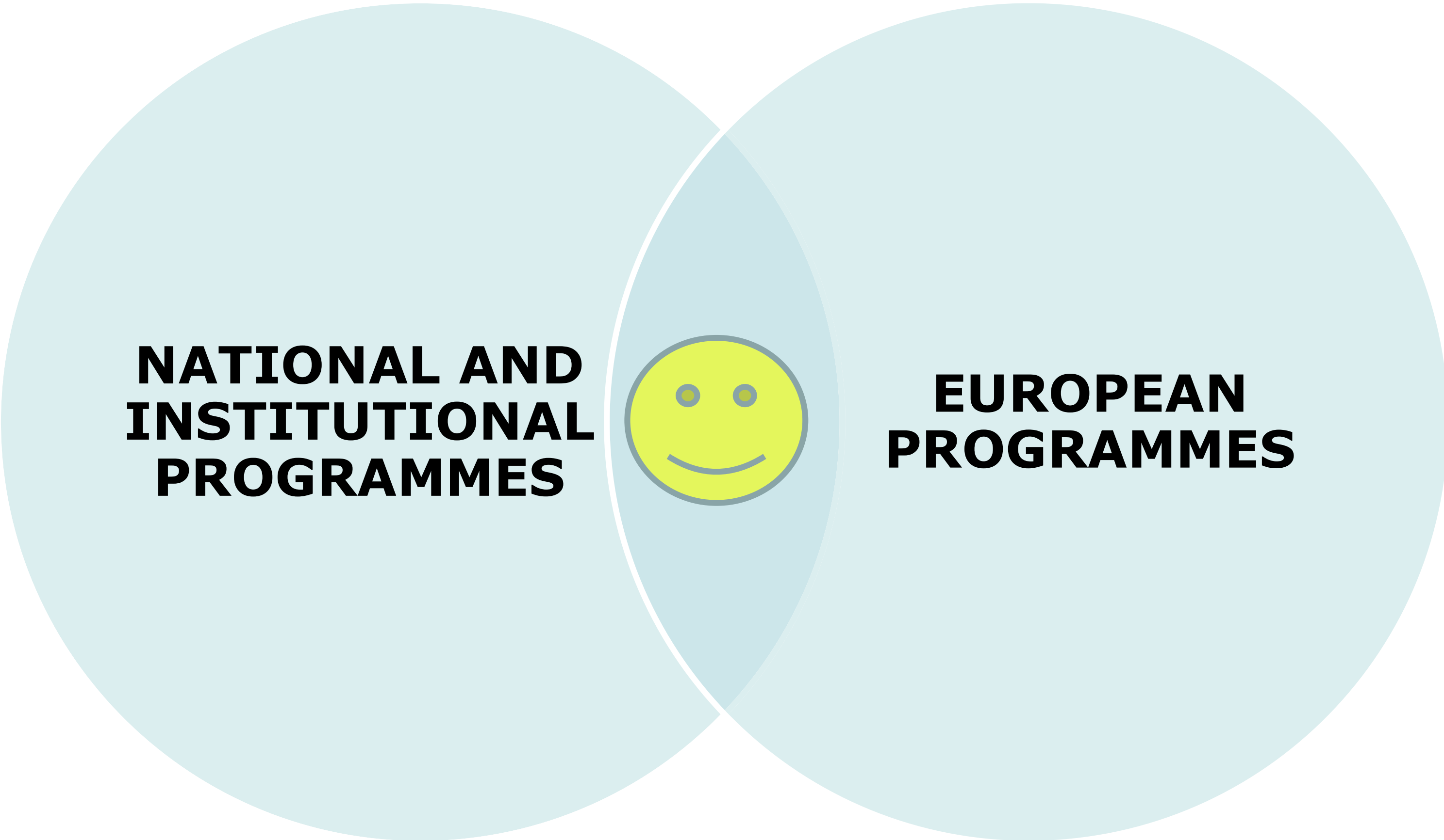

FUTURE SKY

FS

SAFETY

FS

QUIET

FS

ENERGY

FS

INTEGRATION

EREA

FUTURE SKY SAFETY

FUTURE SKY QUIET

ARTEM - Aircraft noise Reduction Technologies and related Environmental iMpact (22 partners)
Development of innovative technologies for the reduction of aircraft noise at the source. Innovative concepts for the efficient damping of engine noise and other sources by the investigation of dissipative surface materials and liners. Noise shielding.

ANIMA - Aviation Noise Impact Management through Novel Approaches (23 partners) Aims to analyze the methods deployed by different types of European airports to manage aircraft noise in order to design and propose the best solutions to reduce the annoyance felt by the local residents.

RUMBLE - Regulation and norm for low sonic Boom Level

FUTURE SKY ENERGY

- **<u>Innovative engines/propulsion systems</u>**
  - hybrid engines/propulsion
  - electrical engines/propulsion
  - distributed electrical engines/propulsion

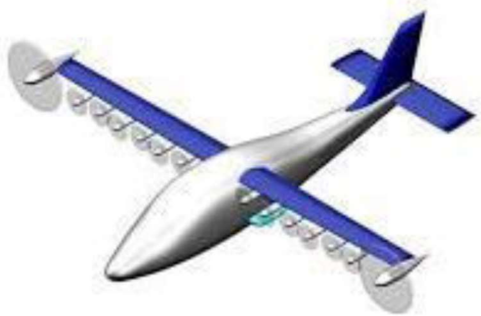

- **<u>Innovative energy sources</u>**
  - Electrical power generation, distribution and conversion
  - batteries
  - fuel cells

- **<u>Innovative configurations of Small and Regional Aircraft</u>**
  breakthrough enabling technologies for the innovative configurations (aerodynamics, aerostructures, flight mechanics etc.)

- **<u>Energy management and on board electric equipment</u>**

FUTURE SKY INTEGRATION

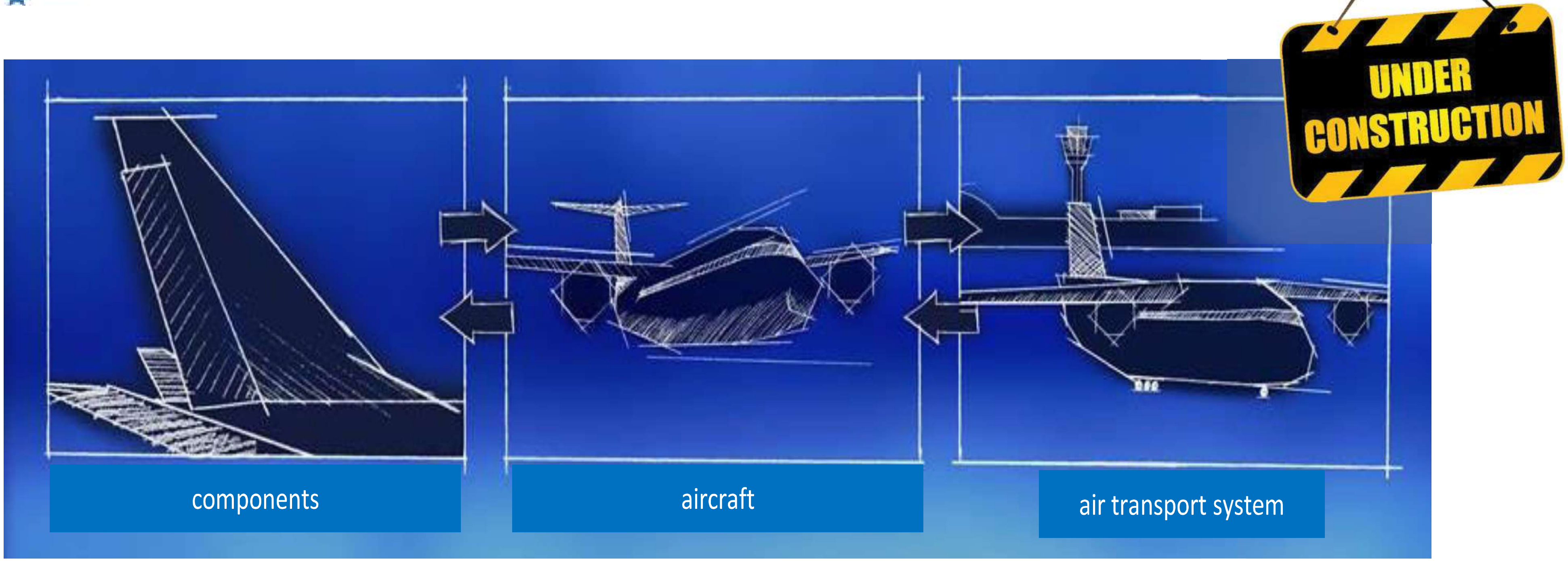

AIR TRANSPORT INTEGRATION =

integration of aircraft into the air transport system (ATS)

+

integration of the ATS into the general transport system

FUTURE SKY INTEGRATION

Create a **virtualization of the ATS**:

- **Development of a model** of the future ATS

- **Derivation** of technical requirements and targets for the design of novel aircraft and infrastructure based on the model and several scenarios

- **Analysis and Assesment** of the impact of novel aircraft integration, infrastructure and processes into the ATS.

www.erea.org

www.futuresky.eu

Presentation 2302

EREA RTDI Capabilities and Infrastructure

Meeting the flightpath challenge on Environment and Energy

The Future Sky Energy Initiative

Marcello Kivel Mazuy
Centro Italiano Ricerche Aerospaziali CIRA

EREA RTDI Capabilities and Infrastructure

Meeting the flightpath challenge on Environment and Energy

The Future Sky Energy Initiative

The Future Sky Energy (FSE) initiative is an EREA proposal for creating a coordinated programme,tackling the Flightpath challenge of Environment Protection and the Energy Supply.

This paper will show an overview of the activities foreseen by EREA Research Establishments in this framework,including enabling technologies and highlighting the main EREA RTD&I competences, and infrastructures for the FSE programme implementation.

As starting point for delivering useful technologies within 2035-2050 framework, in the long term also for 'large passengers aircraft, the targeted innovative vehicles will beSmall Air Transport (SAT) aircraft(CS-23 / 4-19 seats) and regional aircraft (CS-25 / 4-19 seats 19-75 seats).

The final goal is the zero emissions aviation by means of breakthroughpropulsion systems and technologiesintegrated in innovative configurations; this innovation requires intensive validation and experimental testing, real scale on ground demonstrators and scaled Flying Test Beds(FTBs).

In order to design systems ableto fulfill the flightpath goals, *Future Sky Energy* intends to address and explorespecific RTD themes with dedicated enabling technologies that will be detailed in the paper:

- Multidisciplinary design tools
- Advanced Configurations
- New Material and production processes
- New regulatory framework
- New solutions for energy storage
- Hybrid-Electric propulsion
- Electric propulsion

Finally,the three pillar approach (REs Institutional Programmes, EC funded projects, Stakeholdersinvolvement and research programmes) will be highlighted showing the dedicated Roadmap of implementation, whilst main RTD&I capabilities and infrastructures provided by REs will be also highlighted.

Section III

AFloNext

Paper 2404

Design of a Pulsed Jet Actuator for Separation Control

Philipp Schlösser
Airbus Defence and Space GmbH
Researcher, PhD Candidate
81663 Munich, Germany
philipp.schloesser@airbus.com

Design of a Pulsed Jet Actuator for Separation Control

Philipp Schlösser
Airbus Defence and Space GmbH
Research Engineer, PhD Candidate
81663 Munich, Germany
philipp.schloesser@airbus.com

Matthias Bauer
Navasto GmbH
Research Engineer, CEO
Karl-Kunger-Straße 17, 12435 Berlin, Germany
matthias.bauer@navasto.de

ABSTRACT

A pulsed jet actuator for separation control has been developed for application in a real-scale wind tunnel experiment with focus on separation behind the pylon-wing junction. The concept of the actuator bases on fluidic technology and applies pulsed blowing without the help of moving parts. Design parameters are given by numerical simulations of the experimental application case and are validated in ground test. Results of these ground tests are presented and parameters for wind tunnel test settings are derived. The further evaluation of ground test results yields a relation of momentum coefficient, supply mass flow and wind tunnel velocities. It is shown that for the given wind tunnel experiment levels of constant momentum coefficient approximately coincide with levels of constant velocity ratio. All requirements with respect to flow control parameters and model geometry can be satisfied with the presented design.

KEYWORDS: active flow control, separation control, pulsed jet actuator

NOMENCLATURE

Acronyms
AFC – Active Flow Control
CFD – Computational Fluid Dynamics

Latin
c_μ – momentum coefficient
c – chord length
DC – duty cycle
F^+ – normalized frequency
f – frequency
I – momentum flux
$\dot{m}$ – mass flow
M – MACH number
q – dynamic pressure
R – specific gas constant
S – surface area
T – temperature
u – velocity
VR – velocity ratio

Greek
γ – ratio of specific heats
ρ – density

Subscripts
AFC – AFC system property
jet – AFC jet property
peak – maximum value
ref – reference property
0 – stagnation property
∞ – ambient/free-stream condition

1 INTRODUCTION

Separation of air flow over an aerodynamic surface is usually undesirable. The functional limit of an aircraft wing is given by separation on large sections of the wing, commonly known as stall. Active Flow Control (AFC) is a trending technology that can potentially enhance the performance of aircraft and was recently demonstrated in flight test with separation control applied to the vertical stabilizer of an airliner [1]. Previously, the potential of AFC has been proven in wind tunnel tests with a variety of different control systems [2, 3, 4].

This paper describes the design and development of a pulsed jet actuator intended for separation control at the pylon-wing junction. The theoretical background is given followed by a summary of the actuator development. Results of ground testing are shown and evaluated with respect to settings required during wind tunnel testing.

2 SEPARATION CONTROL

The technology of AFC can target many different aspects of aerodynamics, but in this publication the focus is put on separation control. The aim of the presented actuator design is to delay or even suppress separation. Separation control was investigated by Prandtl as early as 1904 in the form of boundary layer control [5] and has since been further researched and improved. This publication further focuses on an *active* separation control approach which means that external energy in the form of pressurized air is required. The basic principle of active separation control can be summarized as adding momentum to the boundary layer to increase its resistance against adverse pressure gradients. It has been shown in numerous publications, that local surface-tangential blowing is successful in adding momentum to the boundary layer and providing the necessary resistance against separation. The momentum addition is further increased by entrainment of surrounding high-momentum flow [6]. Advancing to oscillatory blowing, commonly applied in a periodic form, further increases the effectiveness of separation control through the generation of vortical structures [7]. These additional vortices increase the momentum transfer from high-momentum flow towards the boundary layer. The presented work applies unsteady forcing with high amplitude that reaches beyond the boundary layer, a mechanism that was thoroughly investigated and tested for example by Bauer [8].

Different applications of active flow and separation control depend strongly on local aerodynamics, specific conditions of the boundary layer state and the underlying separation mechanism. A direct comparison is therefore usually difficult but three prominent parameters are commonly used to compare the actuation amplitude, air jet velocity and actuation frequency. The momentum coefficient

$$c_\mu = \frac{I}{q_\infty \cdot S_{\mathrm{ref}}} \tag{1}$$

relates the momentum flux added by the actuation system I to the momentum flux of the free-stream. The latter is calculated as the product of the incidence dynamic pressure q_∞ and a reference area, i.e. the projected model surface S_{ref}. The velocity ratio is defined by [9] as

$$VR = \frac{u_{jet}}{u_\infty} \tag{2}$$

where u_{jet} is the velocity of the jets produced by the AFC system and u_∞ is the incidence velocity. The third parameter relates to the frequency of actuation and is calculated in analogy to a STROUHAL number as the nondimensional frequency

$$F^+ = \frac{f_{AFC} \cdot c}{u_\infty} \tag{3}$$

where f_{AFC} is the actuation frequency of the system and c is the chord length. Previous numerical investigations within the framework of this publication have shown a neglectable effect of F^+ on the aerodynamic effectiveness of the AFC system [10].

3 ACTUATOR DESIGN

Pulsed air blowing with net mass flow is exerted with the help of a two-stage flow control system. For safety-driven industries like ours this concept is attractive due to the lack of moving or electrical components. The present flow control system employs a two-stage design with a fluidic oscillator acting as the driving (or 1st) stage and an array of fluidic diverter elements acting as the outlet (or 2nd) stage. Fluidic oscillators make use of the possibility to switch a primary jet between two stable states by applying a much weaker control jet. Fig. 1a depicts a single diverter element of the outlet stage at an instant in time where the left outlet is active. This instant corresponds to a flow state of the driving stage where the right port is active and therefore pushes the primary mass flow towards the left outlet. At an instant half a period later, this flow state will be reversed, and the right outlet will be active. Fig. 1b shows the final layout of the actuators' internal flow channels. The span-wise structure is the driving stage, based on the principle of a fluidic oscillator. Behind it, seven diverter elements as shown in Fig 1a are aligned that together form the outlet stage. For a more detailed description and application of a similar two-stage system refer to Bauer *et al.* [2].
The possibility to provide unsteady airflow with only one stage of fluidic oscillators has previously been shown in several publications, e.g. with sweeping jets in [11]. The design effort of the two-stage actuator concept significantly increases in contrast to single-stage oscillators like sweeping jets. The reason for choosing the two-stage design regardless is given by three aspects of interest for future application of the technology on an aircraft:

- Increased efficiency – the conversion of total to dynamic pressure is more efficient due to the application of several diverters driven by only one oscillator that produces the most losses due to its internal complexity
- Improved compactness – driving multiple diverters with one oscillator reduces the required installation space, as only the driving oscillator requires feedback lines
- Improved variability – the two-stage actuator design allows for an independent setting (and tuning) of actuation amplitude and frequency

Requirements with respect to flow control parameters, geometry and the test environment are collected in Table 1. These requirements are the basis of a successful design of the actuator. As the functionality of the flow control system relies purely on its internal shaping, it is not possible to design an actuator with any given combination of parameters – e.g. low switching frequencies require a sufficiently large feedback structure, therefore defining a minimum size of the overall AFC system. The design of the two-stage AFC system is undertaken in a three-step process with increasing design fidelity. A theory based approach is used to define the basic features of the flow control system, including its approximate dimensions, the number of elements in the second stage, and the dimensions of critical flow cross-sections. Based on these formulations the design for the second stage elements is derived. The workflow is concluded by the development of the driving stage and the integration of the two stages with experimental testing and refinement of parameters. Employing further experimental testing, the design is modified until all specifications and requirements - i.e. with respect to modulation, frequency and spatial jet homogeneity - are satisfied.

Rapid prototyping and 3D printing are used whenever a prototype is necessary – approximately once per iteration loop. CFD simulations are used mostly to analyse the internal flow topology of the actuators, while the practical experiment-based approach provides information on the flow conditions at the outlet and consequently the actuator's performance.

Table 1: Potential requirements for actuator design

Flow control / physics	**Model / geometry**	**Environment / wind tunnel**
• jet velocity / MACH number range • pulsation frequency range • mass flow rate or outlet slot dimensions • number of slots • geometric jet exit angle • jet quality criterion (jet velocity homogeneity)	• location of AFC system integration: span-wise extent, chord-wise location, local surface curvature • installation space: bounding box for the AFC system, model-internal obstacles • interfaces for structure and pressure supply	• loads on the AFC system • temperature of ambient and working fluid • security factors issued by the wind tunnel operators *Environmental aspects do not necessarily influence the actuator performance, but can act as significant cost drivers for testing and manufacturing!*

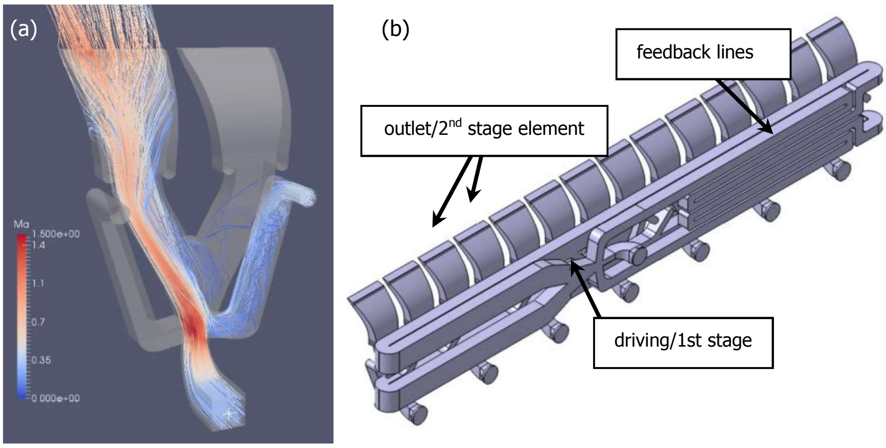

Figure 1: (a) Final design of a second stage diverter element; streamlines colored according to Mach number [13]; (b) Final design of the actuator's internal flow channels

The flow control parameters as well as geometrical constraints both collected in Table 1 are derived from CFD simulations of the wind tunnel model [10, 12]. The resulting system is designed as an insert integrated at ten percent relative chord length inboard of the engine pylon. The outlets of the system are inclined at 30 degrees to the local surface. In total, 14 slots are integrated into the design which produces pulsing jets with a 180 degree phase-shift between adjacent outlets. The total span-wise extent of the insert is approximately one meter. The flow control insert is equipped with a number of pressure sensors to monitor its function and performance. Three major functions have to be monitored: if each of the outlets is supplied with pressurized air; if the fluidic oscillator is providing the necessary control flows and if overall performance is achieved, i.e. if pressure levels are met. In addition to the pressure sensors, a mass flow meter is installed in the supply pipe outside of the wind tunnel model.
The flow control system including all monitoring sensors was optimized in preceding ground-tests. First results of these ground tests show that the system is fully functional (full modulation of jets) and that the desired parameters are possible within given mass flow and pressure limits [13]. In the next chapter the ground tests are revisited and further results are presented.

4 GROUND TESTING OF THE PULSED JET ACTUATOR

After theoretical and numerical development of the pulsed jet actuator, a series of ground tests is performed to optimize and finalize the design. Three stages of ground testing are used to acquire the necessary data. Preliminary results of the first and second test stage, which cover an optimization of the actuation frequency and an investigation of the manufacturing method, are discussed in [13]. In a third stage of the ground test, the final actuator for integration into the wind tunnel model is investigated. All necessary hardware including the monitoring system is included in this final test.

An important step of the actuator design is the integration of the two stages and the following testing of the first complete system prototype. This step of the design process is focused on a final tuning of the actuation frequency by varying the length of the driving stage's feedback lines. For easy variation and tuning of the actuation frequency, a modular system with flexible tubes is incorporated into this first prototype. From this data the required feedback length structure can be directly inferred. In addition, such an experiment on a full system prototype allows validating the prediction of the system limits with respect to lower and upper working mass flow rates. The size of the full AFC system as well as the number of permutations of feedback length and mass flow rates of interest (here: approx. 100 data points) makes the use of CFD for this task uneconomical. Experimental results of this stage of testing are presented in the next section.

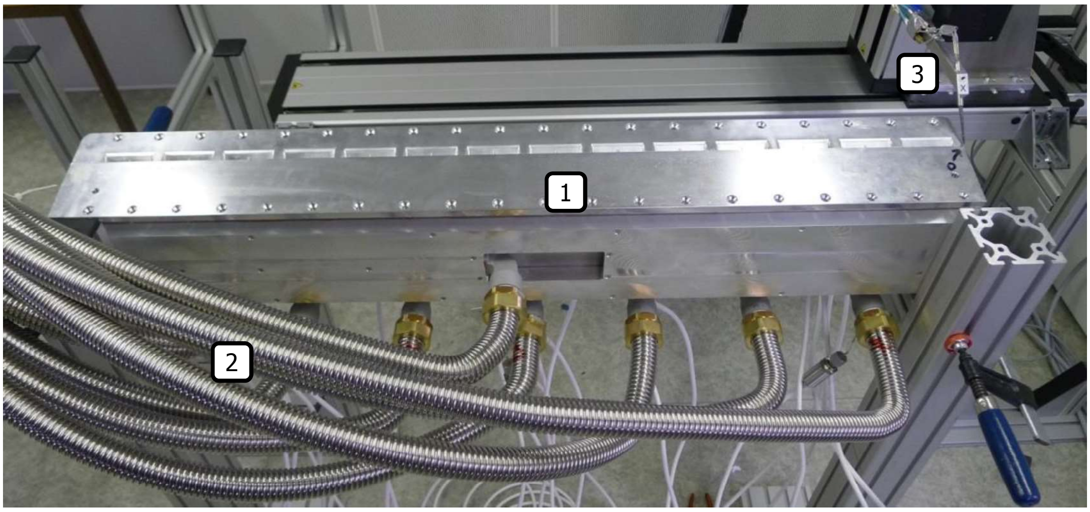

Figure 2: Test setup of the pulsed jet actuator (1) with corrugated pipes (2) and three-hole-probe on a three-axis traverse (3) [13]

Fig. 2 depicts the final pulsed jet actuator (1) during the last stage of ground testing, which focused on a final characterization of the system. The actuator is manufactured from four separate Aluminium layers that incorporate the flow channel geometry (c.f. Fig. 1b). Two layers together form the shell of the outlet and driving stage respectively whereas the inlets are manufactured separately with 3D-printing of Aluminium. The supply air is delivered through eight individual corrugated pipes (2) to the actuator (1). During ground testing, the produced jets are investigated with the help of a three-hole probe (3) on a three-axis traverse. With this setup, the jet MACH number was measured on a field spanning all 14 outlets. In addition, the supply mass flow was logged as well as data of the monitoring sensors. From this data, it can be stated if the corresponding outlet is active, in correct phase with its partner, and if the desired working point is achieved. The three-hole probe was moved across the outlets at a height of 1 mm above the actuator with approx. 2500 measurement points per diverter. Phase-averaging of data logged over one second was used to evaluate and condense the measurements to one "average pulse". Further evaluations based on this time history of the phase-averaged pulsed jet are presented in the following chapter.

5 GROUND TEST RESULTS

During ground tests with the first prototype, frequency data was logged together with a variation of feedback length and mass flow rates. In Fig. 3 the resulting normalized frequencies are plotted versus the mass flow rate normalized with respect to the design point. The dashed lines correspond to several different feedback length settings, where the top line marked with circles represents the initial design. As expected, the actuation frequency decreases with longer feedback lines and increases at higher mass flow rates due to increased flow velocities and therefore shorter switching times. The collection of frequency data is only possible starting at settings of approx. 40% of the design mass flow. At lower mass flow rates, the driving stage (a fluidic oscillator) does not function properly. In the data corresponding to the prototype measurements (dashed lines), the upper limit at approx. 80% is not given by the system but is rather a result of the testing facility. During these first measurements, no higher mass flow rates were available.
The measurement data of nine different feedback lengths was used to extrapolate the desired actuation frequency at the design point and to consequently choose the corresponding feedback length. Due to the given bounding box of the AFC system, the resulting feedback lines were incorporated in the upper layer of the driving stage in a meander-like fashion. The internal flow channels are depicted in Fig. 1b and indicate the final layout with refined feedback lines. The solid black line in Fig. 3 corresponds to data measured with the final actuator as shown in Fig. 2. At the design point, a normalized actuation frequency of $F^{+} = 4.3$ is reached which perfectly satisfies this requirement.

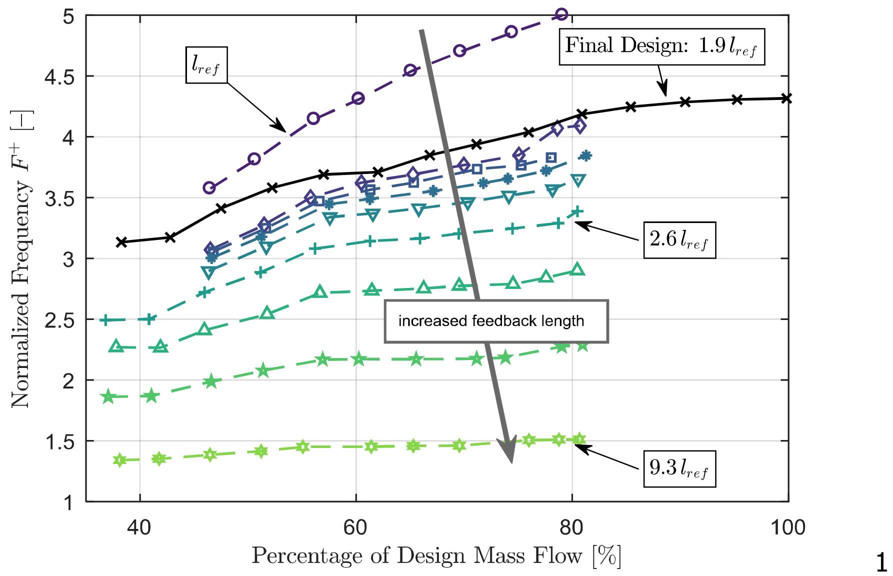

Figure 3: Actuation frequency in relation to mass flow; dashed lines resulting from prototype at variable feedback lengths, solid line resulting from final actuator

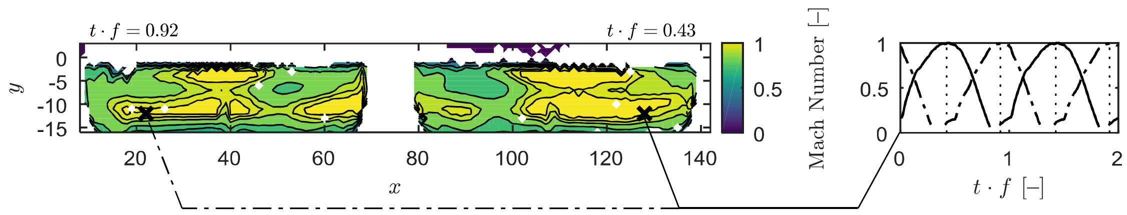

Figure 4: Contours of jet MACH number at time of peak values in each slot with time history of two selected points over two pulses

MACH number data evaluated from the three-hole probe measurement during the last stage of ground testing is presented in Fig. 4. The MACH number contours of one diverter element are shown exemplarily. The data is taken from two instants during one phase-averaged period, with each instant corresponding to the time were peak MACH numbers are reached in the respective slot. It can be noticed, that both outlets produce similar MACH number patterns, while reaching values of $M > 0.8$ across large sections of the slots. In significant sections of the slots, values of $M \approx 0.99$ are evaluated, only limited by the calibration range of the three-hole probe (yellow contour). In addition to the contour plot, the MACH number histories of two selected points are plotted over two pulses. This plot clearly indicates, that full modulation of the jet is achieved, with MACH numbers dropping to zero during the active cycle of the opposite slot. This evaluation shows, that two of the design targets are satisfied: The peak MACH number of $M_{peak} = 1.0$ is reached and full modulation of jets is achieved at the design point.

Resulting from measurements with the three-hole probe, a correlation between the jet MACH number M and the supply mass flow $\dot{m}$ can be extracted, see Fig. 5. This correlation is the most important result of the ground test and is required during wind tunnel experiment, because no velocity or MACH number measurements of the jets can be performed during these tests. An installation of any kind of measurement would interfere with the flow and would distort the actual aerodynamics in the area of interest. In Fig. 5, the mass flow is normalized with respect to the design mass flow. Measurement data starts at approximately 40% because a minimum mass flow through the driving stage is required for the fluidic oscillator to function properly. A cubic polynomial is used to fit a curve in the plotted interval for further evaluation. The target of the further evaluation is the collection of "points of interest" within the operation range of the actuator, i.e. 40 - 100% mass flow. As introduced in section 2, the momentum coefficient c_μ and the velocity ratio VR are of major interest.

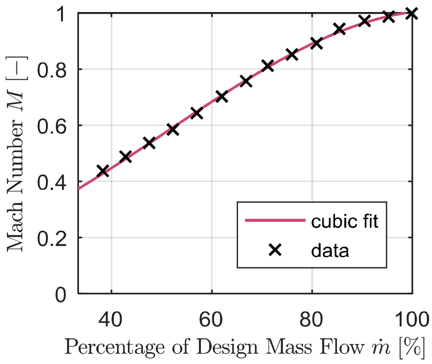

Figure 5: Peak jet MACH number versus mass flow; curve fit based on cubic polynomial

Proceeding from Eq. 1, the momentum coefficient for pulsed blowing can be expressed as

$$c_\mu = \frac{I}{q_\infty \cdot S_{\mathrm{ref}}} = \frac{1}{2\sqrt{DC}} \cdot \frac{\dot{m} \cdot u_{\mathrm{jet,peak}}}{\frac{\rho_\infty}{2} u_\infty^2 \cdot S_{\mathrm{ref}}}, \tag{4}$$

where DC is the duty cycle of the actuation, here fixed at 0.5 with periodic blowing, and where $u_{\mathrm{jet,peak}}$ is the maximum jet velocity achieved during one cycle. The factor $1/(2\sqrt{DC})$ together with the peak jet velocity $u_{\mathrm{jet,peak}}$ represents the root mean square of the periodic pulse. Multiplying this value with the mass flow yields the effective momentum introduced into the flow, c.f. Eq. (1). The peak jet velocity can be calculated from the measurement data and the corresponding fit in Fig. 5 according to

$$u_{\mathrm{jet,peak}} = M_{jet,peak} \cdot \sqrt{\gamma R T_{jet}}\,. \tag{5}$$

Here, T_{jet} is the static jet temperature calculated according to isentropic flow relations with the jet MACH number M and the total temperature of the supply air T_0. With the assumption of constant values for DC, ρ_∞ and T_0 Eq. 4 together with Eq. 5 is reduced to $c_\mu = \mathrm{f}(\dot{m}, u_\infty)$. With the cubic fit plotted in Fig. 5 and the definition in Eq. 2 the velocity ratio can also be expressed as a function of $\dot{m}$ and u_∞ as $VR = \mathrm{g}(\dot{m}, u_\infty)$. This allows plotting a multitude of curves within the operation range of the actuator $\dot{m} \in [0.4,1]$ and the possible range of incidence velocities $u_\infty \in [30, 50]\,\frac{\mathrm{m}}{\mathrm{s}}$.

Fig. 6 depicts seven of these curves, with three of them plotted at constant incidence velocities (solid lines) and four of them plotted at constant velocity ratios (dashed lines). Three defined incidence velocities are used for visualization purposes. The levels with $VR = const.$ are set equidistantly between the maximum and minimum VR at the highest plotted incidence speed.
What is remarkable in Fig. 6 is that levels of constant velocity ratio VR approximately coincide with levels of constant momentum coefficient c_μ. This reduces the number of independent variables and therefore facilitates the analysis during wind tunnel experiments. Only at higher VR and $\dot{m}$ do the curves with $VR = const.$ deviate from levels with constant momentum coefficient. Given the assumptions of this evaluation based on isentropic flow the error is minor in comparison and therefore allows for a selection of "points of interest" from the generated data. The first "points of interest" are selected according their expected aerodynamic effectiveness and a realistic application of the system. First, the maximum possible $c_\mu \approx 0.025$ and $VR \approx 10$ are of interest (lowest incidence speed at highest mass flow), which represents the point of maximum energy the AFC system can introduce with respect to the incidence flow. This setting should achieve the highest aerodynamic effect but is unlikely to be applied in a realistic scenario (low incidence velocity means low REYNOLDS number, VR limited by onboard air supply). In addition, all intersection points on the curve representing the highest incidence speed are of interest because in this case a realistic REYNOLDS number of approx. 11 million is represented. These points should provide an "envelope" of the realistically possible aerodynamic effect and provide the basis of an analysis in terms of "cost/benefit".

Integration and testing of the AFC system are successfully performed in a large-scale wind tunnel facility. Due to the focus of this paper on the actuator design, no further results of the wind tunnel campaign are discussed. The successful installation of the actuator into the wind tunnel model concludes the actuator development with its designated application. Model and geometrical requirements are satisfied and no issues with respect to the test environment are present.

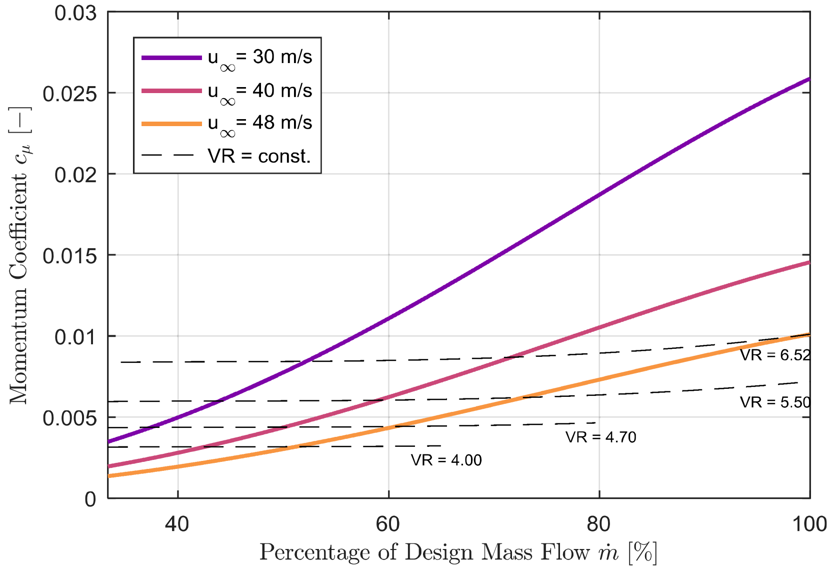

Figure 6: Evaluation of momentum coefficient at several incidence velocities; dashed lines indicate levels of constant velocity ratio

6 CONCLUSION

A pulsed jet actuator for separation control at the pylon-wing junction has been designed, optimized and manufactured for application in a full-scale wind tunnel test. Benefits of the applied two-stage concept are described and the corresponding design work flow is introduced. Design parameters are presented that are based on requirements with respect to flow control physics and performance as well as to the actuator and model geometry. The design target for these parameters is derived from CFD simulations of the wind tunnel model.
Two important steps of the design process are described in more detail, namely the testing of a first full system prototype and the characterization of the final actuator. The first ground test of the prototype is focused on a tuning of the actuation frequency with the help of variable feedback lines. Results of this ground test stage are used to refine the geometry of the fluidic oscillator. A comparison of frequency data of the prototype and the final actuator proves that this design step was successful and that the target actuation frequency range is reached with the final actuator. An evaluation of the three-hole probe data shows that the required peak MACH numbers are reached and that full modulation of the jet is achieved. Jet MACH numbers logged during the last ground test of the final actuator are used to further evaluate the most important parameters of flow control, i.e. the momentum coefficient c_μ and the velocity ratio VR. For the presented actuator it is shown that levels of constant velocity ratio approximately coincide with levels of constant momentum coefficient. This reduces the amount of independent variables and allows for a simplified identification of interesting settings during wind tunnel testing.
Results of the ground test conclude that all parameters with respect to flow control are within their design limits. The first successful installation of the actuator proves that all geometrical requirements are satisfied. Wind tunnel test are performed as planned with flow control settings and parameters derived from the presented evaluation.

ACKNOWLEDGMENTS

The work described in this paper and the research leading to these results have received funding from the European Community's Seventh Framework Programme FP7/2007-2013, under grant agreement n° 604013, AFLONEXT project.

REFERENCES

1. J. C. Lin, M. Y. Andino, M. G. Alexander, E. A. Whalen, M. A. Spoor, J. T. Tran, I. J. Wygnanski; 2016; "An overview of active flow control enhanced vertical tail technology development"; *54th AIAA Aerospace Sciences Meeting*; San Diego; January 1 - 8; pp. 1-13
2. M. Bauer, J. Lohse, F. Haucke, W. Nitsche; 2014; "High-lift performance investigation of a two-element configuration with a two-stage actuator system"; *AIAA journal*; **52**(6); pp. 1307-1313
3. P. Scholz, C. J. Kähler, R. Radespiel, J. Wild, G. Wichmann; 2009; "Active control of leading-edge separation within the German flow control network"; *47th AIAA Aerospace Sciences Meeting*; Orlando; January 5 – 8; AIAA 2009-0529;
4. A. Seifert, A. Darabi, I. Wyganski; 1996; "Delay of airfoil stall by periodic excitation"; *Journal of aircraft;* **33**(4); pp. 691-698
5. L. Prandtl; 1935; "The mechanics of viscous fluids"; *Aerodynamic theory*, Vol. III, pp. 34-208
6. G. Jones, C. Yao, B. Allan; 2006; "Experimental investigation of a 2D supercritical circulation-control airfoil using particle image velocimetry"; *3rd AIAA Flow Control Conference;* San Francisco; June 5 – 8; AIAA 2006-3009
7. D. Greenblatt; I. Wygnanski; 2000; "The control of flow separation by periodic excitation"; *Progress in aerospace Sciences*; **36**(7); pp. 487-545.
8. M. Bauer; 2015; "Design and application of a fluidic actuator system for high lift flow control"; *PhD Thesis;* Technical University; Berlin
9. H. Nagib, J. Kiedaisch, P. Reinhard, B. Demanett; 2006; "Control techniques for flows with large separated regions: A new look at scaling parameters"; *3rd AIAA Flow Control Conference;* San Francisco; June 5 – 8; AIAA-2006-2857
10. S. Fricke, V. Ciobaca, A. Kröhnert, J. Wild, O. Blesbois; 2015; "Active Flow Control Applied at the Engine-Wing Junction"; *5th CEAS Air and Space Conference*; Delft; September 7 -9; No. 249
11. R. Seele, P. Tewes, R. Woszidlo, M. A. McVeigh, N. J. Lucas, I. J. Wygnanski; 2009; "Discrete Sweeping Jets as Tools for Improving the Performance of the V-22"; *Journal of Aircraft*; **46**(6); pp. 2098-2106.
12. S. Fricke, V. Ciobaca, J. Wild, D. Norman; 2016; "Numerical Studies of Active Flow Control Applied at the Engine-Wing Junction"; R. Radespiel; *Advances in Simulation of Wing and Nacelle Stall;* Springer International; Braunschweig; pp. 397-411
13. P. Schloesser, M. Meyer, M. Schueller, P. Weigel, M. Bauer; 2017; "Fluidic actuators for separation control at the engine/wing junction", *Aircraft Engineering and Aerospace Technology*, https://doi.org/10.1108/AEAT-01-2017-0013

Paper 2405

Design of a Synthetic Jet Actuator for Separation Control

Perez Weigel
Fraunhofer Institute for Electronic Nano Systems ENAS
Research Associate
Technologie-Campus 3, 09123 Chemnitz, GERMANY
perez.weigel@enas.fraunhofer.de

Martin Schüller
Fraunhofer Institute for Electronic Nano Systems ENAS
Research Associate
André Gratias
Fraunhofer Institute for Electronic Nano Systems ENAS
Research Associate

Mathias Lipowski
Fraunhofer Institute for Electronic Nano Systems ENAS
Research Associate

Theo ter Meer
NLR – Netherlands Aerospace Centre
R&D Engineer
Anthony Fokkerweg 2, 1059 CM Amsterdam, NETHERLANDS

Michiel Bardet
NLR – Netherlands Aerospace Centre
Senior Application Engineer

Design of a Synthetic Jet Actuator for Separation Control

Perez Weigel
Fraunhofer Institute for Electronic Nano Systems ENAS
Research Associate
Technologie-Campus 3, 09123 Chemnitz, GERMANY
perez.weigel@enas.fraunhofer.de

Martin Schüller
Fraunhofer Institute for Electronic Nano Systems ENAS
Research Associate

Theo ter Meer
NLR – Netherlands Aerospace Centre
R&D Engineer
Anthony Fokkerweg 2, 1059 CM Amsterdam, NETHERLANDS

Michiel Bardet
NLR – Netherlands Aerospace Centre
Senior Application Engineer

ABSTRACT

This paper describes the development of a piezo-electric Synthetic Jet Actuator (SJA) in the AFLoNext project. AFLoNext (Active Flow – Loads & Noise control on Next generation wing) is a project within European Union's 7th Framework Program. One of the main goals is the application of Active Flow Control (AFC) techniques, such as SJAs and Pulsed Jet Actuators (PJAs) in two different application scenarios to evaluate the potential benefit for retrofit of current aircraft and also for future aircraft designs. For large-scale wind tunnel testing, an actuator panel with 85 SJAs including the drive electronics system was designed and pre-tested in a laboratory environment. The performance exceeds 100 m/s with outlet nozzles of 2.5 mm diameter and a span wise clearance of 10 mm. A second actuator design was prepared for the application on the outer wing region and was investigated in an environmental test campaign. Two rows of 5 actuators were integrated in a panel with 10 x 0.5 mm² slotted outlet nozzles. With this design also velocities exceeding 100m/s can be measured. The actuators withstand different harsh environmental conditions including extreme temperature, rain, mechanical vibration and shock. With the results of the project, a Technology Readiness Level (TRL) evaluation will conclude the maturity of the technology. Depending on the final test and evaluation results, achievement of TRL4 is expected.

KEYWORDS: *Synthetic Jet Actuator, separation control, robustness test campaign, wind tunnel evaluation*

1 INTRODUCTION

1.1 AFLoNext technology streams

AFLoNext is a project within the European Union's 7th Framework Program. One of the main goals is the application of Active Flow Control (AFC) techniques, such as Synthetic Jet Actuators (SJA) and Pulsed Jet Actuators (PJA) in two different application scenarios to evaluate the potential benefit for retrofit of current aircraft and also for future aircraft designs. An overview of the different Technology Streams (TS) in the project is depicted in Figure 1. In TS2 the application of Synthetic Jet Actuators on outer wing region is evaluated. For the actuator development in TS2 the focus was on the robustness of the system. A detailed test campaign for the assessment of the system in different harsh environmental conditions was performed. A second application scenario is evaluated in TS3. The actuators are applied on the wing/pylon junction to counter the lift losses caused by the closely-coupled integration of Ultra High Bypass Ratio (UHBR) turbofan engines. The other Technology Streams within the project deal with other approaches for reducing emissions for future aircraft, such as hybrid laminar flow control or noise and vibration mitigation.

Figure 1: Overview of Technology Streams for the AFLoNext project

1.2 State of the Art review

It has been known for two decades that Synthetic Jet Actuators) are able to manipulate an air flow. This effect can be used for fluidic active flow control, especially for aerospace applications. Apart from this this, their possible application field is very wide. SJA can be used for cooling of small surfaces, jet vectoring, pumping, mixing enhancement and for many other purposes. The device consists of a small cavity which is closed on one side by a vibrating transducer element. On the other side of the actuator a nozzle connects the cavity with the external environment. The vibration of the transducer element leads to a periodic suction and exhausting of the surrounding fluid through the nozzle. Due to the pulsed blowing a synthetic jet is formed in front of the nozzle, even if the net mass-flow through the actuator is zero. The advantages of SJAs are that they do not need an external compressed air source, are relatively small and have a low power consumption. Challenging is their limited performance with respect to possible peak velocities and the interdependence of the resonance behaviour and environmental conditions. The development in AFLoNext aims on a progress towards feasible actuators for future aircraft integration. The identified drawbacks of the actuators are addressed and the designs focus on both aspects - high performance as well as high robustness - to meet the industrial requirements.

The majority of the described actuators in literature use piezo-electric transducers (1–6), but also actuators with shape-memory alloy based transducers (7) or mechanical piston actuators (8, 9) are used to drive SJA. Next to this kind of transducers, also actuators with electro-dynamic transducers are described (10). The normal velocity range of the described actuators lies below 50 m/s. The different geometrical parameters of the actuators make an overall benchmark of different prototypes difficult, because the peak velocity depends on drive frequency, nozzle geometry, cavity volume and even the used clamping method for the transducer element. A review of the current state of the art has identified four main aspects for further optimization:

- Transducer element optimization calculations and simulations;
- Modelling and optimization calculation for geometrical parameters for the fluidic resonator;
- Clamping and electrical contact for transducer element integration;
- Increased robustness against harsh environmental conditions.

The requirements given by the industrial partners cover constraints of the following aspects:

- ***System installation and assembly room***
- ***Active flow control performance***
- Energy consumption
- ***Materials***
- Operability
- Redundancy
- ***Structural Considerations***
- Weight

Not all requirements apply to the hardware system which is evaluated in wind tunnel tests. The focus has been the bold marked aspects above to keep the effort in line with the available time. All other aspects will be addressed in further developments of the actuator system towards a future flight test.

2 ACTIVE FLOW CONTROL ON THE WING / PYLON JUNCTION

2.1 Concept for Wind Tunnel Evaluation

The main goal of the system design was the compliance with the requirements that apply to the integration in a 1:1-scale wind tunnel model. Because of the limited budget and time, a cost optimized solution is designed with the option to further miniaturize and integrate the system in future design iterations. The final specification of the actuators was not available during the design phase of the system, so certain assumptions had to be made. This led to the modular approach of the system. Changes on the system can be made more easily than with fully integrated systems.

An overview of the complete system design for the SJA AFC system is shown in Figure 2. It consists of three main parts:

- The SJA Insert for the housing of the actuators and the integration in the wind tunnel model;
- Signal conditioning, actuator excitation and monitoring equipment, located as close as possible near the wind tunnel model (Drive Electronics subracks);
- The HMI (Human Machine Interface) computer for control, data recording and visualisation.

The Drive Electronics system consists of two High Voltage (HV) Amplifier subracks that are controlled by a Measurement & Control (M&C) subrack. It provides high-voltage excitation signals for the actuators and monitors the current status of the system and the individual actuators.

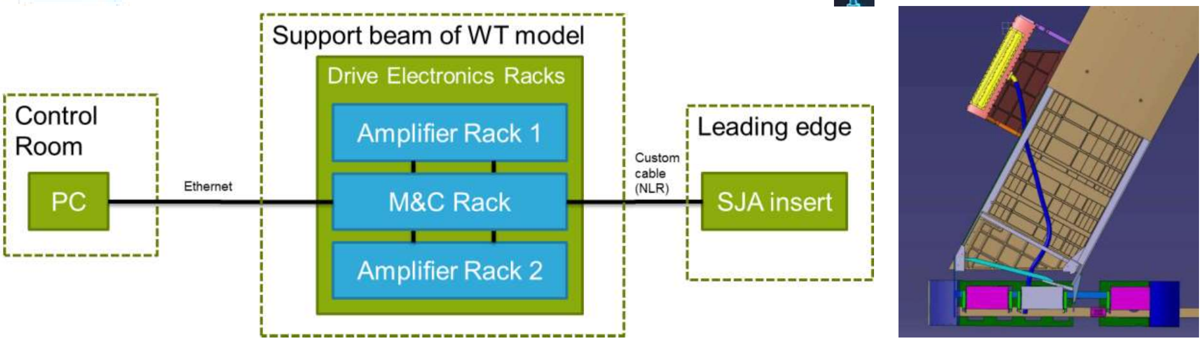

Figure 2: System design concept for the SJA System (left), top view of wind tunnel model CAD model with SJA insert (yellow), custom actuator connection cable (blue), and drive electronics subracks (magenta & grey)

2.1 Wind tunnel test actuator design

The Synthetic Jet Actuators developed in AFLoNext are based on piezo-electric transducers. They are equipped with a two-pin electrical connector for the HV input signal and have a 45° inclined circular outlet with a diameter of 2.5 mm on the upper side of the housing. The outlet has a sealing for an air tight connection with a common top cover plate. The actuators have a polymeric housing.

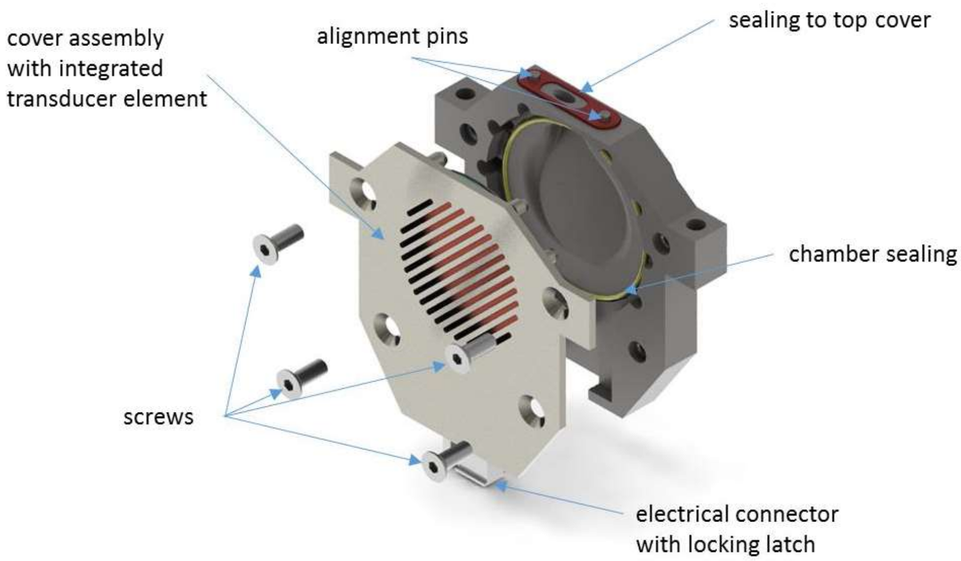

Figure 3: Synthetic Jet Actuator

The electrical parameters of the piezo-electric transducer determinegovern the design of the drive electronics system. The following parameters were used to calculate the required amplifier power:

- Capacitance of transducer element: 200 nF
- Drive frequency in mechanical resonance: 2.0 kHz
- Maximum excitation voltage: 200 V_{pp} (unipolar)

The typical performance of three actuators is shown in Figure 4. Velocities up to 100 m/s are possible with a current consumption of 0.15 A to 0.2 A. At the resonance frequency the power consumption of an actuator can be calculated using the average current $\boldsymbol{I_{av}} = \frac{1}{\pi} \cdot \boldsymbol{I_{pk}}$. With 200 V excitation voltage the power consumption of one actuator is 9.6 to 12.7 W.

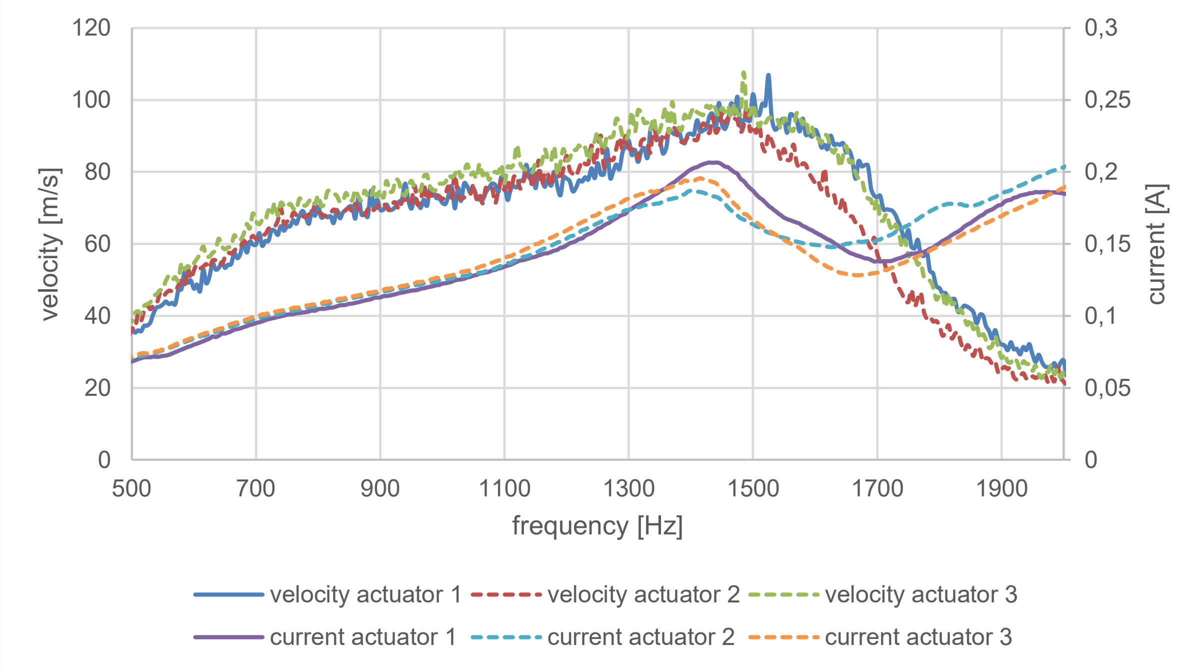

Figure 4: Actuator velocity and current versus frequency

2.2 Drive electronics design

Amplifier subrack

The initial aim of the market survey was to focus on the use of Commercial Off-The-Shelf (COTS) equipment as a complete solution to drive all required actuators. The leading specifications were the ability to drive large capacitive loads (100 SJAs of 200 nF each) in combination with sinewave excitation voltages of at least 150 V_{pp} and a frequency of 3 kHz. Because of the required high full power bandwidth with the associated high slew rate, this leads to HV amplifiers that must be able to deliver a current of about 28 A_p in total. COTS products with such specifications (total power exceeding 2 kVA) were not found on the market. Only high voltage power amplifiers that are specifically designed for driving reactive loads are suitable for this application, as regular amplifiers would suffer from stability issues and have difficulty to cope with the high dissipation in the power stage. Also, flexible grouping of actuators is desired with the option to drive various groups with different signals. The high total power demand and the grouping requirement called for a more flexible custom solution based on smaller COTS HV driver amplifiers.
Various desktop and modular amplifiers were evaluated from such manufacturers as Trek, Physik Instrumente, Sonitron, Tegam, Piezo Systems, and PiezoDrive. The most appropriate amplifiers with regard to technical performance, compactness, and price are manufactured by PiezoDrive. The selected amplifier module is a fan-cooled OEM module from PiezoDrive, type MX200 (11). This module can be configured for a maximum amplitude of 100, 150, or 200 V_{pp}. Maximum output current depends on the selected voltage mode. For the 200 V setting, the maximum output current is 220 mA_{RMS} and 1 A_p. This corresponds to driving 250 nF at 2 kHz at 200 V_{pp}. The output is current limited and tolerates overloading and short circuiting, making it a robust solution.

An Amplifier subrack (Figure 5) is designed and manufactured that contains twelve MX200 amplifier modules and the DC power supplies for the amplifiers. Three amplifier modules are combined on one carrier board; four carrier boards and two COTS power supply modules (12) are incorporated in one amplifier rack. The subrack is a 19" unit with perforated top and bottom panels. They allow ventilation while at the same time shielding the dangerous voltages that exist on the amplifier modules. A fan tray is fixed to the bottom of the rack, in order to remove the heat that is dissipated in the amplifier modules.

Figure 5: Amplifier subrack - front view

Measurement & Control subrack

Monitoring of the actuators is necessary to have a feedback on the actual behaviour during the tests. Different approaches for the monitoring can theoretically be used, but have to be feasible in terms of integration, costs and handling. A characterization of the performance with conventional air speed measurements with hot-wire anemometry is not possible during the tests. Due to the dynamic alternation of the suction and blowing phase in one cycle, a very fast system is needed. Pitot tube systems have the drawback of low-pass filtering the velocity signal due to fluidic capacitance in the tube and therefore can only be used at low frequencies. Also, the integration in the small nozzle structures would be very challenging. A second solution would be to monitor the pressure in the cavity of the actuators and the outer pressure to calculate the velocity through the nozzle based on the pressure difference with common analytical equations. Small pressure sensors which can measure the cavity pressure fast and accurately are however too expensive for integration in each actuator. Therefore only the possibility of measuring the electrical characteristics of actuator voltage and current consumption is available to provide feedback of the actuator behaviour. The dynamic behaviour of the actuator can be observed by measuring the frequency-dependent current consumption and the phase angle between voltage and current signal.

Figure 6 shows the connection between the Amplifier subracks, the Measurement & Control (M&C) subrack and the actuators. The HV signal of the amplifiers is routed through the M&C subrack. In this subrack a measurement circuit monitors the voltage and current signal. From the M&C subrack the HV signal is connected to the actuators. Up to four actuators can be connected in parallel to a single output of the M&C subrack.

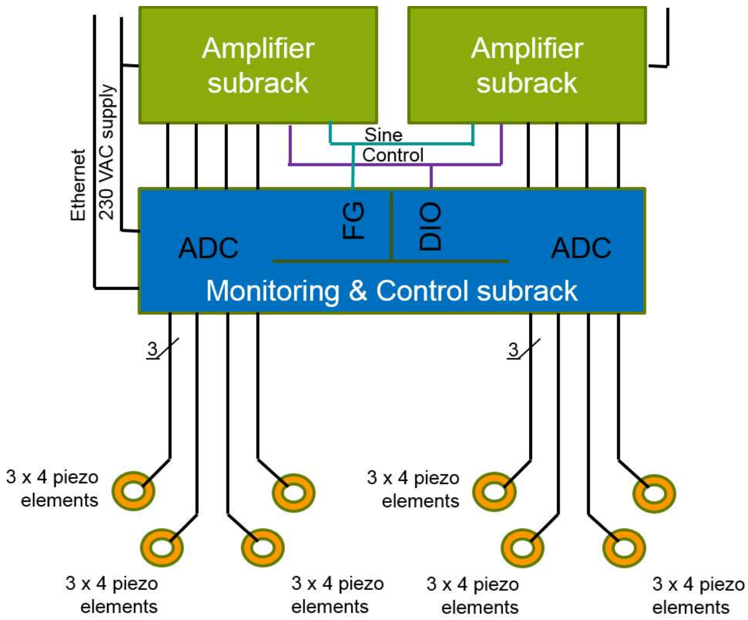

Figure 6: System Design for AFLoNext SJA System (ADC = Analog-Digital Converter, FG = Function Generator, DIO = Digital Input/Output)

The M&C subrack has integrated microcontroller-based data acquisition circuits. The microcontrollers measure the signals' current and voltage. Moreover, they provide an analogue input signal for the HV amplifiers. The subrack is only functional when it is connected to a remote measurement computer. On this computer a software application provides a user interface to control the subrack and setup the drive signals as well as collect the data measured by the microcontrollers.

Figure 7: Measurement & Control subrack (left – HV outputs, middle – connectors for Amplifier subrack, right – power plug and remote Ethernet connection)

Cabling

Cable harnesses were manufactured for the signal exchange between the M&C subrack and the two Amplifier subracks, and also for connecting the actuators to the M&C subrack. The latter cables are five meters long. They carry potentially lethal signals and are manufactured using high-voltage wire in twisted pairs. Sets of these twisted pairs are contained in braids that provide a protective shield that ensures safety even in case a cable is damaged mechanically. Inductance of the long cable needs to be kept below a specified value, in order to avoid resonance with the SJA capacitance at a frequency in or close to the signal bandwidth.

Software

The windows software for control of the M&C subrack is implemented in C# programming language. It can be used to set up the drive parameters for every amplifier and measure the voltage and current on every channel out of the total of 24. Furthermore, it monitors the overload status of the amplifiers and gives the possibility to enable or disable individual amplifiers. To identify the resonance behaviour of the actuators and track if there are changes related to the different outer flow conditions, the software is capable of performing a frequency sweep and providing data for peak current versus frequency plots. This data can be used to check if the resonance frequency has changed and drive parameters can be adapted accordingly. For the wind tunnel test a common time synchronization signal will be provided by the wind tunnel system via the UDP protocol. Therefore the software monitors and logs also the UDP ports so that the acquired data of the measurement system can be easily linked to the specific experiments during the test campaign. Figure 8 shows the software user interface with the different sections:

(1) Enable/Disable of amplifier boards with overload signal indicators;
(2) Setup of drive signal amplitude and frequency;
(3) Setup of Measurement file path and sweep parameters;
(4) Setup of Range for plots;
(5) Current and voltage plots for every amplifier with setup block for;
    a. Drive signal and frequency
    b. Enable
    c. Overload indicator
(6) UDP monitoring.

Figure 8: Software interface

2.3 Laboratory testing of the system

The Drive Electronics system was tested with the SJA Insert that is used for the wind tunnel tests. Figure 9 shows the setup for the laboratory tests.

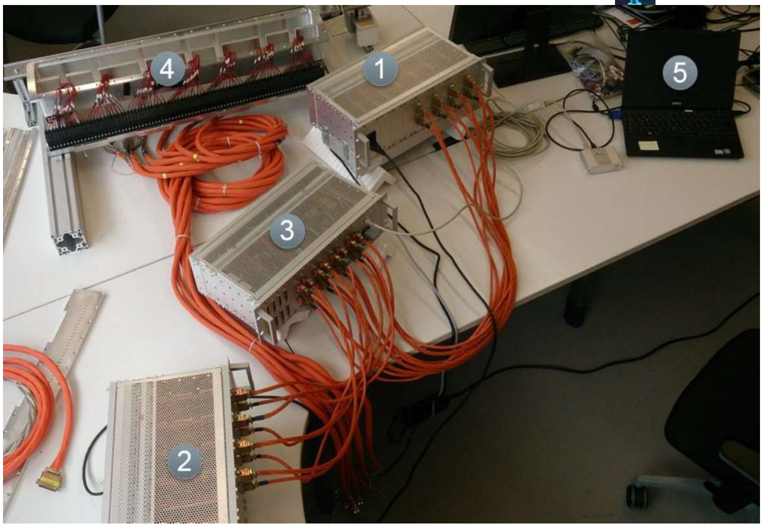

Figure 9: Setup for ground test (1 and 2 – Amplifier subracks, 3 – M&C subrack , 4 – SJA Insert with actuators , 5 – Remote Control Computer)

Due to manufacturing tolerances the performance of the actuators is not identical. The panel was characterized by means of a hot wire anemometer. The results are shown in Figure 10 including the scattering of the performance. The drive electronics system was capable of driving all actuators without going into overload state. The capacitance of one actuator is approximately 85 nF. Up to four actuators are connected to one amplifier in parallel, which this corresponds to a capacitive load of 340 nF.

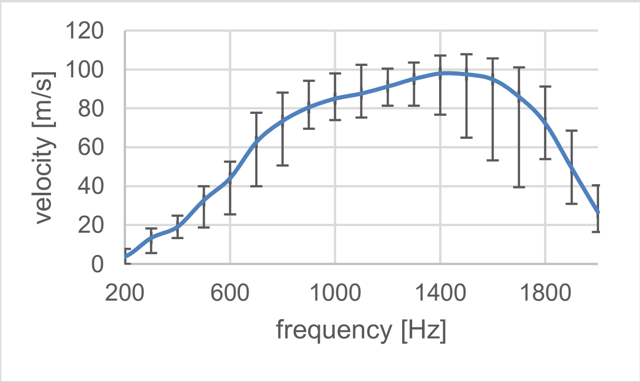

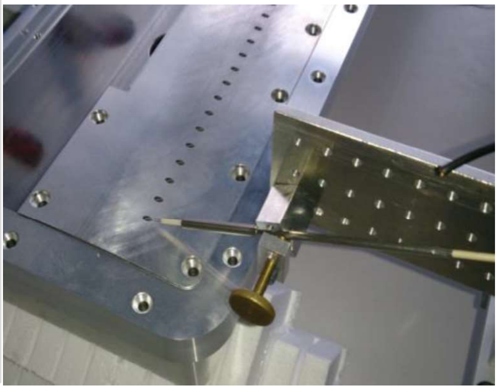

Figure 10: Statistical test results of all 84 actuators (left) / hot-wire velocity measurement setup (right)

3 ACTIVE FLOW CONTROL ON THE OUTER WING

3.1 Concept for Robustness Test Campaign

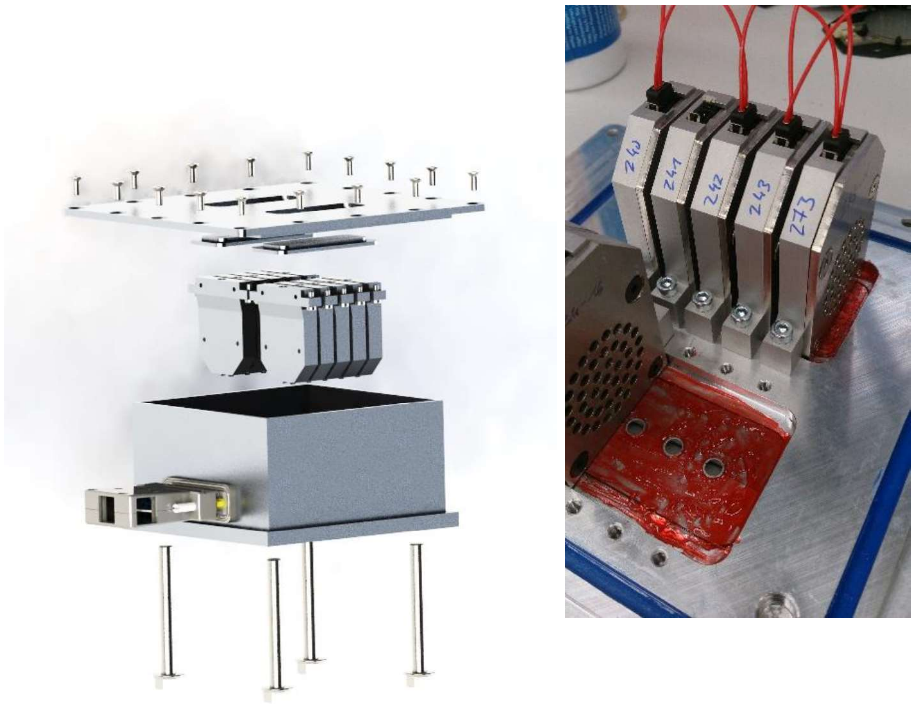

Figure 11: Exploded view of actuator panel for a harsh environmental test campaign (left) and actuators mounted in top cover plate (right)

For the robustness test campaign a panel with ten actuators in two rows was designed and manufactured. The panel integrates two different nozzle geometries. One row has 10*0.5mm² with 30° nozzle inclination. The second row basically has the same geometry, but with a 45° inclination with respect to the surface. All actuators within the panel are connected to one common 25-pin D-Sub connector. Twenty pins are used for connecting every single actuator with a 2-pin electrical interface. The remaining five pins are used for grounding the panel to protective earth, when the drive electronics system is connected. For driving the actuators with a proper HV signal an amplifier system with attached measurement circuit for current and voltage monitoring is used. In contrast to the system described above, this system has only two HV amplifiers (in-house development by Fraunhofer) integrated. The peak output voltage is 150V. Ten channels – five per amplifier output – for voltage and current monitoring are available. The system is connected via USB interface to a control computer and a LabVIEW software is used to set up the drive signal and monitor the actuator signals and their current consumption.

3.1 Robust Actuator design

The actuators are designed with an aluminum housing. The same transducers as for the actuators for wing-pylon integration are used. The interface to the top cover is a circular hole with 4 mm diameter. The within the nozzle the geometry changes to inclined slots of 10*0.5mm² with 30° or 45° inclination. The choice to use aluminum as the housing material was based on the extreme environmental conditions the actuators had to withstand during environmental DO1060 tests.

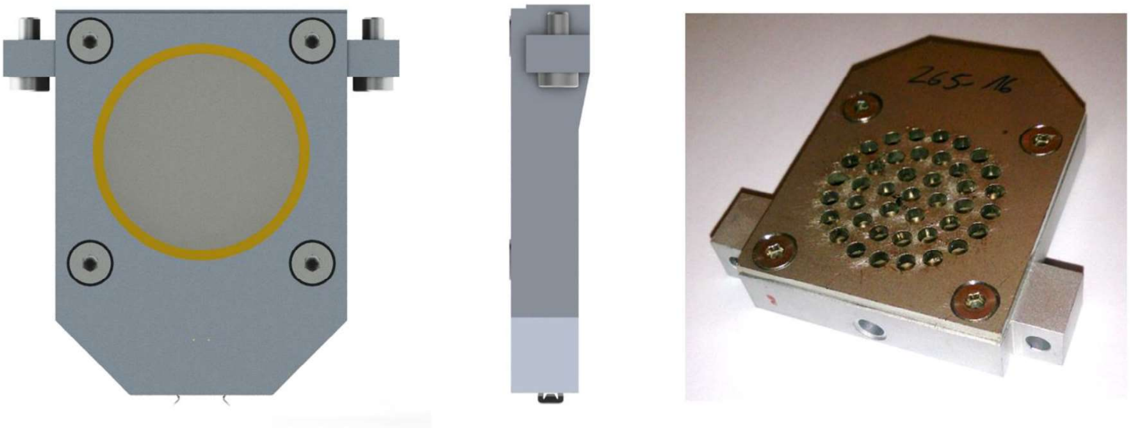

Figure 12: SJA front view (left), side view (middle), prototype actuator (right)

3.2 Results of test campaign

Before starting the tests campaign the performance of every single actuator in the panel was characterized using a hot-wire anemometer. To verify the influence of the harsh environmental tests on the actuator panel the characterization was repeated after every test. The results showed whether the actuators still worked properly or whether the performance had changed. The different tests are an indicator of any critical weak points of the current design and will be detailed to exactly identify the individual failure mechanisms and derive adaptions of the design out of them.

Most of the tests are performed using the EUROCAE ED-14G (RTCA DO-160G) environmental test standard for airborne equipment. More detailed information can be found in (13).

4 OUTLOOK

The goal of the test campaign was the technology evaluation and assessment of the Technology Readiness Level (TRL). With the current results of the environmental test campaign the actuator system is classified as TRL 3. With positive results out of the wind tunnel test TRL 4 may be achieved. The further development on the actuators will focus on aircraft integration and addresses the identified drawbacks of the current design to find more robust solutions. The results of the project AFLoNext will be transferred to future projects to mature the technology towards higher technology readiness levels. This will include a miniaturization of peripheral electronic systems and a further optimization of the actuator performance with integration of additional internal sensors for enhanced monitoring and control.

References

[1] OYARZUM, Matias A., and Loius CATTAFESTA. Design and Optimization of Piezoelectric Zero-Net Mass-Flux Actuators. *AIAA Journal.* 2010.

[2] DENG, Jinjun, Weizheng YUAN, Jian LUO, Dandong SHEN, and Binghe MA. Design and Fabrication of a Piezoelectric Micro Synthetic Jet Actuator. 2011.

[3] GIRFOGLIO, Michele. *On the characterization of a synthetic jet actuator driven by a piezoelectric disk,* 2015.

[4] BHATT, Shibani, Vladimir V. GOLUBEV, and Yan TANG. Design, Modeling and Testing of Synthetic Jet Actuators for MAV Flight Control. *52nd Aerospace Sciences Meeting, 13-17 January 2014,National Harbor, Maryland.* [Reston]: [American Institute of Aeronautics and Astronautics - AIAA], 2014.

[5] GALLAS, Quentin, Ryan HOLMAN, Toshikazu NISHIDA, Bruce CARROLL, Mark SHEPLAK, and Louis CATTAFESTA. Lumped Element Modeling of Piezoelectric-Driven Synthetic Jet Actuators [online]. *AIAA Journal.* 2003, **41**(2), 240-247. Available from: 10.2514/2.1936.

[6] LUCA, Luigi de, Michele GIRFOGLIO, and Gennaro COPPOLA. Modeling and Experimental Validation of the Frequency Response of Synthetic Jet Actuators [online]. *AIAA Journal.* 2014, 1-16. Available from: 10.2514/1.J052674.

[7] LIANG, Yuanchang, Minoru TAYA, and Yasuo KUGA. Design of diaphragm actuator based on ferromagnetic shape memory alloy composite. In: Eric H. Anderson, ed. *Smart Structures and Materials:* SPIE, 2003, p. 45.

[8] ASHRAF, Hamad Muhammad, Karthika Murugan ILLIKKAL, Francis D'SOUZA, Mohamed Alsayed MAHMOOD, Suhail Mahmud MOSTAFA, Young Hwan KIM, Petra DANČOVÁ, and Tomáš VÍT. Design & Development of a High Mass Flow Piston Synthetic Jet Actuator [online]. *EPJ Web of Conferences.* 2015, **92**, 2002 [viewed 24 August 2015]. Available from: 10.1051/epjconf/20159202002.

[9] GILARRANZ, J., and O. REDINIOTIS. Compact, high-power synthetic jet actuators for flow separation control. *39th Aerospace Sciences Meeting and Exhibit,* 2001.

[10] AGASHE, JANHAVI S. *MODELING, DESIGN AND OPTIMIZATION OF ELECTRODYNAMIC ZERO-NET MASS-FLUX (ZNMF) ACTUATORS,* 2009.

[11] PIEZODRIVE. *PiezoDrive MX200* [online]. *200V 1A Piezo Driver* [viewed 17 July 2017]. Available from: https://www.piezodrive.com/wp-content/uploads/2016/01/MX200.pdf.

[12] SCHROFF. *Maxpower MAX180 datasheet* [online]. *document 63972-225_R1.2* [viewed 20 September 2011]. Available from: https://schroff.pentair.com.

[13] BRINZA, Ionut, Johannes KIRN, and Perez WEIGEL. Testing of Active Flow Control Actuators at Harsh Environments. *Proceedings of CEAS2017 conference.*

Paper 2406

Testing of Active Flow Control actuators at harsh environment

Ionut BRINZA
National Institute or Aerospace Research
Research Engineer
Iuliu Maniu Blvd, no 220, Bucharest - ROMANIA
brinza.ionut@incas.ro

Perez WEIGEL
Fraunhofer Institute for Electronic Nano Systems ENAS
Research Associate
Technologie-Campus 3, 09123 Chemnitz, GERMANY
perez.weigel@enas.fraunhofer.de

Phillip SCHLOESSER
Airbus Defence and Space GmbH
Researcher, PhD Candidate
81663 Munich, GERMANY
philipp.schloesser@airbus.com

Testing of Active Flow Control actuators at harsh environment

Ionut BRINZA
National Institute or Aerospace Research
Research Engineer
Iuliu Maniu Blvd, no 220, Bucharest - ROMANIA
brinza.ionut@incas.ro

Perez WEIGEL
Fraunhofer Institute for Electronic Nano Systems ENAS
Research Associate
Technologie-Campus 3, 09123 Chemnitz, GERMANY
perez.weigel@enas.fraunhofer.de

Phillip SCHLOESSER
Airbus Defence and Space GmbH
Researcher, PhD Candidate
81663 Munich, GERMANY
philipp.schloesser@airbus.com

ABSTRACT

During the last two decades active flow control technologies have been developed and matured, and the results showed that this concept has a highly potential for achievement a reduced impact on the environment foot-print, and so, to have a greener future aircraft transportation. [1,2]. One of the goals of AFLoNext (Active Flow Loads & Noise control on Next generation wing) project is to design, manufacture and test two different architectures of actuators –Synthetic Jet and Pulsed Jet- in order to evaluate the benefits of this type of hardware and to secure the path for higher Technology Readiness Level. The present paper presents the results of the harsh-environment testing campaign on the mentioned actuators which was performed in INCAS (Romania National Institute for Aerospace Research) laboratory, based on a testing matrix and standards requirements (environmental conditions and test procedures). Tests on extreme temperature (hot/cold), mechanical vibrations and shocks, artificial rain, solid elements contaminations including dust and sand exposure were performed in order to demonstrate the robustness of the actuators tile.

KEYWORDS: *active flow control, synthetic jet, pulsed jet, harsh environment, EUROCAE ED-14G*

NOMENCLATURE

Acronyms
AFC – Active Flow Control
CFD – Computational Fluid Dynamics
TRL – Technological Readiness Level

Latin
g – Gram
f – Frequency
M – Mach number
q – Dynamic pressure
m – Mass
T – Temperature
v – Velocity

1 INTRODUCTION

1.1 General

Testing of the SJ and PJ actuators in the framework of AFLoNext project (Active Flow – Loads & Noise control on Next generation wing) in the harsh environment conditions were performed in INCAS Laboratory on individual test rigs according to a test strategy agreed by the hardware developers. The ground tests are intended to evaluate the actuators robustness in extreme environment in order to open their way to a mature TRL. Given the actuators panels manufactured by Fraunhofer (Synthetic Jet Actuators Panel) and Airbus Group Innovation (Pulsed Jet Actuators), INCAS defined a test strategy which consists of a series of ground tests: External control of the actuators panel; Testing of functional parameters at normal temperature; Testing at extreme temperatures (-55, +70 Celsius Degrees); Testing at mechanical vibrations exposure; Testing at mechanical shocks exposure; Testing of operational parameters at icing exposure; testing under artificial rain conditions; Testing for exposure to solid elements contamination and Testing at dust and sand winds exposure. All the tests specified above were performed, noting that after each of these tests, the measurements of the actuators functional parameters for nominal operation conditions were again performed for comparison purposes with base line measurements.

1.1 Brief description of the work performed

To allow the mounting of the actuators tiles on the testing equipment it is necessary to design a mechanical interface-testing rig. Design of these testing rigs was carried out, for which a modal analysis was performed for the all three fixing positions on the vibration and shock machine. The air flow measurement methods were reviewed, thus the airflow at exit slots of the actuators panels were measured by hot wire when the air temperature is at ambient temperature, while for the high temperatures (up to 100°C or more) a method based on Pitot tube was used. The mechanical interfaces have to be stiff enough to avoid any influence into vibration and shock test results. Because each actuator panels has a different positioning (arrangement) of the air supply and/or electrical supply outlet(s), additional mechanical machine works (millings) are necessary. This may leads to inadvertent panel-test rig-vibration machine interaction due to weakening of the mechanical strength of the rig.
Design goal: to minimize the test rigs resonant frequencies in testing domain (5 Hz-3000 Hz for SJ, 5 Hz – 1400 Hz for PJ)
The test rig designs are presented in Figure 1. (CAD model and manufactured object)

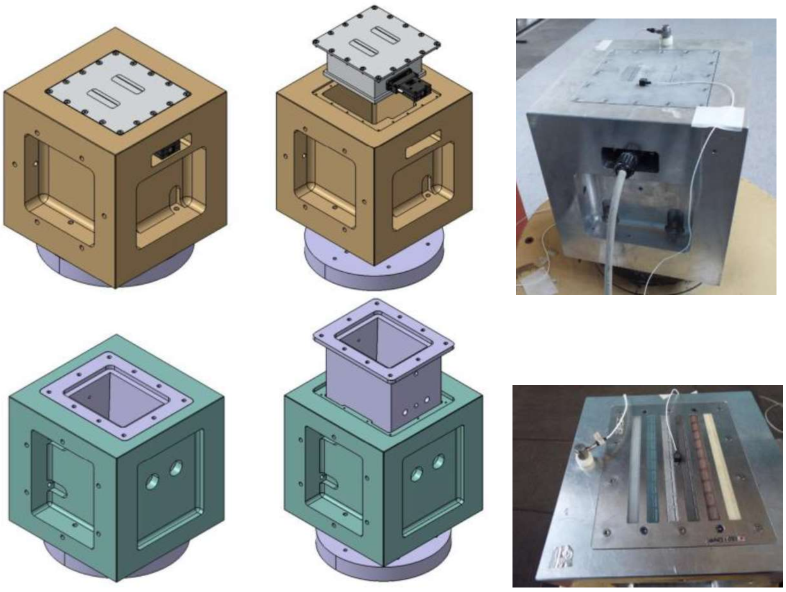

Figure 1: SJA test rig (up), PJA test rig (down)

2 SYNTHETIC JET ACTUATOR

For the harsh environmental test campaign a panel with ten actuators in two rows was designed and manufactured. The panel integrates two different nozzle geometries. One row has 10*0.5mm² outlet area with 30° nozzle inclination. The second row basically has the same nozzle cross section geometry, but with a 45° inclination with respect to the surface. All actuators within the panel are connected with a two-wire electrical interface to one common 25-pin D-Sub connector in the panel housing. Beside the twenty pins for the electrical connection to the actuators, the remaining five pins are used for grounding the panel to protective earth, when the drive electronics system is connected. For driving the actuators with a proper HV signal an amplifier system with attached measurement circuit for current and voltage monitoring is used. The drive electronic system has two HV amplifiers (in-house development by Fraunhofer) integrated. The peak output voltage is a 150V. Ten channels – five per amplifier output – for voltage and current monitoring are available. The measurement system is connected via USB interface to a control computer and a LabVIEW software is used to control the drive signals and monitor the actuator signals and their current consumption.

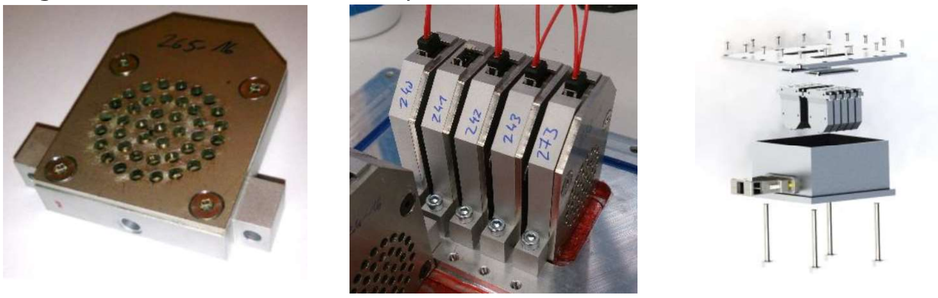

Figure 2: SJA prototype actuator (left), actuators mounted in top cover plate (middle) and exploded view of actuator panel for testing campaign (right)

3 PULSED JET ACTUATOR

The pulsed jet flow control actuators tested under harsh environment conditions are based on fluidic oscillator technology. Their concept eliminates any moving or electrical parts which make the design appealing for safety driven industries like aeronautics. The actuators are comprised of connected fluidic elements; a fluidic oscillator with interface to an array of fluidic diverters. The fluidic oscillator acts as the driving stage which provides pulsing control jets to the fluidic diverters. With the help of the control jets, a primary jet is switched between two stable states, each connected to a separate outlet. Figure 3a depicts a schematic of this two-stage design which was already proven in wind tunnel experiments [3]. A flow control system based on the same concept has been tested in wind tunnel experiments within the AFloNEXT project framework. Please refer to [4, 5] for a more detailed presentation of the two-stage actuator concept. For testing at harsh environment, the actuators are reduced to sizes that fit inside the outer wing section, see Figure 3b. The driving stage is wrapped around five diverter elements to reduce the spanwise extent of one actuator segment.

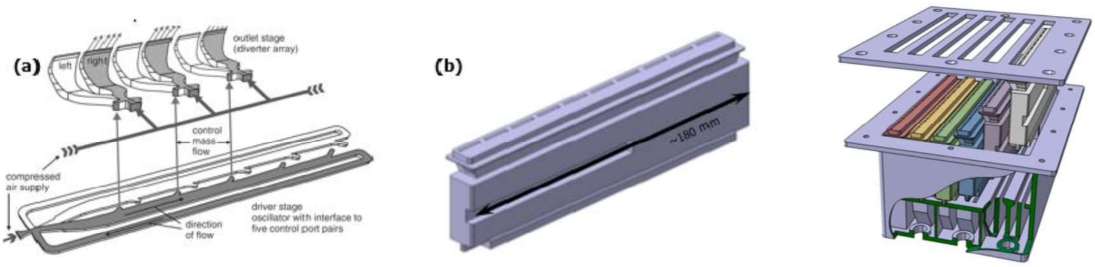

Figure 3: a) Schematic of the two-stage actuator's flow channels: the grayed area illustrates the internal flow when the "right" outlets of the diverter elements are active [3]; b) Adapted actuator geometry for harsh environment testing – cutout shows internal structure chambers

4 DESCRIPTION OF TESTING APPROACH AND TEST SET-UPS

Based on a list of requirements identified at aircraft scale, the most relevant cases for testing in harsh environment were extracted and addressed into the testing campaign. Some of these requirements are described hereafter: the flow control performance shall be robust and predictable; Outside parking at the gate should not be a problem for the AFC device (e.g. minor sand ingestion, rain, ice); Ambient temperature; Fluid through actuator system at high temperature; Vibrations and shocks; Exposure to non-clean fluid; Operation under artificial rain (water exposure). In the following all these test are presented.

4.1 External Control of Actuator Panel

The external control of the actuator panel consist in dimensional verification (Overall size; operational size) and weighing of the aggregate. Actuator panel (1 row of 5 slots with 30° exit angle and 1 row of 5 slots with 45° exit angle) in total mass of 1665.1 g

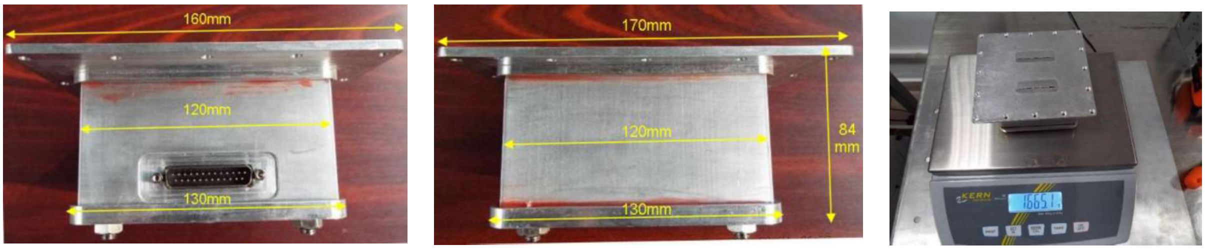

Figure 4: SJA actuator tile – external geometric dimensions and weight

4.2 Testing of functional parameters at normal temperature (baseline measurements)

For the ambient (cold) baseline measurements, the hot wire probe was calibrated at room temperature using the method described below and the Streamware Pro software. The program features an assisted calibration method that allows for data input along with temperature and voltage readouts to ease lifting the calibration characteristic. The DISA M55 calibration system comprising M55D45, M55D46 together with the tubing and 10 bar approx. air supply. The pressure regulator is supplied from the compressor that generates approximately 10 bar and then the regulated output is ran through the miniature wind tunnel M55D45 with the appropriate nozzle to generate air velocities typically between 8 and 300 m/s. Using the pressure indicator with Mach compensation M55D46 we ensure precision through compressible flow conditions. Using the 120, 60, 24 and 12 mm2 nozzles we generate a range of air velocities that are needed for calibration. Mach compensation is used from 50 m/s onwards so to account for the air compressibility. A typical calibration encompasses velocities from 8 to 300 m/s. The calibration for the Pitot tube is also made using the same method for generating the velocities but data will be recorded using the data acquisition system and processed.

The dynamic calibration follows: we expose the probe to the maximum expected flow velocity, we apply a calibrated step signal to the input, and we adjust the CTA bridge amplification and filtering so that the system response is stable. Sensors: Hot-wire and Hot-film Probes (StreamLine Pro CTA / Dantec Dynamics); Kulite pressure-sensors; Mass-flow rate; Thermal resistances. Once the calibration is made, the StreamLine Pro system is ready to measure the airflow velocities at high temperatures. Using the above-mentioned traverse system, we keep the probe and the thermal compensator at the specified distance (4 mm) from the slot. Then we begin to investigate the flow angularity by angling the probe support. Measurements were made for each slot individually, taking into account the system performance and spatial resolution, in a continuous pass across the length of the slot. In order to account for the flow geometry, we placed the probes at a starting position of 4 mm from the slot and 8 mm above it, and take a pass at room temperature, and then modifying the distance we find the most interesting flow profile (maximum speed or maximum speed variation).

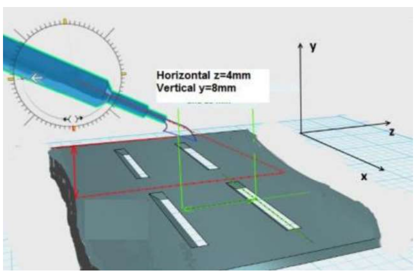

4.2 Testing at mechanical shocks exposure

For mechanical shock the test was performed on a dedicated testing-machine TIRA SHOCK 4110. The

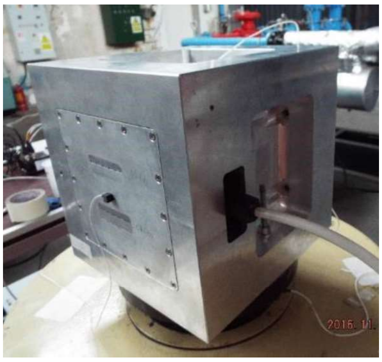

actuators panel was fitted with the same gripping as on the aircraft, in a device that allows it's positioning so that the force resulting from the shock exposure manifests in one of the 6 directions derived from movements in planes parallel to the coordinate axes planes of the airplane. This test is based on EUROCAE ED-14G standard, Section 7. The device on which the actuators panel is fitted shall be so rigid that it does not have resonant frequencies in the 0-3000 Hz range to avoid distorting of the shock transmitted by the mechanical shocks testing-machine. The input shock is measured by an accelerometer, placed as close as possible to the actuators panel attachment point, with an accuracy of ±10% of standard reading.

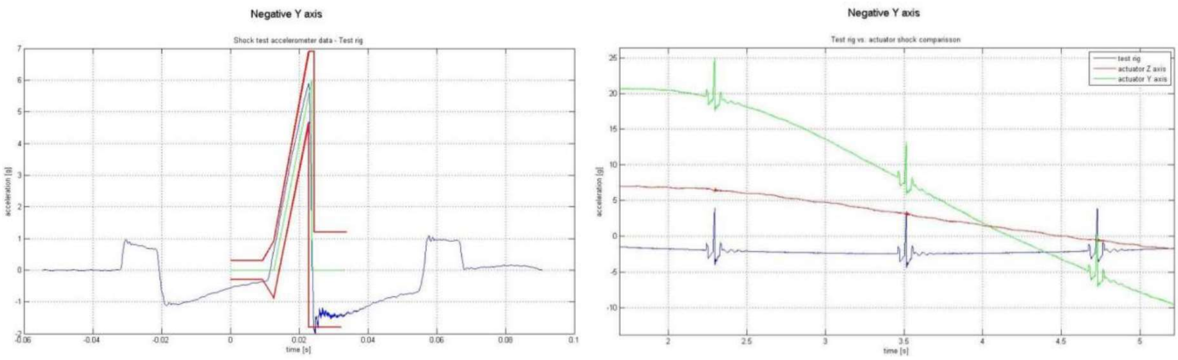

Figure 5: Test rig Y axis (negative acceleration) vs. standard profile and Test rig vs actuator comparison

The drive electronics will be supplied with 230V AC and provide a sinusoidal HV input signal for the actuators with a specific frequency and voltage up to 150V. Also, the actuators panel shall be operational during the mechanical shock event. The actuators panel is subjected to 3 successive saw-tooth pulses of 6 g amplitude, 11 ms for each pulse. The direction of the imposed mechanical shock is reversed and the same tests as mentioned in the previous paragraph are performed. The experiments for the other Y and Z directions of imposed mechanical shocks are repeated.

4.3 Testing at extreme temperatures (+70 Celsius Degrees)

High Temperature: The actuators panel is installed on the specialized test bench. The entire assembly is placed into an enclosure where the working temperature is established at +70°C (EUROCAE ED-14G, Section 4.5.4). Nominated temperature levels will be maintained for 1 hour to stabilize the temperature. The actuator was visually inspected and weighted before its placement in the climatic chamber test rig and equipped with temperature sensors to monitor its surface temperature

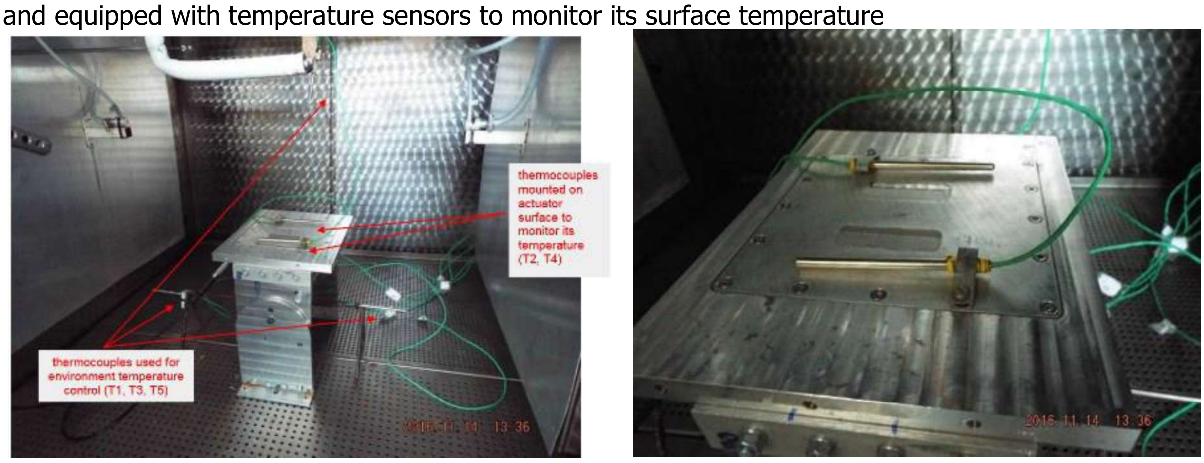

Figure 6: Temperature test bench into climatic chamber-thermocouples installation

4.4 Testing under artificial rain conditions

Testing of operational parameters under artificial rain conditions aims to verify if there is any risk of water penetration inside the actuators panel. The test is performed according to EUROCAE ED-14G standard, Section 10.3.3. The actuators panel is installed on a suitable holder in a similar fitting position and with similar mechanical connections as on the aircraft. The actuators panels are supplied with 230 V AC for electronical components. Showerhead is positioned no more than 2.5 m from the actuators panel and provides 450 l/hour water flow. Mass of the actuator before the test – mi1= 1665.94g mi2= 1665.93g mi3= 1665.94g

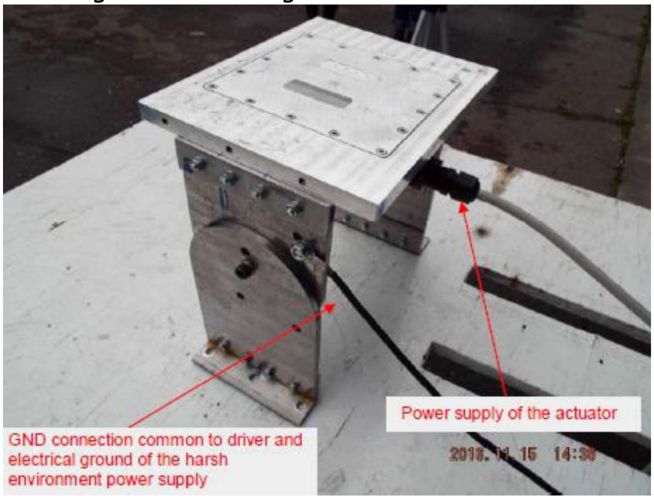

Figure 7: Temperature test bench into climatic chamber-thermocouples installation

4.5 Testing of operational parameters at icing exposure

The icing test aims to determine to what extent the actuators panel is affected by the ice formation and it is performed according to Section 24.4.2, EUROCAE ED-14G standard; The actuators panel is thoroughly cleaned in order to remove the elements that affect adhesion between ice and its surface (such as oil, grease, dirt). The electrical powered actuators panel is installed on a suitable holder in a similar fitting position and with similar mechanical connections as on the aircraft. Test procedure is described hereafter: a.The actuator is installed in the climatic test chamber; b.The temperature inside the climatic test chamber is lowered and the actuators panel temperature is stabilized to -55ºC, at ambient room pressure and humidity. The AFC actuators panel is not operating; c.The temperature inside the climatic test chamber is raised to 30ºC and the environmental humidity is set at least 95%, as quickly as practicable, while the surface temperature of the actuators panel is monitored; d.The environmental conditions of 30°C and 95% humidity in the climatic test chamber are maintained until the surface temperature of the actuators panel reaches 5ºC. After this surface temperature is achieved the environmental conditions in the climatic test chamber are changed to -55°C and to ambient pressure and humidity, as quickly as practicable. e. Tests *b.* to *d.* to are repeated 2 times (in total, 3 cycles are performed); f. At the end of 3th cycle, the temperature of the actuators panel is stabilized to -55ºC, then the temperature in the climatic test chamber is set (and maintained) to -10°C, until the surface temperature of the actuators panel reaches -10±5ºC when the actuators panel is put into operating state.

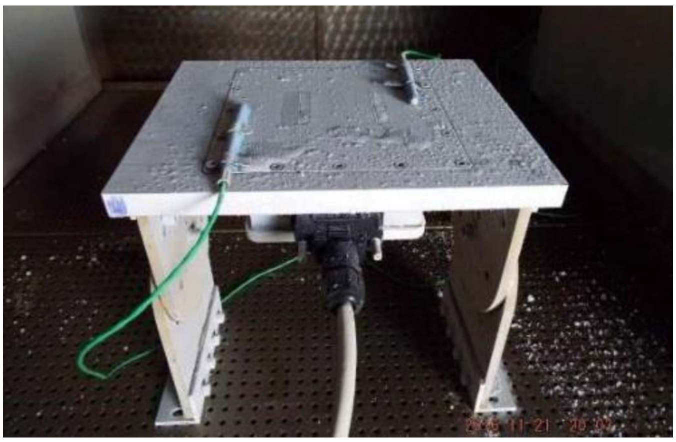

Figure 8: Temperature test bench into climatic chamber after the icing test

4.6 Testing for exposure solid elements contamination

The actuators panel is installed on the specialized test bench and will be supplied by a HV signal from the drive electronics. For this experiment the solid elements used are non-uniform quartz (A), spherical steel (B) and spherical glass (C). One of the output windows of the actuators panel is completely blocked and the actuator is powered up. 2. Step 1 is repeated successively blocking up to half of the actuators panel windows. 3. Then, blocked windows in steps 2 and 3 are released. 4. Bodies of A type are placed in all active rooms of the actuators panel final stage through the exit slots. Then the actuators panel is supplied by pressure or voltage. It is kept running for 30 minutes or until the complete elimination of the elements inserted into the actuators panel. The time at which bodies are removed from the actuators panel is recorded in the report attached to the experiment. 5. Step 4 is repeated by replacing Type A bodies with Type B bodies. 6. Step 4 is repeated by replacing Type A bodies with Type C bodies.

Figure 9: Solid elements contamination: quartz, steel and glass

4.7 Testing at dust and sand winds exposure

Testing at dust and sand winds exposure aim to determine the actuators panel functionality in an atmosphere filled with sand and dust. These tests are based on EUROCAE ED-14G standard, Section 12. The actuators panel was installed in a climatic testing chamber of the facility. The length of the chamber section and the position of the equipment under test within it, should be such as to avoid the turbulent flow upstream and if possible also downstream the actuators panel. The characteristics of the environment in the climatic test chamber are: Temperature: +25±2 ºC, First Cycle, +55±2 ºC Second Cycle and Relative humidity no more than 30%. The dust used during the test is Silica Flour, 97% to 99% silicon dioxide, and is maintained in the chamber at a concentration of 3.5 to 8.8 g/m³. Size distributions of 100% by weight less than 150 µm, median diameter (50±2% by weight) of 20±5 µm. Dust/Sand Test Procedure: The first cycle parameters are stabilized in the climatic test chamber: Temperature, +25±2 ºC; Relative humidity, no more than 30%; Airflow speed along the +x direction, between 0.5 and 2.4 m/s - DUST and between 18 and 29 m/s - SAND. These parameters are maintained for an hour, along each of the three orthogonal axis, in succession.

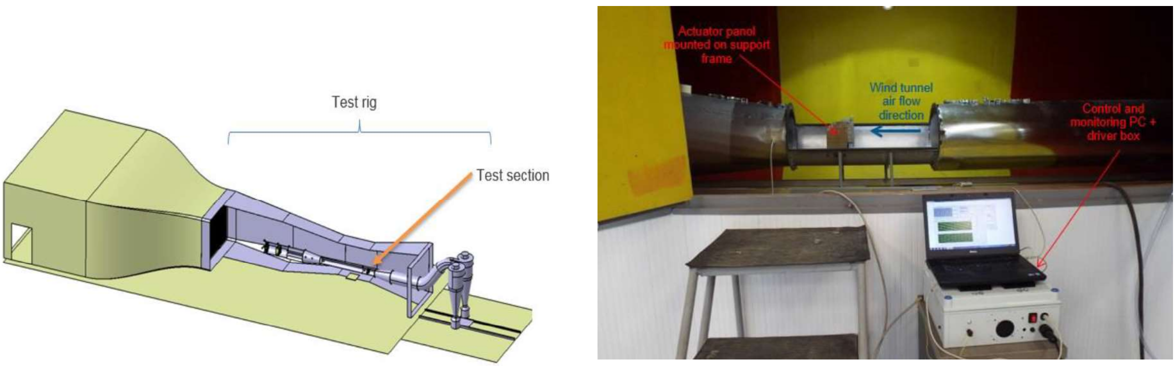

Figure 10: Sand and dust testing facility and test set-up

4.8 Testing at mechanical vibration exposure

The actuators panel was installed on the vibration machine table ensuring a gripping as on the aircraft. Control accelerometers were fixed in the attachment points of the actuators panel. Fastening of the actuators panel on the vibration machine table was made using a device which allows its successive positioning so that the vibrations direction changes along three orthogonal axes x, y, z which are parallel to the airplane ones. The actuators panel was mounted in aircraft configuration and was supplied with 230V AC as specified by the supplier. Figures below show the mounted actuator panels on vibration machine and the accelerometers positioned for Z axis test setup.

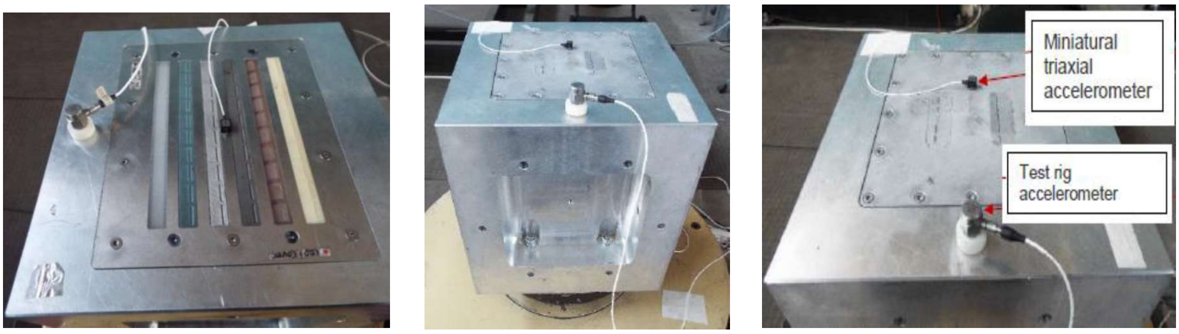

Figure 11: Test specimen ready for vibration test

4.9 Testing de-icing fluid

This test determine whether the materials used in the construction of the equipment can withstand the un-wanted effects of fluid contamination. This test was based on EUROCAE ED-14G standard, Section 11. The actuators panel was installed on a specialized test bench and the equipment was not required to operate during this test and the test was performed at ambient temperature.
The actuators panel is sprayed for minimum 15 minutes to the entire surface with De-Icing fluid Safewing MP II FLIGHT, a propylene glycol based SAE type II aircraft deicing / anti-icing fluid, which meets or exceeds the current revision of SAE specification AMS 1428. The flow of De-Icing fluid for spraying the actuators panel was Q = 200g/min.
The surfaces were maintained in a wetted condition for 8 hours followed by a drying period of 16 hours at 65°C.

Figure 12: Drying of the actuator tile inside climatic chamber

5 RESULTS AND SOME DISCUSSIONS

Synthetic Jet Results and discussions after the testing campaign:

- During the solid elements contamination test, we observed changes in the air velocity of the actuator panels. After the contamination with the first two elements type (1 - quartz, 2 - spherical steel 0.6-1.18mm), representing pictures, video of power up after filling the slots and velocities measured with the Pitot tube. For the 1st slot of the 45º row, the measurements in the center of the slot didn't record any air flow, and by passing on a grid of 1mm starting at 3mm left to the center we achieved a velocity profile for the respective slot. Because of the change in velocities for all slots we conclude that some of the elements remained in the slot channel and blocked/modified the normal air flow of the actuator;
- After the sand test, there has been observed the following changes in actuator panel behavior:
    - For the 1st row, 45° slots - the 3rd and 4th actuators are not working;
    - For the 2nd row, 30° slots – only the 2nd actuator is working but in poor conditions compared to baseline measurements
- The dust contamination test was carried out in good conditions, following the requirements of the test procedure, according to the EUROCAE ED-14G Standard. By weighing of the actuators panel has been noticed a negligible mass compared to its initial, of 0.67 g, this meaning that this quantity of dust was remained inside the actuators. This, however, did not influence the subsequent operation of the actuators panel, the values of air velocity measured after the dust test being comparatively similar to the initial ones.
- The vibration test on Z axis was performed under normal conditions, according to the procedure and EUROCAE ED-14G standard. At the beginning of the test the noise produced by the actuators panel was sensed by the vibration machine's controller as displacement, at 18.69 mm. To avoid this problem, the actuators panel started at 1200 Hz and stopped it at 820 Hz, during sweep-down. 4 critical frequencies were identified and the actuators panel was tested for 30 min on each ones. After air velocity measurements at the end of the vibration test on Z axis, one of the D-Type electrical connector was broken.

Pulsed Jet Results and discussions after the harsh environment testing campaign:

- As a general note, the Hybrid Jet Actuators worked OK, except the Sand & Dust test (which has failed - some of the actuators stop or worked with very small velocity). Formlabs HT row were broken and this fact influenced the velocity measurements
- After high temperature test the slots of Bluestone row increased the values of velocity, up to 66.44 m/s;
- After vibration test on X axis for PerFORM row, the slot number 9 indicated a reduced air velocity. The reason was a deformation in slot geometry due to changes of inner profile. This fact did not influenced the measurements for this row.
- After the sand test all slots of Formlabs HT row were broken. This fact influenced the air velocity measurements;
- After vibration test on Z axis the velocity measurements of Formlabs HT row have undergone a change, in the sense of decreasing values toward the baseline;
- After artificial rain tests, contamination with solids elements, de-icing, and sand & dust tests, the contaminants were removed during the actuators panel operation, having insignificant amounts inside of the samples at the end of the tests.
- Contaminating elements do not affect the actuators panel operation -only on a small scale- at the beginning of their operation – and after 15-30 minutes of testing, the remaining elements were exhausted.

6 SUMMARY – TRL EVALUATION - CONCLUSIONS AND FUTURE DEVELOPMENT

In general the harsh environmental testing went well, some problems were encountered during the sand and dust tests, but the more critical conditions were intentionally positioned in the test matrix towards the end of the campaign, so this was not critical. After an inspection of the hardware, the aerodynamic baseline (actuator prior to exposure to harsh conditions) was measured (hot wire, Pitot tube), this defines the reference. After each test (and for some tests also during the test), the measurements of aerodynamic properties were repeated in order to detect any deficiencies of actuator performance caused by the harsh conditions. In addition some specific tests were made (e.g. weight) in order to derive e.g. mass increase due to ice formation inside the hardware. [6]

One can conclude in general that the harsh environmental testing provided very valuable and detailed data sets, to compare the SJA properties before and after exposure to harsh conditions. These conditions are representative enough for aircraft applications, that conclusions regarding TRL3 (area Operations) are possible [7].

The recommendation out of these tests is to further improve the current design concepts of HJA and SJA, taking the "deltas" of aerodynamic properties into account. Specific care might be necessary for sand and dust conditions, since the essential feature of the active flow approach is a powerful control jets expelled out of a small orifice. Any blocking and/or remaining material inside the chamber could impact the functionality.

ACKNOWLEDGEMENT
The authors would like to thank all the partners in AFLoNext Work Package 2.2 for cooperation. The work described in this paper has received funding from the European Commission Seventh Framework Programme FP7/2007-2013, under grant agreement n° 604013, AFLoNext project.

7 REFERENCES

1. V. Ciobaca, J. Wild; 2013; "An Overview of Recent DLR Contributions on Active Flow-Separation Control Studies for High-Lift Configurations" Aerospace Lab Journal, AL06-12, Issue 6
2. C. Nae; 2009; "Flap gap oscillatory blowing on wings", INCAS Bulletin 2/2009, ISSN 2066- 8201
3. M. Bauer, J. Lohse, F. Haucke, W. Nitsche; 2014; "High-lift performance investigation of a two-element configuration with a two-stage actuator system"; *AIAA journal*, **52**(6), pp. 1307-1313.
4. P. Schloesser, M. Meyer, M. Schueller, P. Weigel, M. Bauer; 2017; "Fluidic actuators for separation control at the engine/wing junction", *Aircraft Engineering and Aerospace Technology*, https://doi.org/10.1108/AEAT-01-2017-0013
5. P. Schloesser; 2017; "Design of a Pulsed Jet Actuator for Separation Control"; 6th *CEAS Conference*; Bucharest; October, 16-19
6. I. Brinza; 2017; "AFC technology testing and TRL evaluation plan AFLoNext Deliverable WP 224"
7. H. Bieler; 2017; "Summary Conclusions from WP22 for Transport Aircraft Application" AFLoNext Deliverable WP 225"

Paper 2421

A CFD Benchmark of Active Flow Control for Buffet Prevention

Fulvio Sartor
ONERA - Applied Aerodynamics Department. Meudon, France
fulvio.sartor@onera.fr

Mauro Minervino
CIRA - Fluid Mechanics Department. Capua, Italy
m.minervino@cira.it

Jochen Wild
DLR - Institute of Aerodynamics and Flow Technology. Braunschweig, Germany
jochen.wild@dlr.de

Stefan Wallin
KTH - FLOW Centre, Dept. of Mechanics. Stockholm, Sweden
stefanw@mech.kth.se

Hans Maseland
NLR - Netherlands Aerospace Centre. Amsterdam, The Netherlands
hans.maseland@nlr.nl

Julien Dandois
ONERA - Applied Aerodynamics Department. Meudon, France
julien.dandois@onera.fr

Vitaly Soudakov
TsAGI - Department of Aerodynamics. Zhukovsky, Moscow Region, Russia
vit_soudakov@tsagi.ru

Petr Vrchota
VZLU - Aeronautical Research and Test Institute. Prague, Czech Republic
vrchota@vzlu.cz

A CFD Benchmark of Active Flow Control for Buffet Prevention

Fulvio Sartor
ONERA - Applied Aerodynamics Department. Meudon, France
fulvio.sartor@onera.fr

Mauro Minervino
CIRA - Fluid Mechanics Department. Capua, Italy
m.minervino@cira.it

Jochen Wild
DLR - Institute of Aerodynamics and Flow Technology. Braunschweig, Germany
jochen.wild@dlr.de

Stefan Wallin
KTH - FLOW Centre, Dept. of Mechanics. Stockholm, Sweden
stefanw@mech.kth.se

Hans Maseland
NLR - Netherlands Aerospace Centre. Amsterdam, The Netherlands
hans.maseland@nlr.nl

Julien Dandois
ONERA - Applied Aerodynamics Department. Meudon, France
julien.dandois@onera.fr

Vitaly Soudakov
TsAGI - Department of Aerodynamics. Zhukovsky, Moscow Region, Russia
vit_soudakov@tsagi.ru

Petr Vrchota
VZLU - Aeronautical Research and Test Institute. Prague, Czech Republic
vrchota@vzlu.cz

ABSTRACT

This paper will present the main results of the aerodynamic design and analysis for flow control applied to trailing edge of wings and profiles. This work has been conducted in the framework of the European project AFLoNext aiming at developing technologies allowing for an improvement of the performance and loads situation in the operational domain. The technologies are expected to provide an increase in aerodynamic efficiency and a structural weight reduction for the design flight conditions with a potential for 1-2% fuel savings and corresponding emission reduction. Numerical simulations are performed on 2D and 3D test cases. Where available, a comparison with experimental data is performed. High-speed flow is considered, in order to investigate a transonic configuration representative of cruise conditions. Trailing edge devices (TED) such as fluidic Gurney flaps or micro-jets for circulation control are used for assessing the possibility of delaying the buffet onset or increasing the maximum achievable lift, thus extending the flight envelope of an aircraft. The purpose of the present paper is to present the result of the work performed by the different partners involved in the project.

KEYWORDS

RANS, transonic buffet, flow control, Trailing Edge Device

NOMENCLATURE

α	angle of attack	c	chord of the profile
CFD	Computational Fluid Dynamics	C_p	Pressure Coefficient
C_D	Drag Coefficient	C_L	Lift Coefficient
Pi_{TED}	Total pressure of the TED	TED	Trailing Edge Device

1 INTRODUCTION

The current growth of air traffic worldwide (expected to double every fifteen years) emphasizes clearly the stakes of fuel-burn reduction, both from an environmental and economical perspective. The operating costs of transport aircraft are largely affected by the aerodynamic performance of the wing. Because of rising fuel costs and lower emissions targets there is an increasing need to exploit the full aerodynamic potential of the wing, either across the entire operating envelope, or at design flight conditions. In the past, the ability to modify the detailed flow at the trailing edge of a wing has been shown to potentially provide aerodynamic benefits by and adaptive change of camber during flight and to improve aircraft performance across the entire flight envelope.

A number of trailing edge devices for the control of trailing edge flows have been proposed: these include a variety of "Gurney" flaps [12, 2, 6] or "Mini-Trailing Edge Device" [18]. More recently, the use of fluidic injection at the trailing edge of a wing has been suggested [11, 10] and, to a limited extent, evaluated both theoretically and experimentally [3]. These fluidic devices include concepts such as normally blown fluidic Gurney flaps and tangentially blown "Circulation Control" concepts [8]. The basic idea is to replace the mechanical trailing edge deflector, which has shown to be able to increase the wing aerodynamic performances and delay the onset of buffet by altering the load distribution [3], using a fluidic devices.

In the case of transonic buffet phenomenon, it has been shown that fluidic vortex generators located upstream of the shock foot can reduce the extent of the separated area and are very efficient to postpone the buffet onset [22]. However, the effect of the fluidic TED is different, the separation is not suppressed, but the rear wing loading is increased and consequently the buffet onset is not delayed to higher angles of attack, but only to higher lift coefficient [13]. Fluidic TED have also found applications on nozzle engines: fluidically enhanced chevrons have also shown promising results for supersonic jet noise reduction [20].

One of the goals of the AFLoNext project is to explore the potential of active mechanical and pneumatic trailing edge flow control concepts for application in a multi-function role at both high- and low-speed operating conditions. This is done by application of numerical simulation together with targeted simple experiments to understand the potential aerodynamic performance benefits achievable together with design parameters such as pneumatic supply pressures/mass-flows and the required speeds/frequencies of operation.

The partners involved in the project focussed on the numerical assessment of the flow-control devices and their effect on a reference configuration. The numerical simulation is a central part of this collaborative project, and is done to understand both the flow inside a control device and the impact on the total aerodynamic field in each considered case. Parametric investigation is used to assess the effect of the control-device location on the global system, while optimisation is applied in order to assist the design of the actuator and define its geometric characteristics. Different goal functions have been considered for the optimisation process, aiming at maximising the total lift, the aerodynamic efficiency, or at obtaining an increase of the lift without incurring in buffet conditions. The design variables were the jet orientation, the slot width, its position, and the stagnation pressure intensity. In order to investigate the multi-functional use of the TED, a low-speed application was also considered on a high-lift aerofoil equipped with a simple single-slotted trailing-edge flap with TED.

The paper is structured as follows: first, the numerical benchmark is presented in section 2, where the partners evaluated the performance of their code by comparing RANS results on cases with and without flow control against an existing experimental database. The results are then presented: first in section 3 in the case of a 2D profile with TED, then in section 4 for a half wing-body configuration equipped with a 3D slot acting as a fluidic Gurney flap on the outer part of the wing.

2 NUMERICAL BENCHMARKS

The design of an efficient control device needs an accurate description of the aerodynamic field of the uncontrolled configuration as well as a correct representation of the control device itself. The work performed in this article is based on numerical simulations. A validation process is necessary to assess the capability of modern CFD techniques of correctly predicting the behaviour of the flow in the presence of control devices. For this reason, two numerical benchmarks have been proposed and a comparison with available experimental data allows for code validation. Different codes are used by the partners involved in the simulations, for example U-ZEN by CIRA [1], elsA by ONERA [19], TAU by DLR [5], Edge by KTH and VZLU[21]. The results by KTH has been obtained in cooperation with FOI, the Swedish Defence Research Agency.

The benchmarks focus on a 2D profile and a 3D half wing-body configuration in transonic conditions, with and without control device at the trailing edge. When the angle of attack is small, the interaction between the shock and the boundary layer yields to a steady flow field. When increasing the angle of attack, periodic shock motions known as transonic buffet occur, and the flow is unsteady. The experimental results are available from the European FP6 project AVERT, were two wind tunnel testing campaigns have been performed, aiming at studying buffet and delaying its onset by means of several control devices. The first one was performed at VZLU A4 test section wind tunnel with an existing ONERA 2D OAT15A aerofoil [14]. The second test campaign was performed at the ONERA S2MA wind tunnel on a 3D half-model [15, 16].

3 RESULTS OF THE 2D TEST CASE

The aerofoil geometry is based on a modified ONERA OAT15A cross-section. The chord length and span of the used wind tunnel model are equal to 0.200 m and 0.390 m, respectively. This model, visible in figure 1, is equipped with a removable mechanical TED that can be easily modified and thus has been adapted to integrate a fluidic TED. Moreover, its wing span was compatible with the dimensions of the VZLU-A4 test section with a few adjustments. This model was tested at the transonic ONERA T2 wind tunnel in two campaigns in 1998 and 1999 [14].

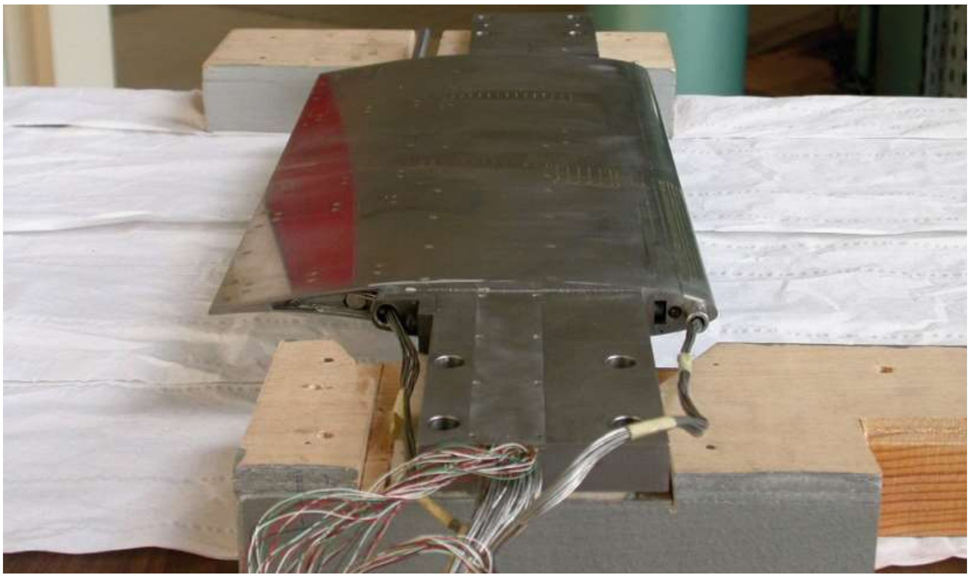

Figure 1: OAT15A aerofoil for 2D buffet characterisation tested in the VZLU A4 wind tunnel.

The test conditions were a variable Mach number between 0.730 and 0.739, stagnation pressure of 1 bar and a Reynolds number based on the chord of 2.6 million. The transition was fixed at 7%

of chord length on both upper and lower side. The main part of the test program was related to the aerodynamic evaluation of the reference configuration (reference standard trailing edge, and/or baseline configuration with fluidic TED without blowing) and, above all, aerodynamic evaluation of fluidic TED with blowing. Static pressure (pressure taps) and unsteady pressure (Kulite transducers) measurements were performed, while some specific oil-flow visualizations allowed to check side walls interferences. For the baseline configuration, the buffet characteristics (onset, shock position and intensity) obtained at the VZLU A4 transonic wind tunnel are very consistent with the former ones recorded at the ONERA T2 transonic wind tunnel testing campaigns, allowing then to pursue on fluidic TED investigations.

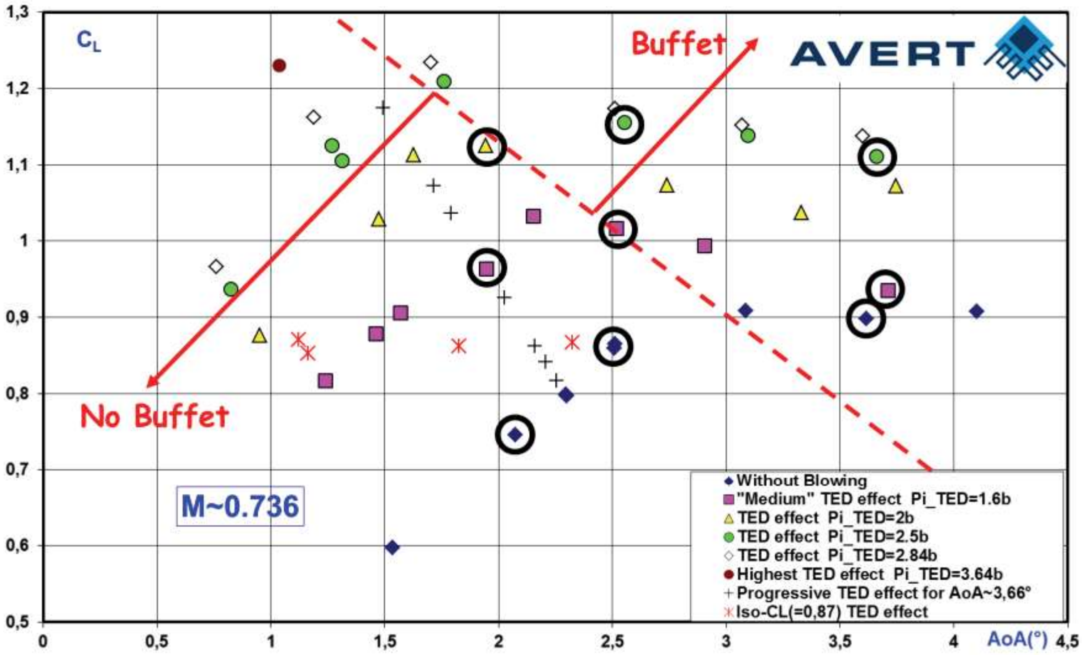

Figure 2: Polar curves with the selected test cases for the 2D benchmark exercise.

Nine test cases are proposed before and after buffet onset, for the baseline configuration and for two levels of TED mass flow rate. They can be clearly identified (rounded by black circles) in figure 2. The following angles of attack will be presented in this paper:

- $\alpha = 1.5°$ (no buffet), without blowing
- $\alpha = 3.4°$ (buffet), without blowing
- $\alpha = 2.0°$ (no buffet) blowing at Pi$_{TED}$ = 1.6
- $\alpha = 3.7°$ (buffet), blowing at Pi$_{TED}$ = 1.6

The partners were provided with the geometrical characteristics of the 2D aerofoil and the slot, and for each test case with the lift coefficient (obtained by pressure integration) and chord-wise distributions of C_p and C_p RMS. To simulate the different test cases all the partners generated a multi-block structured C-type hexahedral mesh appropriately refined in the proximity of the TED slot and around the expected shock location. The flow control device was either simulated using a surface boundary condition on the profile, which imposes the stagnation pressure and temperature at the TED slot outlet, (CIRA, TsAGI, VZLU), or with total pressure and temperature imposed at the inlet of an idealized slot geometry (DLR, ONERA), or with total pressure and temperature imposed at the inlet of the provided slot geometry (ONERA). The three approaches are summarised in figure 3. Almost identical results were obtained for the first two modelling techniques, while the ONERA slot geometry yielded to an under estimation of the flow control effect.

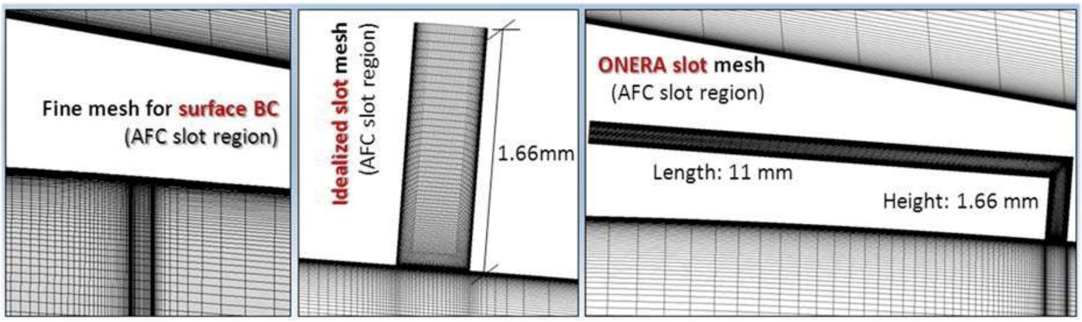

Figure 3: Different strategies for TED representation: surface boundary condition (left), idealized slot geometry (middle) or ONERA slot geometry (right).

Several turbulence models were considered, with most of the partners preferring the Menter k-ω SST model or the Spalart-Allmaras model. The spatial discretisation was based upon a finite volume formulation, with second and fourth order artificial dissipation.

Figure 4 shows on the left the pressure and skin friction coefficient distributions for the case at low angle of attack without blowing. The C_p exhibits a very good agreement between all partner's results on the plateau level as well as on the shock position and the compression downstream of the shock. The shock is just located a bit too far downstream (2% of chord) in the CIRA computation. The discrepancies between partner's results are higher on the skin friction coefficient, presented on the right side of figure 4, but the agreement is still reasonable.

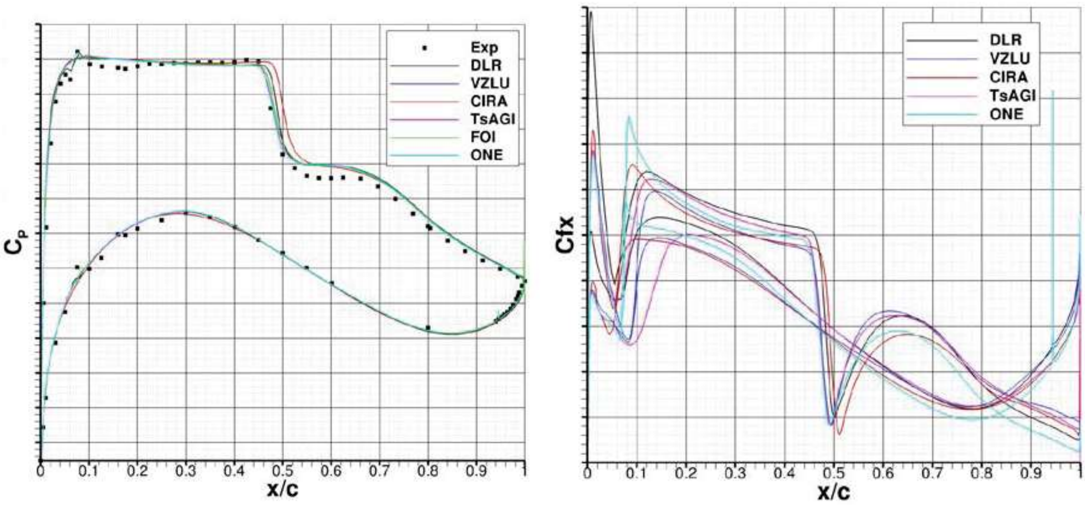

Figure 4: Pressure (left) and skin-friction (right) coefficients: low angle of attack, without TED.

The second test case is in the buffet regime and corresponds to a Mach number equal to 0.7385 and $3.4°$ angle of attack. Figure 5 shows on the left the time-averaged wall pressure coefficient. Much effort has been put in looking for modified flow conditions, in order to take into the account wind-tunnel corrections. CIRA computed both the original and modified flow conditions with a lower angle of attack in order to correct the wall effect in the wind tunnel. The shock is located too far downstream for both CIRA and TsAGI and the plateau level is a little bit too high. The ONERA computation is in better agreement with the experimental data. The RMS values of the wall pressure coefficient are shown on the right side of figure 5. There is a problem in the experimental data for the three sensors located between 40% and 45% of aerofoil chord, since there should be a peak like in the computations. There is also a problem on the position of the peak which seems more upstream in the experimental data than in the computations although there is a good agreement on the shock location.

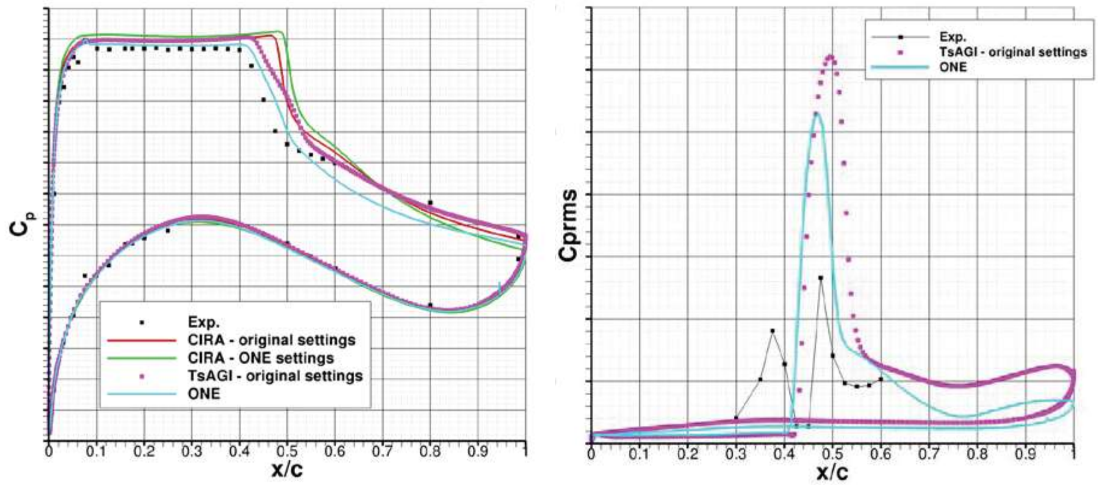

Figure 5: Mean (left) and RMS (right) values of pressure coefficient: high angle of attack, without TED.

The first case with the control device blowing is presented on the left side of figure 6. The flow conditions are a Mach number of 0.727 and $2.02°$ angle of attack. ONERA performed two computations: one for which the flow is computed in the full cavity of the TED and the second one for which only the flow in the slot is computed like for DLR. In the VZLU, CIRA and TsAGI, the blowing boundary condition is applied at the wall, so the flow in the blowing slot is not computed. The pressure coefficient distribution shows a good agreement between all partner's results on the plateau level as well as on the shock location. The ONERA computation with the full cavity predicts a shock which is too upstream compared to the ONERA computation with just the slot and all the other computations too. This is due a separation in the $90°$ corner in the cavity. On the contrary, for the simulations with just the slot (ONERA, DLR) or the boundary condition applied directly on the wall (VZLU, CIRA and TsAGI), the velocity profile has a top-hat shape and the numerical simulations are in better agreement with the experimental data. The best agreement on the wall pressure on the pressure side between $x/c = 95$% and 100% is obtained for the DLR and ONERA computation with the simplified slot. This region corresponds to the separated zone downstream of the fluidic TED.

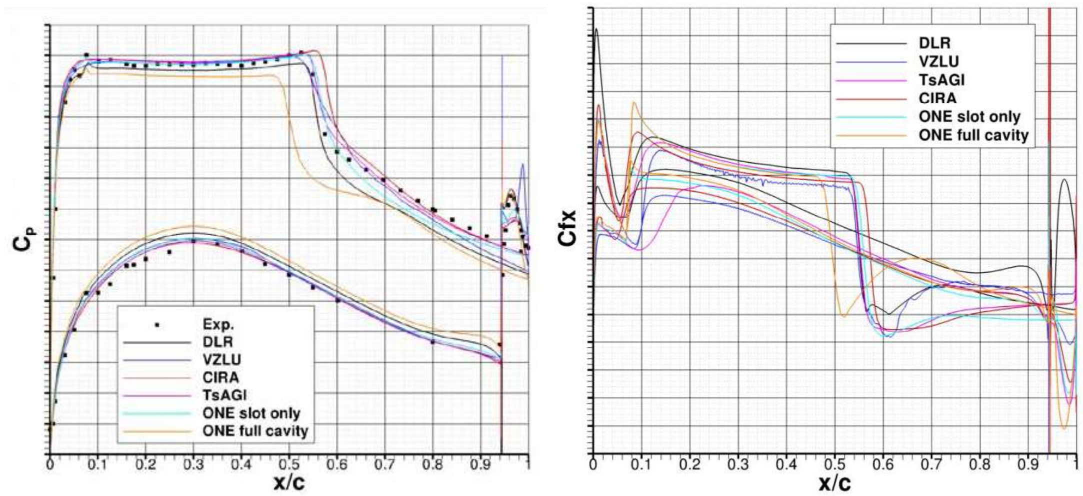

Figure 6: Pressure (left) and skin-friction (right) coefficients: low angle of attack, with TED.

The last case is in the buffet regime with the fluidic TED blowing, the original flow conditions were Mach equals 0.73657 and $3.71°$ angle of attack. ONERA proposed a corrected condition with same Mach number but lower angle of attack. The left side of figure 7 shows that VZLU, TsAGI and ONERA computations predict a shock oscillation as expected but not the CIRA one. The time-averaged shock location is well predicted by TsAGI and ONERA computations and is a slightly too far downstream and with a lower amplitude for the VZLU one. Concerning the C_p RMS distribution, presented on the right side of figure 7, the TsAGI and ONERA computations predicted a good agreement in terms of C_p RMS peak amplitude but this peak is located slightly too far downstream, which is surprising because the time-averaged shock location was well predicted on the C_p distribution.

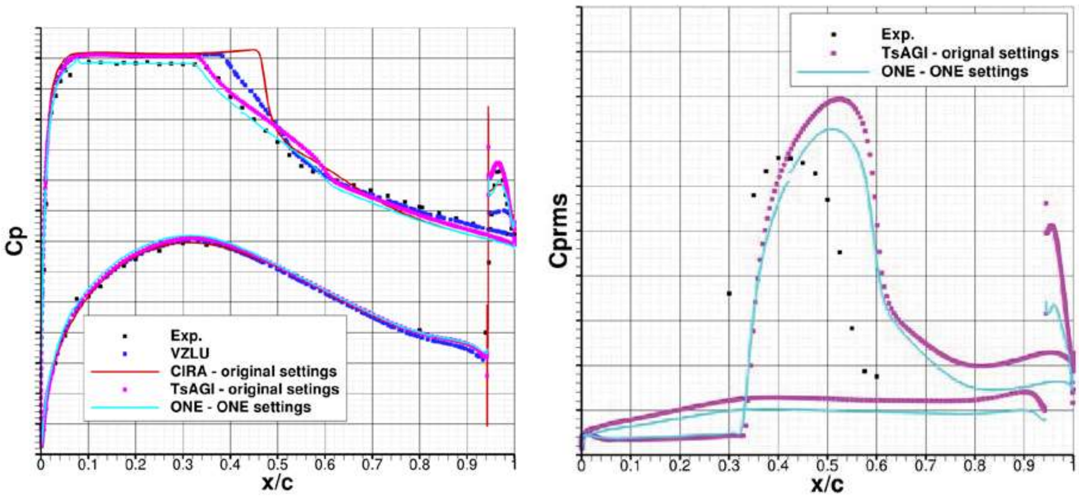

Figure 7: Mean (left) and RMS (right) values of pressure coefficient: high angle of attack, with TED.

Globally, a good agreement between each partner's results and the experimental data has been observed on the wall pressure distribution as well as on the plateau level and the shock location. There are more discrepancies on the skin friction distribution and for the unsteady cases in buffet regime which are more challenging. Concerning the modelisation of the fluidic TED, different solutions have been chosen. Applying an injection boundary condition at the wall leads to a good prediction of the plateau level and shock location but the pressure distribution downstream of the fluidic TED is not very well predicted. Computing the flow in the full cavity, even if it seems more realistic compared with the wind tunnel tests, leads to the prediction of a shock which is too upstream. Computing the flow only in the slot leads to an overall better prediction as well as on the shock location and the pressure distribution downstream of the fluidic TED. Concerning the prediction of the buffet onset, this onset is delayed to a higher angle of attack ($0.5°$ to $1°$) than in the experimental data. The angle of attack correction depends on the turbulence model which is used.

4 RESULTS OF THE 3D TEST CASE

The present section concerns the assessment of the active flow control approach applied to a swept wing in transonic conditions. As for the 2D test case presented in the previous section, different test cases are investigated, with a combination of angles of attack and blowing momentum of the control devices. The approach is based on continuous blowing through a span-wise slot on the lower surface in the vicinity of the trailing edge, employed to modify the span-wise aerodynamic loading in order to increase the lift-to-drag ratio for a rigid wing. As in the previous case, the fluidic trailing edge device is developed and demonstrated for separation control to increase the buffet margin at transonic conditions by increasing the rear-loading of the wing.

RANS approaches are used, without imposing any constraint on the numerical method or turbulence model for the simulations. The test cases are selected from an available experimental data base ob-

Figure 8: 3D model in the ONERA S2MA wind tunnel.

tained in the S2MA wind tunnel of ONERA. The comparison of numerical and experimental data concerns sectional pressure distributions on the wing and force coefficients for the entire configuration. Subsequently, lift curves are computed for the fluidic TED configurations at the design Mach number as a function of the jet momentum coefficient. The aerodynamic efficiency is determined in terms of the lift-to-drag ratio and compared to that of the baseline configuration. The half-model geometry consists of a wing, a fuselage and a peniche (see figure 8). The wing cross-section geometry is based on the OAT15A aerofoil.

The fluidic TED is equipped with a slot, the jet exit flow being normal to the lower surface. Its geometry is similar to the one used in the VZLU wind tunnel tests described above and has a slot width of 0.5 mm. The chord-wise position of the slot center is at $x/c = 95\%$, while the span-wise length is 490 mm. The slot is thus located between 45% and 85% of wing span. The design of the plenum that supplies the slot with air is based on the TED design for VZLU tests.

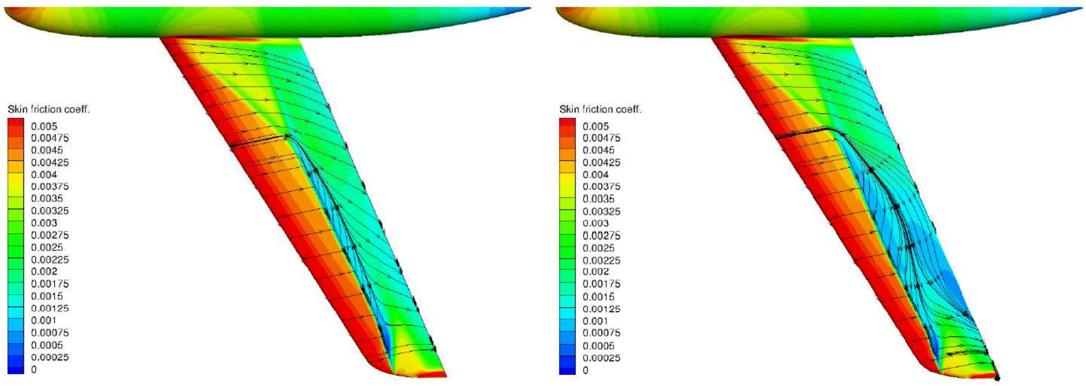

Figure 9: Skin friction on the 3D model from NLR: low (left) and high (right) angle of attack, no control.

The mesh provided by ONERA consists of 249 blocks and 16.86 million grid points, including a description of the whole cavity of the TED and, contrarily to the 2D case in the previous section, is the same for all partners. A set of deformed grids were provided, taking into the account the static deformation of the wind-tunnel model. The boundary condition used for the jet computation can be either based on the specification of the total pressure, total temperature and velocity direction or on the direct specification of the mass flow rate though the control device. The actual values of pressure and temperature are prescribed in terms of the total pressure ratio and need to be adjusted in order to obtain the correct mass flow rate. NLR and TsAGI performed the simulations using this boundary condition, while ONERA used the second method.

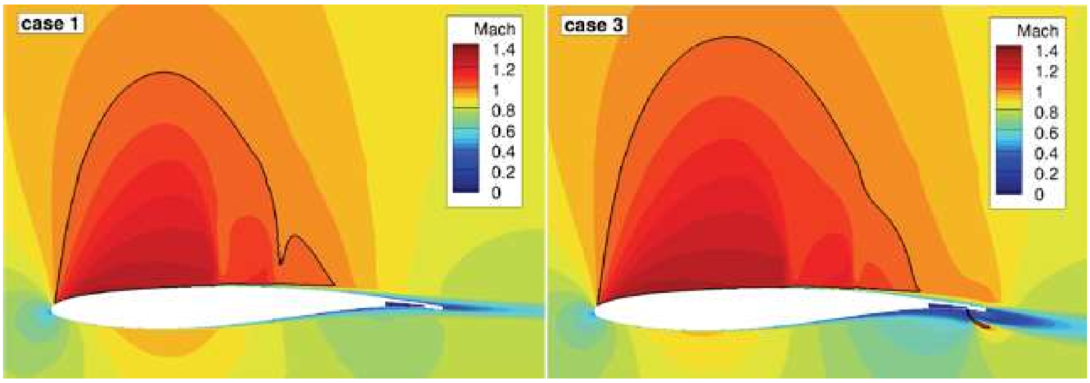

Figure 10: Mach field at y/b = 55.0% for the cases at low angle of attack, with (left) and without (right) flow control.

Figure 9 shows a typical flow solution, obtained by NLR using the baseline EARSM k-ω model at low (left side) and high (right side) angle of attack, indicating the flow pattern on the upper surface of the wing in terms of limiting stream-lines and illustrates the existence of a large separation bubble downstream of the shock location. When considering a lower angle of attack, the separated zone has a limited extension. As it can be seen in figure 10, showing the Mach distribution on a slice at y/b = 55.0% of the span, the shock has a more downstream position. When the TED is active, the shock moves even further downstream, increasing the value of the total lift coefficient.

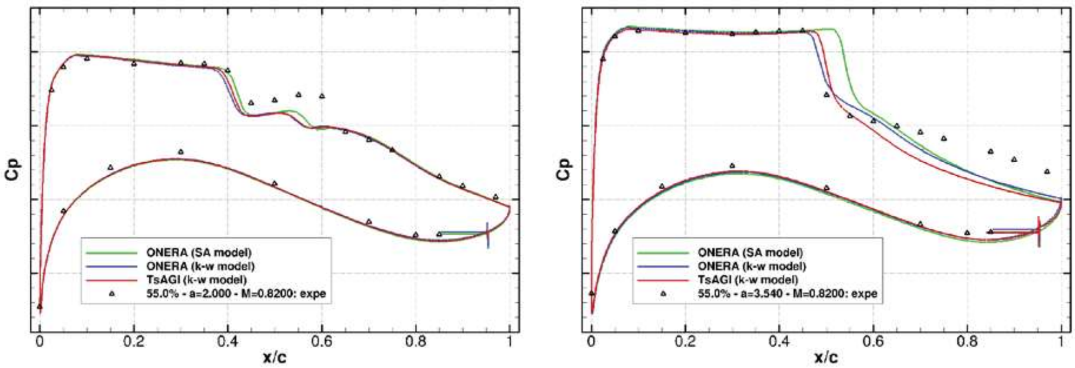

Figure 11: Pressure coefficient at y/b = 55.0%: low (left) and high (right) angle of attack, no control.

A comparison between the pressure coefficient distribution is presented in figure 11 for the uncontrolled cases: the agreement between the partners when using the same turbulence model is excellent, indicating that the failure to correctly reproduce the pressure distribution on the profile should not be sought in a specific code, but could be the consequence of the approach: RANS simulations, wall corrections, model deformations, and so on. On the same plot, the green line indicates a result obtained with the SA turbulence model: one can see that the comparison with the experimental data yields a better agreement when the angle of attack is small (case 1, on the left of the figure). However, when comparing the configurations at high angle of attack, the SA turbulence model predicts a shock position too far downstream, and the k-ω SST turbulence model yields a better agreement (case 4, right of the figure).

Figure 12 shows the pressure distribution for the span-wise location at y/b = 72.5% obtained for the two cases at low angle of attack, with and without control. The first case, on the left side of the image, presents the results for the case 1 (no TED) and indicates that taking into account the mesh deformation barely impacts the pressure distribution downstream of the shock. The shock wave however moves upstream when taking into the account the mesh deformation, yielding a less favourable comparison.

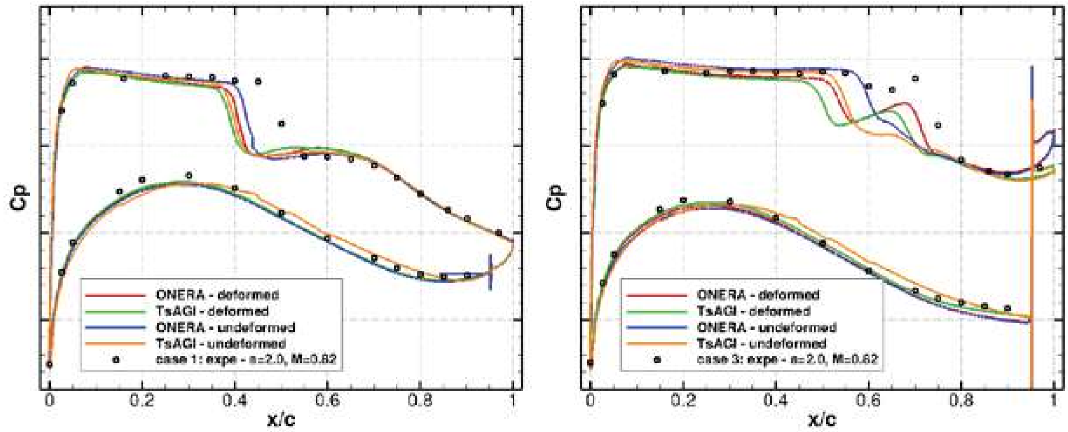

Figure 12: Pressure coefficient at y/b = 72.5%: low angle of attack, uncontrolled configuration (left), and case with flow control (right).

Case 3 (low angle of attack, high momentum through the TED) is presented on the right side of figure 12. The TED directly impacts the pressure distribution of this wing section: the shock wave moves downstream with increasing momentum of the TED. Consequently, the shock-induced separation decreases its size thanks to the control device. The pressure in the trailing edge region is also decreased, inducing higher wing load and pitching moment. In this configuration the wing deformation is the most important, and a more favourable comparison with the experimental data can be observed when taking into the account the bending and twisting of the wing. Contrarily to the undeformed geometry, the secondary expansion seen in the pressure distribution downstream of the shock wave is correctly reproduced by the numerical simulations.

In conclusion, the selected simulation approach for the characterization of 3D buffet is based on RANS calculations in combination with different turbulence models. Assessment of numerical results in a comparison with experimental data obtained in the S2MA wind tunnel of ONERA show a good agreement in terms of wing sectional pressure distributions and aerodynamic force coefficients for the entire configuration. The evaluation of the fluidic TED as a trailing edge variable camber device shows an aerodynamic efficiency for a wing-body configuration in terms of an increase of the lift-to-drag ratio along the entire lift curve.

The benefit offered by the fluidic TED scales with the mass flow rate. Although a satisfying agreement is generally achieved with the original conditions, some more challenging cases exist, where the numerical simulation is not able to accurately reproduce the pressure distribution observed in the experiments at both span-wise locations. In most cases at low angle of attack, the modified conditions provided by ONERA to take into account the wind tunnel correction and the model deformations do not improve the agreement with the experimental data. The reason for this could be sought either on the wind tunnel corrections, or on the RANS approach, which fails to correctly predict the flow field on the wing surface. However, satisfying agreement is often already achieved when using the non corrected aerodynamic conditions.

In order to assess the effect of the fluidic TED on the aerodynamic performance at cruise conditions, the drag behaviour is computed for the clean and fluidic TED configurations at the design Mach number. The design point is defined as $C_L = 0.5$. The clean configuration serves as a reference. The mass flow rate is varied for the TED configurations in order to identify the effect of the mass flow rate on the aerodynamic performance of the wing-body configuration. Figure 13 depicts the drag at two angles of attack for the clean and fluidic TED configurations. The mass flow rate is increased by considering the cases with higher momentum of the TED. The plot shows a reduction of the drag at a given value of the lift coefficient, which implies an enhancement of the aerodynamic efficiency.

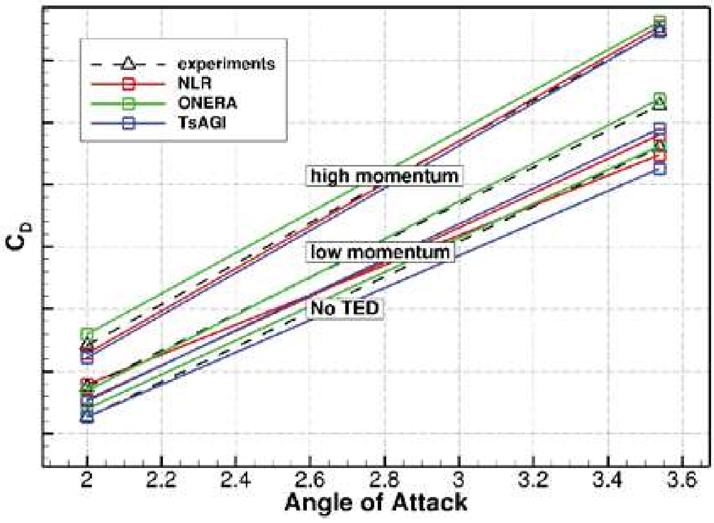

Figure 13: Comparison of drag coefficients between partner's results for all cases.

Finally, it is relevant to remark that relatively small drag increase is found for relatively small values of the jet momentum coefficient. These observations underline the multi-functional use of the fluidic TED for separation control and overall cruise performance enhancement. The fluidic TED seems a promising concept for future wings based on composite structures that feature larger flexibility than conventional wings. The aero-elastic deformations that originate from the variation in fuel load during the cruise segment result in aerodynamic performance degradation. The fluidic TED is capable to increase the local aerodynamic loading by increasing the rear-loading at the wing section. Therefore, the fluidic TED can be exploited to alter/restore the aerodynamic load distribution and act on the induced drag to limit the aerodynamic performance degradation.

5 CONCLUSIONS

The purpose of this article was to present the main results of the investigation on the potential of active mechanical and pneumatic trailing edge flow control concepts. This was done in the framework of the European project AFLoNext by application of numerical simulations together with targeted simple experiments to understand the potential aerodynamic performance benefits achievable together with design parameters.

A benchmark between different partners involved in the project has been considered. Overall, the results of both 2D and 3D benchmarks show a good agreement between parters. An improvement of the lift-to-drag ratio for the considered lift coefficient range which is representative for the entire cruise segment of the flight, confirming the conclusion of the AVERT program. The benefit of the fluidic TED is relative large even for small values of the jet momentum coefficient. Most importantly, the results presented indicate that the numerical simulations compare favourably to the experimental results. Thus, CFD can be used as a reliable tool to predict the behaviour of the flow in the presence of control devices.

In terms of perspectives, a great advantage of the TED when compared to other classical control devices such as vortex generators is that the TED can be used as a pulsed device, either in an open or a closed loop approach. The efficiency of a closed-loop approach using mechanical TED depends on the choice of the control law, which is not trivial, and could be the subject of future studies, who will prove the ability of a pulsed device to obtain the same beneficial effect as the classical continuously-blowing device, but using less mass flow rate.

Acknowledgements

The work described in this paper and the research leading to these results has received funding from the European Commission Seventh Framework Programme FP7/2007-2013, under grant agreement n°604013, AFLoNext project. The authors are also grateful to Lars Tysell from FOI for providing some of the results for this study, and to Mark Nichols from BAE Systems for managing the work package.

REFERENCES

[1] Marongiu C., Catalano P., Amato M., and Iaccarino G. U-zen: A computational tool solving U-RANS equations for industrial unsteady applications. In *34th AIAA Fluid Dynamics Conference and Exhibit*, page 2345, 2004.

[2] Van Dam C.P., Yen D.T., and Vijgen P.M. Gurney flap experiments on airfoil and wings. *Journal of aircraft*, 36(2):484–486, 1999.

[3] Caruana D., Mignosi A., Corrège M., Le Pourhiet A., and Rodde A.M. Buffet and buffeting control in transonic flow. *Aerospace science and technology*, 9(7):605–616, 2005.

[4] Quagliarella D. and Vicini A. Gas for aerodynamic shape design. I: General issues, shape parameterization problems and hybridization techniques. *Lecture series-van Kareman Institute for fluid dynamics*, 7:O1–O24, 2000.

[5] Schwamborn D., Gerhold T., and Heinrich R. The DLR TAU-code: recent applications in research and industry. In *ECCOMAS CFD 2006: Proceedings of the European Conference on Computational Fluid Dynamics, Egmond aan Zee, The Netherlands, September 5-8, 2006*. Delft University of Technology; European Community on Computational Methods in Applied Sciences (ECCOMAS), 2006.

[6] Jeffrey David., Zhang Xin., and Hurst David W. Aerodynamics of gurney flaps on a single-element high-lift wing. *Journal of Aircraft*, 37(2):295–301, 2000.

[7] D. Dolgopyat. On the feasibility of hinge-less flow control manoeuvring system. *Tel Aviv University, Israel*, Master Thesis, 2014.

[8] Dvorak F.A. and Choi D.H. Analysis of circulation-controlled airfoils in transonic flow. *Journal of Aircraft*, 20(4):331–337, 1983.

[9] Arwatz G., Fono I., and Seifert A. Suction and Oscillatory Blowing actuator. In *IUTAM Symposium on Flow Control and MEMS*, pages 33–44, 2008.

[10] Browaeys G., Collin E., Deniau H., and Bonnet J.P. Numerical study of closed loop control of transonic buffet by means of fluidic trailing edge device. In *CEAS/KATnet (Key Advances Technologies) Conference 2009*, 2009.

[11] Browaeys G., Deniau H., Collin E., and Bonnet J.P. Pneumatic control strategies for transonic buffet. a numerical approach. In *7th International Symposium on Engineering Turbulence Modeling and Measurement (ETMM7), Limassol, June 4-6, 2008.*, pages pp–805, 2008.

[12] Liebeck Robert H. Design of subsonic airfoils for high lift. *Journal of aircraft*, 15(9):547–561, 1978.

[13] Dandois J., Lepage A., Dor J.B., Molton P., Ternoy F., Geeraert A., Brunet V., and Coustols É. Open and closed-loop control of transonic buffet on 3d turbulent wings using fluidic devices. *Comptes Rendus Mécanique*, 342(6):425–436, 2014.

[14] Dandois J., Gleyzes C., Dor J-B., Ternoy F, and Coustols E. Report on the VZLU wind tunnel test analysis and report on the 3D RANS and URANS computations of mechanical/fluidic VGs and fluidic TEDs. *AVERT Deliverables D1.3-3 & D1.3-8*, June 2010.

[15] Dandois J., Dor J.-B., Lepage A., Brunet V., Eglinger E., Ternoy F., and Coustols E. AVERT: ONERA S2MA wind tunnel test report. *AVERT Deliverable D4.3-4*, June 2010.

[16] Dandois J., Molton P., Lepage A., Geeraert A., Brunet V., Dor J-B., and Coustols E. Buffet characterisation and control for turbulent wings. *Aerospace Lab Journal*, 6, 2013.

[17] Hellsten Antti K. New advanced kw turbulence model for high-lift aerodynamics. *AIAA journal*, 43(9):1857–1869, 2005.

[18] Richter Kai. and Rosemann Henning. Steady aerodynamics of miniature trailing-edge devices in transonic flows. *Journal of Aircraft*, 49(3):898–910, 2012.

[19] Cambier L., Heib S., and Plot S. The ONERA elsA CFD software: input from research and feedback from industry. *Mechanics and Industry*, 14:159–174, 1 2013.

[20] Heeb N., Gutmark E., Liu J., and Kailasanath K. Fluidically enhanced chevrons for supersonic jet noise reduction. *AIAA Journal*, 52(4):799–809, 2014.

[21] Eliasson P. EDGE, a Navier-Stokes solver for unstructured grids. *Proceedings to Finite Volumes for Complex Applications III*, pages 527–534, 2002.

[22] Molton P., Dandois J., Lepage A., Brunet V., and Bur R. Control of buffet phenomenon on a transonic swept wing. *AIAA journal*, 51(4):761–772, 2013.

[23] Wallin S. and Johansson A.V. An explicit algebraic reynolds stress model for incompressible and compressible turbulent flows. *Journal of Fluid Mechanics*, 403:89–132, 2000.

[24] P. Vrchota, A. Prachar, P. Hospodar, D. Dolgopyat, and A. Seifert. Development of simplified boundary condition of saob actuator based on high-fidelity cfd simulations. In *Proceedings of the 52nd 3AF International Conference on Applied Aerodynamics*, Lyon - France, 2017.

Section IV

Space Technologies and Advanced Research

Presentations 2501, 2502 and 2515

Siemens Convergence Creators

Space Activities under the Incentive Scheme

CEAS 2017

Siemens Convergence Creators

Space Activities under the Incentive Scheme

www.convergence-creators.siemens.com

Agenda

SIEMENS

Topic	Content
• **Who are we?**	Siemens Convergence Creators short presentation
• **Siemens Convergence Creators Romania and the Space Business**	Siemens Convergence Creators Romania and the space domain
• **Earth Observation** • Enhancement of Earth Observation Service Access • Federated Identity Management • Cloud-based Identity and Access Management	ESA Earth Observation related projects part of the Romanian Incentive Scheme
• Mission Planning and Mission Control • Visual XML Editor • Lightweight Interface for SPAN infrastructure • Java implementation of Language for Mission Planning • Mobile UI for EMS Portal	Projects related to ESA Mission Planning and Mission Control
• **Q&A**	Q&A related to any of the topics. Other relevant discussion or technical details

Who are we?

Siemens Convergence Creators

Siemens Convergence Creators provides the middleware that handles the “logistics” of data in digital businesses

SIEMENS

Goods logistics in the 21st century

Data & information logistics in the Internet of Things

Transport

Networks

Flow of Data

Flow of Goods

Addresses

Devices

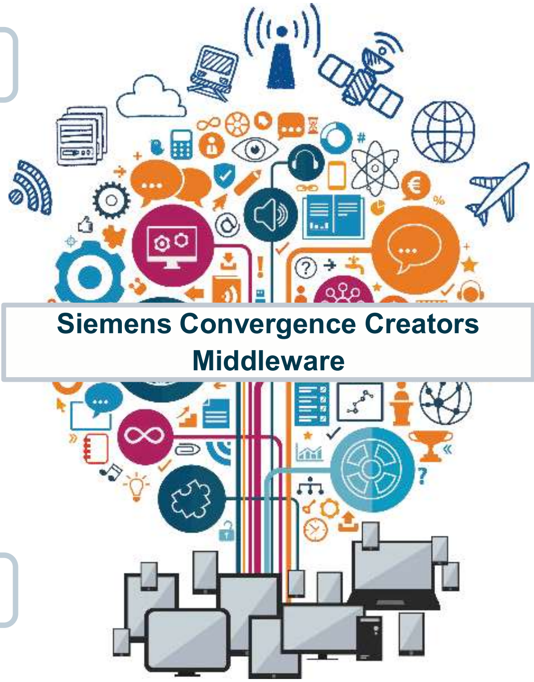

Superior data logistics represents a key competitive factor in a digital business
Our converged platforms deliver tangible value to our customers

Our portfolio: Focusing on solutions for the target industries

SIEMENS

Our solutions

Target industries

Our solutions	Energy	Media	Public Safety & Security	Space	Telecom	Transportation
Aerospace			✓	✓		✓
Infrastructure Solutions	✓		✓		✓	✓
LTE & Broadband Technologies	✓		✓		✓	
Media-Infotainment		✓			✓	✓
Professional Services	✓	✓	✓	✓	✓	✓

A strong partner for the space industry

Space

At a glance

Satellite manufacturers, carriers and network operators face a multitude of requirements that we help to meet with our proven and reliable **satellite monitoring** and **testing** solutions.
Our **SIECAMS®** solutions **identify interference** and **manage carriers** with minimal investment, while the **Electrical Ground Support Equipment** portfolio allows for efficient **space environment testing** and **calibration** of multiple satellite subsystems.

Customer value

- OPEX savings
- CAPEX savings
- Allows satellite operators to fulfill their SLAs
- Cost-efficient investment for public & corporate sectors

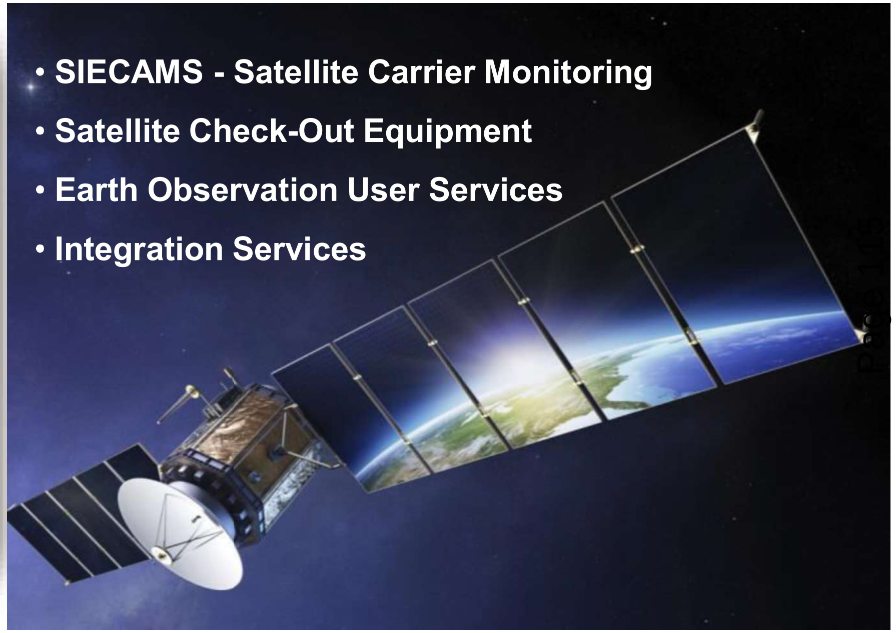

SIEMENS

Siemens Convergence Creators Romania and the Space Business

Siemens Convergence Creators

About Siemens Convergence Creators Romania

SIEMENS

- **Who we are**

Embedded into the strongest European technology player

- **What we do**

Unique R&D, telecommunication, software development and IT services portfolio in Romania
Cross-industry offerings that bring value to your business

- **What we know**

Benefit from more than 15 Years of ICT industry experience and certified expertise

- **Where we are**

Worldwide on-site support and near shore presence in Eastern Europe

Siemens Convergence Creators Romania

SIEMENS

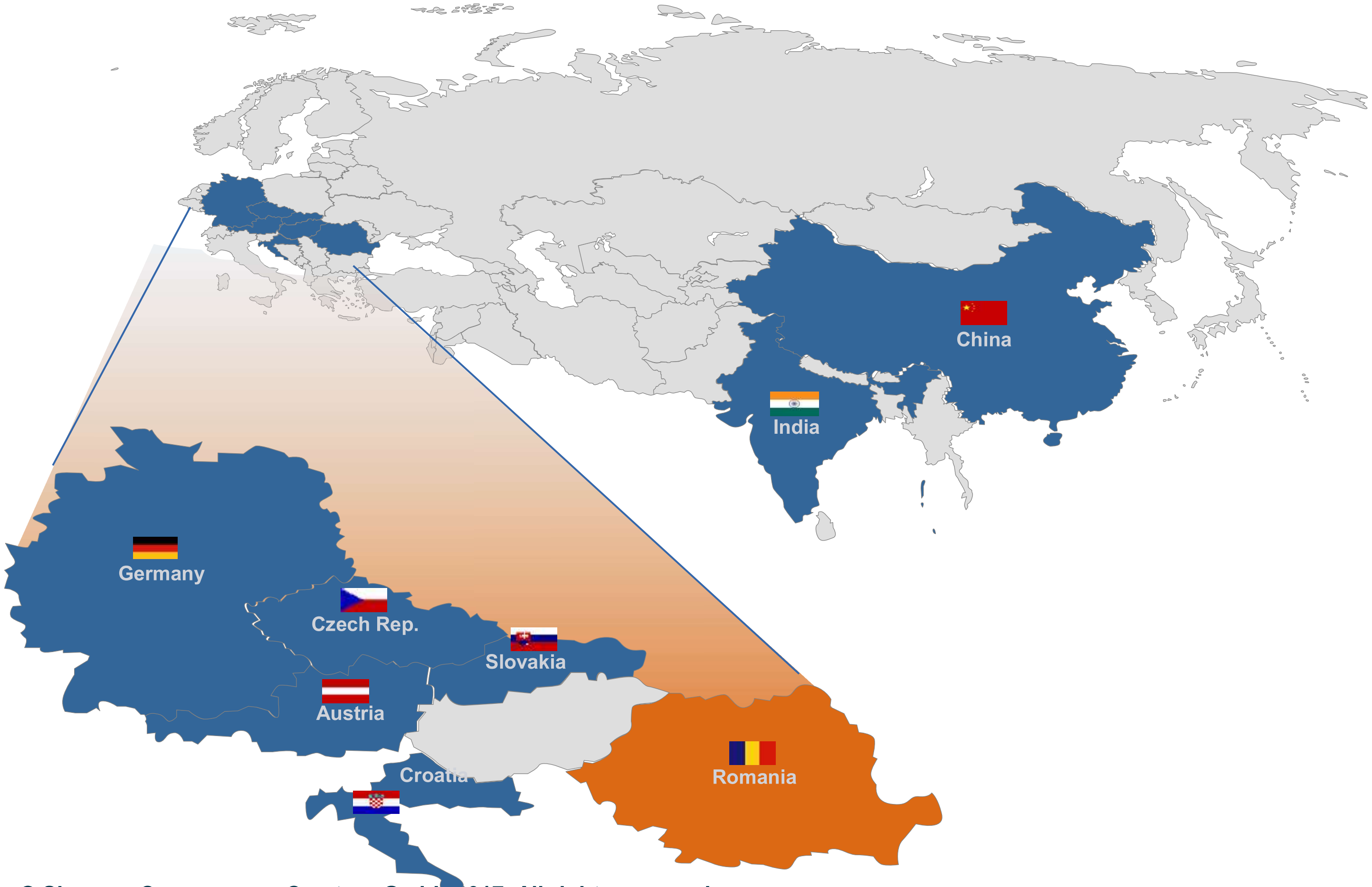

Siemens Convergence Creators Romania

230 Employees

ISO 9001:2000

ISO 14001:1997

ISO 27001

OHSAS 18001

CMMI Level 3

Established in 2001

Located in Brasov (HQ) and Cluj-Napoca

Telecommand, Telemetry & Control (TT&C) Tests
Herschel Satellite

SCOE - Special Check-Out Equipment

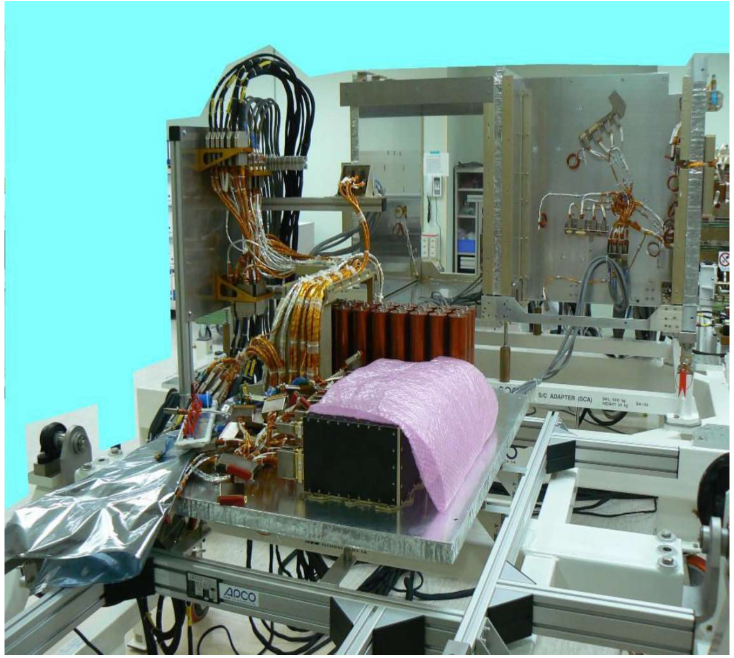

Platform

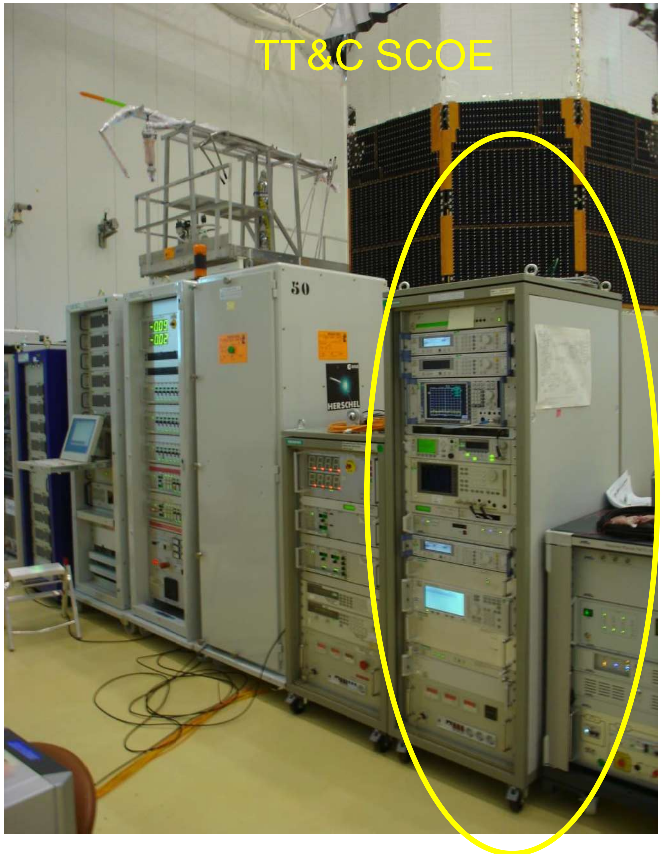

Page 119

SIEMENS

Power Subsystem Tests
Planck and SWARM Satellites

Launch Base Tests
Ariane5 – Herschel Planck Launch

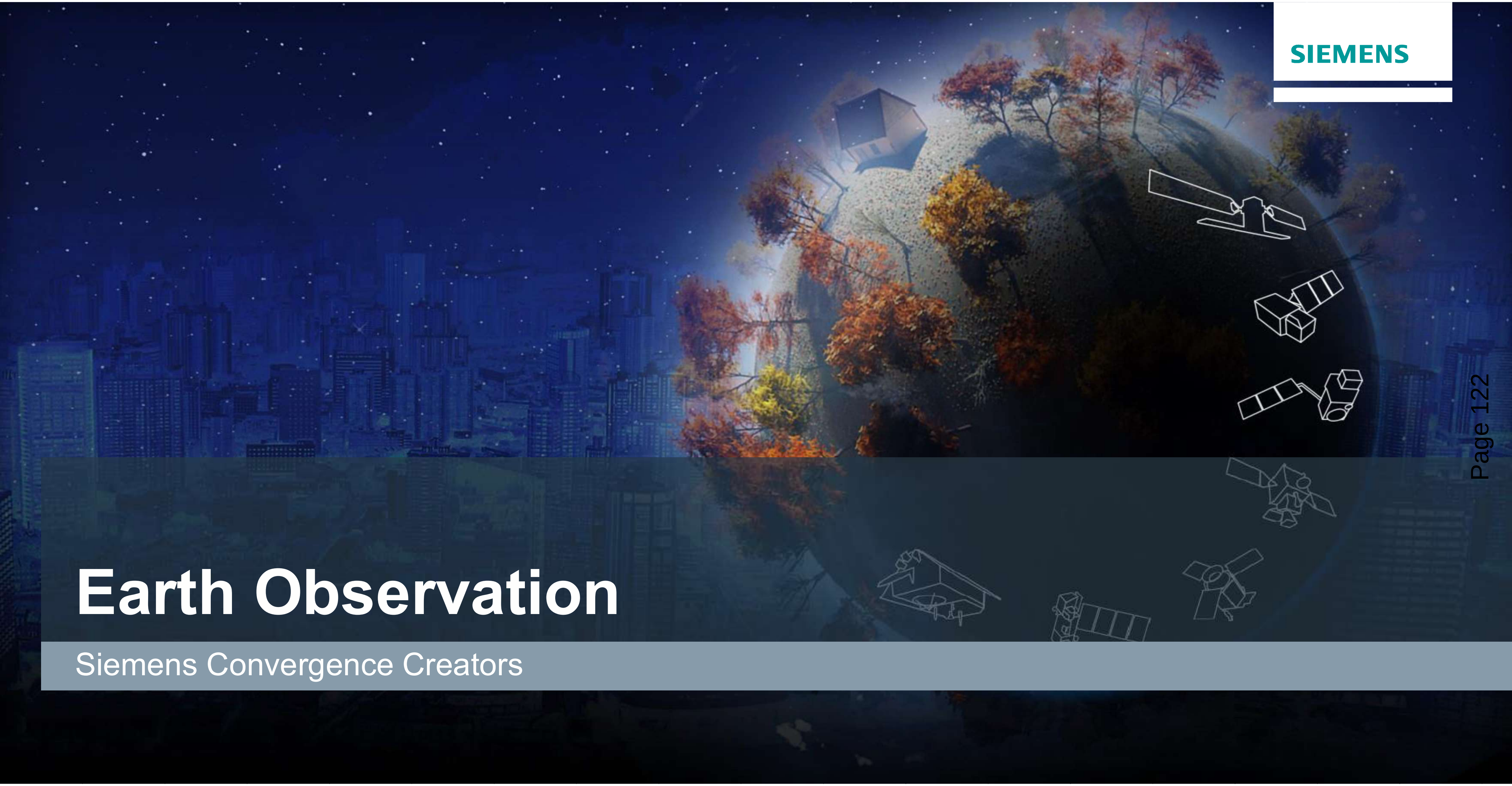

Earth Observation

Siemens Convergence Creators

The ESA Earth Observation Satellite Fleet

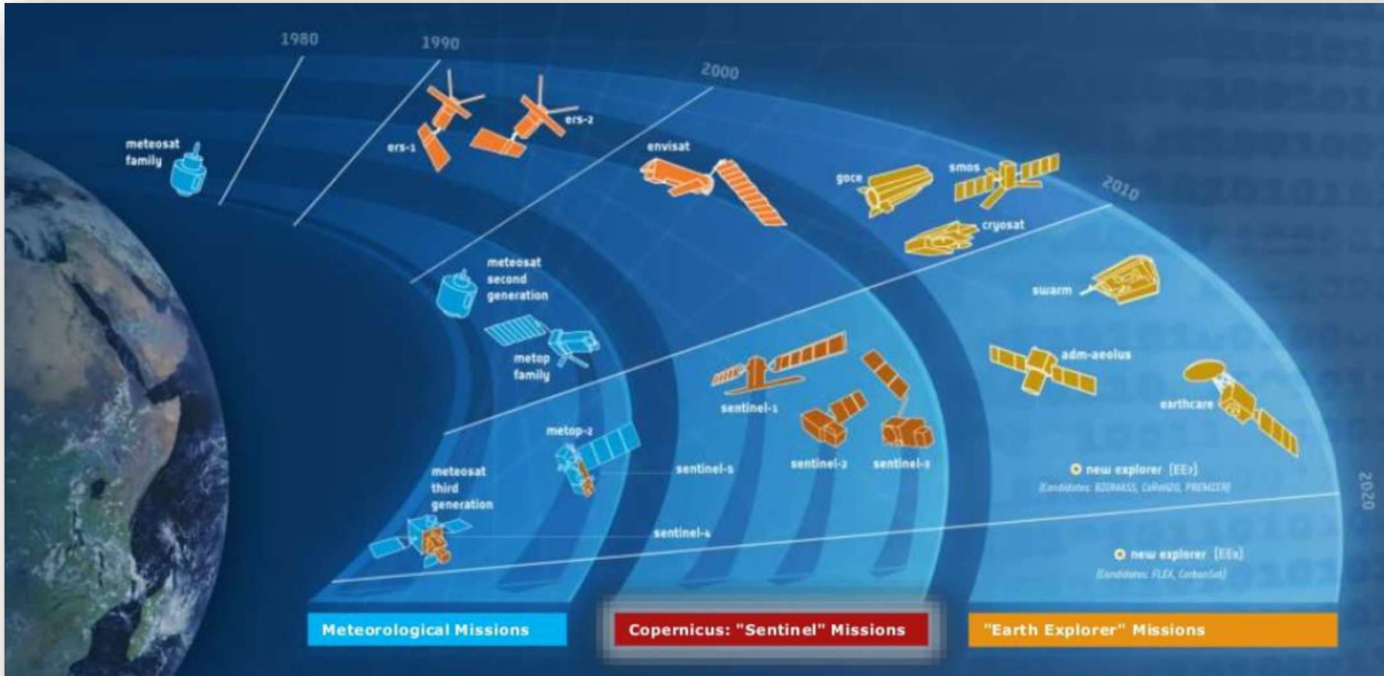

- Lots of data are transmitted to Earth
- ESA makes the data available to EU users
- Concepts like Single Sign On, SAML, federations are used

Page 123

Enhancement of Earth Observation Service Access

EEOSA

Structure and Scope of the EEOSA Project

SIEMENS

EEOSA general info:

- First Siemens Convergence Creators Romania Incentive project
- Agile methodology
- 1 year project
- 4 iterations
- 3 months / iteration

Investigate and split the ESA user communities into dedicated domains, Multi Mission (ESA projects) and Copernicus (ESA/EU projects)

Integrate the test services in the IDEM Test Federation

Study and deploy the necessary tools to manage the ESA Internal Federation

Pilot implementation for the EO FIM internal domains

Before domain split

After domain split

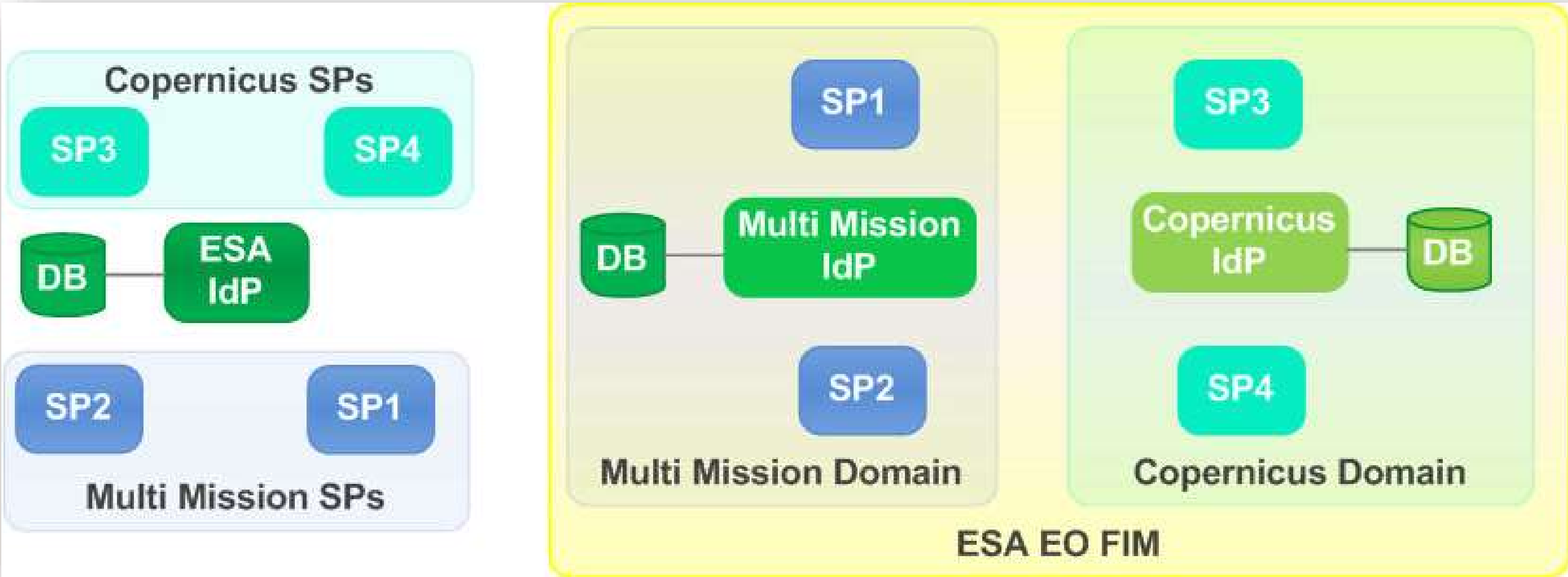

Page 126

Test environment after domain split

To fully function, the domains need to cooperate → new services and tools need to be introduced:

- Attribute Authority Service
- Discovery Service
- Metadata Aggregator
- Federation Management Tool

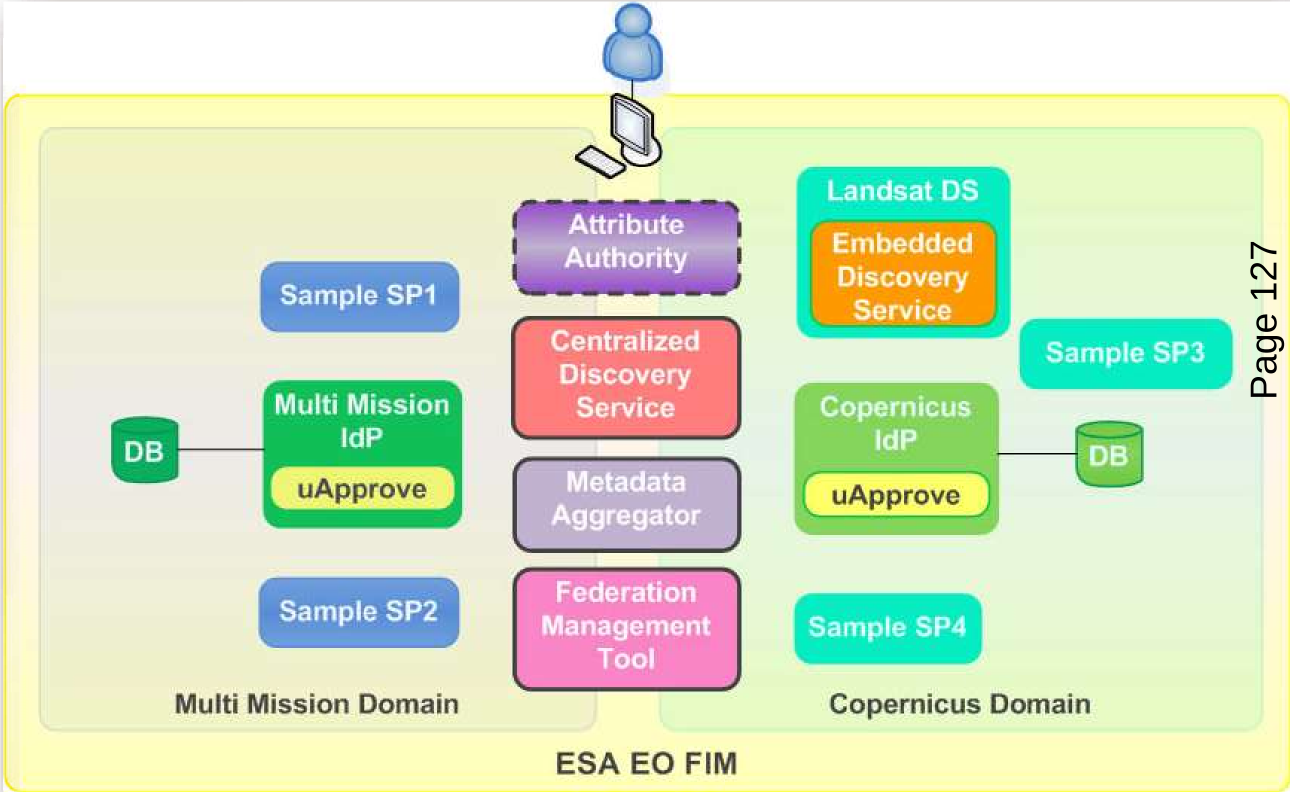

Federated Identity Management

FIM

SIEMENS

Structure and Scope of the FIM Project

FIM general info:

- Agile methodology
- 1 year project + 3 months extension
- 4 iterations
- 3 months / iteration
- 35 progress meetings

Iteration 1: Implement an AAI that is functionally equivalent to the existing EO-SSO but using vanilla Shibboleth products, standard tools and best practices

Iteration 2: Extend the AAI from Iteration 1 with methods for accessing resources on the Service Provider via OAuth 2.0 using an existing SSO account

Iteration 3: Host the AAI from Iteration 1 (EO Data Service and EO Data IdP) on the IPT to connect to Sentinel-2 products and extend the AAI capabilities for the IDEM/GARR and eduGAIN integration

Iteration 4: Extend the AAI to integrate federation administration tools in the IPT in order to ease the domain management and enhance the EO Data Service

FIM Architecture Overview

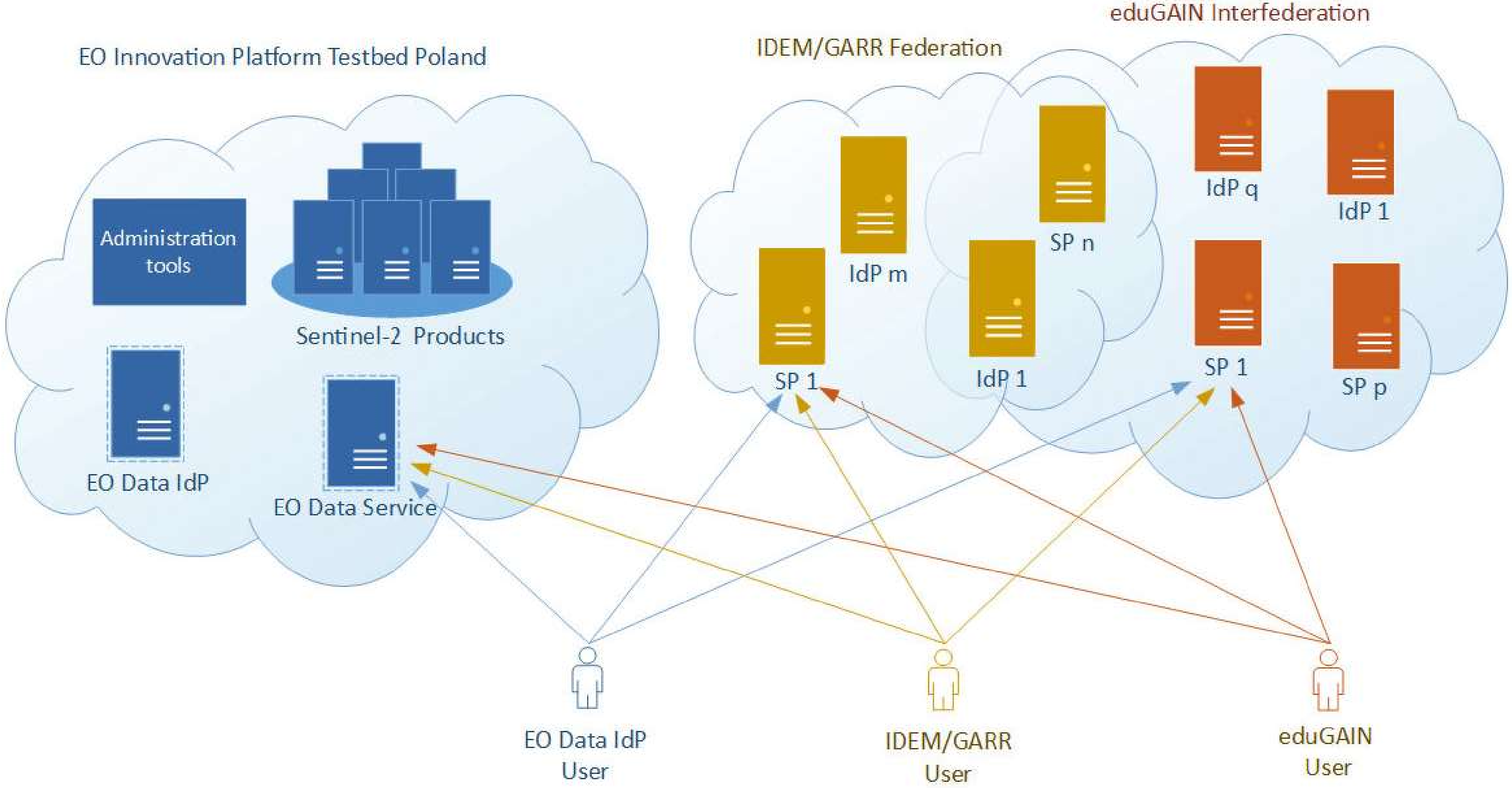

Page 130

Bigger, Better, Stronger - eduGAIN

Interfederation inter-connects federations without establishing one rule to bind them all.

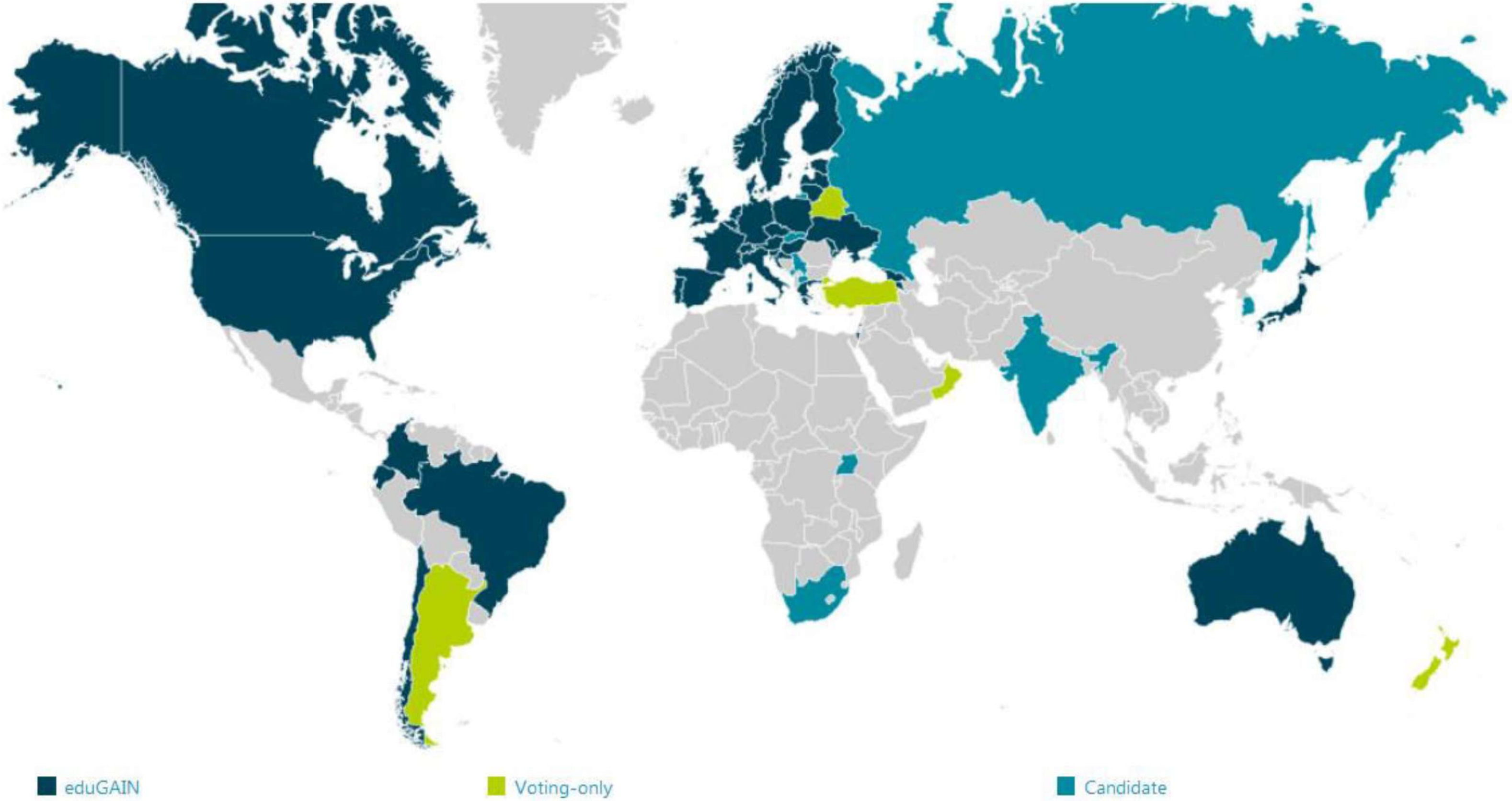

SIEMENS

Cloud-based Identity and Access Management

CloudIAM

Structure and Scope of the CloudIAM Project

SIEMENS

CloudIAM general info:

- Ongoing project
- Agile methodology
- 1 year project
- 4 iterations
- 3 months / iteration

Scope: Study how to extend the capabilities and evolve the existing Identity and Access Management solution at ESA/ESRIN

Iteration 1: Extend the infrastructure with methods for accessing resources on the Service Provider via OpenID Connect, keeping the existing functionalities

Iteration 2: Analyse homeless users products and deploy them in a test environment similar with the ESA SSO infrastructure

Dual protocol access

Access to satellite imagery resource via both SAML and OpenID Connect

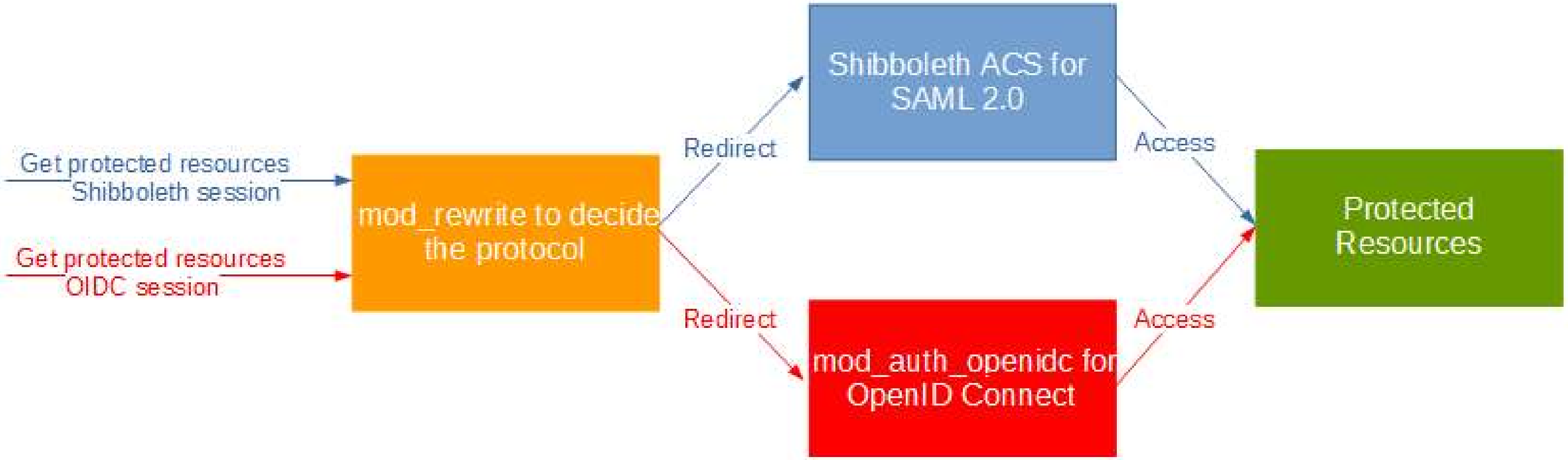

Page 134

Mission Planning and Mission Control

Siemens Convergence Creators

Page 135

Mission Planning and Mission Control

The extensive ESTRACK station network and the large number of missions require advanced Mission Planning and Control tools.

SIEMENS

Visual XML Editor (for Mission Planning)

ViXE

ViXE Scope

SIEMENS

Page 138

Currently, the EPS uses an XML editor based on *XMLMind XML Editor* (XXE). This solution has proved to be cost effective, but ESA considers to supersede this approach for various reasons such as the change of the license terms and inefficient handling of large tables.

ViXE is a replacement and an enhancement of this solution, a tool for opening, editing and saving XML/XMI files.

ViXE Epics (mapped to Work Packages),Tasks and Output

SIEMENS

Epic	1. Analyze current solution (WP2000)	2. Evaluate alternative solutions (WP3000 and WP4000)	3. Implement and customize the chosen solution (WP5000)
Tasks	• Check XMLMind UI components layout • Check XMLMind main toolbar functionalities • Check XMLMind right-click actions on UI elements (insert, copy/paste etc.)	• Studied tools: VEX, ECP, EEF, jquery. xmleditor, CAM, XERLIN, XMLGrid, Rinzo etc. • Rate each capability of the alternative depending on how well it fits the requirements • Strong and weak points of each tool • Choose technical solution for the prototype implementation	• Implement ViXE based on EMF Client Platform (ECP) 1.8.0
Output	• Requirements Document	• Technical Note Document	• ViXE Prototype • Software Design Document • Software Validation & Test Document

Comparison between XMLMind and ViXE

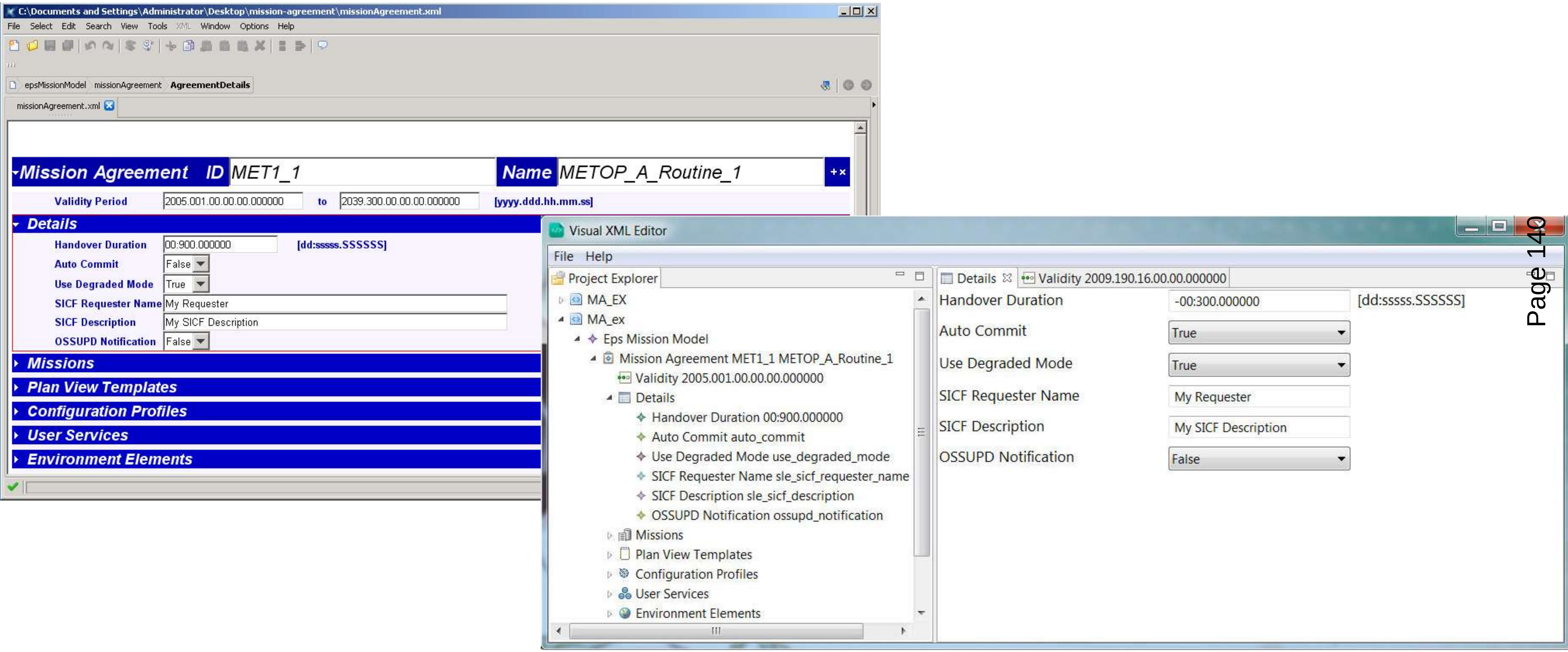

Page 140

Lightweight Interface for SPAN infrastructure

LIFESPAN

LIFESPAN Scope

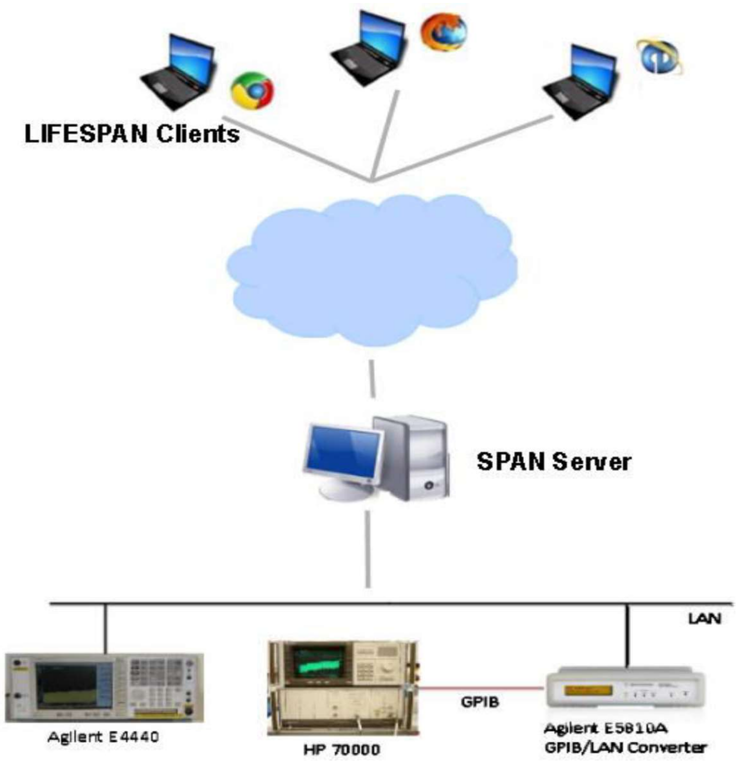

Currently ESA is using the Spectrum Analyzer which is a distributed client-server application fully developed in Java by Rhea System. The existing solution is a stand-alone desktop application.

The Spectrum Analyser Interface (SPAN) application remotely monitors and controls Spectrum Analyser devices located at ESA groundstations.

The server part is run on a suitable computer at the groundstation and is capable of interfacing to two different SPAN models, the HP 70000 series and the Agilent E4440 models.

LIFESPAN is the web based alternative application of the existing SPAN Client, a tool used for monitoring and control of Spectrum Analysers through a web-based GUI.

Organizational overview of the LIFESPAN Project

SIEMENS

LIFESPAN general info:

- Agile methodology
- 15 months project
- 5 work packages (WP)
- 13 iterations
- 2 weeks / iteration
- 15 progress meetings

Baseline General Analysis

Analyze the existing EUD and SPAN source code and documentation

Software Design

Preparation of the SW Development & Runtime Environment (VMs)

Prototype overview

Software Implementation

Implementation of the selected solution for the LIFESPAN project

Fixes and modifications according to the incremental delivery feedback

Acceptance & Delivery

Evaluation and testing of the developed software

Delivery of the complete software and documentation

Warranty

Analyses and Fixes

Preparation of the warranty delivery patch and final delivery

LIFESPAN User Interface

Menu bar

Parameters tabs

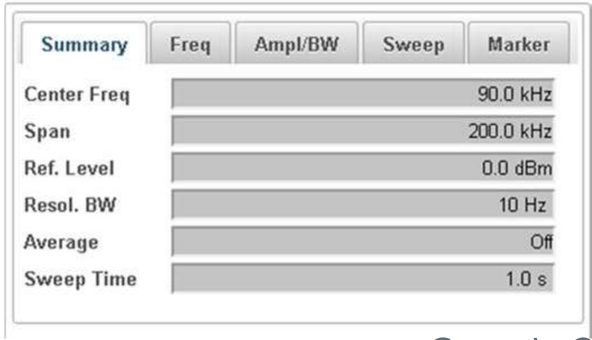

Generic Command

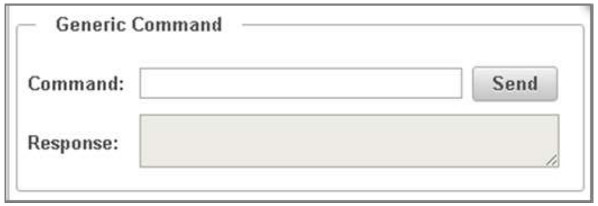

Player Panel

Chart area

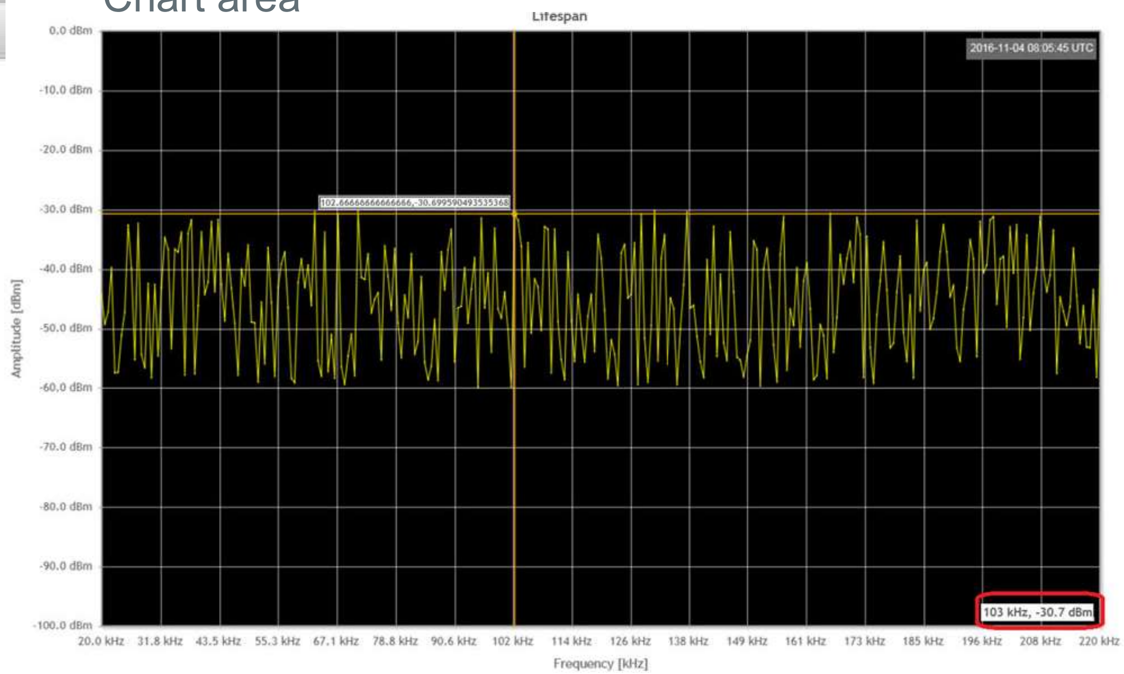

Status line

Page 144

SIEMENS

Java implementation of Language for Mission Planning

jLMP

jLMP Overview

SIEMENS

Language for Mission Planning (LMP) is used by many mission planning systems in use today at ESOC, especially European Space Tracking Planning System (EPS). The grammar of LMP is currently implemented in C++, while the upcoming Mission Planning System Framework is implemented in Java.

The scope of jLMP project is to analyze the requirements, technologies and possible architecture for implementing a Java replacement implementation of LMP. All these findings will be implemented into a prototype that could be integrated into the ESTRACK Planning System.

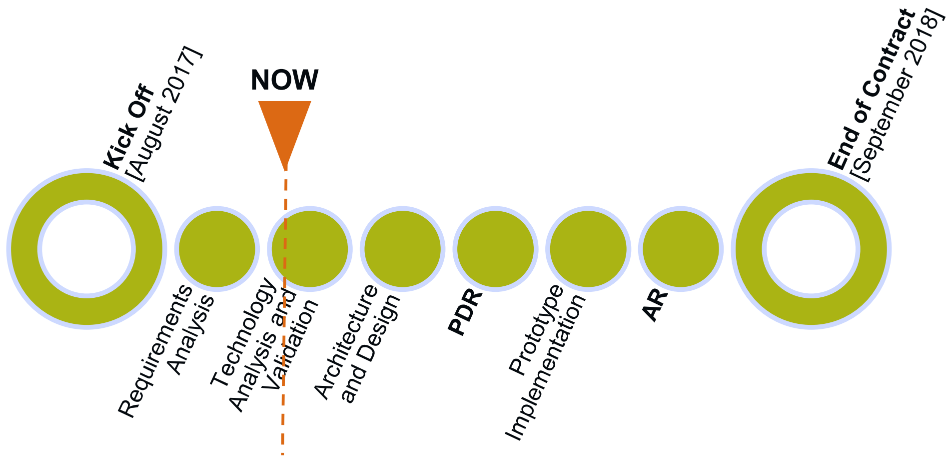

Page 146

SIEMENS

Page 147

Mobile UI for EMS Portal

mEMS

mEMS Overview

ESTRACK (**E**uropean **S**pace **Track**ing) Management System translates requests from multiple missions into a schedule for the ground stations and monitors both the execution of the schedule and the general health of ground stations. The EMS Portal enables users to inspect the produced plans and to issue and track change requests, while allowing special service requests, management of configuration profiles and overall mission awareness about the ESTRACK service allocations.

The scope of mEMS project is to analyze the current (heavyweight) implementation of the EMS Portal, the user experiences and expectations in order to produce an architecture and to implement a prototype. The target design is responsive web, for availability on a wide range of devices: phone, tablet and laptop.

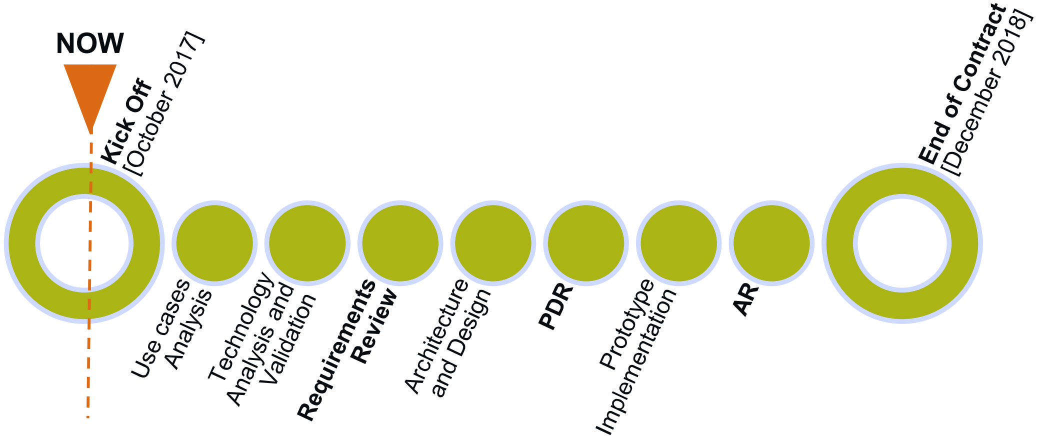

Summary of the Siemens Convergence Creators Romania Activities in the ESA Incentive Scheme

SIEMENS

EEOSA

Enhancement of Earth Observation Service Access

FIM

Federated Identity Management

CloudBasedIAM

Cloud-based Identity and Access Management

ViXE

Visual XML Editor

LIESPAN

Lightweight Interface for SPAN infrastructure

mEMS

Mobile UI for EMS Portal

jLMP

Java implementation of Language for Mission Planning

Thank you for your attention!
Q&A

SIEMENS

Raluca Botez
Siemens Convergence Creators

System Engineer

Siemens Convergence Creators SRL
B-dul Mihail Kogalniceanu 21, Bl. C6
RO-500090 Brasov, ROMANIA
Tel.: +40 (0)268 409 083

raluca.botez@siemens-convergence.com

Presentation 2503

Stepper motors for space applications – ICPE activities

Mircea Modreanu
ICPE, Romania

Ioana Ionica
ICPE, Romania

Cristian Boboc
ICPE, Romania

Stepper motors for space applications – ICPE Activities

Mircea MODREANU

Ioana IONICĂ

Cristian BOBOC

Stepper motors for space applications ICPE Activities

- The development of stepper motors (SMs) for space applications in ICPE has beginning within two contracts with ESA, EMSIS and SM MADPM MKII.

- The approach towards product development was chosen based on a preliminary survey that established the particularities of the market from the electric motors' point of view that leads to choose SM and seems to indicate a need for high detent torque, this requirement being another indication towards the use of SMs in keeping orientation (for solar panels, antennas, or instrumentation), where is indicated as preferred a precise position control.

- There are three SM types, based on the type of construction:
  - Variable-reluctance (VR – SM);
  - Permanent-magnet (PM – SM);
  - Hybrid (H – SM).

Stepper motors for space applications
ICPE Activities

Background

- Theoretical and experimental work was devoted to study and compare the SMs with conventional closed-loop positioning systems, and deploy the SMs to a variety of applications (for solar panels, antennas, or instrumentation).

- The market of actuators for the space sector covers a wide range of products and there is a clear need for such mechanism in the industry.

- The probability of being selected as a supplier for space applications is strongly dependent on the maturity of the products or services being procured.

- ICPE, as a well-established manufacturer of electric motors at an international level, is in an entering position on this new market with harmonization of the existing electric motor technology with the standard required for the space applications.

Stepper motors for space applications
ICPE Activities

- EMSIS is a project through which ICPE was awarded a contract with ESA for evaluating the suitability of its electric motors for the space sector. The main focus of the project was developing a product for operations in space.

- ICPE run a technology survey to identify specific needs for primes and/or end users. The answers related all to SMs and seem to indicate a need for high detent torque.

- The usage scenario most likely involves actuators for deployment and pointing of various equipments.

- Accordingly to the conclusions of the survey report, a Permanent Magnet (PM) or a Hybrid Stepper Motor (H-SM) were chosen to be developed in the EMSIS project, supplied in a frameless configuration (rotor and stator separately), in order to integrate them within space mechanism applications.

Stepper motors for space applications
ICPE Activities

- SM MADPM MKII is a project through which ICPE was awarded with a contract with ESA for study and develop a new version of SM.
- The main objective is to develop a product for applications involving a precise position control.
- ICPE has the opportunity to develop a product needed in the space mechanism market.
- According to project plan, the activities for first milestone, SRR, were realized. Thus, the SM requirements specification document was established. Also, from the design stage, the electromagnetic modeling for SM was completed.

Electric Motor Technology Spin Into Space – EMSIS ICPE Activities

- The main characteristics of the motor are divided into three categories:

Main dimensions:

Parameter	Unit	Tolerance	Value
Total mass	g	+/- 10%	TBD
Stator OD	mm	h6	90 max.
Rotor ID	mm	H6	50 min.
Step angle	deg	Nom	1.0
Thickness	mm	+/-0.1	30 max.

Mechanical characteristics:

Configuration / Parameter	2-phase // (1 phase ON)	4-phase (1 phase ON)
Min Net output torque (Running) at 20°C, 1 phase ON, 23.4 V	TBC 0.6 Nm (Goal)	
Net output torque (Running) at 20°C, 1 phase ON, 20.8 V		TBC 0.16 Nm (Goal)
Detent torque	TBC 0.1 Nm (Goal)	TBC 0.1 Nm. (Goal)

Electrical characteristic

Configuration / Parameter	Unit	2-phase // (1 phase ON)	4-phase (1 phase ON)
Voltage	V	26 ± 10%	20.8 to 31.2 (26 +/- 20%)
Max. Peak power	W	20	N/A
Winding resistance (half phase) @ 20°C	Ω		TBC
Winding inductance (@ 20°C)	Mh		TBC
Electrical time constant	ms	TBC	
No load angular error (peak to peak)	arcmin	4 Max.	

Electric Motor Technology Spin Into Space – EMSIS ICPE Activities

The motor shall have the possibility to be configured in two ways:

- As a 2-phase motor
- As a 4-phase motor

The switch from 4 to 2 phases will be made at the connector level.

Main winding configuration:

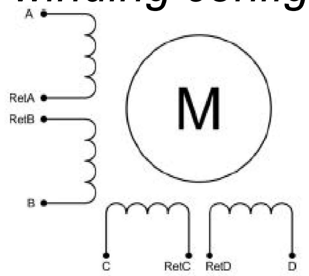

MDE Duty Cycle

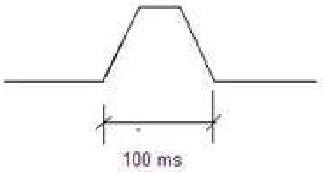

Motor Drive Electronics (MDE) characteristics

These electronics are able to drive 2 phases SMs. This is intended for the 2 phases configuration. The motor is driven with following characteristics:

Parameter	Value
Command line	Bipolar
Duty cycle	From 25% up to 100 %
Command frequency	< 10 Hz
Voltage	26 V ± 10 %

EMSIS stepper motors – Breadboarding process

First breadboarding stage – Iron-Silicon

- There are three type of SMs.
- Three breadboarding (BBs) stages and an engineering model (EM) were considered.
- In the first breadboarding stage (BB1), both PM and H-SM variants were realized.
- The following materials were used: iron-silicon lamination for the stator and magnetic iron for the rotor, as per ICPE industrial production.

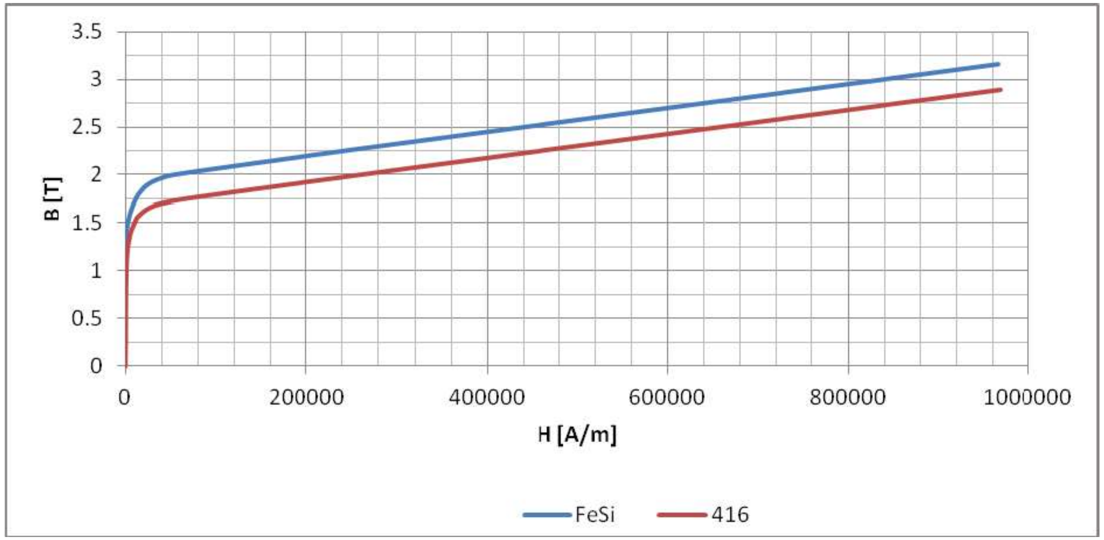

B-H characteristics of the materials

EMSIS stepper motors – Breadboarding process

First breadboarding stage – Iron-Silicon

- In order to optimize the geometry and to obtain the required characteristics according to Specification, numerical modeling based on FEM was largely used.

- For the PM SM model, the bi-dimensional models gave accurate results. Due to their construction, this type of SMs can be studied through a bi-dimensional model in a simple planar-parallel problem.

- Three BBs were manufactured, two with Neodymium – Iron – Boron magnets and one with Samarium-Cobalt PMs. All these BBs did not satisfy all the requirements regarding the winding configuration mentioned in Specification.

- Therefore, the H-SM variant was chosen and for it, is mandatory to use three-dimensional modeling because it has longitudinal magnetization in rotor PM and radial and longitudinal in the stator magnetic circuit.

Hybrid Stepper Motor – Constructive elements for BB1

The magnetic circuit of the motor

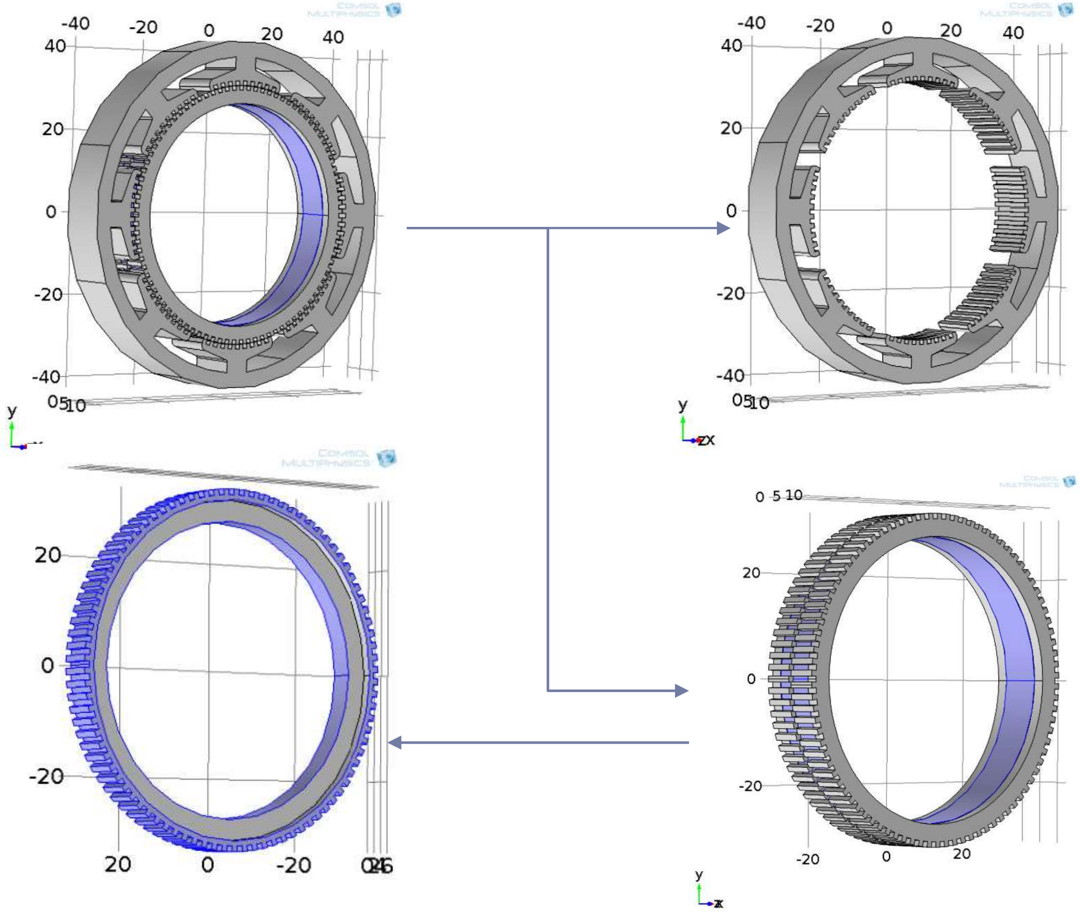

The stator

The rotor semi-armature

The stepper rotor

Hybrid Stepper Motor – Detent Torque
Results of numerical modeling

➢ For numerical modelling a specialized equipment and a software based on the finite element method, Comsol Multiphysics were used.

➢ For the detent torque (T_D) computation, the winding is not supplied, so the magnet is the only magnetic source.

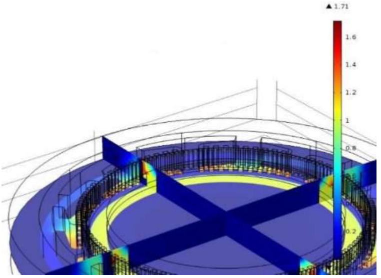

Detail of Magnetic flux density. Values are in tesla.

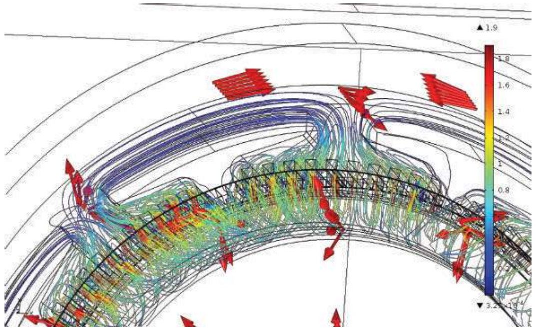

The magnetic flux density. Values are in tesla.

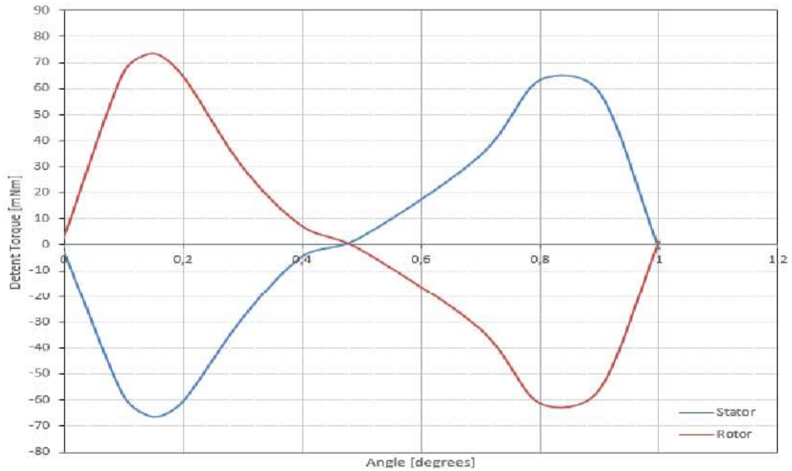

➢ The teeth are charged at airgap where flux concentrators appears.

➢ The value of T_D is about 70 mNm. This version was been chosen for execution of BB1.

Calculated T_D – angle characteristic over 1 step

Hybrid Stepper Motor – BB 1

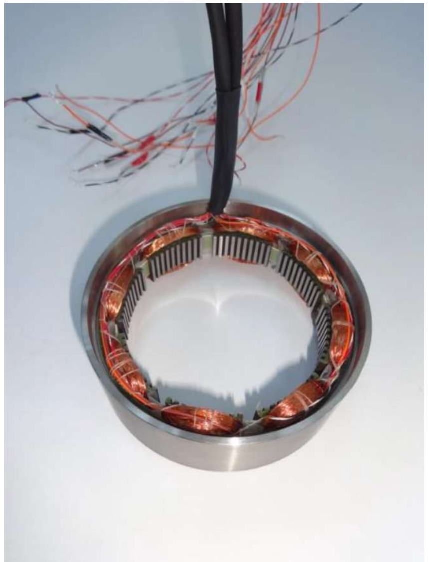

The stator

The rotor

- The main winding is spread on half of the stator stack and the redundant winding is spread on the other half.
- The rotor has two components with 90 teeth each. The two components of the rotor have an offset of 2 degrees.
- Between this two components (made of Steel 416), there is one magnet with longitudinal magnetization (the magnet is of the neodymium type).

EMSIS stepper motor – Breadboarding process
Second breadboarding stage – Iron-Cobalt

- In the second breadboarding (BB2) stage, a new version for H-SM, different from the material and geometric point of view, was realized.
  - The following materials were used:
  - iron-cobalt lamination for the stator;
  - magnetic iron for the rotor.
  - The variant of calculation is in accordance with the overall dimensions of the motor specification, except inner diameter that was increased to 55mm.

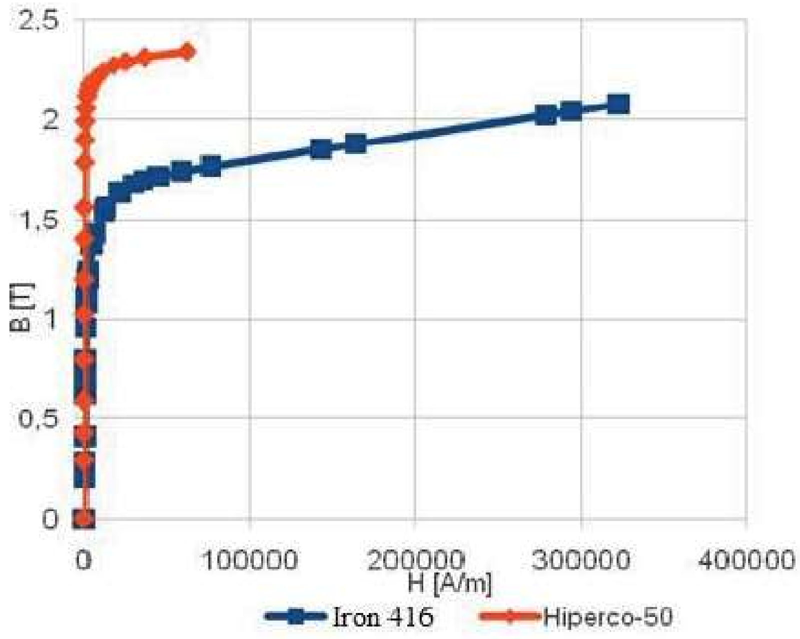

B-H characteristics of the materials

Hybrid Stepper Motor – Constructive elements for BB2

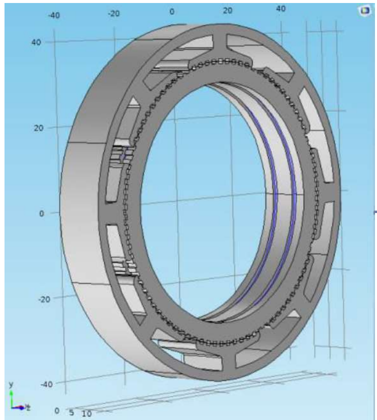

The magnetic circuit
of the motor

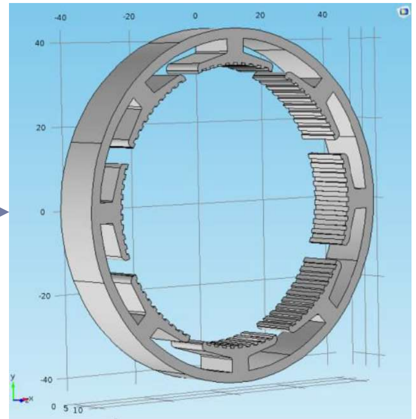

The stator

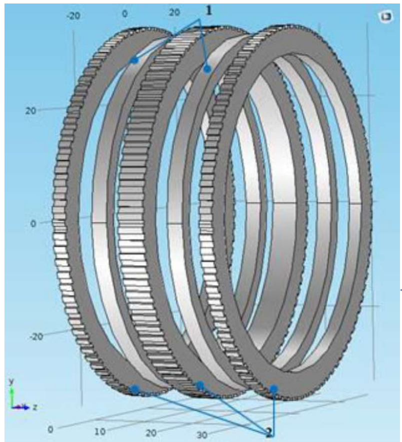

The rotor components

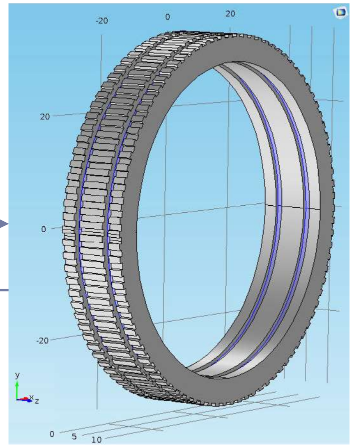

The stepper rotor

Hybrid Stepper Motor – Detent Torque
Results of numerical modeling

- For T_D computation, the winding is not supplied, so the magnets are the only magnetic source.

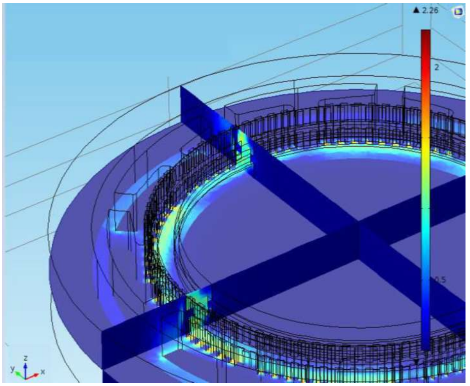

Detail of Magnetic flux density. Values are in tesla.

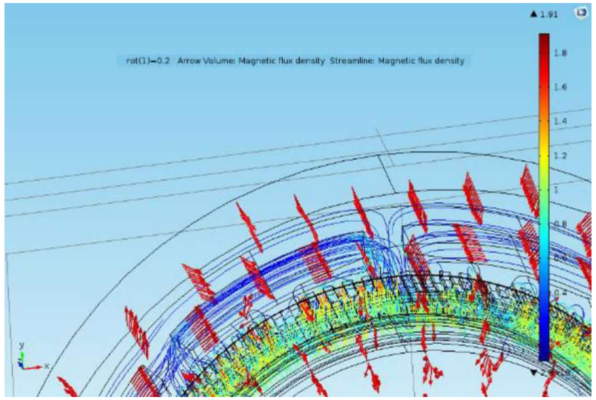

The magnetic flux density. Values are in tesla.

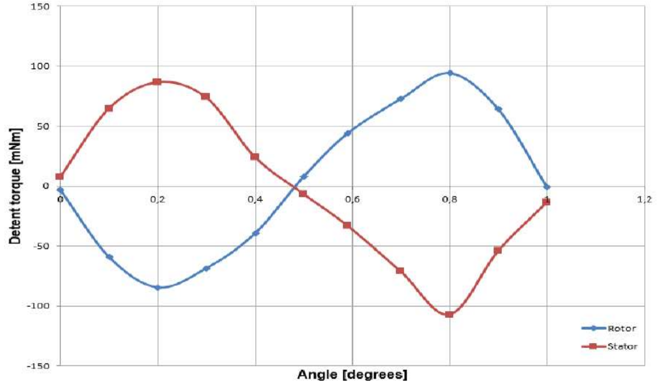

Calculated T_D – angle characteristic

- The teeth are charged at airgap where flux concentrators appears.
- The postprocessing results for BB2 present the calculated T_D – angle characteristic. The value of T_D is about 90 mNm. This version was been chosen for execution of BB2.

Models for Holding Torque calculation

- For BB2, a numerical model for T_H calculation was developed.
- Because we kept the solution for redundancy from BB1 (the main winding is spread on half of the stator stack and the redundant winding is spread on the other half), for T_H calculation, only half of the main winding which is spread on two poles (half-phase configuration), was considered.

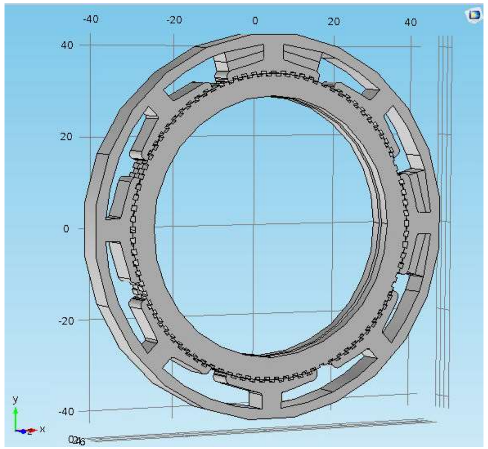

The magnetic circuit of the motor

Results of numerical modeling

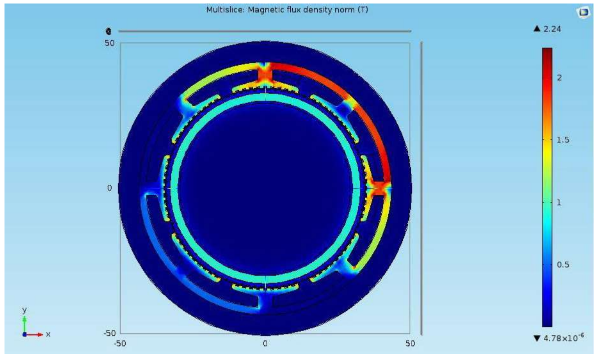

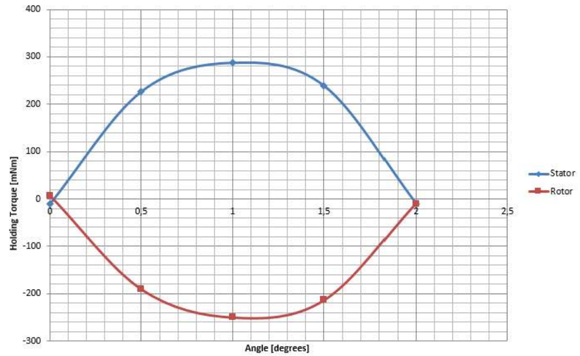

- Magnetic flux density xOy plane   Calculated T_H – angle characteristic - Half-phase option, U=26V

Hybrid Stepper Motor – BB 2

- BB2 was manufactured. The wound stator stack is only varnished, not embedded.

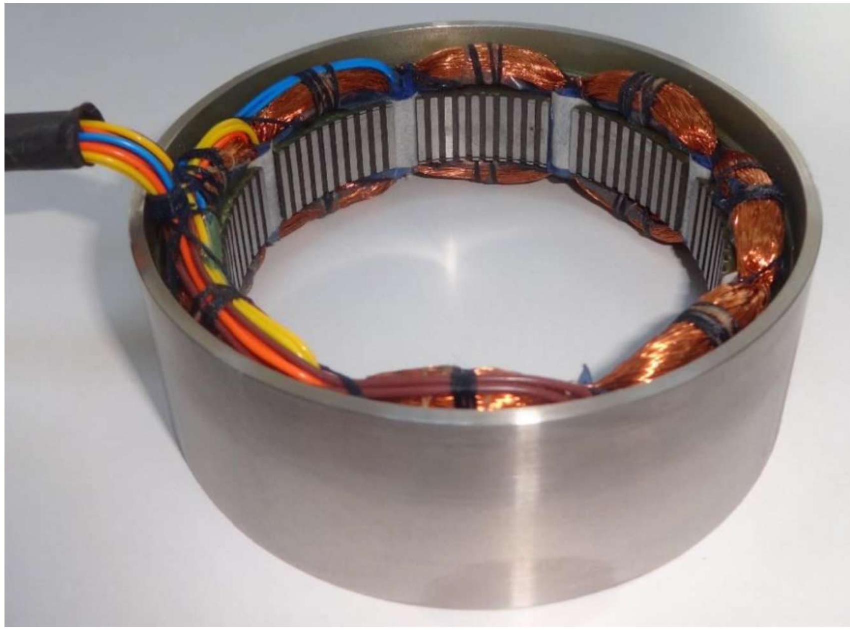

Wound stator stack

Rotor

Breadboard 3 and Engineering Model (EM)

- In Breadboard 3 (BB3) and EM, the redundancy solution was changed. The first solution has some disadvantages, i.e. the use only of half of magnetic circuit and heating of half of motor.

The constructive elements of the motor **Numerical modeling results for BB3 T_H model**

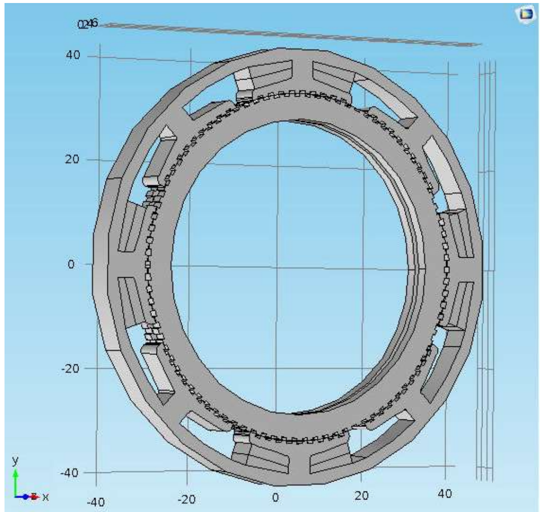

The magnetic circuit of the motor

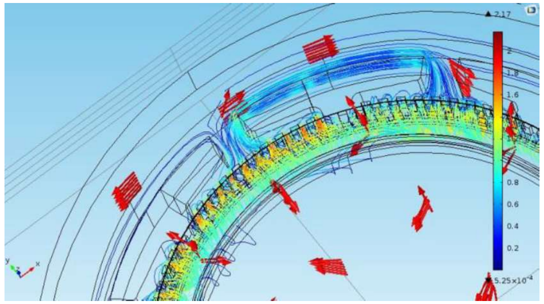

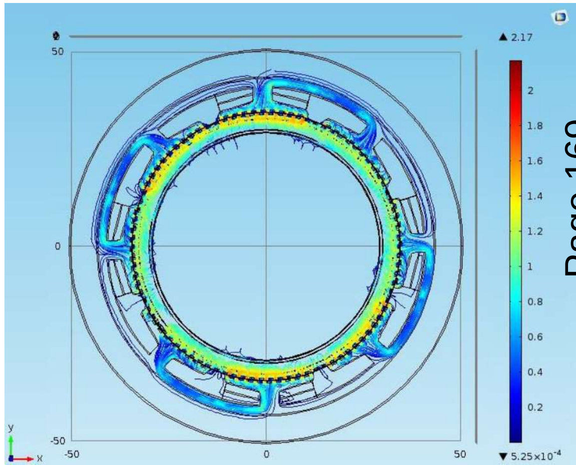

The magnetic flux density. Values are in tesla.

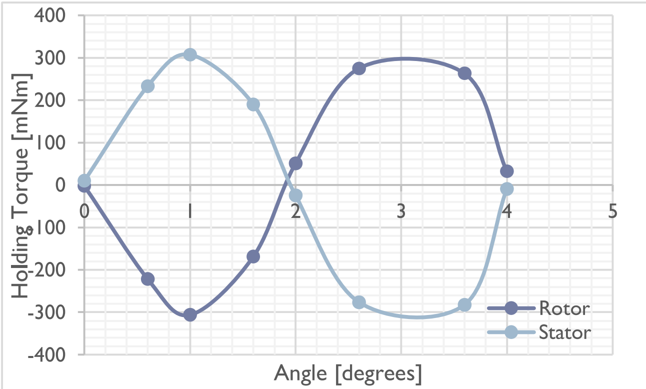

Calculated T_H – angle characteristic – Half-phase option, U=26V

BB3 and Engineering Model (EM)

- The wound stator stack is embedded and on the main and redundant windings thermistors are placed for the motor thermal monitoring.

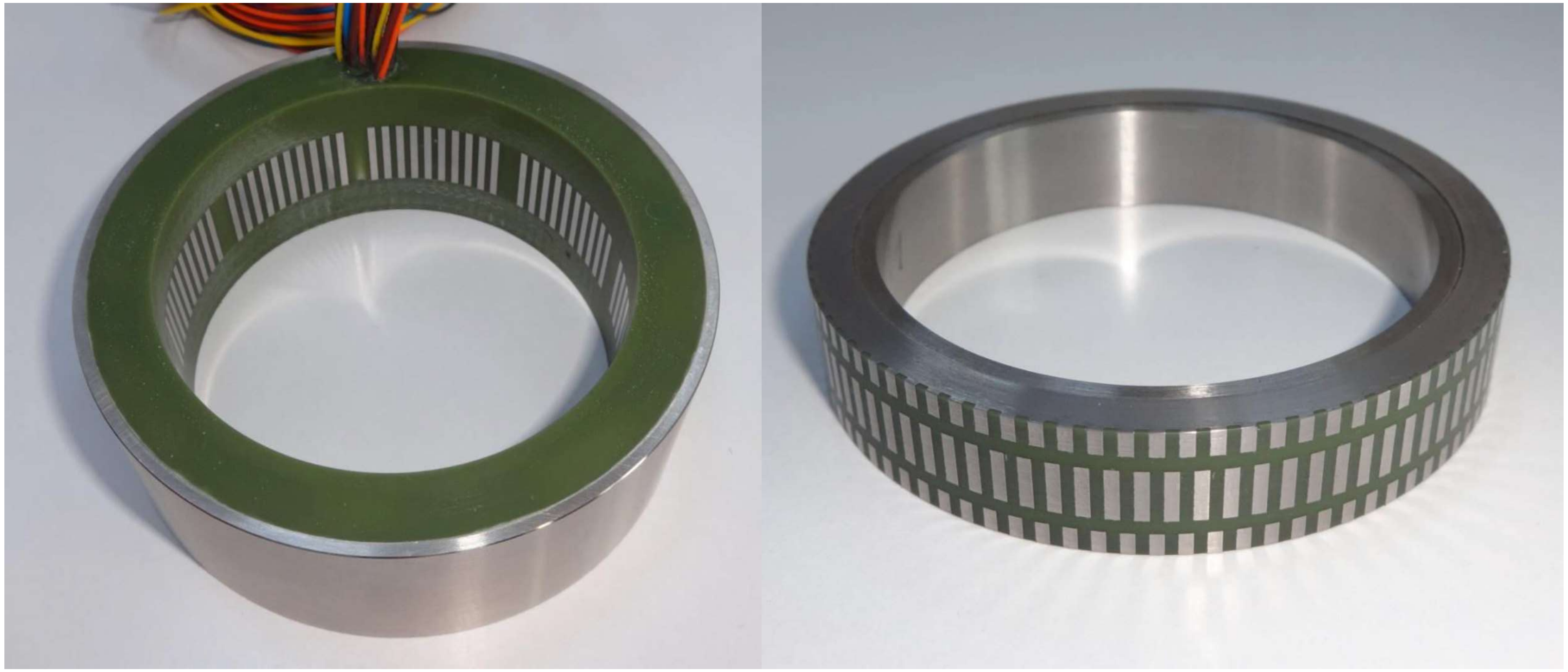

The magnetic circuit of the motor

Motor tests

- For all BBs and EM, the physical dimensions, the electrical properties and then, the performances of the motor (T_D, T_H and on load torque (T_L)), were measured.

❖ First measurement method

- For BB1, T_D and T_H were measured with a digital dynamometer and the device with the mounted motor fixed on a rotating head.
- Method disadvantages:
- ❑ Difficulty of measurements repeatability
- ❑ mounting difficulty.

- For T_L torque, a pulley having a known diameter and a measuring masses kit were used. Due to elasticity of the measuring thread, step vibration appears that affects the measurements results.

❖ Second measurement method

- The second measurement method for T_D and T_H uses a torque transducer with angle transducer (with the angle resolution of 1 degree) and the rotor of the motor is rotated with a motoreducer.

Motor tests

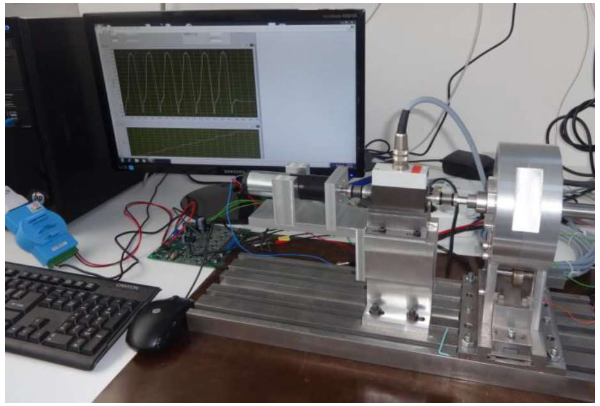

Measurement device for T_D and T_H

➢ Measurement method disadvantages:

- ❑ Impossibility to measure entire T_H characteristic (the instable part) due to an increased backlash of reducer. This problem will be solved by replacing the actual reducer with another one with reduced backlash.
- ❑ Increased frictions in the slide bearings.

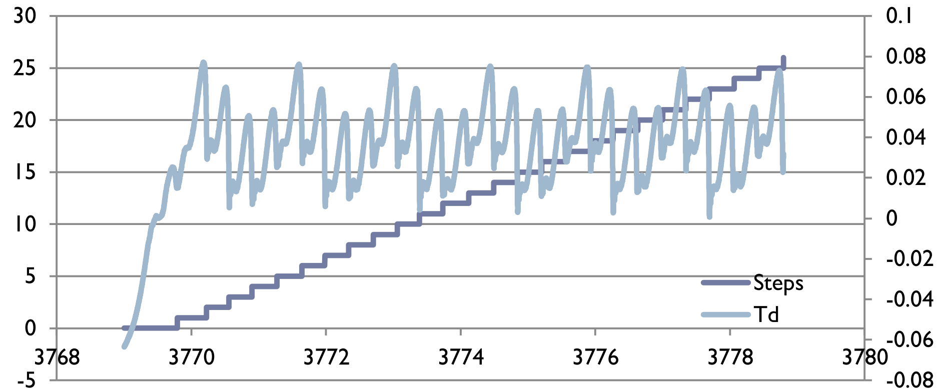

T_D – stator windings unpowered

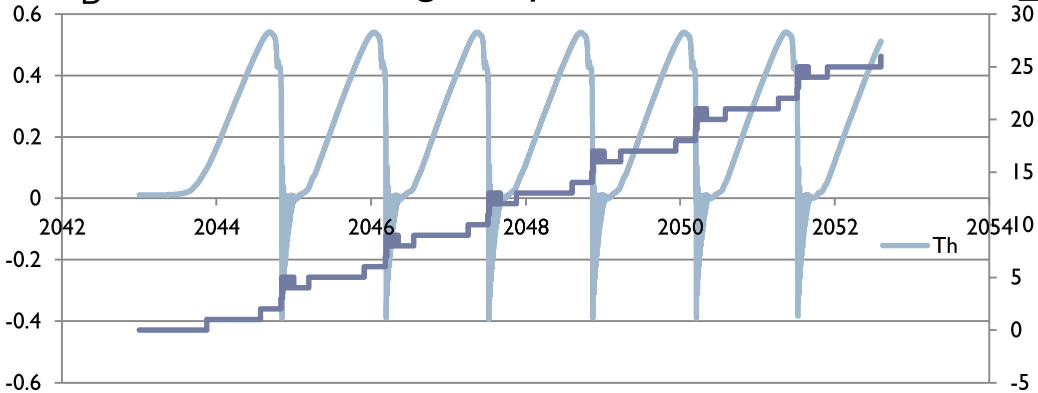

T_H – Parallel option, redundant winding disconnected, U=26V

Motor tests

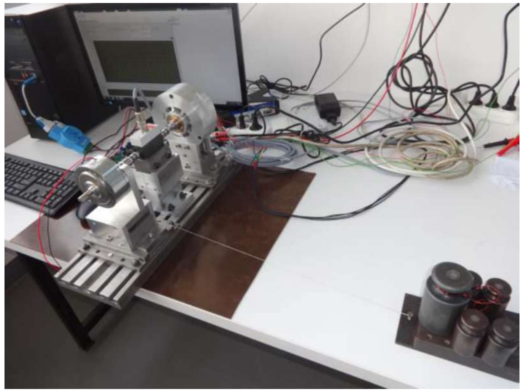

- T_L torque was measured with powered motor (main winding), using the device presented, which uses a friction load and a torque transducer for T_L measurements.

Measurement device for T_L

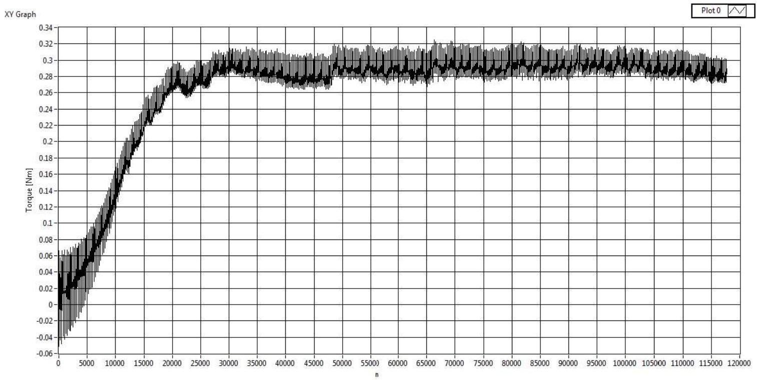

T_L – Parallel option, redundant winding in short circuit, U=26V, f=10Hz

- Measurement method disadvantages:
- ❑ T_L is not constant due to a variable friction coefficient
- ❑ The difficulty to appreciate the inertia of the load.

Motor tests

❖ **Third measurement method**

- The previous measurement device for T_D and T_H was improved by replacing the slide bearings with ball bearings having very low friction. This device will be improved by using a reducer with a small backlash.
- The last measurement device for T_L (a brushless AC motor controlled in torque, working like a brake) and the measured diagram are presented. This method allows us to measure the pull-in and pull-out torque.

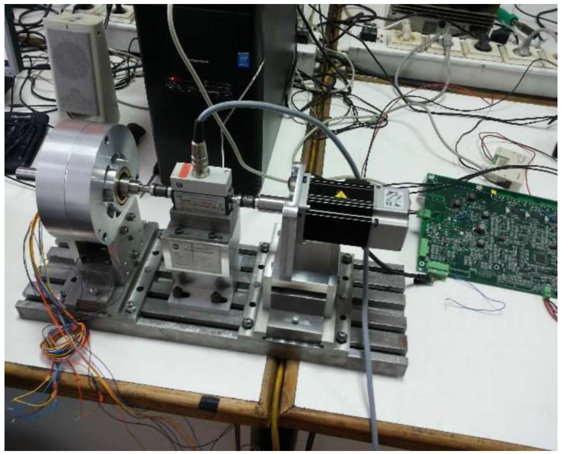

The last measurement device for T_L

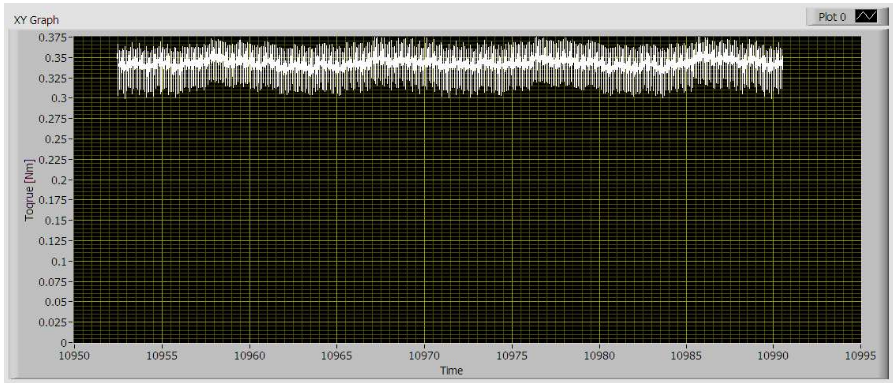

T_L – Parallel option, redundant winding in short circuit, U=26V, f=10Hz

Motor tests – Environmental Test Campaign

- The last objective of EMSIS project is a test campaign which includes the activity presented in the following flowchart. The entire program of EMSIS project was completed, except TV tests on the EM.

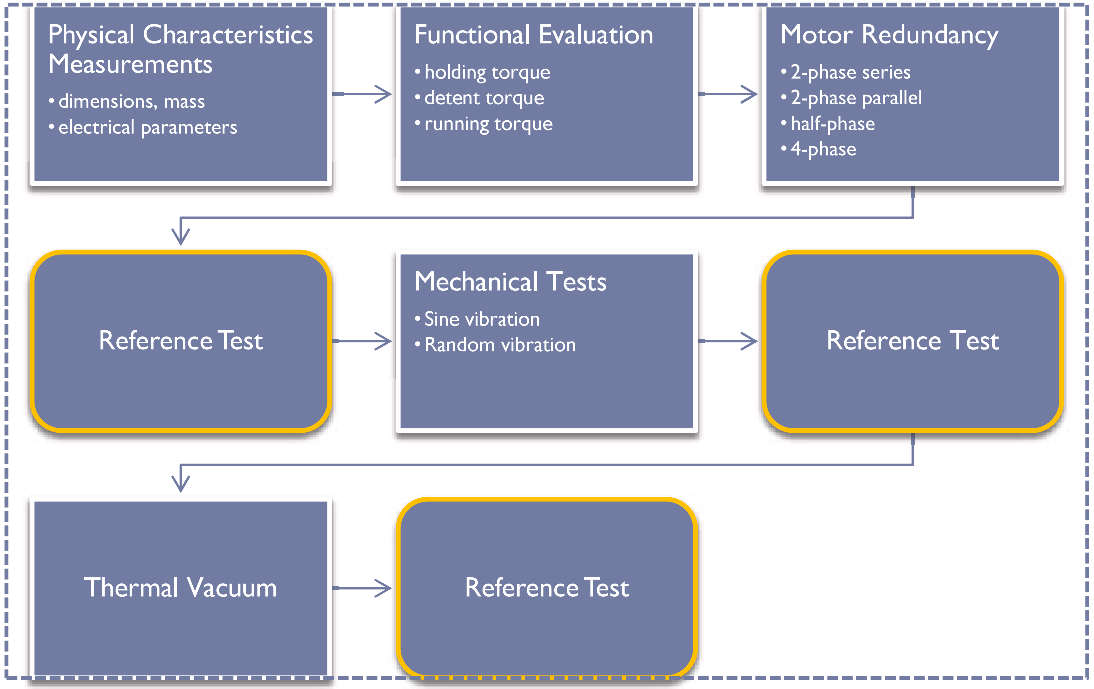

SM MADPM MKII

- The project activities are divided into eight work packages with a total duration of 18 months subdivided in five milestones.

- Functional and performance requirements of SM have been established and consolidated via SRR:

- Motor type: Redundant, bi-phase, frame-less and hybrid stepper motor.
- Voltage supply (voltage/full step): 26 V ±10%
- Output wires: 4
- Total mass: Mechanical part ≤ 215 g
- Step angle (zero friction): 1,0° (360 steps by revolution)
- Position accuracy ≤ 4 arc min
- Winding resistance: 86 Ω ± 10 % (@ +20°C)

SM MADPM MKII

- Speed:

  Ω_{max} from 0 to ±120 steps/s (Ω_{max} is used when the motor is used as a motor).

  Ω_{model} from 0 to ±250 steps/s (Ω_{model} is used when the motor is used as a load).

- Functional and performance requirements of SM were established:
- Holding torque $\geq$ 0,38 Nm
- Running torque $\geq$ 0,25 Nm
- Irreversibility from one step to another $\geq$ 0,012 Nm
- According to project plan, the activities for first milestone, SRR, have been achieved in which the SM requirement specification document was established. “Statement of Compliance & Verification Control Document” (Technical Requirements only) was prepared, at which was annexed the verification sheet of the requirements included in the Specification document.

SM MADPM MKII – Design process

- Currently, we are at SM design phase. Accordingly to this, numerical models were developed.
- **H-SM first model**
- The geometry characteristics are: rectangular teeth both on stator and rotor, tooth width/tooth pitch ratio (t/λ) is 0.5 both on stator and rotor.
- Used materials: iron-cobalt lamination for the stator and magnetic iron for the rotor semi-armatures. B-H characteristics of the materials were already presented in EMSIS project.
- Constructive elements

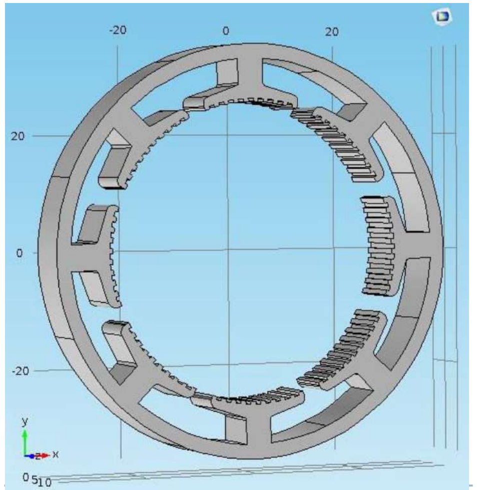

The stator

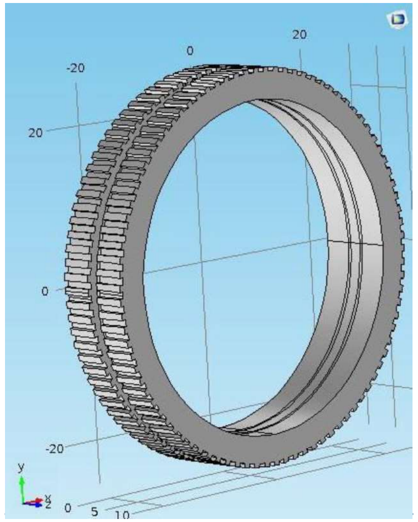

The stepper rotor

Results of numerical modeling
Detent Torque

➢ For T_D computation, the winding is not supplied, so the magnet is the only magnetic source.

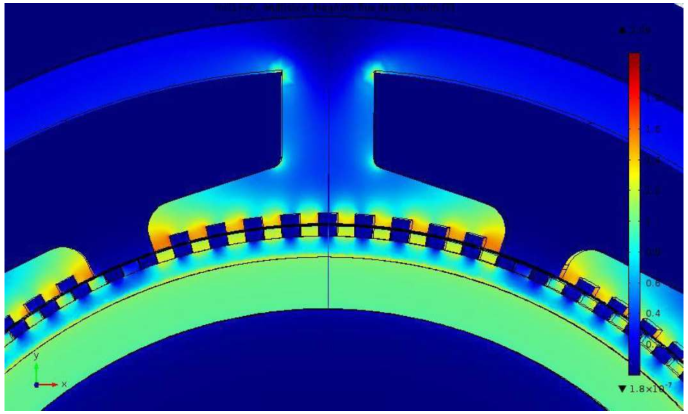

Detail of Magnetic flux density.

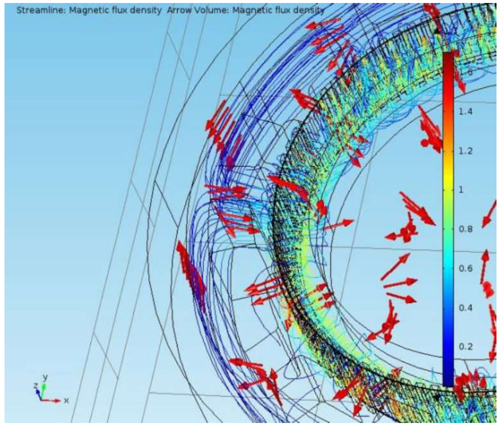

The magnetic flux density.

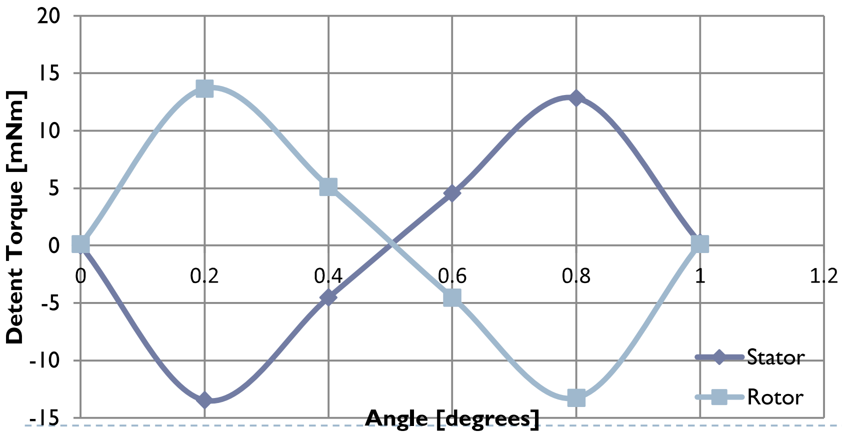

➢ The teeth are charged at airgap where flux concentrators appears.

➢ The maximum calculated value for T_D is about 14 mNm.

➢ Due to the work frequencies that are approximately 10 times bigger than EMSIS Project, this variant is not recommended.

Calculated T_D – angle characteristic over 1 step

Results of numerical modeling
Holding Torque

Constructive elements

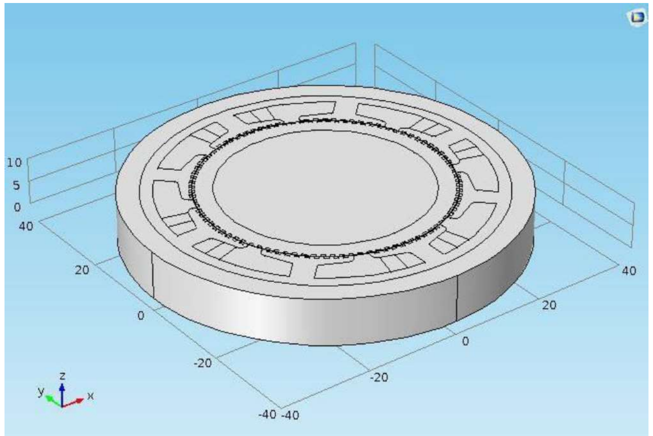

The magnetic circuit of the motor.

T_H results for H-SM first model

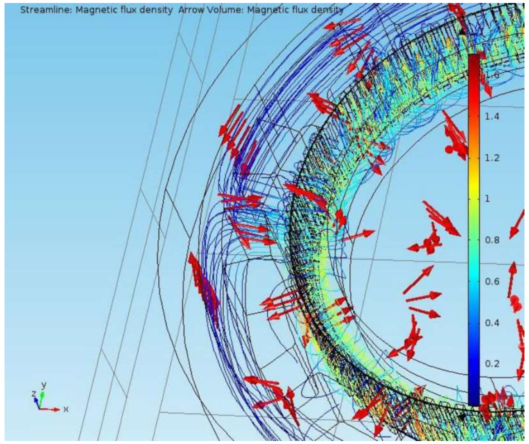

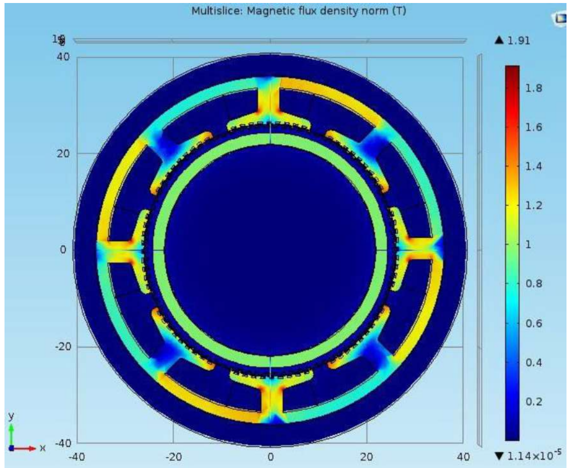

The magnetic flux density.

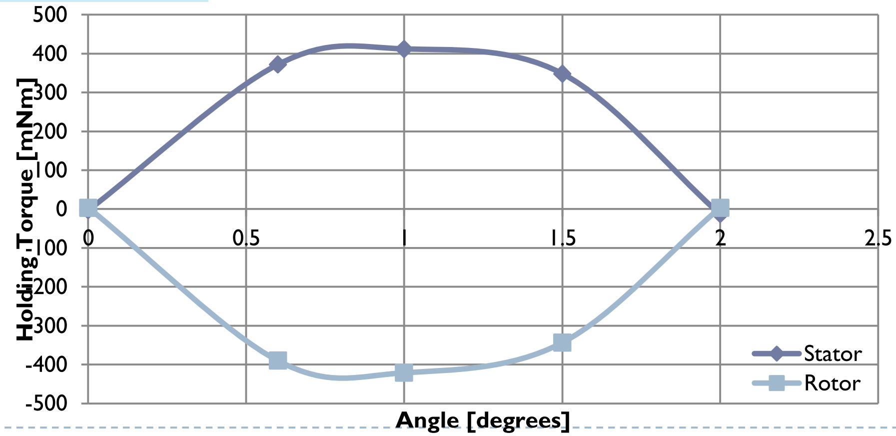

The maximum calculated value for T_H is about 400 mNm.

Calculated T_H – angle characteristic.

SM MADPM MKII – Design process
Results of numerical modeling - Detent Torque

❖ **H-SM second model**

- The geometry characteristics are: rectangular teeth both on stator and rotor, tooth width/tooth pitch ratio (t/λ) is 0.5 both on stator and rotor.
- Used materials: iron-cobalt lamination for the stator and for the rotor semi-armatures.
- Detent Torque

Detail of Magnetic flux density.

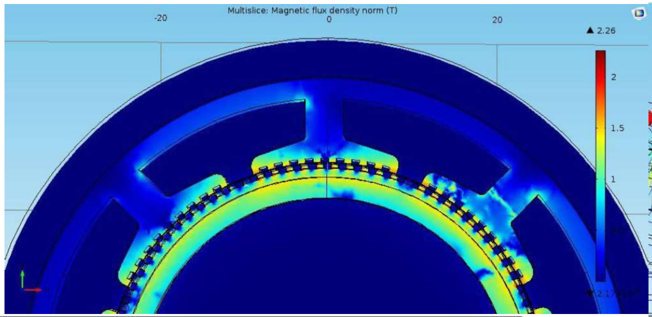

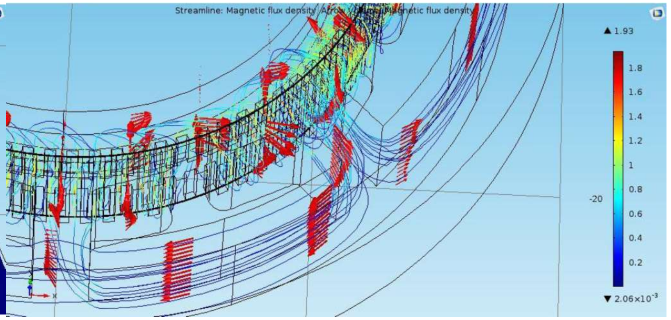

The magnetic flux density.

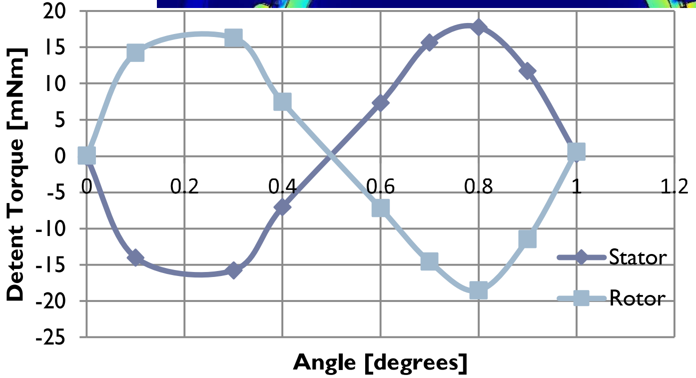

➢ The maximum value for T_D is about 17 mNm.

➢ The teeth are charged at airgap where flux concentrators appears.

Calculated T_D - angle characteristic over 1 step

Results of numerical modeling
Holding Torque

Constructive elements

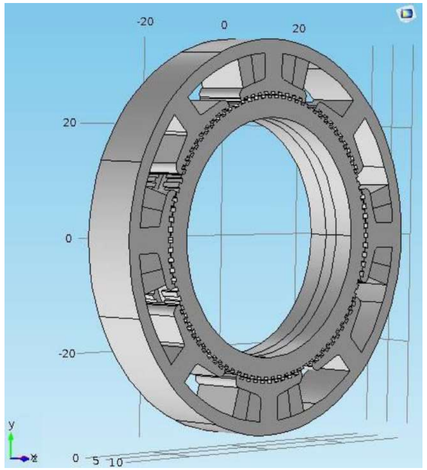

The magnetic circuit of the motor.

T_H results for H-SM second model

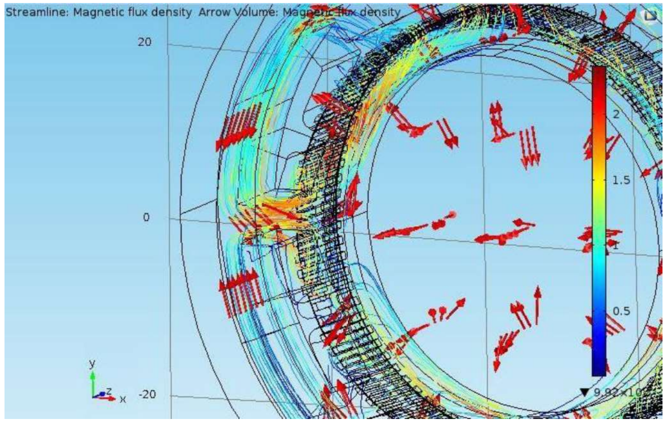

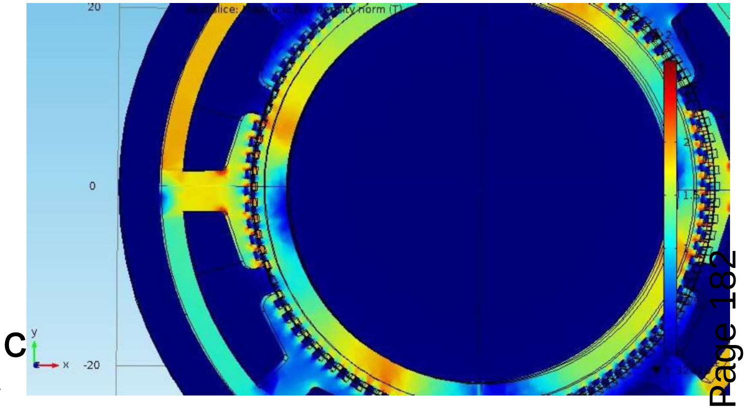

The magnetic flux density.

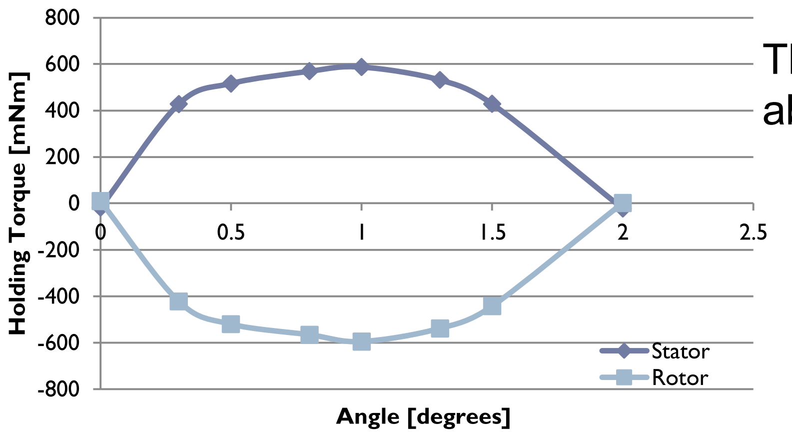

The maximum calculated value for T_H is about 590 mNm.

Calculated T_H – angle characteristic.

SM MADPM MKII – Design process
Results of numerical modeling - Detent Torque

- **H-SM third model**
- The geometry characteristics are: rectangular teeth both on stator and rotor, tooth width/tooth pitch ratio (t/λ) is 0.5 on rotor and 0.38 on stator.

Detent Torque

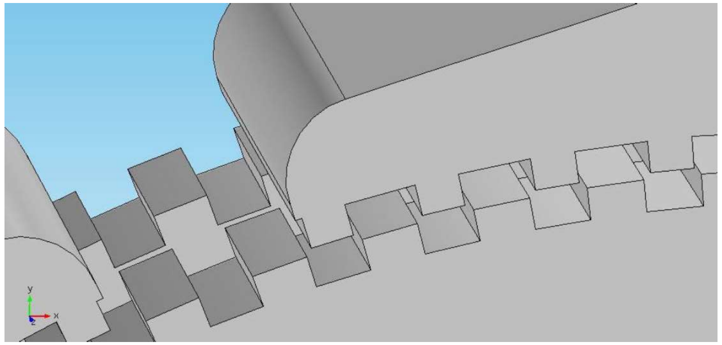

Constructive elements

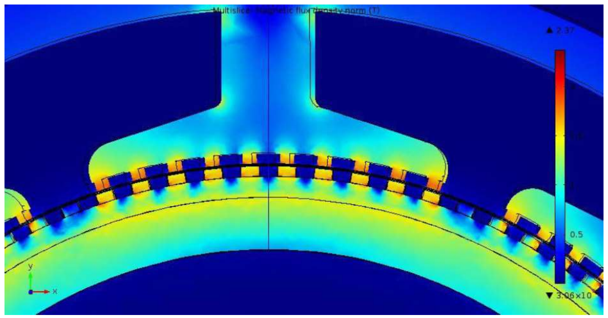

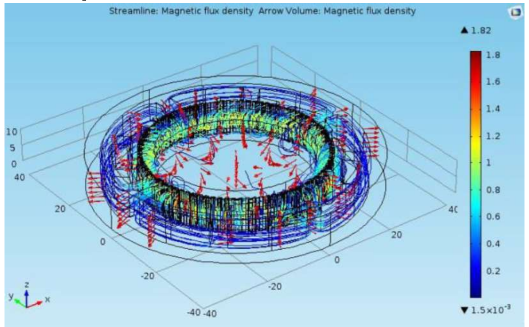

The magnetic flux density.

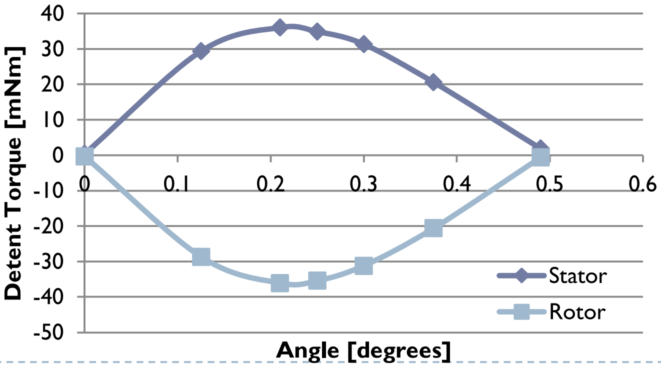

- The maximum value for T_D is about 36 mNm.
- The teeth are charged at airgap where flux concentrators appears.

Calculated T_D – angle characteristic

Results of numerical modeling
Holding Torque

Constructive elements

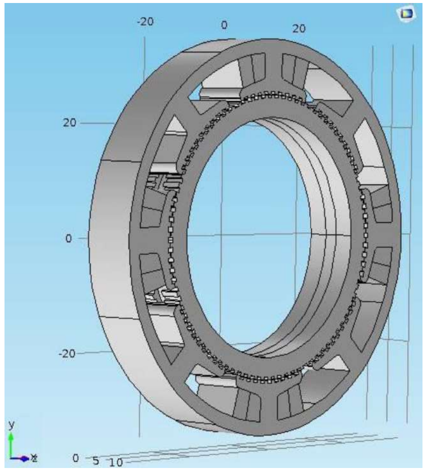

The magnetic circuit of the motor.

T_H results for H-SM third model

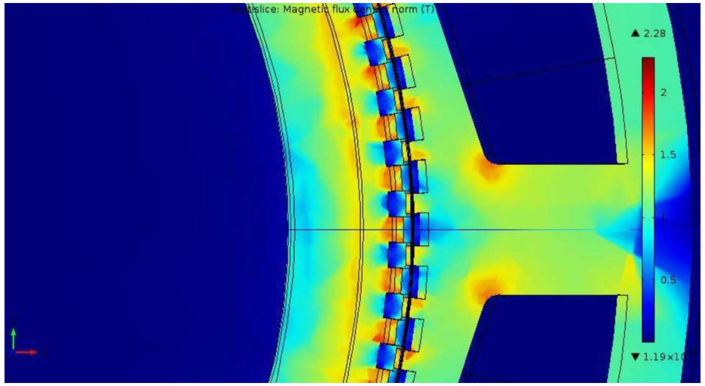

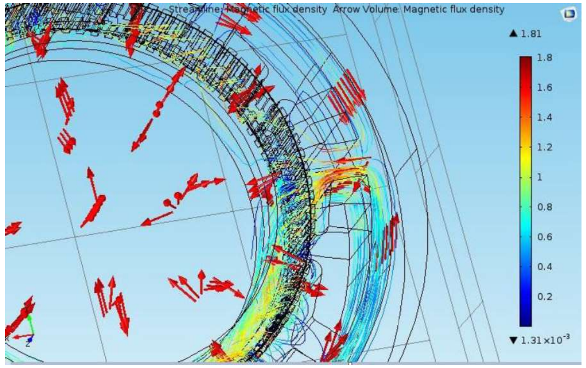

The magnetic flux density.

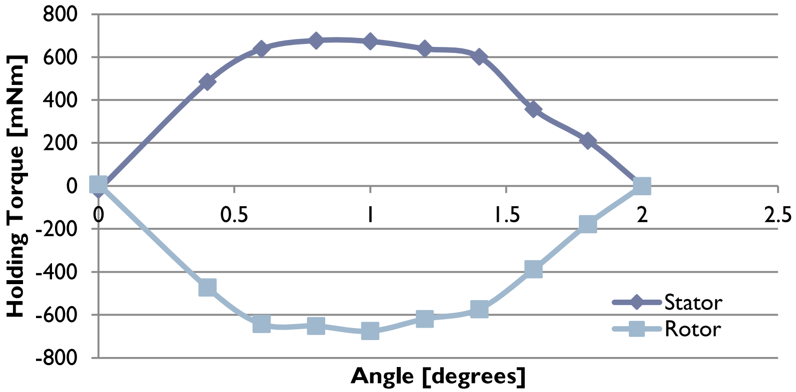

The maximum calculated value for T_H is about 670 mNm.

Calculated T_H – angle characteristic.

SM MADPM MKII – Design process
Results of numerical modeling - Detent Torque

- **H-SM fourth model**

- The geometry characteristics are: rectangular teeth both on stator and rotor, tooth width/tooth pitch ratio (t/λ) is 0.4 on rotor and 0.38 on stator.

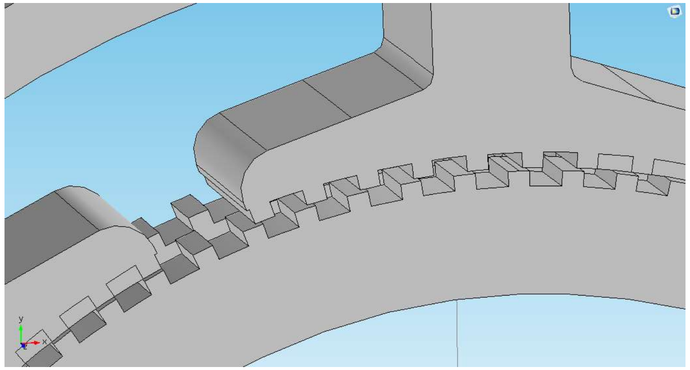

Constructive elements

Detent Torque

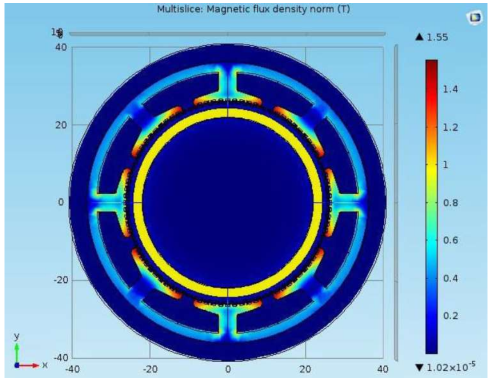

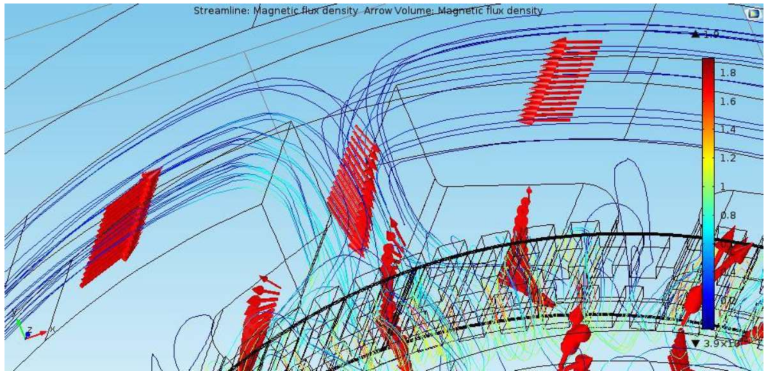

The magnetic flux density.

- The maximum value for T_D is about 34 mNm.
- The teeth are charged at airgap where flux concentrators appears.

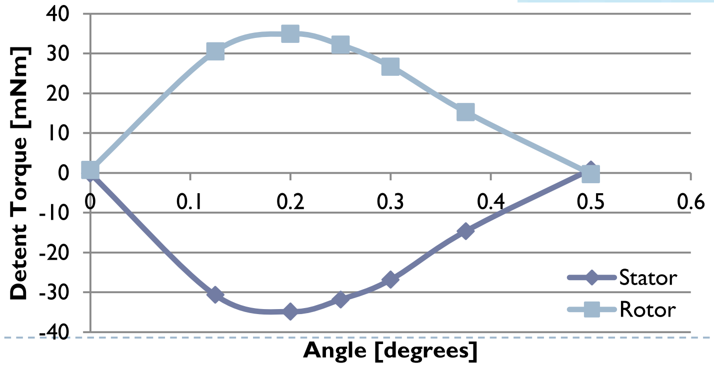

Calculated T_D – angle characteristic

Results of numerical modeling
Holding Torque

Constructive elements

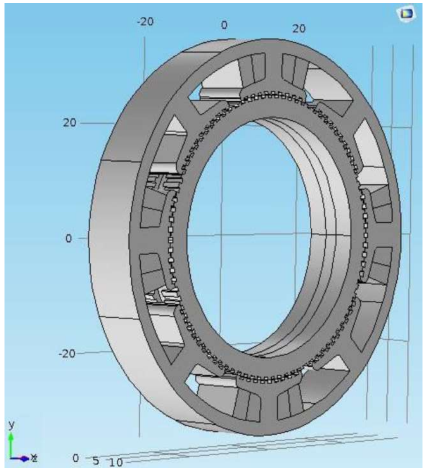

The magnetic circuit of the motor.

T_H results for H SM fourth model

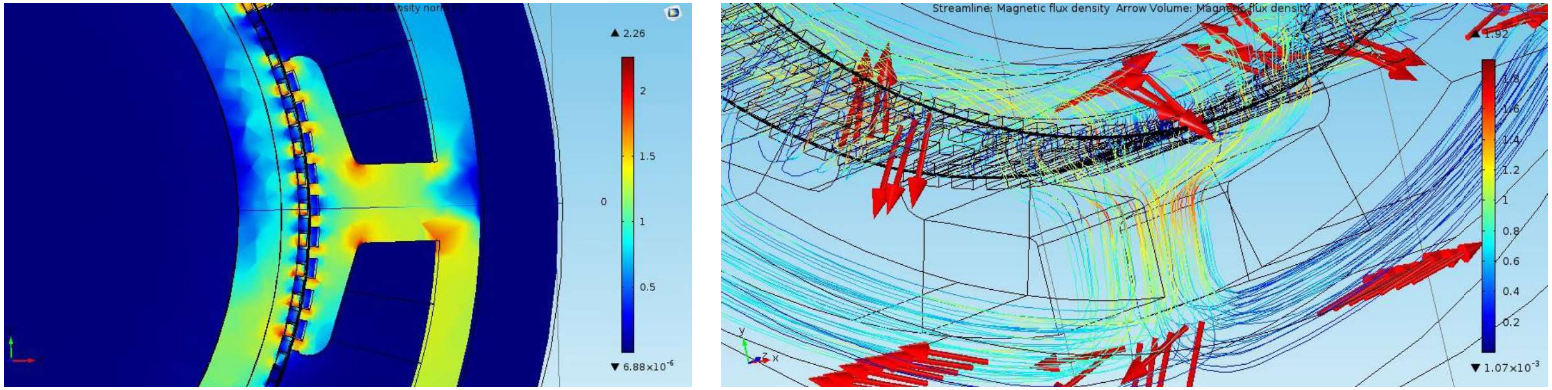

The magnetic flux density.

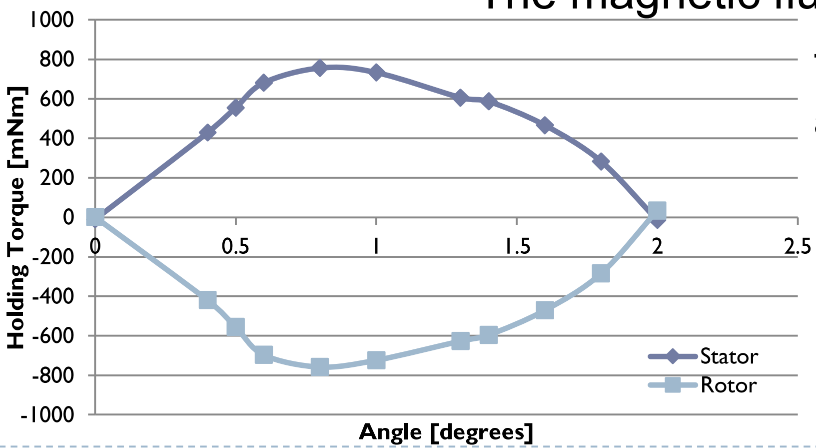

The maximum calculated value for T_H is about 760 mNm.

Calculated T_H – angle characteristic.

SM MADPM MKII – Design process
Results of numerical modeling - Detent Torque

- **H-SM fifth model**
- The geometry characteristics are: trapezoidal teeth both on stator and rotor, tooth width/tooth pitch ratio (t/λ) is 0.4 on rotor and 0.38 on stator.

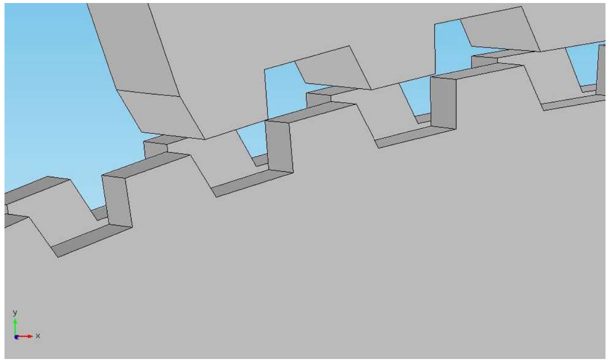

Constructive elements

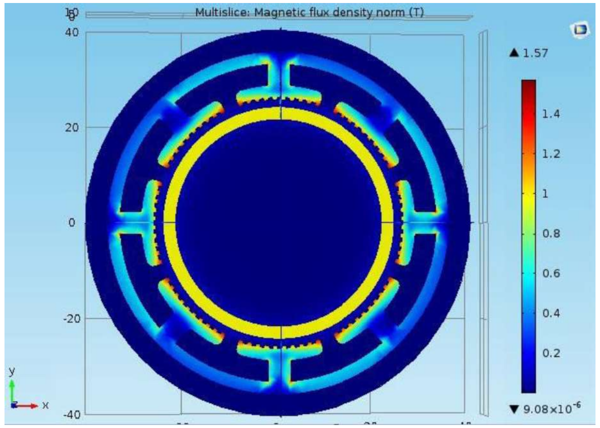

Detent Torque

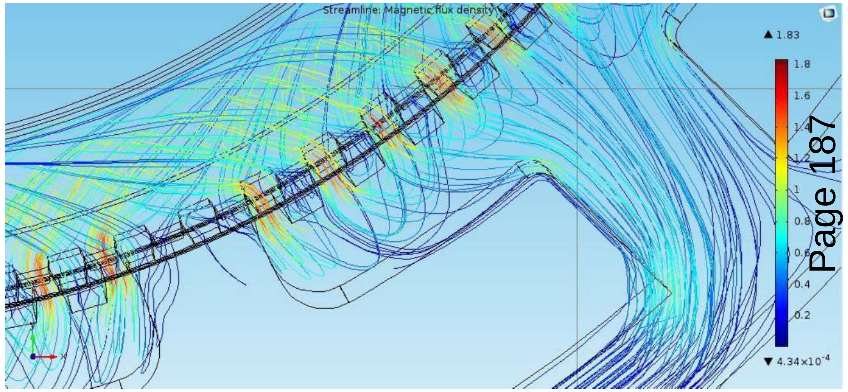

The magnetic flux density.

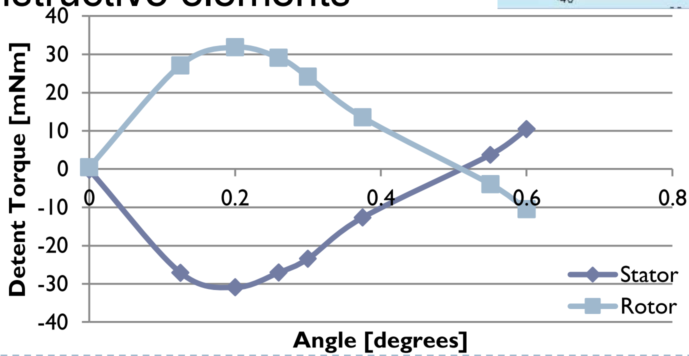

Calculated T_D – angle characteristic

- The maximum value for T_D is about 32 mNm.
- The teeth are charged at airgap where flux concentrators appears.

Results of numerical modeling
Holding Torque

T_H results for H SM fifth model

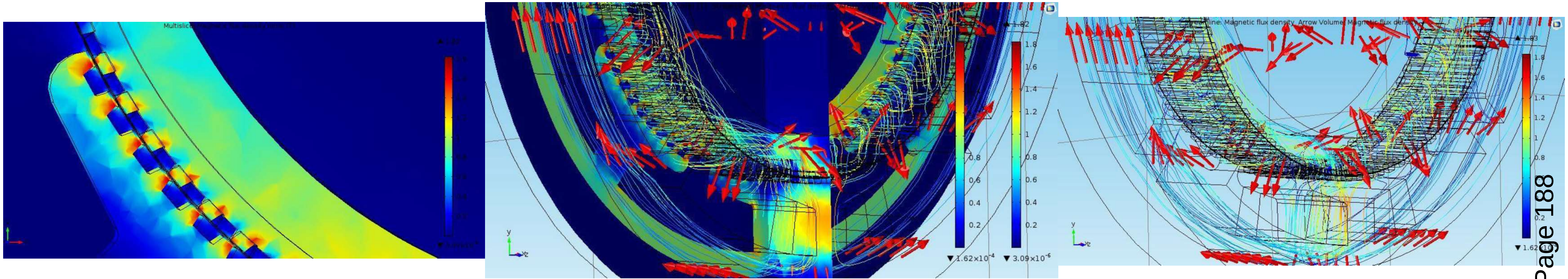

The magnetic flux density.

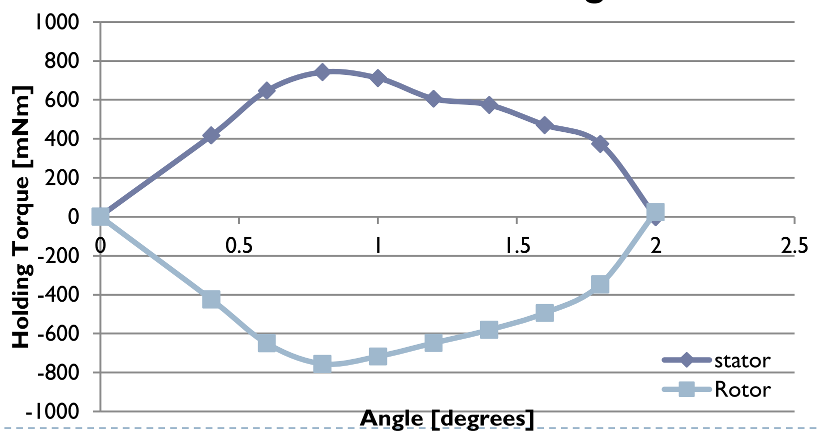

The maximum calculated value for T_H is about 740 mNm.

Calculated T_H – angle characteristic.

Conclusions

- This paper presents ICPE activities in two ESA projects for SM development.

- For each studied case, the computation results were been highlighted.

- Currently, accuracy tests of computation results are performing. A higher uniformity of the torque - angle characteristics was obtained without major modification of maximum torque values.

- Both project`s activities made possible reaching a TRL 4-5 for SM. More activities are needed, especially in experimental field, in order to bring the SMs manufactured at ICPE on the space market.

REFERENCES

- L. Bogdan; 2017;"Steppers"; http://web.ulbsibiu.ro/laurean.bogdan;
- M. Scarpino; November 2015;"*A Guide to Steppers, Servos, and Other Electrical Machines*", 1st ed., Que, pp.59-61;
- NASA; 2017; https://ntrs.nasa.gov/archive/nasa/casi.ntrs.nasa.gov/19690011418.pdf;
- NMBTC; 2017; http://www.nmbtc.com/hybrid-step-motors/;
- J. C. Nicklas; Jan. 25, 1962;"*Analysis, Design and Testing of a Position Servo Utilizing a Stepper Motor*". Tech. Rep. 32-206, Jet Propulsion Lab.; California Inst. Tech.
- S. Giles, A. A. Marcus; Dec. 15, 1964;"*SNAP-8-Control-Drum Actuators*". Rep. NAA-SR-9645, Atomics International;
- S. J. Bailey; *Incremental Servos.* 11, Nov. 1960;"*Part I - Stepping vs Stepless Control. Control" Eng*., vol. 7, no., pp. 123-127; Dec. 1960;"*Part II - Operation and Analysis*", vol. 7, no. 12, pp. 97-102; Jan. 1961;"*Part III - How They've Been Used*", vol. 8, no. 1, pp. 85-88; Mar. 1961;"Part IV - Today's Hardware", vol. 8, no. 3, pp. 133-135; May 1961;"*Part V - Interlocking Steppers*", vol. 8, no, 5, pp. 116-119;

- Thank you for your attention!

Presentation 2504

Development of a new reaction wheel using up-to-date technologies

Development of a new reaction wheel using up-to-date technologies

Development of a new reaction wheel using up-to-date technologies

Objectives:

- preliminary concept of a reaction wheel (RW) that will take maximum benefit of new technologies
- preliminary validation of most critical issues
- establish a detailed development plan

Project Consortium:

- ICPE as Prime Contractor
- Thales Alenia Space France SAS (TAS-F) as Sub-contractor

Requirements for the reaction wheel

Type of requirements	Requirement		Value
Capacities for AOCS	Torque (at SC level)		0.2 Nm
	Momentum		6 Nms
Interfaces And environment	Mass		5 kg
	Volume		200 x 200 x 90 mm^3
	Power consumption (at max speed)		Typical: 20W Max: 150 W @ 0.2 Nm
	Temperature: Qualification vs acceptance: [Tmin-5° Tmax+5°]	OFF	[-35 +75]°
		ON	[-35 +65]°
		Operating (ON)	[-25 +65]°
	Supply voltage		27-50V
	Data interfaces		Digital (RS-422 ideally)
Performances	Momentum bias		0.1% * Hmax
	Momentum stability (RMS)		0.04% * Hmax
	Microvibrations	Static imbalance	0.15 g.cm
		Dyn. imbalance	2.2 $g.cm^2$
		Max force over [0 500] Hz	0.5 N (ambitious)
Design	ITAR free		Yes
	Zero-crossing		1e6
	Reliability & lifetime		7 years

Development of a new reaction wheel using up-to-date technologies

Electric machine based on a Direct Drive Permanent Magnet (PM) Synchronous Motor with Outer Rotor and Ironless Winding Configuration

- high rotor inertia → substitute the flywheel → compact RW with reduced weight
- large rotor diameter → maximizes output torque
- shorter axial length
- smooth speed/torque characteristics → zero cogging torque → very low torque ripple
- eliminated stator iron losses → increased motor efficiency → high speed operation
- Halbach array configuration of high energy SmCo PMs → increase power density of electric motor and decrease the yokes thickness

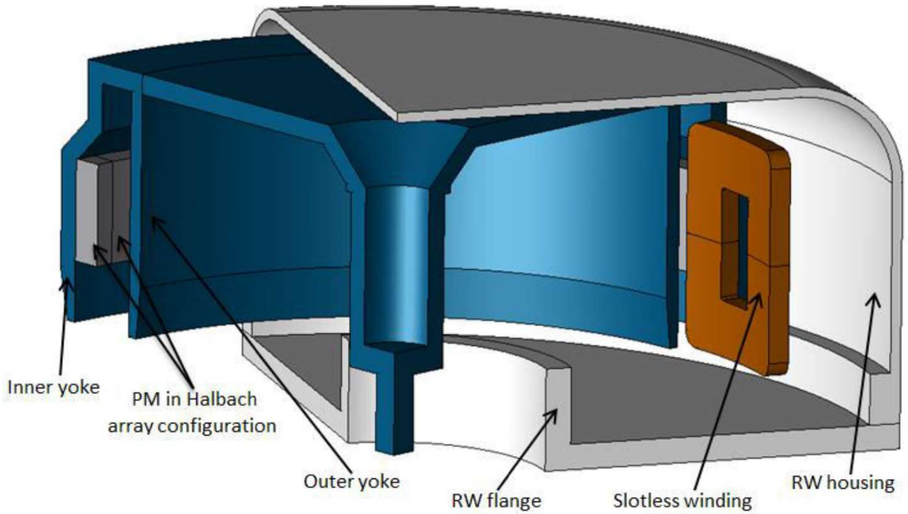

Configuration of the PM synchronous motor

Development of a new reaction wheel using up-to-date technologies

Electric machine optimization based on 3D FEM:

- sinusoidal induced voltage
- 0.5 % ripple of electromagnetic torque
- 11.5% increased of airgap magnetic flux
- 22.5% decrease of the rotor yokes thickness
- Reduced AC losses → Litz wires winding

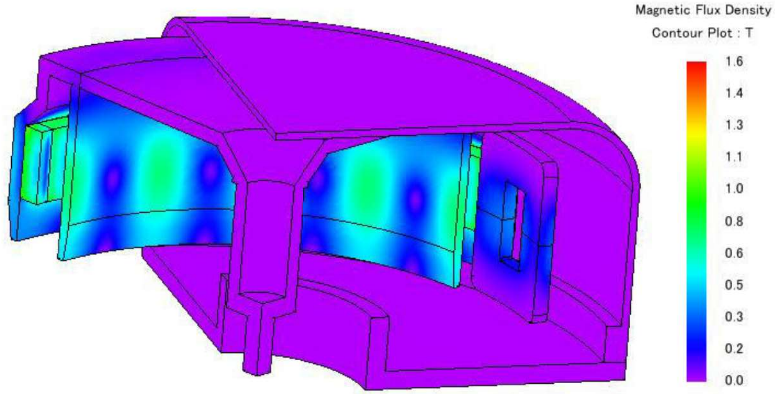

Magnetic flux density distribution

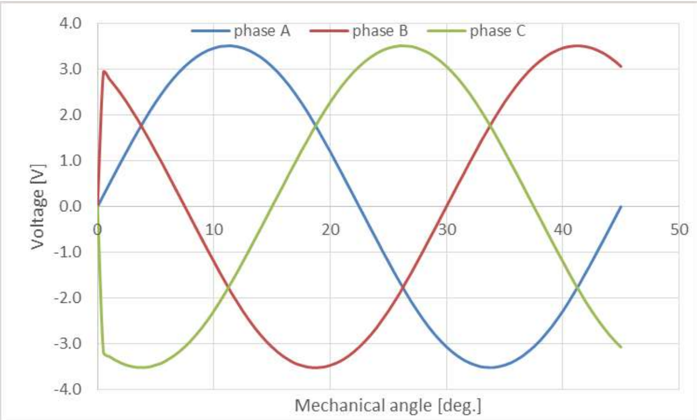

Phase Electromotive Force @ 1000 rpm

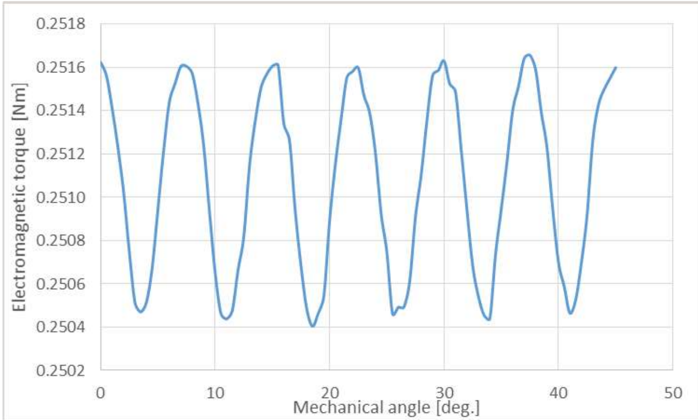

Electromagnetic torque

Development of a new reaction wheel using up-to-date technologies

Electromagnetic losses analysis

Resistive losses (cooper losses)	0.6 W
Rotor yokes losses	0.3 W
Permanent magnets losses	0.3 W
Housing losses	0.4 W
TOTAL	**1.6 W**

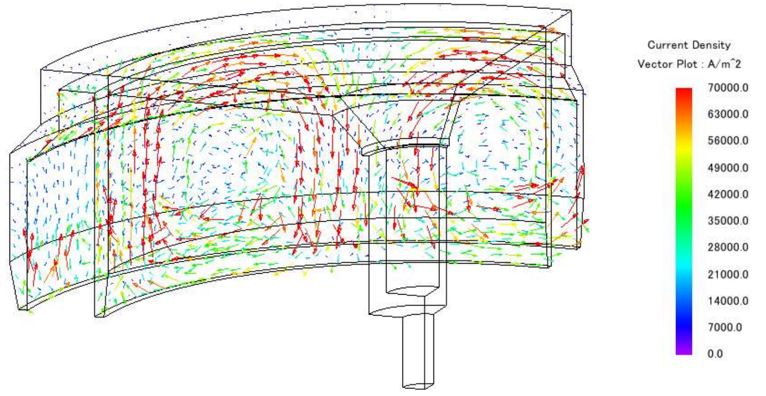

Density of the Eddy current induced in the rotor magnetic core

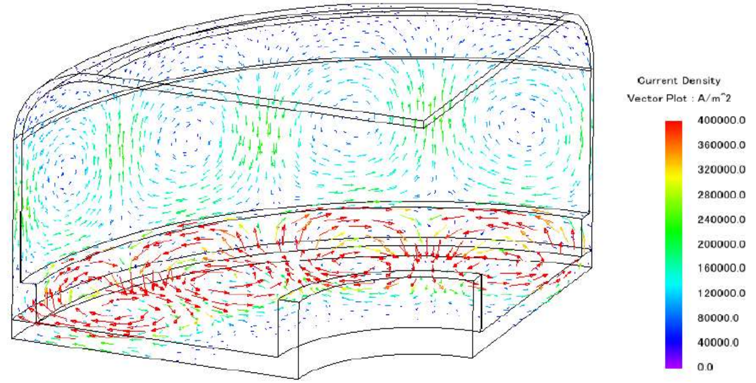

Density of the Eddy current induced in housing

Development of a new reaction wheel using up-to-date technologies

Temperature analysis

- 11 ^{0}C average temperature rise after 5 cycles
- 21.5 ^{0}C peak local temperature rise after 5 cycles

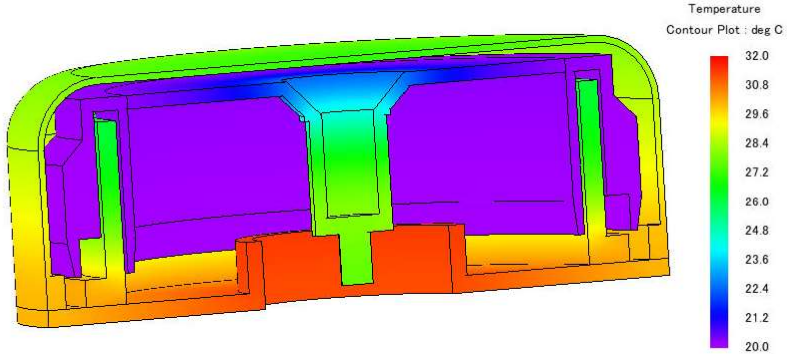

Temperature distribution after 5 cycles

Average electromagnetic losses	1.6 W
Average bearings friction losses	4 W
Average power electronic losses	5 W
Average braking resistor losses	18 W

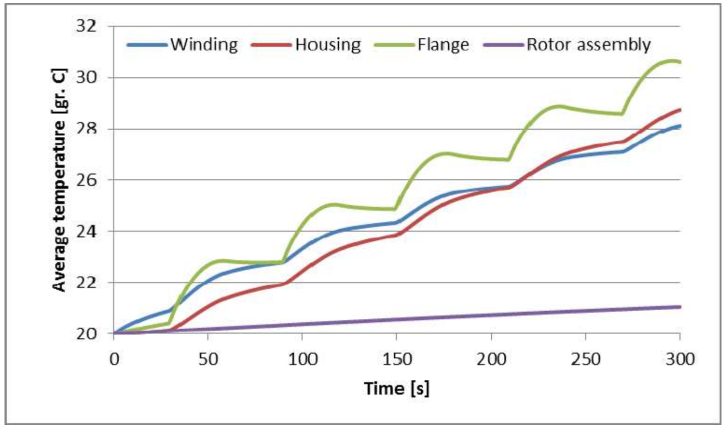

Average temperature rise in the RW during 5 cycles

Development of a new reaction wheel using up-to-date technologies

Mechanical design and optimization:

- First bending mode > 140 Hz → increased bearing cartridge stiffness
- Sinus loads: 25g (20-100Hz), 1000g shock load → hard preload and fluid lubrication
- Reduced weight < 5 Kg → compact design
- Static imbalance: 0.15 gcm and dynamic imbalance: 2.2 gcm2 →laser balancing of the flywheel

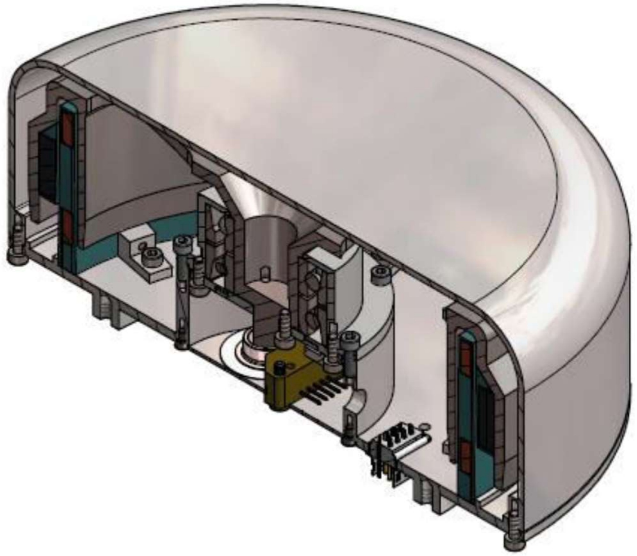

Configuration of the RW

Development of a new reaction wheel using up-to-date technologies

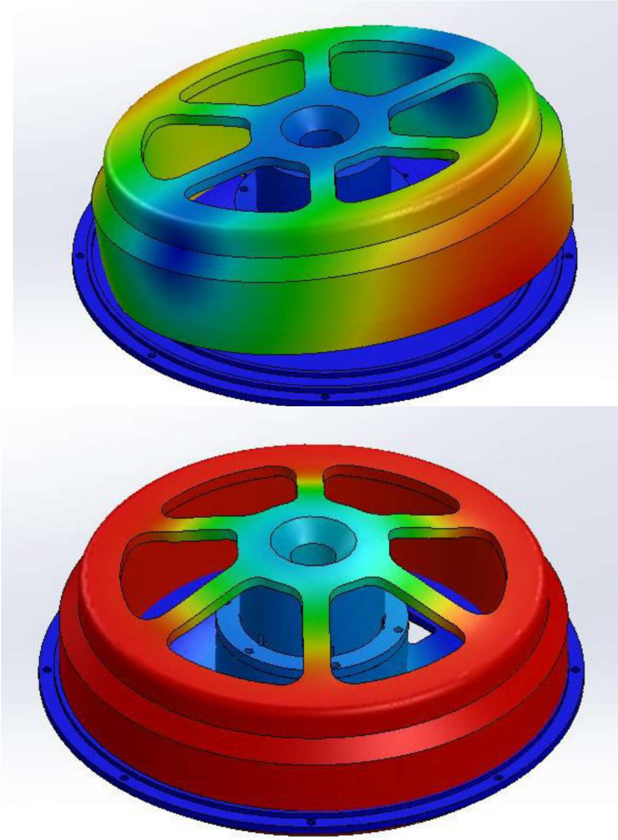

First (223 Hz) and second (330 Hz) mechanical modes

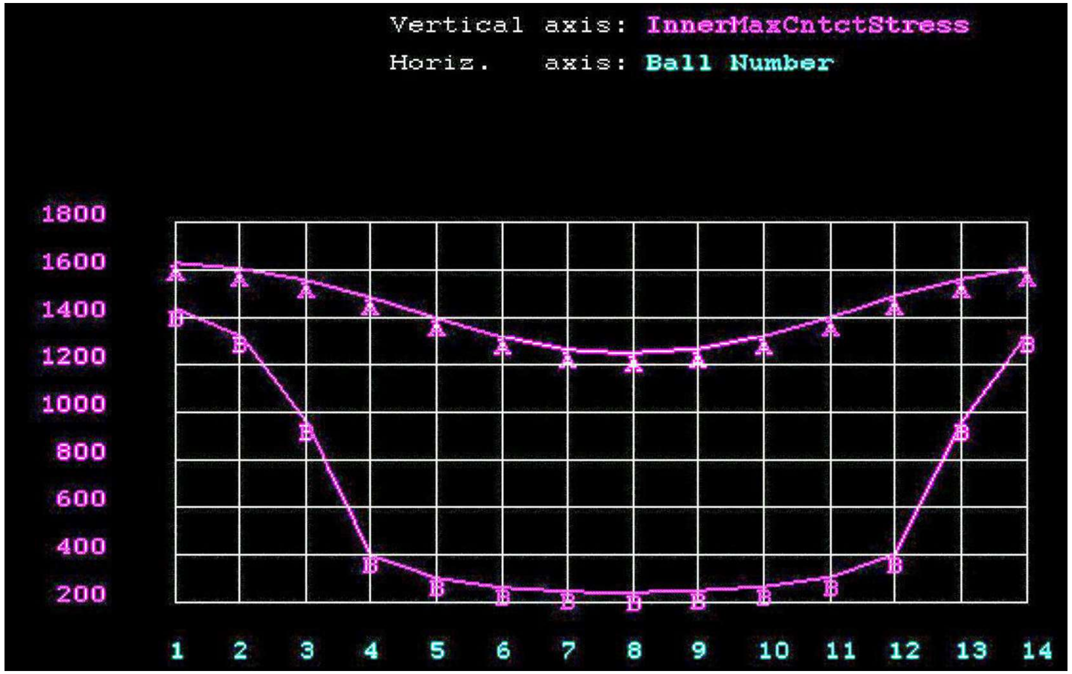

Hertz contact stress for 25g quasistatic loading

Development of a new reaction wheel using up-to-date technologies

Digital control through an FPGA:

1 x NI cRIO-9035

→ 40 MHz / 80 MHz onboard clock
→ Xilinx Kintex-7 70T Reconfigurable FPGA

1 x NI 9220

- 16 differential channels Simultaneous AI, 100 kS/s per channel sample rate
- ±10 V measurement range, 16-bit resolution

→ electric motor currents

2 x NI 9401

- 8-channel, 100 ns high-speed digital I/O
- 5 V/TTL, sinking/sourcing digital I/O

→ power switch control
→ drivers states
→ Hall-effect sensors states

1 x NI 9402

- 4-channel, 55ns high-speed digital I/O
- LVTTL, sinking/sourcing digital I/O

→ optic/magnetic signals in quadrature with index

Development of a new reaction wheel using up-to-date technologies

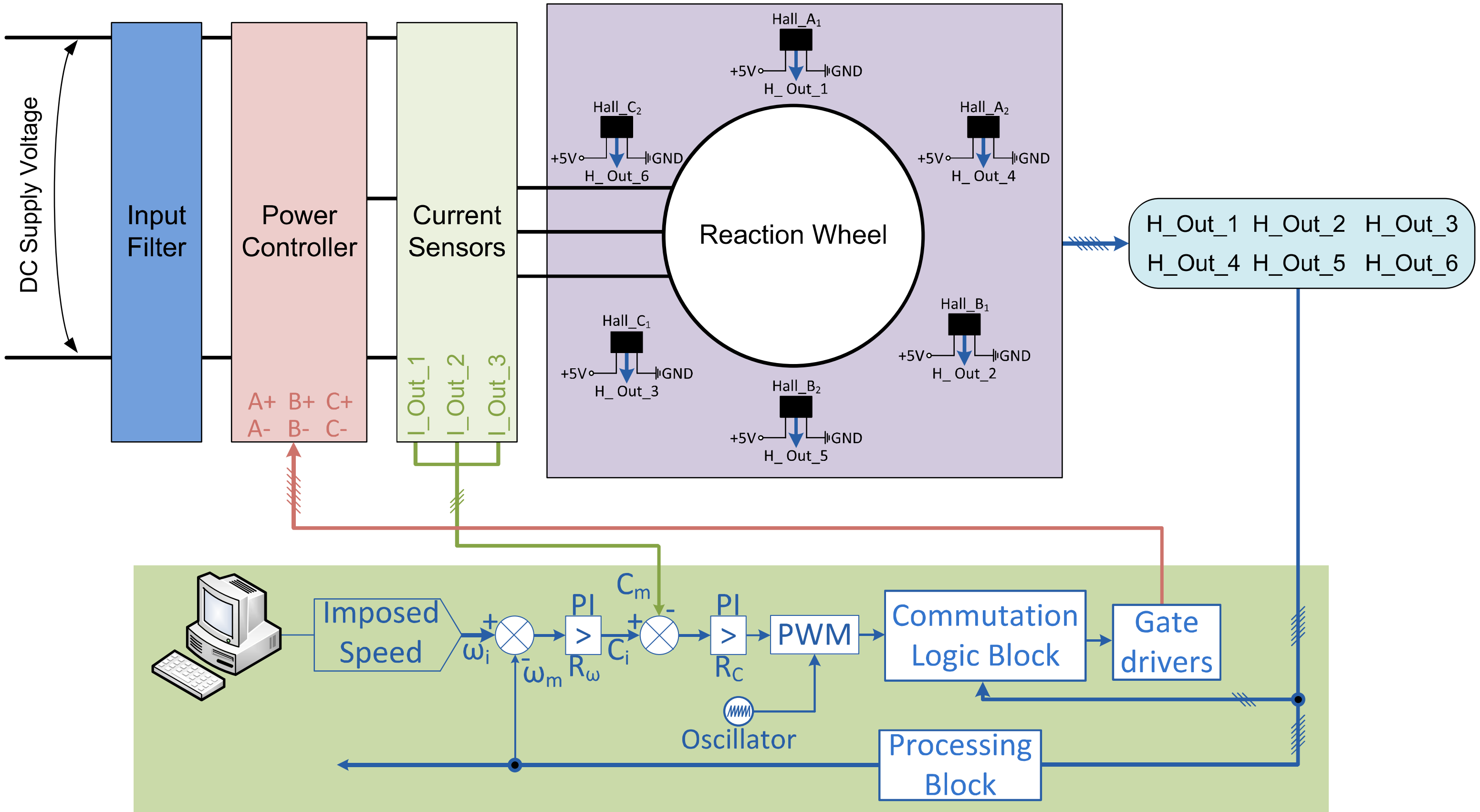

RW Control – SVM algorithm implemented with LabVIEW

- Thank you for your attention!

Presentation 2505

New Technologies on Developing Wide Range Thermic Facilities Based on Low Pressure Temperature Controlled Helium Environment

Dan Ifrim
Romanian Research and Development Institute for Gas Turbines COMOTI
220D, Iuliu Maniu Blvd, sector 6, 061126, Bucharest, Romania

New Technologies on Developing Wide Range Thermic Facilities Based on Low Pressure Temperature Controlled Helium Environment".

Romanian Research and Development Institute for Gas Turbines COMOTI, Bucharest, Romania

Dan IFRIM, MSc

Content

- Project and mission overview
- Sealing methods analysis and trade-off
- Seals characteristics – system dimensioning
- System components
- Closing operation analysis
- Further steps

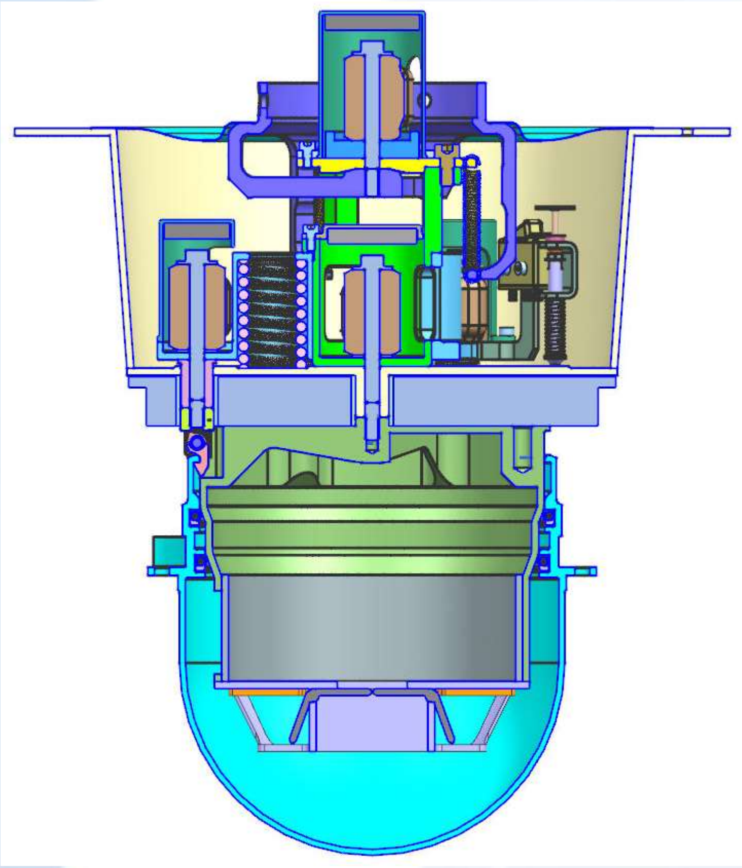

Mission

JUICE - JUpiter ICy moons Explorer

Cosmic Vision Themes

• What are the conditions for planet formation and emergence of life?

• How does the Solar System work?

Primary Mission Themes

•Emergence of habitable worlds around gas giants Jupiter system as an archetype for gas giants.

Lifetime

•7.6 years cruise & 3.5 years in the Jovian system

Type

•L-class candidate mission

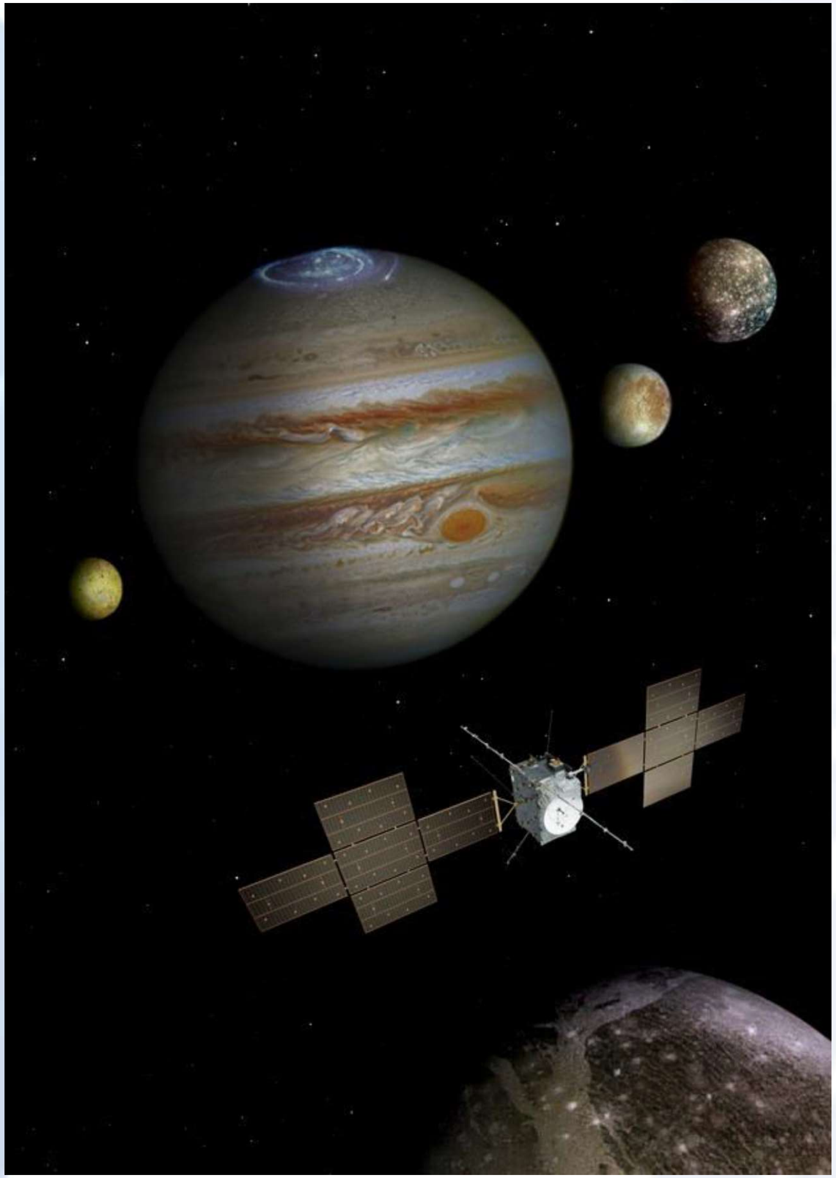

WRTF – Wide Range Thermal Facility

• Wide Range Thermal Test Facility (WRTF) serve the JUICE mission and space applications requiring testing at low temperature in a short timescale.

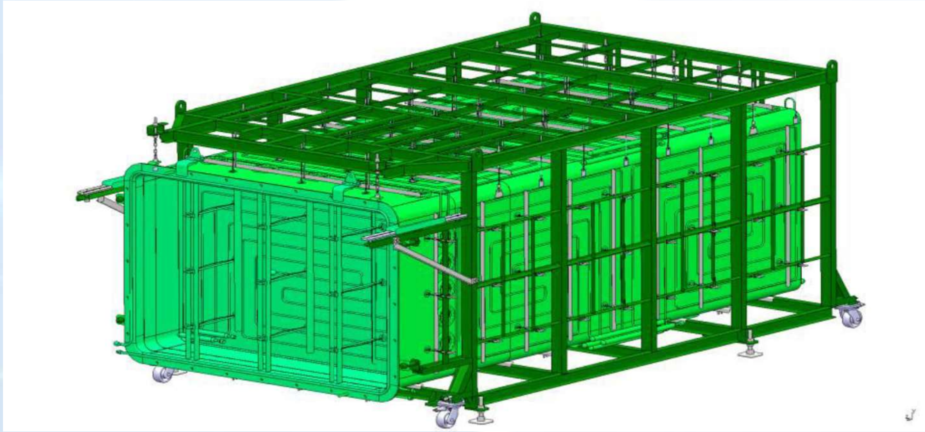

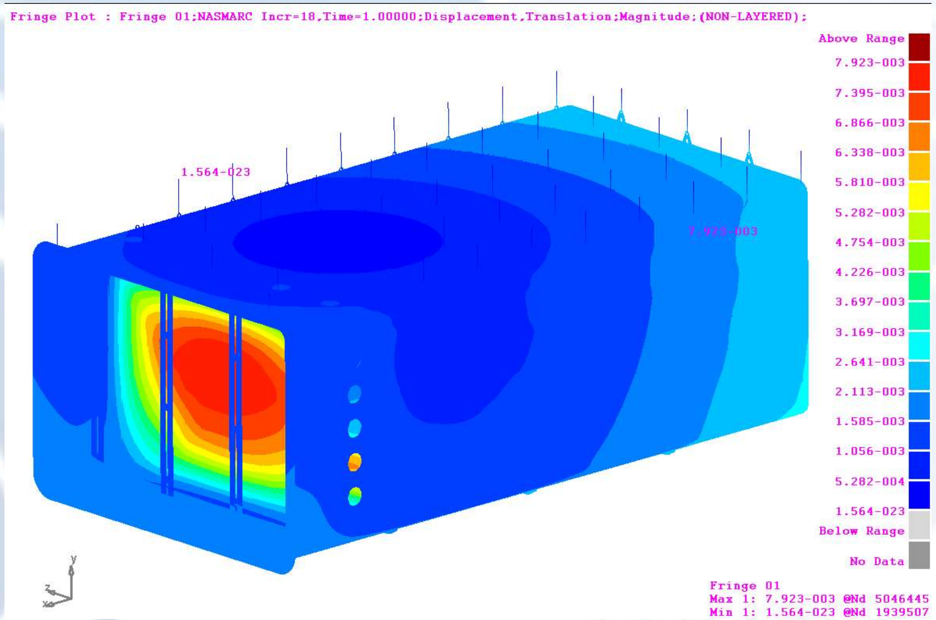

Page 208

Concept & Thermal requirements

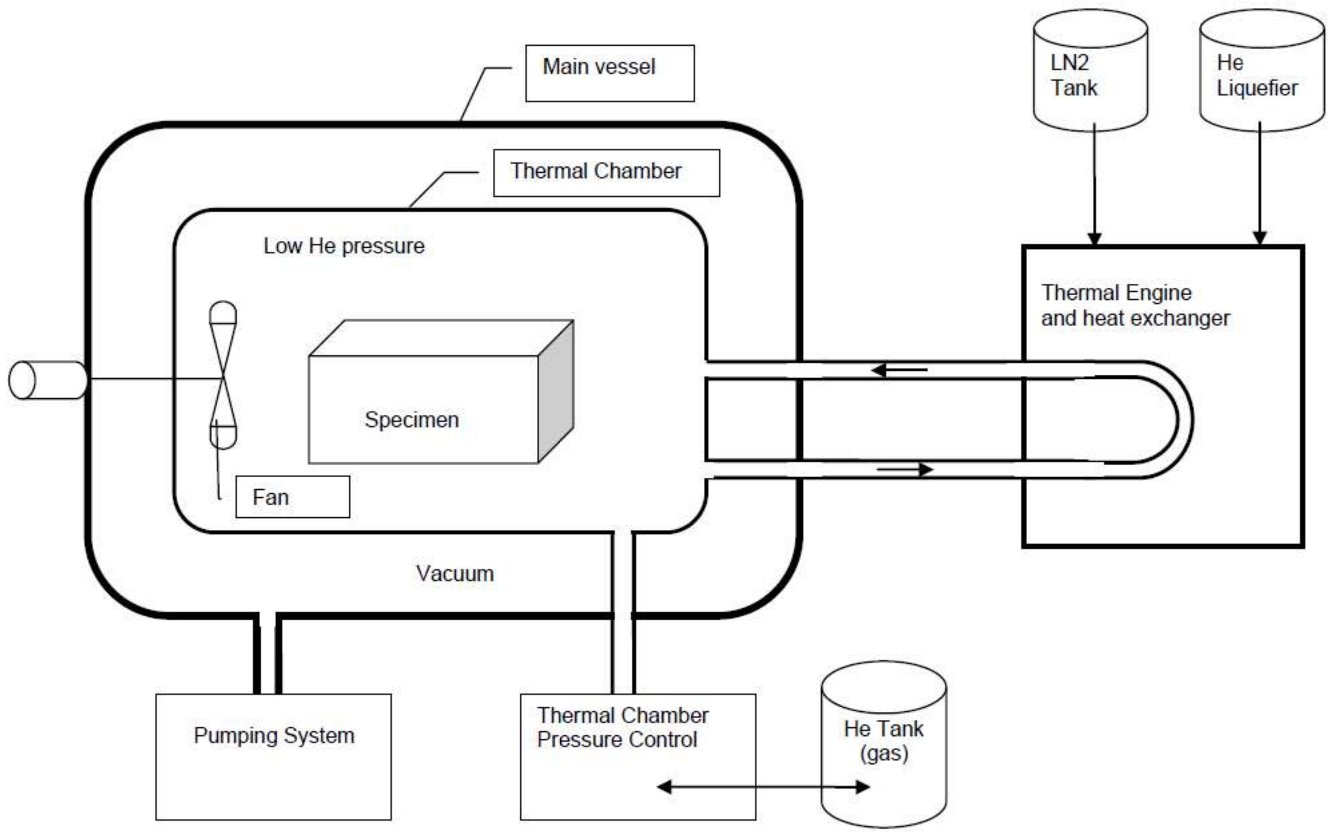

THERMAL REQUIREMENTS

- Temperature Range : 43 Kelvin (- 230 °C) - 433 Kelvin (160 °C).
- Cooling and heating rate: less than 3 K/min
- Temperature Control Accuracy: +/- 1 K
- Spatial Homogeneity : less than 5 K (TBC)

Concept & mechanical requirements

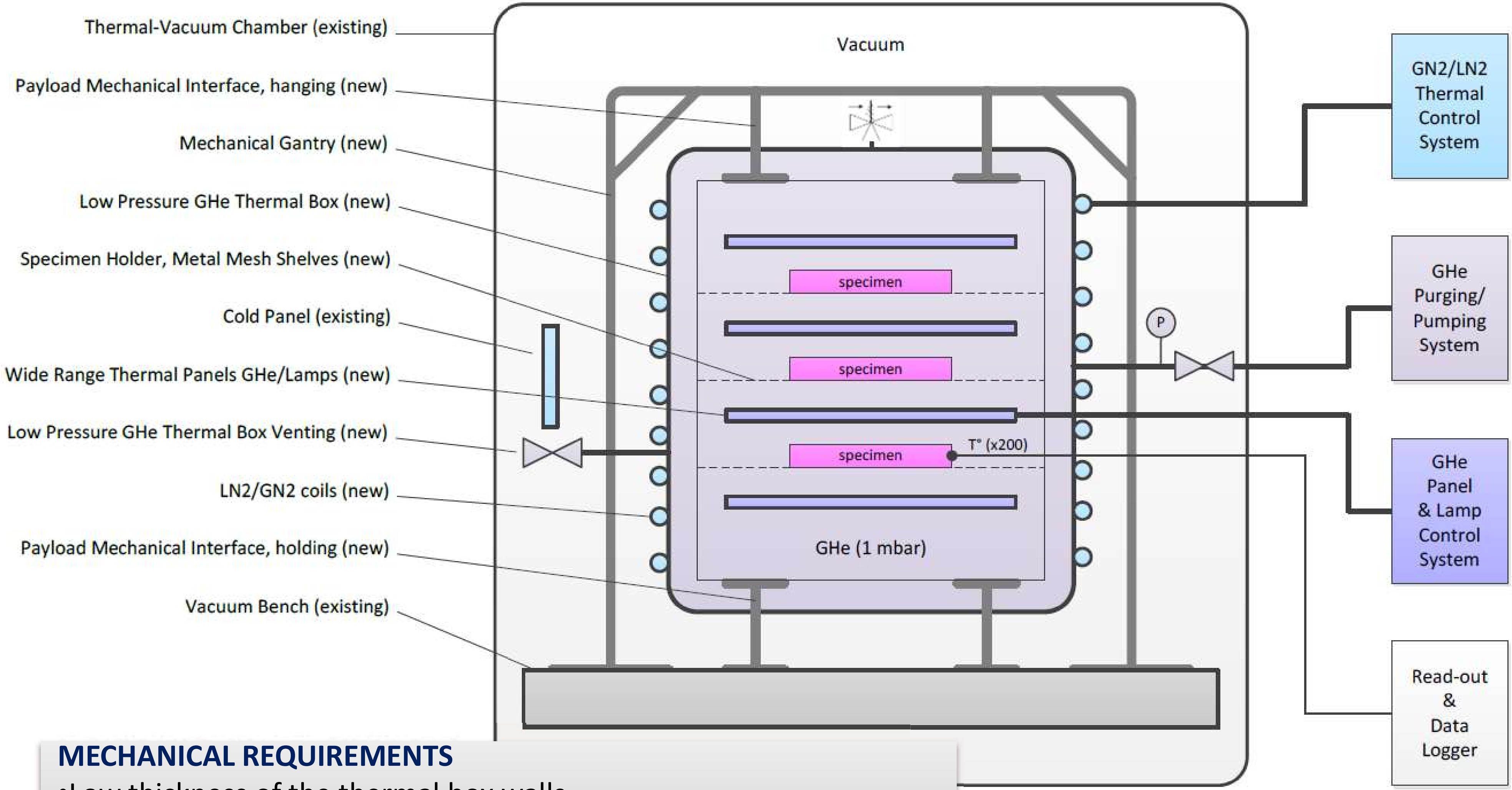

MECHANICAL REQUIREMENTS

- Low thickness of the thermal box walls
- Low thermal conductivity between box and frame (mechanical gantry)
- No leakage on pipes welded on plates
- No losse of pressure

Chalenges

-Temperature range : 43 Kelvin to 433 Kelvin;
- Pressure difference:
  - outside ≤10^{-5} hPa
  - inside 2 hPa
- Necessity of a high conductivity between LN2/GN2 pipes and box surfaces
- Low transfer of conductivity between the gantry /frame and box
- capability to resist to the themperature cycles.

Phases

Phase 1: Developing a small box

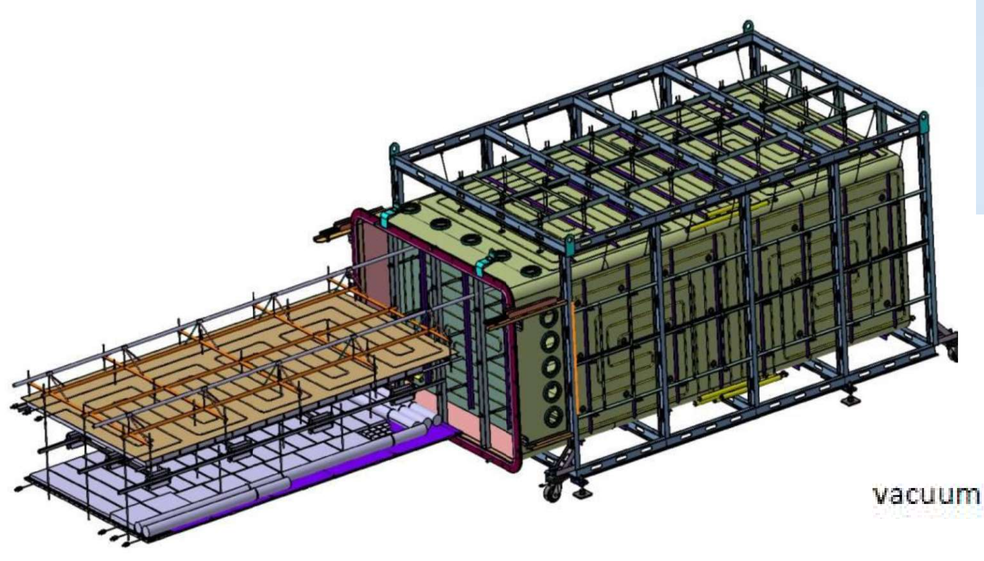

Phase 2: Developing a large box

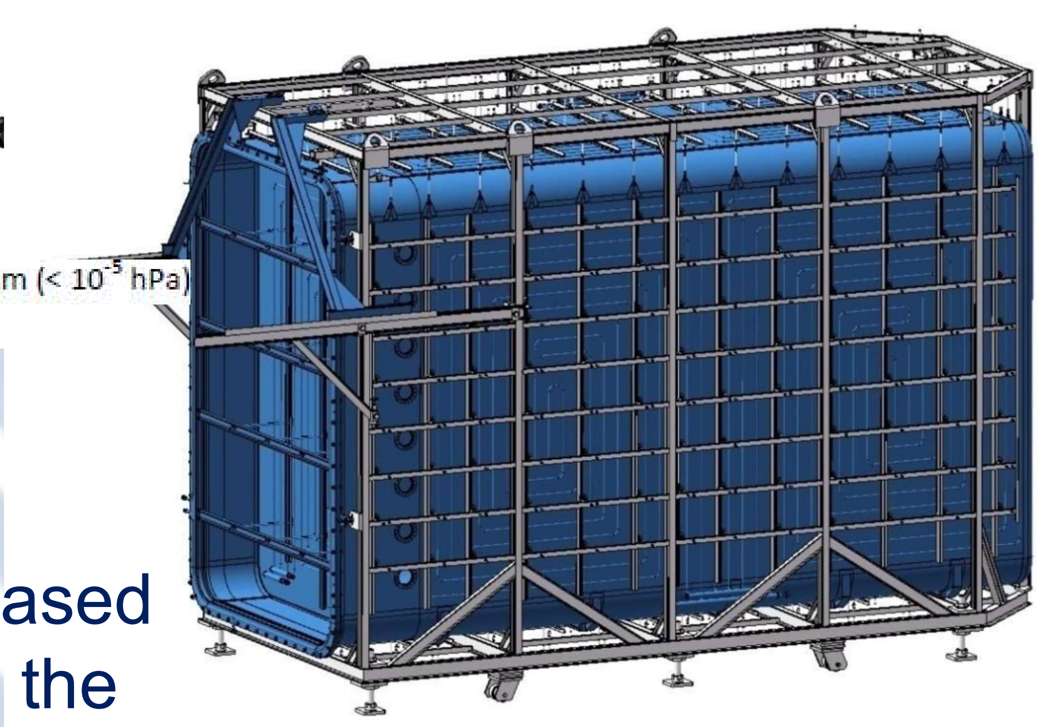

Large box development is based on the experience gained in the realization of the small box

Small box concept

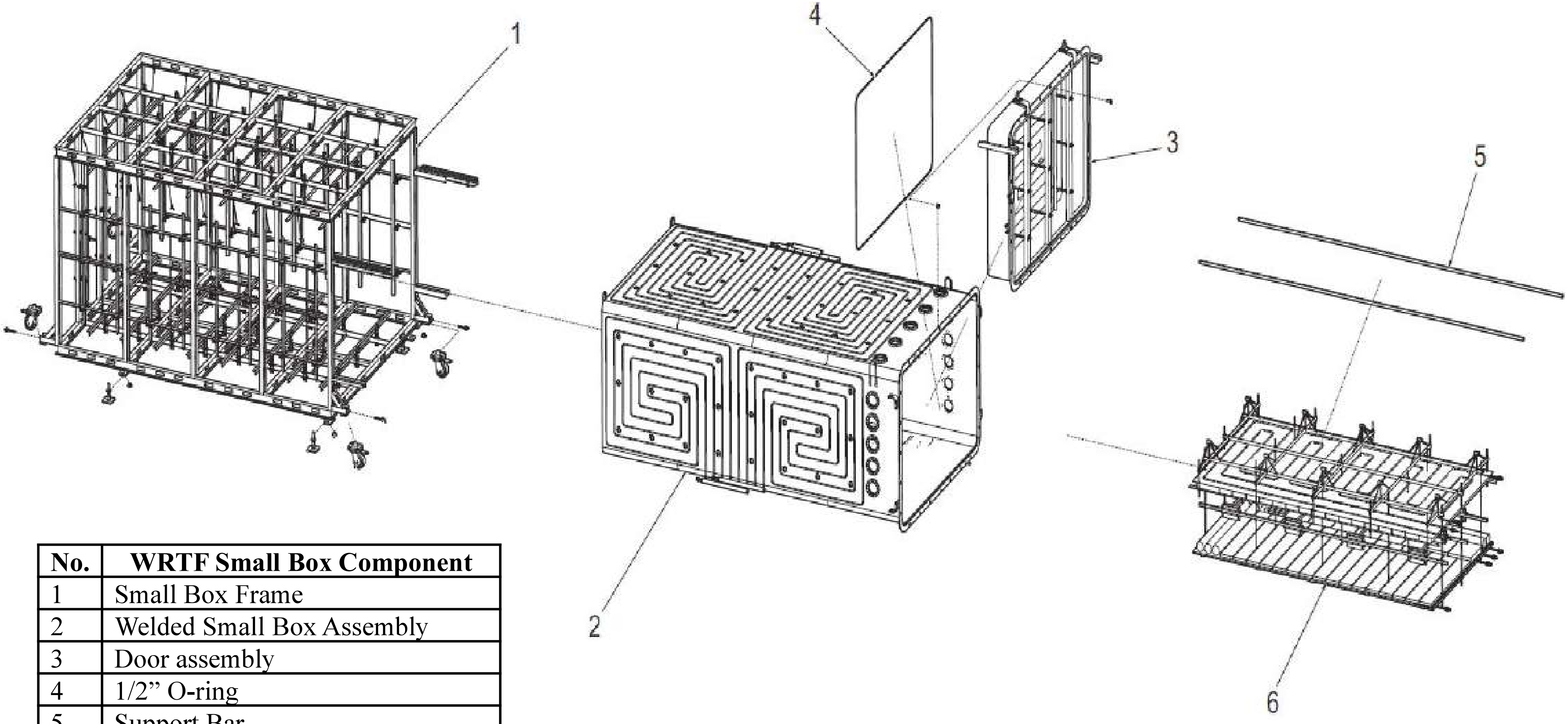

No.	WRTF Small Box Component
1	Small Box Frame
2	Welded Small Box Assembly
3	Door assembly
4	1/2” O-ring
5	Support Bar
6	Shelves Assembly

Small box set

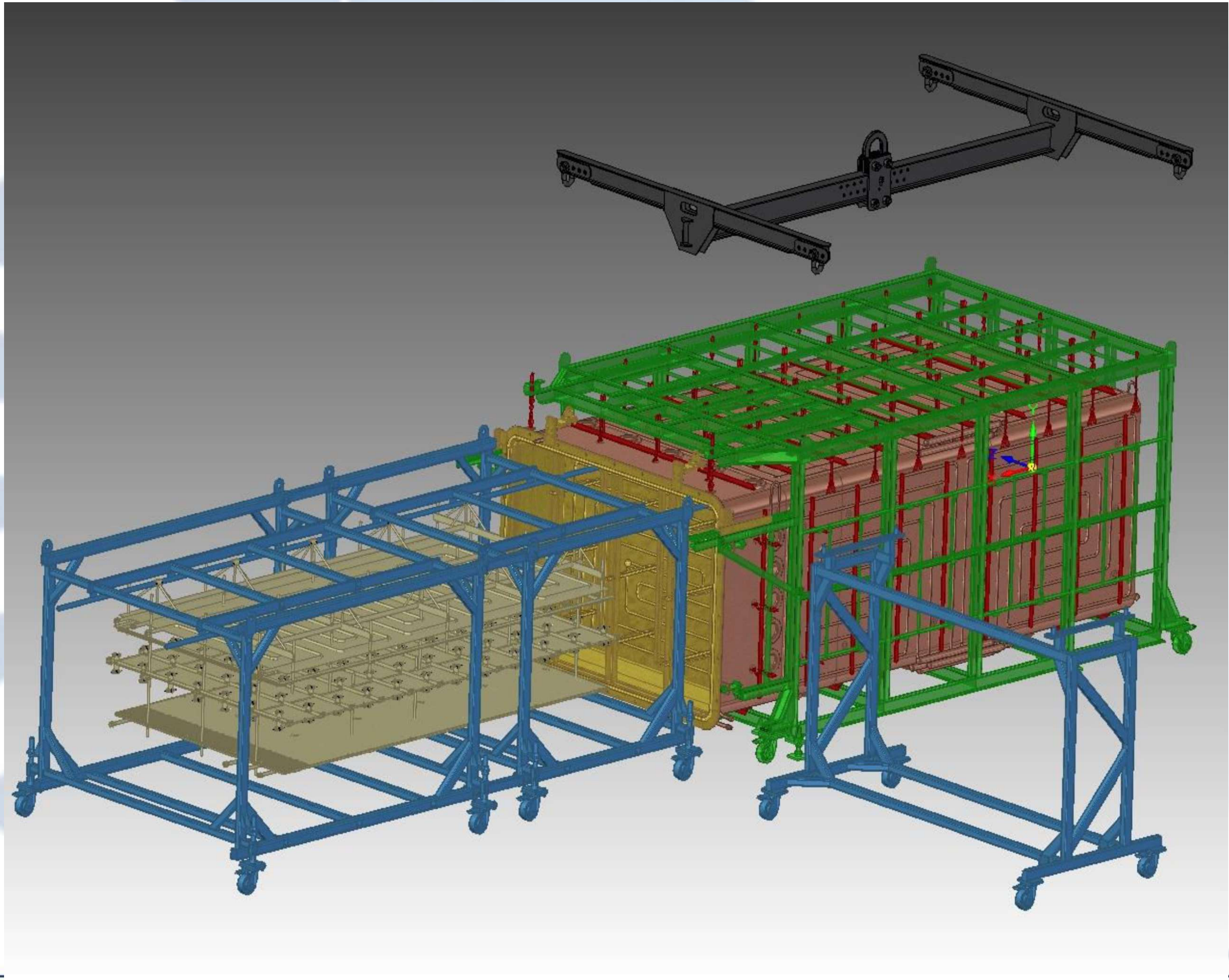

FEM Analyse

First iteration

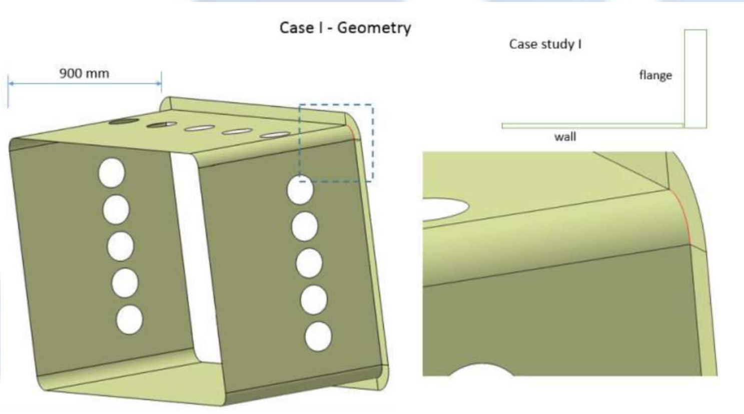

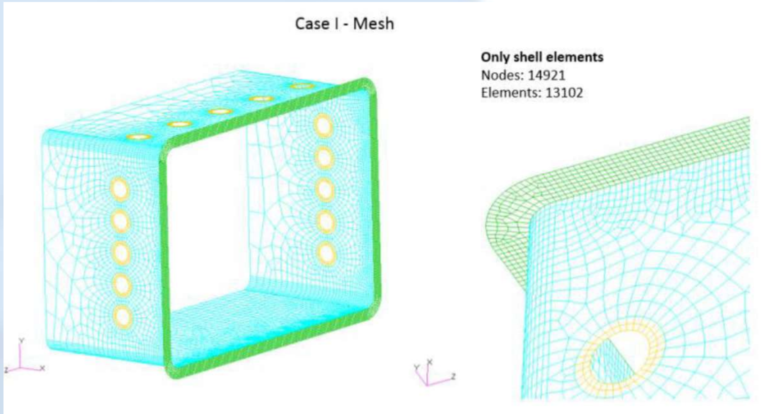

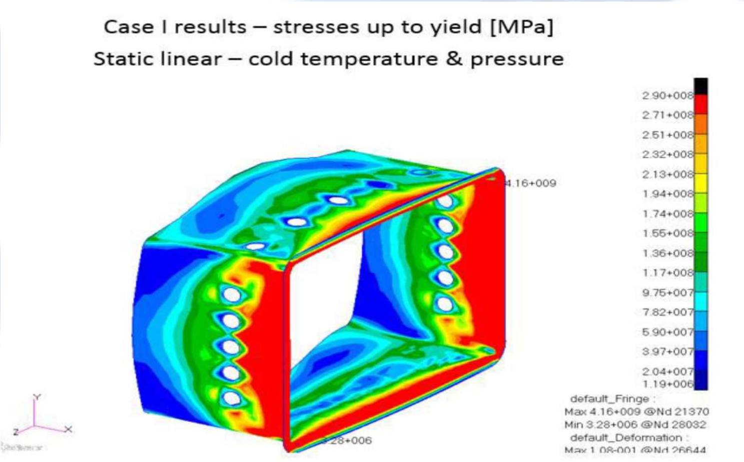

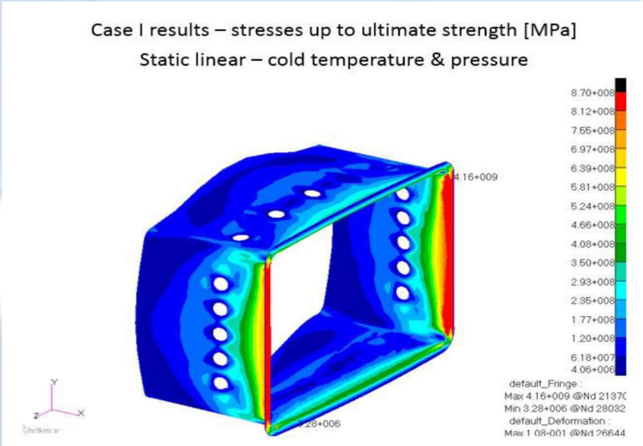

Conclusion : the small box should not have resisted !

Final aproach: Progressive thickness variation in the box

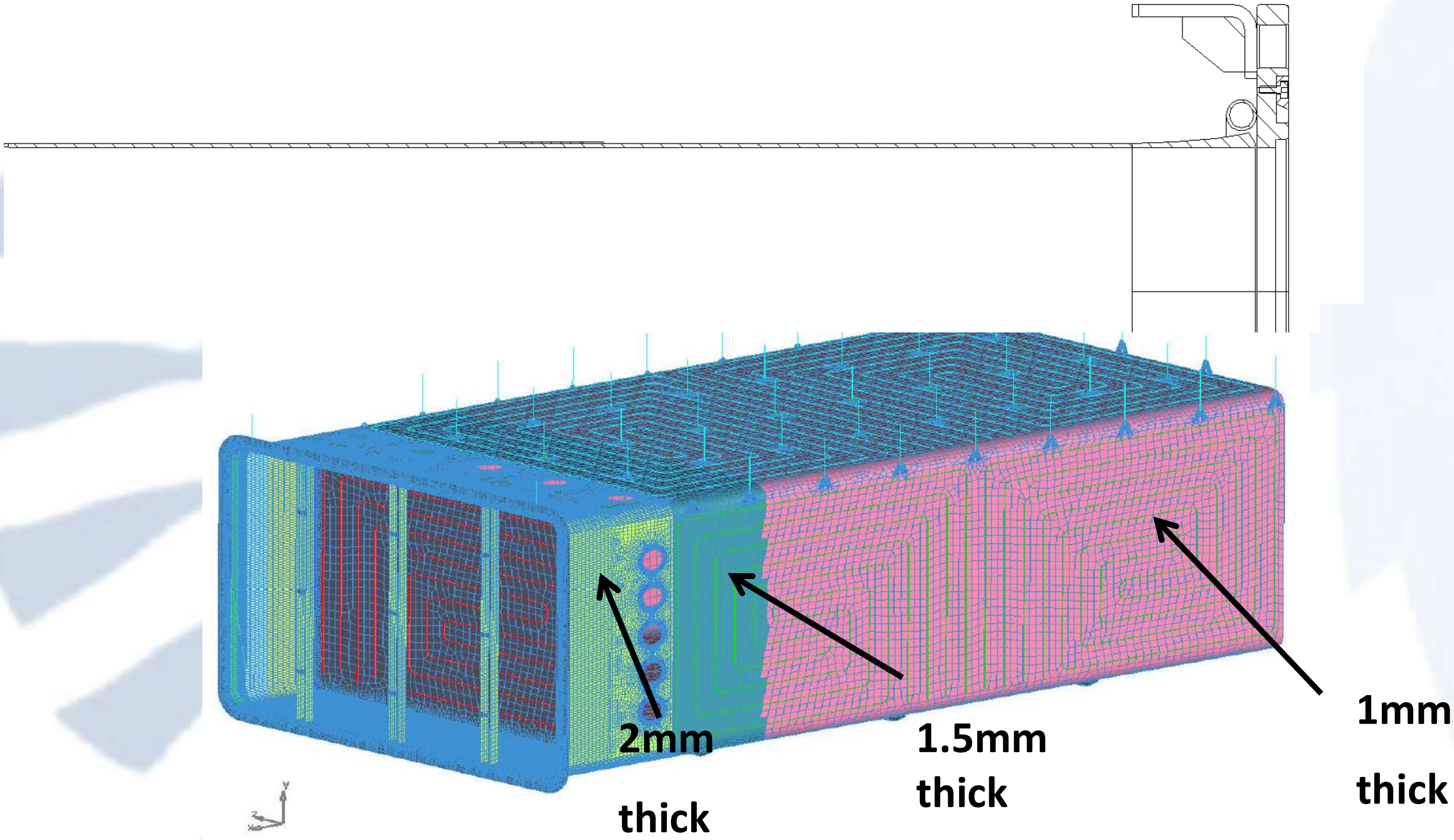

FEM Analyse

Conclusion: Small box resist

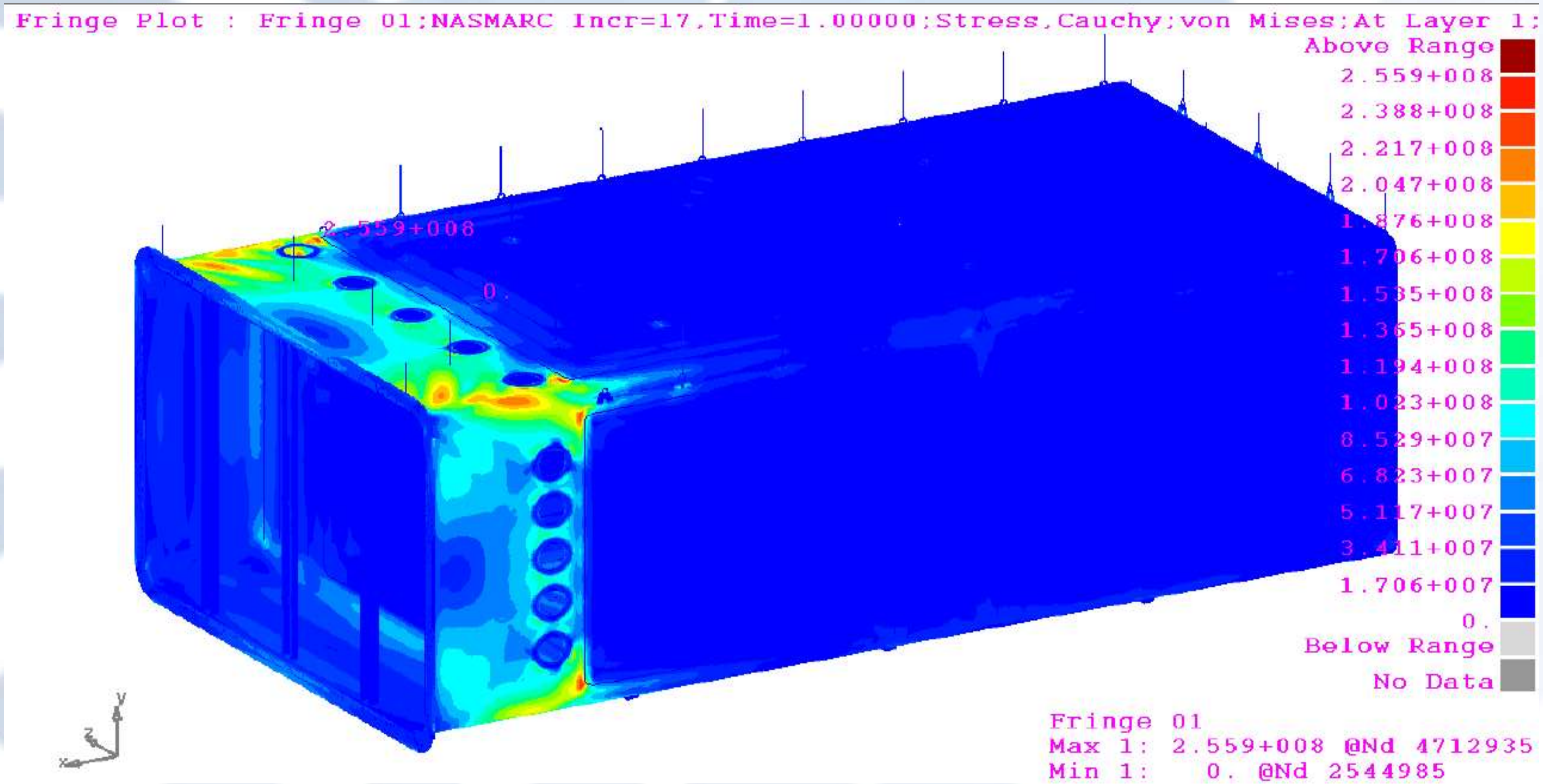

Small box technological solutions

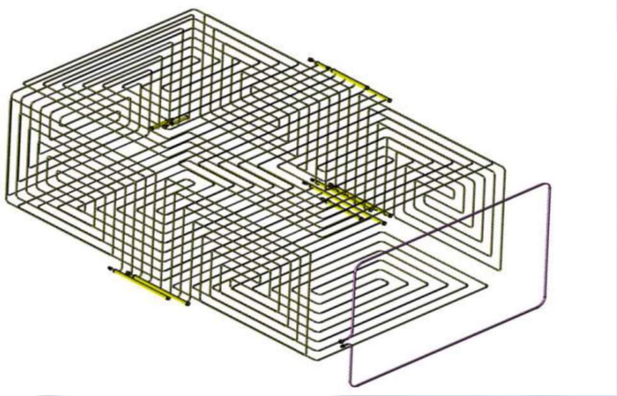

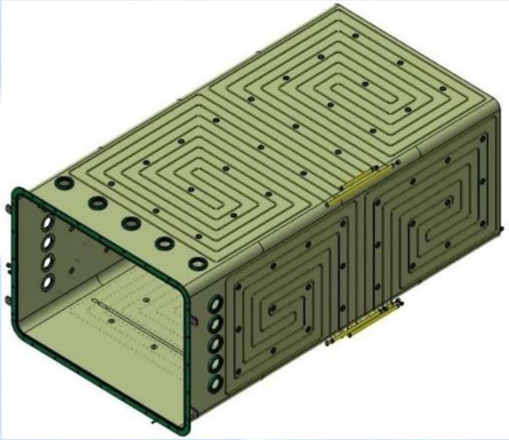

External pipes welded on small box

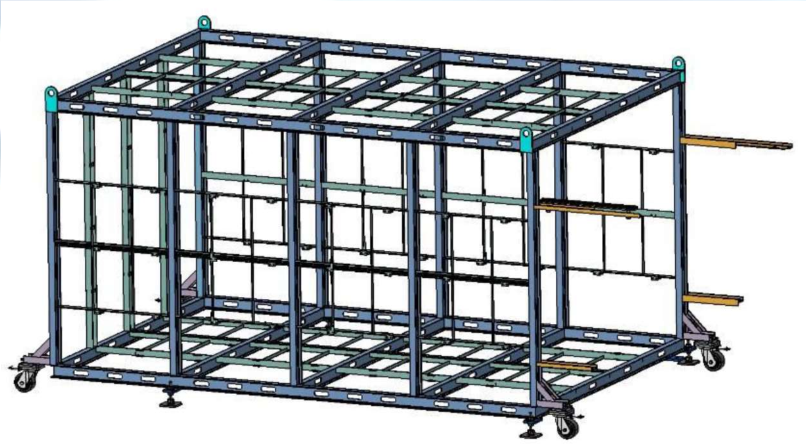

Small box is suspended on a solid frame

Small box technological solutions

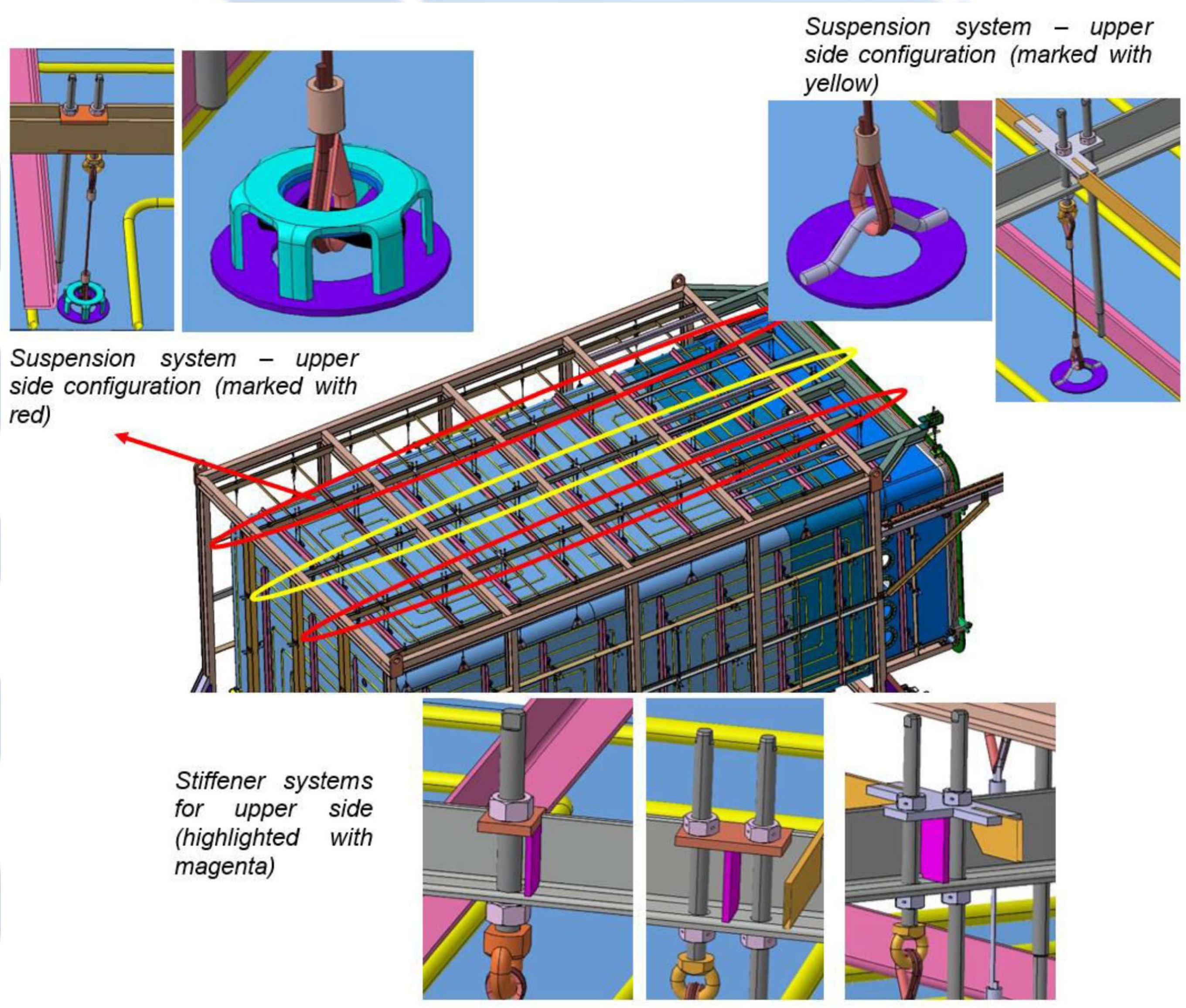

Small box technological solutions

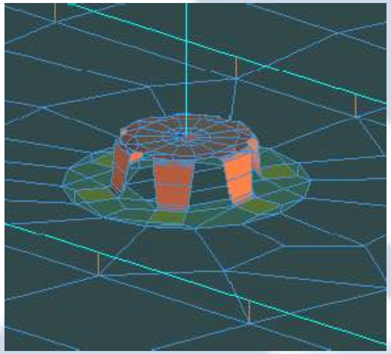

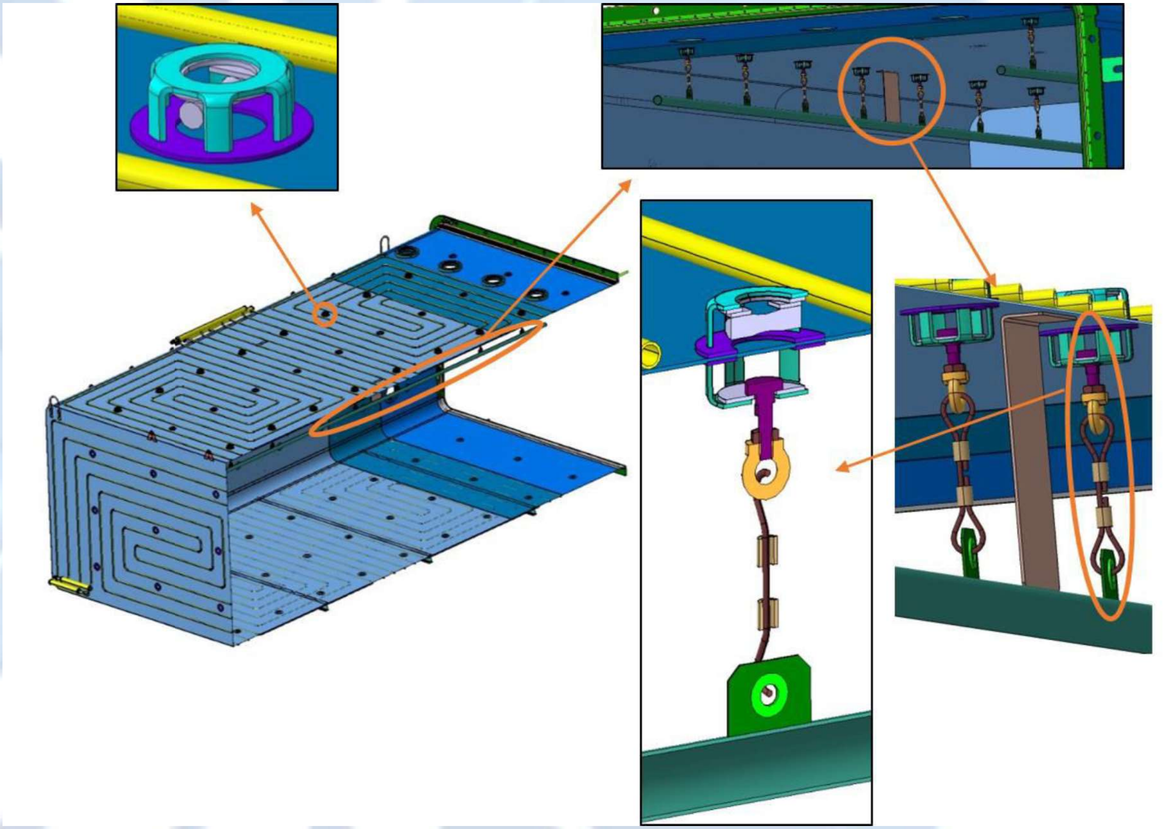

Small box technological solutions

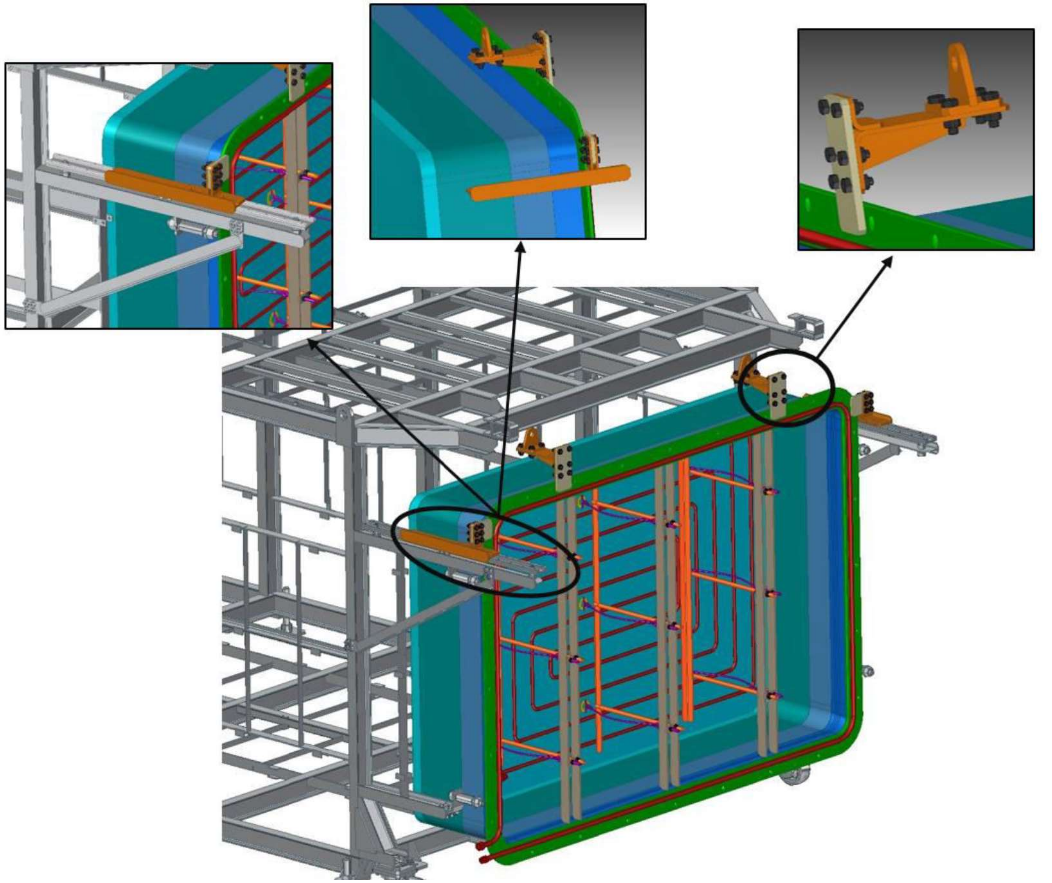

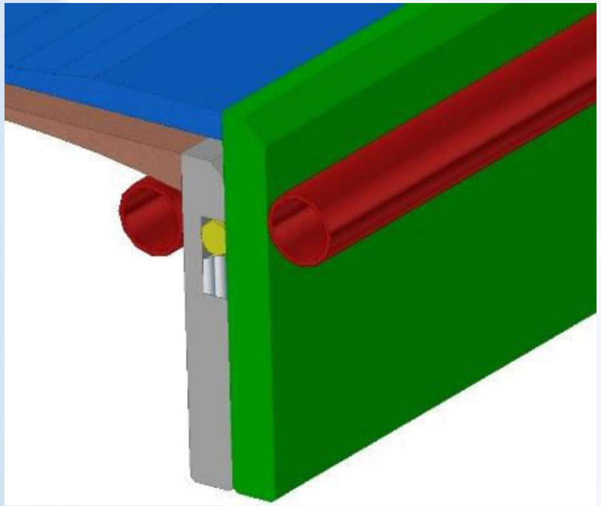

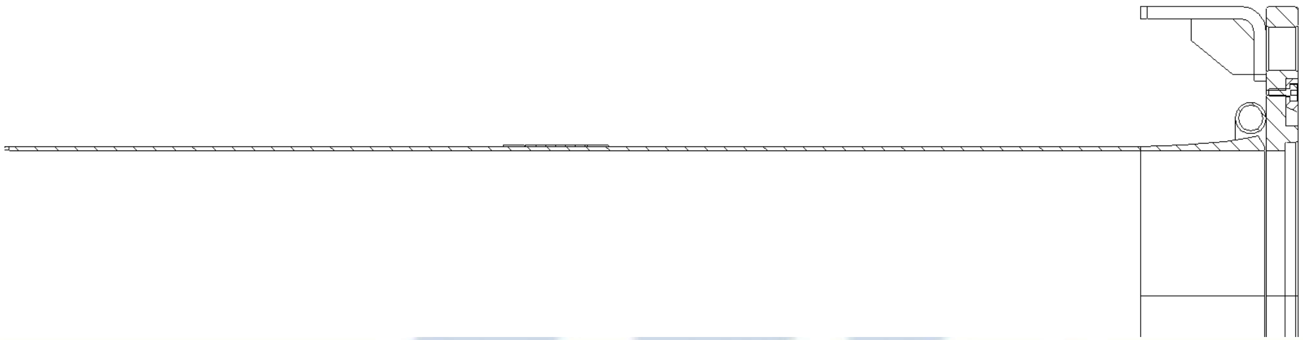

Large box concept

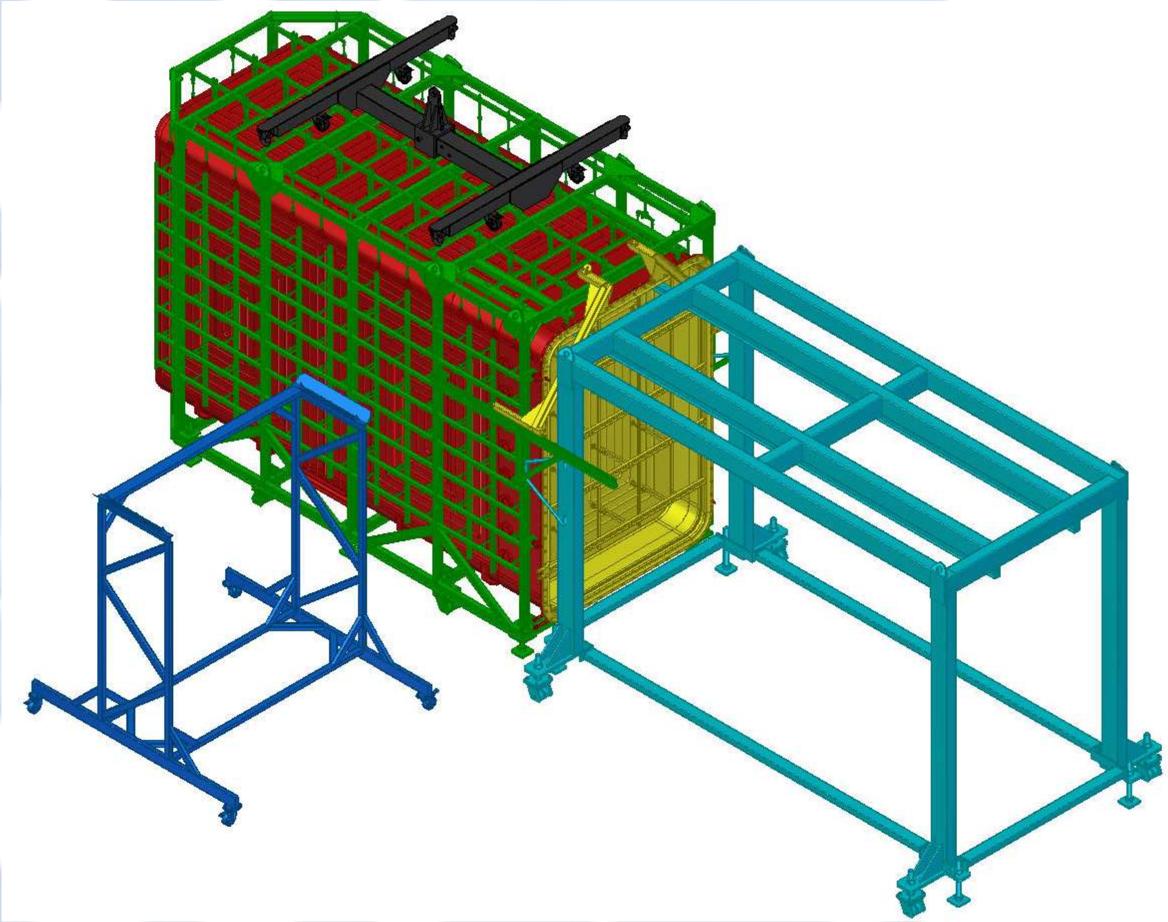

Large box suspending sollutions

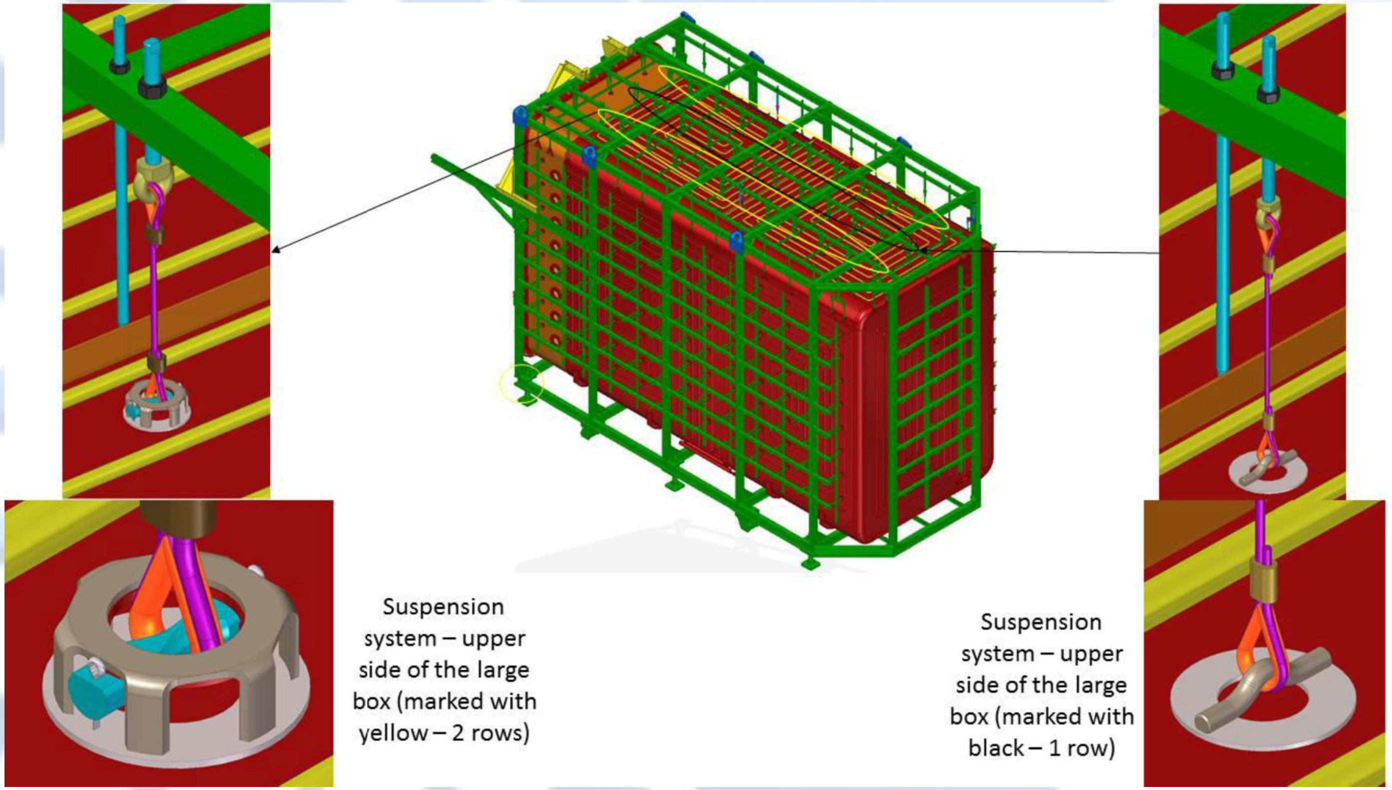

Suspension system – upper side of the large box (marked with yellow – 2 rows)

Suspension system – upper side of the large box (marked with black – 1 row)

Large box insid eframe

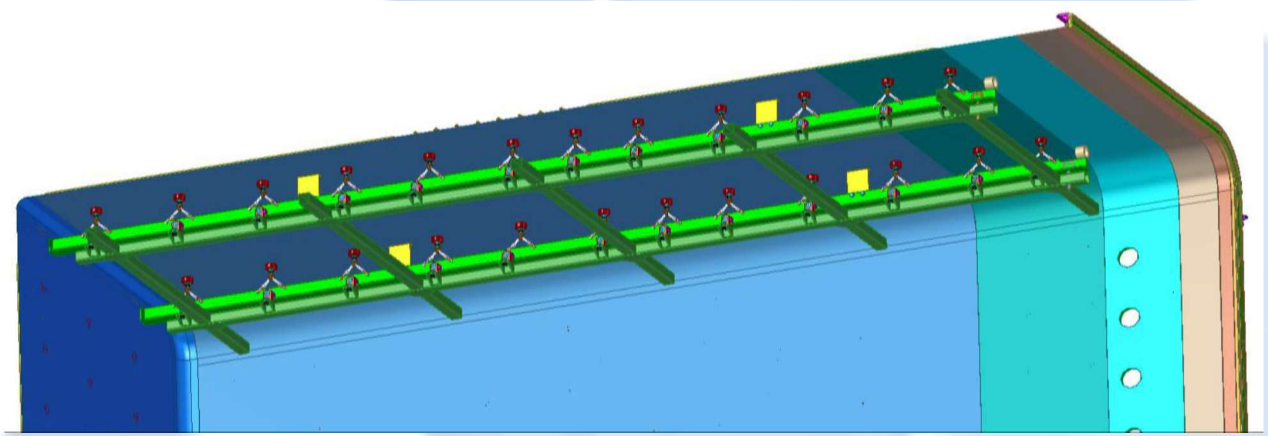

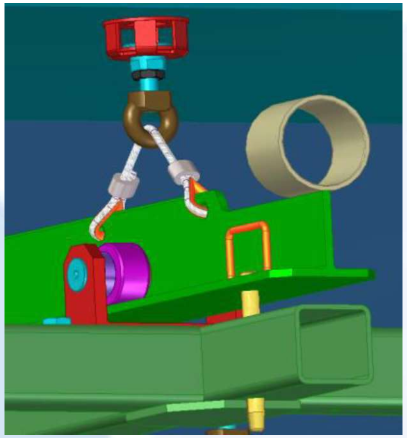

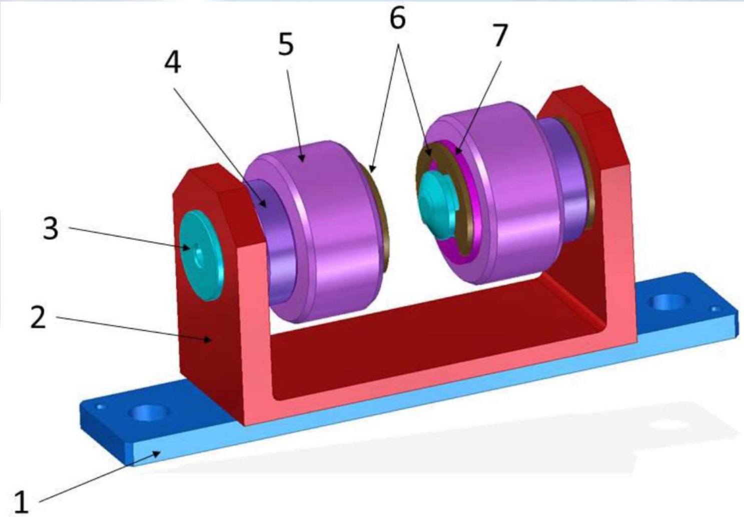

1 – Support plate
2 – Wheels support
3 – Ax
4 – Spacer
5 – Wheel
6 – Seeger retaining rings
7 – Washer

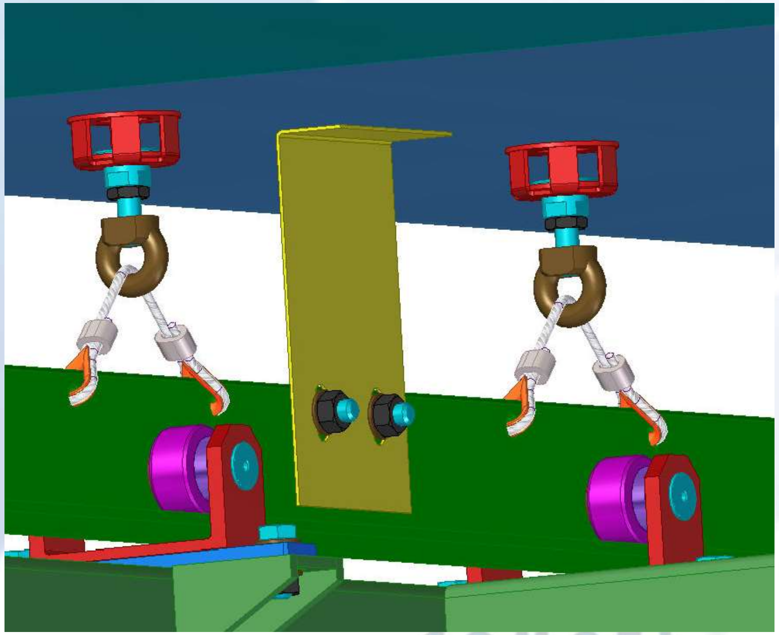

Thank you for your attention

Presentation 2506

COMOTI contribution on sealing system development

Radu Mihalache
Romanian Research and Development Institute for Gas Turbines COMOTI
220D, Iuliu Maniu Blvd, sector 6, 061126, Bucharest, Romania

Breadboard of Sealing Systems for a Phobos Sample Return Mission

Contract no. 4000115017/15/NL/Pa

COMOTI contribution on sealing system development

Romanian Research and Development Institute for Gas Turbines COMOTI, Bucharest, Romania

Eng. Radu Mihalache

Content

- Project and mission overview
- Sealing methods analysis and trade-off
- Seals characteristics – system dimensioning
- System components
- Closing operation analysis
- Further steps

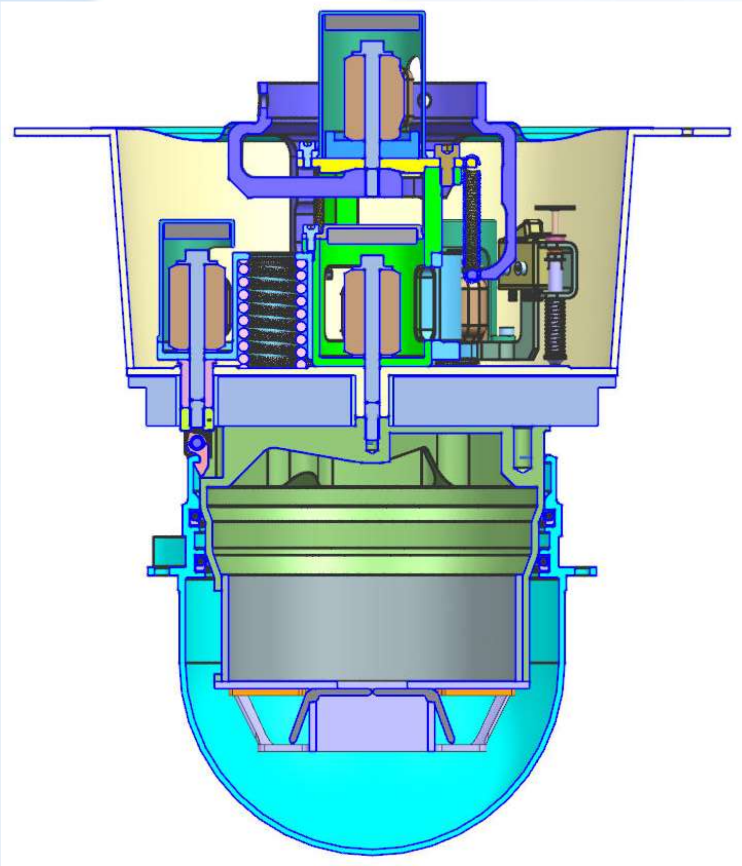

Project and mission overview

MREP 2 – Mars Robotic Exploration Preparation -2

Objectives:
- to reinforce the Europe's position in Mars robotic exploration
- to prepare for a European contribution to future international Mars Sample Return mission

Phobos Sample return mission

Objective
- to collect and return Phobos' surface material in access of 100 g to Earth

Mars

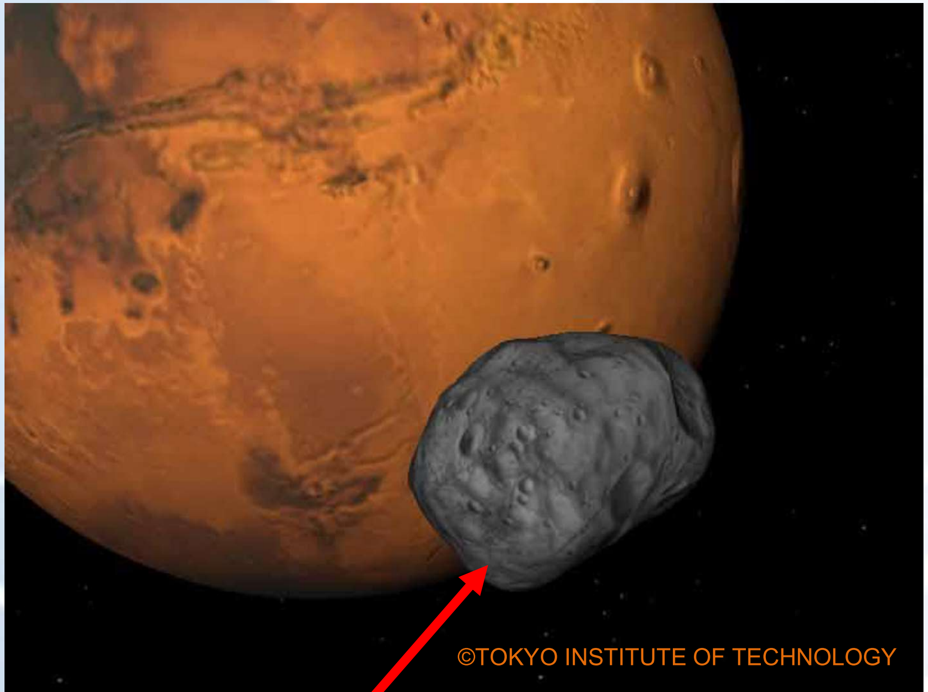

Phobos

Evaluation of Sealing Systems for a Phobos Sample Return Mission
Contract no. 4000115017/15/NL/Pa

Project and mission overview

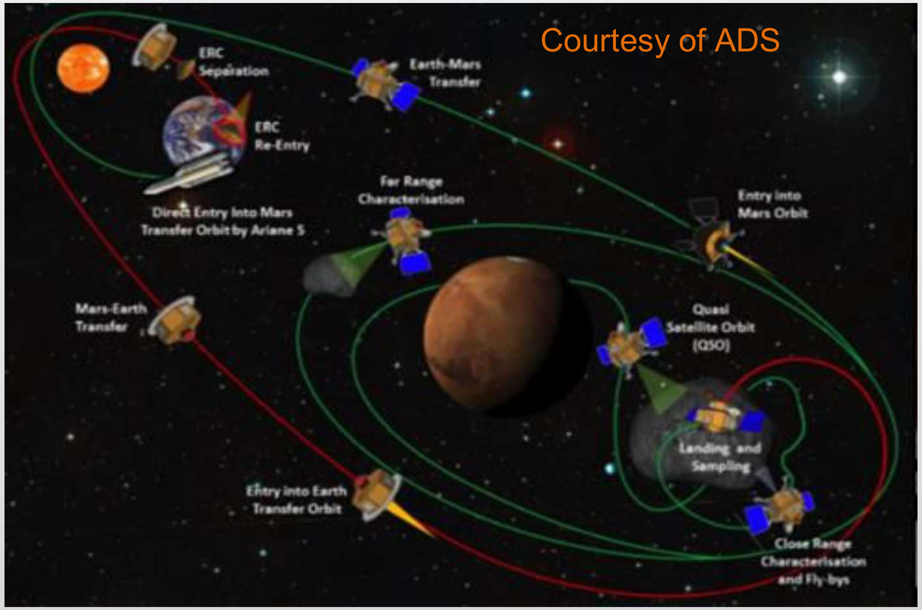

Landing module

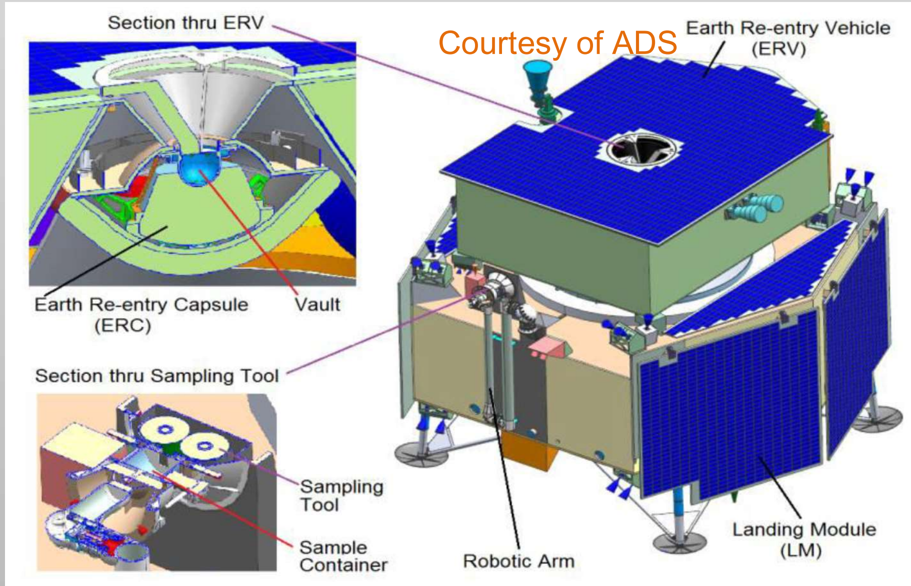

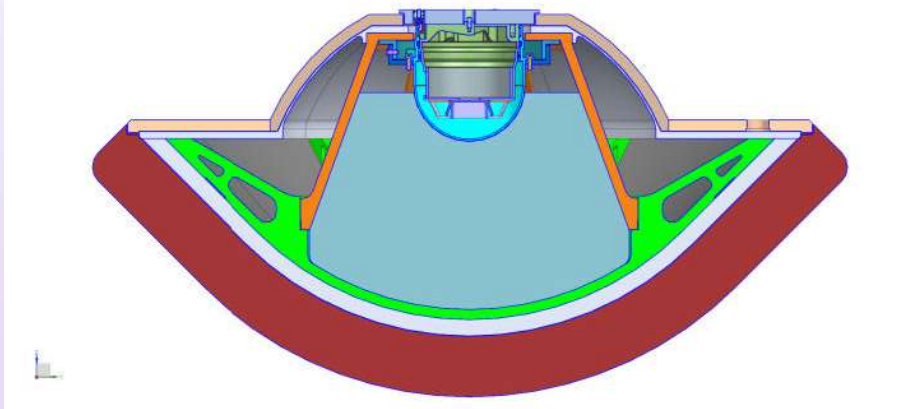

Earth Re-entry Capsule

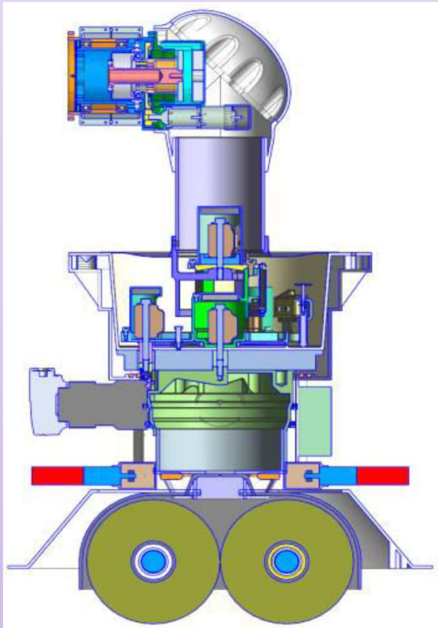

Robotic Arm and Sampling tool

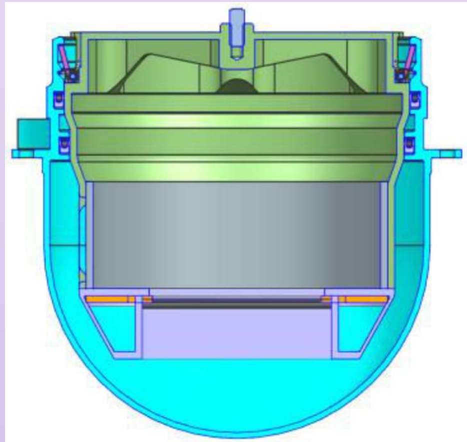

Vault closed

Project and mission overview

Phase 1: Evaluation of Sealing Systems for a Phobos Sample Return Mission

Kick-Off Meeting – 1st October 2015

11 months – phase finished

TRL: 2-3

Phase 2: Breadboard of Sealing Systems for a Phobos Sample Return Mission

Kick-Off Meeting – 1st October 2016

23 months – phase under implementation

Target TRL: 5

Specific requirements

- No particle or droplet of a fluid > 1μm shall escape or enter the vault
- The vault shall have a maximum mass of 2.0 kg including 20% margin
- Robotic arm capabilities (for vault closing) – 40 N pushing force and 5 mm radial misalignment
- The vault shall withstand a shock load of 2000g for 10 ms without failure

Sealing methods analysis and trade-off

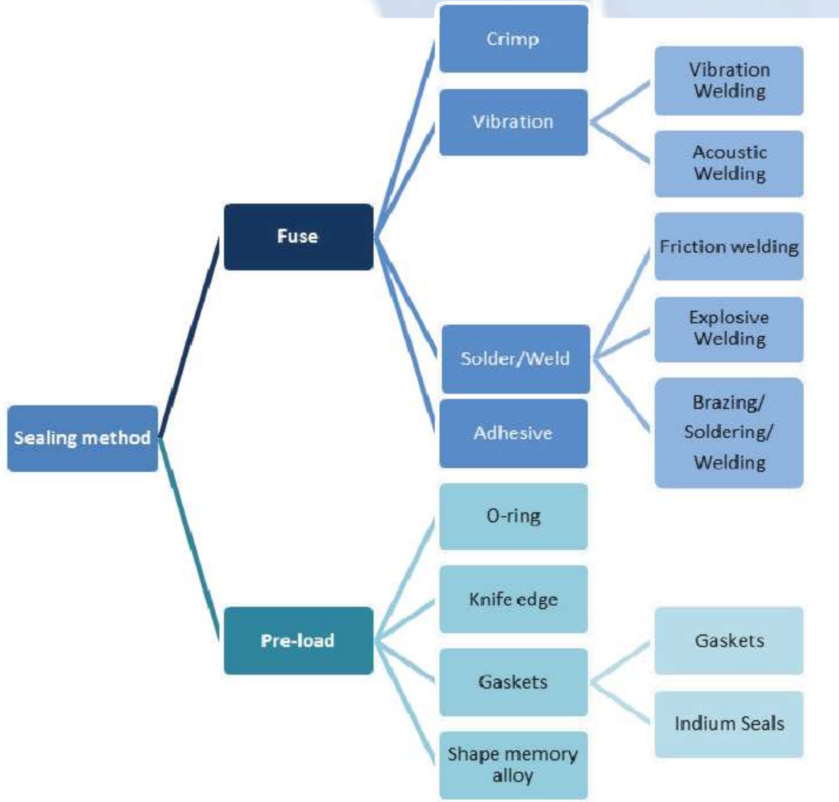

Criteria used in sealing methods analysis

- Introduction and general presentation;
- Advantages and disadvantages;
- Relevant values;
- Other uses of the method in space applications;
- Conclusion.

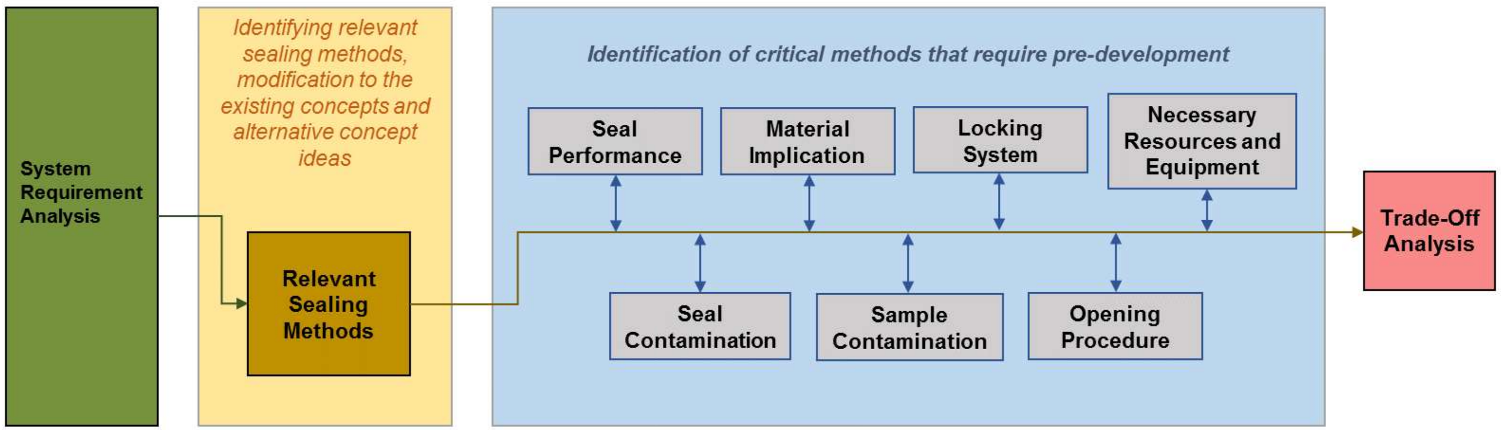

Sealing methods analysis and trade-off

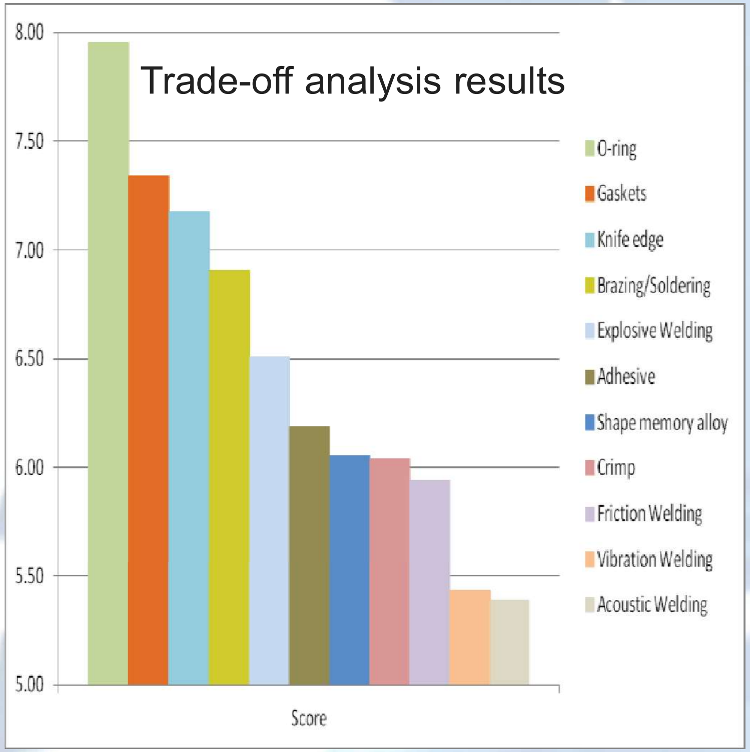

- Sealing system trade-off results
- Required pushing forces for:
  - ✓ face seal with O-ring;
  - ✓ radial seal with O-ring;
  - ✓ radial seal with composite gasket;
  - ✓ metallic gasket;
  - ✓ radial seal with metallic gasket;
- *Minimum required force for 2 radial seals – around 2000 N*
- Robotic arm capabilities

Mechanical press device is needed

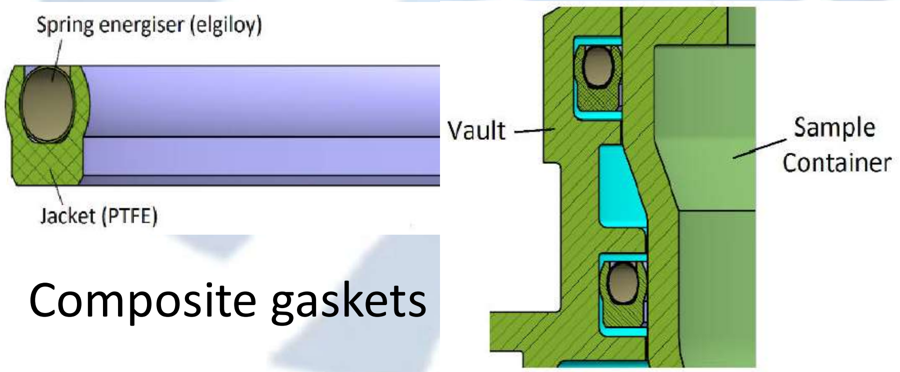

Composite gaskets

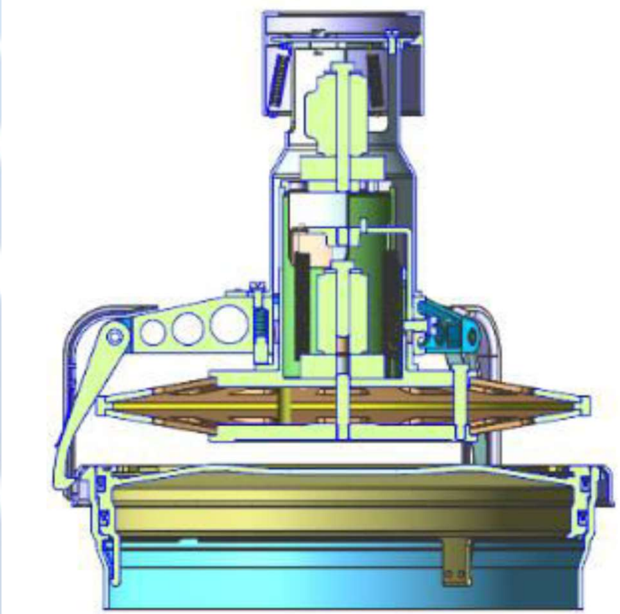

Mechanical press concept

Seals characteristics – system dimensioning

Initial concept

Mechanical Press with Diaphragm springs

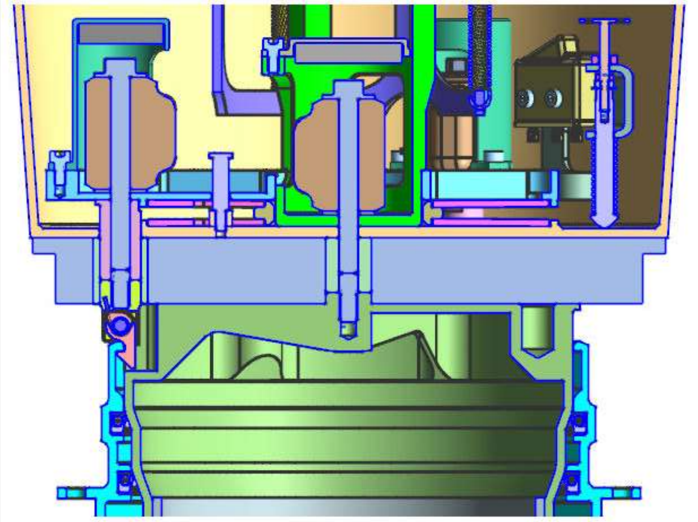

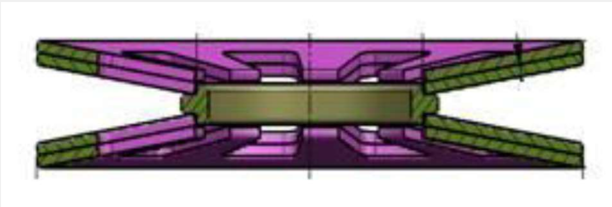

Specifications

-a diameter > 160mm is required;

-special design and calculus are necessary;

-spring characterization tests are required;

-impossibility of obtaining forces larger than 1000N.

Actual concept

Mechanical Press with Helical compression springs

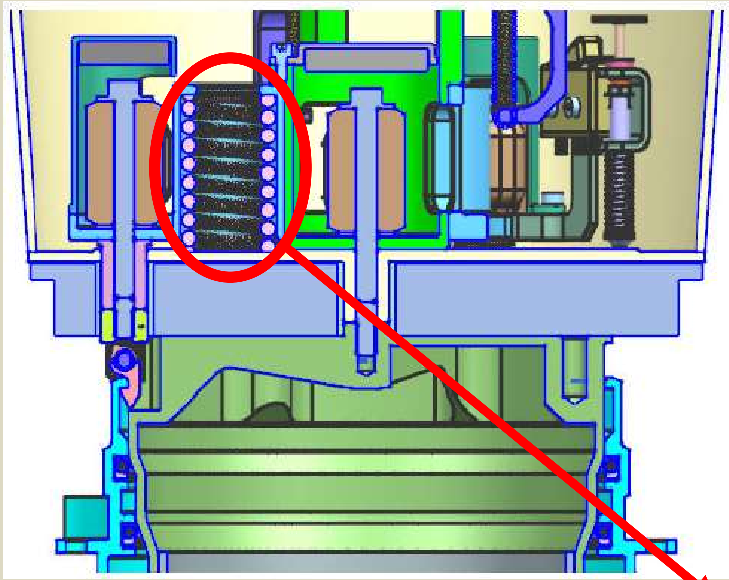

Diameter = approx. 100mm

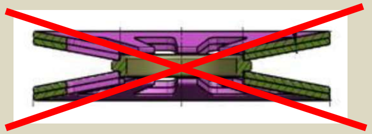

Specifications

-COTS elements;

-characterization tests are not required;

-low risks;

-available in different dimensions and specifications.

System components

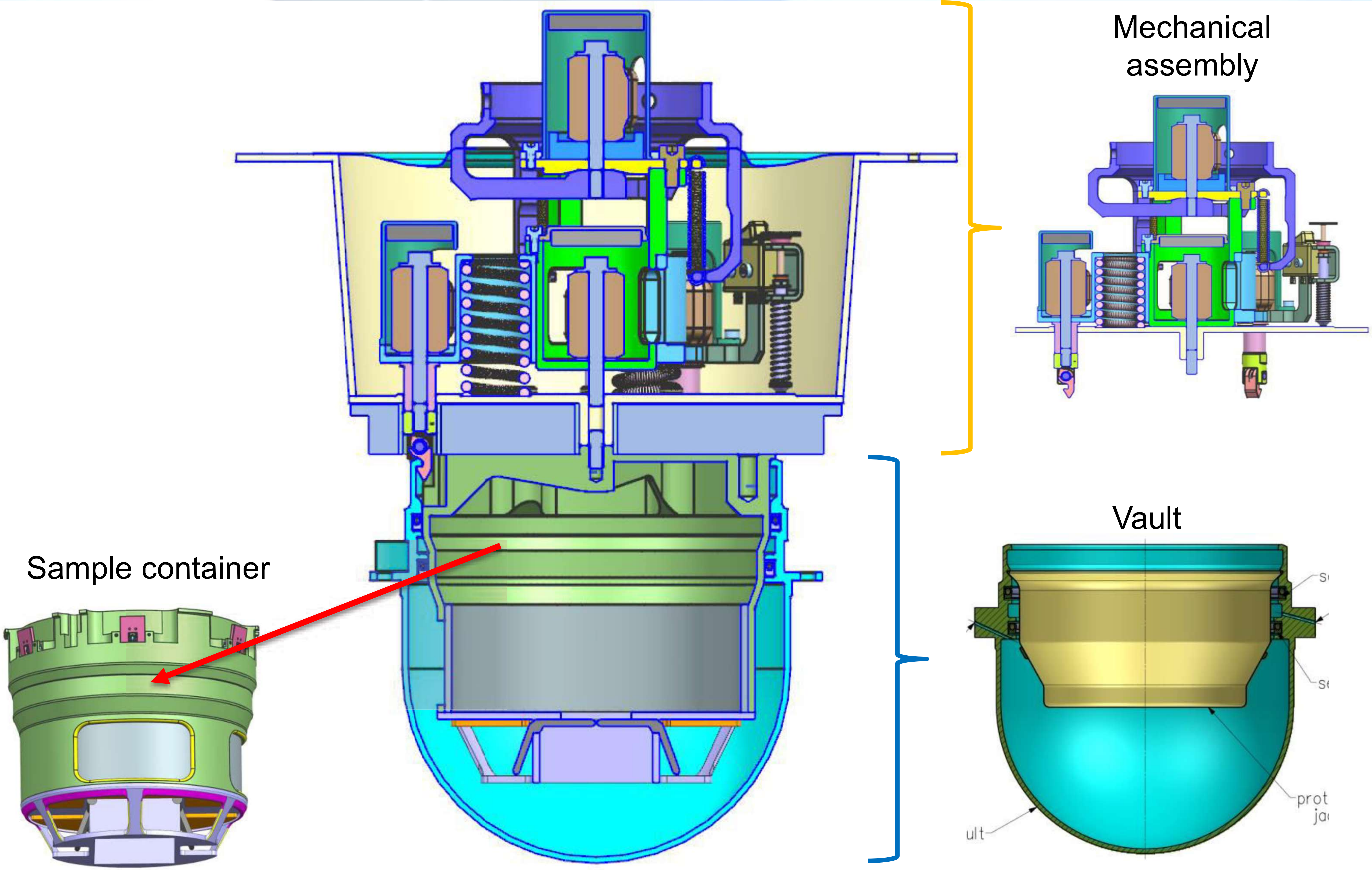

System components – Vault

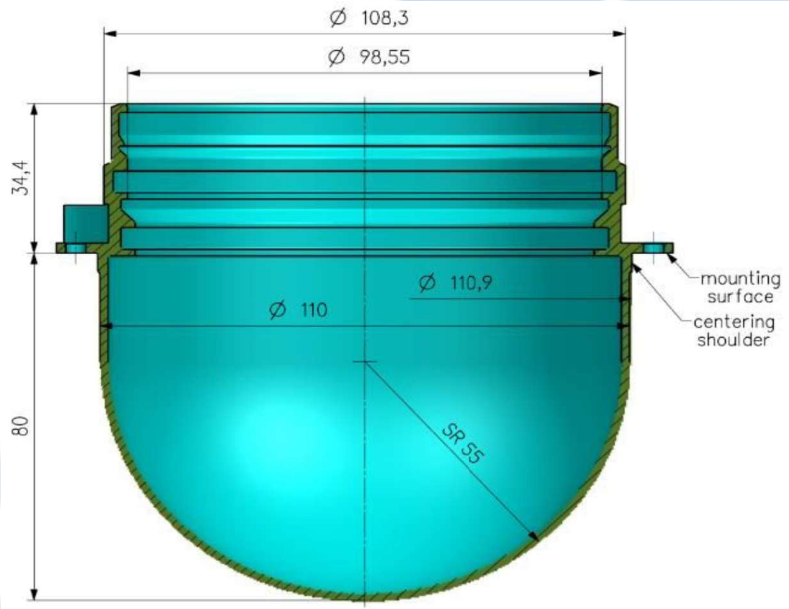

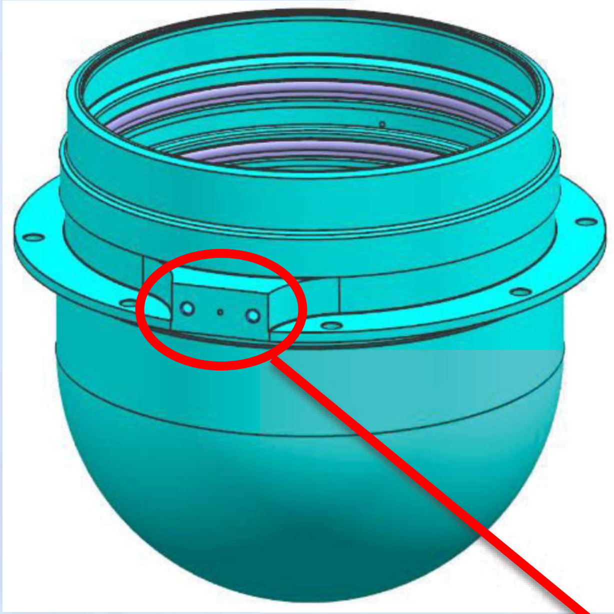

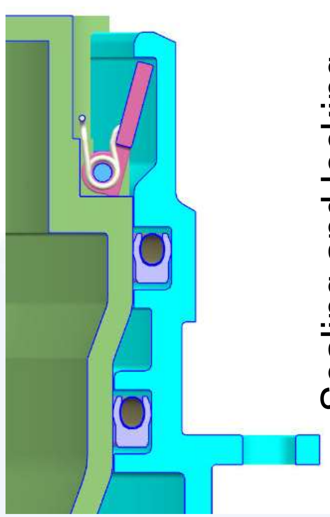

Sealing and locking elements detail

Leak ports for qualification and acceptance.

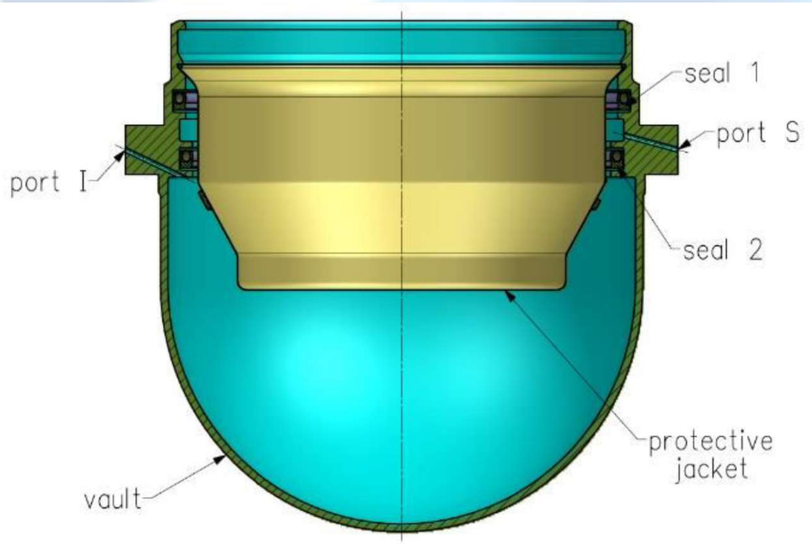

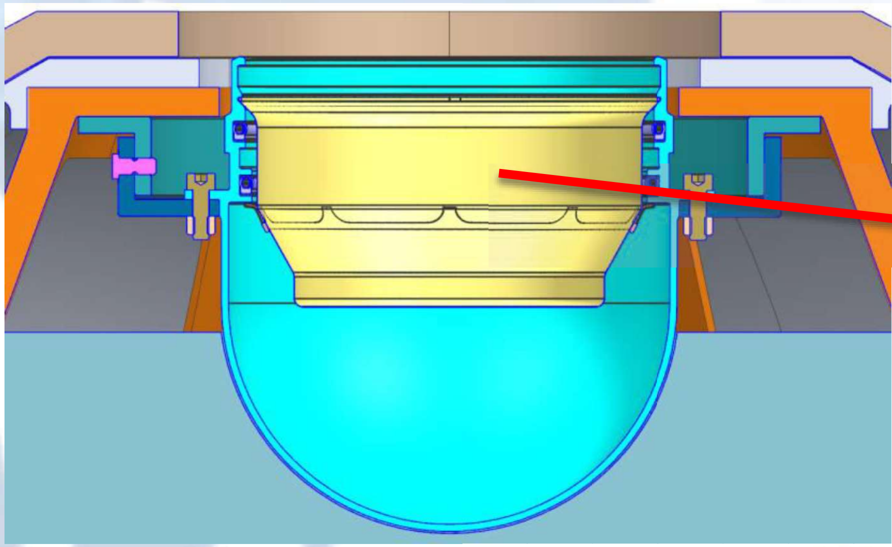

Dust (Regolith) Protection Jacket

System components – Sample Container

COMOTI design (green)

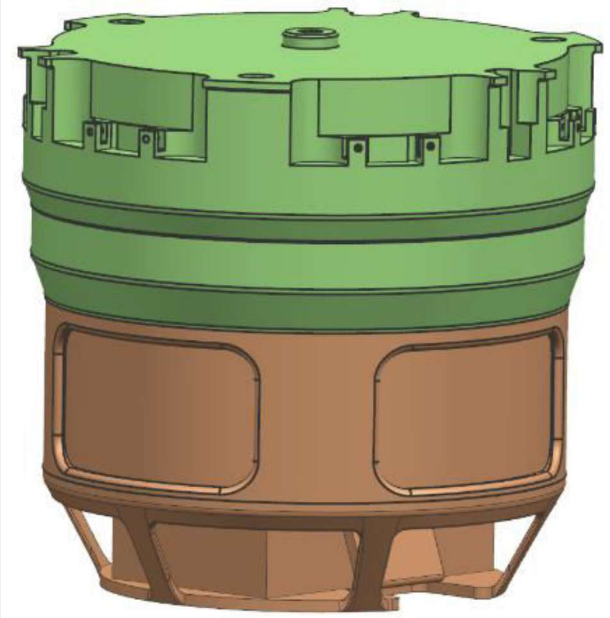

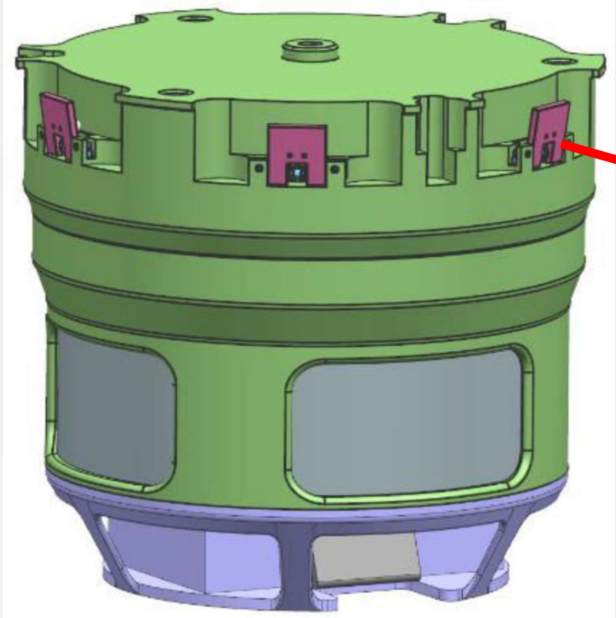

Pawl assembly

Airbus design (brown)

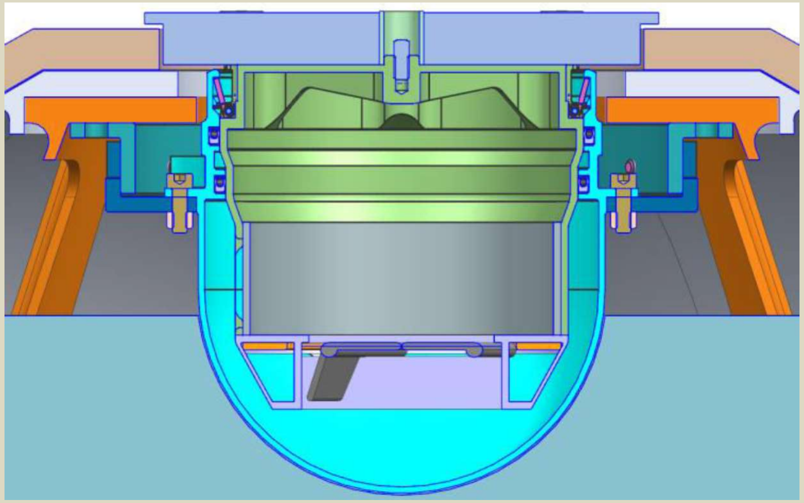

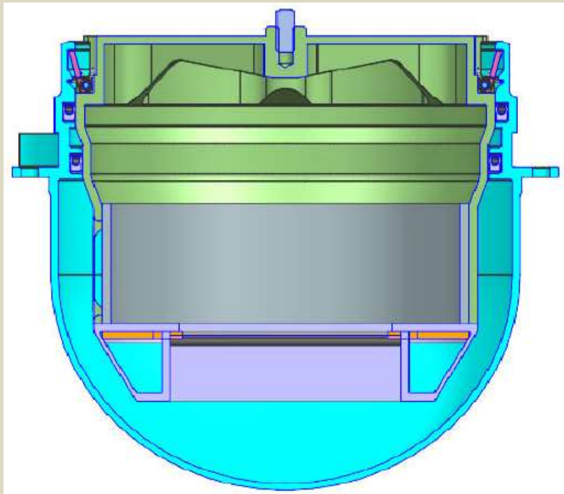

Vault closed with SC

System components – Mechanical assembly

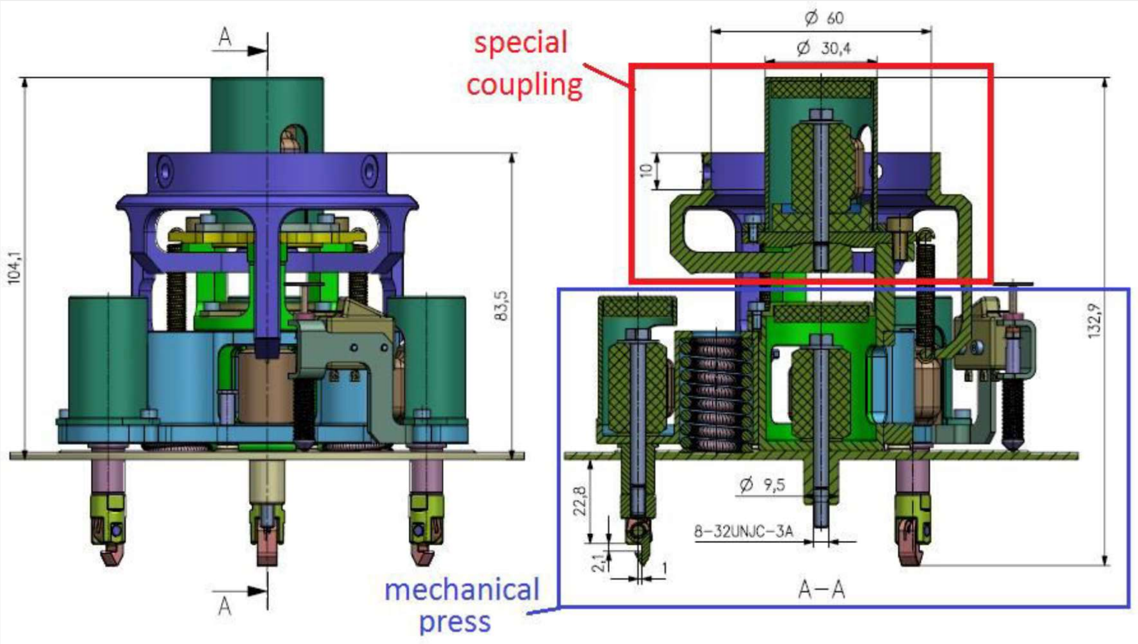

Mechanical Assembly:

- ➢ Special coupling
- ➢ Mechanical press

Mechanical Assembly:

- ❑ Mechanical parts
- ❑ Electrical parts
  - ❖ Frangibolts
  - ❖ Micro-switch

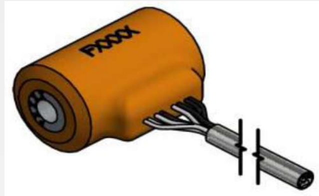

TiNi Aerospace Frangibolt FC2

Main Joints foreseen in the mechanical assembly

a) **Joint S** between Sample Container and Spring Body

b) **Joint H** between the Hook support and the Spring Body

c) **Joint C** between the special coupling's bodies

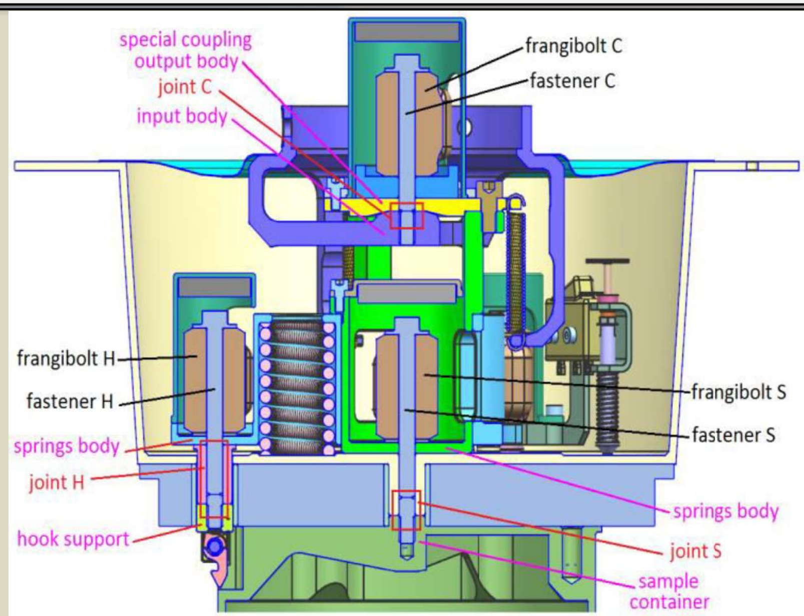

System components – Special Coupling

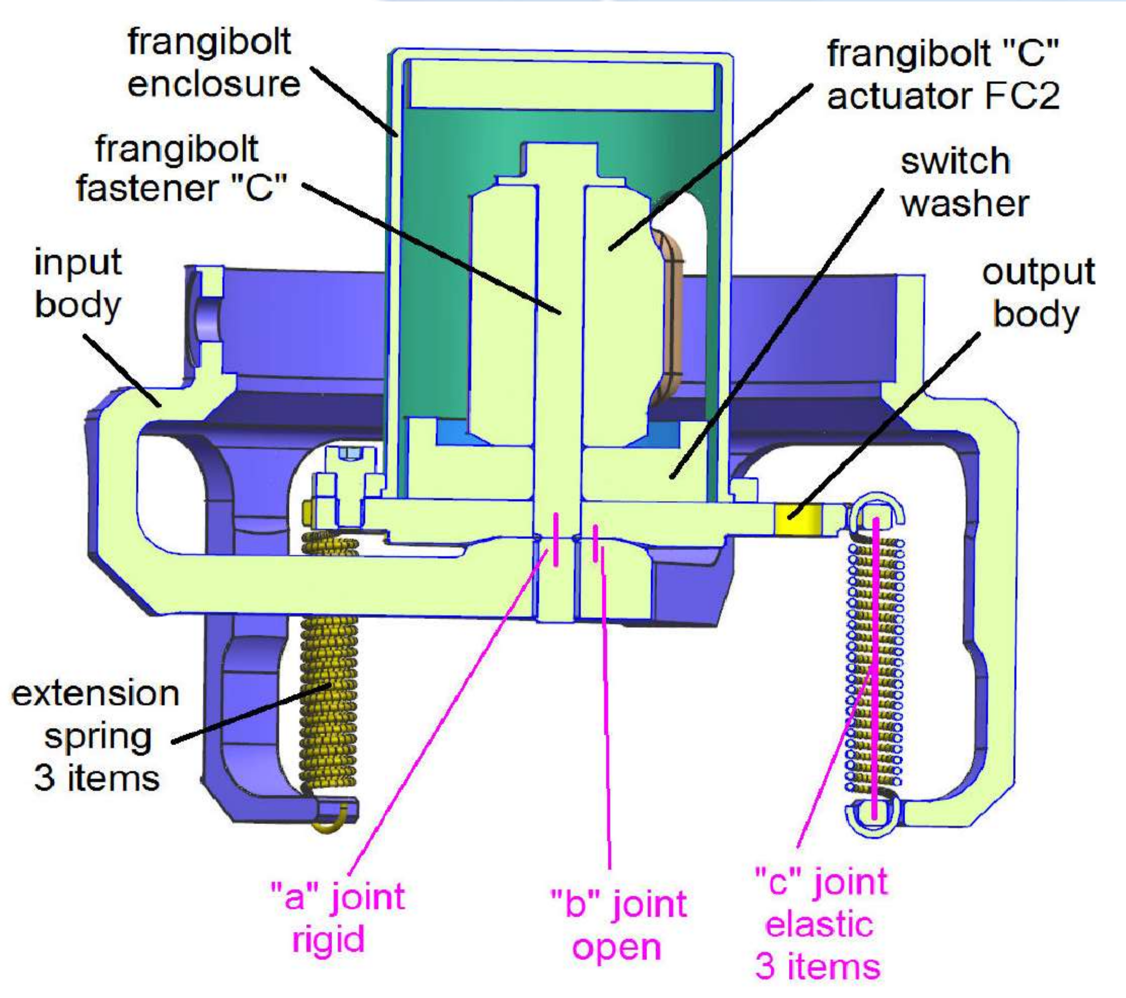

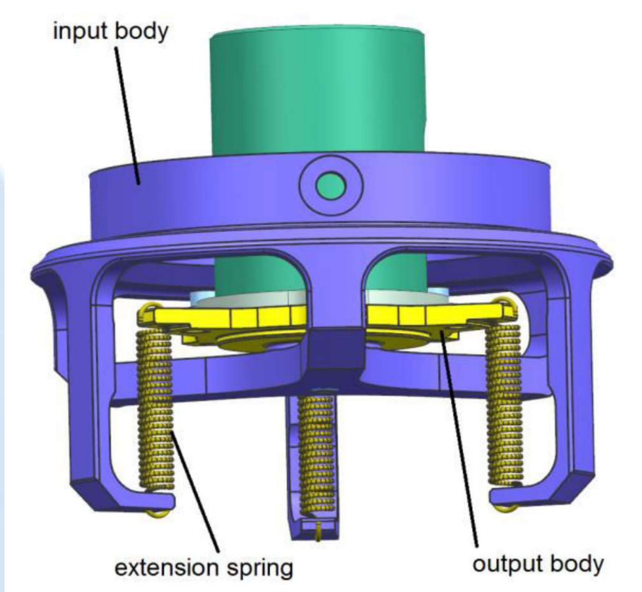

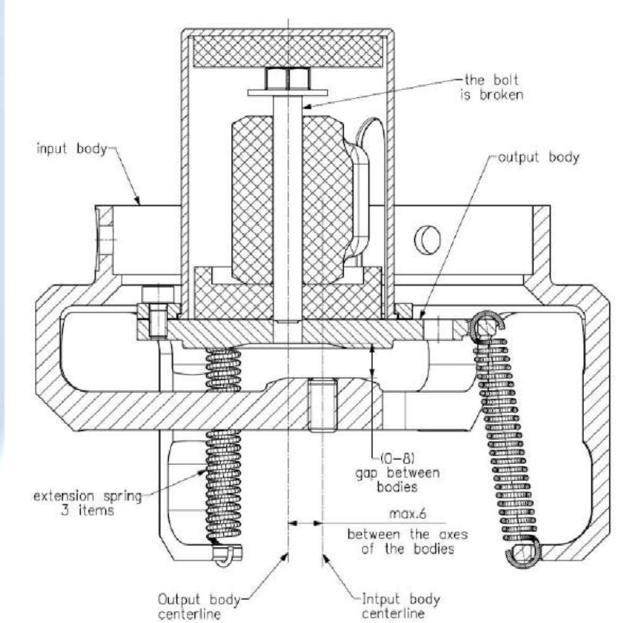

Special Coupling in free state

Position errors of the Robotic arm which should be compensated:
- max. 5 mm radial;
- max.1,5º angular.

Breadboard tests are required

System components – Mechanical Press

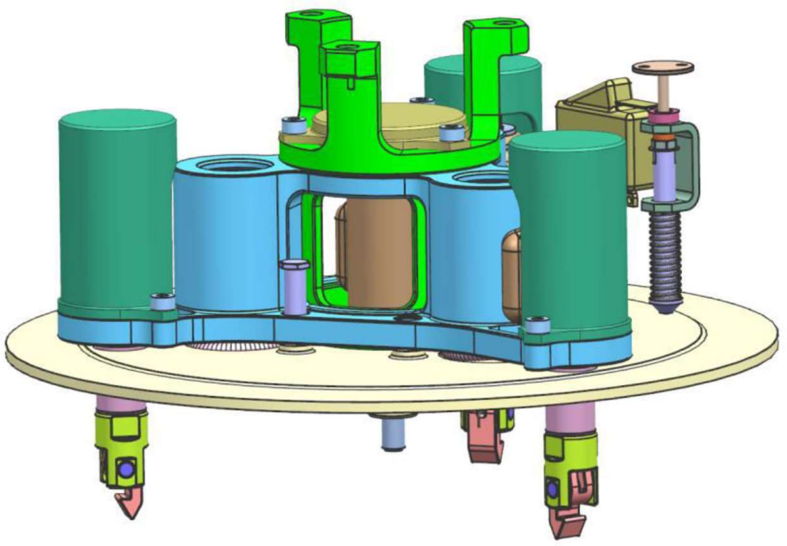

Mechanical Press (compressed springs)

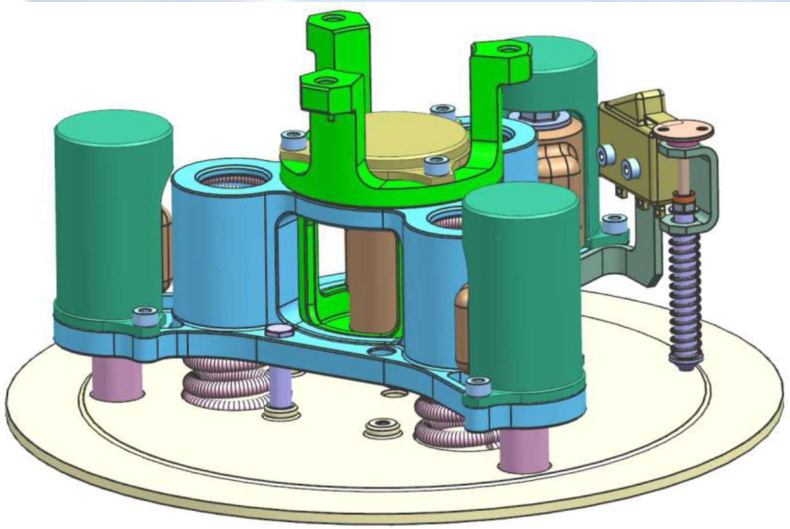

Mechanical Press (extended springs)

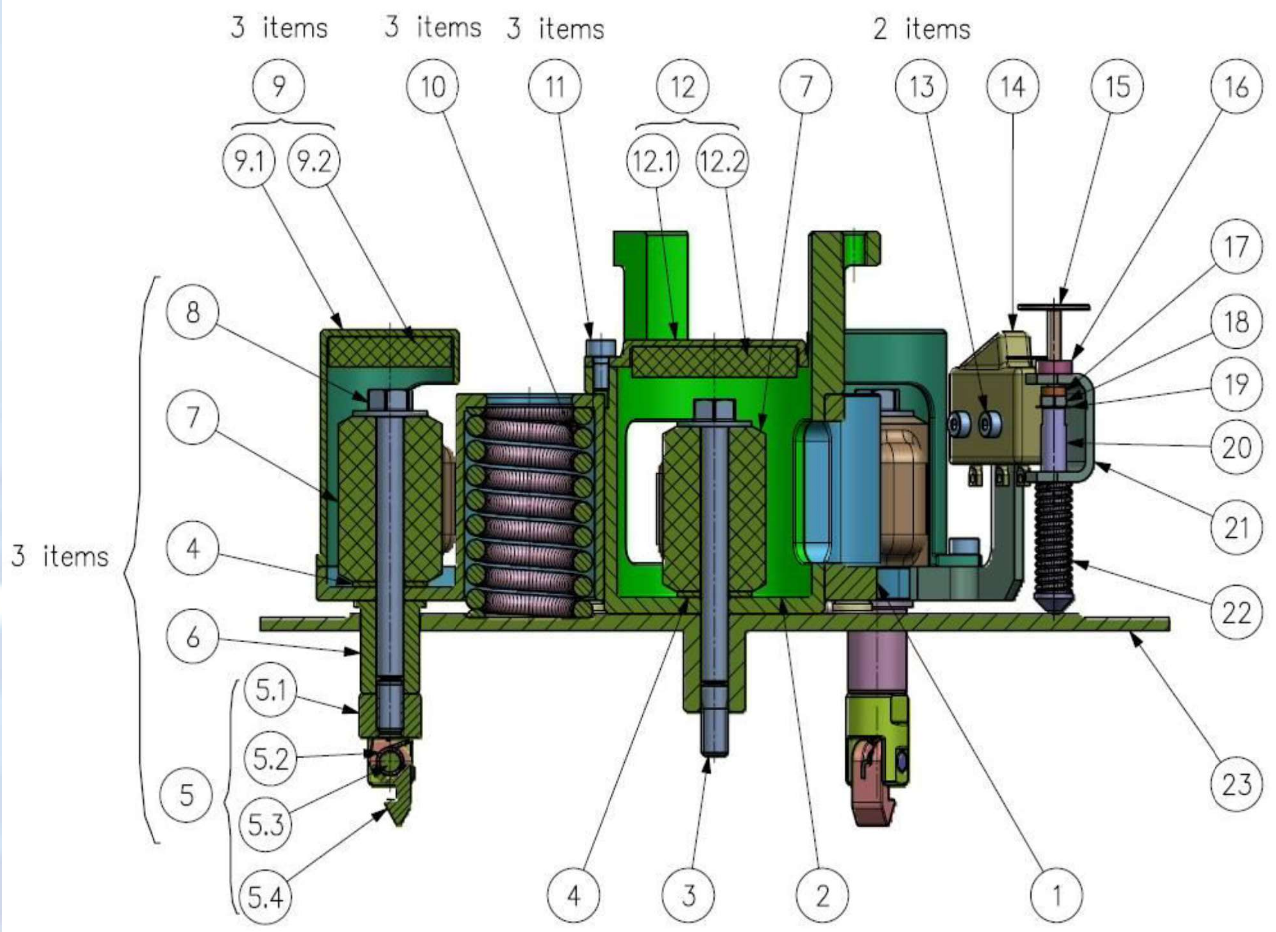

- One shot device;
- Contains mechanical and electrical components;
- Estimated mass: 573,5 grams;
- Overall dimensions: ϕ140 x 87,5 mm

Closing operation - paths

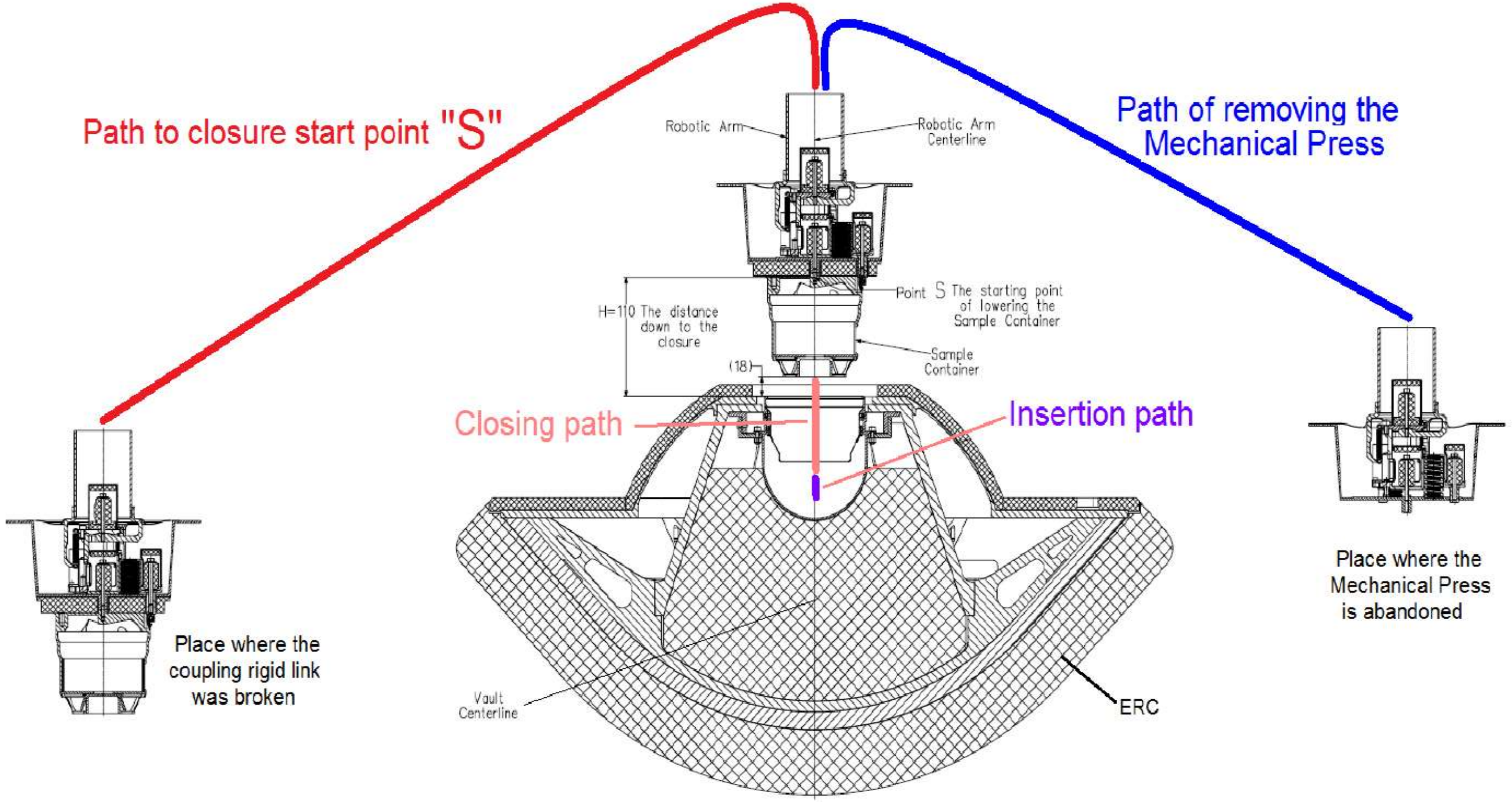

-Robotic Arm: Bringing path, Closing path and Removing the Mechanical Press
- Mechanical Press: insertion path

Sample Container paths run for the closing operation

Vault closing phases

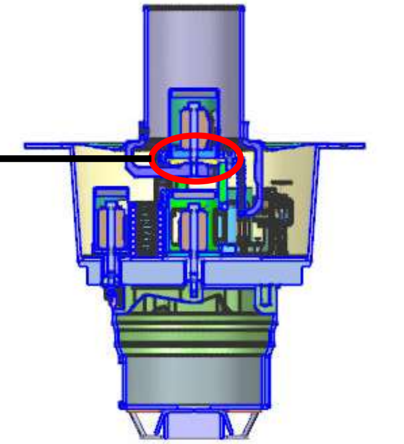

Phase A
breaking the rigid joint of the special coupling only coupling is shown

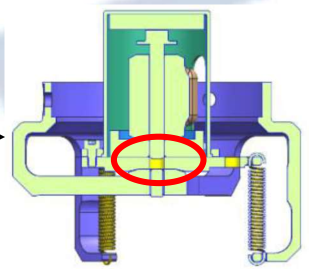

Special coupling almost free state

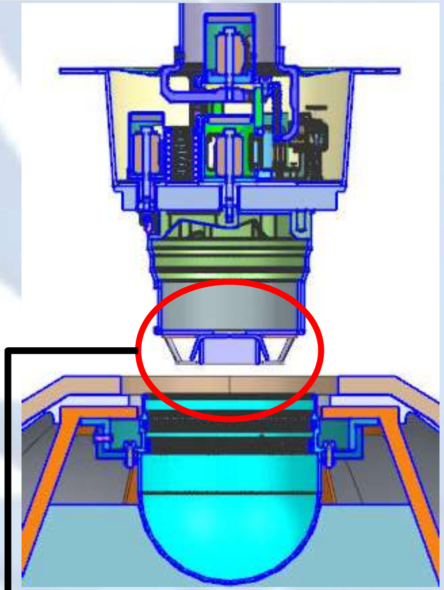

Phase B
placing the Sample Container over the ERC

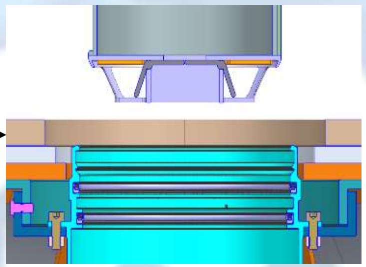

Sample Container position before closing

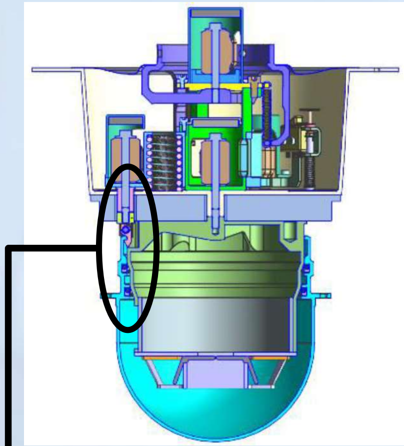

Phase C
capturing the Vault with the Mechanical Press, using the hooks

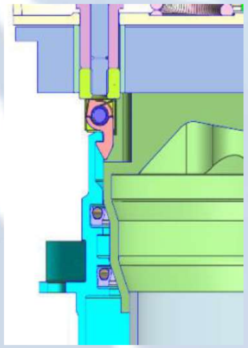

Sample Container attached to the Vault

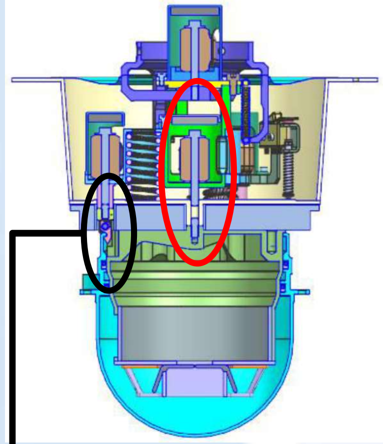

Phase D
inserting the Sample Container in the Vault

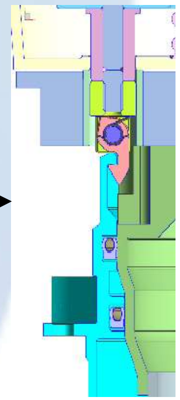

Vault closed with the MP attached

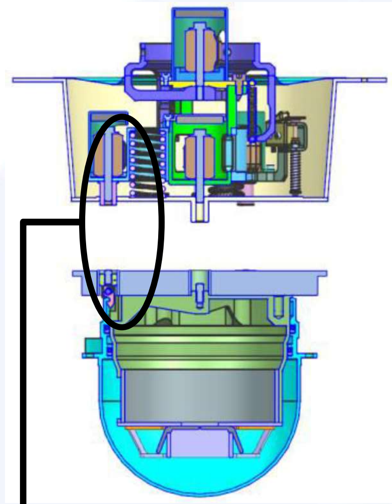

Phase E
remove the Mechanical Press

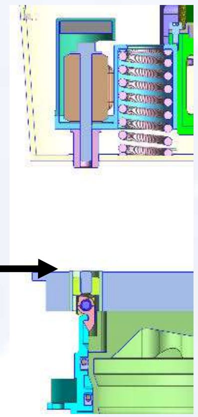

Vault closed and MP detached

Further steps

Design optimization

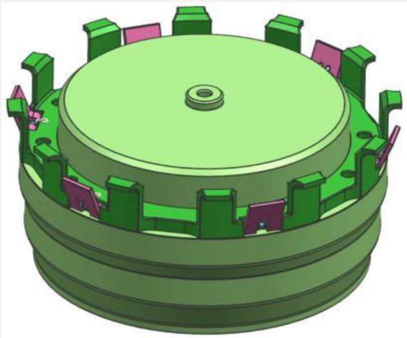

Development tests

- Closing forces measurement;
- Insertion forces measurement;
- Compression spring stress relaxation.

Breadboard manufacturing

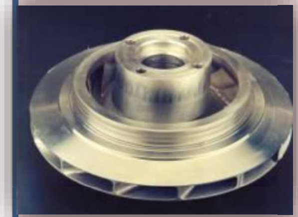

Validation tests

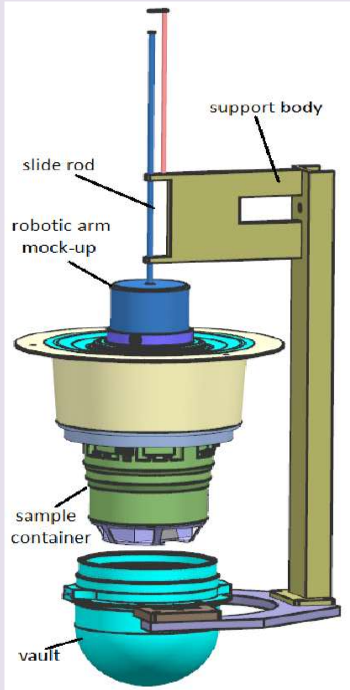

Closing device used for testing

Further steps – Test plan

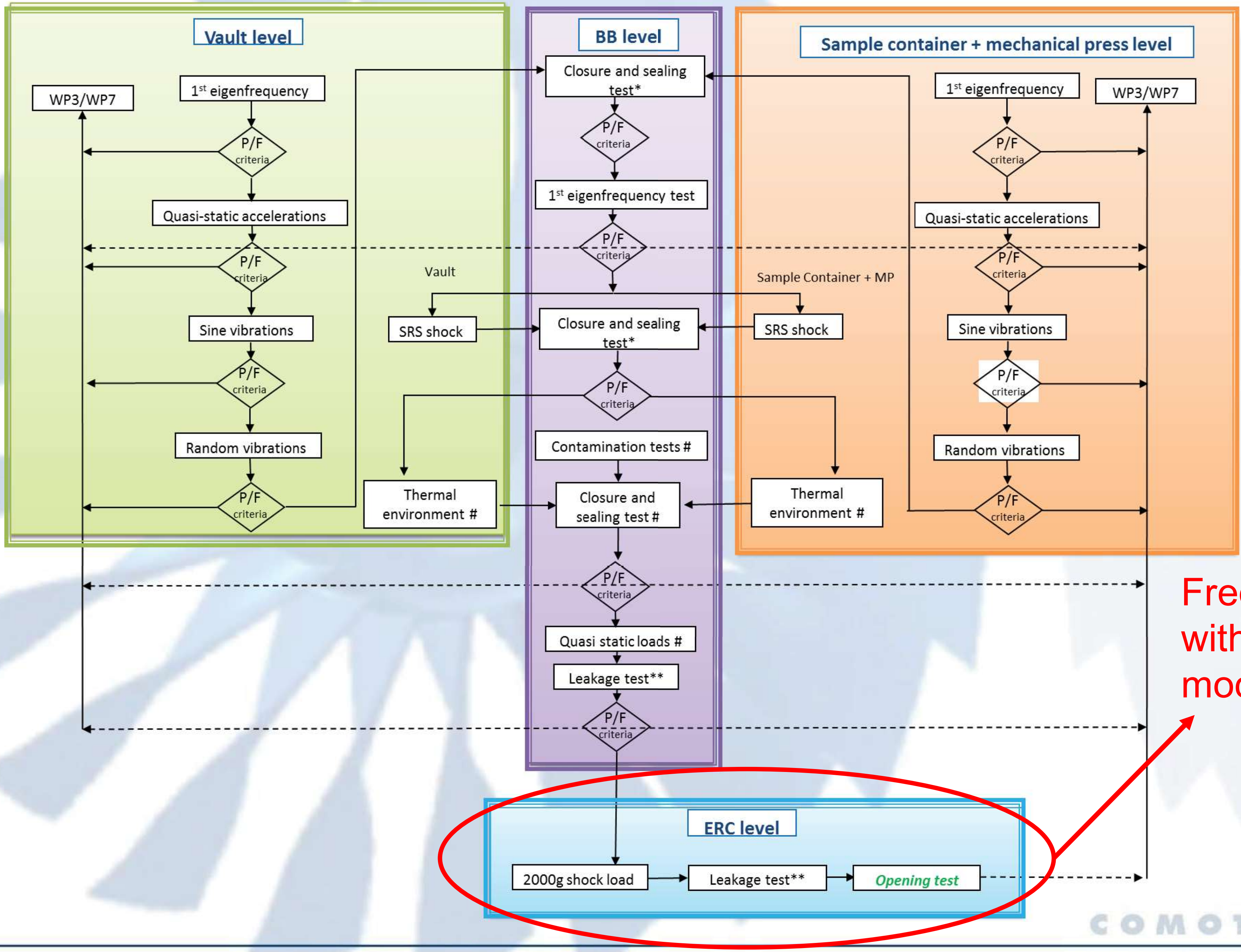

Free fall test with ERC mock-up

Further steps – Free fall test

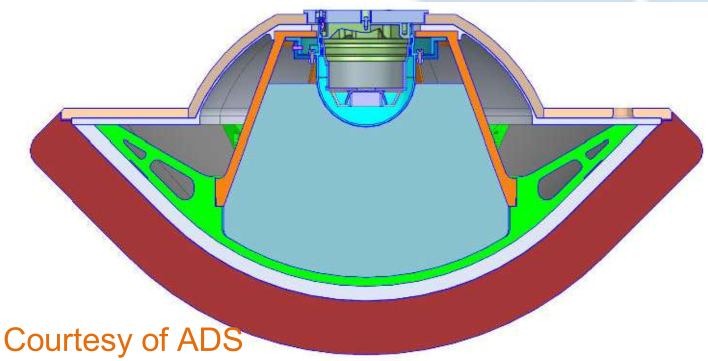

Courtesy of ADS

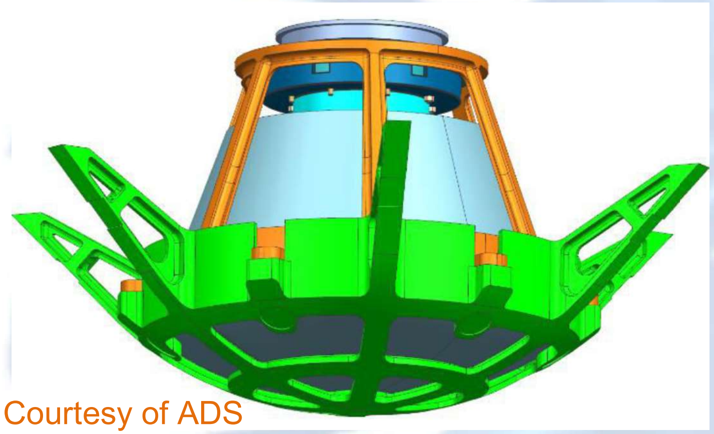

Courtesy of ADS

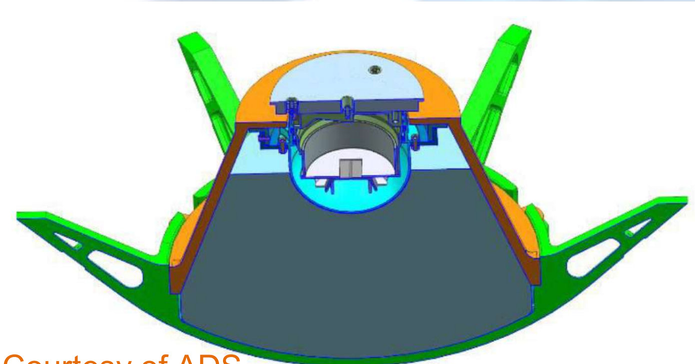

Courtesy of ADS

ERC structure

Fuse system
(800g, 1600g, 2000g)

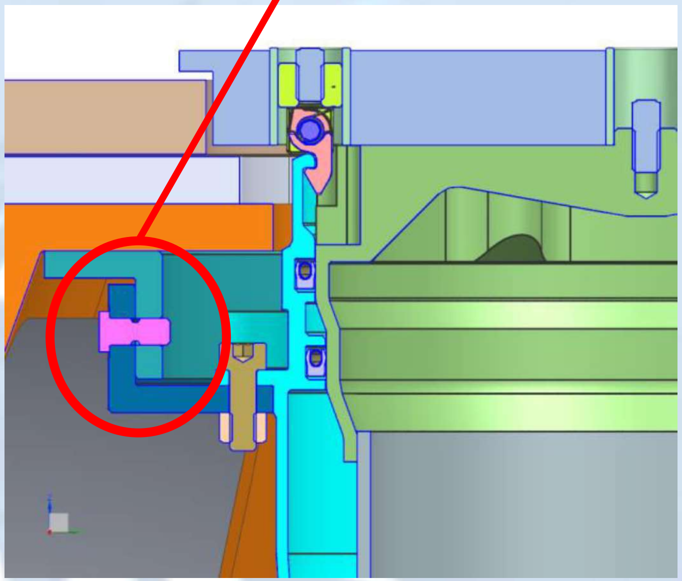

ERC mock-up will be manufactured by COMOTI

2000 g free fall –trade-off

-chimney tower

-crane

-helicopter

-mountain gorgeous

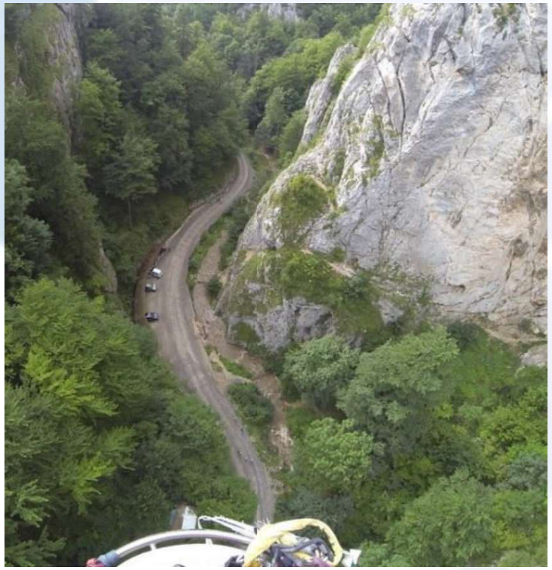

140m height

Acknowledgments

- ESA and Airbus Defense and Space UK
- Special thanks to Mr. Sanjay Vijendran and Emanuele Piersanti for their continued support and patience

Thank you for your attention

- Questions?

Presentation 2507

OrbiPro - accurate orbital propagator for modelling the effect of various perturbations for GNC and AOCS system's design

Lucian Bărbulescu, Alin Buțu, Mădălin Mămuleanu, Sorin Scorțan – CS ROMANIA
Thierry Ceolin, Roberto Alacevich – CS Systčmes d'Information
Jonathan Grzymisch – ESA/ESTEC

OrbiPro - accurate orbital propagator for modelling the effect of various perturbations for GNC and AOCS system's design

Lucian Bărbulescu, Alin Buțu, Mădălin Mămuleanu, Sorin Scorțan – CS ROMANIA
Thierry Ceolin, Roberto Alacevich – CS Systèmes d'Information
Jonathan Grzymisch – ESA/ESTEC


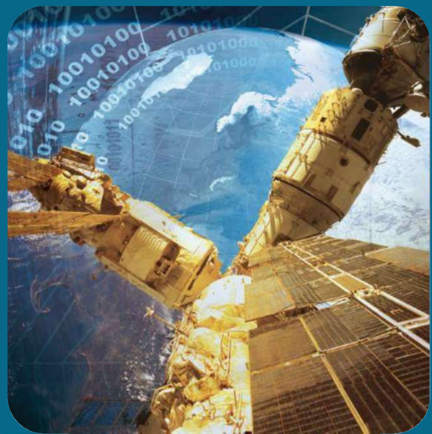

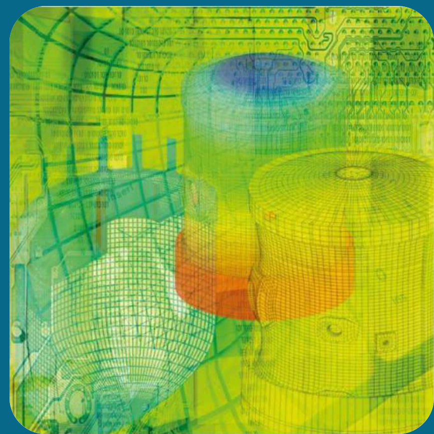

CEAS 2017, 16-20 OCTOBER 2017

AGENDA

- Introduction
- OrbiPro features
- Validation
- Conclusions and Future Works

INTRODUCTION

1

Page 250

MOTIVATION

- An accurate propagator is required for the computation of spacecraft's trajectory and attitude

- Additionally, the propagator should be
  - Flexible and configurable
  - Able to compute trajectories around main celestial bodies
  - Able to compute inter-planetary trajectories

- OrbiPro toolbox
  - A Matlab toolbox which implements a numerical propagator with configurable perturbations, attitude profiles, frames and time scales
  - Follows an object oriented programming approach
  - Requires MATLAB R2016b or newer

ORBIPRO FEATURES

2

Page 252

ORBIPRO FEATURES

- The main features of OrbiPro are
  - Numerical propagator
  - Different representations of orbital elements
  - Different spacecraft representations
  - Perturbations
  - Attitude profiles
  - Event detection
  - Several inertial and non-inertial frames
  - Several timescales
  - Determination of global perturbing force and torque for a given trajectory

ORBIPRO FEATURES

➔ Numerical propagator

- Numerical integration of the equations of motion
- Can use any of the Matlab ODE Suite functions for solving nonstiff differential equations
  - Explicit Runge-Kutta (2,3) - the Bogacki–Shampine method (ode23)
  - Explicit Runge-Kutta (4,5) - the Dormand-Prince method (ode45)
  - Adams-Bashforth-Moulton PECE solver of orders 1 to 12 (ode113)
- It is possible to add new solvers if they have the same format
- Can detect events during propagation
- Configurable perturbations considered during integration
- Configurable format of the orbital elements during integration

ORBIPRO FEATURES

- Representation of the orbital elements
  - Three formats supported
    - Keplerian with true, eccentric or mean anomaly
    - Equinoctial with true, eccentric or mean longitude
    - Cartesian
  - Easy conversions between formats

- Spacecraft representation
  - Two formats
    - Spherical spacecraft
    - Convex body and solar panels

ORBIPRO FEATURES

➔ Perturbations

› Gravity potential of the central body

- Holmes-Featherstone model with user defined degree and order
- The spherical harmonics coefficients are read from a configurable external file
- The following formats are supported:
  - Eigen and EGM gravity field for Earth
  - SGM100i (SELENE mission) and PDS (GRAIL mission) for Moon
  - PDS (Messenger mission) for Mercury
  - PDS (Magellan mission) for Venus
  - PDS (Mars Reconnaissance Orbiter mission) for Mars

› Solid Earth Tides

- With or without pole tides

› Ocean Tides

- With or without pole tides and with user defined degree and order
- The harmonics coefficients are read from a configurable external file
  - FES2004 model supported

ORBIPRO FEATURES

➔ Perturbations

› Third Body

- Support for Sun, Moon and all major planets of the solar system
- Planetary ephemerides read from a configurable external file
  - Supported format: JPL DE 4xx
- Other formats can be added by implementing a file reader

› Atmospheric Drag

- Based on an atmospheric model
- Currently available atmospheric models
  - Jacchia-Bowman 2008 model for Earth
    - Geomagnetic storm and solar indices files provided by user or read from the official site
  - Martian Climate Database atmosphere model for Mars
    - Density read from user provided files in MCD format
  - VIRA model for Venus

ORBIPRO FEATURES

- Perturbations
  - Solar Radiation Pressure
    - Takes into account the penumbra/umbra of the central body
  - Albedo and Infrared Pressure
    - Value computed based on latitude and longitude for Earth
    - Average albedo and infrared for other planets (Mercury, Venus, Mars, Jupiter, Saturn, Uranus, Neptune)
  - Maneuvers
    - Impulsive maneuvers
    - Constant thrust maneuvers
    - Variable thrust maneuvers
      - Variable direction and thrust force
      - Interpolation is used to compute the maneuver direction ant thrust at a required date

ORBIPRO FEATURES

➔ Attitude profiles

- Predefined laws
  - Nadir pointing with possible Yaw compensation with respect to ground velocity or Yaw steering with respect to Sun
  - Celestial body center pointing, with possible spin
  - Fixed Cardan offsets with respect to Local Orbital Frames LVLH, VVLH or VNC
  - Inertially fixed
  - Tabulated from a file

- Computed by integration of the dynamic equations of motion
  - Rotation, rotation rate and rotation acceleration is computed along the propagation
  - The contribution of several torques is considered:
    - Gravity Gradient Torque
    - Magnetic Torque (for Earth only)
    - Aerodynamic Torque (for Earth, Mars and Venus)
    - Solar Radiation Torque

ORBIPRO FEATURES

➔ Event detection

- Several events are detected during propagation
  - Eclipse (umbra, penumbra and antumbra entry and exit)~~,~~
  - Ascending and descending node crossing~~,~~
  - Apogee and perigee crossing~~,~~
  - Alignment with some body in the orbital plane (with customizable threshold angle)~~,~~
  - Raising/setting with respect to a ground location (with customizable triggering elevation)~~,~~
  - Date~~,~~
  - Altitude crossing~~,~~
  - Impulse maneuvers occurrence
- It offers the possibility of slightly shifting the event occurrence time
  - Useful when some decisions must be made before or after the exact moment of an event

ORBIPRO FEATURES

➔ Frames

- Several frames are implemented
  - Geocentric Celestial Reference Frame (GCRF)
  - Celestial Intermediate Reference Frame (CIRF)
  - Terrestrial Intermediate Reference Frame (TIRF)
  - International Terrestrial Reference Frame (ITRF) with precession and nutation models from IERS 2010
  - EME2000 (J2000)
- Earth Orientation Parameters (EOP) are read from configurable external files
- The frames are organized in a tree-like structure with GCRF as root
- Each frame (except GCRF) defines the transformation to its parent
- New frames can be easily added

ORBIPRO FEATURES

- Time scales
  - Several time scales are implemented
    - International Atomic Time scale (TAI)
    - Terrestrial Time scale (TT)
    - Universal Time Coordinate scale (UTC)
      - Leap seconds are read from a configurable external file
    - Universal Time 1 scale (UT1)
  - Each time scale defines its offset from and to TAI
- Determination of global perturbing force and torque for a given trajectory and attitude profile
  - Spacecraft state and attitude read from external files
    - ESOC attitude and orbit format
    - Proprietary ASCII format

VALIDATION

3

Page 263

VALIDATION

- Several features validated against Orekit (www.orekit.org)
  - Low level space dynamics library written in Java
  - Open-source code developed and maintained by CS SI, currently at version 8.0
  - Selected by CNES for its next generation of flight dynamics systems, both for operational systems and for studies and mission analysis systems
  - Successfully used during the real time monitoring of the rendez-vous phase between the Automated Transfer Vehicle (ATV) and the International Space Station (ISS), by CNES and ESA
- For features not available in Orekit
  - Results validated against expected behavior from the literature

VALIDATION – TESTING METHODOLOGY

ROMANIA

- Use of Matlab R2016b for OrbiPro
- Several Matlab applications that uses OrbiPro toolbox are created and executed for each test
- OrbiProTester application written in Java, for running the equivalent tests in Orekit
  - JRE 1.8
  - Orekit version 7.1 and Apache Commons Math version 3.6
  - JFreeChart version 1.0.13 and JCommons version 1.0.16 (required by JFreeChart) for the plots
  - Apache Log4j version 1.2.17 for log messages
- Comparing the results obtained by OrbiPro toolbox with the results obtained by using the Orekit library

VALIDATION – TESTING METHODOLOGY

- Input data
  - Initial conditions of an orbit
  - The perturbation model
  - The initial date
  - The frame
  - The attitude used
  - The events
  - The duration of propagation
  - The state generation step
- Output data
  - The generated orbit ephemerides for the orbit initial date and for the duration proposed as initial conditions
  - Plots generated and saved as PNG files

VALIDATION – SOME EXAMPLES

- Validation test
  - Elliptical retrograde orbit with high inclination and high altitude apogee (Borealis 3hr)
- Other tests – see annex
  - Low Earth Orbit with Geopotential 2x0 and 30x30
  - Geostationary orbit with Third Body (Sun and Moon)
  - Geostationary orbit with Solar Radiation Pressure
  - Low Earth Orbit with Atmospheric Drag
  - Aerodynamic torque in Mars atmosphere
  - Interplanetary trajectory - Rosetta

VALIDATION

- Elliptical retrograde orbit with high inclination and high altitude apogee (Borealis 3hr)
  - Initial conditions:
    - Epoch: 1st, July 2000, 0 h, 0 min, 0 sec
    - Time scale: UTC
    - Orbit type: keplerian
      - $a = 10559.2710$ km — $\Omega = 280.0°$
      - $e = 0.345705$ — $\omega = 270.0°$
      - $i = 116.565°$ — $M = 0.0°$
  - Frame: EME2000
  - Satellite characteristics: Mass = 1000 Kg, Shape: 1.0 x 1.0 x 1.0 m, No Solar Arrays
  - Attitude: EME2000 Aligned
  - Duration: 7 days
  - Forces model:
    - Central body: Earth Newtonian force
    - Central body: Gravity potential 8 × 8
    - Atmospheric drag: Cd = 2.1
    - Solar radiation pressure: Cr = 1.2
    - Third body: Lunar-Solar point mass

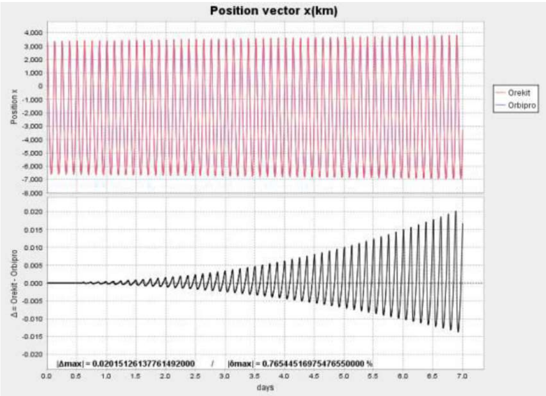

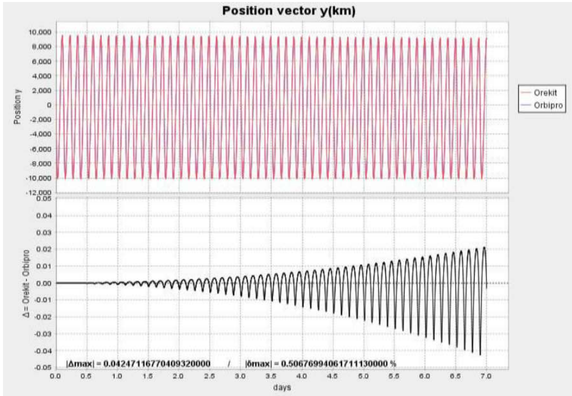

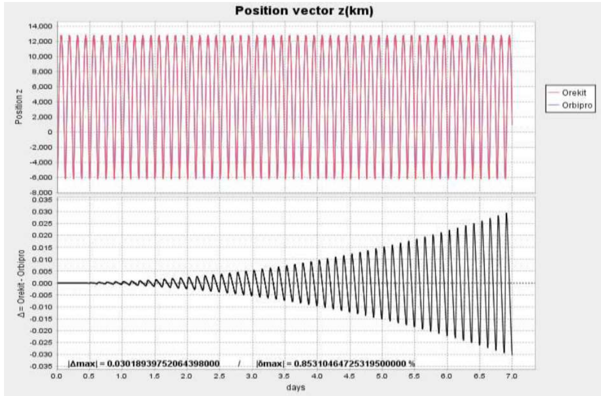

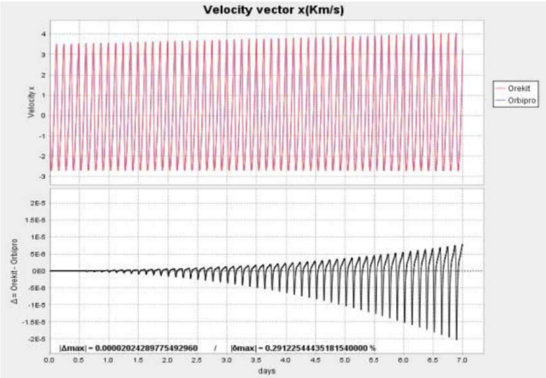

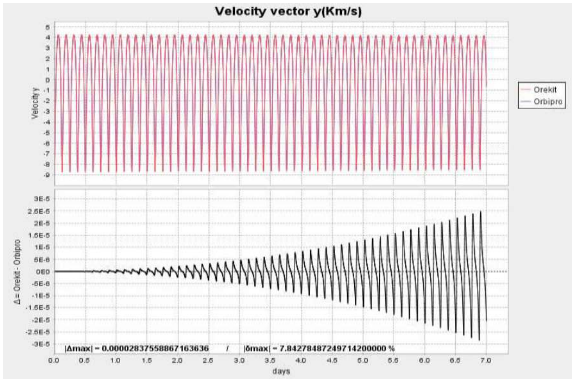

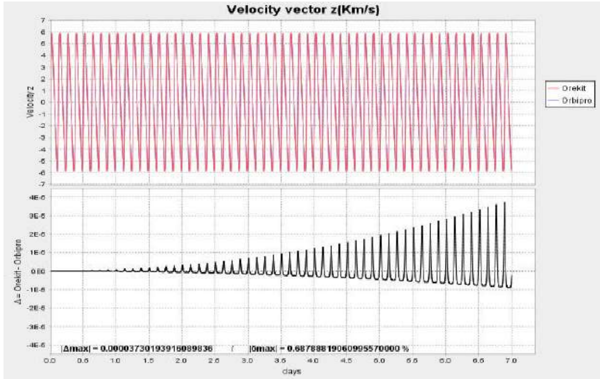

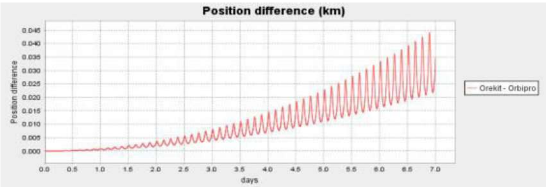

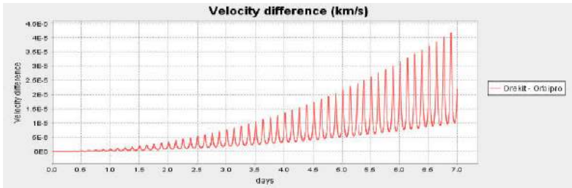

Orekit vs. OrbiPro differences:

Position vector x(km): 0.020 / 7.654E-1%
Position vector y(km): 0.042 / 5.068E-1%
Position vector z(km): 0.030 / 8.531E-1%
Velocity vector x(Km/s): 2.024E-5 / 2.912E-1%
Velocity vector y(Km/s): 2.838E-5 / 7.843E0%
Velocity vector z(Km/s): 3.730E-5 / 6.879E-1%
Position difference Orekit - Orbipro (Km): 0.044 / 6.378E-7%
Velocity difference Orekit - Orbipro (Km/s): 4.168E-5 / 4.731E-7%

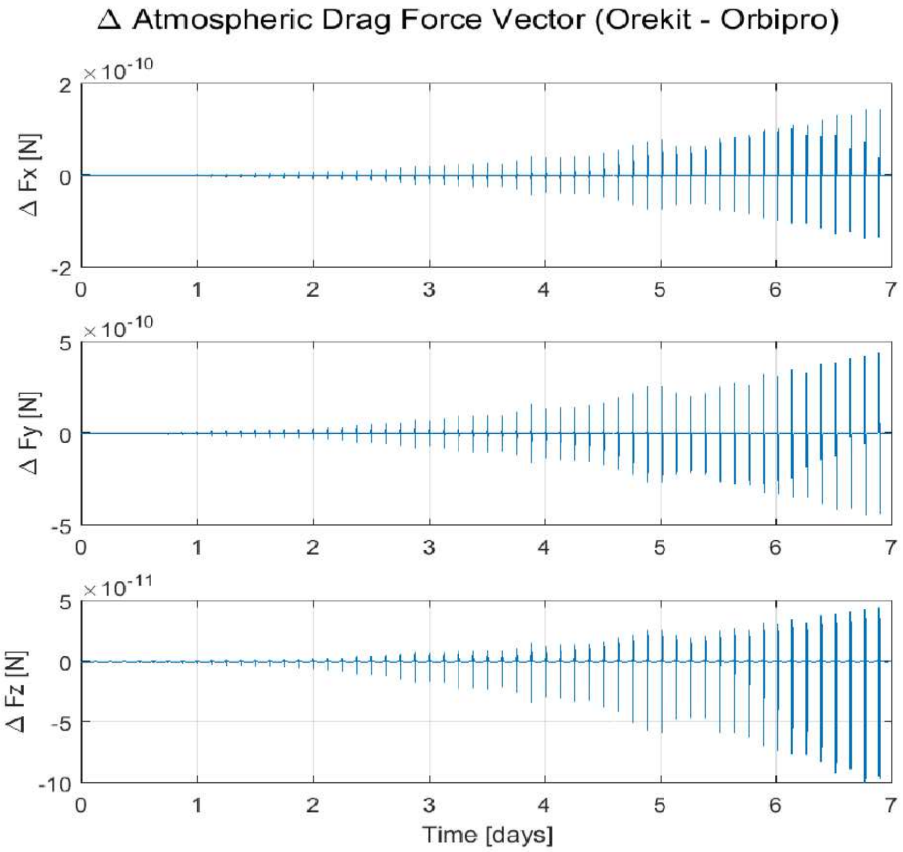

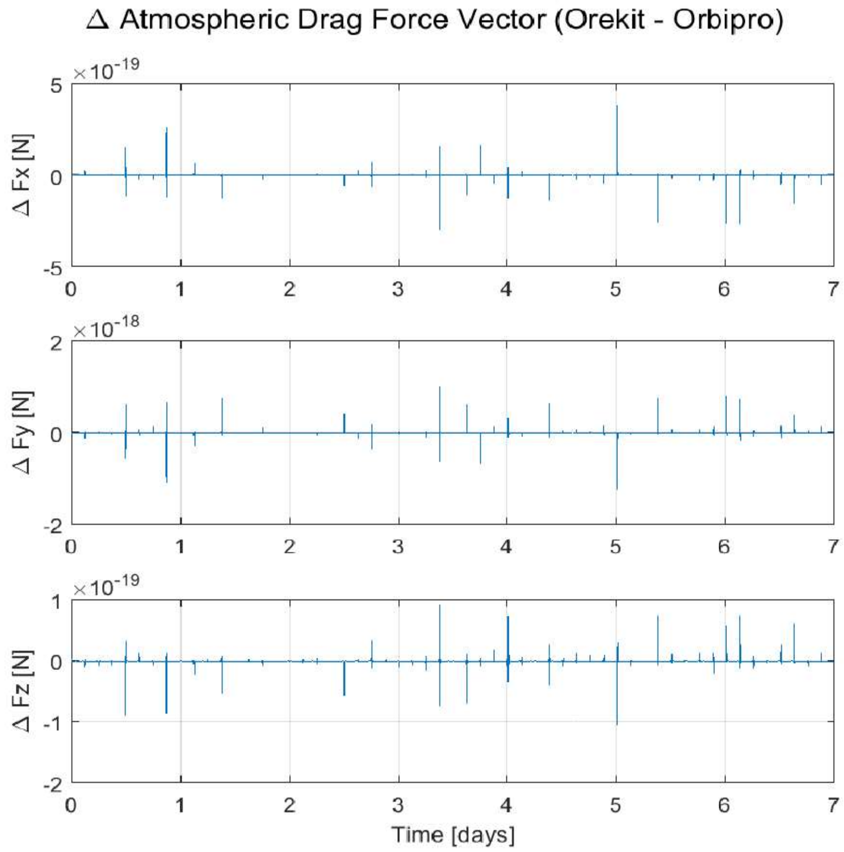

Orekit vs. OrbiPro differences:
Atmospheric drag force - same propagation time

Orekit vs. OrbiPro differences:
Atmospheric drag force - same spacecraft state as input

CONCLUSIONS AND FUTURE WORKS

4

CONCLUSIONS AND FUTURE WORK

- OrbiPro is a good alternative to Orekit if Matlab is required
- The results were successfully validated against Orekit
- Further improvements of the OrbiPro toolbox
  - Implementation of some mathematical functions in C
  - Support for TLE files
  - Development of a semi-analytical propagator for mean and short periodic elements
  - Implementation of a fixed step integrator for all the propagators
  - Development of an Orbit determination module using various on-board measurement sources, batch least squares estimations and Kalman filters

THANK YOU!




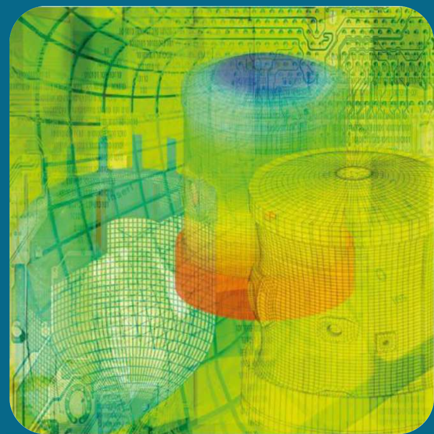

ANNEX – OTHER VALIDATION TESTS

5

VALIDATION

➔ Low Earth Orbit with Geopotential 2x0 and 30x30

- Initial conditions:
  - Epoch: 23th, July 2013, 03h, 03min, 05.970 sec
  - Time scale: UTC
  - Orbit type: keplerian
    - a = 7698.4832626 km
    - e = 0.092750114
    - i = 98.6894245º
    - Ω = 263.17707959º
    - ω = 56.9237741458º
    - M = 303.21338071º
- Frame: EME2000
- Satellite characteristics: Mass = 4085 Kg
- Attitude: EME2000 aligned
- Duration: 10 days
- Forces model:
  - Central body: Newtonian force
  - Central body: One of:
    - Gravity potential 2 × 0
    - Gravity potential 30 × 30

LEO orbit propagation – Contribution of Earth’s gravity potential 2x0 (model EGM2008)

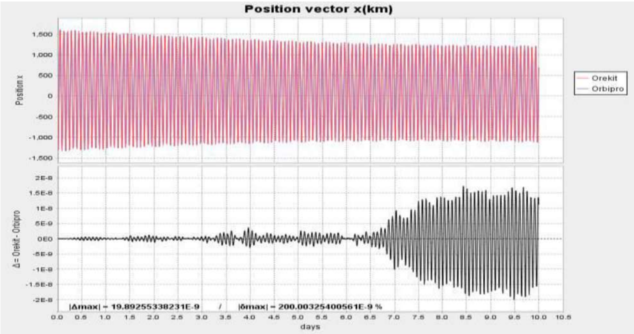

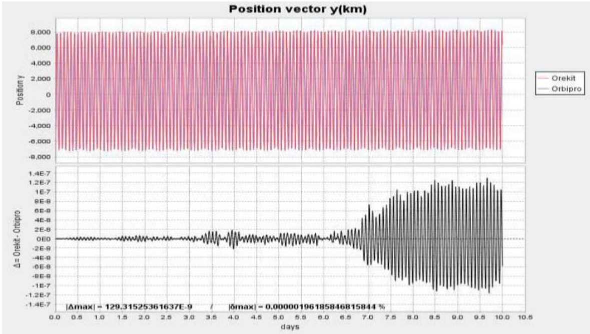

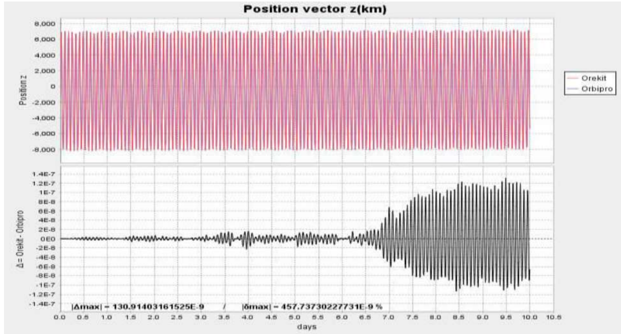

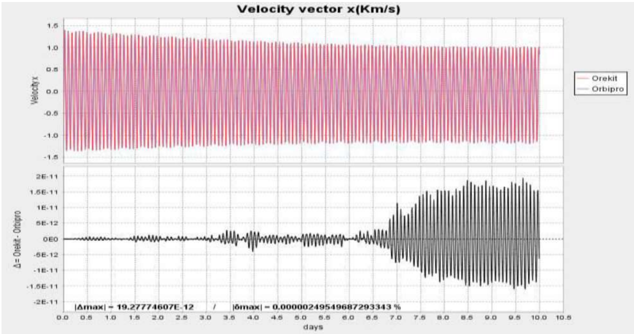

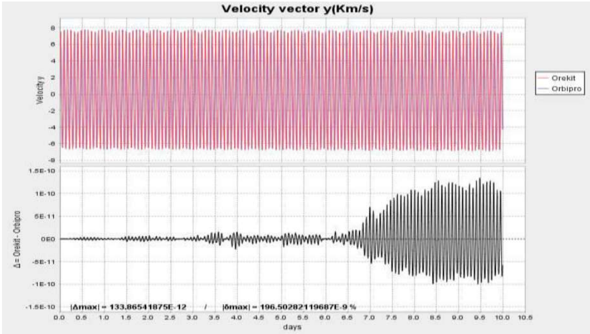

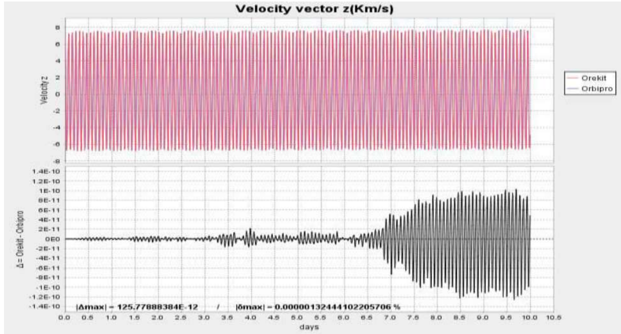

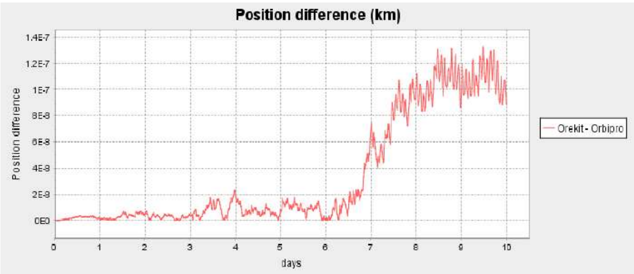

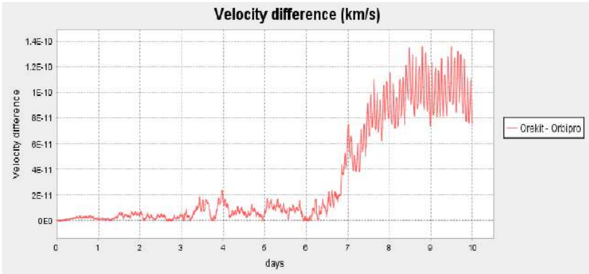

Orekit vs. OrbiPro differences:

Position vector x(km): 1.989E-8 / 2.000E-7%
Position vector y(km): 1.293E-7 / 1.962E-6%
Position vector z(km): 1.309E-7 / 4.577E-7%
Velocity vector x(Km/s): 1.928E-11 / 2.495E-6%
Velocity vector y(Km/s): 1.339E-10 / 1.965E-7%
Velocity vector z(Km/s): 1.258E-10 / 1.324E-6%
Position difference Orekit - Orbipro (Km): 1.325E-7 / 1.883E-12%
Velocity difference Orekit - Orbipro (Km/s): 1.361E-10 / 1.732E-12%

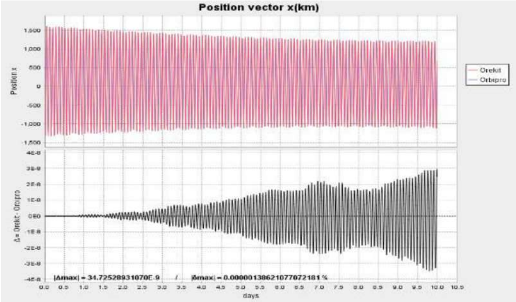

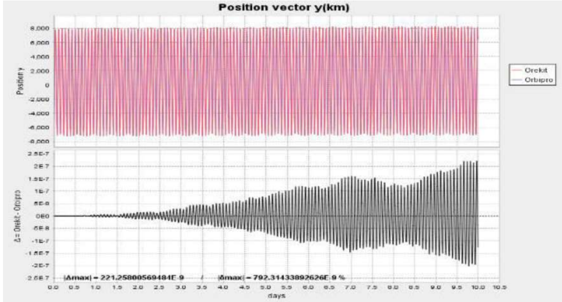

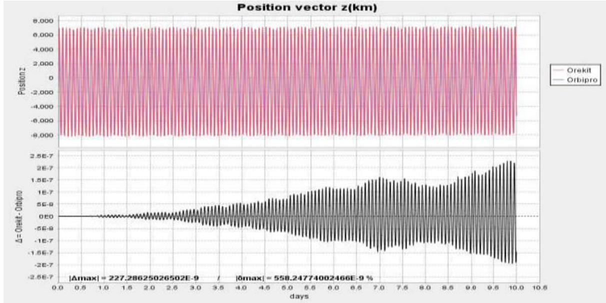

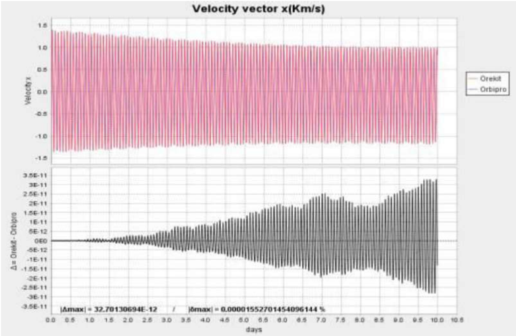

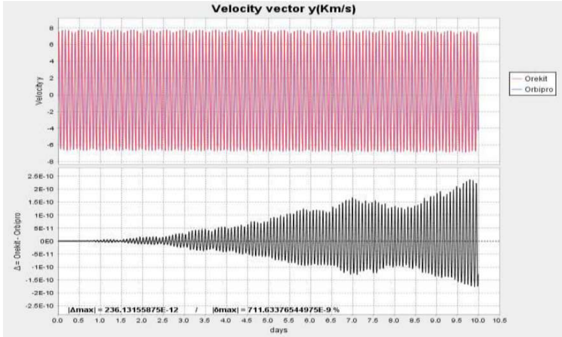

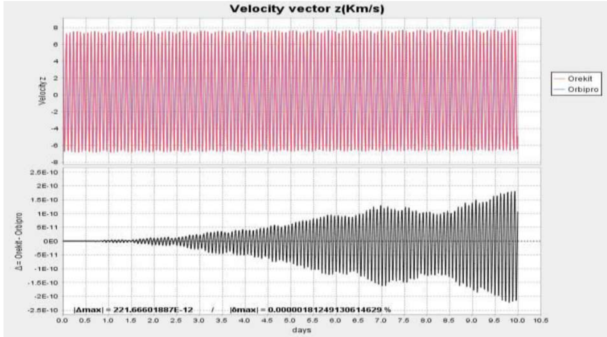

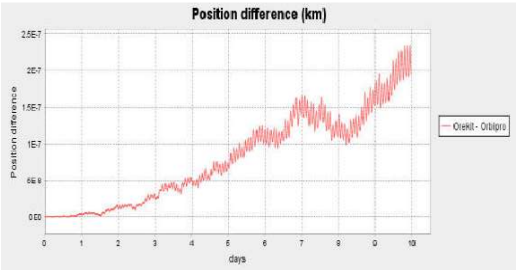

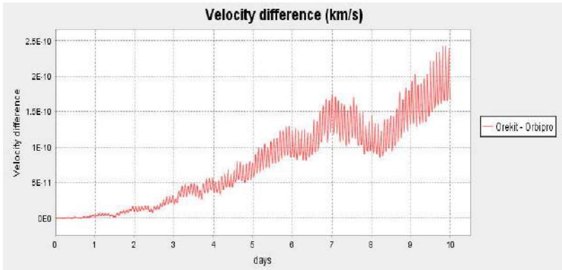

Orekit vs. OrbiPro differences:

Position vector x(km): 3.473E-8 / 1.386E-6%
Position vector y(km): 2.213E-7 / 7.923E-7%
Position vector z(km): 2.273E-7 / 5.582E-7%
Velocity vector x(Km/s): 3.270E-11 / 1.553E-5%
Velocity vector y(Km/s): 2.361E-10 / 7.116E-7%
Velocity vector z(Km/s): 2.217E-10 / 1.812E-6%
Position difference Orekit - Orbipro (Km): 2.337E-7 / 3.348E-12%
Velocity difference Orekit - Orbipro (Km/s): 2.420E-10 / 3.059E-12%

Geostationary orbit with Third Body (Sun and Moon)

- Initial conditions:
  - Epoch: 23th, July 2013, 03h, 03min, 05.970 sec
  - Time scale: UTC
  - Orbit type: keplerian
    - $a = 42163.476$ km — $\Omega = 263.17707959°$
    - $e = 0.00012750114$ — $\omega = 56.9237741458°$
    - $i = 1.3864°$ — $M = 303.21338071°$
- Frame: EME2000
- Satellite characteristics: Mass = 4085 Kg
- Attitude: EME2000 aligned
- Duration: 10 days
- Forces model:
  - Central body: Earth Newtonian force
  - Third body: Sun point mass, Moon point mass

Geostationary orbit with Third Body (Sun and Moon)

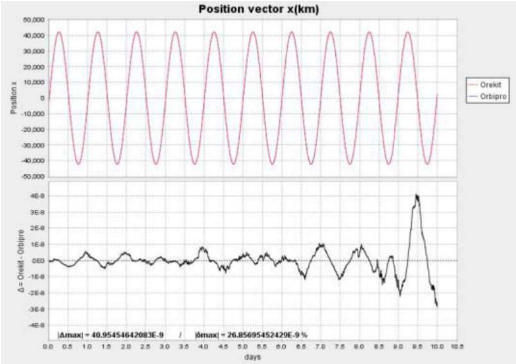

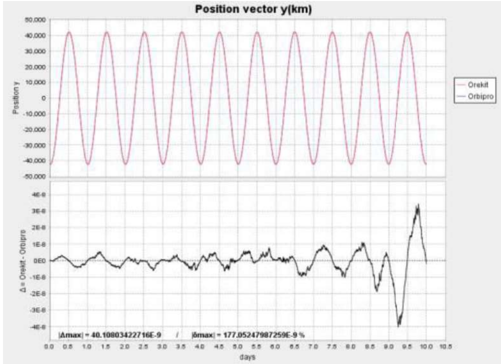

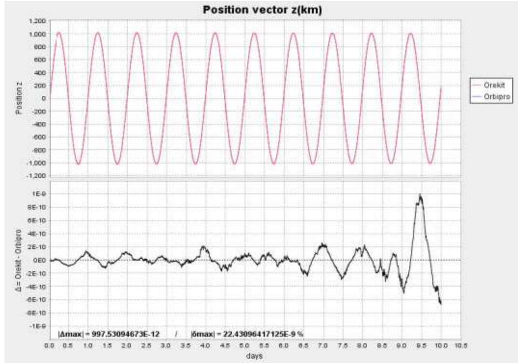

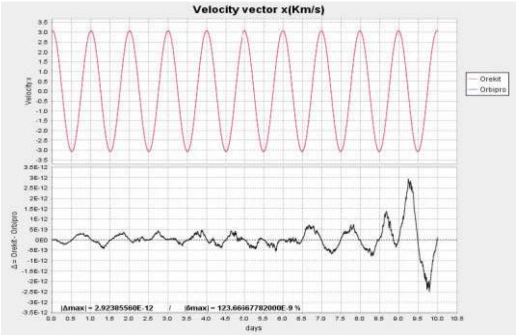

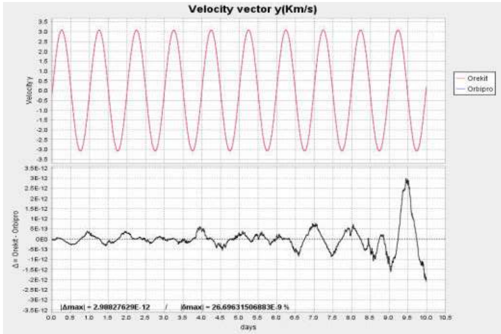

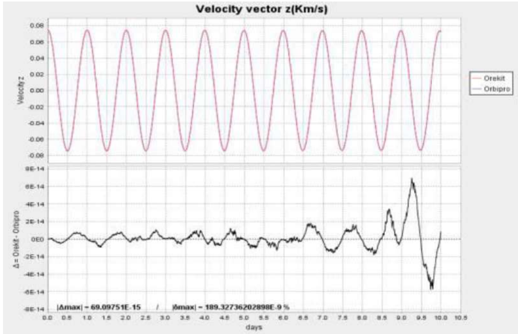

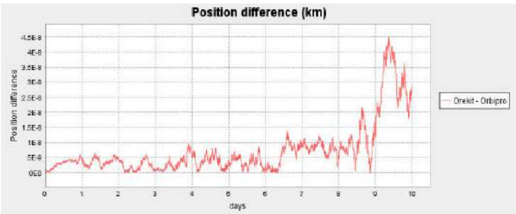

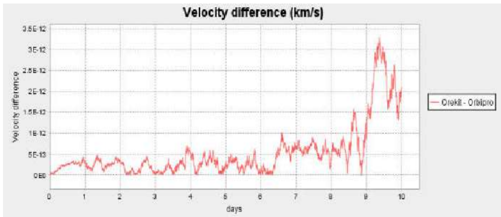

Orekit vs. OrbiPro differences:

Position vector x(km): 4.095E-8 / 2.686E-8%
Position vector y(km): 4.011E-8 / 1.771E-7%
Position vector z(km): 9.975E-10 / 2.243E-8%
Velocity vector x(Km/s): 2.924E-12 / 1.237E-7%
Velocity vector y(Km/s): 2.988E-12 / 2.670E-8%
Velocity vector z(Km/s): 6.910E-14 / 1.893E-7%
Position difference Orekit - Orbipro (Km): 4.493E-8 / 1.066E-13%
Velocity difference Orekit - Orbipro (Km/s): 3.277E-12 / 1.066E-13%

Geostationary orbit with Solar Radiation Pressure

- Initial conditions:
  - Epoch: 23th, July 2013, 03h, 03min, 05.970 sec
  - Time scale: UTC
  - Orbit type: keplerian
    - $a = 42163.476$ km — $\Omega = 263.17707959°$
    - $e = 0.00012750114$ — $\omega = 56.9237741458°$
    - $i = 1.3864°$ — $M = 303.21338071°$
- Frame: EME2000
- Satellite characteristics: Mass = 4085 Kg
- Attitude: EME2000 Aligned
- Duration: 10 days
- Forces model:
  - Central body: Earth Newtonian force
  - Perturbation: Solar radiation pressure

Geostationary orbit with Solar Radiation Pressure

ROMANIA

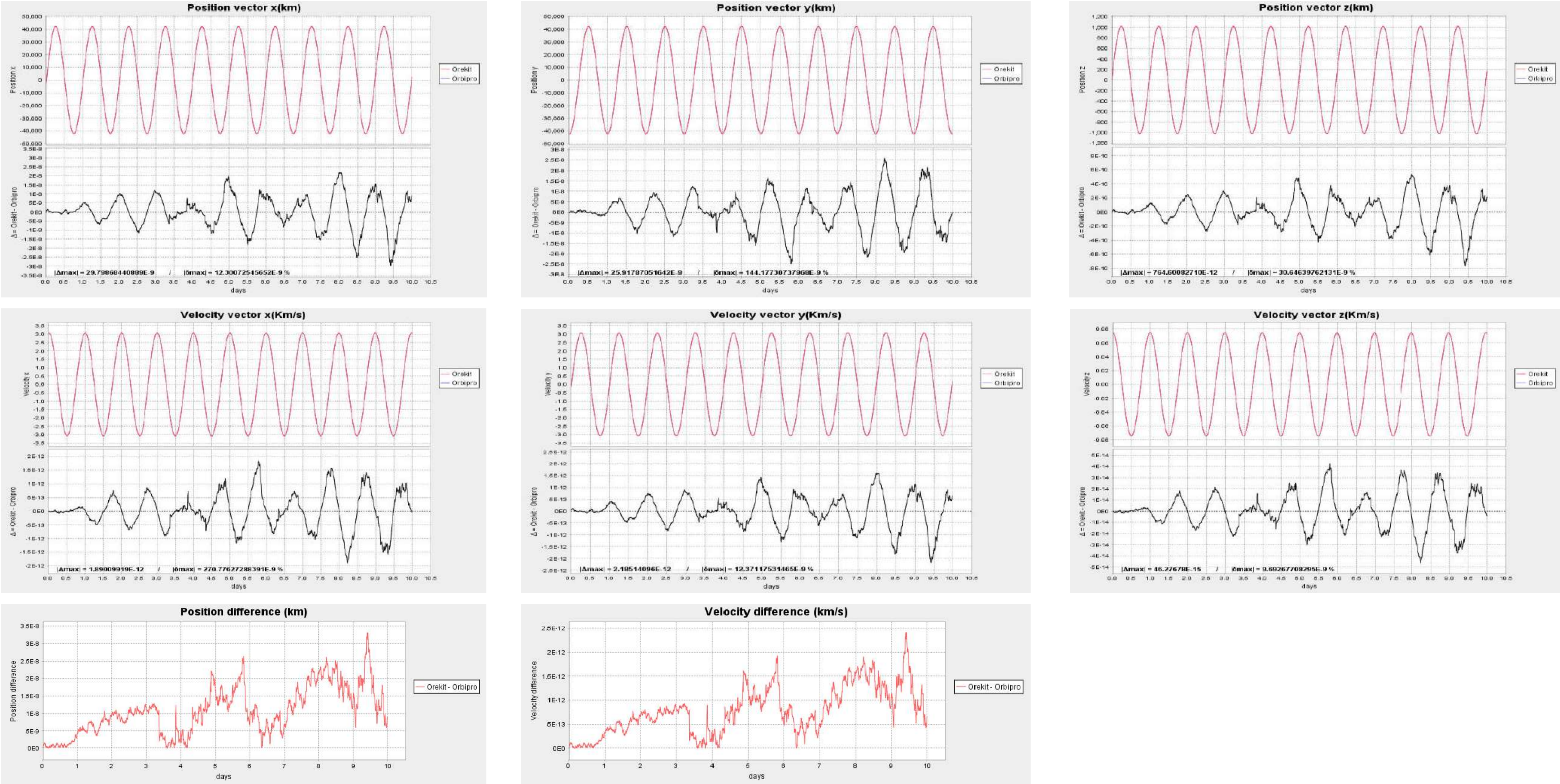

Orekit vs. OrbiPro differences:

Position vector x(km): 2.980E-8 / 1.230E-8%
Position vector y(km): 2.592E-8 / 1.442E-7%
Position vector z(km): 7.646E-10 / 3.065E-8%
Velocity vector x(Km/s): 1.890E-12 / 2.708E-7%
Velocity vector y(Km/s): 2.185E-12 / 1.237E-8%
Velocity vector z(Km/s): 4.628E-14 / 9.693E-9%
Position difference Orekit - Orbipro (Km): 3.296E-8 / 7.817E-14%
Velocity difference Orekit - Orbipro (Km/s): 2.403E-12 / 7.817E-14%

VALIDATION

➔ Low Earth Orbit with Atmospheric Drag

- Initial conditions:
  - Epoch: 23th, July 2013, 03h, 03min, 05.970 sec
  - Time scale: UTC
  - Orbit type: keplerian
    - a = 6798.400 km   Ω = 281.661404104º
    - e = 0.00000001   ω = 230.123714157º
    - i = 0.00000001º   M = 1.195159217º
- Frame: EME2000
- Satellite characteristics: Mass = 985 Kg
- Attitude: Nadir pointing (to have the same area facing the incoming air flux during propagation)
- Events: Perigee detector (to study the orbit decay)
- Duration: 10 days
- Forces model:
  - Central body: Earth Newtonian force
  - Perturbation: Earth atmospheric drag force
- For each detected perigee starting with 2nd occurrence:
  - The delta (Semi-major axis, Period revolution, Velocity) is computed as current detection data - previous detection data;
  - Using previous detection data, the estimated delta is computed.

Low Earth Orbit with Atmospheric Drag

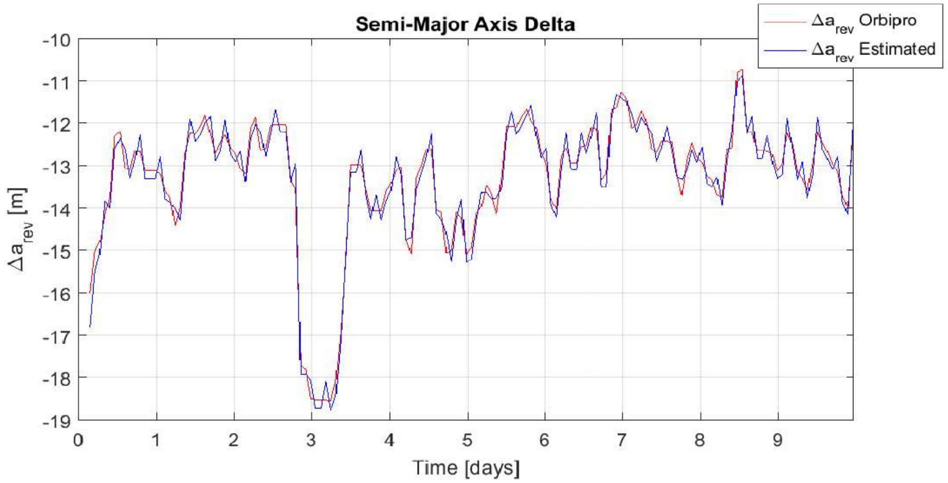

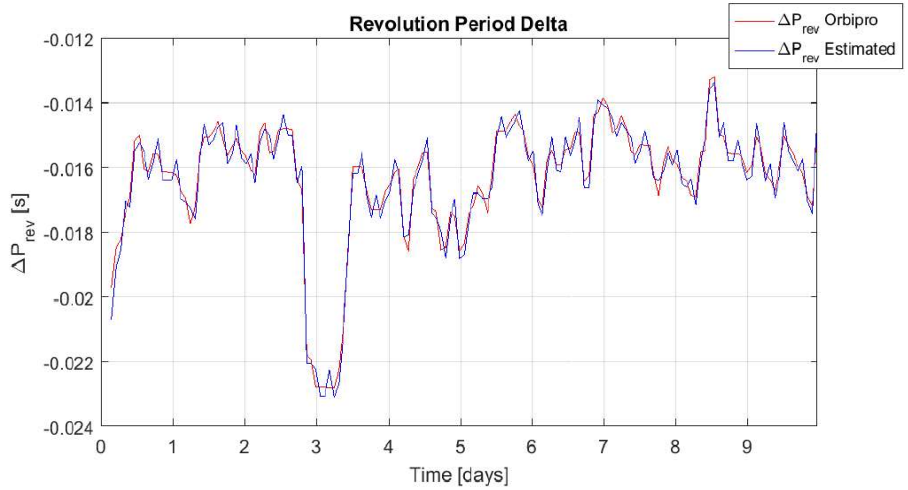

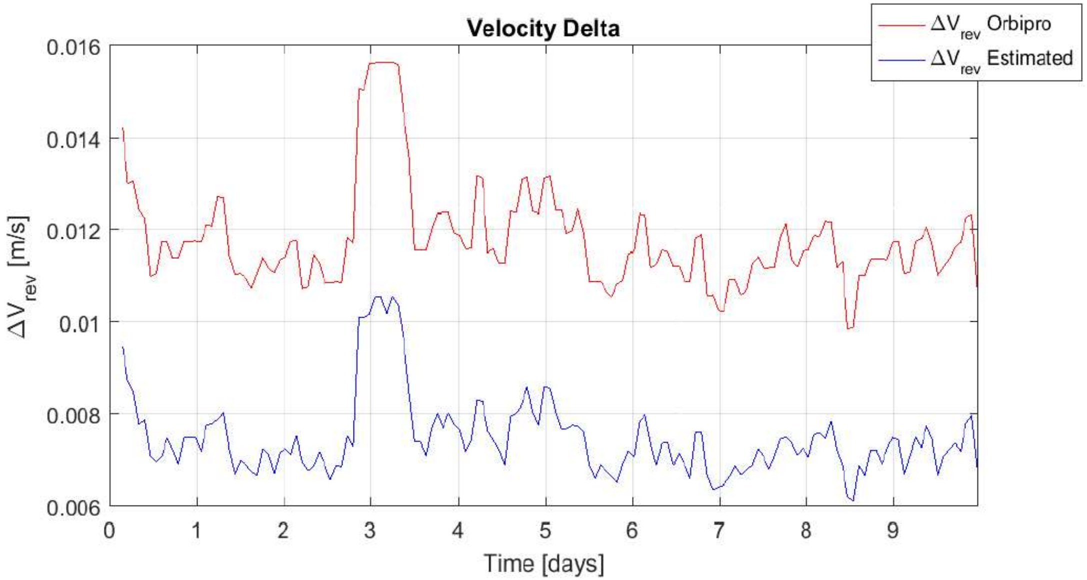

➔ Aerodynamic torque in Mars atmosphere

- Initial conditions:
  - Epoch: 23th, July 2013, 03h, 03min, 05.970 sec
  - Time scale: UTC
  - Orbit type: keplerian
    - a = 3635.0105 km — Ω = 281.661404104º
    - e = 0.000001 — ω = 230.123714157º
    - i = 1.86438067644º — M = 1.195159217º
- Frame: Mars inertial frame
- Satellite characteristics: Mass = 285 Kg
- Attitude: Uncontrolled attitude profile under aerodynamic disturbance torque
- Duration: 2 days
- Forces model:
  - Central body: Mars Newtonian force

Aerodynamic torque in Mars atmosphere

- Testing approaches:
  - Given a spacecraft state, a manual computation of aerodynamic torque was done,
  - Given the shape of the spacecraft and the shape of the orbit, an estimation of minimum and maximum torque value was done

- Spacecraft: a cube with side length of 1 m, solar panels with 8×2 m^2

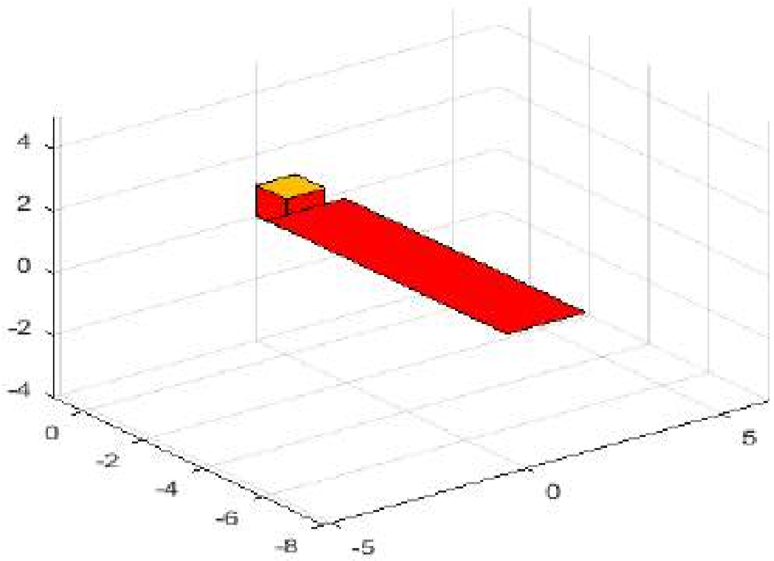

Aerodynamic torque in Mars atmosphere

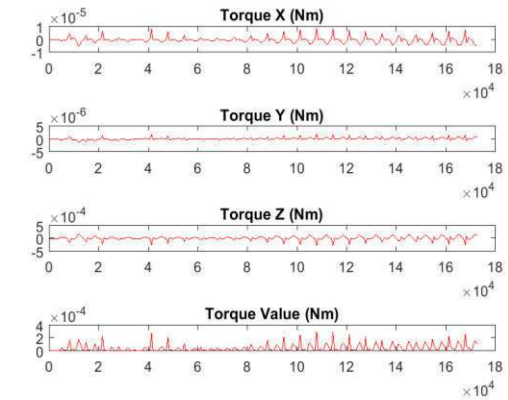

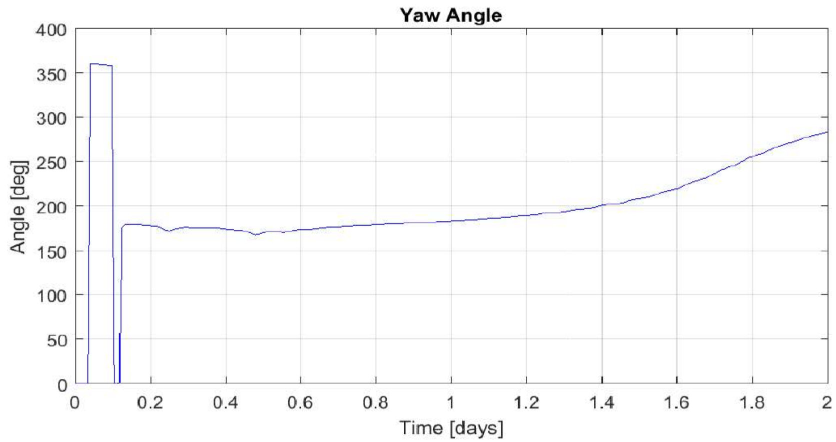

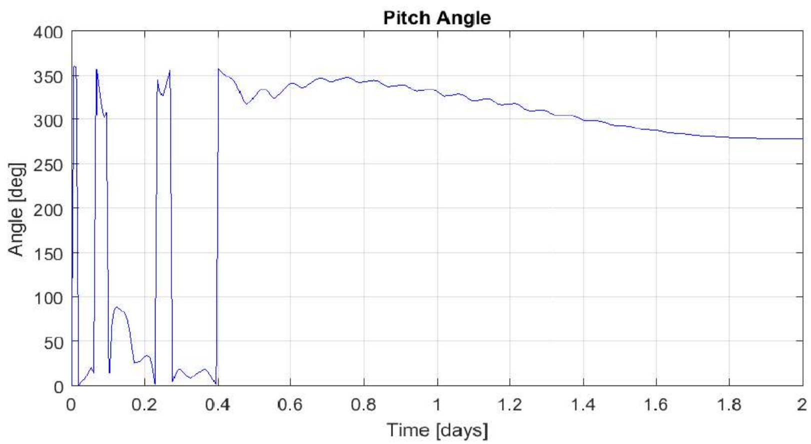

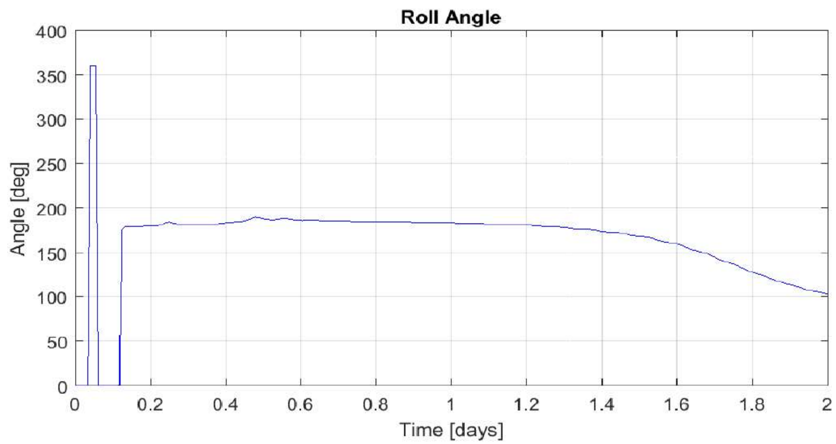

Orbipro – Computed:
ΔTorque X: 7.940933880509066e-23
ΔTorque Y: -3.639594695233322e-23
ΔTorque Z: -2.117582368135751e-22

VALIDATION

➔ Interplanetary trajectory – Rosetta

- Input files: position, velocity and solar panels rotation of Rosetta spacecraft retrieved from ESOC files
- Initial conditions:
  - Epoch: 12th, July 2011, 07h, 33min, 58.00 sec
  - Time scale: UTC
- Frame: Sun inertial frame
- Spacecraft shape: box-type central structure (2.8 m x 2.1 m x 2.0 m) and two solar panels, with a combined area of 64 m^2
- Attitude: Tabulated from a file
- Duration: 935 days
- Forces model:
  - Central body: Sun Newtonian force
  - Third body: Mercury point mass, Venus point mass, Earth point mass, Mars point mass, Jupiter point mass, Saturn point mass, Uranus point mass, Neptune point mass, Pluto point mass
  - Perturbation: Solar radiation pressure

Interplanetary trajectory – Rosetta (ESOC files data)

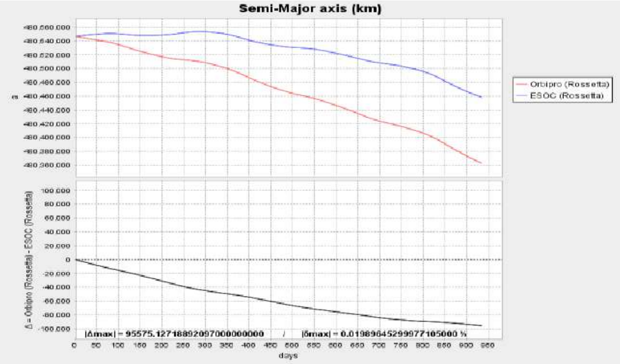

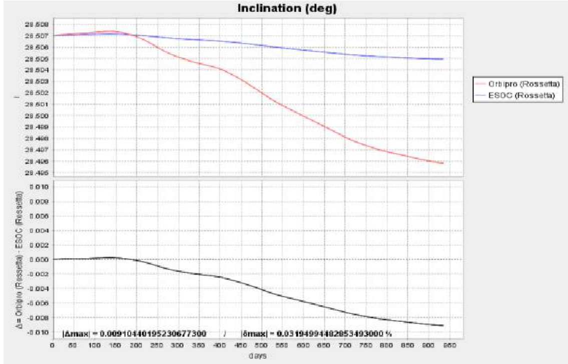

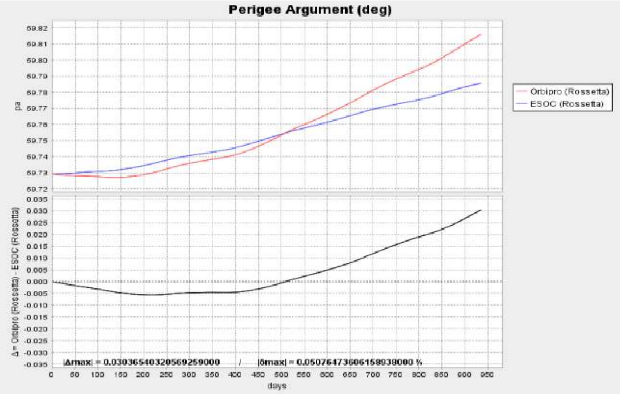

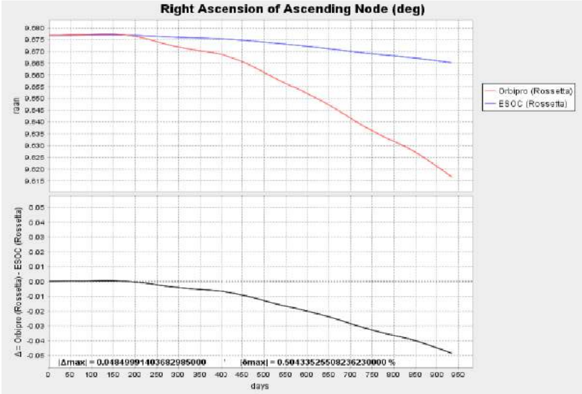

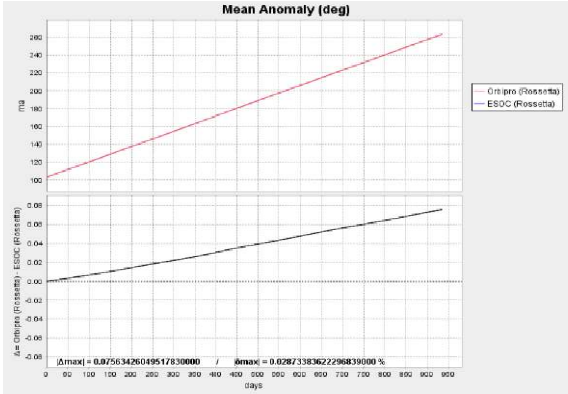

OrbiPro vs. Spice data

Increasing difference due to Rosetta maneuvers, but similar shape of the plots

Page 288

Interplanetary trajectory – Rosetta

ROMANIA

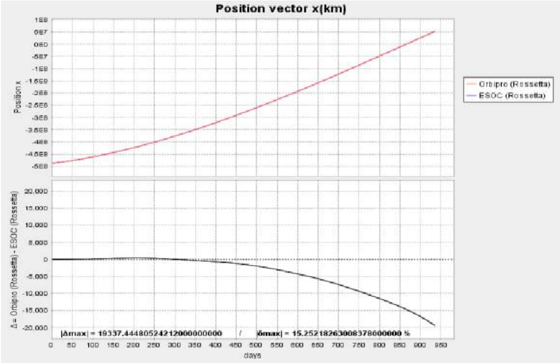

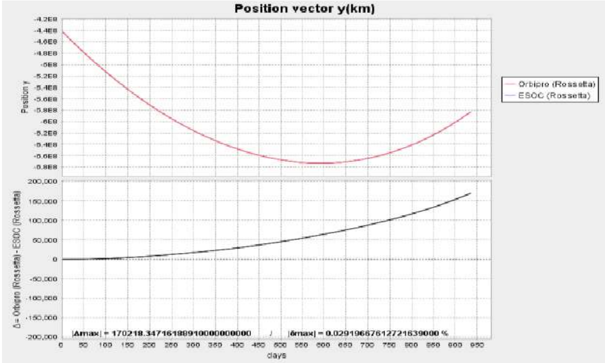

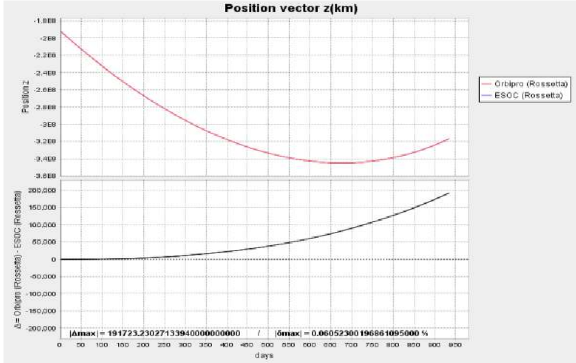

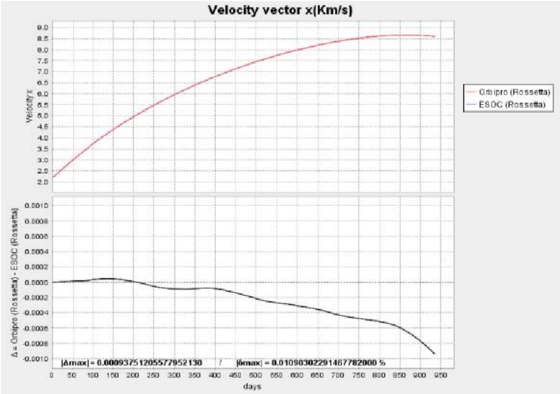

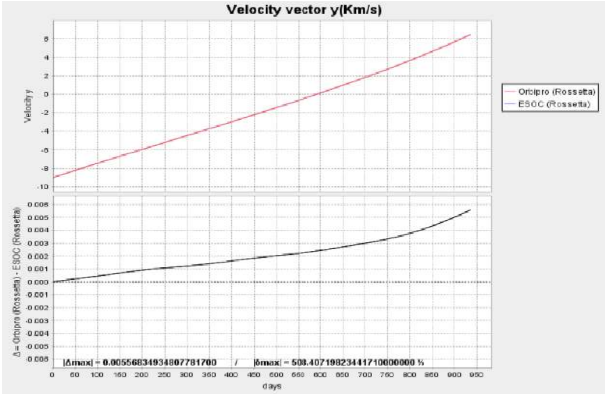

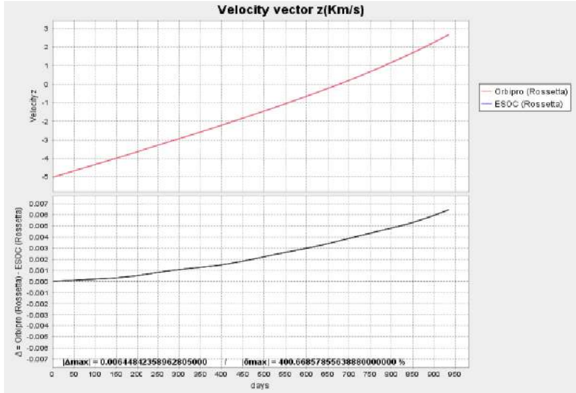

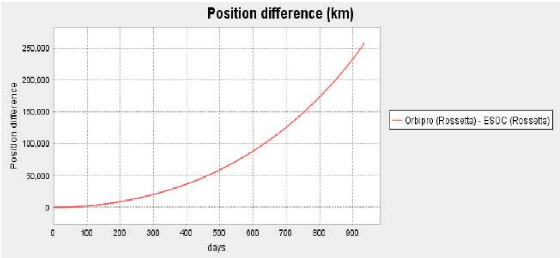

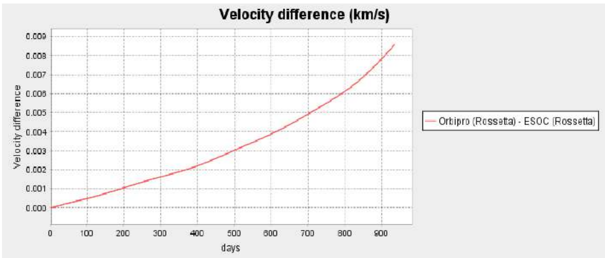

OrbiPro vs. Spice data

Increasing difference due to Rosetta maneuvers, but similar shape of the plots

Presentation 2508

Advances in visual based navigation approach and landing scenarios

CEAS 2017

Advances in visual based navigation approach and landing scenarios

Oct 16th , 2017

INNOVATING SOLUTIONS

Presentation outline

- Visual navigation activity background
- AbsNav system description
- Landmark database
- AbsNav breadbording
- RelNav system description
- RelNav breadbording
- RelNav Testing Campaign
- Conclusions

Visual Navigation background

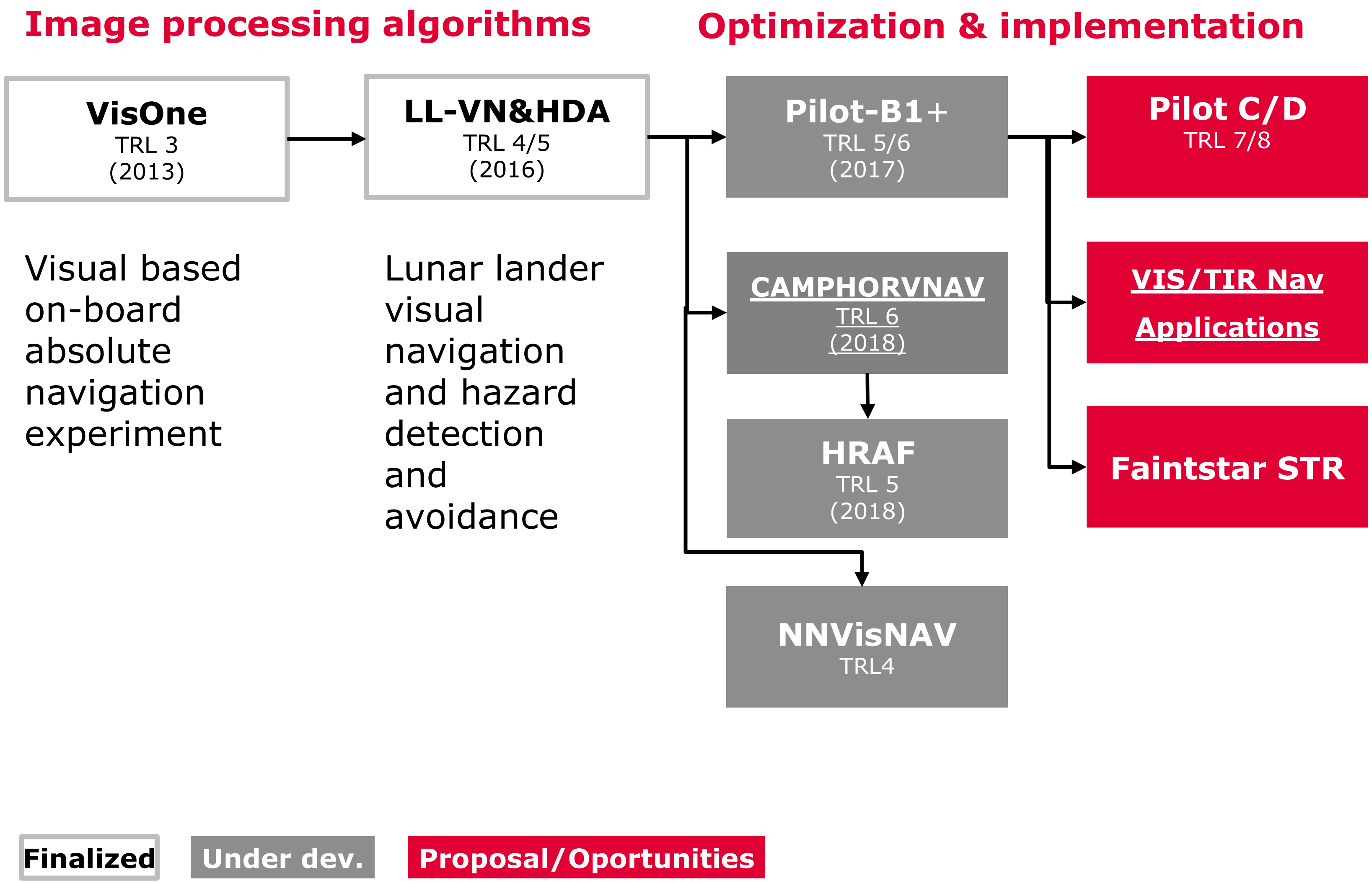

AbsNav System Description

INNOVATING SOLUTIONS

AbsNav System

- Absolute navigation system for Entry Descent and Landing phases (ED&L)
- In charge of receiving images from S/C camera and providing precise position estimation for achieving pin-point landing accuracy (PPL) requirements
- Limits Navigation errors derived by pure IMU propagation
- Measurements based on single camera images
- Uses image processing techniques:
  - Landmarks detection and matching between camera acquired images and onboard stored data
  - Onboard database created offline starting from DEMs and geo-referenced images
- Landmarks used: craters – due to scale, rotation and illumination invariance properties
- <u>**Winning point**</u>: Database can be validated/verified on-ground thanks to the use of physical features in the lunar surface.

Functional Description

- Online and offline functionalities
- Offline feature consists in creating the landmarks database using DEM only for higher altitudes and geo-referenced images together with DEM for lower than 3 km altitudes
- Online feature is tasked with:
  - Detecting the landmarks from the onboard camera images
  - Matching the detected landmarks with the ones stored in the database
  - Provide the Landmarks correspondence to the Navigation Filter

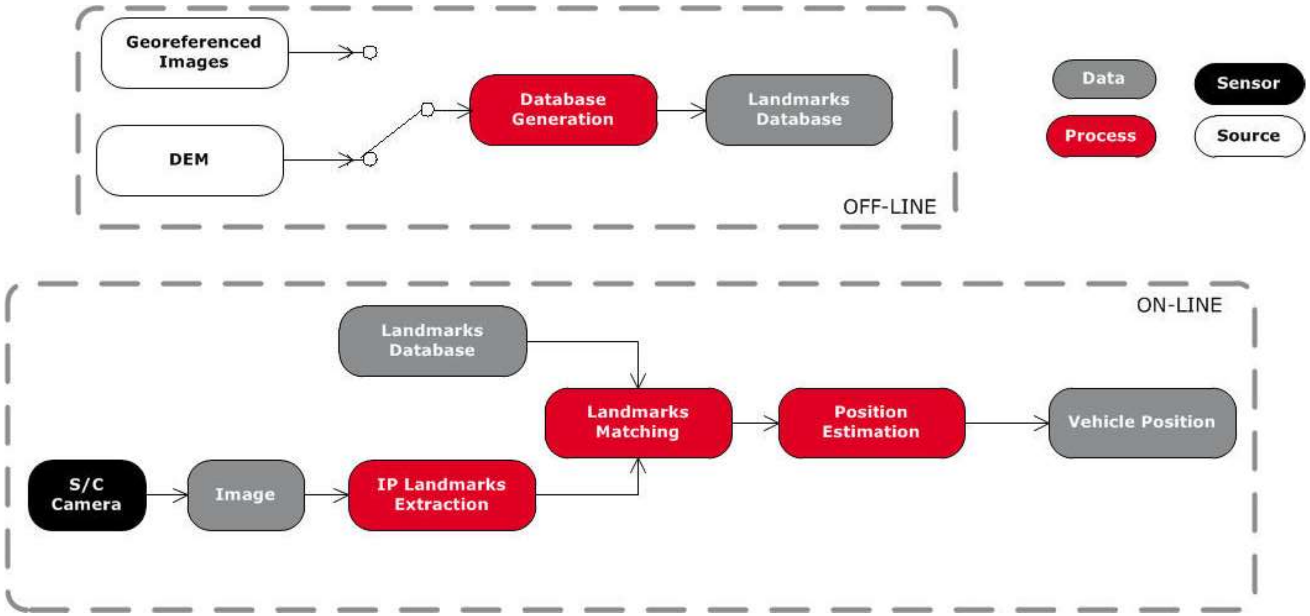

Offline: Landmark Database Creation (DEM case)

- Sources: Kaguya, LRO and DEMs that can be treated as images
- Craters
  - Craters catalogued by area and dimension
  - Impact craters: steep-sided circular depressions

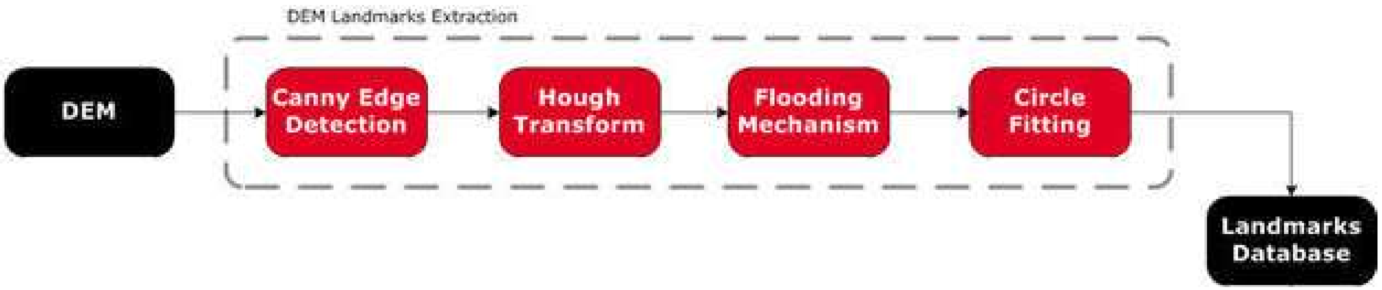

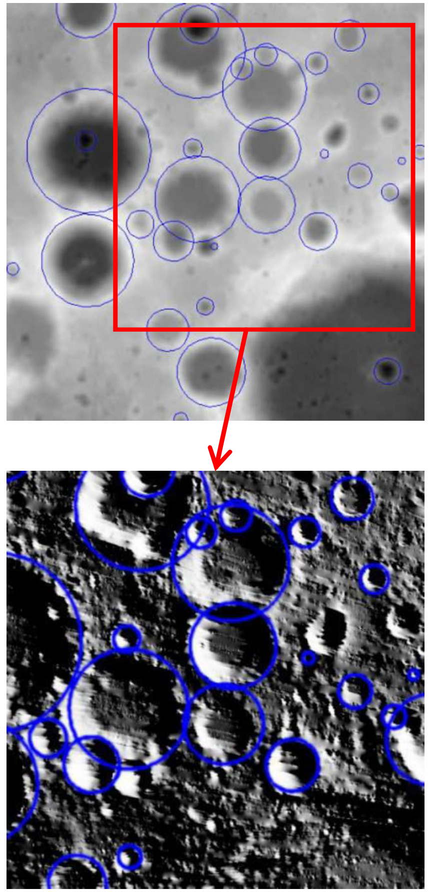

Online: Landmark Extraction

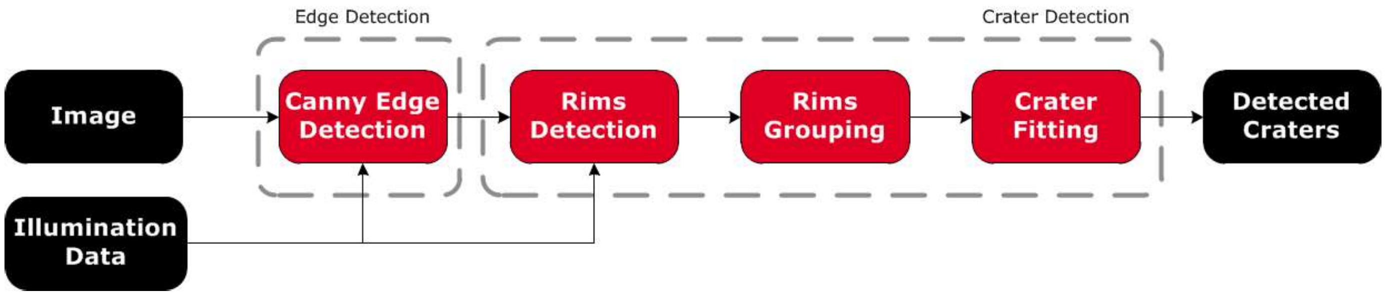

- Four stages present in the algorithm
  - Edge Detection implemented in HW
  - Rim Detection
  - Rims Grouping
  - Crater fitting

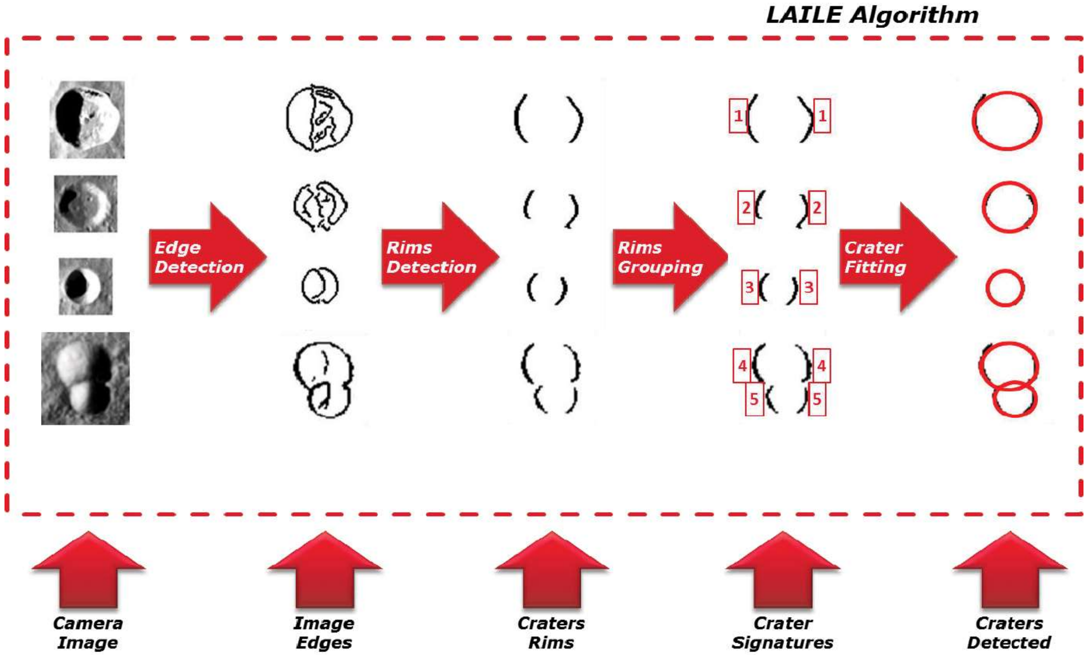

Online: Landmark Matching

- Typical Point-Matching Problem

- Point matching between two sets of points:
  – Robust solution based on outliers discarding

- Associates the detected craters (red) to the database craters (black)

- Outputs pairs of craters

- False matches are eliminated by a landmark integrity check function, using a database 2D projection:
  – Removes craters from the subset
  – Corrupted subset if there are less than 4 craters remaining

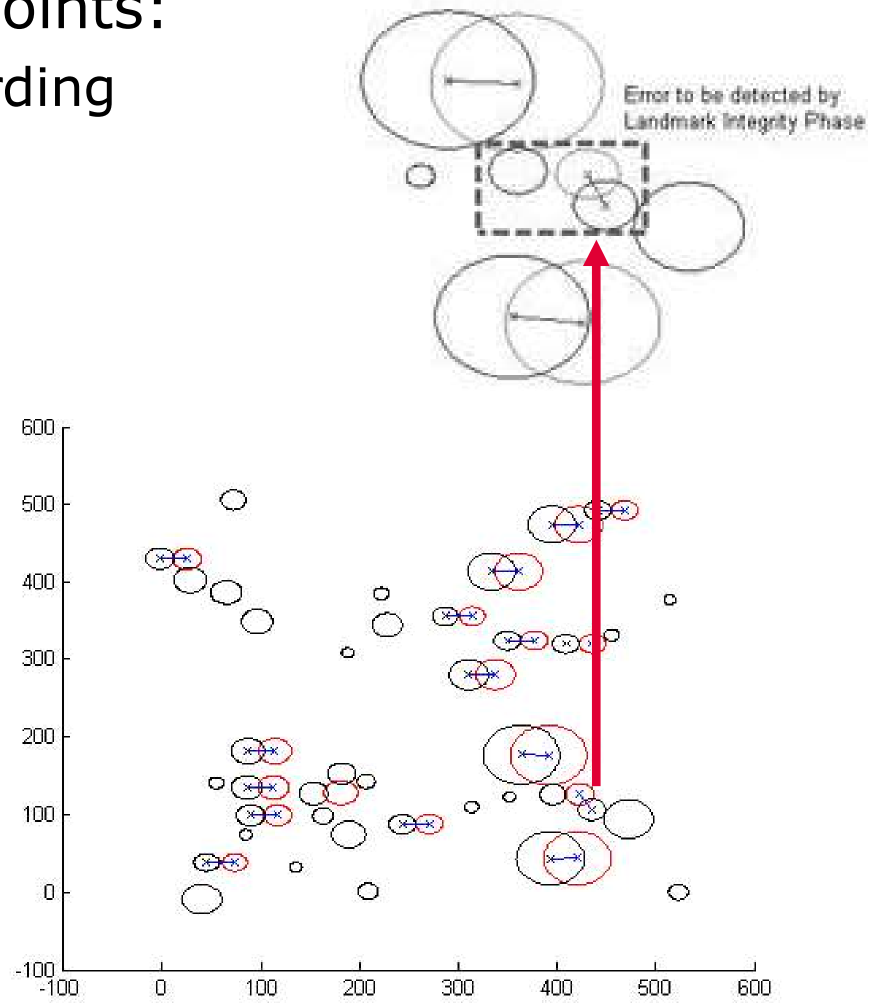

AbsNav BB: Set-up Preparation

AbsNav SW Validation Environment integrates the following:

- The WindRiver Workbench Environment with the VxWorks RTOS
- The PowerPC BSPs
- The CPCI-CPU/750 board

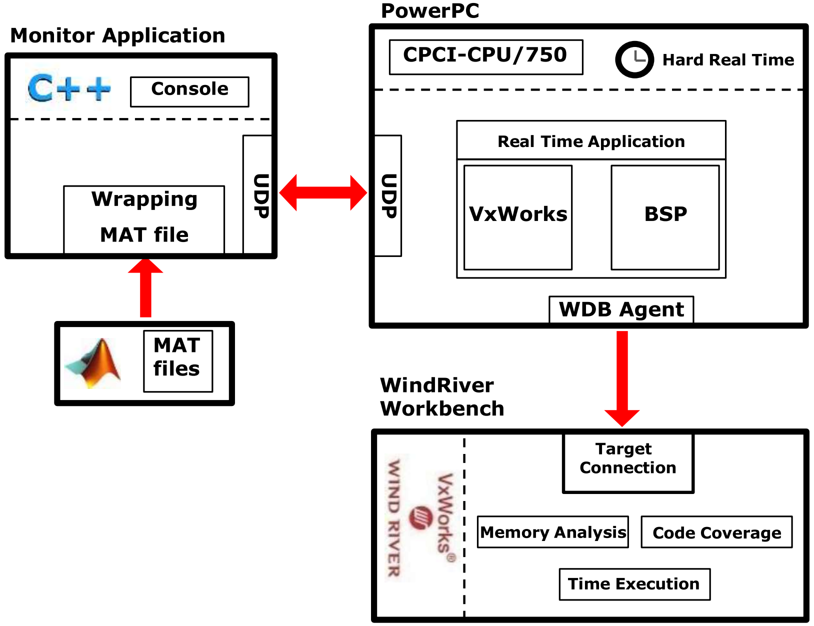

AbsNav SW Validation Plan for Simulation includes the following:

- AbsNav SW Unitary Testing
- AbsNav SW Incremental Testing

AbsNav BB: Validation

AbsNav SW Unitary Testing:

- Development Environment Settings
  - WindRiver Workbench Preparation
  - Workbench connected to PPC with WDBAgent
- Upgraded functions
  - Execution time improved maintaining accurate results
  - Preliminary validation of the Upgraded functions
- AbsNav SW sub-functions Unitary validation
  - Most of the sub-functions have been preliminary validated in RTEMS
  - Modifications are required according to ADS interface requirements
- AbsNav SW complete module validation

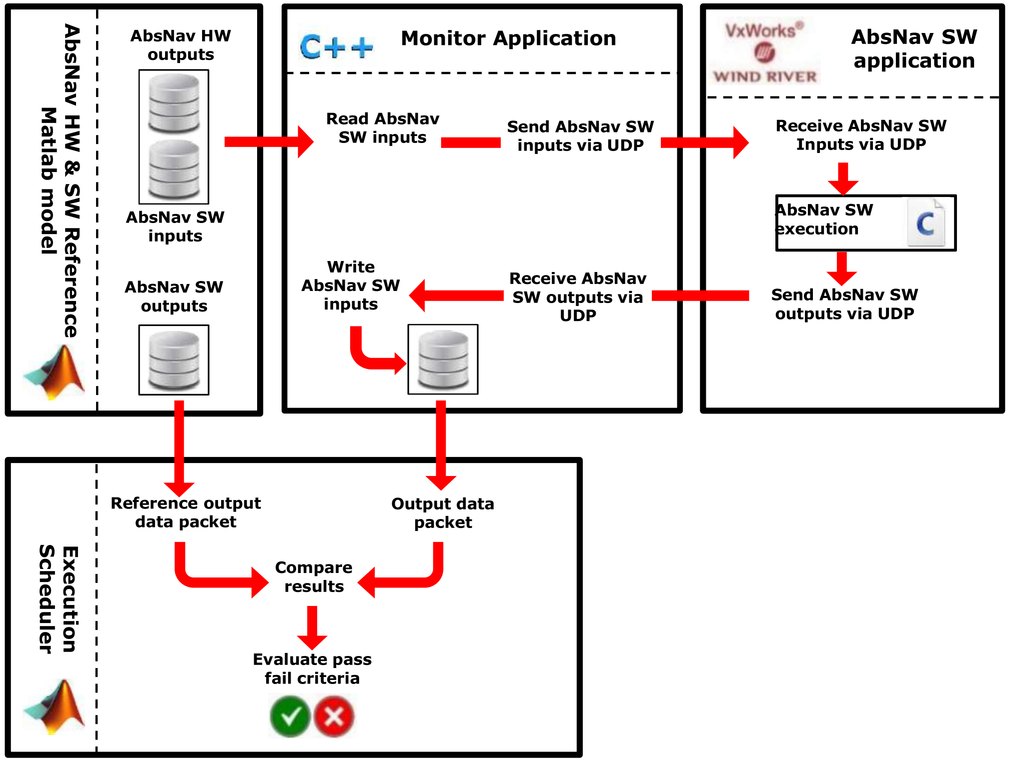

AbsNav SW Incremental Testing:

- Unitary validation of the AbsNav SW part and AbsNav HW part, executed together

RelNav System Description

SCOPE & OBJECTIVES

Develop a navigation camera for Phobos Sample Return (PhSR) Mission i.e a Vision-Based Navigation Camera (VBNC) composed of:

- Camera Optical Unit (COU)
- Image Processing Board (IPB)

- The final goal of the activity, the development of the EM of the VBNC for PhSR, comprises the following elements:
  - an Engineering Model (EM) version of the IPB (TRL 5/6)
  - a BreadBoard (BB) version of the COU

- In addition, the activity will develop the required test bench to validate the VBNC EM:
  - flight representative oBC emulator with the required navigation software and potentially part of the low level navigation algorithms
  - Ground support equipment to power, operate and stimulate the VBNC EM (EGSE).

TECHNICAL APPROACH

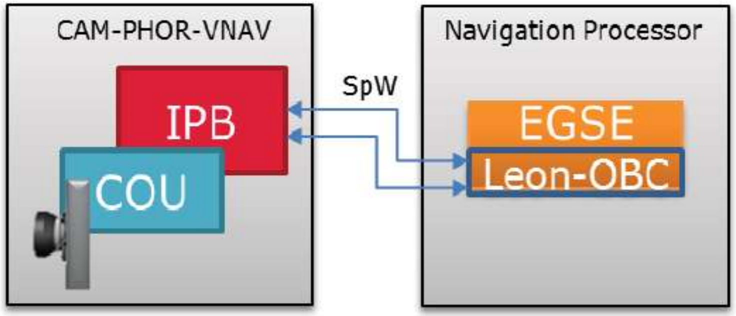

- Vision-based Autonomous Navigation developed following Architecture Avionics of Processor + FPGA
- Profiling:
  - HW acceleration is needed for the Image Processing
- FPGA-VHDL Image Processing implementation in IPB
  - Image calibration
  - Processing of calibrated images to extract navigation data
- IPB is the main contribution of this activity.
- Final interfaces: SpaceWire link connects both the COU-IPB and IPB-OBC.

IPB BASELINE

- Processing FPGA: GMV RelNav IP-core (high-performance & high-density SRAM-based FPGA)
  – AMBA bus based system
  – Memory controllers
  – Data Acquisition and Synchronization
  – FPGA-FPGA parallel communication

- Interfaces FPGA: Deals with the interfaces of the IPB to the external world (smaller Flash-based FPGA)

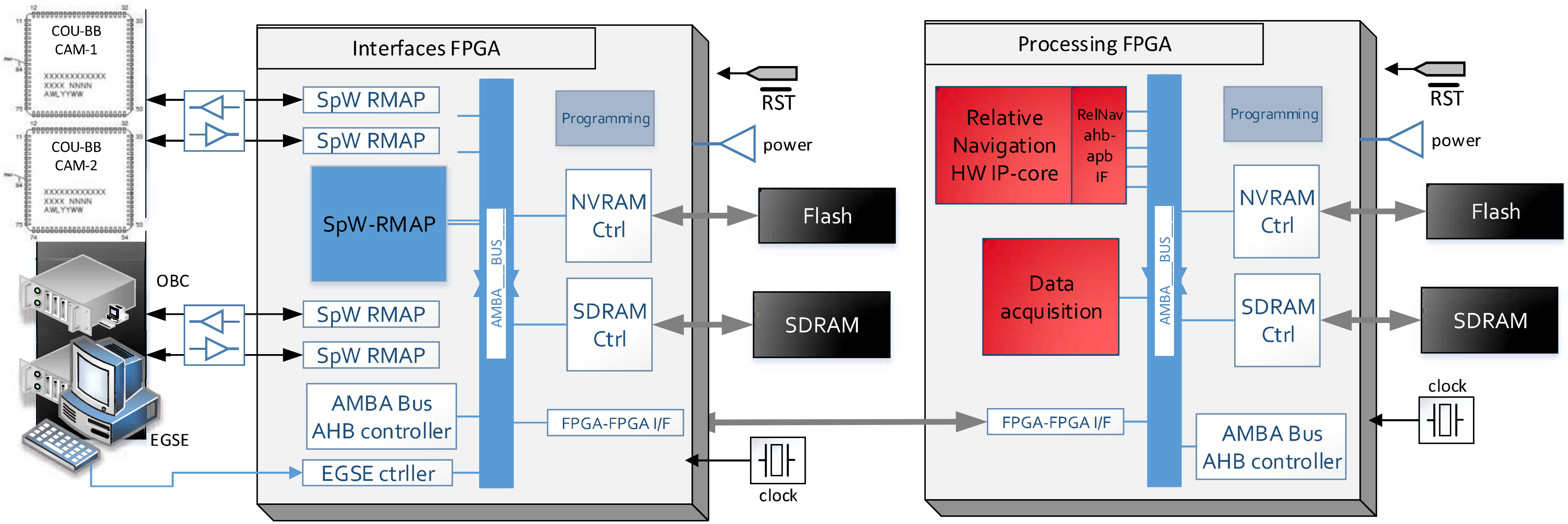

IPB – FEATURE TRACKING ALGORITHM

- No input feedback is needed from GNC filter.
- Features Detection generates a list of features
- Pyramids computation helps reduce time and increase track lengths
- Multi-level images are generated as intermediate data to match features between different image frames.
- Feature Tracking tracks the features in the multi-level images by computing the displacement between two consecutive frames in a mean square error sense.

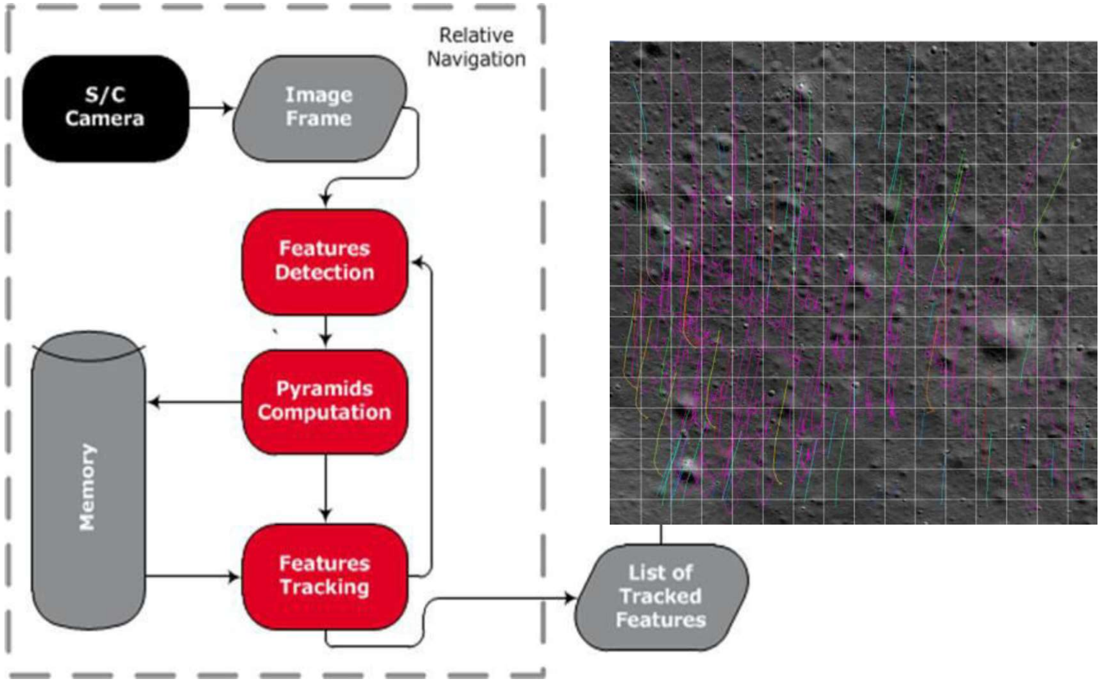

IPB ENGINEERING MODEL

- Evolution of an existing design
- COTS components that have flight equivalent parts
- Commercial Virtex-5 FPGA
- SpaceWire Interface
- Synchronisation signal

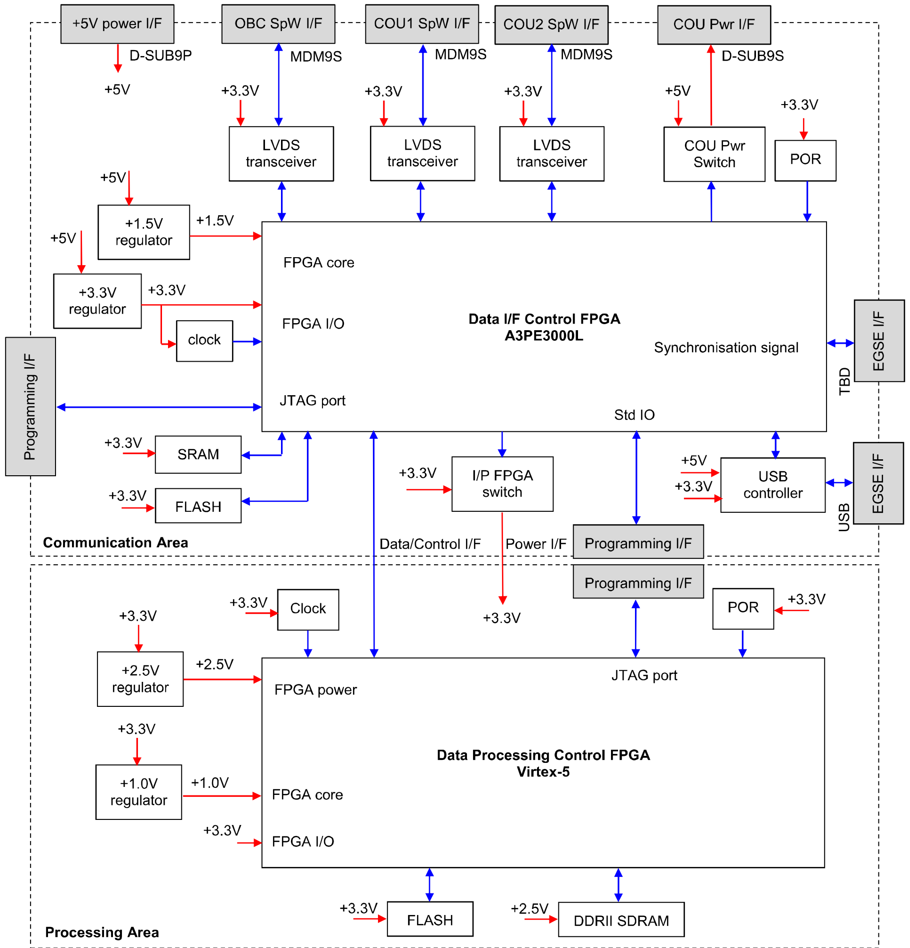

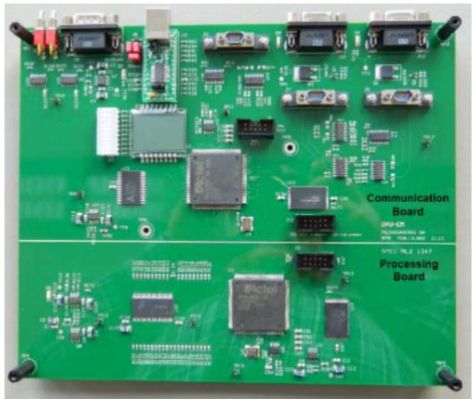

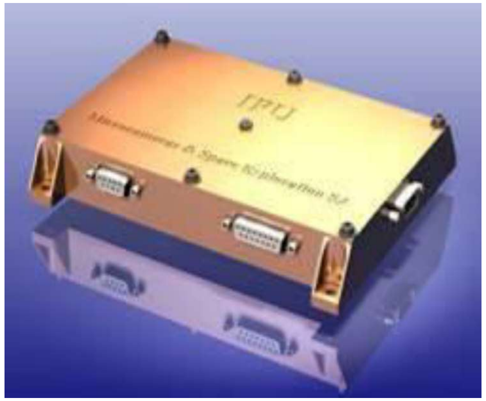

Existing breadboard and possible flight configuration

Page 307

TEST CAMPAIGN

- Unitary Tests (modules)
- Integration Tests (Incrementally, subsystems)
- Simulator for closed loop data generation
- System Tests: FPGA-in-the-loop
- System Tests: HW-In-the-Loop
  - ViSOS (PANGU-4 new Phobos model images)
  - platform-ART® (Phootprint Mock-up as in GMV-NPAL tests)
- IPB EM Mechanical and Thermal Tests
- IPB Radiation Test Analysis
- COU Functional and performance tests campaign including Calibration Tests
- VBNS Acceptance Tests

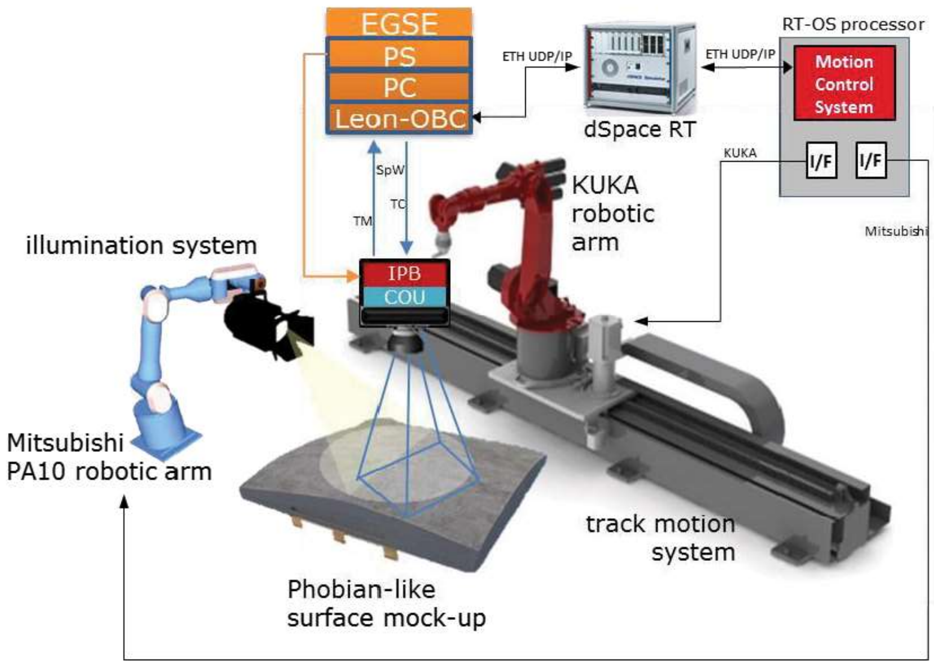

Conclusions

- Absolute Navigation and Relative Navigation techniques are considered key technologies for future planetary explorations;
- The visual navigation systems has a relatively high TRL (5/6) and has been evaluated very promising in term of performance and robustness;
- Ongoing breadbording activities for PIL and HIL validation shall increment the technology TRL in GMV Romania;
- GMV Romania has acquired expertise in AbsNav and RelNav through projects like VISONE, LL-VN&HDA, DAFUS-AIM, TAIM, CAMPHORVNAV and PILOT-B+ and will receive support from GMV through continuous transfer of know-how and technology.

Thank you

www.gmv.com

INNOVATING SOLUTIONS

Presentation 2509

Open Loop Verification of Guidance and Navigation System for an Asteroid Mission

Tudor Muresan, Massimo Casasco
European Space Agency

Open Loop Verification of Guidance and Navigation System for an Asteroid Mission

Tudor Mureșan

Massimo Casasco

GNC Section of ESA

Agenda

- Introduction
- Problem definition
- Previous work
- Simulator design and setup
- Planet and Asteroid Natural scene Generation Utility (PANGU)
- Results, discussion, observations
- Future work
- Questions

Introduction

- The work shown here was performed as part of the Young Graduate Trainee programme
- The outline is the Asteroid Impact Mission (AIM)
- The project sought to integrate and test a simplified GNC simulator
- Vision-based navigation
- Image processing

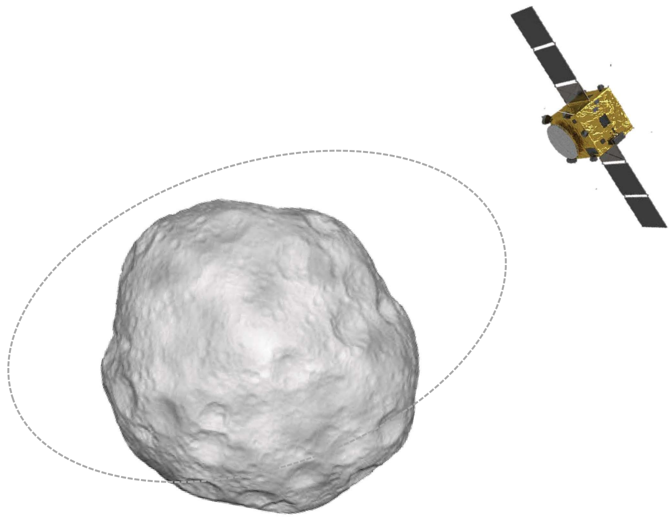

Page 314

GNC definitions and concepts

- GUIDANCE (G): establishment of the desired path to follow
- NAVIGATION (N): establishment of the current and future state
- CONTROL (C): actions to match the current state (navigation) with the foreseen path (guidance)

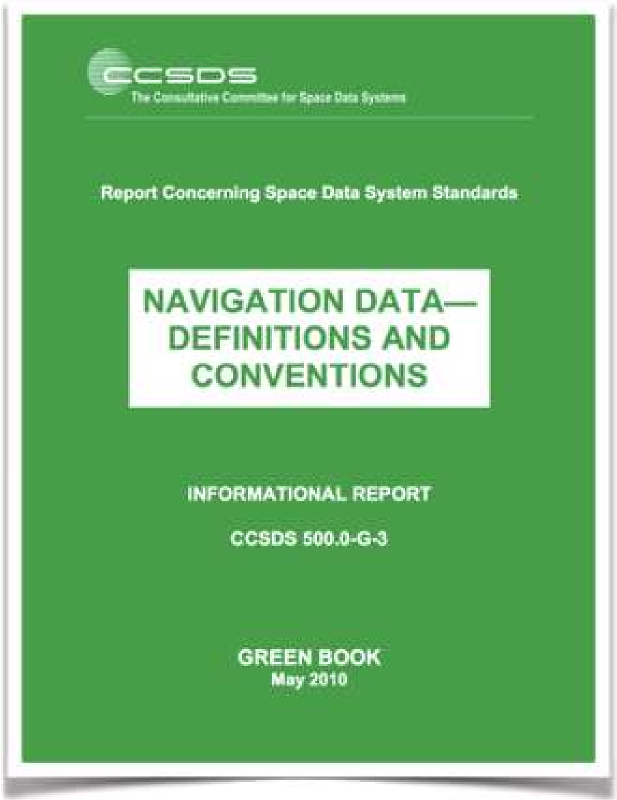
CCSDS
The Consultative Committee for Space Data Systems

Report Concerning Space Data System Standards

NAVIGATION DATA—
DEFINITIONS AND
CONVENTIONS

INFORMATIONAL REPORT
CCSDS 500.0-G-3

GREEN BOOK
May 2010

http://public.ccsds.org/publications/archive/500x0g3.pdf

Guidance, Navigation, and Control for Asteroid Mining

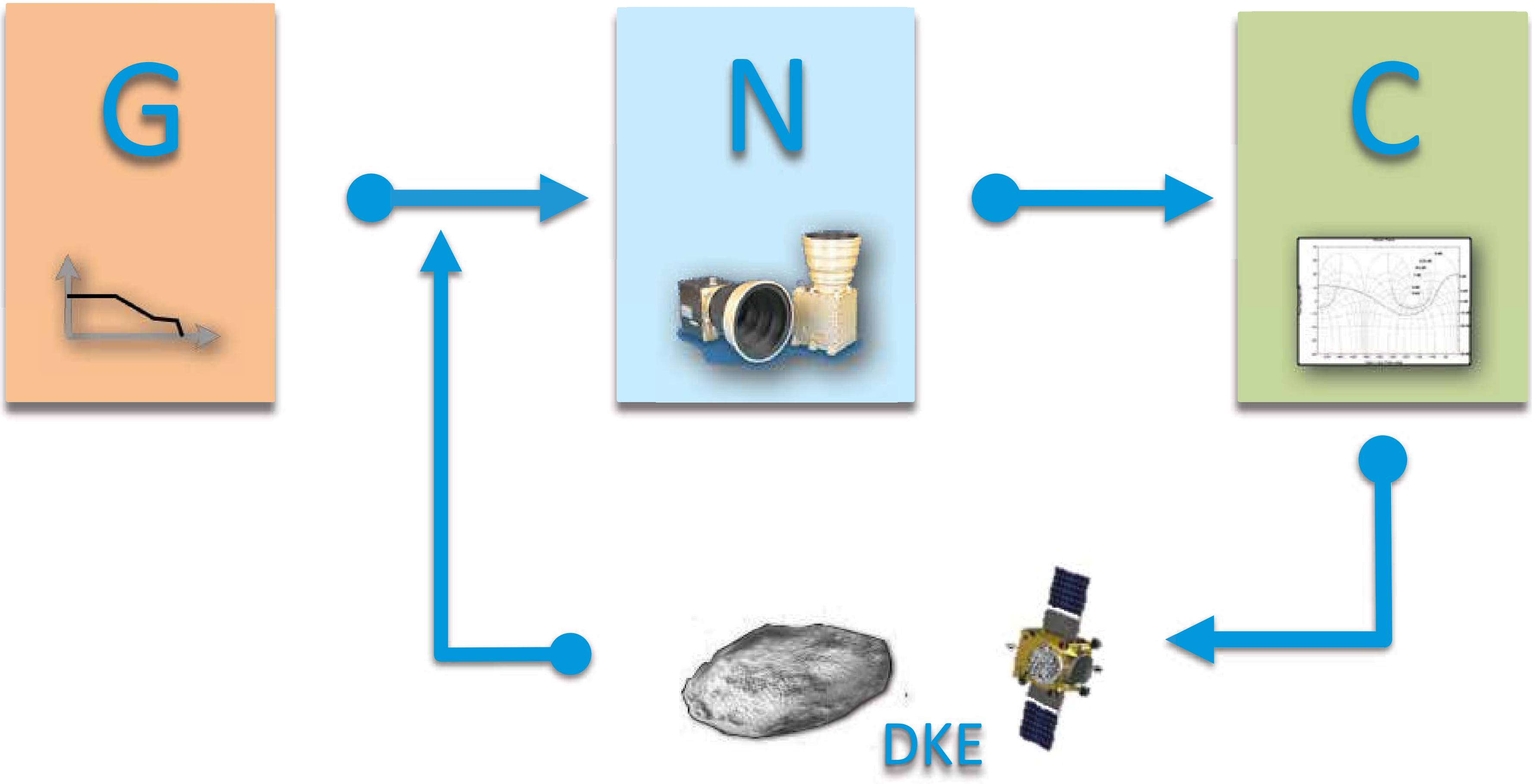

AIM mission phases

aim

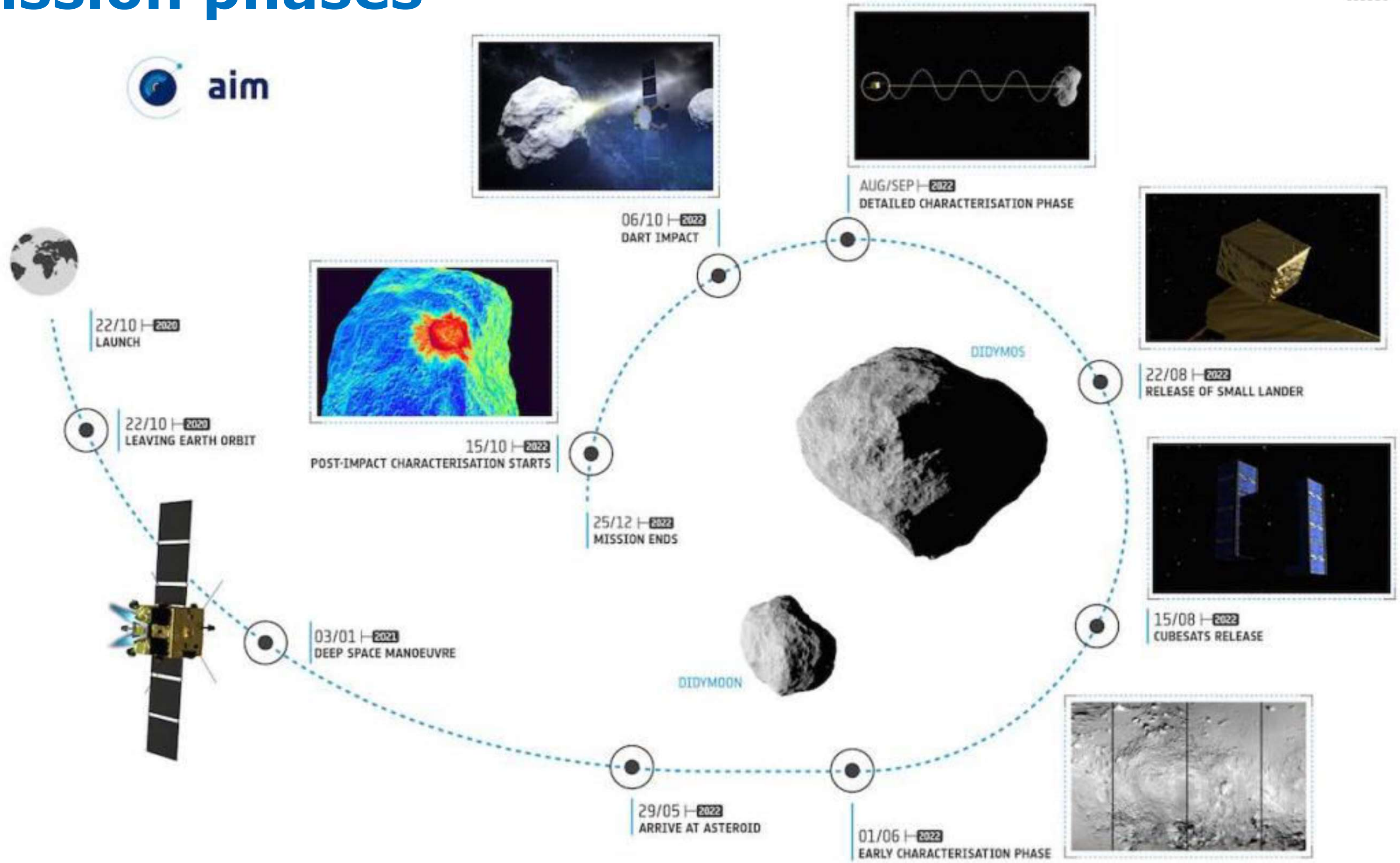

Page 317

Problem definition

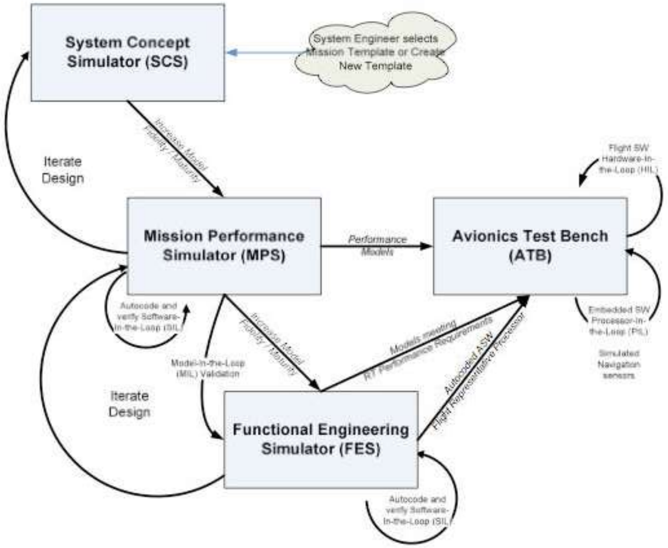

- Relative navigation in the proximity of a binary asteroid is required
- Visual navigation is very important
- Image processing is crucial
- The scope of this project was the development and validation of a simulator for the Guidance, Navigation and Control (GNC) subsystem of the Asteroid Impact Mission (AIM)
- The principal focus was the verification and integration of the previously developed MASCOT lander simulator with a new AIM spacecraft simulator
- The previous work was performed by YGT Bruno Brito

Page 318

GNC building blocks used on the AIM mission

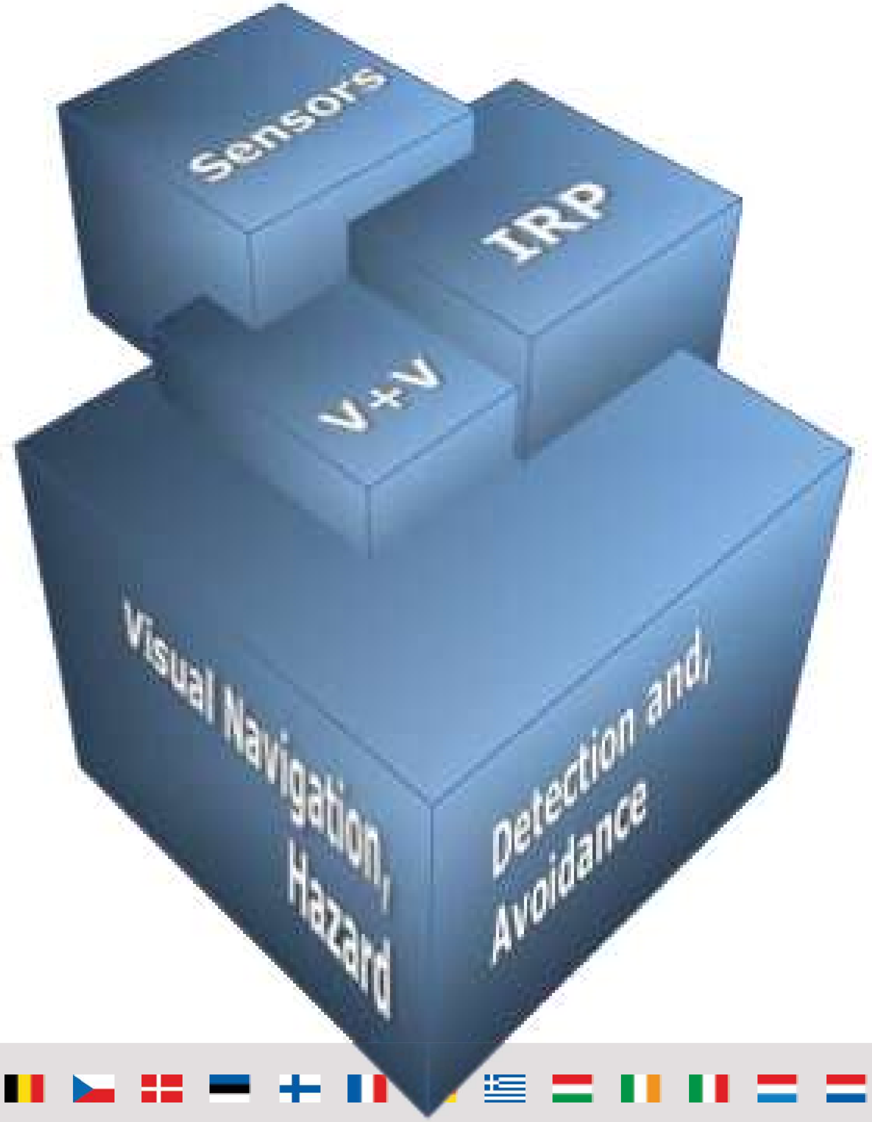

- GNC building blocks that are tested under the AIM mission

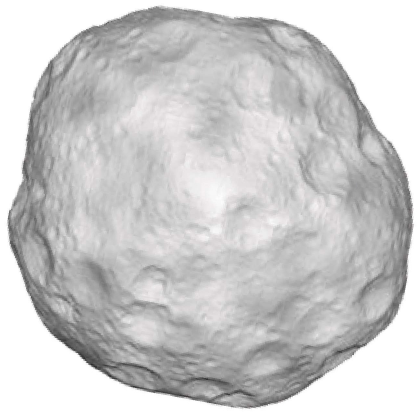

AIM Guidance technologies

- Interplanetary trajectory guidance: mid course correction maneuvers, computation of delta-V and energy to reach the required asteroid, ground contact
- Rendezvous and close approach guidance: relative trajectories between chaser and asteroid target, collision avoidance maneuvers, mission phases and transitions, retreat to safe hold points

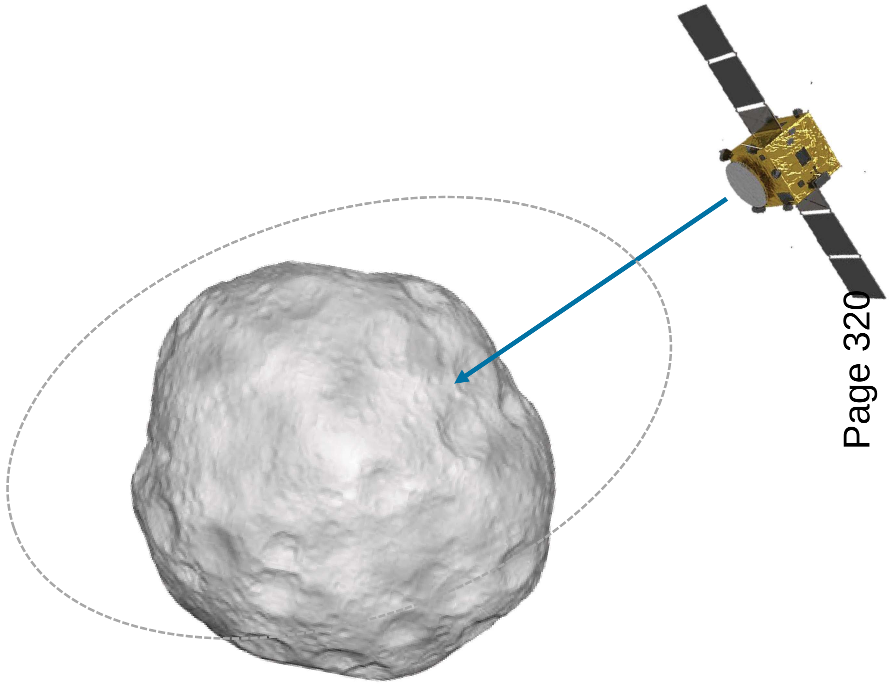

AIM Navigation technologies

- Target acquisition and identification: vision-based cameras (wide and narrow fields of view), infrared cameras, multi-spectral, altimeters, LIDAR, IMU, STR
- Image processing for navigation: feature Extraction and image correlation, optical flow
- Estimation and data fusion for navigation: sensor data fusion, deterministic and stochastic filtering, Kalman

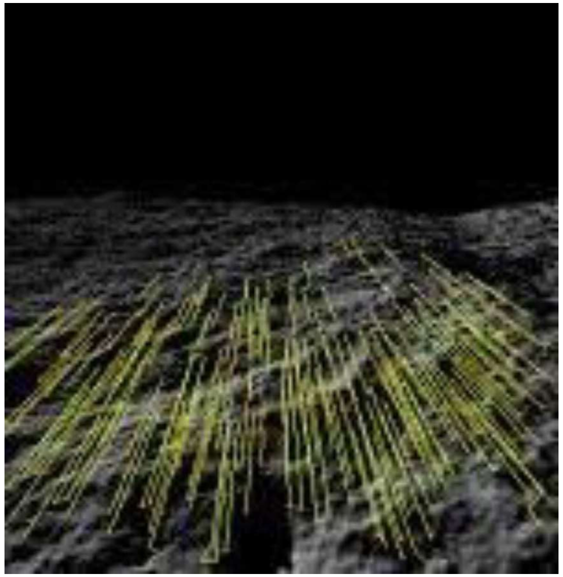

AIM Control technologies

- Optimal and robust control: optimal guidance profiles for descent and landing, re-targeting functions, on-board real-time trajectory optimization, advanced robust multi-variable control
- Failure detection, isolation, and recovery: fault detection and accommodation, recovery procedures, modes transitions, mission vehicle management
- GNC testing facilities

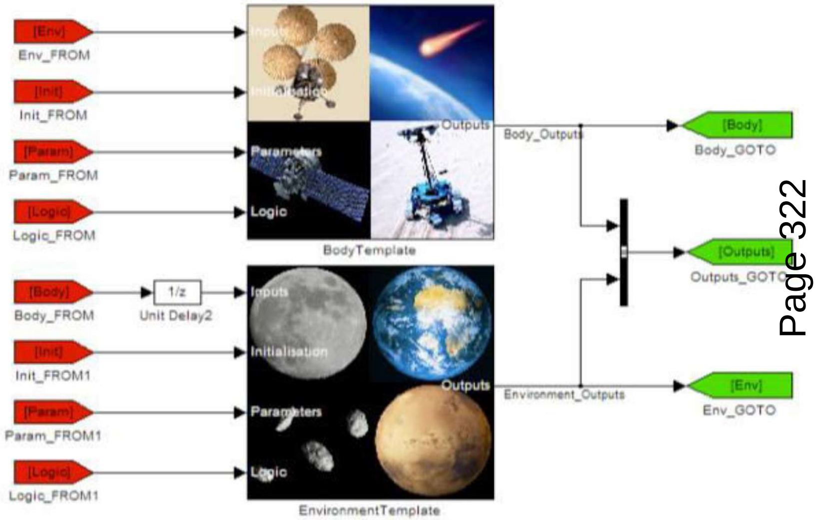

AIM DKE technologies

- Environment modelling: gravity model of asteroids, dust environment, lighting conditions, spectral signatures of the targets
- AIM vehicle design and knowledge: matrix of inertia, perturbation sources

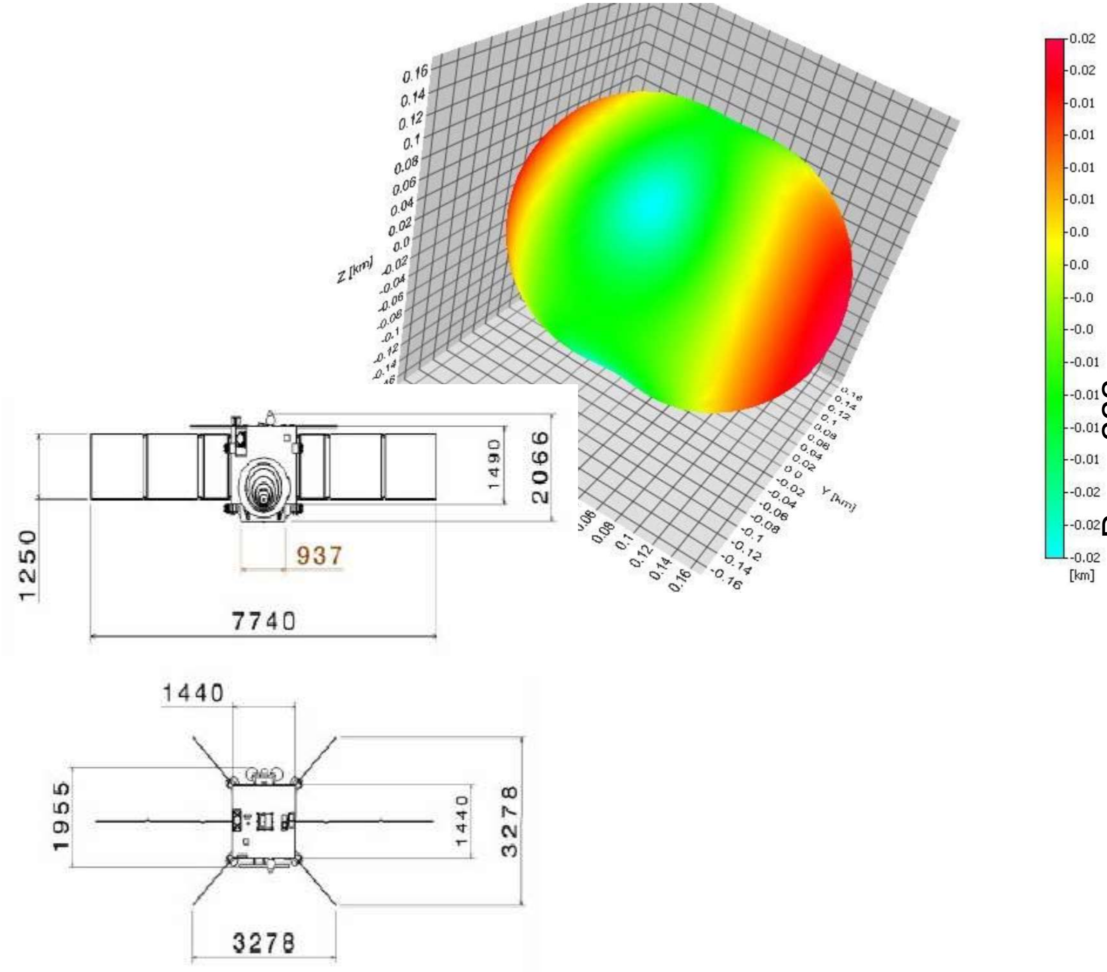

Simulator design and setup

- Complete model-based Reaction Wheel design, based on Bepi Colombo
- Commutation delay
- Generated torque
- Spike torque
- Viscous and magnetic friction
- Stiction and coulomb friction
- White noise
- Propagator
- Tachopulses generator

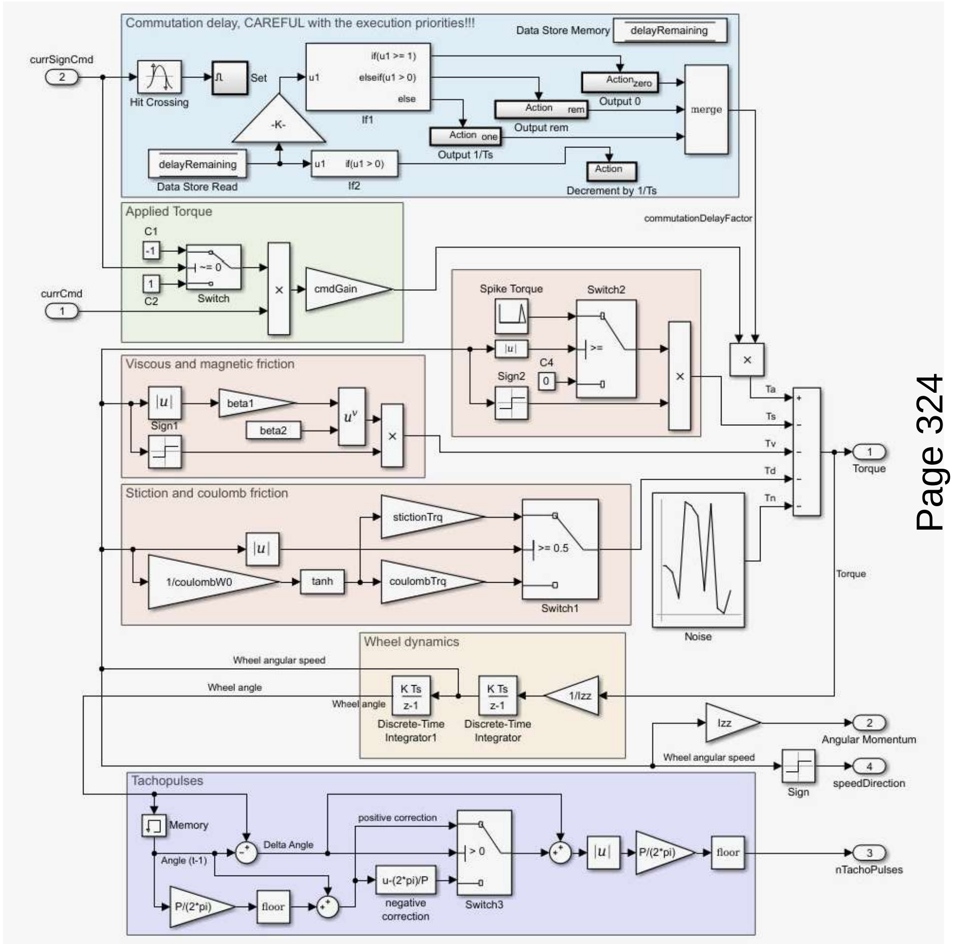

Page 324

Simulator design and setup

- Complete empirical bipropellant thruster model, based on Bepi Colombo

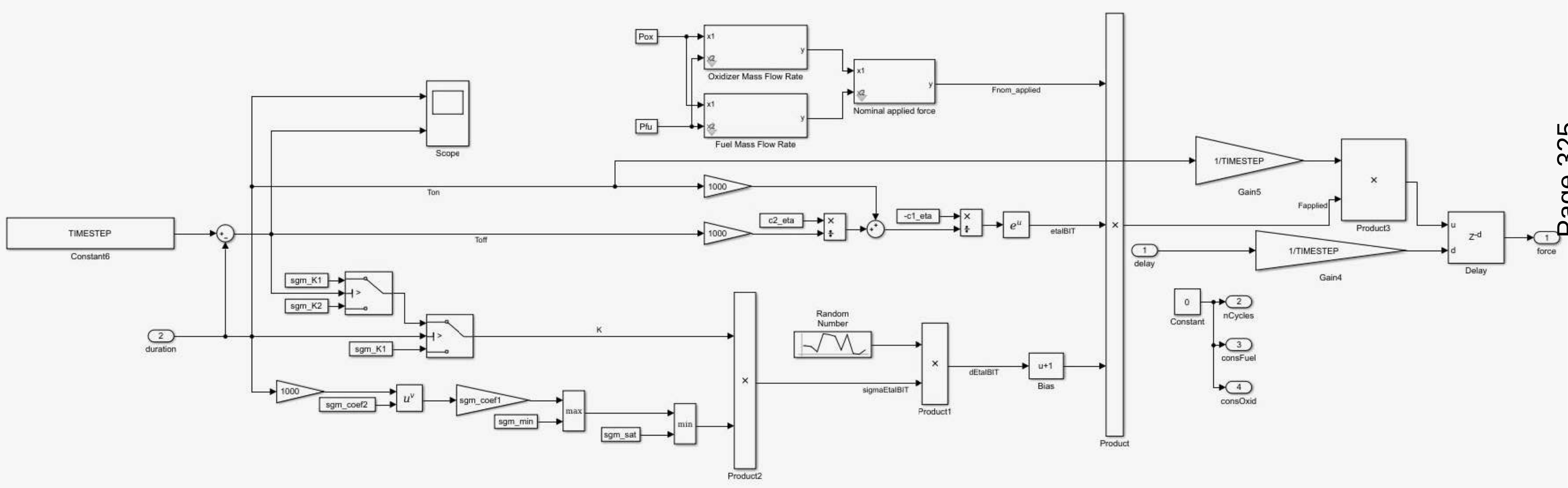

Page 325

PANGU v4

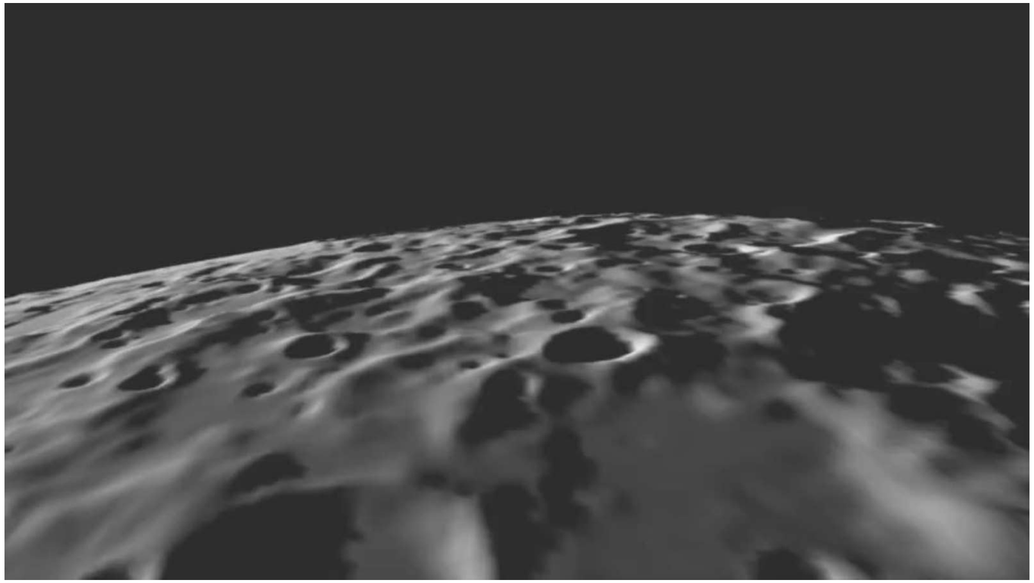

- Surface modeller: realistic surfaces (MLI, OSR, solar cells…); Generate surface file and shadow maps from scratch or from existing Digital Elevation Maps (DEM); Features available are craters, boulders and dunes
- Whole planet and asteroid models are also possible; Viewer to render the surface; Fog / atmospheric dust; Dust devils, Dust kicked off by thrusters; Sky colour, stars, Earth, moon visible
- Rendering of the surface with a shadow map; Dynamic shadows; DEM completion (filling holes, adding craters…); Surface analysis (illumination, boulder coverage…); Rover surface navigation (experimental feature)
- Asteroid simulation: Fast rendering of surface boulders on asteroid now possible, multiple bodies casting dynamic shadows
- Virtual Spacecraft Image Generator Tool
- Import of CAD/3D model
- University of Dundee

PANGU 4 Itokawa orbit simulation

PANGU v4 simulation of a rotation of
Itokawa by Hayabusa/AMICA 2005-Oct-01

Created: 2016-Jun-17

Modelling: Iain Martin/PANGU v4.00
Rendering: Martin Dunstan/PANGU v4.00

(c) Space Technology Centre,
University of Dundee, Scotland, UK

With thanks to ESA

Flyby and release trajectory

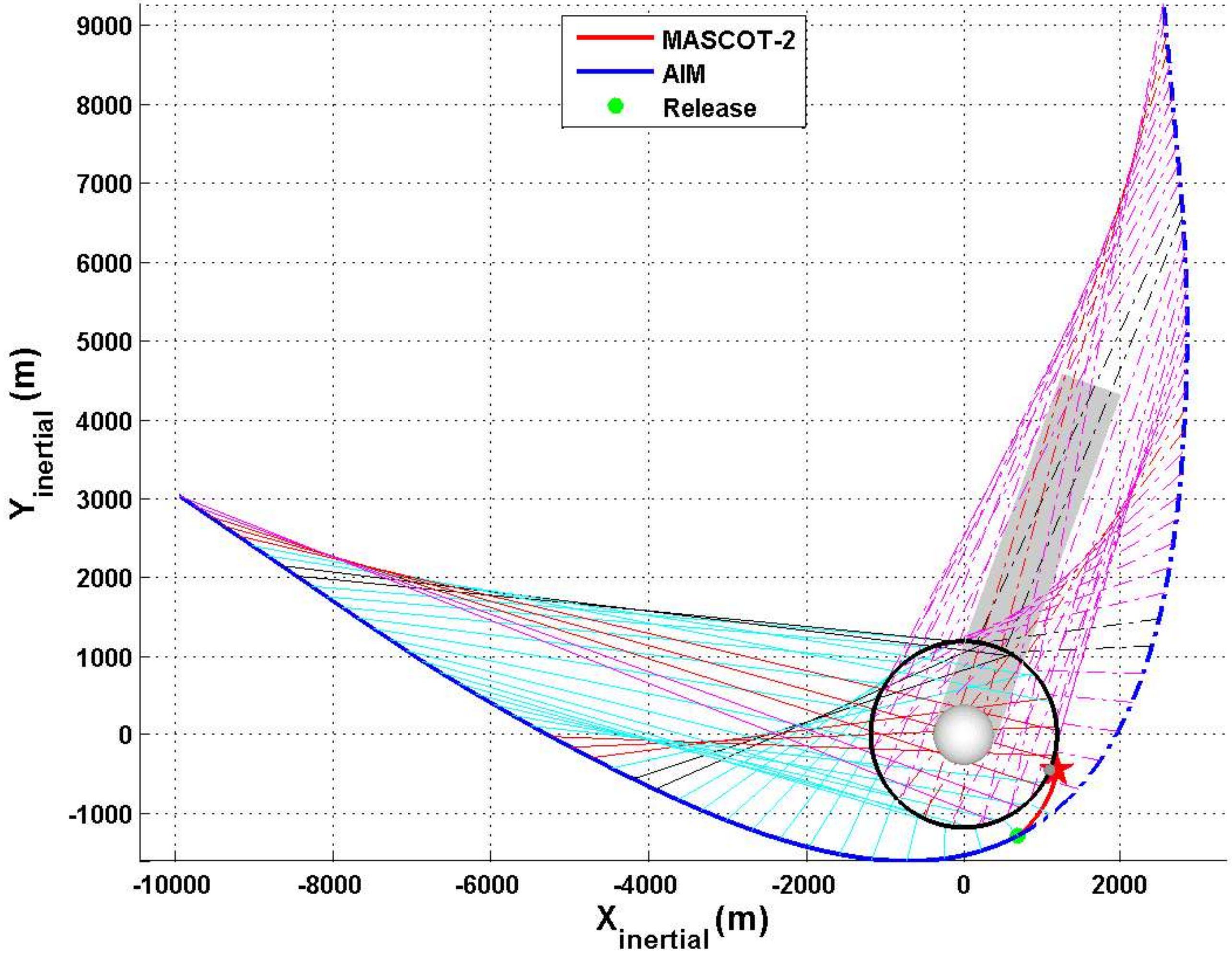

Page 328

MASCOT release Monte Carlo results

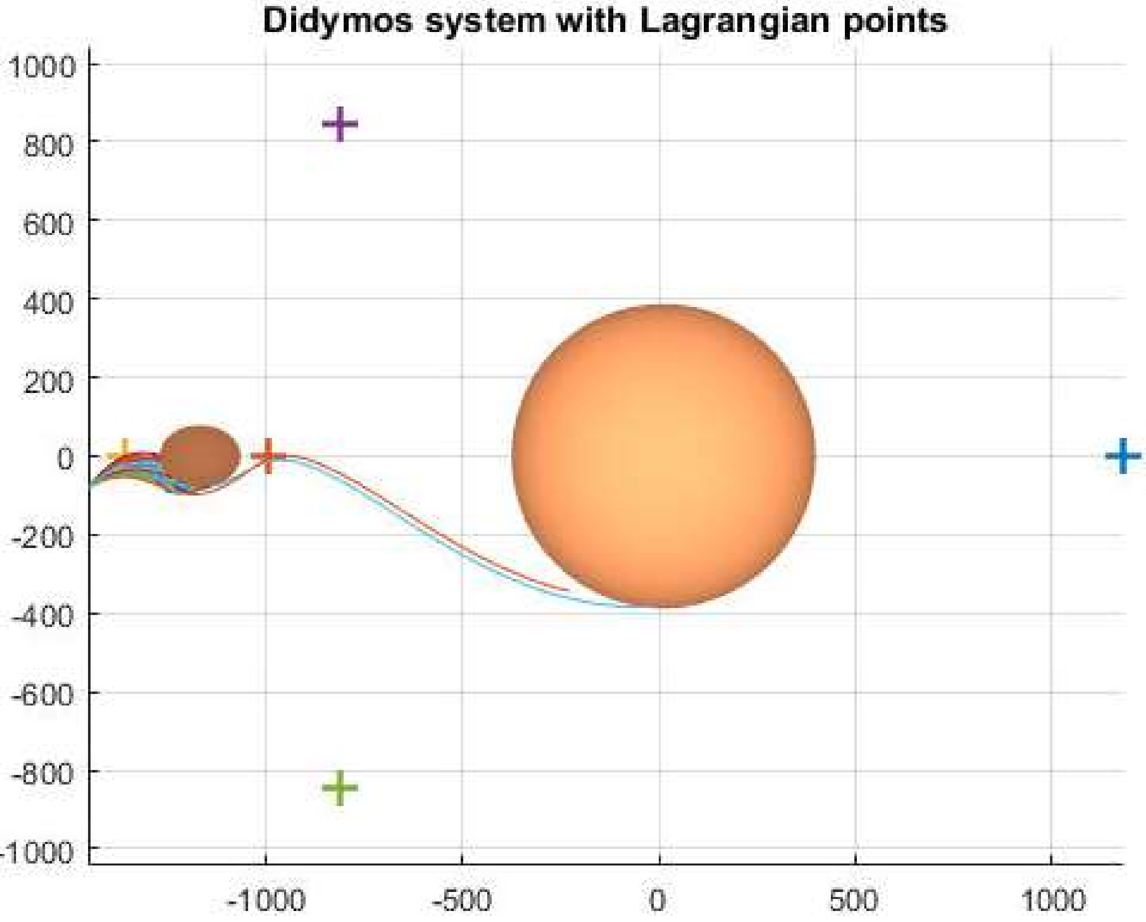

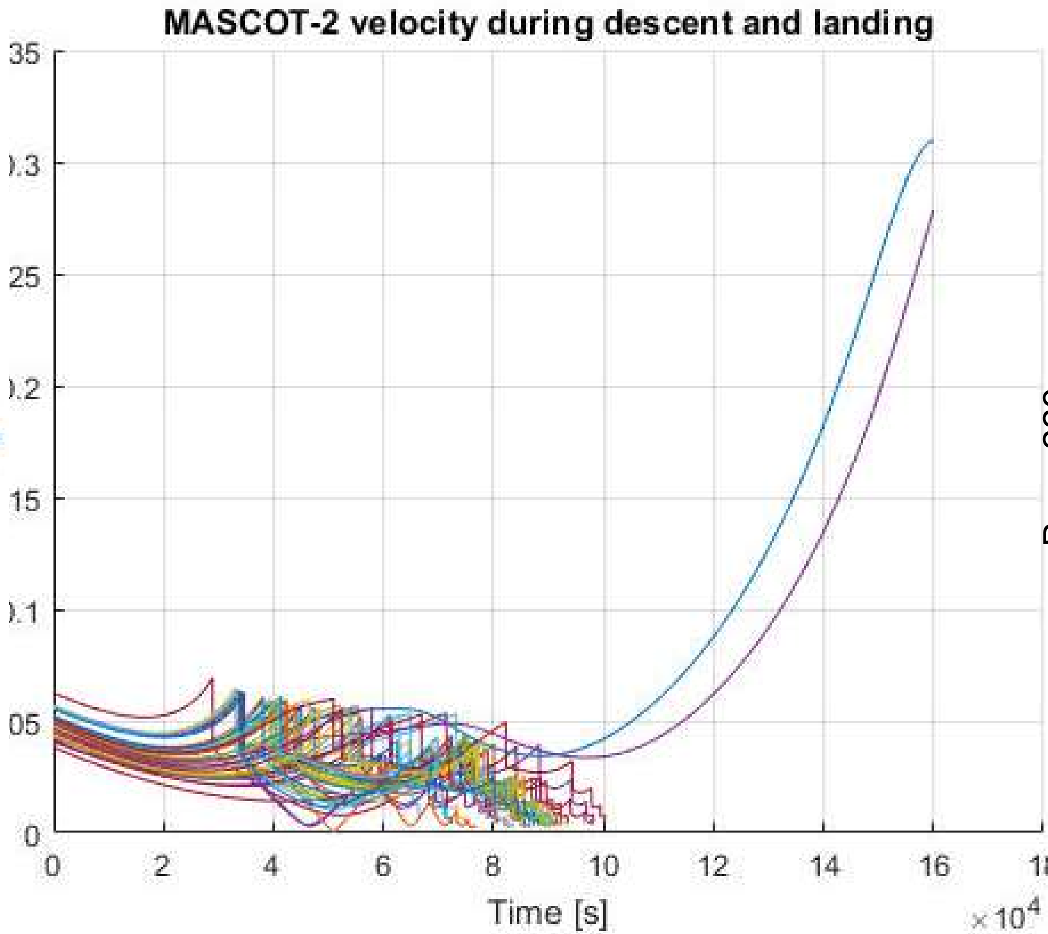

Processor In the Loop (PIL) testing facility

- (Auto-)coding of GNC algorithms into C-code and compilation to upload in flight-representative boards (LEON-2 and LEON-4 processors, FPGAs, etc.)
- Guidance algorithms
- Navigation algorithms, filters
- Image Processing algorithms
- Control algorithms
- Verification and validation of GNC code and functionality
- Performance testing

Page 330

AIM testing facilities for GNC

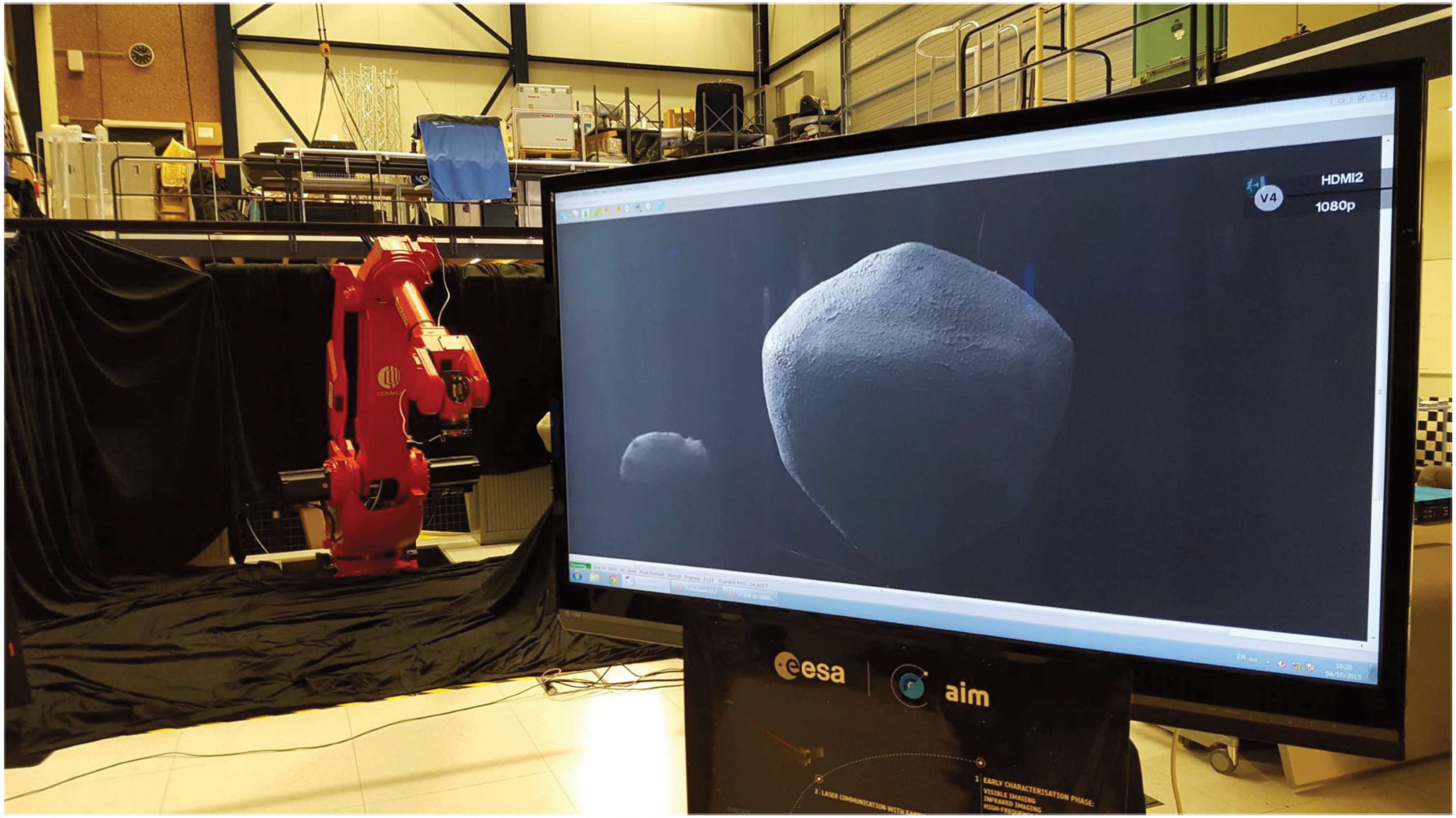

Future work

- Image processing integration
- Filter implementation
- Closed loop simulations

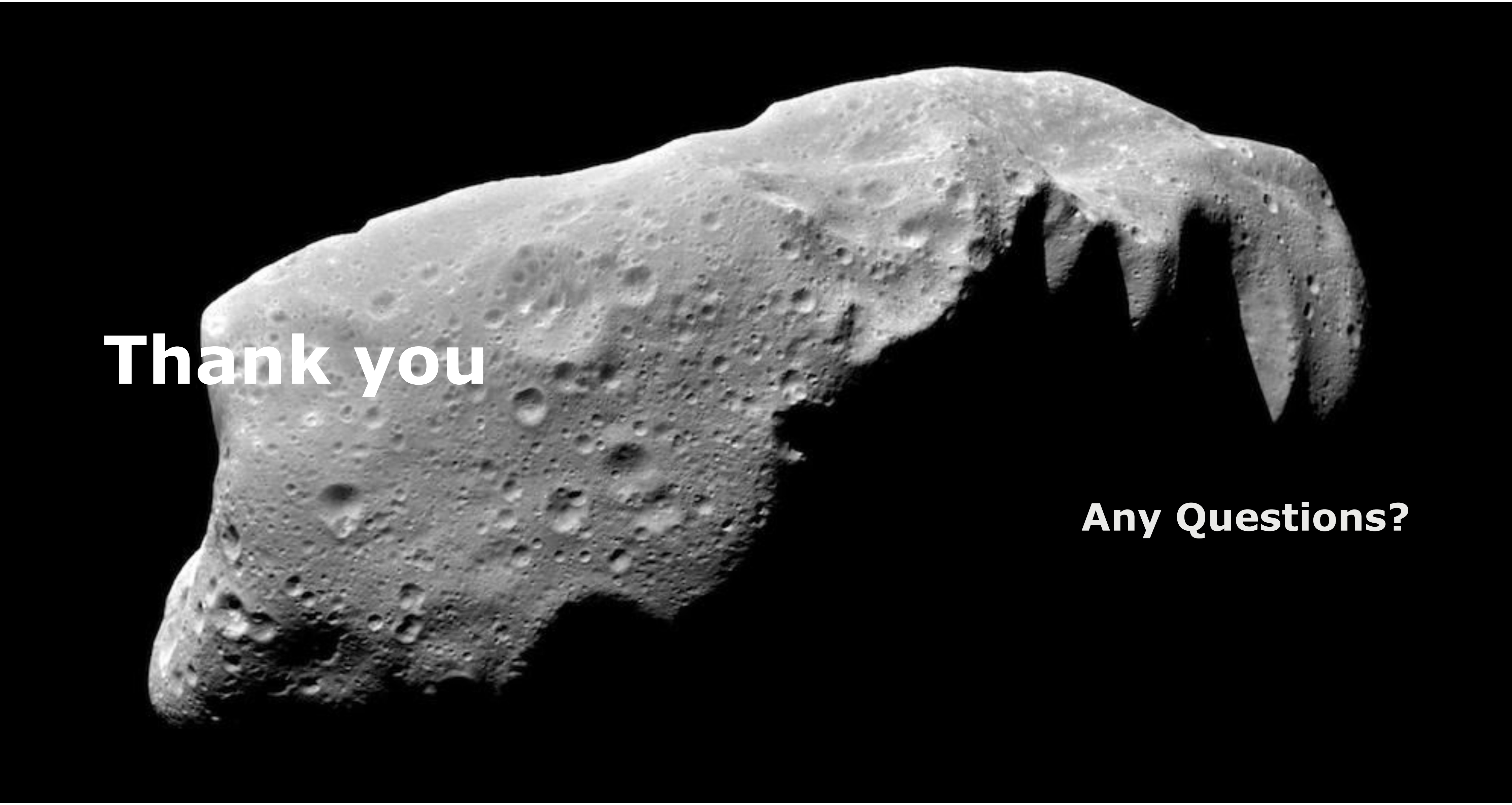
Thank you
Any Questions?

Presentation 2510

IMFUSING

GNSS Localization in Constraint Environment by Image Fusing Techniques

Universitatea Politehnica Timişoara

Pia]a Victoriei nr. 2
RO 300006 - Timi[oara
Tel: +40 256 403000
Fax: +40 256 403021
rector@upt.ro
www.upt.ro

ThalesAlenia Space
a Thales / Leonardo company

Politehnica University of Timisoara

IMFUSING

GNSS Localization in Constraint Environment by Image Fusing Techniques

16-20.10.2017
Bucharest, Romania

CEAS COUNCIL OF EUROPEAN AEROSPACE SOCIETIES

Aerospace Europe
6th CEAS Conference

AKNOWLEDGMENTS

- This work has been supported by **IMFUSING (Quality of Services Improvement for GNSS Localization in Constraint Environment by Image Fusing Techniques**), a contract part of the Romanian Industry Incentive Scheme aimed at supporting the participation of Romania in **ESA/ESTEC** mandatory activities.
  - Number of the contract: ESA - 4000111852/14/NL/Cbi
  - Contractor: Politehnica University of Timisoara (UPT)
  - Subcontractor: Thales Alenia Space-France (TAS-F)
  - Participants:
    - From UPT: Ciprian David, Vasile Gui, Andrei Campeanu, Corina Nafornita, Alexandru Isar, Ioan Nafornita, Marius Otesteanu, Monica Nafornita;
    - From TAS-F: Guillaume Carrié, Michel Monnerat, Pauline Martin

AGENDA

1. Urban Navigation – General Problem
2. Navigation Algorithms / Image Hybridisation
   1. Image Processing module
   2. GNSS Processing Module
   3. Fusing module
3. Performances assessment with real world data
   1. Experimental Campaign
   2. Results
4. Conclusions

Piața Victoriei nr. 2, RO 300006 - Timișoara, Tel: +40 256 403000, Fax: +40 256 403021, rector@upt.ro, www.upt.ro

Universitatea Politehnica Timişoara

Urban Navigation
–
General Problem

Piața Victoriei nr. 2, RO 300006 - Timișoara, Tel: +40 256 403000, Fax: +40 256 403021, rector@upt.ro, www.upt.ro

Urban Navigation –General Problem

- In urban environment, the LoS of a satellite is frequently disrupted by obstacles
  - Inaccurate information provided to a GNSS receiver
  - Location errors
- The first objective of the project is to eliminate or weight the signals coming from these satellites
  - GNSS sensors are unable to identify masked satellites (case of NLoS with strong MP resulting en nominal C/N0 or vegetation affecting most of links C/N0)
  - Identification of the critical satellites by using a supplementary sensor : the fish eye camera
- The segmentation of the image provided by the fish eye camera should permit to identify the satellites that are not on the LoS of the GNSS receiver

Exemple of expected results of segmentation of the image provided by the fisheye camera.

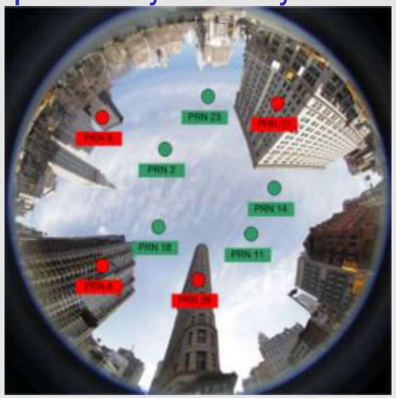

Urban Navigation – General Problem
User requirements

- Issue: impact of Multipath in an urban environment and especially NLoS
- User needs :
  - Continuity => need of satellites in LoS
  - Accuracy => limited positioning error
  - Integrity => computation of protection levels and warnings
  - Availability
- Standard RAIM initially designed for civil aviation => Need to handle specifically local environment for ground applications

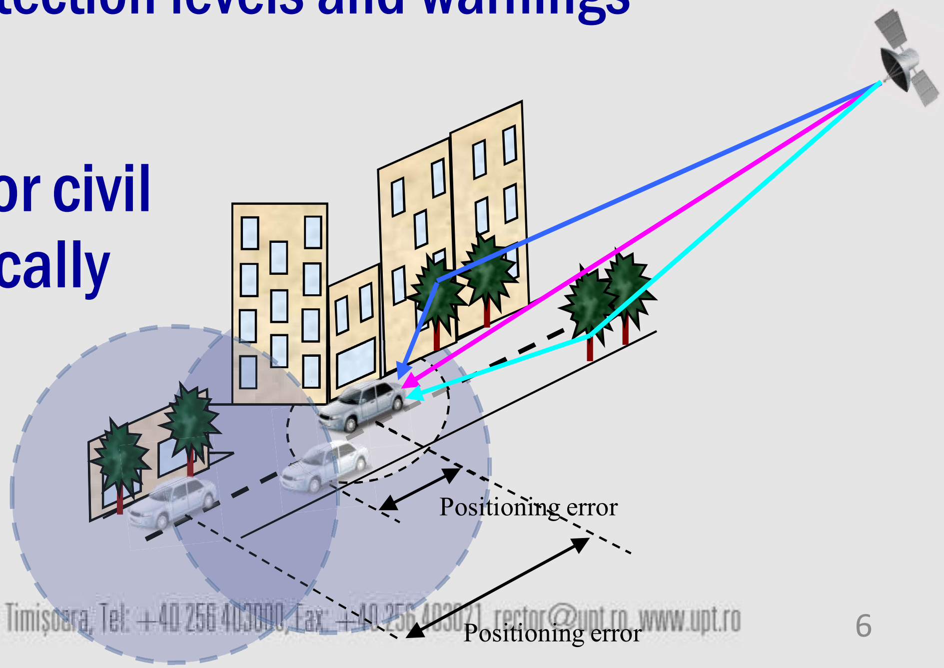

Page 340

Navigation Algorithms
/
Image Hybridisation

Image Processing Module

- Image processing module block diagram

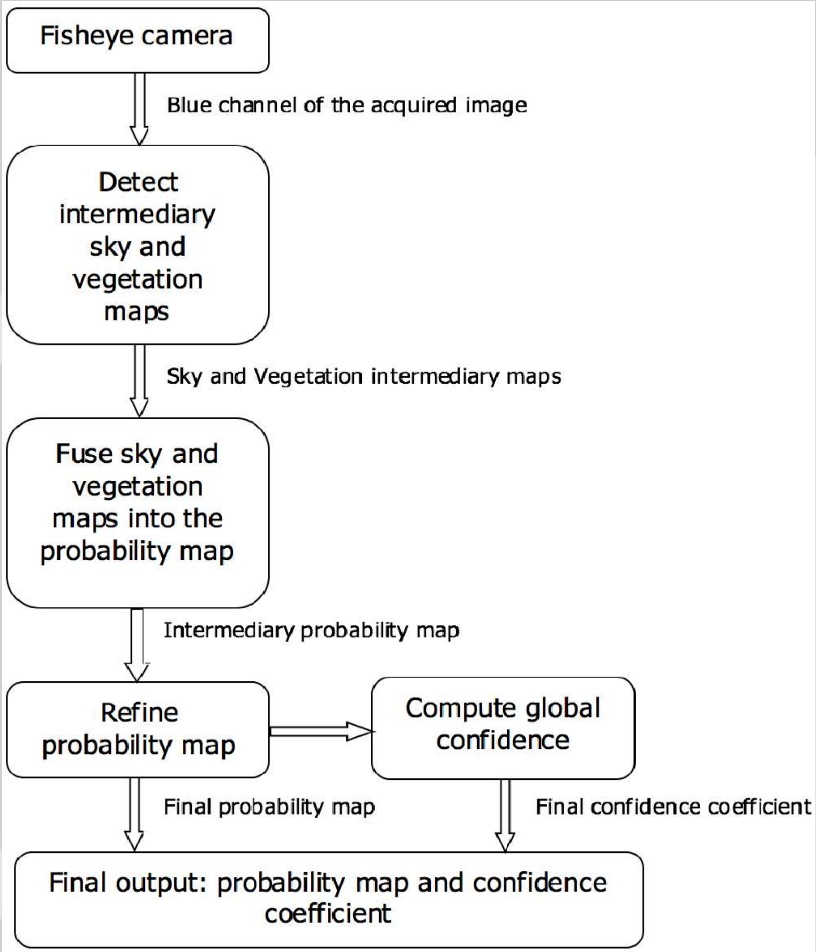

Piața Victoriei nr. 2, RO 300006 - Timișoara, Tel: +40 256 403000, Fax: +40 256 403021, rector@upt.ro, www.upt.ro

Image Processing Module

- Final output : LoS Probability Map

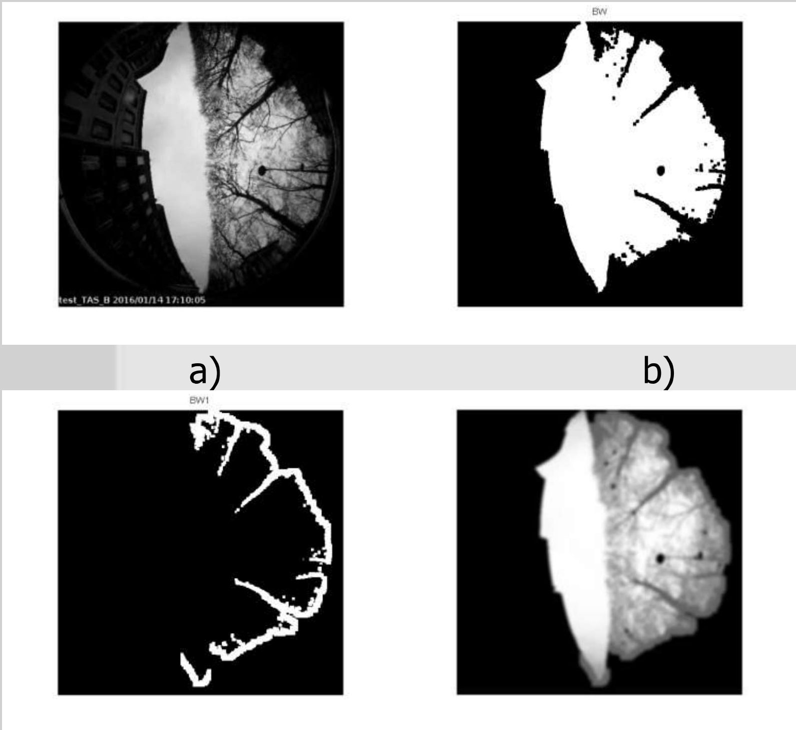

a) b)

c) d)

Figure 4: Image processing module results: a) blue channel image; b) intermediary sky map; c) intermediary vegetation map; d) final probability map

Image Processing Module

- Validation across different weather conditions

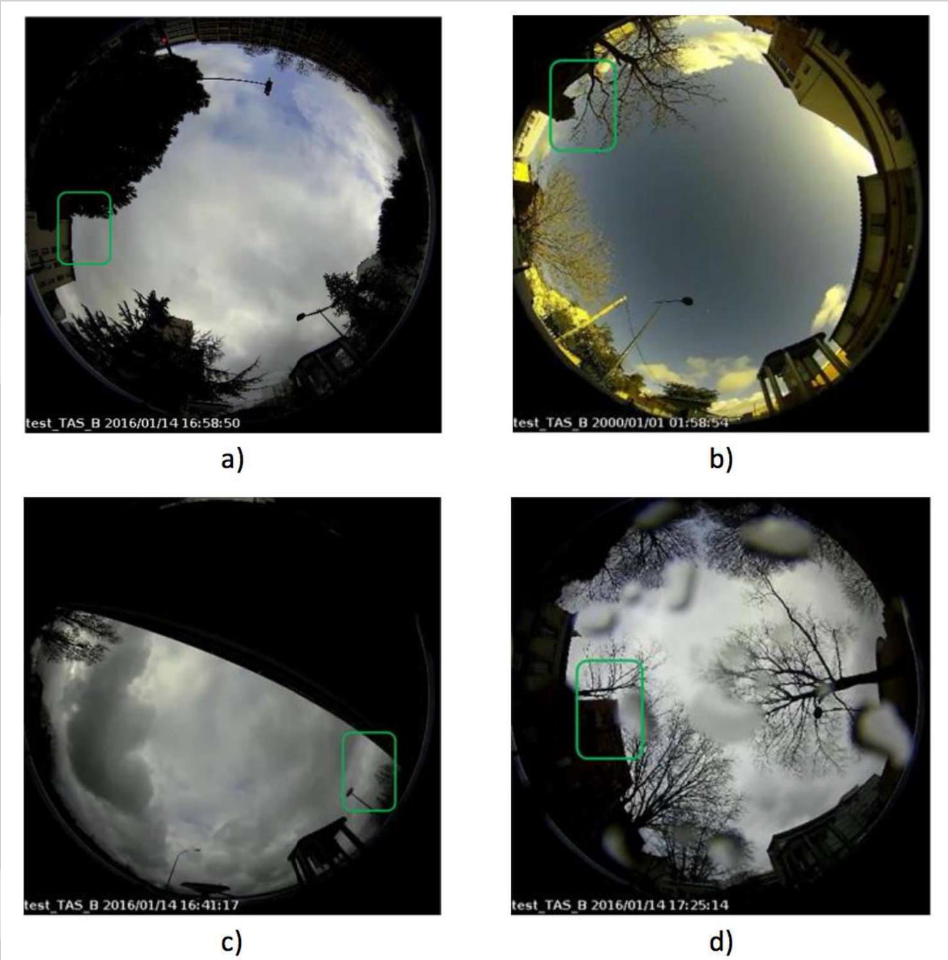

Page 344

Piața Victoriei nr. 2, RO 300006 - Timișoara, Tel: +40 256 403000, Fax: +40 256 403021, rector@upt.ro, www.upt.ro

Image Processing Module

- Validation across different weather conditions

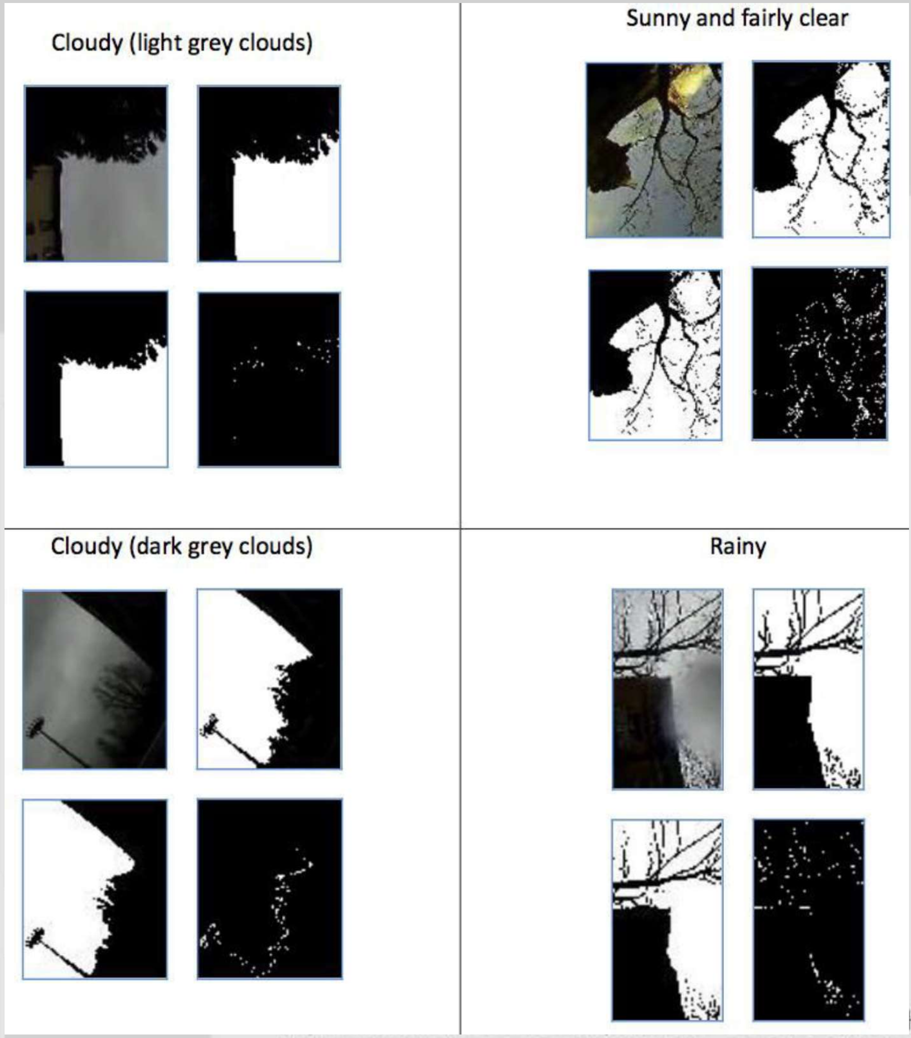

Image Processing Module

- Validation across different weather conditions

Table 4. Quantitative assessment of the segmentation in various weather conditions

Weather condition	Cloudy (light grey clouds)	Sunny and fairly clear	Cloudy (dark grey clouds)	Rainy
Patch size	81 x 100	83 x 107	76 x 95	53 x 97
Segmentation accuracy	99.66%	95.30%	98.60%	97.89%
Overall segmentation accuracy	**97.86%**			

Page 346

Piața Victoriei nr. 2, RO 300006 - Timișoara, Tel: +40 256 403000, Fax: +40 256 403021, rector@upt.ro, www.upt.ro

GNSS Processing Module

- 1 Navigation algorithm : Kalman Filter + RAIM
- Multicorrelator discriminator :
  - High performances
  - MP detection and mitigation
  - See [1] for details
- Tri-constellation GNSS Rx
  - Galileo / GPS / Glonass
- Multipath & KPI overweithing strategy
  - See [2] for details

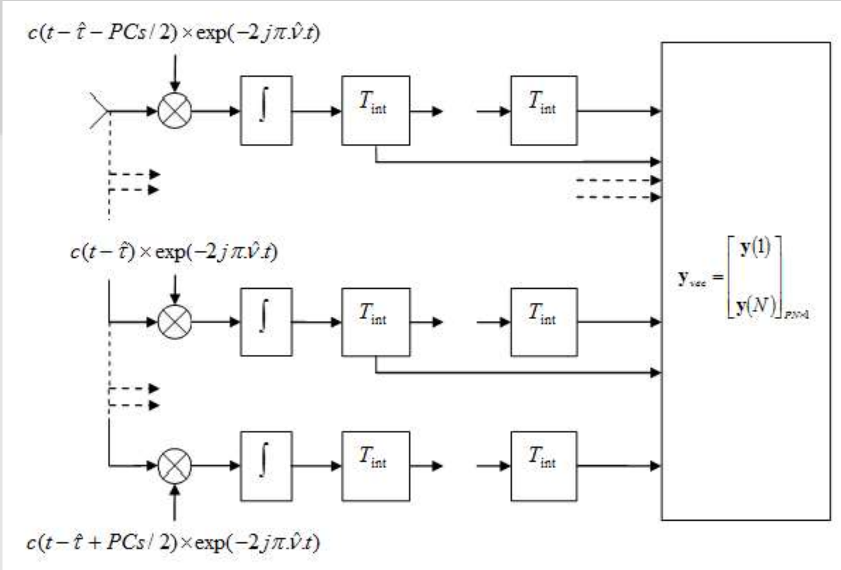

[1] G. Carrie, D. Kubrak, M. Monnerat; 2014; "Performances of Multicorrelator-Based Maximum Likelihood Discriminator"; ION GNSS+ 2014; Tampa, Flo; September

[2] G. Carrie, D. Kubrak, M. Monnerat, J. Lesouple; 2014; "Toward a new definition of a PNT trust level in a challenged multi frequency / multi-constellation environment"; NAVITEC 2014; Noordwijk, The Netherlands; December

GNSS Processing Module

Example of GNSS autonomous PVT

- Using GEMS SW Receiver from Thales Alenia Space
- GPS L1 C/A; Galileo E1 OS; Glonass G1 - PVT KF Tight with RAIM

GBox-Ref trajectory
GEMS EMLP
GEMS Multicorr-0
GEMS Multicorr-Auto

Page 348

Piața Victoriei nr. 2, RO 300006 - Timișoara, Tel: +40 256 403000, Fax: +40 256 403021, rector@upt.ro, www.upt.ro

Fusing Module (1/2)

- The GNSS pseudoranges and pseudorange rates are computed with the software receiver GEMS using the Multicorrelator tracking loop.
- These measurements are fed into a first KF GNSS autonomous PVT and its associated RAIM can thus exclude faulty satellites.
- The vehicule heading is computed.

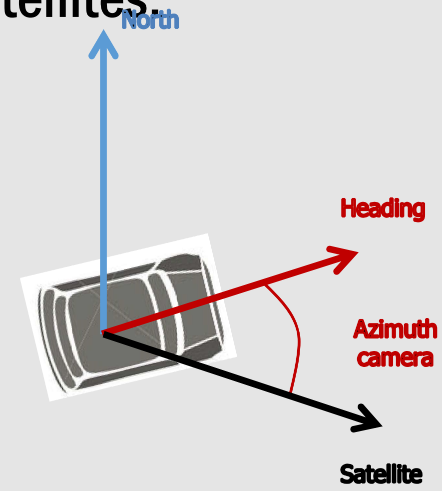

- For each satellite left, the elevation and the azimuth are computed in the vehicule/camera reference frame.

Fusing Module (2/2)

- The camera LoS probability is computed for each satellite and compared to **two** thresholds → 3-levels discretization of LoS probability :
  - <u>LoS level</u>: When pLoS is between 0.75 and 1, the received signal is considered as the LoS, the measurements are kept unchanged.
  - **<u>Doubt level</u>: When the pLoS is between 0.25 and 0.75 (most likely related to building edges or vegetation), there is a doubt on the quality of the received signal, so an overweighting is applied on the measurements as $\sigma^2 = \sigma^2 + w^2$ with**

$$w(SV,t) = f \cdot L \cdot cos(el(SV,t))$$

  - <u>NLoS level</u>: Finally, when pLoS is between 0 and 0.25, the received signal is considered as NLoS and the measurements are excluded if there are enough LoS space vehicles, otherwise they are kept and overweighted as above.
- The remaining GNSS data goes through the Kalman filter correction step, which provides the final PVT solution.
- The Horizontal Protection Level (HPL) is computed from the output of the Kalman filter as:

$$HPL = K_H \cdot D_{major}$$

Piața Victoriei nr. 2, RO 300006 - Timișoara, Tel: +40 256 403000, Fax: +40 256 403021, rector@upt.ro, www.upt.ro

Performances assessment with real world data

Experimental Campaign

- Fish eye camera : VIVOTEK FE8181/81V;
- RF capture system to record GNSS raw signals (GDAS-2);
- The SW receiver GEMS
- The reference trajectory was obtained using GUIDE GBOX that embeds a high grade Inertial Navigation System (INS)

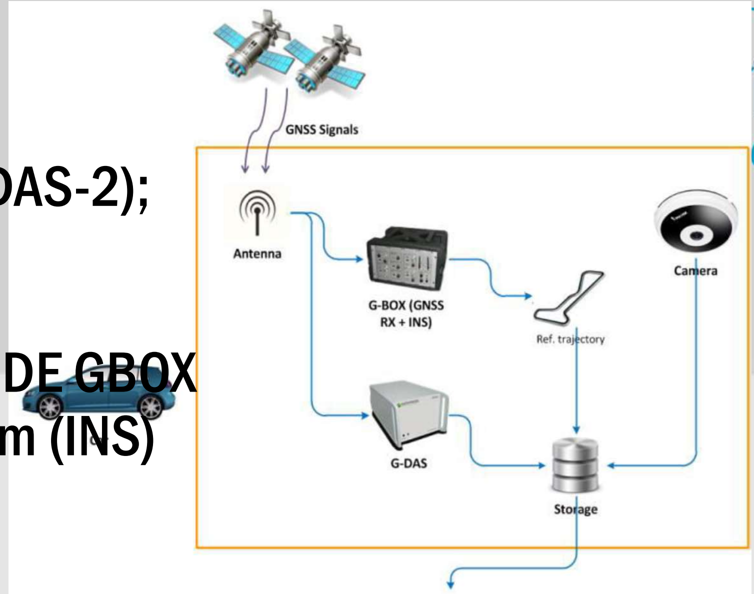

- The campaing occurred on Ja… se
  - The main trajectory lasted 1800s in urban environement
  - 18 SV from 3 constellations (8 GPS; 2 Galileo; 8 GLONASS) among which a maximum of 12 SV were used simultaneously in the PVT.

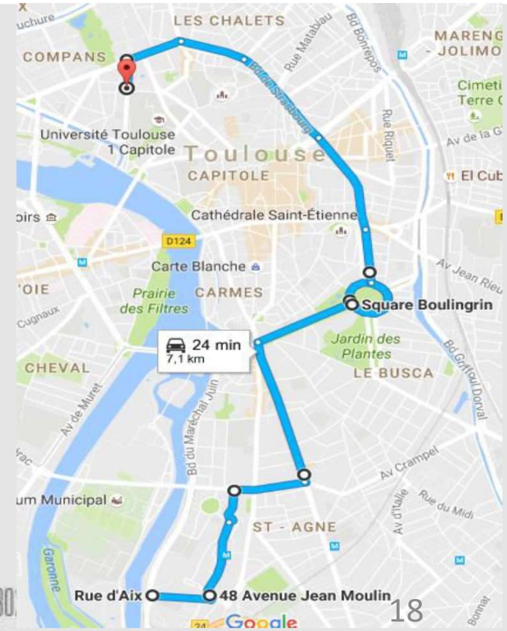

Results : whole trajectory

Universitatea Politehnica Timişoara

ThalesAlenia Space
a Thales / Leonardo company

- Environment: light urban to deep urban

- Camera improves PVT accuracy by more than 1σ (4,27m)
- No significant impact of camera
- Camera degrades PVT accuracy by more than 1σ (4,27m)

Piaţa Victoriei nr. 2, RO 300006 - Timişoara, Tel: +40 256 403000, Fax: +40 256 403021, rector@upt.ro, www.upt.ro

Results : whole trajectory

- Environment: light urban to deep urban

Discri	Camera Module	OW MP coeff	HPE			HPL			I+A (%)	MI+UA (%)	I+UA (%)
			67%	95%	99%	67%	95%	99%			
MC	OFF	Inf	4.27	8.79	12.17	31.71	41.56	58.45	0	0	100
MC	ON	Inf	3.85	6.59	10.14	36.64	47.62	78.28	0	0	100

Legend :

HPE : Horizontal Positioning Error

HPL : Horizontal Protection Level

A : Availability of the system (defined as HPL <20m)

I : Integrity of the measure

Piața Victoriei nr. 2, RO 300006 - Timișoara, Tel: +40 256 403000, Fax: +40 256 403021, rector@upt.ro, www.upt.ro

Results : whole trajectory

- HPE vs HDOP

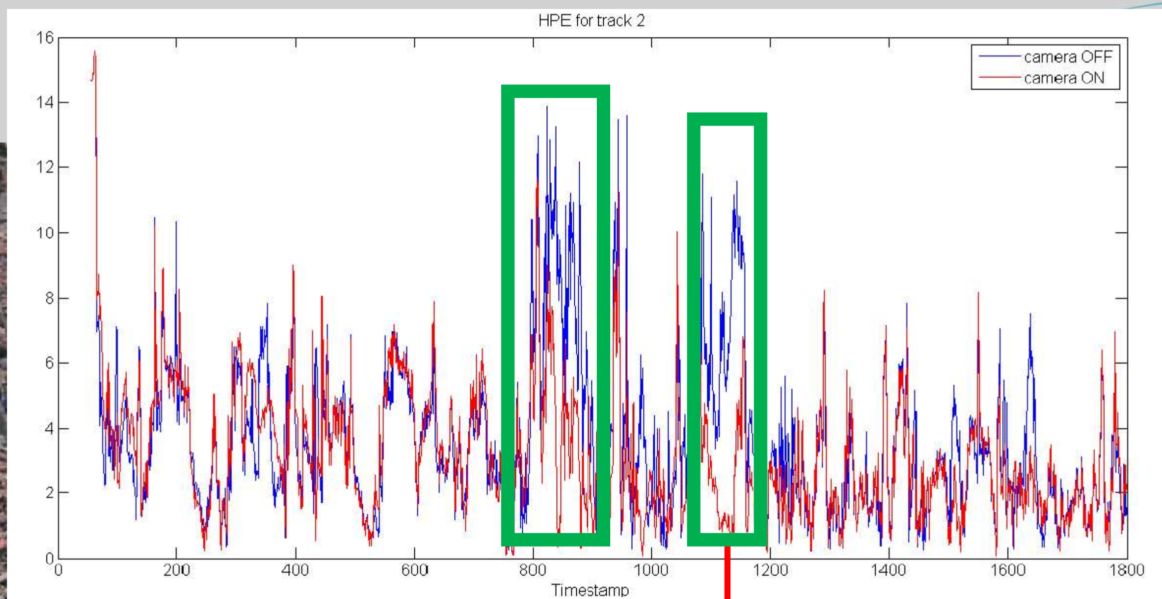

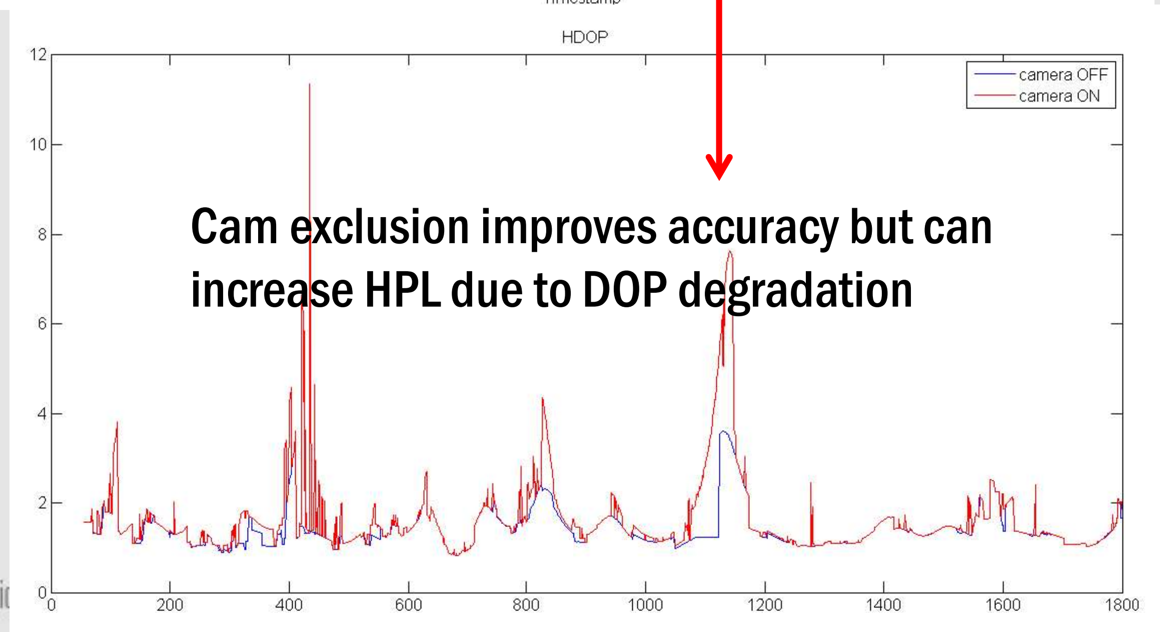

Results : focus around 850s

- HPE improved by Cam Exclusion
- Evidence impact of Cam exclusion on HDOP and then on HPL (but « smoothed » by KF)

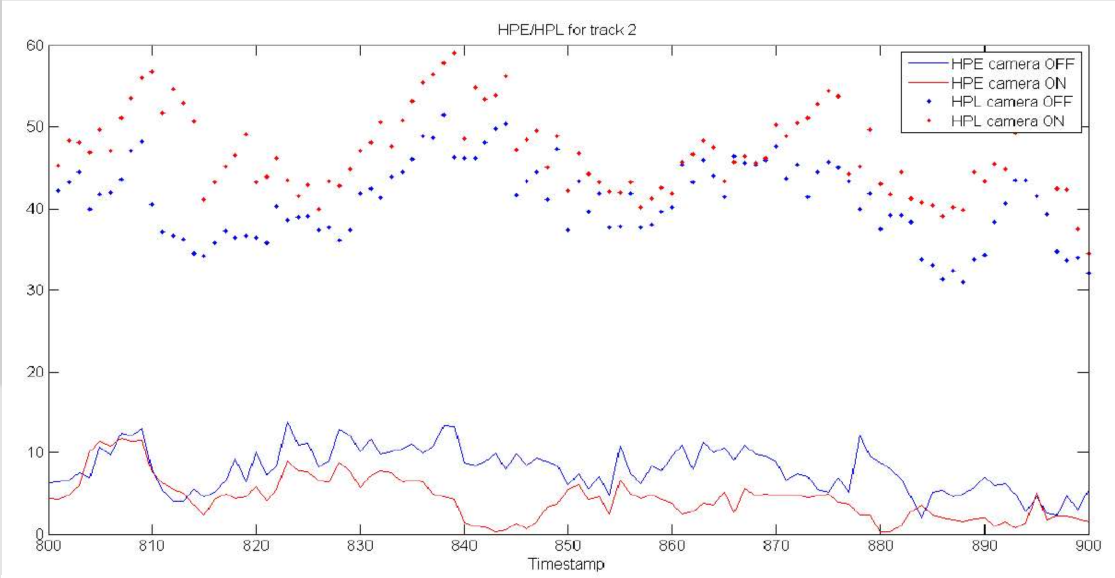

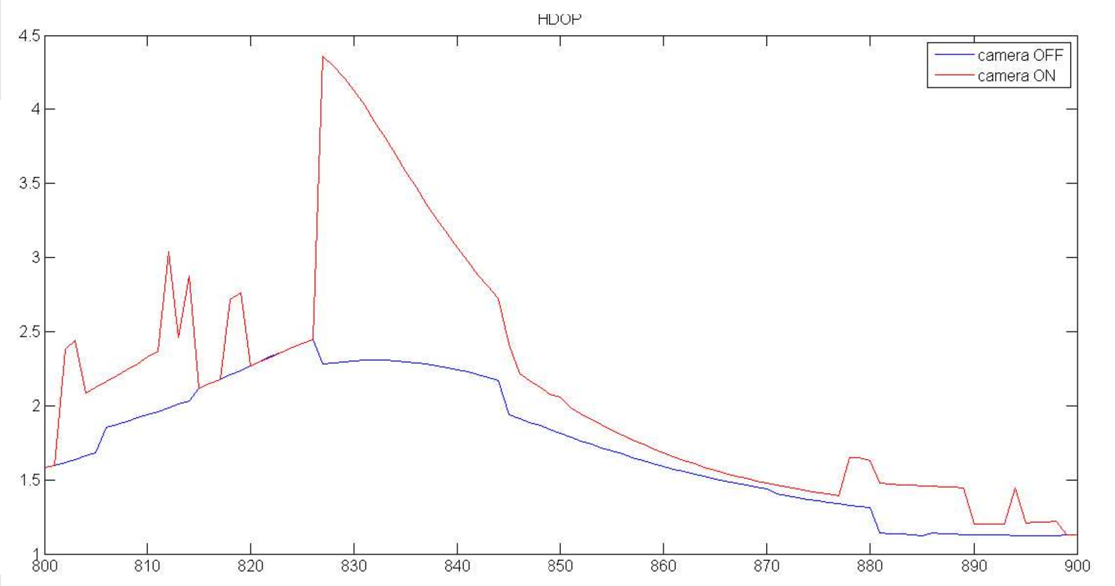

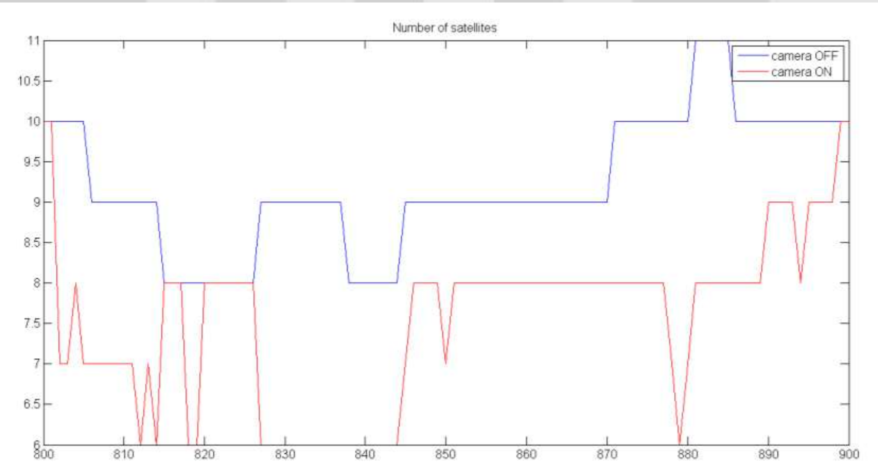

Page 356

Results: focus at 850s

- Examples of good and bad exclusions
- C/N0 cannot be an exclusion criterion

(PR biased while C/N0 very good near 400s)

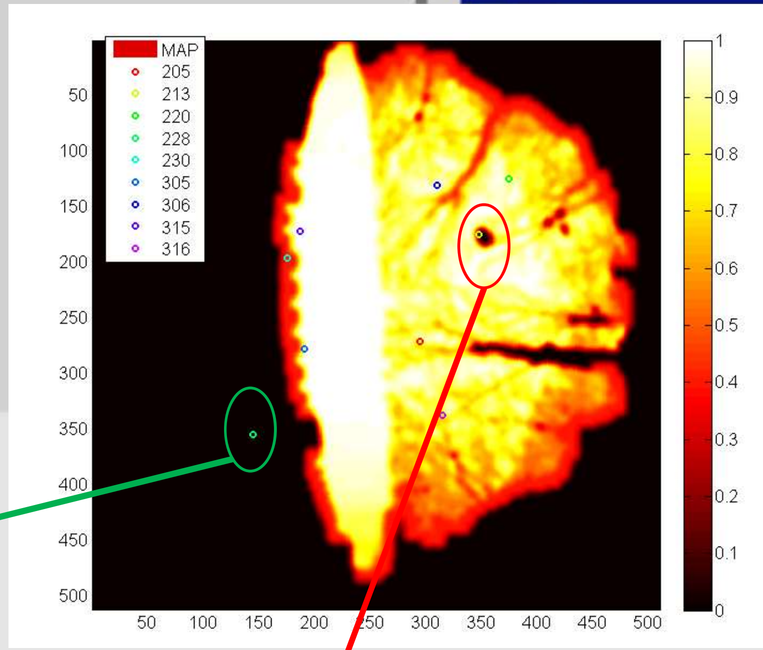

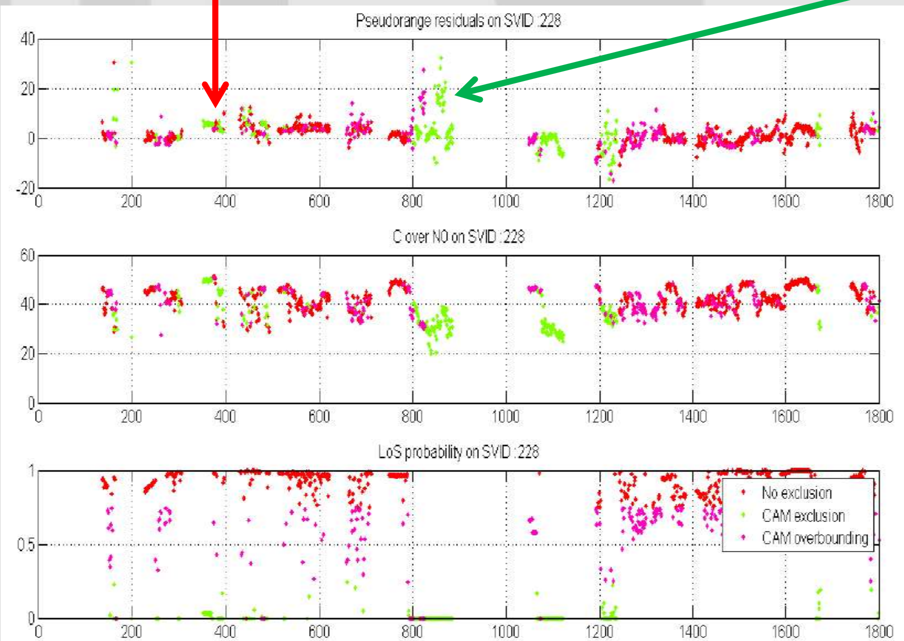

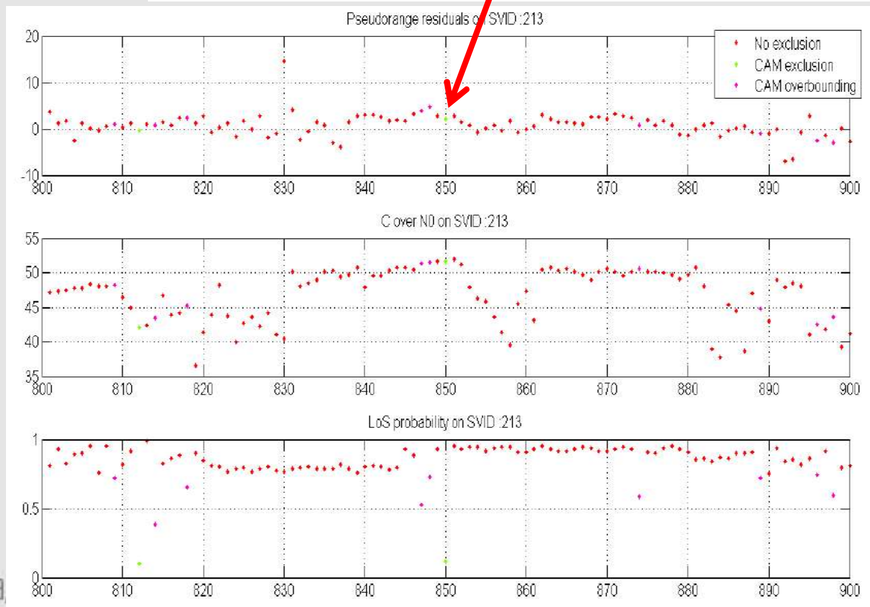

Page 357

Results: statistics on PVT Residuals

Universitatea Politehnica Timişoara

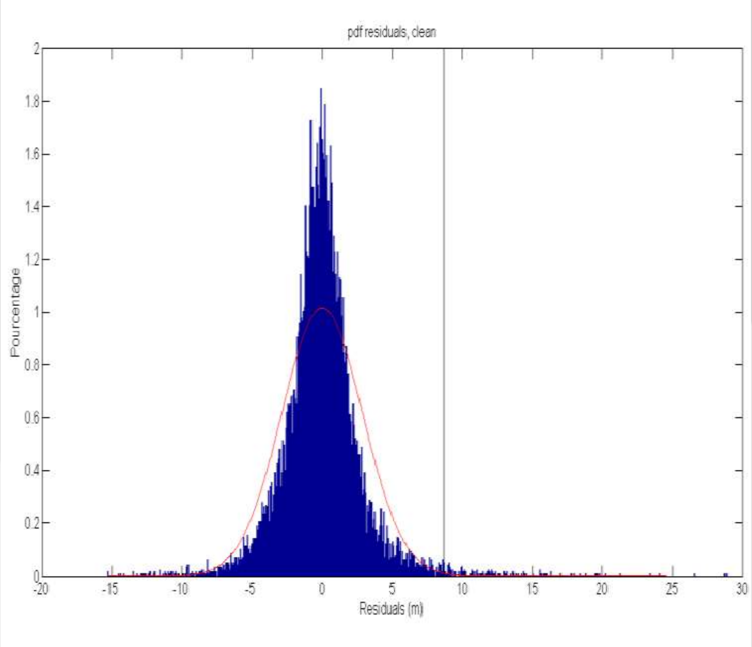

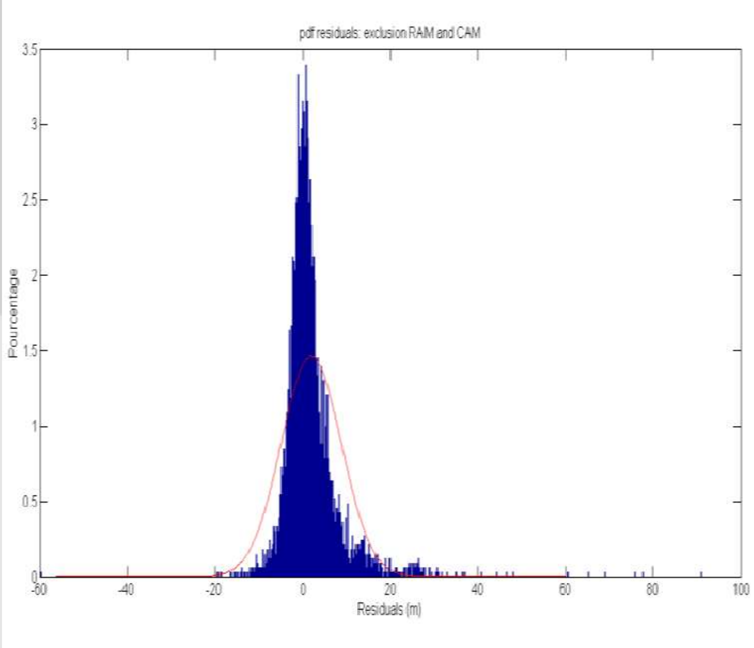

The residuals larger than 8.6m (3σ of the "clean" distribution, represented by a vertical line) are considered as due to NLoS conditions. They represent about 2% of the whole distribution. 70% of these residuals are marked as NLoS by the camera.

100% of the residuals greater than 29 meters are marked as NLoS by the camera, which represents 0.13% of the measurements.

From the measurements of whole track, 7.52% were excluded by the camera and 22% were excluded or overweighted by the camera.

Conclusions

Piața Victoriei nr. 2, RO 300006 - Timișoara, Tel: +40 256 403000, Fax: +40 256 403021, rector@upt.ro, www.upt.ro

Conclusions

- Camera **improves integrity**
- Camera module is useful to **detect NLOS** space vehicles
  - **Solve miss-integrity** problems
  - **Correct KF+RAIM+MC deficiency** when locking on a NLOS MP measurement

Piața Victoriei nr. 2, RO 300006 - Timișoara, Tel: +40 256 403000, Fax: +40 256 403021, rector@upt.ro, www.upt.ro

Conclusions

- Problems with degraded results could be solved by appropriate tuning of the parameters involved
- Additional constraints for some cases could prove useful
- Future improvements:
  - Better tune the video analysis module;
  - include additional assumptions that can discriminate between buildings and vegetation;
  - 3 class segmentation: sky, vegetation and other;
  - feedback loop and additional criteria for adaptively tuning the parameters;

Piața Victoriei nr. 2, RO 300006 - Timișoara, Tel: +40 256 403000, Fax: +40 256 403021, rector@upt.ro, www.upt.ro

Presentation 2511

RTXM Debug & trace tools for RTOSes on GR740

Valentin Picos, Andrei Paval
ENEA

RTXM Debug & trace tools for RTOSes on GR740

Aerospace Europe CEAS 2017 Conference

Authors: Valentin Picos
Andrei Paval

Agenda

1. RTXM: Debug & trace tools for RTOSes on GR740 - “What is RTXM?”
2. Project overview

   - budget, tasks, milestones, standards, challenges

3. Technical approach
4. Q&A

“What is RTXM?”

– RTXM provides the capability to execute RTOSes in a time and space virtualized environment on the Gaisler GR740 board

– The RTOSes are RTEMS and FreeRTOS and the hypervisor is Xtratum

– It also includes a set of debug & trace tools

“What is RTXM?”

– The RTOSes are isolated into independent partitions over Xtratum whose executions do not interfere, preserving spatial and temporal isolation

– This hypervisor facilitates the running of guest multiple applications on the same hardware

– The system will provide specific tools for debugging and tracing software applications that use the API provided by the RTOSes

Project overview
(budget)

Original contract: 250K Eur

Start Date: February 2017

End Date: February 2018

PROJECT CONTEXT

ENEA is prime contractor and Airbus subcontractor

Project overview
(scope)

C implementation required (class 1, class 2, SFO and latest modification of the standard)

Linux (x86)

RTEMS (Leon 4-SPARC V8)

FreeRTOS (Leon 4-SPARC V8)

Project overview

Item	Description	1	2	3	4	5	6	7	8	9	10	11	12
M 0	Project Kick-Off												
WP 1.1	Management and reporting												
WP 2.1	System Software Specifications												
WP 2.2	Requirement Specification												
M 1	SRR												
WP 2.3	Detailed Design												
M 2	PDR												
WP 3.1	XtratuM build and configuration												
WP 3.2	Add Leon4 support for tiny RTOS												
WP 3.3	Add XM pava-virtualization support for selected RTOS												
WP 3.4	Add trace support for selected RTOS												
WP 3.5	Extend and optimize GRMON2 debug-link support for LEON4												
WP 3.6	Convert plugin from raw trace to CTF												
WP 3.7	Debug and trace tools												
M 3	CDR												
WP 4.1	Exectuion of Debug tests												
WP 4.2	Execution of Trace tests												
WP 5.1	Implementation of Live Debug&Trace DEMO												
M 4	QR												
WP 5.2	Execution of Live Debug&Trace DEMO												
M 5	AR												

Project overview
(timeline)

- SRR milestone : 30 March 2017
- PDR milestone : 27 June 2017
- CDR milestone : 23 November 2017
- QR milestone : 15 January 2018
- AR milestone : 22 February 2018

Project overview
(standards)

ECSS-E-ST-40C (tailored)

ECSS-Q-ST-80C (tailored)

Project overview
(challenges)

ECSS-E-ST-40C (tailored)

ECSS-Q-ST-80C (tailored)

ENEA

esa
European Space Agency

AIRBUS
DEFENCE & SPACE

Technical approach
(Applied standards)

[1] XM4 User manual. XtratuM 4. Fent Innovative Software Solutions. 16-010.006.sum.01. 02/02/2017

[2] RTEMS C User’s Guide. On-Line Applications Research Corporation. Edition 4.10.99.0, for RTEMS 4.10.99.0. 17 July 2015

Technical approach
(Modular design)

RTEMS partition

FreeRTOS partition

Xtratum

Demo application

Trace System

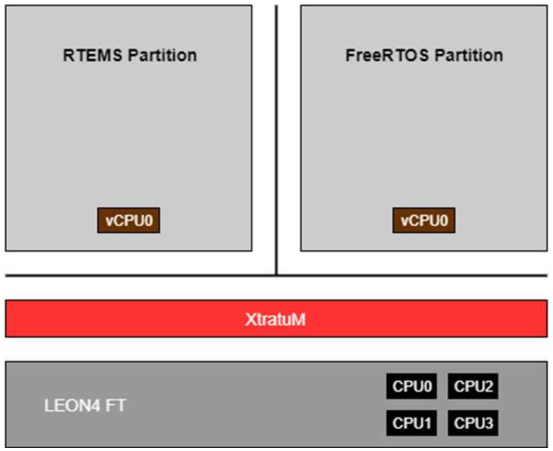

Technical approach
(Logical Model Description)

The RTXM implementation software consists of four major components:

RTEMS Partition – the RTEMS OS and Demo Application
FreeRTOS Partition – the FreeRTOS OS and Demo Application
Xtratum – embedded bare-metal hypervisor
Trace System – reads and decodes the data from the trace buffer, presents the information to the user

Technical approach
(Logical Model Description)

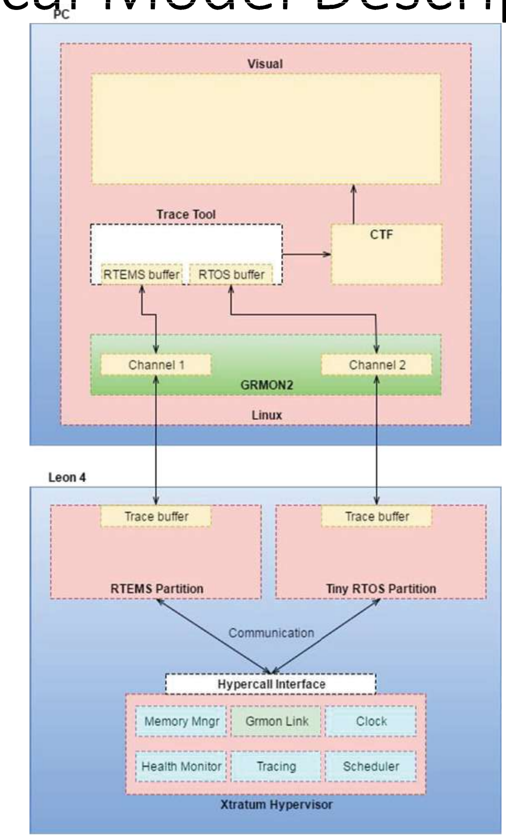

Technical approach
(Process overview)

- Each RTOS and application executes independently
- Each system function call is traced into the corresponding trace buffer
- The trace buffers are read out from the host trace application
- The data is decoded and presented to the user

Technical approach
(Process overview)

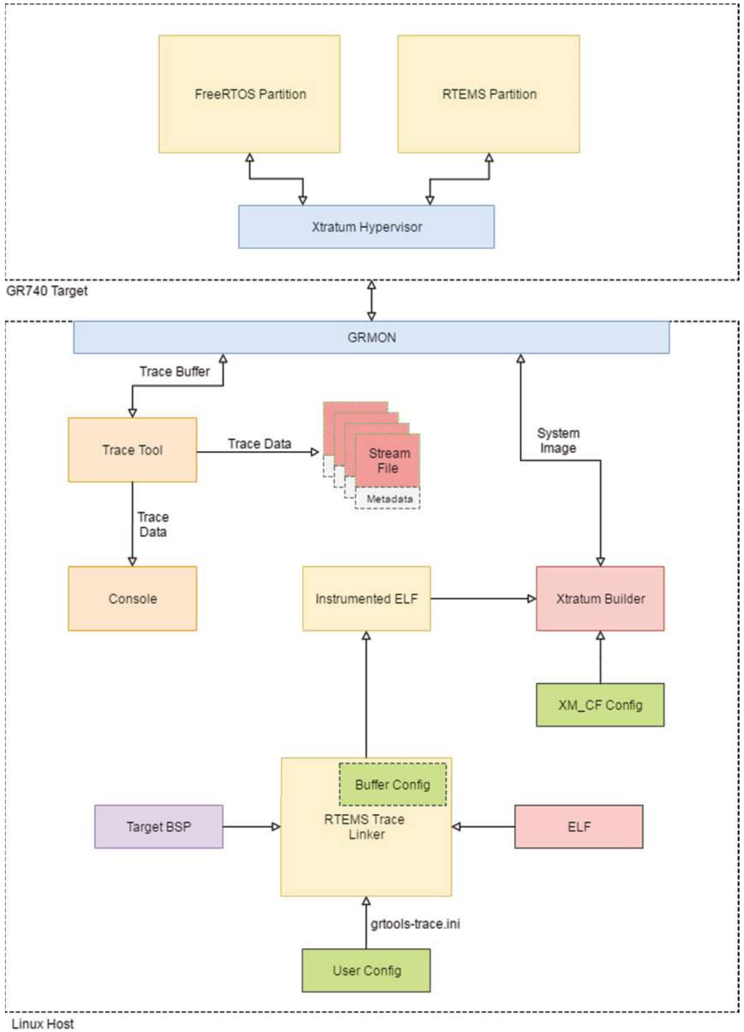

Technical approach
(Validation - Applied standards)

[1] Procedures Manual for the Consultative Committee for Space Data Systems.
CCSDS A00.0-Y-9. Yellow Book.

Technical approach
(Validation)

Test environment:

- 1XRegular PC x86 and 1xLeon4-GR740 (quad core) board connected by FTDI USB and Ethernet

Test setup:

- Trace System software running on x86 (Ubuntu VM)
- One C RTXM embedded image running on Leon4 board (Xtratum)

Technical approach
(challenges)

-Add support for multicore SMP RTOSes

-Extend and optimize GRMON2 debug-link support for LEON4

QA?

Presentation 2512

CFDP FILE TRANSFER PROTOCOL

Valentin Picos, Serban Vatavu
ENEA

CFDP FILE TRANSFER PROTOCOL

Aerospace Europe CEAS 2017 Conference

Authors: Valentin Picos
Serban Vatavu

Agenda

1. CFDP file transfer protocol - "What is CFDP?"
2. Project overview
   - budget, tasks, milestones, standards, challanges
3. Technical approach
4. Q&A

“What is CFDP?”

– CFDP provides the capability to transfer ‘files’ to and from a spacecraft mass memory.

– The content of the files may be anything

– Offers multi-hop capabilities (SFO – store and forward overlay)

ENEA

esa
European Space Agency

AIRBUS
DEFENCE & SPACE

“What is CFDP?”

– Files can be transferred reliably, where it is guaranteed that all data will be delivered without error (class 2), or unreliably, where a ‘best effort’ delivery capability is provided (class 1).

– Files can be transmitted with a unidirectional link, a half-duplex link, or a full-duplexlink

– File transfer can be triggered automatically or manually

Project overview
(budget)

Original contract: 199,878 Eur

Extension: 42 000 Eur

Start Date: 16 April 2014

End Date: 14 April 2016

PROJECT CONTEXT

ENEA is prime contractor and Airbus subcontractor

Project overview
(scope)

C implementation required (class 1, class 2, SFO and latest modification of the standard)

Linux (x86)

PikeOS (Leon 4-SPARC V8)

RTEMS (Leon 4-SPARC V8)

Project overview
(tasks)

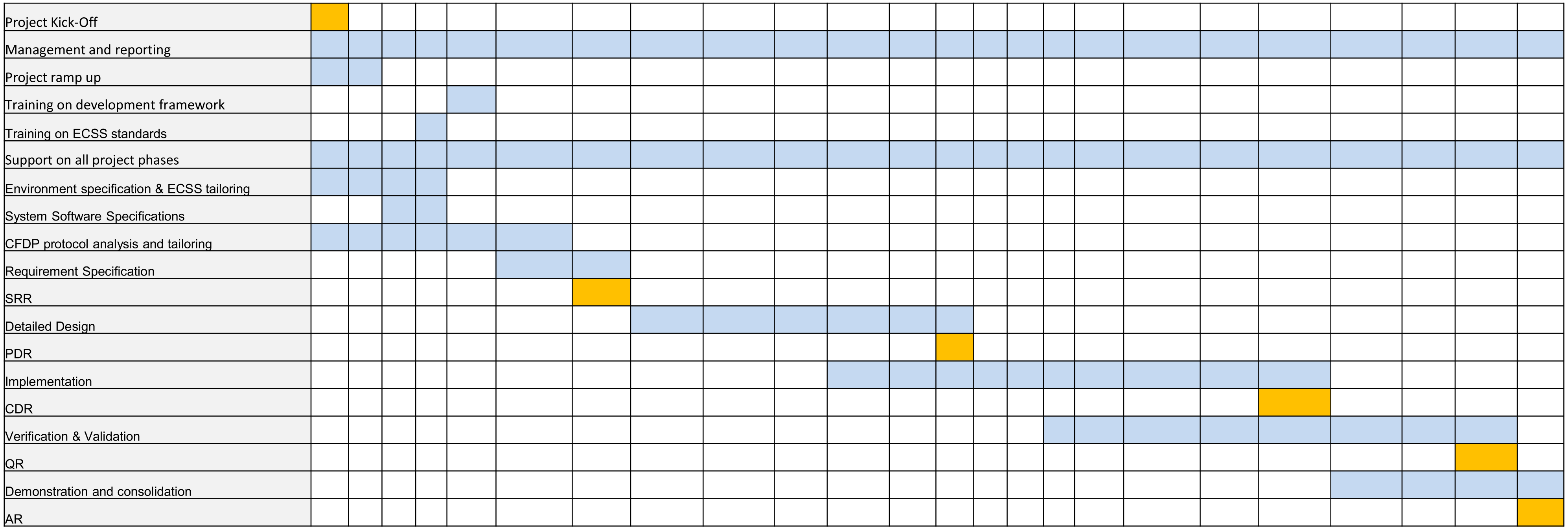

Project overview
(timeline)

- SRR milestone : 07.11.2014
- PDR milestone : 29.05.2015
- CDR milestone : 11.12.2015
- QR milestone : 03.03.2016
- AR milestone : 14.04.2016

Project overview
(standards)

ECSS-E-ST-40C (tailored)

ECSS-Q-ST-80C (tailored)

Project overview
(challenges)

ECSS-E-ST-40C (tailored)

ECSS-Q-ST-80C (tailored)

Technical approach
(Applied standards)

[1] CCSDS File Delivery Protocol (CFDP). Recommendation for Space Data SystemStandards, CCSDS 727.0-B-3. Blue Book.

[2] CCSDS File Delivery Protocol (CFDP)—Part 2: Implementers Guide. Report Concerning Space Data System Standards, CCSDS 720.2-G-3. Green Book.

Technical approach
(Modular design)

CFDP library

OSAL library (POSIX-Linux and RTEMS, Kars-PikeOS)

UT library

cfdpuser

Testsystem framework

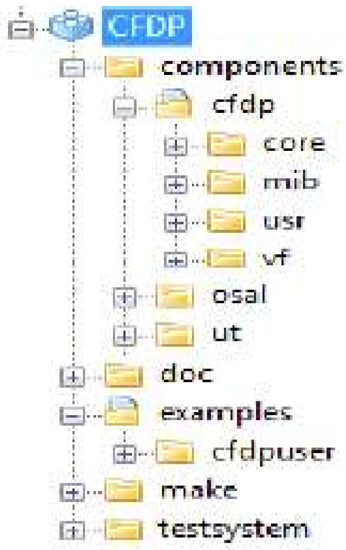

Technical approach
(Logical Model Description)

The CFDP implementation software consists of three major components:

CFDP Core – this implements the CFDP class 1 and class 2 ans sfo
CFDP User – this is using the CFDP User library to exercise the CFDP Core features
UT – this component is transferring the in/out CFDP PDUs of CFPD Core.

Each component is available as standalone executable application.

Technical approach
(Logical Model Description)

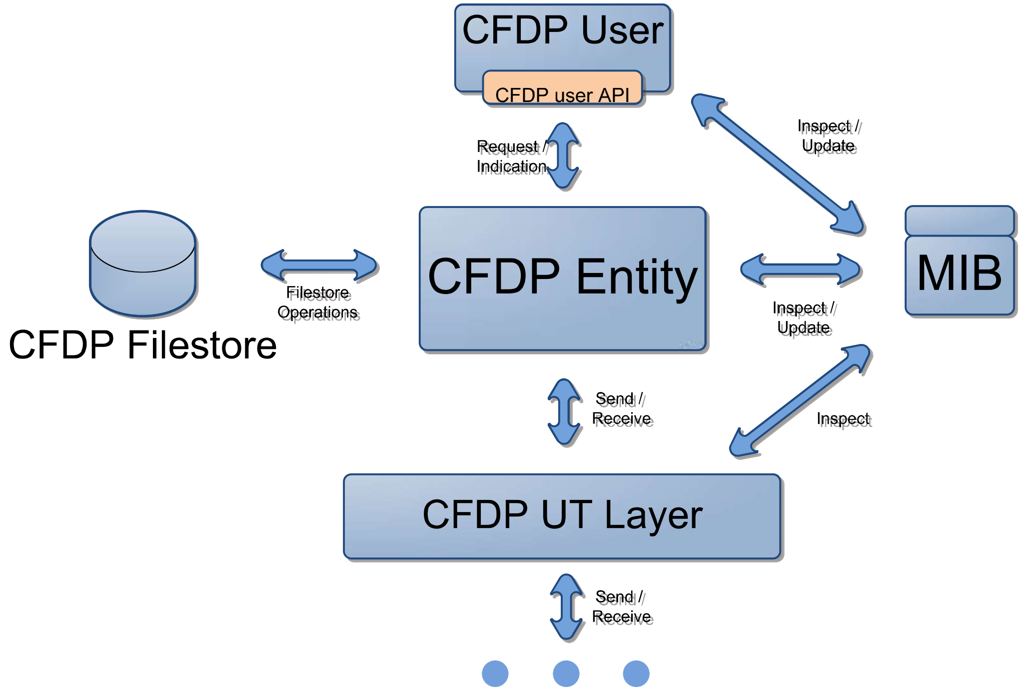

Technical approach
(Process overview)

- Processes communicates through message queues
- Transaction with priorities
  - Named priority message queues
  - Starvation avoidance algorithm
- CFDP Entity process uses state machine for Class 1&2 receiver&sender
- CFDP Entity process uses a thread for timer events
- UT support both Ethernet (UDP) and SpaceWire

Technical approach
(Process overview)

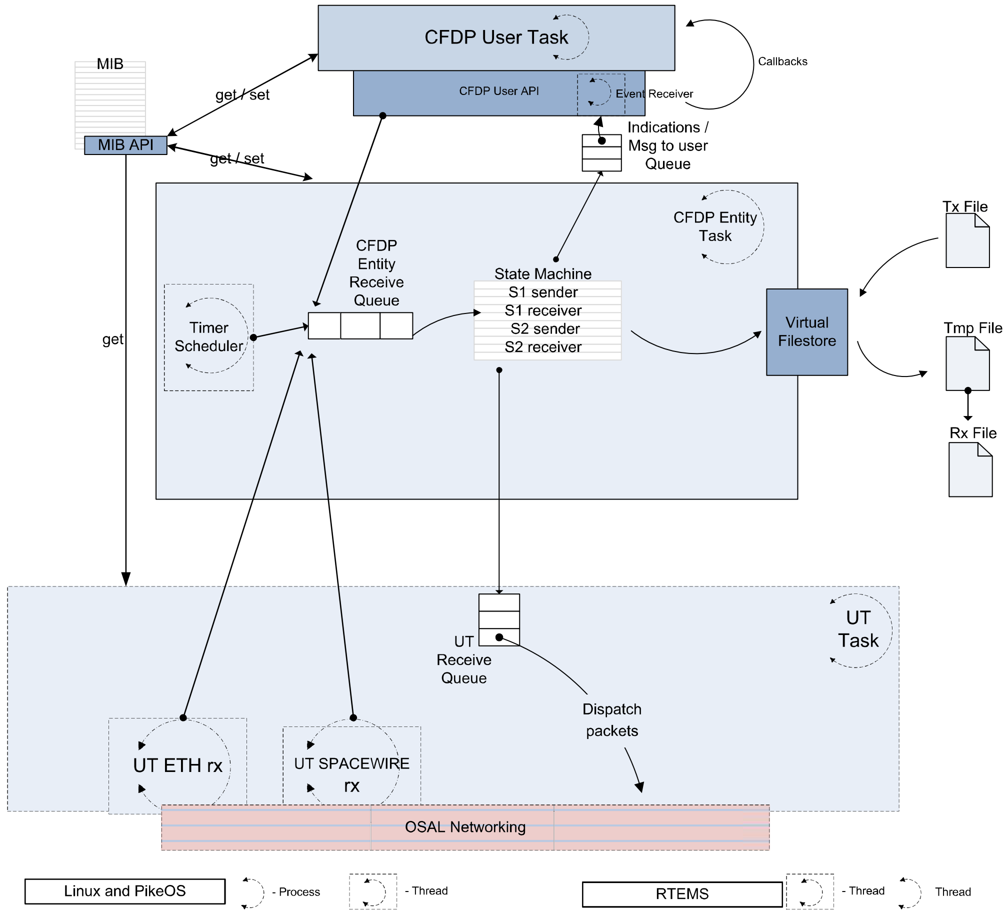

Technical approach
(Validation - Applied standards)

[1] Procedures Manual for the Consultative Committee for Space Data Systems. CCSDS A00.0-Y-9. Yellow Book.

Technical approach
(Validation)

Java reference implementation

Develop test framework for test automation

Packet Control Bridge (PCB) – from Java implementation integrated in our test framework

Full Yellow Book coverage

Technical approach
(Validation)

Test environment:

- 1XRegular PC x86 and 1xLeon4-N2X-DS (quad core) board connected by Spacewire and Ethernet

Test setup:

- Multiple C CFDP instances running on x86 (Ubuntu VM)
- Multiple Java CFDP instances running on x86 (Ubuntu VM)
- One C CFPD instance running on Leon4 board (RTEMS)

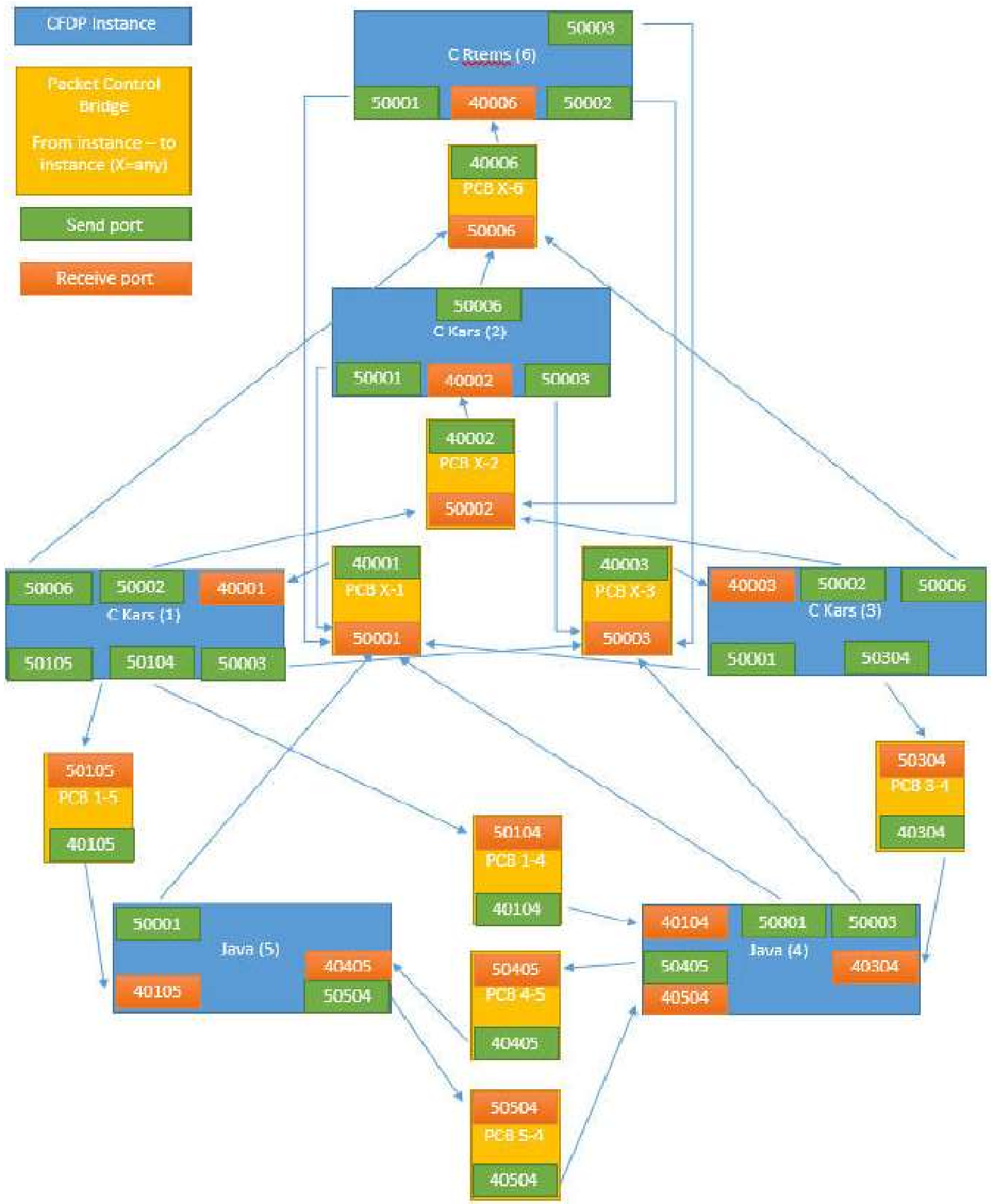
CFDP Instance
Packet Control Bridge
From instance – to instance (X=any)
Send port
Receive port
C Rtems (6)
50003
50001
40006
50002
40006
PCB X-6
50006
50006
C Kars (2)
50001
40002
50003
40002
PCB X-2
50002
40001
PCB X-1
50001
40003
PCB X-3
50003
50006
50002
40001
C Kars (1)
50105
50104
50003
40003
50002
50006
C Kars (3)
50001
50304
50105
PCB 1-5
40105
50104
PCB 1-4
40104
50304
PCB 3-4
40304
50001
Java (5)
40405
40105
50504
40104
50001
50003
Java (4)
50405
40304
40504
50405
PCB 4-5
40405
50504
PCB 5-4
40504

Technical approach
(challenges)

-Add support for multiple architectures (x86, SPARC) and OSes (RTEMS, PIKEOS and Linux)

-Write unit tests to achieve high code coverage numbers

-Develop a flexible functional test system able to handle complex test setup (see SFO functional tests)

QA?

Presentation 2513

PLANAR HEATER BASED ON ELECTROCONDUCTIVE CARBON FIBBERS DESIGNED FOR SATELLITE THERMAL MANAGEMENT"

Aristofan TEISANU
National Institute for Research and Development in Electrical Engineering,
INCDIE ICPE-Advanced Researches,
313 Splaiul Unirii, 030138, Bucharest-3, Romania
aristofan.teisanu@icpe-ca.ro steisanu@gmail.com

Rosu DORIN
Compozite Limited
Brasov, Plevnei no 3, Romania

Alina CARAMITU
National Institute for Research and Development in Electrical Engineering,
INCDIE ICPE-Advanced Researches,
313 Splaiul Unirii, 030138, Bucharest-3, Romania

Sorina MITREA
National Institute for Research and Development in Electrical Engineering,
INCDIE ICPE-Advanced Researches,
313 Splaiul Unirii, 030138, Bucharest-3, Romania

Chart for the final report at the end of the ESA contract:

"PLANAR HEATER BASED ON ELECTROCONDUCTIVE CARBON FIBBERS DESIGNED FOR SATELLITE THERMAL MANAGEMENT"

Authors:

[1]Aristofan TEISANU, [2]Rosu DORIN, [1]Alina CARAMITU, [1]Sorina MITREA

1National Institute for Research and Development in Electrical Engineering, INCDIE ICPE-Advanced Researches, 313 Splaiul Unirii, 030138, Bucharest-3, Romania
2Compozite Limited Brasov, Plevnei no3

Contact details: aristofan.teisanu@icpe-ca.ro steisanu@gmail.com

Short description of the contract objectives

This proposal was aim to develop a new type of planar heater, designed for space vehicle application, with improved characteristics. Unlike the current heater, in which the heating element is made of various metals, carbon fibre will be use to replace copper or tungsten. The current metallic heater has a major disadvantage: the heating element surface is always smaller then the total contact & thermal transfer surface of the heater, due to the high electric conductivity of metals. This topology conducts to a non uniform thermal profile of the surface, and also is subject to supplementary mechanical stress in the insulation system and possible malfunction and earlier faller. The main advantage of the use of carbon fibre instead of metals for heater elements manufacturing is higher specific resistivity of graphitized carbon fibre (in range of $5.10^{-6}\Omega\cdot m$) instead of $1.72.10^{-8}\Omega\cdot m$ for copper. This high specific resistivity allow that the heating element to cover the entire area of the heater, diminishing thermal non uniformity and the mechanical stress induced by temperature difference between the heater element and the insulation system. Another important advantage relay in the structure of the carbon based heating element. In contrast the current heater, which have up to 4 grade redundancy, which means that the heater have up to 4 elementary heating elements placed in a parallel configuration, for the carbon fibre based solution, each heating element consist in hundreds of tiny carbon filaments. That conducts to a redundancy grade in range of thousand, following that the rehabilitee of such heater if greater by design then any present technical solution.

The main objective of this proposal was as fallow:

1. To establish minimum three different topologies, thermally and electrically characteristics for planar heaters, designed for three different applications.
2. To establish the carbon fibre type and morphology of the heating elements related to the specific application.
3. To solve the problem of the electrical contact between the carbon fibre heater and copper terminals and to establish the technical solution.
4. To establish the characterization and testing procedure for heater materials and heater element assembly.
5. Establishing the insulation system type and morphology of the heating elements related to the specific application and selecting the materials for each insulation part.
6. Establishing the specific design and the manufacturing procedure for each type of heater.
7. Establishing the methodology for testing of the planar heaters in similar condition with space environment (function temperature range and ionizing radiation comportment).
9. Final results dissemination.

The work to this contract was divided in three stages as follow:

WP1. Manufacturing preparation and selecting the precursors and the technological solutions. Achieving of three planar heater models KAPTON based insulation system, in respect with ESA demands
WP2. Achieving and validation of planar device heaters based on carbon fibres
WP3. Achieving and validation of planar device heaters based on carbon fibbers and organic insulation system (KAPTON and 3M 966 adhesive) in order to obtain high electrical resistance heaters

WP1. Manufacturing preparation and selecting the precursors and the technological solutions. Achieving of three planar heater models KAPTON based insulation system, in respect with ESA demands

Carbon fibre planar heater specification

Main objectives of the technology

The main objective of the technology for this stage of the project is to establish laboratory manufacturing methods which allow achieving the planar heater model, as follow:

-1 type of heater, large size (125 x 125 mm), flexible frame, for the reference voltage 28 V +/-5 DC, as follow:

- 5 W, at 125 x 125 mm, for the reference voltage specified above, minimum 5 pieces in order to prove repeatability of the electrical and thermal parameters and also of the manufacturing technology;
- 80 W, at 125 x 125 mm, minimum 5 pieces, in the same condition;
- 1 type of heater, small size (25 x 25 mm), flexible frame, 5 W for the reference voltage 28 V +/-5 DC, minimum 5 pieces.
- 1 type of double active layer heater (for redundancy), at 80 W at 28 V DC (large size, 125 x 125 mm), with complete separated electric terminals for each active element, minimum 5 pieces;

At this preliminary stage, the following heater types are available:

- large type, 124 x125mm, active thermal area 111x125mm;
- large type 124 x135mm, active thermal area 111x125mm, double active layer heater,), with complete separated electric terminals for each active element;
- Small type, 63 x 50mm, active thermal area 50x50mm.

The range of the electrical resistance starts from 2Ω up to 2500Ω for the large size type and from 4Ω up to 2500Ω for the small type.

Considering the surface area of the copper current lines, which is non active from the thermal point of view, the smallest recommended size for this type of heater is in range of 30 x 30mm (thermal active surface).

The insulation material for those entire heater models is KAPTON, with thickness staring from 25μm up to 125μm.

The repeatability

- For the dimension parameters, all variation values not exceed 0.5%.

- For the electrical parameters, all variation values not exceed 5%.

TN2 Title: Carbon fibre planar heater design report

Main features of carbon fibre planar heaters

A carbon fibre planar heater consists in two main parts:

- The heating element, based on carbon materials;
- The insulation system, based on thermal resistant organic polymers.

The experimental work in this WP was conducted as follow:

1. To establish all the necessary materials and devices to produce the heater in respect with ESA demands;
2. To establish a procedure for laboratory level heaters manufacturing.

1. Establishing materials and devices

The heating element

For the heating element, many carbon fibre materials are studied, in order to choose the best for this application. The most important parameter is the linear electrical resistance, which depends of the number of micro fibres contained in fibre strand and also of precursors and the graphitization conditions. In order to optimize the thermal transfer between the heating element and the support of the heater, the surface area of the heating element has to cover a maximum percentage reported to entire surface of the heater. Following this idea, the best candidate for carbon heating elements is carbon fabric and carbon felts. From the studied materials, two are selected, in respect with the power specification mentioned above: a carbon fibre (1k type/strand, which means 1000 individual carbon micro fibres per strand) and a composite carbon fabric. Those two materials are situated on the extremes of electric resistivity, as follow:

- Carbon fiber strands with different electrical properties.
- Composite carbon fabric, heaving in composition three types of wires: carbon fibre, KEVLAR and glass fibre.

From those materials, the carbon fibre has the lowest resistivity and the composite carbon fabric has the highest resistivity, in a range of three orders of magnitude.

The exact tuning of the resistance was still a problem at that time, related to the incidence on the market to a specific necessary carbon material.

The insulation material

Following the results established by the state of the art study, the best choice for the insulation material was KAPTON foil, heaving the thermal properties for this job. The thickness of the KAPTON foil was in this laboratory level of experimental work of 100μm (4mils).

The current collector

To solve the problem regarding the connection to power supply of the individual carbon fibre strands, a thin copper ribbon (35μm thickness) was used.

The electrical contact between the current collector and the carbon fibre heaters

The electrical contact between the carbon material and the copper ribbon (the current collector) was solved perfectly, using a conductive adhesive based on silver filer and an epoxy resin. After a carefully analyzing, was selected a DuPont product, especially designed for space application.

As the best choice for the adhesive, was selected an imides based material, product by MINCO. After two months of negotiations, the companies eventually deny the possibility to acquire this product. The next selected product with a significant lower thermal stability was a solid adhesive from 3M, which we succeed to purchase. This material has good adherence properties and a fair thermal stability (up 120◦C).

2. Establishing laboratory level procedure for heaters manufacturing

The manufacturing procedure for the both dimensional types of carbon heater following the same procedure, as follow:

- Cutting the KAPTON foil to the required dimensions;
- Attaching the copper ribbon on the support;
- Adding the polyacetal adhesive layer;
- Adding the carbon fibre heating element or adding the carbon fabric heating element;
- Making the electric connection between carbon fibres and copper ribbon or making the electric connection between carbon fabric and copper ribbon;
- Closing the electrical connection area by banding the copper ribbon over the joining points or over the joining line;
- Achieving a fully assembled carbon heater by adding the upper layer of KAPTON insulating foil.

The manufacturing path is presented bellow.

2.1 Cutting the KAPTON foil to the required dimensions

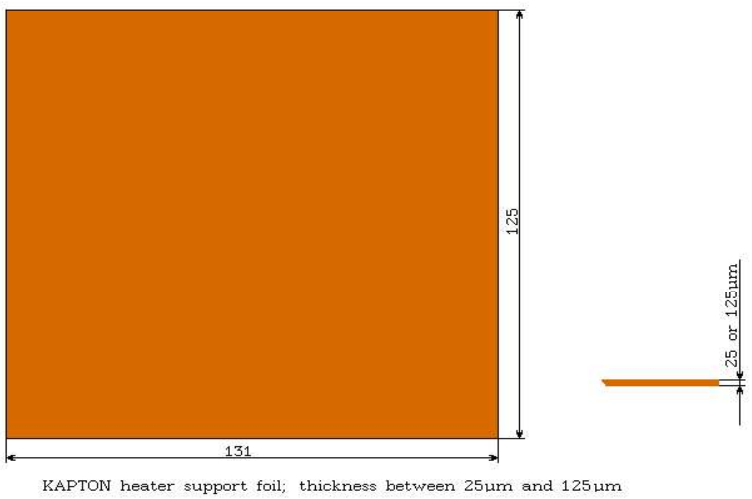

Figure 1

2.2. Attaching the copper ribbon on the support

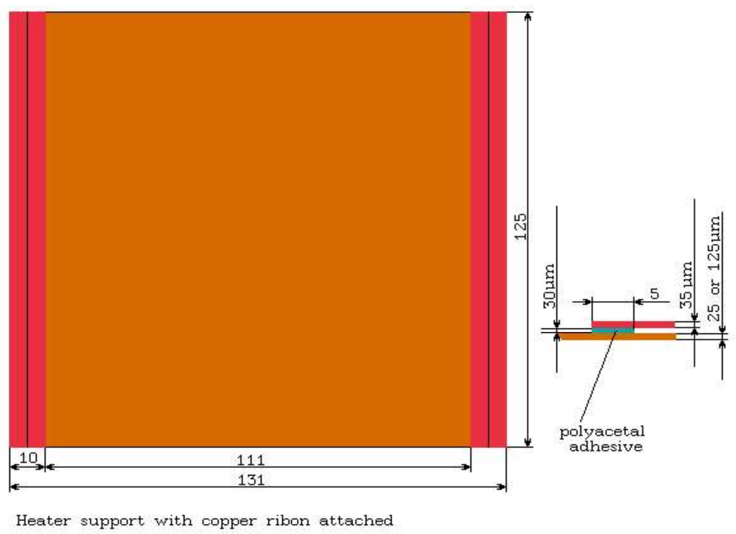

Figure 2

2.3. Adding the polyacetal adhesive layer

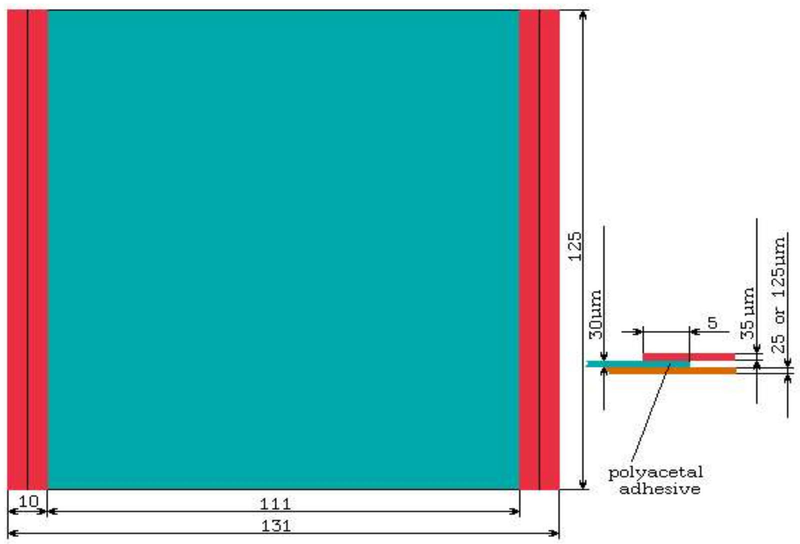

Polyacetal adhesive layer added

Figure 3

2.4. Adding the carbon fibre heating element

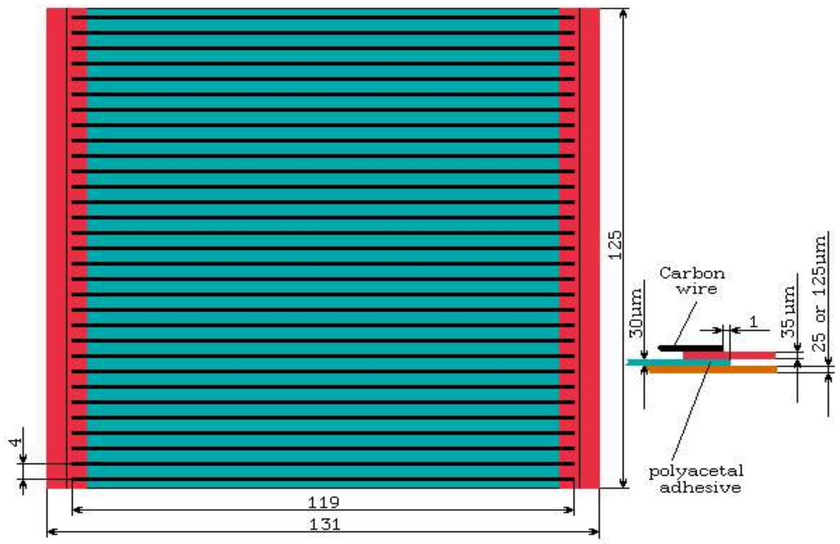

Carbon wires heating element added

Figure 4

2.5. Adding the carbon fabric heating element

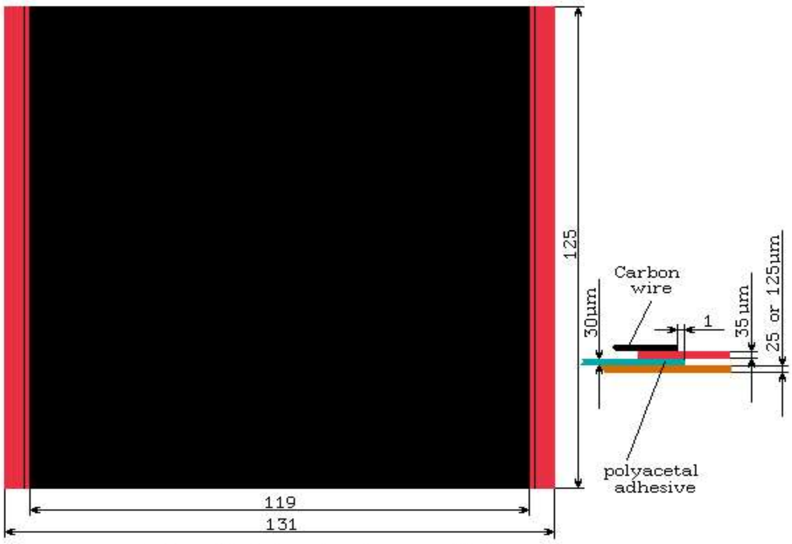

Carbon fabric heating element added

Figure 5

2.6. Making the electric connection between carbon fibres and copper ribbon

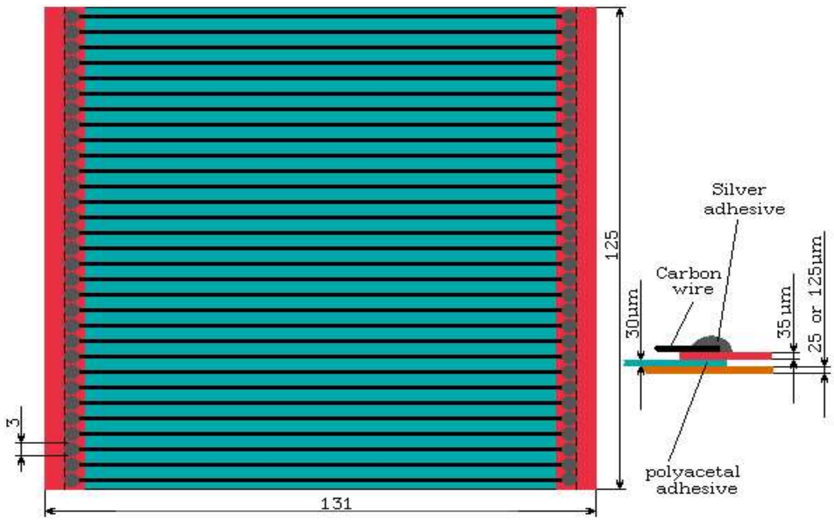

Electricaly connection between copper ribons an carbon heating element performed with silver based conductive adehesive

Figure 6

2.7. Making the electric connection between carbon fabric and copper ribbon

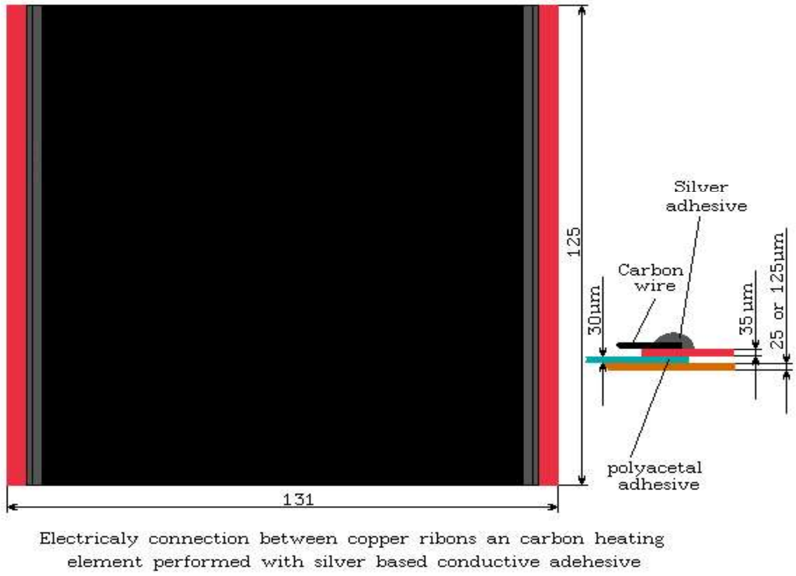

Figure 7

2.8. Closing the electrical connection area by banding the copper ribbon over the joining points

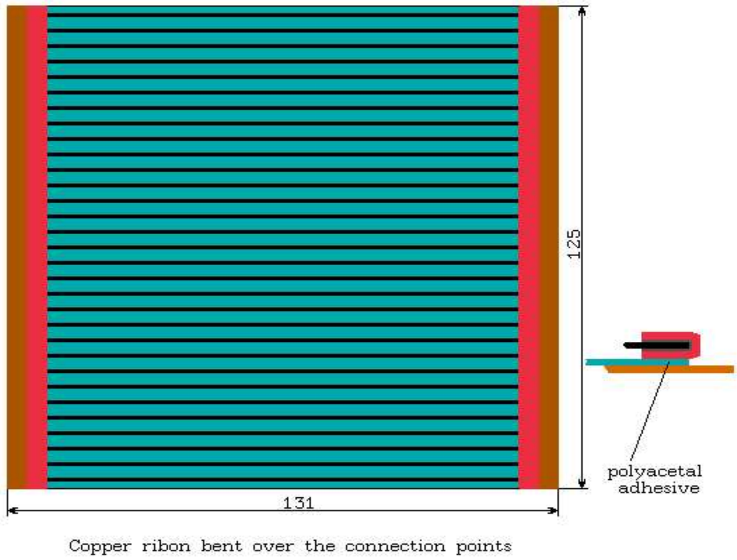

Figure 8

2.9. Closing the electrical connection area by banding the copper ribbon over the joining line

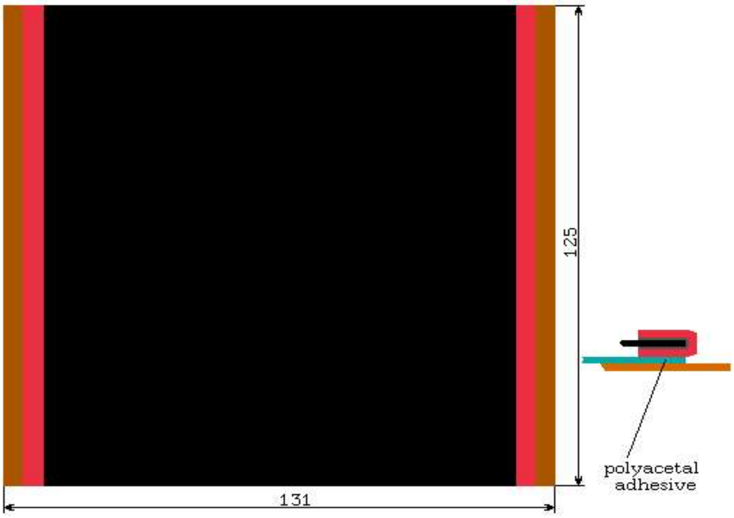

Copper ribon bent over the connection points

Figure 9

2.10. Achieving a fully assembled carbon heater by adding the upper layer of KAPTON insulating foil.

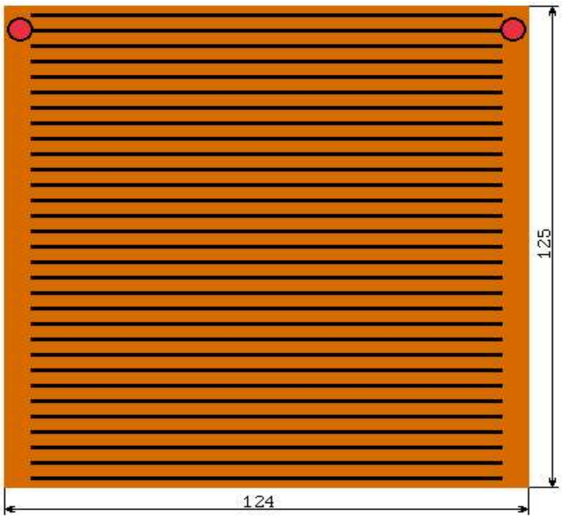

Fully asembled carbon heater,
with uper insulation added

Figure 10

10

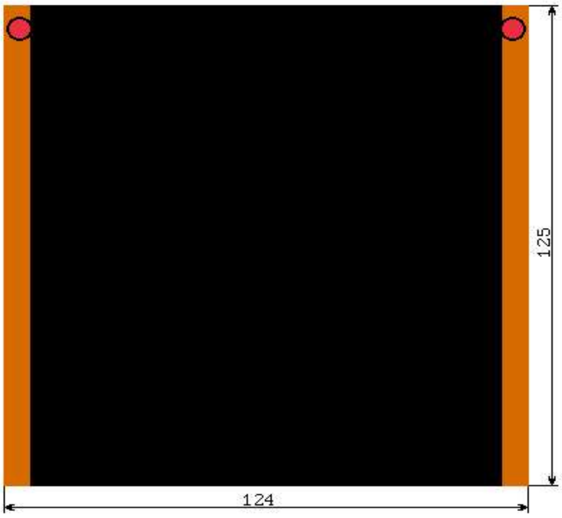

Figure 11

As it is shown in the pictures above, there are to manufacturing path, namely for carbon fibre and carbon fabric.

When discrete carbon fibre heating element are involved, the heating element greed is achieved using a frame like in the picture below (Figure 12)

Figure 12
Heating element carbon fibre grid before embedding in adhesive

Results at the end of the first stage of the contract

Figure 13
Large size heater (124x125mm), based on 1k carbon fibre strand, heaving the electrical resistance in range of 2Ω

Figure 14
Large size heater (124x125mm), based on 0.5k carbon fibre strand, heaving the electrical resistance in range of 4Ω

Figure 15
Large size (124x138mm), based on 0.5k carbon fibre strand, heaving the electrical resistance in range of 4Ω, double heating element, redundant

Figure 16
Large size (124x125mm), based on carbon fibre strand, heaving the electrical resistance in range of 14.5Ω, with carbon material produced in ICPE-CA starting from 6k PAN strand (Blue Star, England)

Figure 17
Large size (124x125mm), based on composite carbon fabric, heaving the electrical resistance in range of 2000Ω; the heater was cut in two pieces in order to prove that, after cutting, the remaining connected part can still working, heaving a power proportional with the remaining surface area

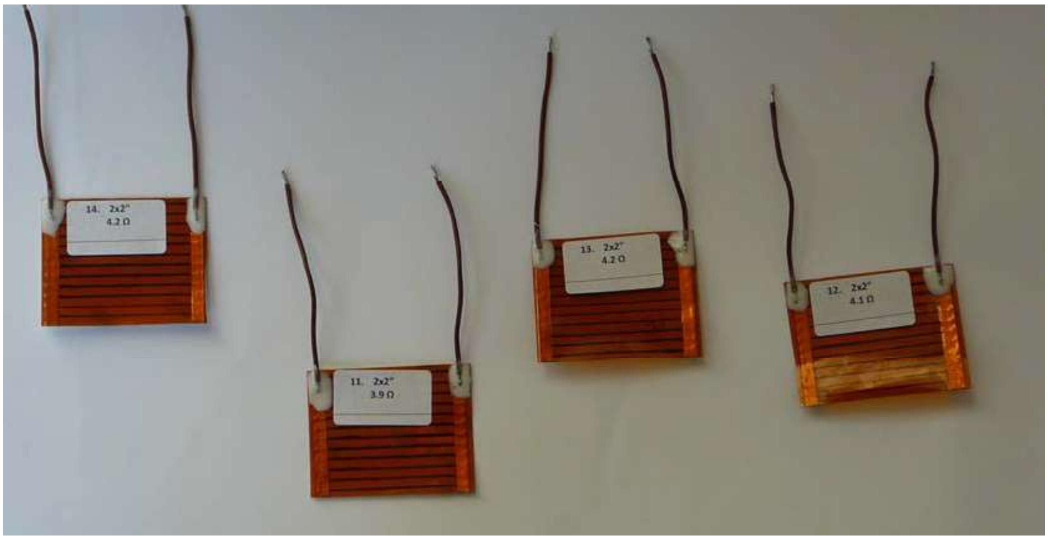

Figure 18
Small size (63x50mm), based on carbon fibre strand, heaving the electrical resistance in range of 4Ω

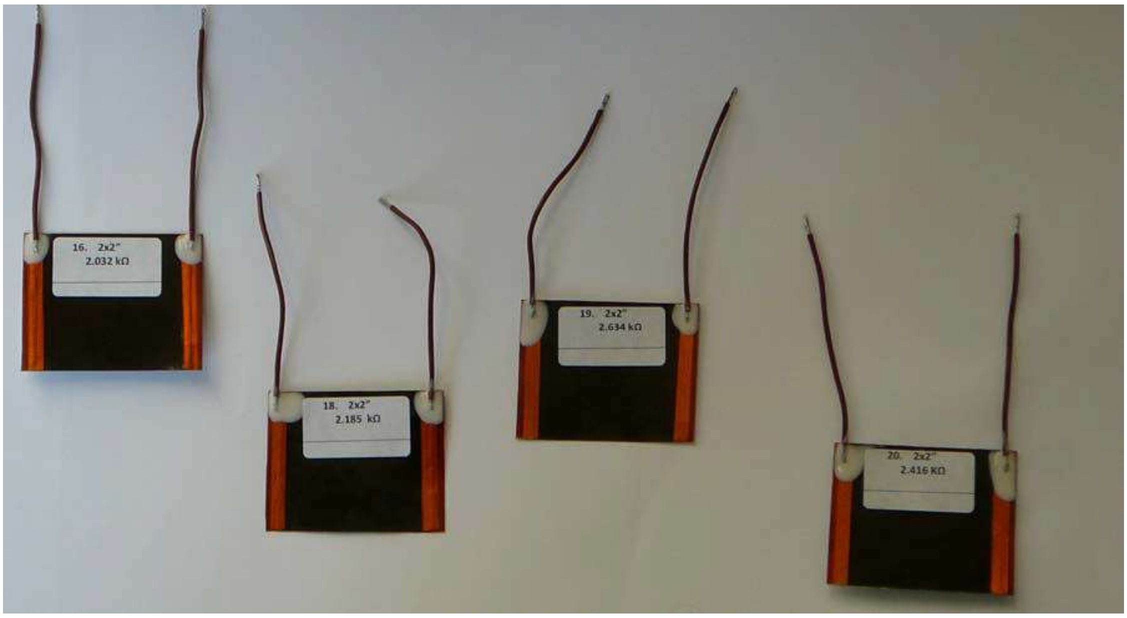

Figure 19
Small size (124x125mm), based on composite carbon fabric, heaving the electrical resistance in range of 2000Ω

Characterization tests

Electrical resistance
The measurements of the electric resistance are listed in the Table 1, bellow.

Table 1

No.	Heater type	Measured resistance (Ω)	Medium Value (Ω)	Tolerance (%)	Repeatability (%)
1	Large size (124x125mm), based on 1k carbon fibre strand, heaving the electrical resistance in range of 2Ω	2.2	2.14	4.5	95.5
2		2.1			
3		2.2			
4		2.1			
5		2.1			
6	Large size (124x125mm), based on 0.5k carbon fibre strand, heaving the electrical resistance in range of 4Ω	4	4.08	2.4	97.6
7		4.1			
8		4.1			
9		4.1			
10		4.1			
11	Large size (124x138mm), based on 0.5k carbon fibre strand, heaving the electrical resistance in range of 4Ω, double heating element,	4.1/4.1	-	-	-

	redundant				
12	Large size (124x125mm), based on carbon fibre strand, heaving the electrical resistance in range of 14.5Ω, with carbon material produced in ICPE-CA starting from 6k PAN strand (Blue Star, England)	14.5	-	-	-
13	Large size (124x125mm), based on composite carbon fabric, heaving the electrical resistance in range of 2000Ω	1988	-	-	-
14	Small size (63x50mm), based on carbon fibre strand, heaving the electrical resistance in range of 4Ω	3.9	4.1	4.88	95,12
15		4.1			
16		4.2			
17		4.2			
18		4.1			
19	Small size (124x125mm), based on composite carbon fabric, heaving the electrical resistance in range of 2000Ω	2032	2293.2	22.86	77.14
20		2199			
21		2185			
22		2416			
23		2634			

The electrical resistance of the heaters was measured with a C.A 6250 Chovin Arnoux micro ohm meter.
The larger tolerance of the type 7 heaters is due to higher influence of conductive adhesive gluing on smaller sizes.

At the end of first stage, we were unable to achieve the electrical resistance for the heaters, as was required (see *Main objectives of the technology*). The reason was the lack of available materials on the market.
However, from the power density point of view we have overcome the required values. Also, the electrical parameters repeatability and the stability were good.

WP2. Achieving and validation of planar device heaters based on carbon fibres

The research activities in the second stage of the contract were conducted as follow:

2.1. Solving the problem regarding the resistance values, in order to obtain the following powers:

There are two different technological ways to deal with this problem;

- A. To use a manufactured material from a supplier;
- B. To produce a material with "on demand" resistivity, starting from PAN precursor.

A. Using a material from a supplier

The thinnest carbon fibre which we can achieve was a 1 K fabric material with a resistivity at around 1Ω/mm.
From consideration regarding the maximum power density for the given insulation system and the thermal resistance of the electrical insulation, thermal homogeneity and redundancy of the heating elements, the minimum power that can be achieved for this material was the 80W, for both small and medium size heaters.

All the heaters are realized following a design as is shown in figure 1.

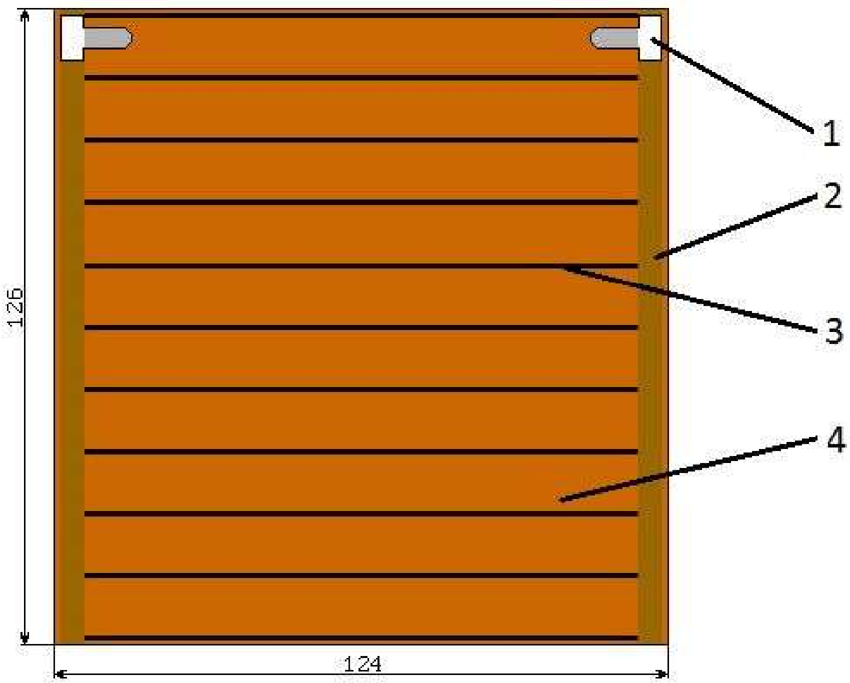

Figure 20
Design used in present for medium size heaters manufacturing; 1.Electric terminal, made from 300μm silver plated brass sheet, attached to the copper ribbons by copper rivets; 2.Current collector, made from 35μm copper ribbon; 3.Heating element, consisting in carbon fibre strand; Insulating system, made from 50μm KAPTON foil, all elements glued together with 3M 966 acrylic solid adhesive

As is shown in *Figure 20*, a medium size heater has 11 carbon fibre strand heating elements, configured in a parallel grid. Each strand consists in around 500 elementary carbon fibres, heaving a diameter of above 3μm. The small size heaters type has a similar design, heaving only 5 carbon fibre strands in order to achieve the desired resistance.

As I already shown, the market available carbon fibre not allows lower power densities.
In order to maintain a redundancy at least at four orders (which is already achieved for the common metallic element planar heaters), the resistance of a single strand, $\boldsymbol{R_{cs}}$, heave to be $\boldsymbol{R_{cs}}$ = 627.2Ω
Following the present design of the heaters, which consists in parallel carbon fibre strands connected to copper ribbons current collectors, because the low electrical resistance of the available carbon fibre strands, it's impossible two achieve lower powers keeping the redundancy and not to exceed the maximum thermal transfer values, which are dependent to the insulation system.
However, I found a way to increase de heater resistance and decrease the power density, affecting only de redundancy of the heating elements. Indeed it is possible to obtain a higher electrical resistance values by change the shape of the carbon strands, in order to increase the strand length, as is shown in the picture bellow.
Considering a heater with only four carbon strands (5 x5" size) and following the specific resistivity of the carbon strand value, the length of a single strand, $\boldsymbol{L_{cs}}$, should be: L_{cs} = 636mm.
That is feasible with the existing frame, with minimum modifications, but only for the medium and large size heaters.

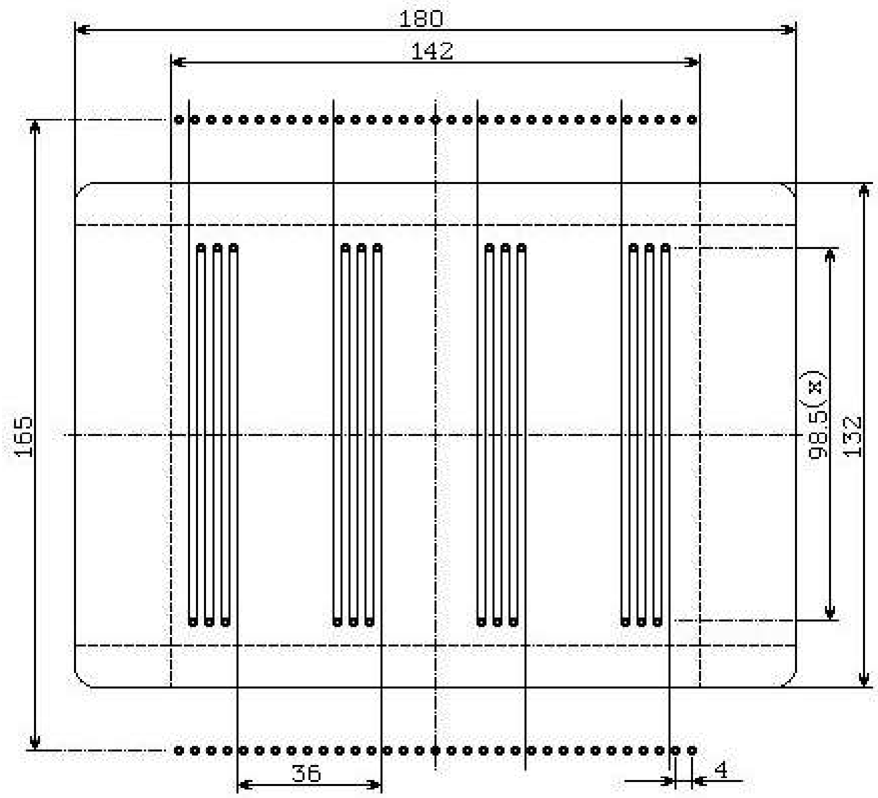

Figure 21

18

Proposed design of the carbon strands form in order to increase length to achieve higher electrical resistance values

The modification consist in inserting a number of removable needles, as is shown in Fig. 2, which allow to make turns with carbon strand in order to increase the electrical resistance. Considering the medium size heater dimensions, the resulting number of "turns" is 7, because the maximum length of the carbon strand is 111mm.
To calculate the distance between the needles line (x), I used the following relation, which result from Fig. 20: $L_{cs} = 6x + 2(111-x) + 3\pi\cdot d_{\text{needle}}$ in which d_{needle} is the needle diameter. By replacing the values, it results x = 98,5mm.
This design was subject of many laboratory trials and was considered to complicate and heaving a big failure potential and therefore, was develop further.

B. To produce a material with "on demand" resistivity, starting from PAN precursor.

Even in the first stage of the contract, we made some trials to produce carbon fiber starting from 6K PAN precursors. Following these trials, we were able to produce a material having a specific resistivity 20-40 times greater then common commercial carbon fibre, but with poor mechanical properties. We used this material to produce one test heater. However, the thickness of the 6K material is too high to be use for this purpose. We achieved a 2K PAN precursor and tried to use in our frame in order to produce low graphitized carbon fiber with high resistivity, but machine prove to be useless for this kind of material, for reason related to the mechanical tensile applied in the PAN strand. In order to manufacture carbon fibre starting from PAN precursor, in each technological step, a mechanical tensile should by applied in the PAN strand, in order to align the resulting molecules of aromatic intermediary to the fibre direction (stage I, oxidation), and to align the resulting graphite conglomerate in stages II and III. We started to modify our equipment, in order to maintain constant the mechanical tensile at very lower values (under 0.2N), but we haven't finished yet this works. To obtain the desired tensile value, we use a system based on an Eddy current clutch. The problem was the mechanical tensile variation due to an inconstant friction forces between the PAN strand and the guiding element of the oxidation oven. To overcome this problem we have replaced all fixed guiding parts with guiding rolls provided with high quality ball bearings.
In order to increase the mechanical strength of the resulting carbon fibre, we have to mitigate between graphitization degree (if the graphitization degree increase, the specific resistivity decrease) and the mechanical properties, by increasing the final temperature in pre graphitization oven up to 1400°C.
To do so, we have to change partial the technical solution for this oven (to replace the oven tube, which in present is made from stainless steel, with a ceramic one, which can endure this temperature. Also, we have to replace the

three heating element, which are made of Khantal, with heating element made from molybdenum.
All these modification take more time then I have initially allocated for this job.
I have succeeded with the modification regarding the mechanical tensile control, but is still to work in order to fit the parameters and to fine tune the temperature inside the first oven.
In first stage of the PAN graphitization process, predominate chemical reaction is the oxidation one, which depend mostly of the oxygen diffusion speed in PAN.
Due to the first test with the 2K PAN precursors, I have established the three temperatures corresponding to the three thermal stages of the oxidation oven, which are different to those corresponding to the 6K PAN precursor, used in the past.

Figure 22
First stage oven (Oxidation stage)
In the left and right side of the oven, can be seen the modification these I mentioned before

Figure 23
Second stage oven (Pregraphitization stage)

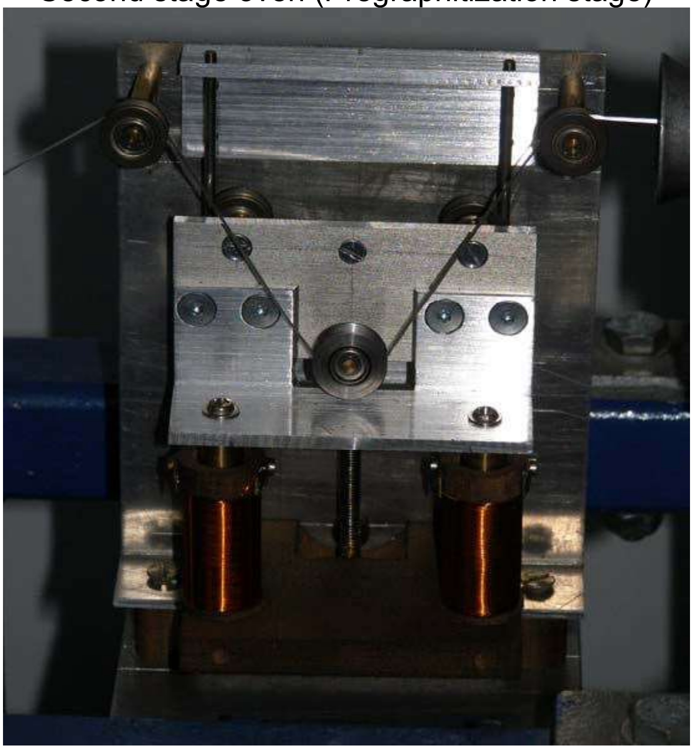

Figure 24
Part of automatic tensile system for 2K PAN precursor

Other problems were related to the friction between the fibre and guiding parts. We have also solved these problems by replacing all friction guidance gauges with ball bearing rolls.

Figure 25
Ball bearing rolls guidance system

Solving the problem regarding the electrical terminals
As electrical terminals, to ending parts (terminals) was attached with rivets, one for each copper ribbon.
The laboratory manufacturing procedure was modified as follow:

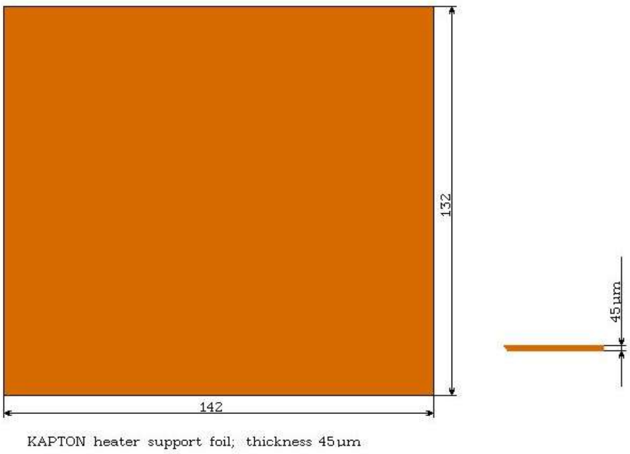

Figure 26
KAPTON heater support for the medium size, manufactured using a cutting stencil

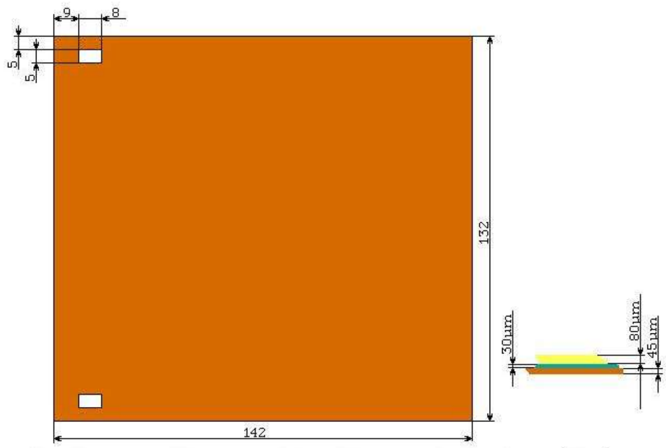

Figure 27
Upper heater part for the medium size, manufactured using a cutting stencil

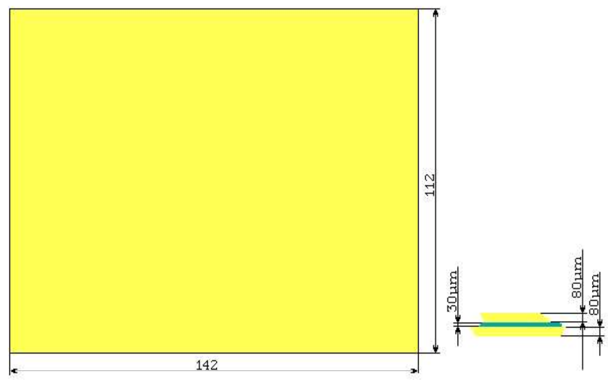

Figure 28
Also manufactured by stencil cutting

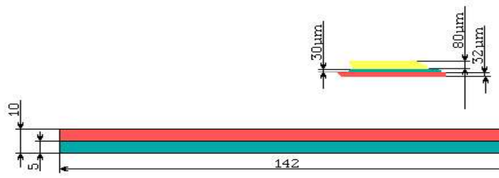

Figure 29
Copper ribbon, with adhesive attached, manufactured by guillotine cutting.

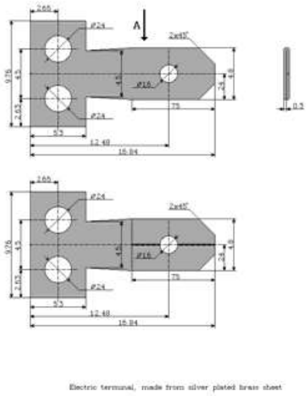

Figure 30
Manufacturing electric terminals

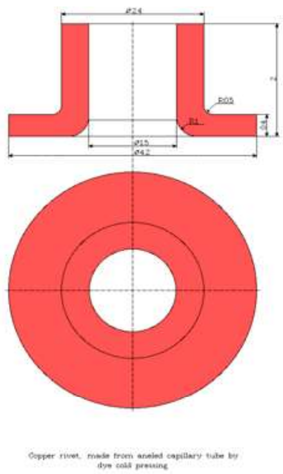

Figure 31
Manufacturing copper rivets

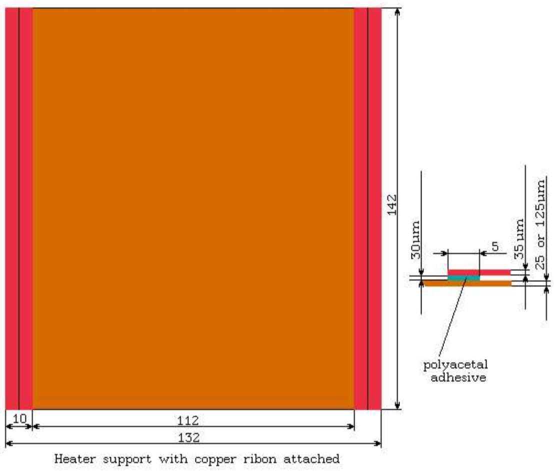

Figure 32
Attaching the copper ribbon

24

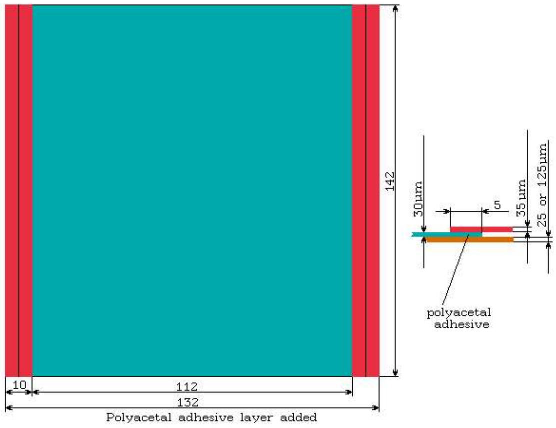

Figure 33
Adding the middle adhesive layer

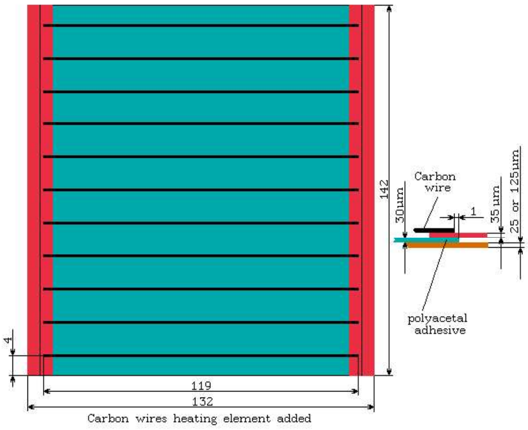

Figure 34
Adding the carbon fibre strands

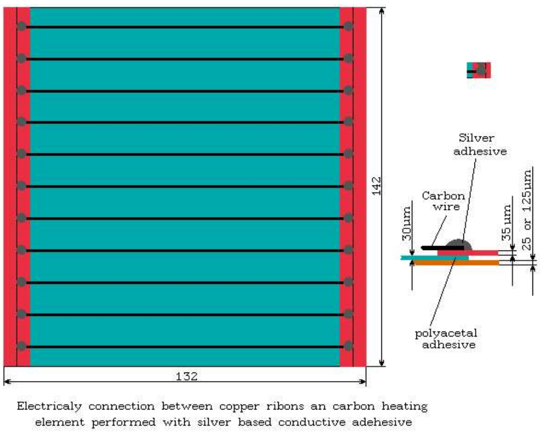

Figure 35
Making the electrical bond between the copper ribbon and the carbon fibre strands

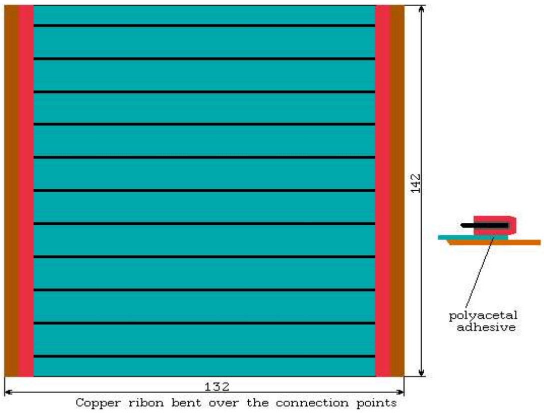

Figure 36
Closing the joints by bending over the copper ribbon

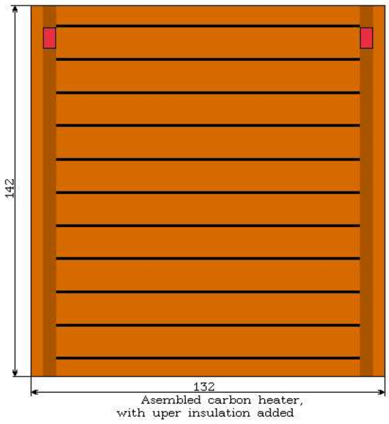

Figure 37
Adding the upper layer

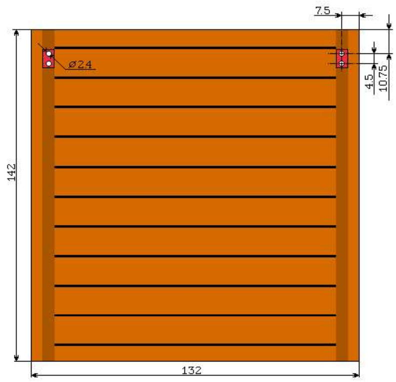

Figure 38
Drilling holes to attach electrical terminals

26

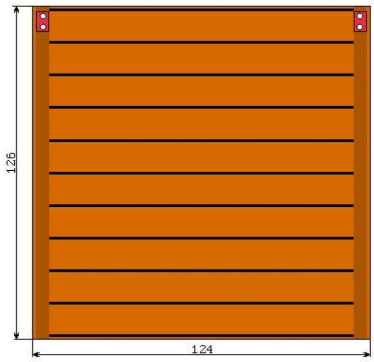

Figure 39
Cutting to final dimensions

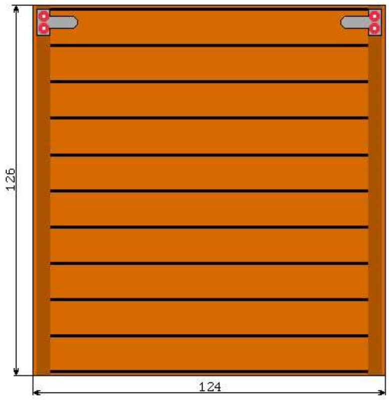

Figure 40
Attaching electrical terminals by rivets

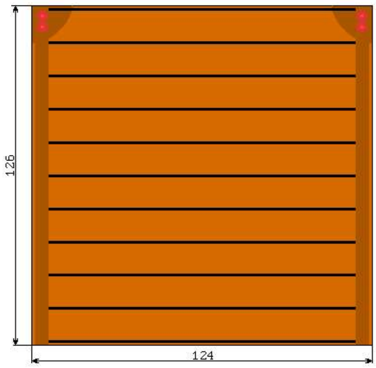

Figure 41
Insulating the rivet heads

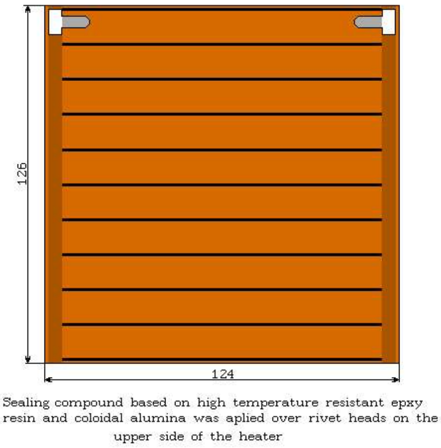

Figure 42
Sealing the rivets joint

Experimental results

80W Heaters, medium size (125x125mm)

Heater visual aspect

Table 2
Medium size heaters visual aspect

1	
2	*Glued on aluminum plate and placed in the qualification device chamber
3	

28

4	
5	
6	
7	
8	

9	

Table 3
80W, medium size (5 x 5”), heaters resistance and power values

No	Resistance (Ω)	Resistance deviation (%)	Power	Power deviation (%)
1	9.457	-3.5	82.902	+1.29
2	10.547	+7,62	74.334	-7.08
3	9.288	-5.22	84.410	+5.51
4	9.635	-1,68	81.370	+1.71
5	9.664	-1.39	81.126	+1.41
6	9.499	-3.07	82.535	+3,17
7	9.025	-7.91	86.870	+8.59
8	9.861	+0.62	79.505	-0.62
9	9.546	-2.59	82.129	+2.66

Table 4
Small size (5 x 5”) heaters visual aspect

1	
2	

3	
4	
5	*Glued on aluminum plate and placed in the qualification device chamber
6	
7	
8	
9	
10	
11	
12	

Table 5
80W, small size (2 x 2”), heaters resistance and power values

No	Resistance (Ω)	Resistance deviation (%)	Power	Power deviation (%)
1	8.893	-9.26	88.159	+10.19
2	9.066	-7.49	86.477	+8.09
3	9.157	-6.56	85.618	+7.02
4	8.621	-12.03	90.941	+13.67
5	10.786	+10.06	72.687	-9.14
6	9.417	-3.91	83.254	+4.07
7	9.721	-0.81	80.650	+0.81
8	9.056	-7.59	86.572	+8.22
9	8.976	-8.41	87.344	+9.18
10	10.300	+5.11	76.117	-4.85
11	9.972	+1.76	78.620	-1.73
12	10.134	+3.41	77.363	-3.29

Another issue, which has been solved in the second stage, was related to the maximum size of the heater that can be achieved through the laboratory procedure presented above. During this stage, a hot press provided with auto alignment plates, was designed and manufactured. This new device allows heater sizes up to 12 x 12”.

Figure 44
50 tones auto aligned plates hot press

Figure 45
12 x 12” large heater

Proving that the obtained heaters can endure the function condition

In order to perform the heaters thermal cycling, to prove that they can work in space like environment, our first approach was to use a liquid nitrogen injection system, which has the following characteristics:

- 2l inner volume, cylindrical shape, 28cm diameter;
- High vacuum operated, with fast operating enclosure (Morse cone sealing);
- 210mm diameter copper plate, with inside liquid nitrogen injection system & electric heaters, capable to achieve temperatures starting from -180°C up to 250°C, computer controlled.
- Thermal stability in isotherm operation mode, ±0.1K, high precision Lake Shore PT100 temperature measuring system;
- Very fast cooling (reach -180°C in less then five minutes)

This system, which I designed and used in the past years for polymer materials characterization at very low temperatures, has to disadvantages for this purpose:

1. Can work with only one heater at the time;
2. Has tremendous liquid nitrogen consumption (over 10l/h during cooling time and about 1l/h after reaching the lower limit temperature, without any heating generation process inside.

The other option was to use a deep freezer machine (Inova101), which can achieve temperatures up to - 80°C, without liquid nitrogen, being a Freon based cryocooler type machine.
The inner volume of this freezer is quite big (140l), and can rich - 80°C in about 5h.

However, the maximum thermal power inside have not to exceed 20W.
To solve the problem I designed and build a stainless steel vessel, provided with a removable cover, sealed with an o-ring VITON gasket. The electrical connection, necessary to power up the heaters and to monitor the temperature and the vacuum connection, is assembled to the cover.
On the inner side of the cover, is assembled a system which consist two thermal plates, each one having his own thermal sensor (T type thermocouple), which are connected to the cover trough four thermal shunts made from stainless steel. The total thermal resistance of these four shunts is designed so, that at maximum working temperature of the plates, the outside transferred power not to exceed 10W.
Two heaters are placed on the palates, and can operate thermally independent. The plates temperature is controlled using a PLC system, connected to a PC. The temperature versus time diagram is shown in fig.1. At the begging of simulation process, the heater temperature is equal with could source (-80°C). When the PLC initializes the process, the heaters temperature starts to rise, up to 80°C. At this temperature, the PLC start the isotherm mode, and maintained the temperature constant for 1h, and after that, begin the cooling step, until the heater temperature reach again -80°C and so on.
The process is designed to take place for two month.
In order to make a comparative analyze of the heaters behavior, at one plate is placed an irradiated heater and at the other plate a normal one.
At the end of the simulation, the main characteristics of the heaters (nominal resistance an insulation resistance versus thermal plate) are measured again, in order to establish that they work still properly. Also, the visual aspect of the heaters will be compared with initial one.

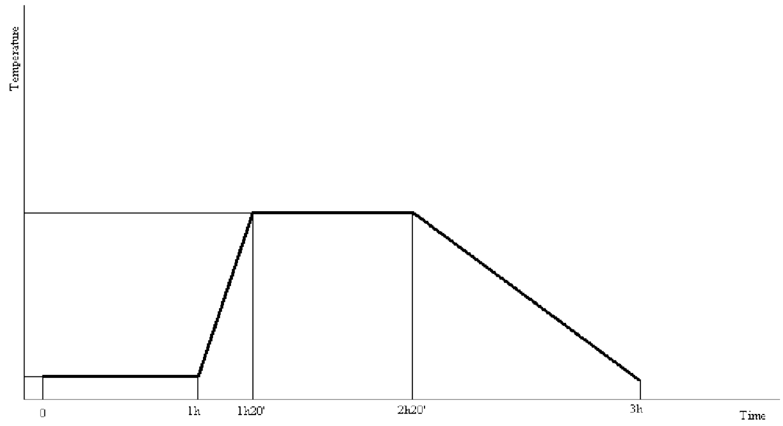

Figure 46
Temperature versus time diagram

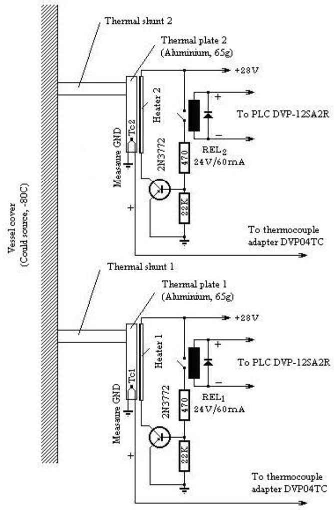

Figure 47
Automation Schematics

Figure 48
Ultra low deep freezer U101 Inova with automation and power heaters supply above

Inside the cool chamber, I placed a vacuumed device:

Figure 49
Vacuumed device for thermal cycling

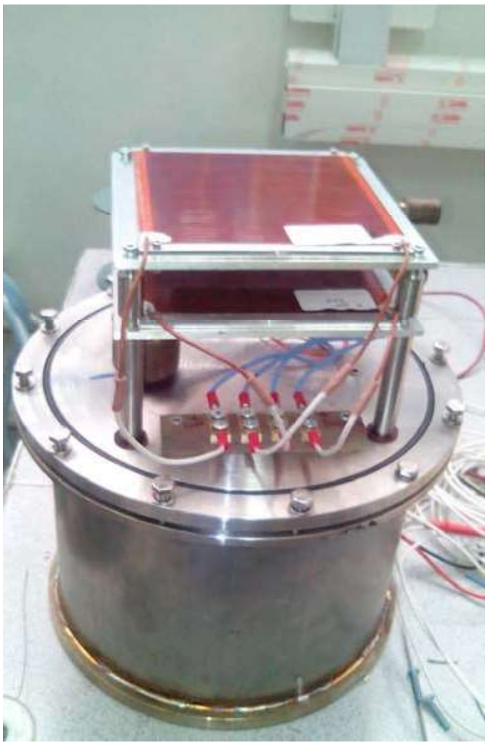

Figure 50
Inside of the thermal cycling device

Another task related to heaters characterization was to be irradiated at a similar ionizing radiation level with the space condition (corresponding to the LEO irradiation conditions.

The Ob-Servo Sanguis type irradiator is self-contained, dry source storage Category I. equipment. The irradiator in which the sealed source is completely enclosed in a dry container constructed from solid materials and is shielded at all times, and the human access to the sealed source and the volume undergoing irradiation is not physically possible in the designed configuration. The shielding of the irradiator is made of lead.
The irradiator is a multipurpose one to be utilized mainly for irradiation of medical (blood, etc.), or other research products with maximum 12 liter volume. The equipment can be operated automatically in accomplished by a PLC (Programmable Logical Controller) system.

Figure 51
The Ob-Servo Sanguis type irradiator

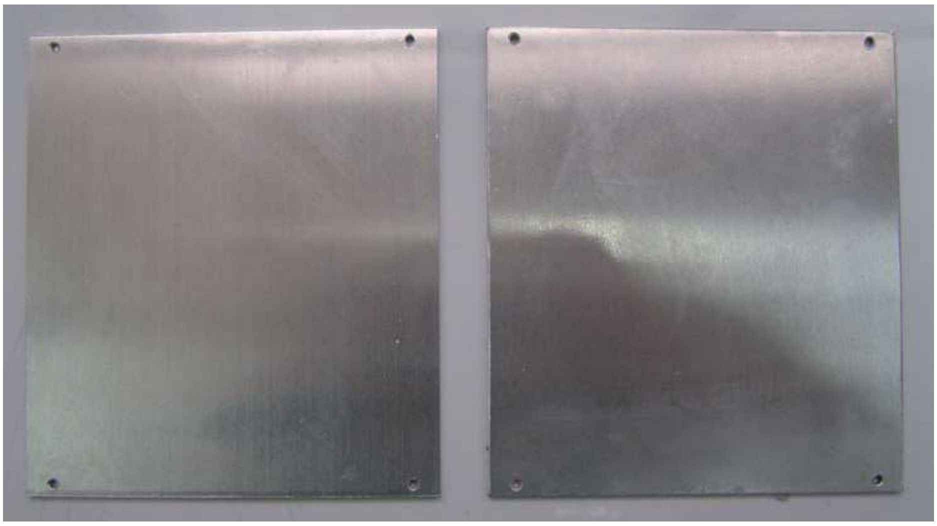

Figure 52
Aluminum plate supports for heater attached

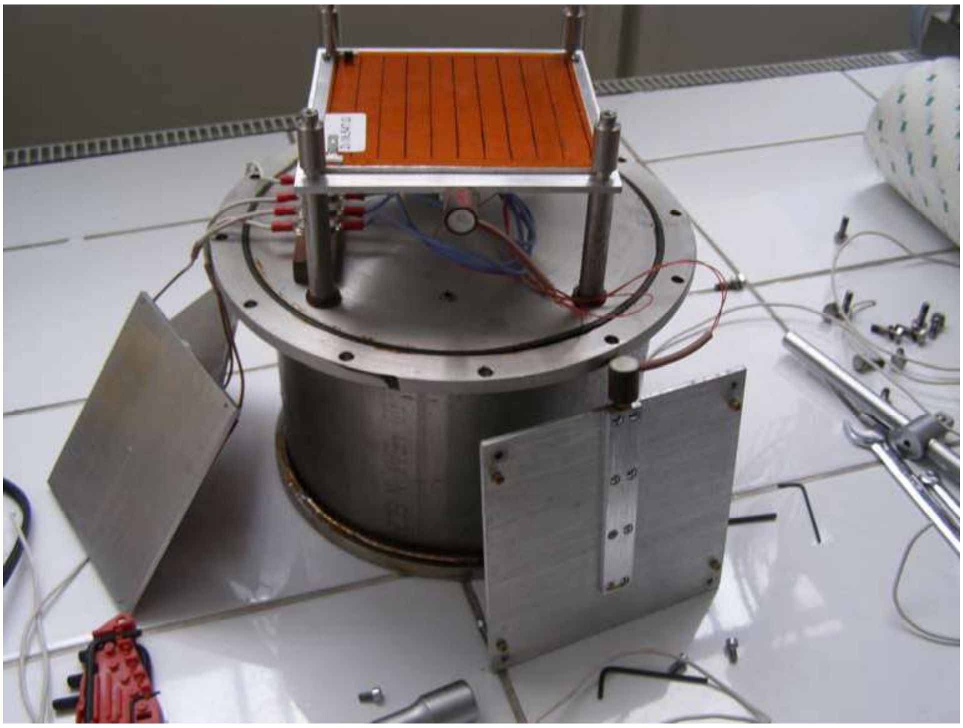

Figure 53
Replacing the heaters in order to continue characterizations;
Those heaters were irradiated with 3KGreys

The irradiated heaters were tested in parallel with similarly unirradiated. The test results have shown no differences between from the electrical point of view.

Furthermore, after the endurance tests ended (they have been carried out for 3600 hours), also no changes from the point of view of electrical parameters and visual aspect were to report.
That proves the rightness of the elaborated technical solution.
At the end of the second stage of the contract, the problem regarding small power densities in respect with local power density to protect the insulation system remain unsolved.

WP3. Achieving and validation of planar device heaters based on carbon fibbers and organic insulation system (KAPTON and 3M 966 adhesive) in order to obtain high electrical resistance heaters (as has been redefined)

During the second stage of the contract, we start to develop a laboratory method to produce targeted resistivity starting from 2K PAN fibre precursor. Unfortunately, the lack of time prevents as to fully succeed in this direction. However, the modified graphitization installation allow to produce small quantities of carbon fibre which electrical resistivity that can be tuned in very large ranges, starting from $10^3\Omega\cdot m$ up to $2\cdot10^{-6}\Omega\cdot m$. The remaining problem is that characteristics are still subject of experimental research from the point of view of reproducibility. Also, the mechanical properties of the resulted carbon fibre strand are still pore.

Hardly at the end of November 2016, had my industrial partner finally succeeded to procure from a Holland company a carbon felt that allows the small power density heaters manufacturing.
The material cam in 10’ rolls, heaving a witness of 1’. The thickness of the felt is in range of 350μm.
This carbon felt has good electrical properties for my propos. Also, the surface electrical isotropy is good. The measured specific resistivity for the carbon felt type material was $\rho = 2.7027\cdot10^{-2}\Omega\cdot m$. Collected samples, from the border and from the middle of the carbon felt sheet present a variation of electrical resistivity less then 2%.

Small power density heater design
The heater design follows the path that has been already established in the second stage of the contract.
All the heaters 5W was realized following a design as is shown in figure 54.

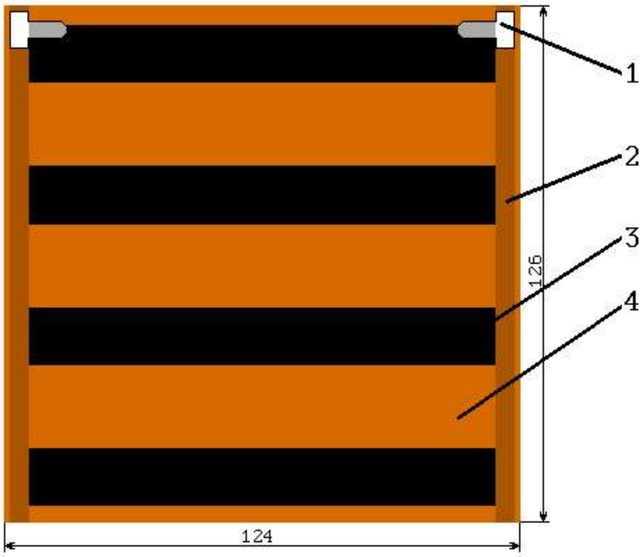

Figure 54
Design used in present for all 5w power heaters manufacturing; the dimensions refers to the medium size heaters; 1.Electric terminal, made from 300μm silver plated brass sheet, attached to the copper ribbons by copper rivets; 2.Current collector, made from 35μm copper ribbon; 3.Heating element, consisting in carbon felt strip, 350μm thickness; Insulating system, made from 50μm KAPTON foil, all elements glued together with 3M 966 acrylic solid adhesive

Experimental results

Heater visual aspect

Table 6
Medium size (5 x 5”) heaters visual aspect

1	
2	

3	
4	
5	
6	
7	
8	

9	
10	

Table 7
5W, medium size (5 x 5”), heaters resistance and power values

No	Resistance (Ω)	Resistance deviation (%)	Power [W]	Power deviation (%)
1	163.109	+4.023	4.807	-3.860
2	169.562	+8.139	4.624	-7.520
3	166.534	+6.208	4.708	-5.840
4	168.423	+7.413	4.655	-6.900
5	164.098	+4.654	4.778	-4.440
6	162.459	+3.609	4.826	-3.480
7	161.527	+3.015	4.854	-2.920
8	162.395	+3.568	4.828	-3.440
9	163.748	+4.431	4.788	-4.240
10	161.317	+2.881	4.860	-2.800

Table 8
Small size (2 x 2”) heaters visual aspect

1	
2	

3	
4	
5	
6	
7	
8	
9	
10	
11	

Table 9

5W, small size (2 x 2") heaters resistance and power values

No	Resistance (Ω)	Resistance deviation (%)	Power	Power deviation (%)
1	159.543	+1.749	4.914	-1.720
2	161.834	+3.211	4.844	-3.120
3	163.903	+4.529	4.783	-4.340
4	162.901	+3.891	4.813	-3.740
5	152.549	-2.712	5.139	+2.780
6	158.711	+1.219	4.940	-1.200
7	153.218	-2.284	5.117	+2.340
8	161.542	3.024	4.853	-2.940
9	154.765	-1.298	5.066	+1.320
10	154.212	-1.651	5.084	+1.680
11	162.232	+3.464	4.833	-3.340

As is shown in the electrical characterization Table 3 and 5, the electrical results are better then the results obtained using carbon fibres for 80W power heater, from the point of view of deviation from the required power. Also, the aria surface covered by the heating element is about ten times higher compared with first technical solution, which relay on carbon fibres, being in concordance with ESA recommendations. However, for the carbon felt technical solution, there some aspects which create problems to be solved, such as:

- The flexibility of the heaters is lower then for the heaters based with carbon fibres;
- Due to some constituents of the carbon felt, during the hot pressing procedure (160°C, 7MPa), the gluing quality was affected, and also some small surface puckering occurs.
- The thickness of this carbonic felt type is too high (350μm). The desire thickness will be in range of 50-100μm.

In order to find out data about the procured carbon felt, an investigation via DTA analysis was made. The test was performed using a STA 449 F3 Jupiter NETZSCH DTA apparatus.
The result for this test is shown in the Figure3.

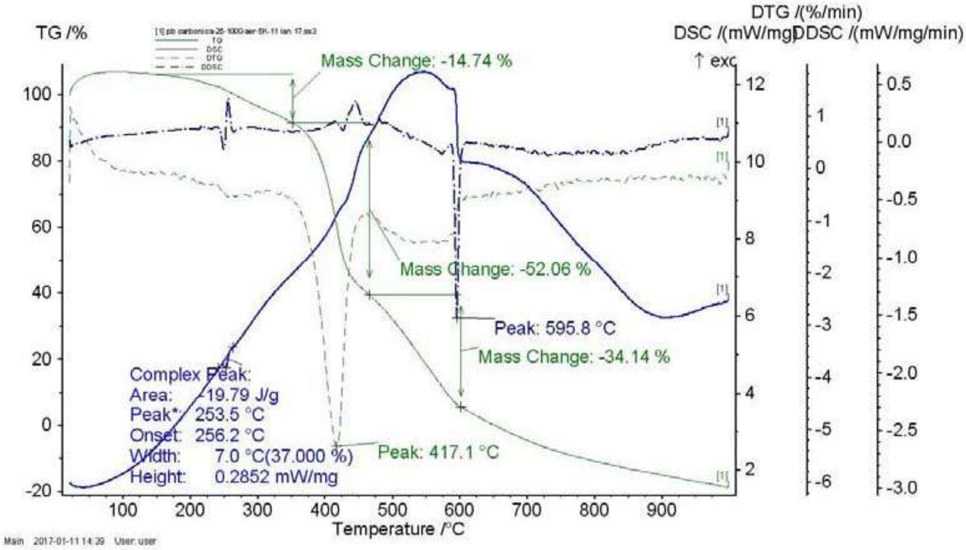

Figure 55
Carbon felt DTA test result

The green line in this chart, which represents the sample mass variation versus temperature, show that this felt has some other constituents, other then carbon. Indeed, the carbon oxidation, in static air (which is the case for this investigation), occurs at a temperature higher then 373°C, when the material has an already mass loss of 14.74%. To establish for sure which are the component which cause this mass loss, a further investigation (elementary analyses) has to be carried out. The result are important, because may allow me to establish the cause which affect the gluing capacity of 3M 966 adhesive.

All main necessary materials in the manufacturing process are listed in the Table 10 bellow.

Table 10
List of all materials used in carbon based heaters manufacuring

No	Material	Producer	Supplier	Main Characteristics	Price (Euro, VAT included)
1	KAPTON foil Type: **KAPTON 200 HN[1]**	**DuPont, USA**	***LOHMANN TECHNOLOGIES LIMITED*** Mr. Manjinder Sidhu - Sales Dept. **KAPTON AND TEFLON FILMS** Email: Manjinder.Sidhu@lohmann-tapes.com	width: 610mm thickness: 50.8μm	199.75 65.49/ sqm

			Phone: +441296337772	Roll @5 meters	
2	**3M™ High Temperature Acrylic Adhesive 100** Type: **966**[2]	**3M, USA**	MDE Group SRL, Oltenita, Romania Email: office@mdegroup.ro Phone:+ 40342220083	width: 12" (304.8mm) thickness: 60µm Roll @180yards	348.70 27.80/ sqm
3	**Copper foil** Type: **JTC-HTE**	**GOULD Electronics Inc., USA**	**GOTTLE GmbH &Co** Email: info@goettle.de Phone: +490823194960 Fax: +498231964622	width: 300mm thickness: 35µm Roll @20m, PCB type, one face preared to be glued	145 24.17/ sqm
4	**Conductive adhesive** Type**:** Master Bond Polymer Adhesive SUPREME 10HT/S[3]	**Master Bond Inc., USA**	**Master Bond Inc.**, USA Email: esther@masterbond.com Fax: **+**0012013432132	50g, sealed jar	1051.10 ($1200) 21.022/ g
5	**Conductive adhesive** Type: Loctite MR 3863	**Loctite Corporation, Germany**	**ASPAD COM SRL,** Romania Email: contact@aspad.eu Phone: **+**40314253651	2g, sealed jar	14 $7/g
6	**Carbon fibre** Type: 90g/m² fabric	**Havel Composites, Poland**	**Havel Composites** Email: biuro@havel-composites.pl Phone: +3833 8513327		157 $78.5/ sqm
7	**Carbon felt**	**LANTOR, Holland**	Po box 45 - 3900 AA Verlaat 22 - 3901 RG Veenendaal	1 x 10' rolls,	$26/ sqm

CONCLUSION OF FINAL STAGE

So far, my work related to this ESA contract succeeded to solve the following issues:
Hard points:

- To prove that the concept regarding planar heaters designed for thermal management of space vehicle is viable, and heaters with demanded characteristics can be manufactured, using carbon fibres or carbon felt as heating elements, glued on current lines made of copper ribbons with silver epoxy or polyester conductive adhesives, and insulated in KAPTON films, all glued together using 3M 966 adhesive.

- The technical solution, as concept and resulting heaters made over this concept was qualified in space like condition (irradiated with a γ rays doze equivalent of ten years for LEO), high vacuum working condition, under a temperature variation starting from -80 and up to 120°C, in repeated cycle (over 1200 cycles was performed), without any changes in electric characteristics of the heaters.
- The chosen technical solution has the advantage of a higher redundancy over the existing technical solution, which relays on metallic heating elements. Indeed, the carbon heating elements consist in tens of thousands of micro carbon filaments, all put in an electric parallel configuration, so if a part of these filaments are damaged, the other remaining part continue to work properly.

Drawbacks:

- The tuning of required value for the heater resistance is still a problem, when a small number of heaters have to be manufactured. During the contract evolution, I have a number of discussions with carbon fibres and carbon felt producers, which shown the availability to produce carbon with on demand grad of graphitization, also said, with dedicated electrical resistivity, if the required quantities are high enough.
- The manufacturing technology is more complicated then the current manufacturing procedure, based on metallic heating elements.

Achievable power densities

Following the technologies and taking count of the percentage of total area surface covered by the heating element, are available to power classes:

1. High power densities, starting from 40W per dm^2 up to 200W per dm^2.
2. Low power densities, starting from 2W per dm^2 up to 15W per dm^2.

The manufacturing procedure was passed to the industrial subcontractor, SC COMPOZITE Limited, which has the capability to manufacture all type of heaters, based on the experience and knowledge accumulated during the applied research for this work.

Presentation 2514

Corner cube retro-reflectors

Corner cube retro-reflectors

Development under "Romanian incentive scheme" funded by ESA

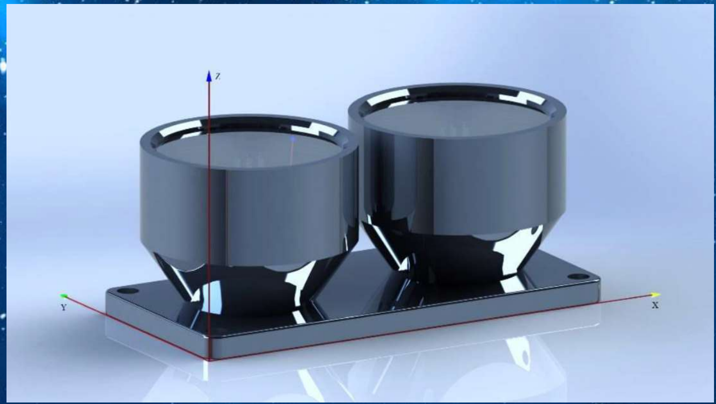

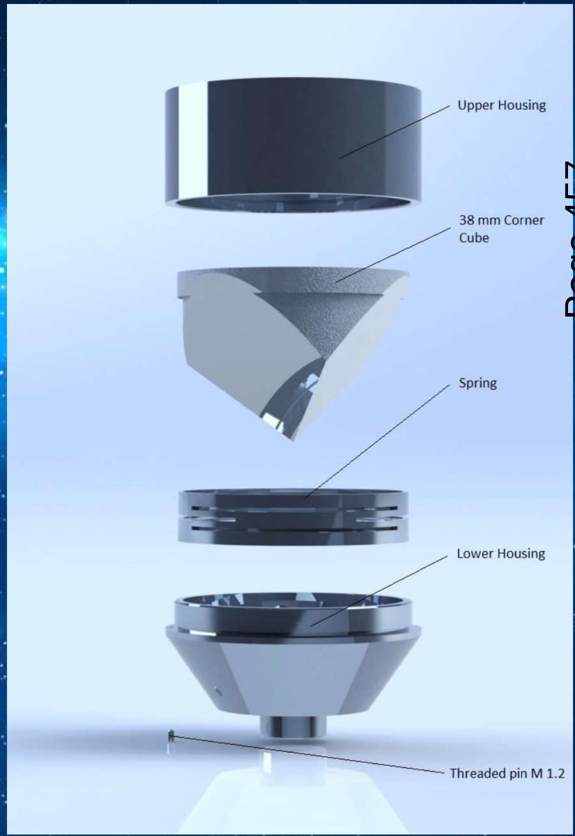

Short introduction

The ESA contract **No. 4000111454/14/NL/CBi** with Pro Optica S.A. was signed in order to help the contractor (Pro Optica S.A.) to improve its facilities and capabilities to become able to achieve retro-reflector assemblies with corner cubes as per ESA requirements, from technical specification and subsequent agreements. The final delivery has included three corner cubes made from fused silica with a diameter of 38 mm and two corner cubes made from fused silica with a diameter of 60 mm. Every CCRR was mounted in an individual mechanical housing. Two of the mounted CCRRs of 38 mm was integrated in an assembly with a flat breadboard. The assembly provide a mechanical and thermal interface to a perfectly flat panel.

Short introduction

A corner cube retro-reflector is a device that reflects light back to the source area with a minimum of scattering. In a retro-reflector, an electromagnetic wavefront is reflected back along a vector that is parallel to but in opposite direction with the wave's source. Arrays of such optical components are commonly used on satellites in order to periodically locate them on their orbits, acting as so called ”cat eyes” 

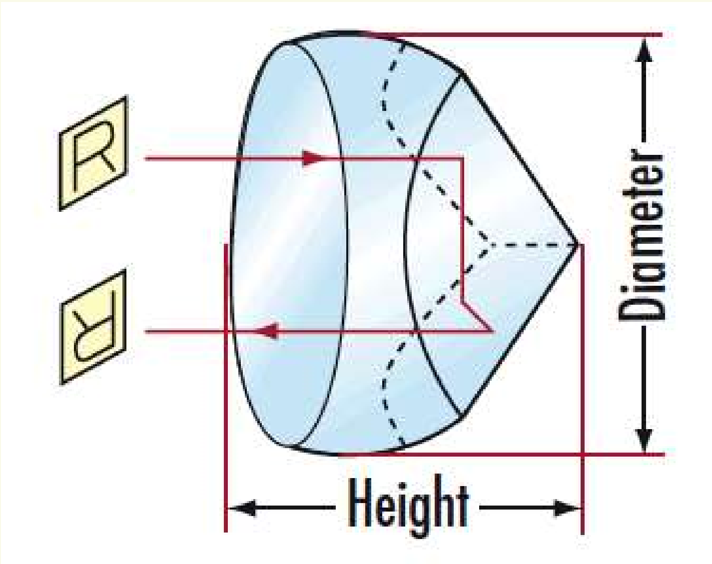

Achieved capabilities

- The project help us to really improve our capabilities in terms of glass processing, optical coatings and assembling.

- The most important achievement was a top level lapping machine "Lapmaster" – this equipment is used to perform high quality flat surfaces, with shape deviations until λ/20 and roughness around of 2 nm.

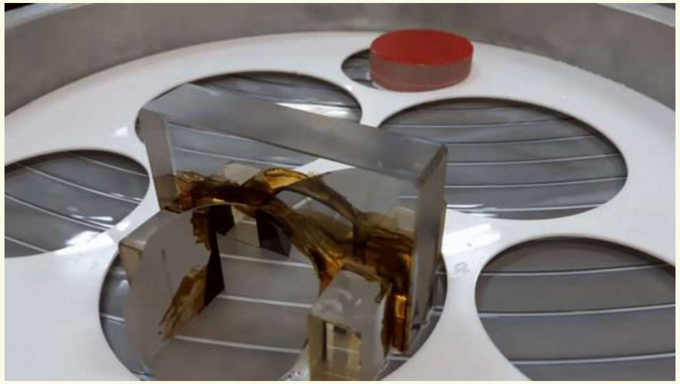


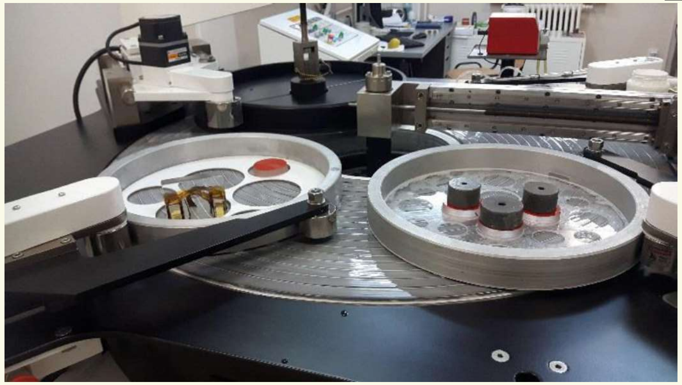

Achieved capabilities

- The second capability achieved was the ion source “Mark II” from VEECO – this equipment is used to enhance the compactness and, consequently, the resistance of optical coatings, by “Ion assisted deposition” technics (IAD). As a consequence, using this equipment, the performed silver-based reflective coatings passed all required environmental and mechanical tests.

Achieved capabilities

- Clean room - equipment assembled in order to ensure the accuracy of optical parts when these are prepared for coating and for final mounting.

Achieved deliverables

- The picture below shows the deliverable hardware, achieved during the project and the table shows a description of each component.

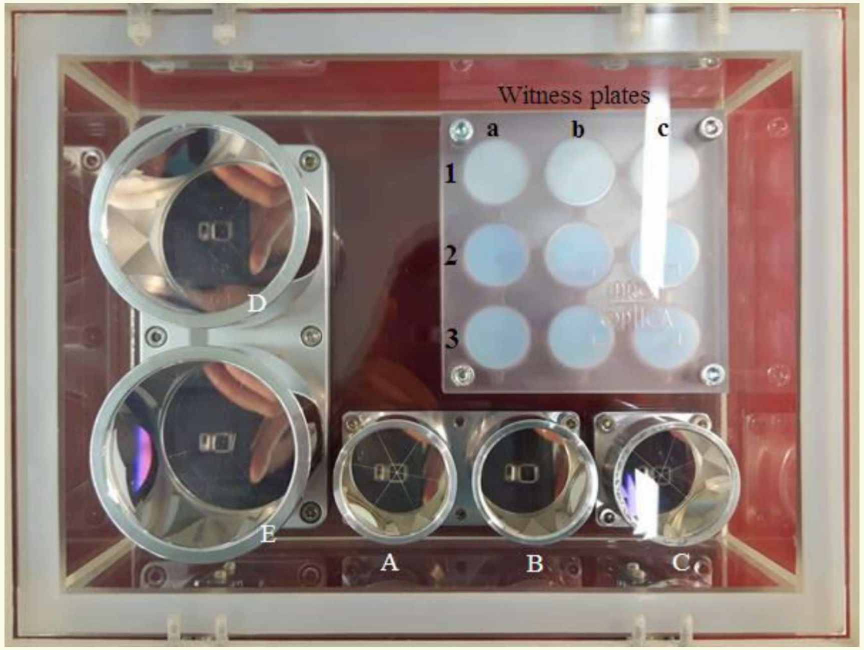

CCRR No.	Base parameters
A F(38)	ε_{AB} = 1.83"
	ε_{BC} = 1.66"
	ε_{CA} = 1.95"
	Coating Type 1 (R = 80%)
B F(38)	ε_{AB} = 2.44"
	ε_{BC} = 1.55"
	ε_{CA} = 2.23"
	Coating Type 3 (R = 75%)
C F(38)	ε_{AB} = -2.96"
	ε_{BC} = -6.16"
	ε_{CA} = -2.62"
	Coating Type 2 (R = 88%)
D F(60)	ε_{AB} = 0.47"
	ε_{BC} = 3.14 "
	ε_{CA} = 5.50 "
	Coating Type 3 (R = 75%)
E F(60)	ε_{AB} = -2.79 "
	ε_{BC} = -7.40 "
	ε_{CA} = 2.05 "
	Coating Type 3 (R = 75%)

Achieved deliverables

- Deliverable hardware, achieved during the project.
- Three corner cubes made from fused silica with a diameter of 38 mm mounted in an individual mechanical housing. Two of the mounted CCRRs of 38 mm was integrated in an assembly with a flat breadboard.
- Two corner cubes made from fused silica with a diameter of 60 mm. These was integrated in an assembly with a flat breadboard.
- The assemblies provide a mechanical and thermal interface to a perfectly flat panel.

38 mm Corner Cube Retroreflector

- Details

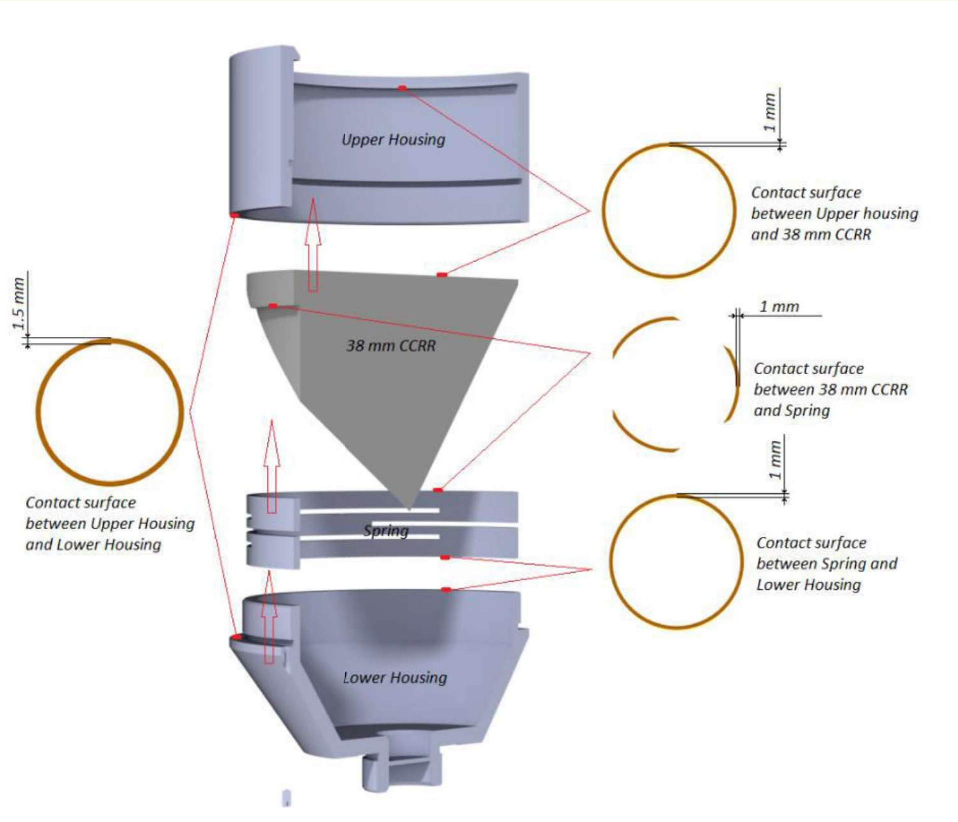

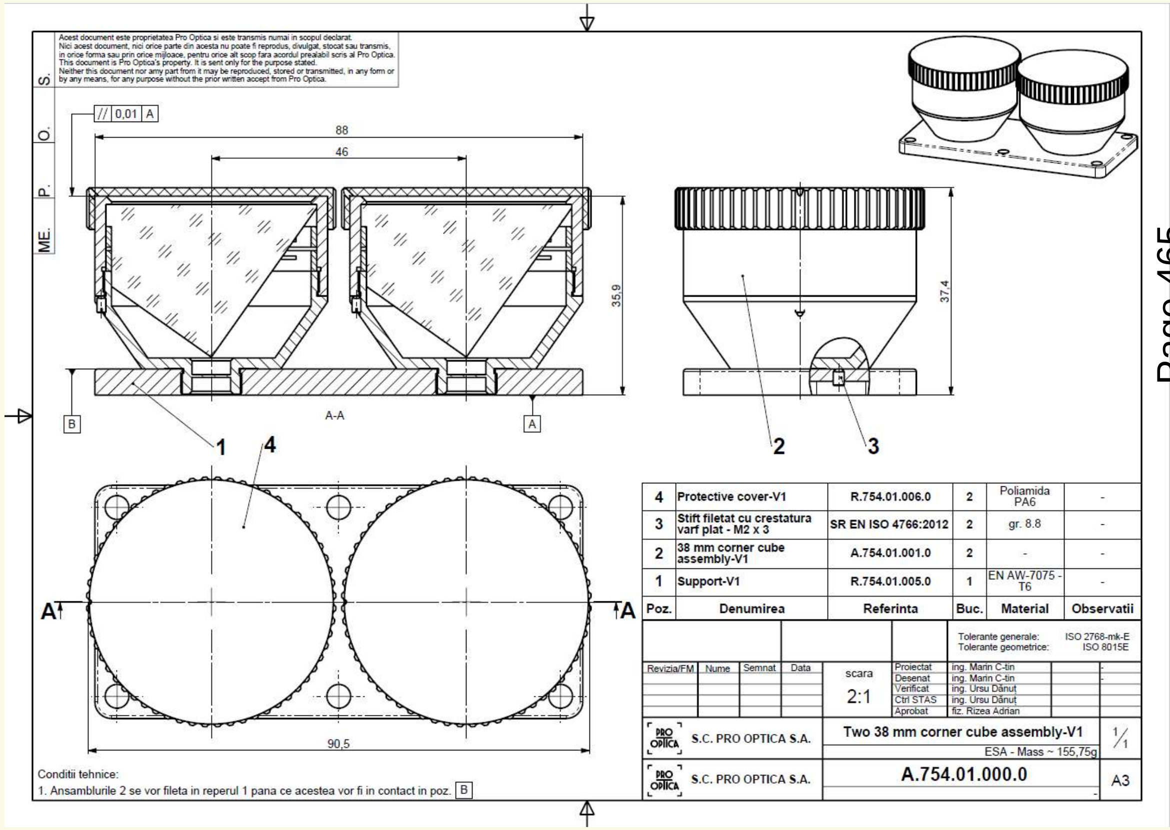

Mechanical tests

- ❑ Mechanical tests.
- ▪ Mechanical tests were done in collaboration with Electric Products Certification Independent Body (OICPE) and National Institute for Research and Development for Micro-technologies (IMT). These tests were executed according to the requirements from the technical specification.
- ▪ After testing, the mechanical housing and optical parts were carefully verified and checked for damages. No damages or other changes were found.

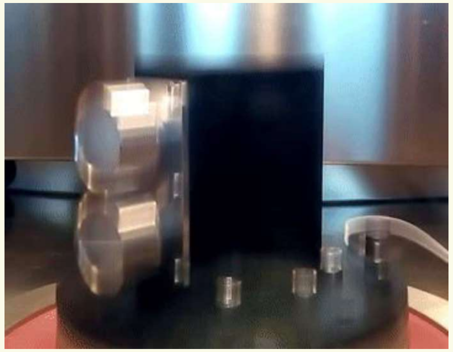

Environmental tests

❑ Environmental tests.

Environmental tests were done in collaboration with National Institute for Research and Development for Micro-technologies (IMT). The parts subjected to this test were:

- An assembly of two coated CCRRs (one of them made from BK7 and the second one made from fused silica);
- A panel containing 6 witness plates

No.	Test	Levels	Duration	Cycles per test
4.	Thermal ambient	-60°C to 100°C The temperature will change by 10°C/min, until the temperature reaches the upper or lower limit where it will stay for 4 min (see Fig. 21).	40 min (10 deg / min)	8 cycles
5.	Humidity	Humidity level 95% Temperature level 40 °C	48h	1 cycle

Coating Type 1 = upper row (two plates → fused silica and one plate → BK7)
Coating Type 2 = second row (two plates → fused silica and one plate → BK7)

Observations & Conclusions

- The project "*Preparatory Activity for the Design, Manufacturing and Testing of Laser Retro-Reflectors*" was an important opportunity for Pro Optica to see the real level of its technological capabilities, to understand our position in this domain and to make important steps in order to achieve highly competitive optical components for outer-space applications.
- The project helped us to improve our capabilities, acquiring and installing new, advanced, equipment and to obtain the associated knowhow. As a consequence we became able to achieve a good roughness on the optical surfaces (2 nm), a better flatness (up to $\lambda/20$), dihedral angles corrections (many times, with deviations lower than 1 arcsec), reliable reflective coatings (R = 88%) etc.
- In conclusion, we appreciate that the project has been very useful for Pro Optica to improve its capabilities and knowledge and also hope for future collaborations that will help to develop more advanced technologies in the niche of optical components for space applications.

Thank you for your attention!

Regarding glass processing contact: Roxana DAMIAN e-mail: roxana.damian@prooptica.ro
Regarding optical coatings contact: Adrian RIZEA e-mail: adrian.rizea@prooptica.ro
Regarding mechanical components and assembly contact: Constantin MARIN e-mail: constantin.marin@prooptica.ro

Presentation 2516

Data Fusion Algorithm for Multispectral Satellite Data

Sorin CONSTANTIN, Catalin CUCU-DUMITRESCU, Florin SERBAN, Anca Liana COSTEA
TERRASIGNA

TERRASIGNA™

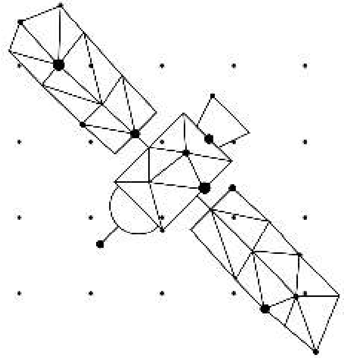

Data Fusion Algorithm for Multispectral Satellite Data

Sorin CONSTANTIN,
Catalin CUCU-DUMITRESCU,
Florin SERBAN,
Anca Liana COSTEA

TERRASIGNA

CEAS 2017 Conference
16-20 October 2017
Bucharest

Context

Developed within the *Data Fusion System for Black Sea Water Quality Monitoring* (***DaFSys***) project financed by the European Space Agency under the Romanian Industry Incentive Scheme.

Period: Dec 2015 – May 2017

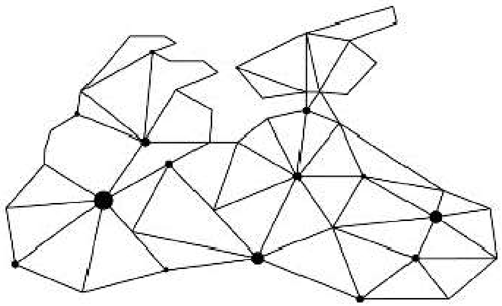

Consortium:

- TERRASIGNA (Romania) - leader
- Thales Alenia Space (France) - partner
- Faculty of Geography, University of Bucharest (Romania) - partner

Page 472

Data fusion products necessity

- Ocean color applications require specific spectral bands with high temporal, spectral and radiometric resolutions (IOCCG reports 1 & 13)
- Coastal areas monitoring should rely on satellite products with increased spatial resolution (tens of meters) compared to open ocean areas
- In optical complex waters a minimum number of well-chosen thin spectral bands is needed to retrieve specific bio-physical properties
- No current satellite sensor meets all the above criteria

Satellite data available

	Landsat 8 (OLI)			Sentinel-2 (MSI)			Sentinel-3 (OLCI) / Envisat (MERIS)			Aqua and Terra (MODIS)		
	Band center (nm)	Bandwidth	SNR	Band center (nm)	Bandwidth	SNR	Band center (nm)	Bandwidth	SNR	Band center (nm)	Bandwidth	SNR
							400*	15	2188			
							412.5	10	2061	412	15	880
	440	20	130	443	20	129	442.5	10	1811	443	10	838
										469	20	243
	480	60	130	490	65	154	490	10	1541	488	10	802
							510	10	1488	531	10	754
										551	10	750
VIS	560	60	100	560	35	168	560	10	1280	555	20	228
							620	10	997	645	50	128
	655	30	90	665	30	142	665	10	883	667	10	910
				705	15	177	673.75*	7.5	707			
				740	15	89	681.25	7.5	745	678	10	1087
				783	20	105	708.75	10	785			
							753.75	7.5	605	748	10	586
							761.25	2.5	232			
							764.375*	3.75	305			
							767.5*	2.5	330			
							778.75	15	812			
				842	115	172				859	35	201
NIR	865	30	90	865	20	72	865	20	666	869	15	516
							885	10	395			
							900	10	308	905	30	167
										936	10	57
				945	20	114	940*	20	203	940	50	250
							1020*	40	152			
										1240	20	74
	1370	20	50	1375	30	50				1375	30	150
SWIR	1610	80	100	1610	90	100				1640	24	275
	2200	180	100	2190	180	100				2130	50	110

*Additional bands for Sentinel-3, compared to MERIS

DaFSys data fusion prototype

- Because data fusion over water surfaces is a very difficult task, multiple algorithms for data merging have been evaluated

- Extended ARSIS (Amélioration de la Résolution Spatiale par Injection de Structures) (D. Sylla et al.,2013) algorithm was chosen as most appropriate for water application

- DaFSys implementation is based on ARSIS, but was highly improved and is more versatile

- The whole logic of DaFSys prototype was oriented toward speed and a user friendly graphical interface

DaFSys data fusion prototype

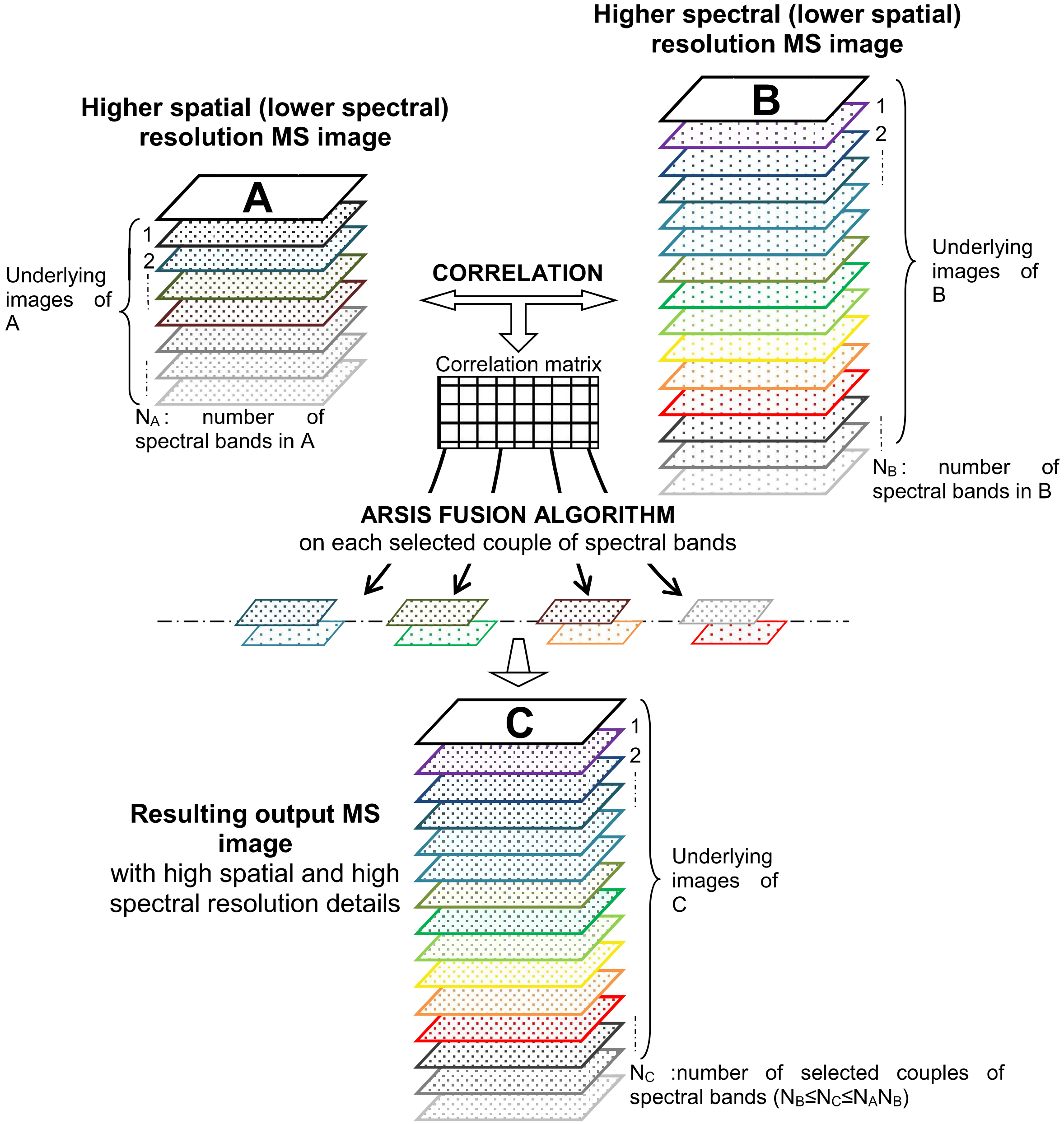

Scheme credit: Sebastien Pacteau (TAS)

Improvements made by DaFSys

Initial ARSIS recommendations	With DaFSys implementation
Low spatial resolution (*LR*) must be a multiple of the high spatial resolution (*HR*).	**Resolution ratio must be a rational number (*LR*/*HR* = *m*/*n*, with *m* and *n* integers).**
Resolution ratio must be a power of 2 (i.e. *LR*/*HR* = 2 or 4 or 8 etc.)	**No limitations for the value of the resolution ratio, as long as it stays rational.**
Images must have square dimensions.	**Images can be rectangular.**
Resolution ratio must not exceed 10 in order to obtain a good result.	**The value of the resolution ratio is not important, more important for a good result is to have a high correlation coefficient (>0.8, our recommendation).**
~	**Surprisingly good results can be obtained even for 1:1 resolution ratio**
The result of the fusion has the spatial resolution *HR*.	**The result of the fusion can have any integer spatial resolution in the interval [*HR*,*HL*].**

DaFSys interface

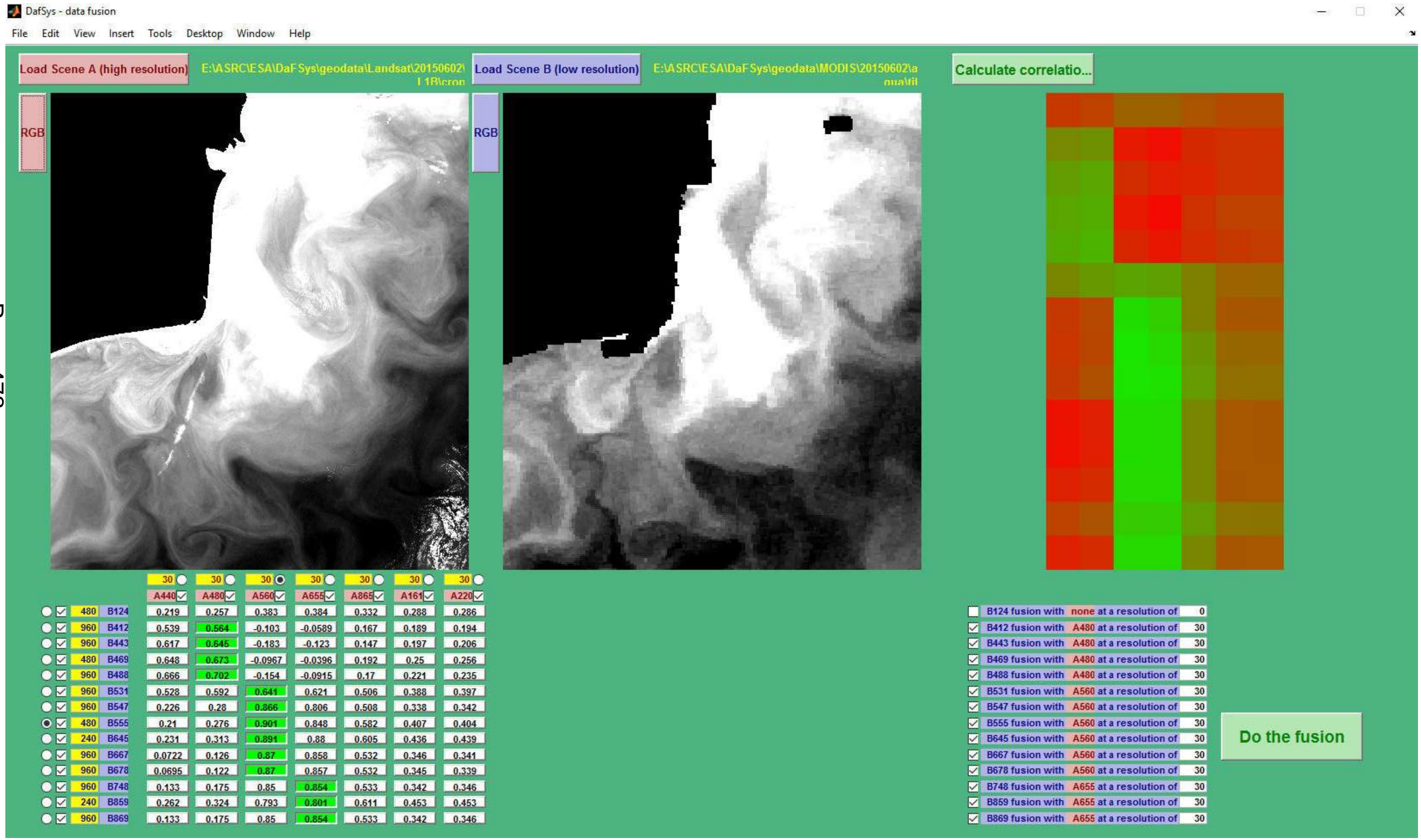

DaFSys interface

Page 479

DafSys - data fusion

File Edit View Insert Tools Desktop Window Help

Load Scene A (high resolution) E:\ASRC\ESA\DaFSys\geodata\Landsat\20150602\cropped\crop

Load Scene B (low resolution) E:\ASRC\ESA\DaFSys\geodata\MODIS\20150602\terra\tif

Calculate correlatio...

B869 fusion with A560 lasted 26 s.

RGB

RGB

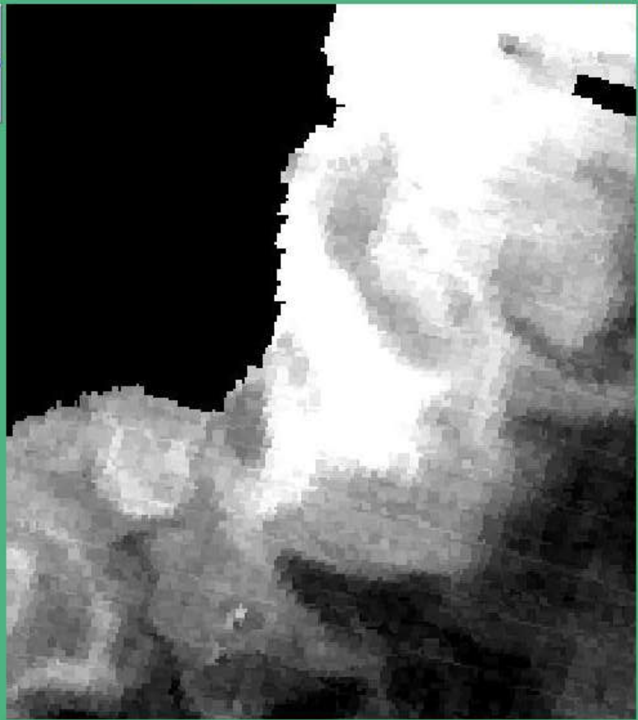

RGB

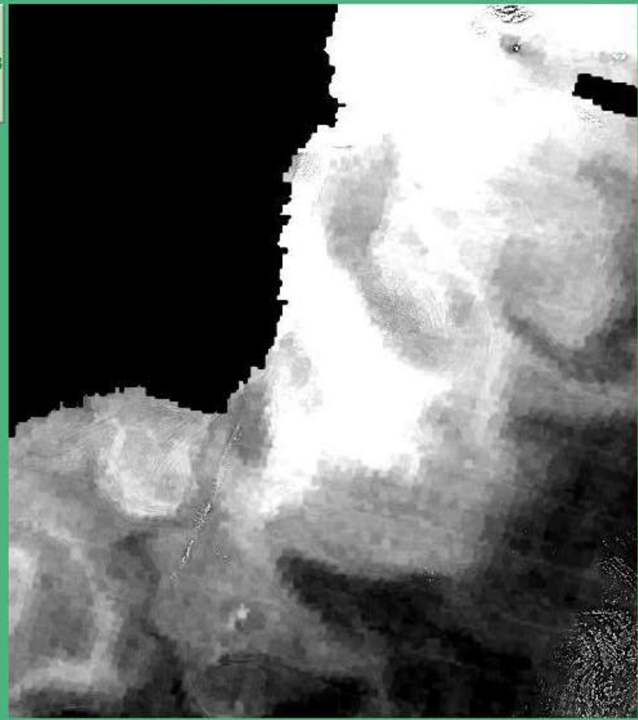

		30	30	30	30	30	30	30
		A440	A480	A560	A655	A865	A161	A220
480	B124	0.0737	0.0738	0.108	0.109	0.0718	0.054	0.0619
960	B412	0.582	0.606	0.0599	0.0692	0.278	0.245	0.231
960	B443	0.637	0.668	-0.0947	-0.0598	0.218	0.229	0.224
480	B469	0.667	0.69	-0.0349	-0.00327	0.221	0.244	0.244
960	B488	0.721	0.76	-0.0644	-0.0332	0.244	0.257	0.258
960	B531	0.478	0.518	0.684	0.617	0.478	0.333	0.318
960	B547	0.154	0.181	0.881	0.783	0.447	0.265	0.247
480	B555	0.157	0.211	0.917	0.84	0.513	0.333	0.325
240	B645	0.186	0.26	0.895	0.871	0.524	0.368	0.363
960	B667	0.016	0.0426	0.868	0.837	0.445	0.255	0.235
960	B678	0.0218	0.0478	0.864	0.832	0.447	0.256	0.236
960	B748	0.114	0.129	0.838	0.83	0.493	0.292	0.272
240	B859	0.163	0.204	0.533	0.545	0.566	0.423	0.367
960	B869	0.114	0.129	0.838	0.83	0.493	0.292	0.272

B124 fusion with	none	at a resolution of	0
B412 fusion with	A480	at a resolution of	120
B443 fusion with	A480	at a resolution of	120
B469 fusion with	A480	at a resolution of	60
B488 fusion with	A480	at a resolution of	120
B531 fusion with	A560	at a resolution of	120
B547 fusion with	A560	at a resolution of	120
B555 fusion with	A560	at a resolution of	60
B645 fusion with	A560	at a resolution of	30
B667 fusion with	A560	at a resolution of	120
B678 fusion with	A560	at a resolution of	120
B748 fusion with	A560	at a resolution of	120
B859 fusion with	A865	at a resolution of	30
B869 fusion with	A560	at a resolution of	120

Do the fusion

Save selected

It's all in the details….

- Water fronts, eddies and other details are visible in the fusion product

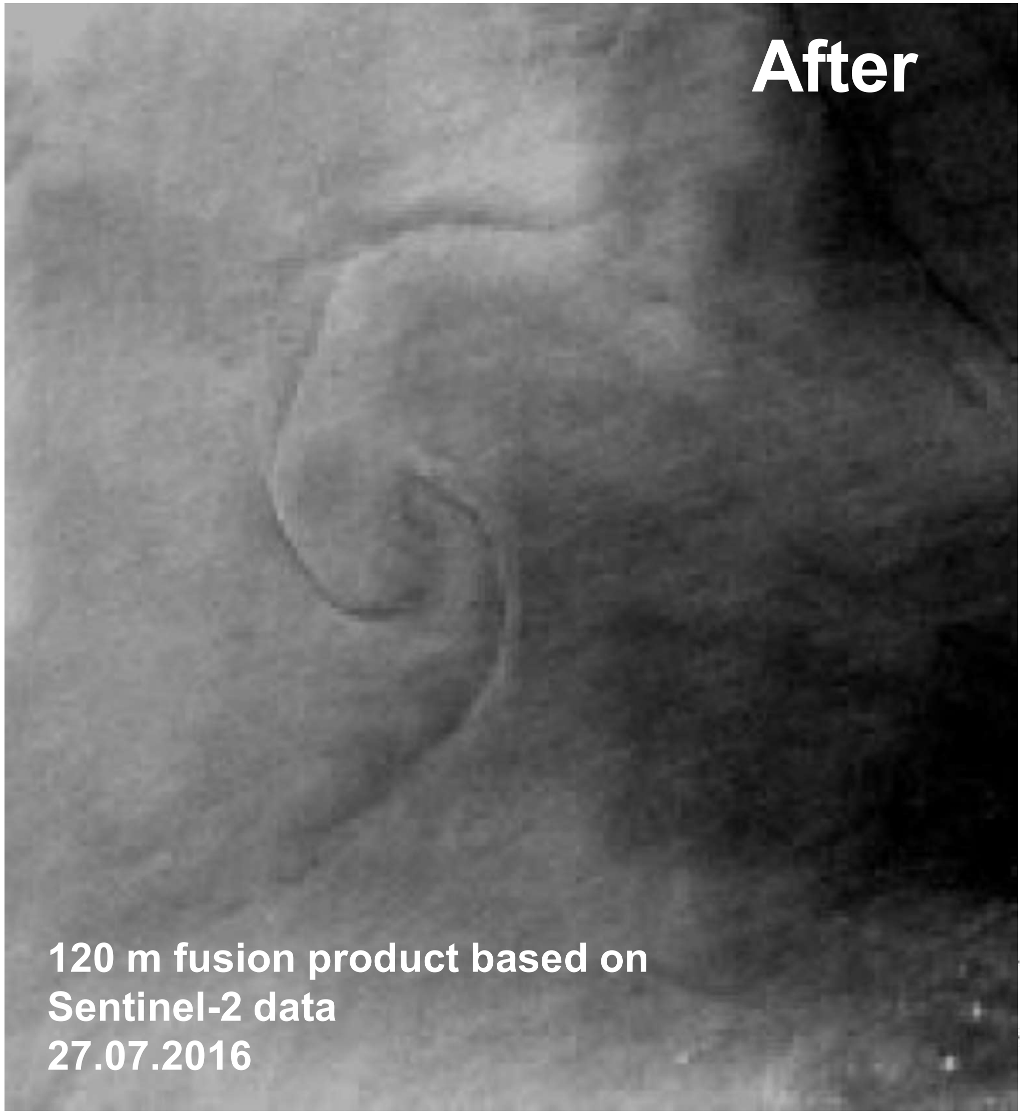

Page 481

It's all in the details….

- Relation between values of the initial image and of the fusion product (down-sampled to 1 km)

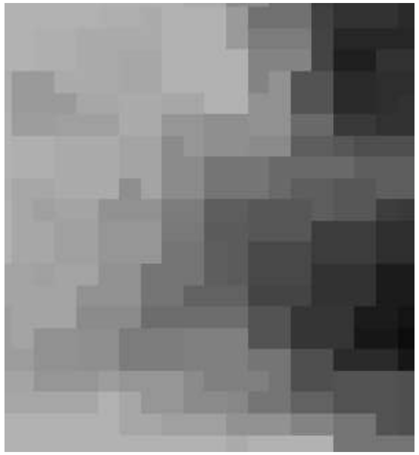

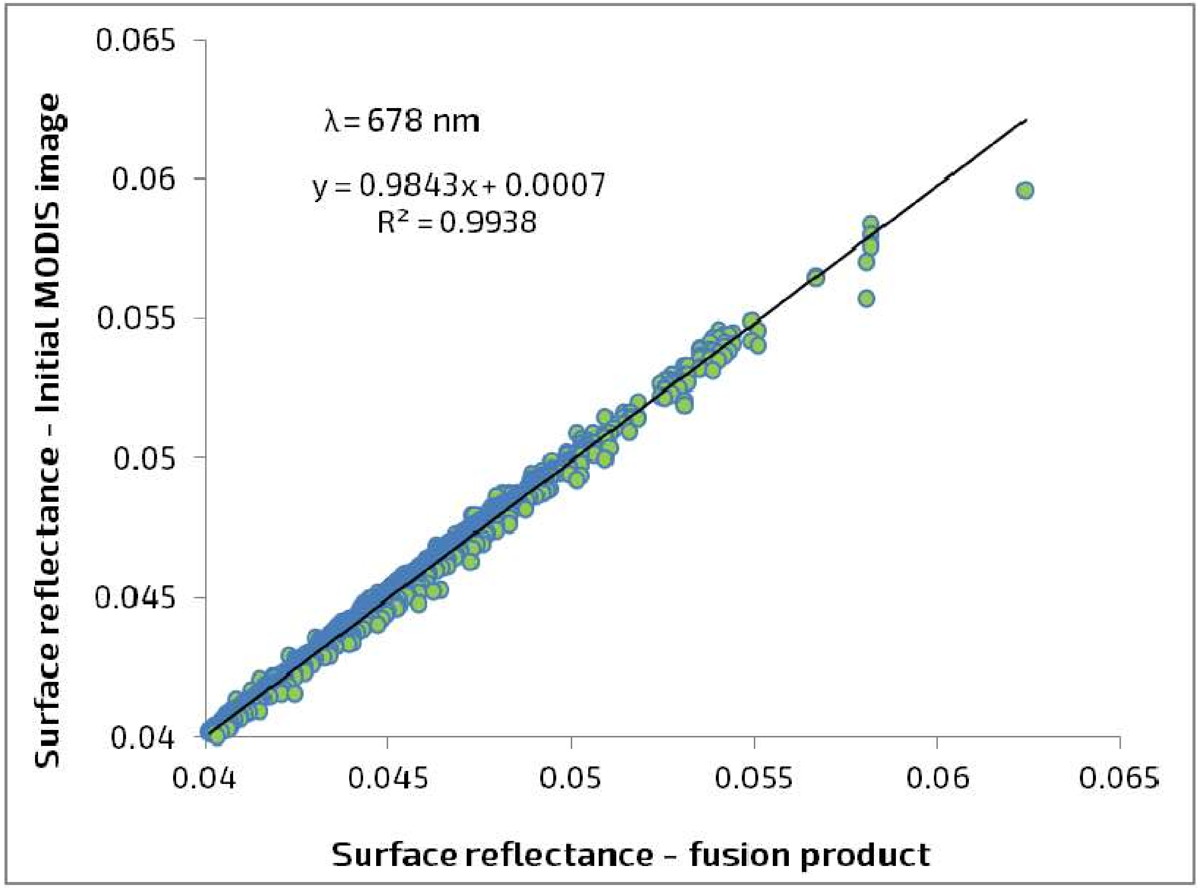

It's all in the details….

- *Chlorophyll front – **Before**: MODIS Terra (1 km), 02.06.2015. **After**: 120 m fusion product based on Landsat 8, 02.06.2015*

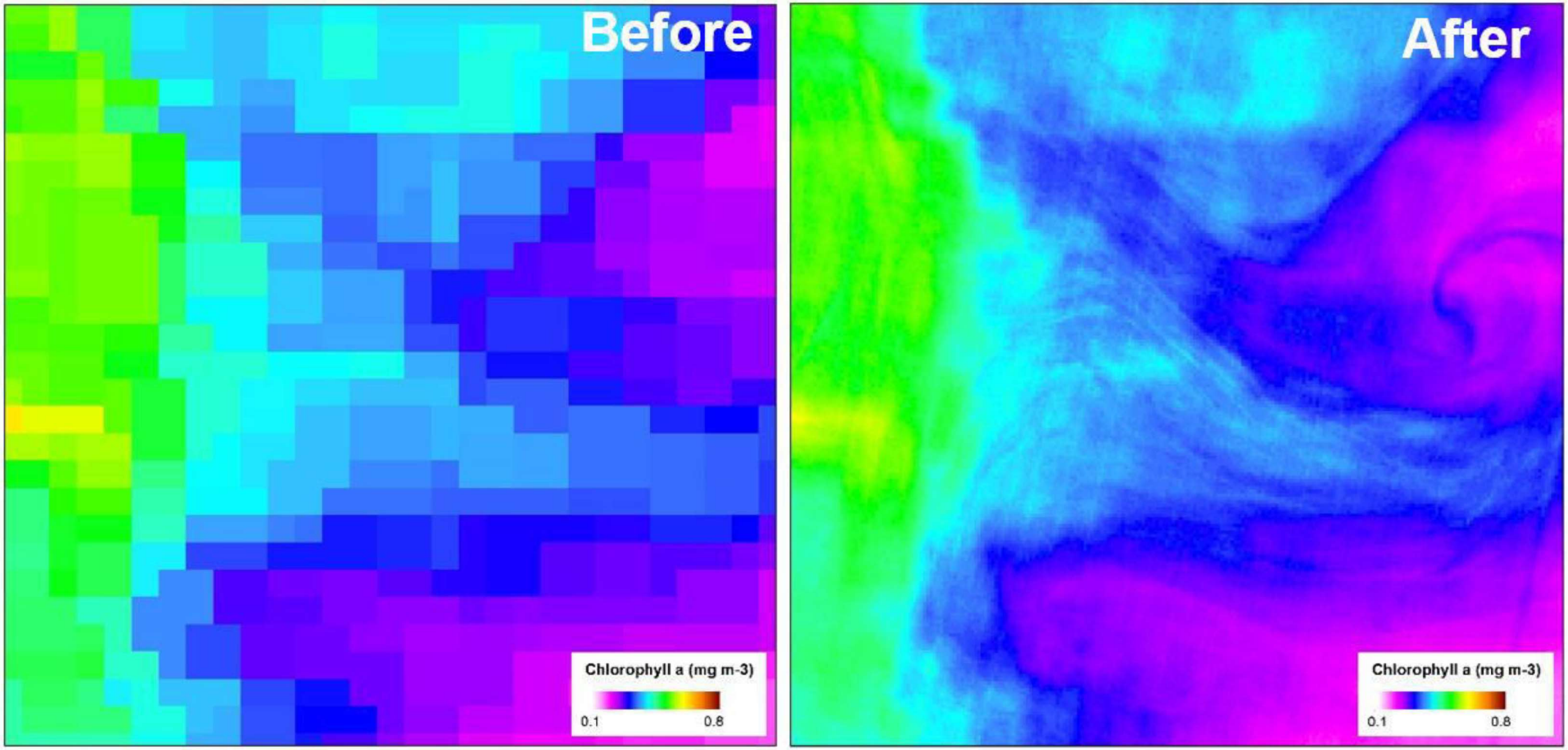

What about spectral improvements?

- **Spectral profile** more detailed after fusion, with **high spatial** resolution

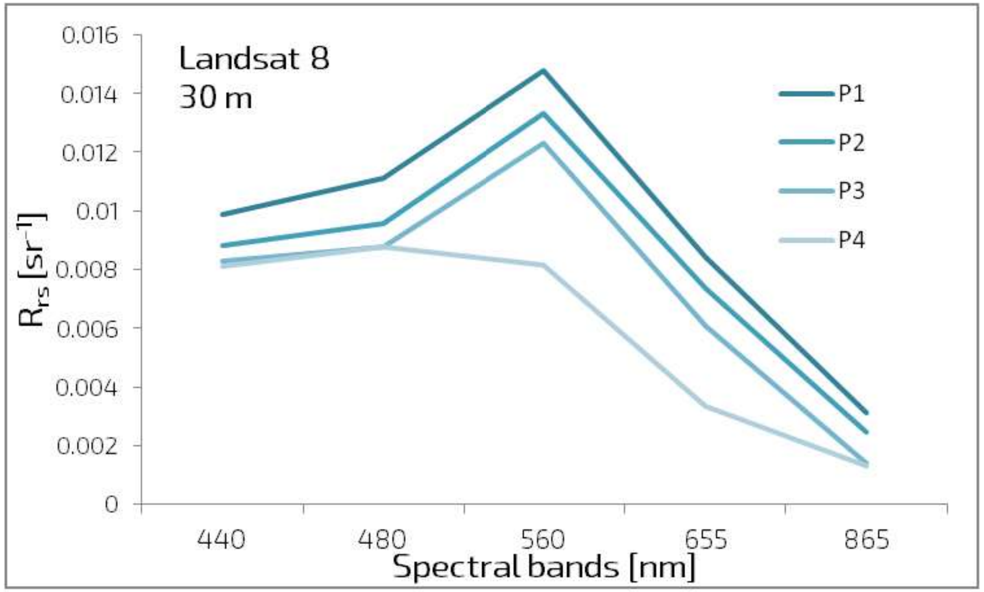

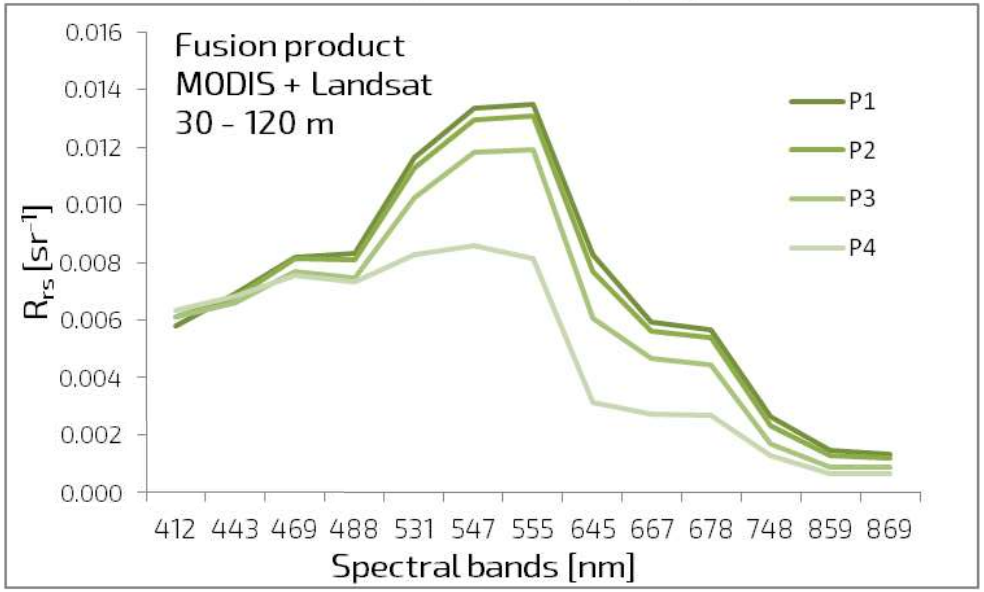

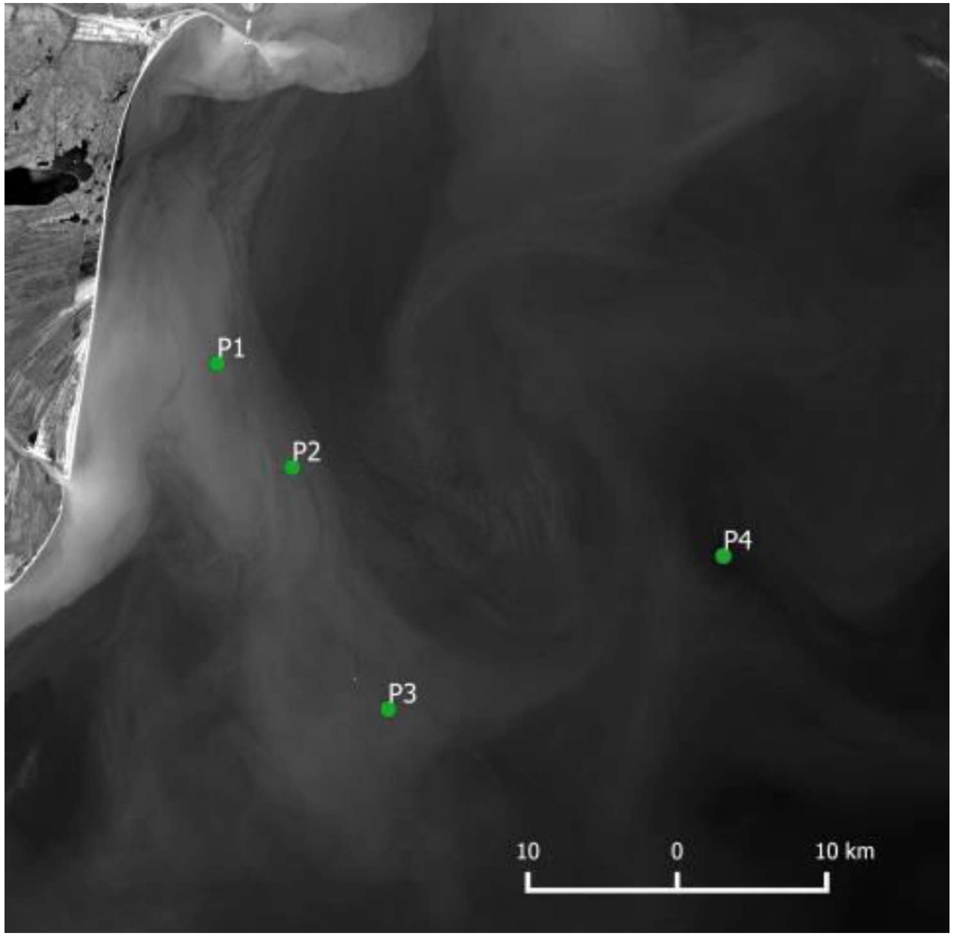

Impact / benefits for the users

- Easy to use data fusion prototype, with interactive graphical user interface that gives access to multiple functionalities

- Possibility to merge satellite datasets with different spectral, radiometric and spatial resolution and obtain a final product that inherits the best characteristics from the inputs

- Ability to derive water quality products (e.g. chlorophyll concentration, suspended particulate matter) at better spatial resolution that before and with improved accuracy

- Small scale ocean color events and phenomena are easier to be detected and analyzed

Conclusions

- The implemented methodology is robust and can be applied to **any type of satellite imagery**

- Data fusion on water is more complex than for land surfaces (where the dynamic of changes is reduced). **In fact, the fusion technology here presented, was applied with very good results also on land areas**

- The quality of the final product depends on the input datasets, thus good products are required, together with proper pre-processing steps

- Artifacts from input images are transmitted in the final product

- Useful for application of regional algorithms for water constituents estimation (generally based on R_{rs} values from coarse spatial resolution sensors) at finer scales

Thank you for attention

www.terrasigna.com
sorin.constantin@terrasigna.com

Presentation 2517

Fragmentation events analysis making use of Fragmentation Event Model and Assessment Tool (FREMAT)

Roxana Larisa Andrișan
Alina Georgia Ioniță
Raúl Domínguez González
Noelia Sánchez Ortiz
Fernando Pina Caballero
Holger Krag

Fragmentation events analysis making use of Fragmentation Event Model and Assessment Tool (FREMAT)

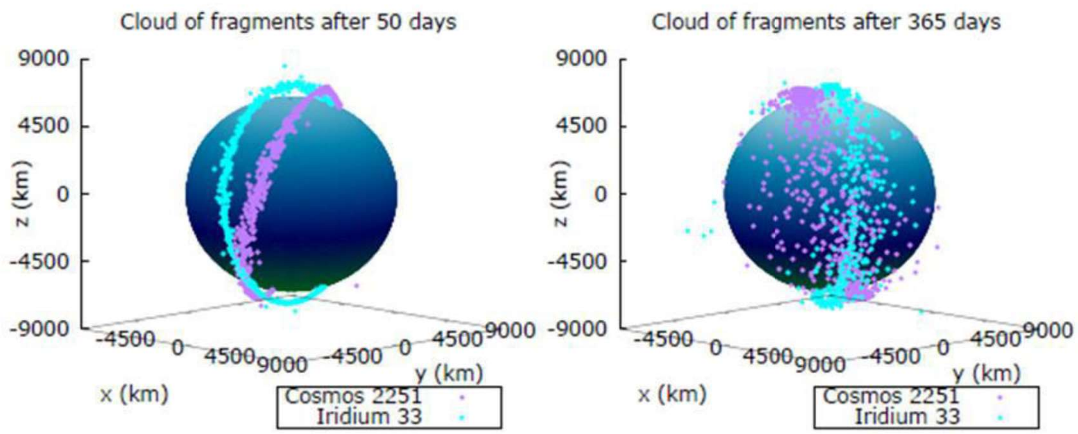

Authors:

Roxana Larisa Andrișan
Alina Georgia Ioniță
Raúl Domínguez González
Noelia Sánchez Ortiz
Fernando Pina Caballero
Holger Krag

1. INTRODUCTION

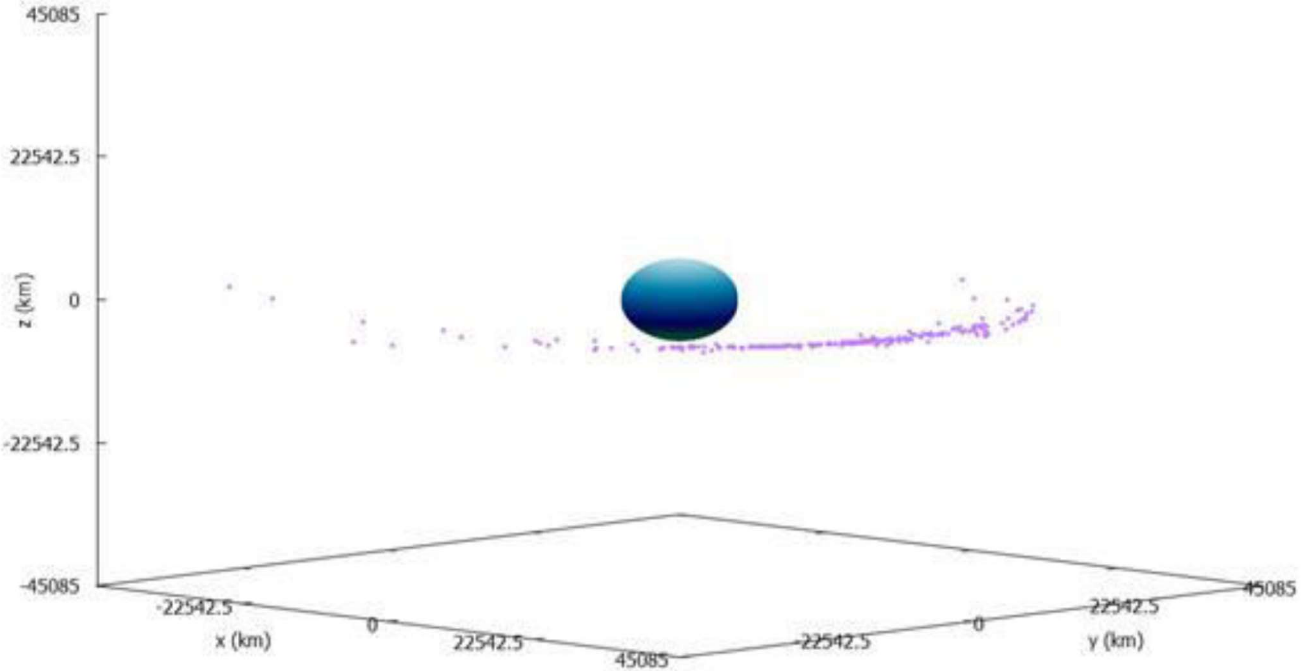

Page 489

1. Introduction

- The **Fragmentation Event Model and Assessment Tool (FREMAT)** project for ESA was completed with the objectives of:
  - simulating on-orbit fragmentations
  - assessing their impact on the space population
  - evaluating the capability of identification of fragmentation events from existing surveillance networks

- FREMAT encompasses three individual tools:
  - Fragmentation Event Generator (FREG)
  - Impact of Fragmentation Events on Spatial density Tool (IFEST)
  - SOFT (Simulation of On-Orbit Fragmentation Tool).

- The tools:
  - can be used independently, or in a chain.
  - are delivered for windows and linux platforms
  - are script friendly

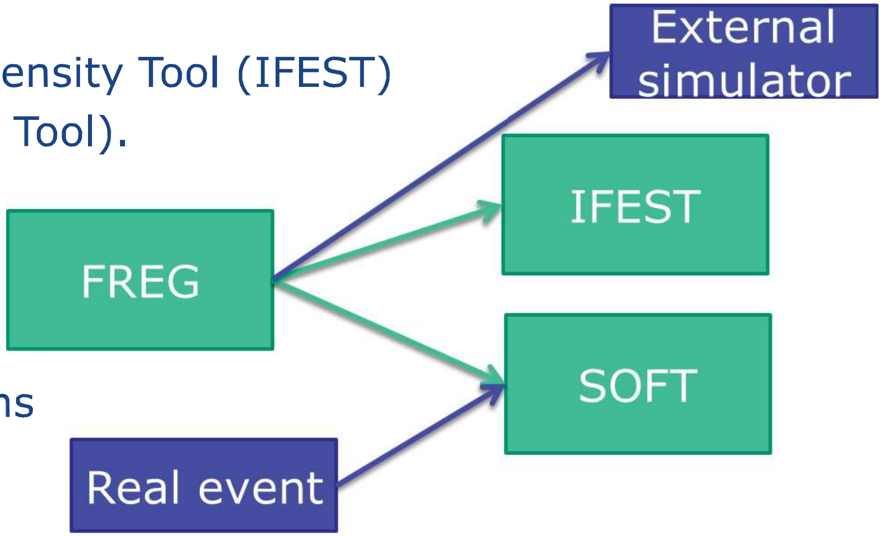

Page 490

2. DESCRIPTION OF THE TOOLS

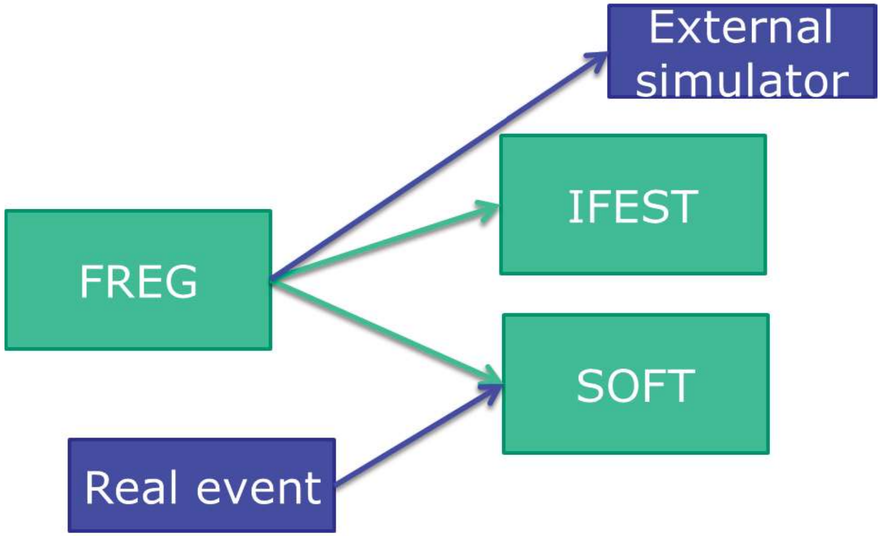

Page 491

2.1 Fragmentation Event Generator (FREG)

- FREG has been conceived to simulate fragmentation events (explosion and collisions)
- MASTER 2009 NASA Breakup Model was employed as the baseline model for this tool
- The baseline model was enhanced in order to ensure the consistency of mass and momentum in the created fragment clouds.
- The user must specify the following inputs for the tool:
  - Type of event (explosion/collision)
  - Type of object (spacecraft/ rocket body)
  - Mass of the parent(s) object(s)
  - State vector(s) of the parent object(s) at event epoch
  - Scaling factor (for explosion)
  - FREG also requires a discretization as input for the computation of representative fragments
- Its output is one or two clouds of fragments (original or representative) that can later be fed into IFEST or SOFT, or to any other propagator.

2. Description of the tools

2.1 Fragmentation Event Generator (FREG)

- Fragmentation Event Generator (FREG) has been created to simulate the generation of space debris as an outcome from fragmentation event (explosion and hypervelocity collisions).
- MASTER 2009 NASA Breakup Model was employed as the baseline model for this tool
  - It is a statistical model based on space surveillance data and a few ground-based test data
    - Size distribution model
    - Shape and consistency model
    - Velocity distribution model
- The baseline NASA break up model was improved during the implementation, in order to ensure:
  - the consistency of mass
  - that two cloud of fragments are obtained in case of collision
  - ensure the kinetic energy is pseud-conserved in case of collisions

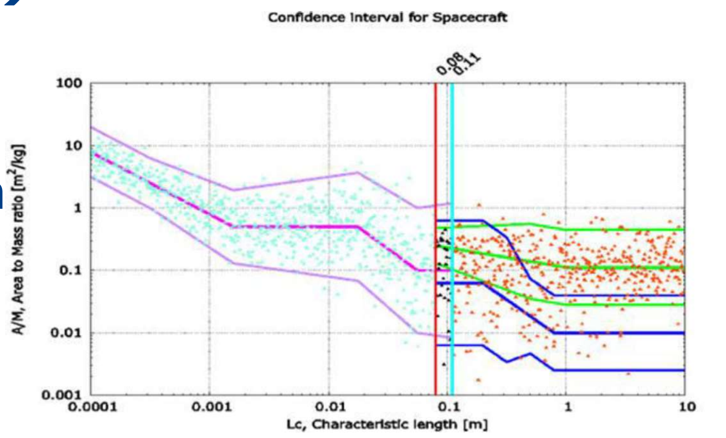

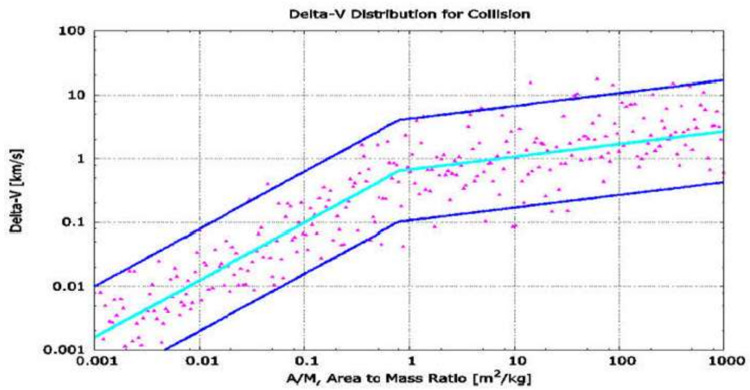

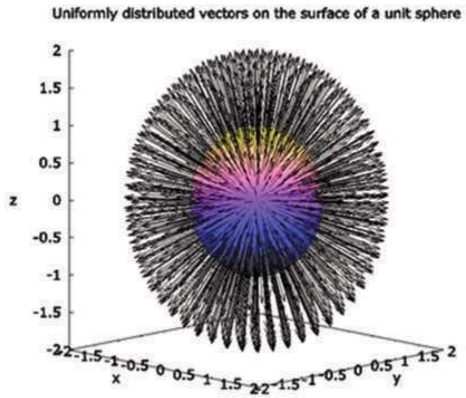

2. Description of the tools

2.1 Fragmentation Event Generator (FREG)

- The user must specify the following inputs for the tool:
  - Type of event (explosion/collision)
  - Type of object (spacecraft/ rocket body)
  - Mass of the parent(s) object(s)
  - State vector(s) of the parent object(s) at event epoch
  - Scaling factor (for explosion)
  - FREG also requires a discretization as input for the computation of representative fragments

- Its output is one or two clouds of fragments (original or representative) that can later be fed into IFEST or SOFT, or to any other propagator.

Parent Object Type	s
PROTON (SL-12) ullage motors (SOZunits)	0.1
Other (non-SOZ) rocket bodies	1.0
EORSATs (Soviet/Russian Electronic Ocean Reconnaissance Satellites)	0.6
Molniya type early warning satellites	0.1
All Soviet/Russian battery-related events	0.5
All Soviet/Russian anti-satellite tests (ASAT)	0.3
Other payloads	1.0

Scaling factors for the revised NASA breakup model as used for future fragmentations.

2.2 Impact of Fragmentation Events on Spatial density Tool (IFEST)

- IFEST (Impact of Fragmentation Events on Spatial density Tool) allows the evaluation of the impact of on-orbit fragmentations in the space debris population.
- It tool employs a fast semianalytic propagator (DSST from Orekit library) for computing the long-term evolution of the clouds of fragments (up to hundreds of years) obtained from FREG
- Computes the 3D spatial density of the fragments (as a function of altitude and/or longitude and time)
  - allows defining discretizations for altitude and longitude

Page 495

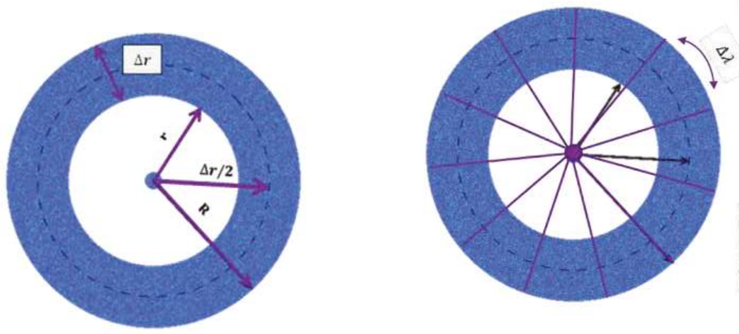

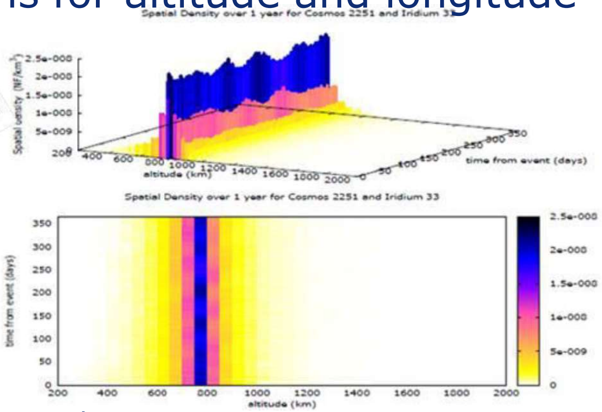

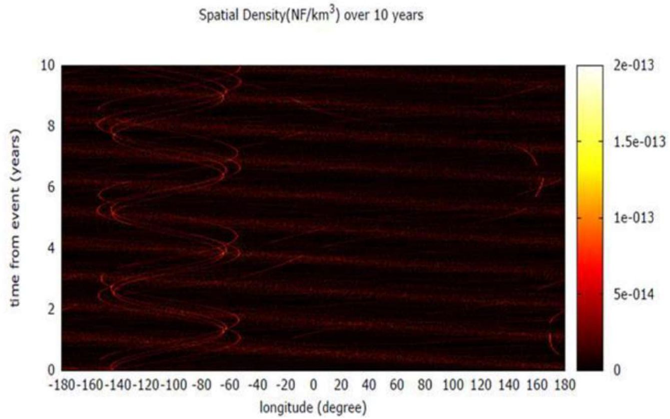

Spherical shell and longitude cells for spatial density computation

2.2 Impact of Fragmentation Events on Spatial density Tool (IFEST)

- Computes the percent increase in the background spatial density obtained from MASTER
- The computation of the spatial density within this tool is validated against results provided by ESA's POEM tool.

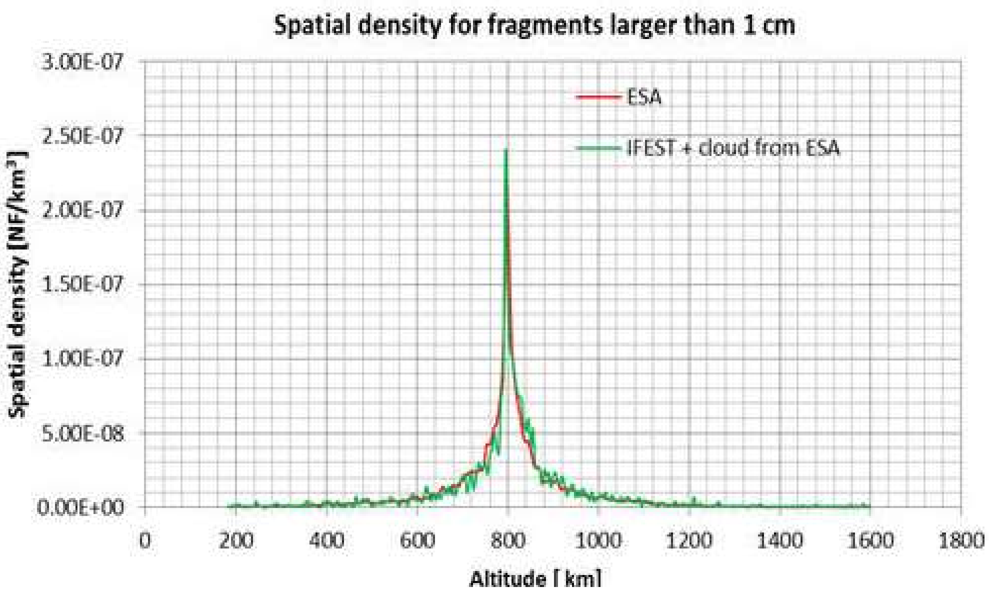

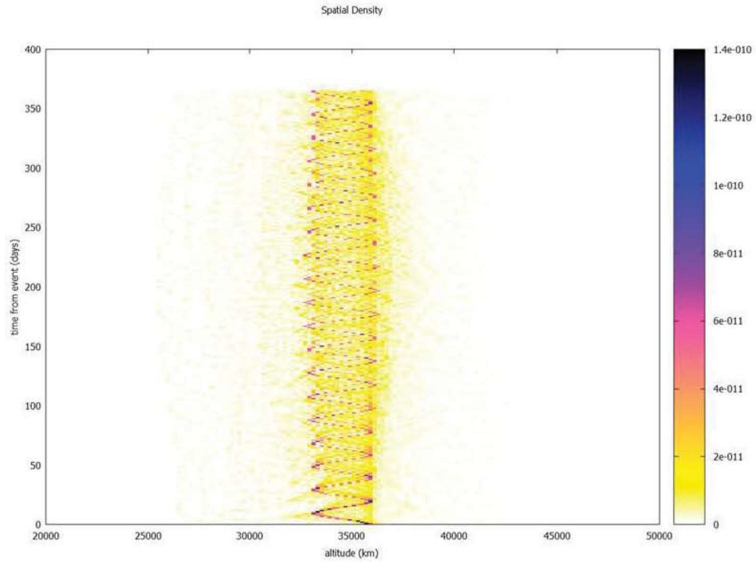

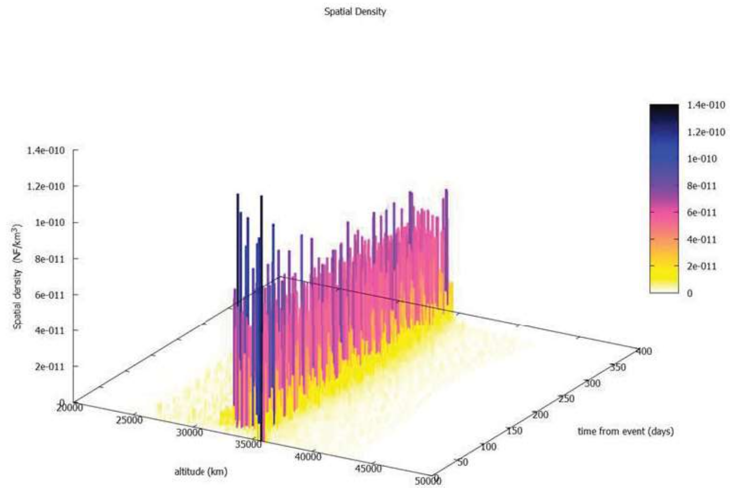

Page 496

2. Description of the tools

2.3 Simulation of On-Orbit Fragmentation Tool (SOFT)

- SOFT simulates the identification of a fragmentation event when a space surveillance network detects a number of unexpected new objects and a fragmentation event is considered a possible cause.
- The tool can be fed with clouds from FREG or from other tools in FREG or AS4 formats
- Uncertainties in the knowledge of the orbits of the fragments and the presence of foreign objects is also considered.
- Starting from a cloud with fragments the tool identifies a fragmentation event following these steps:

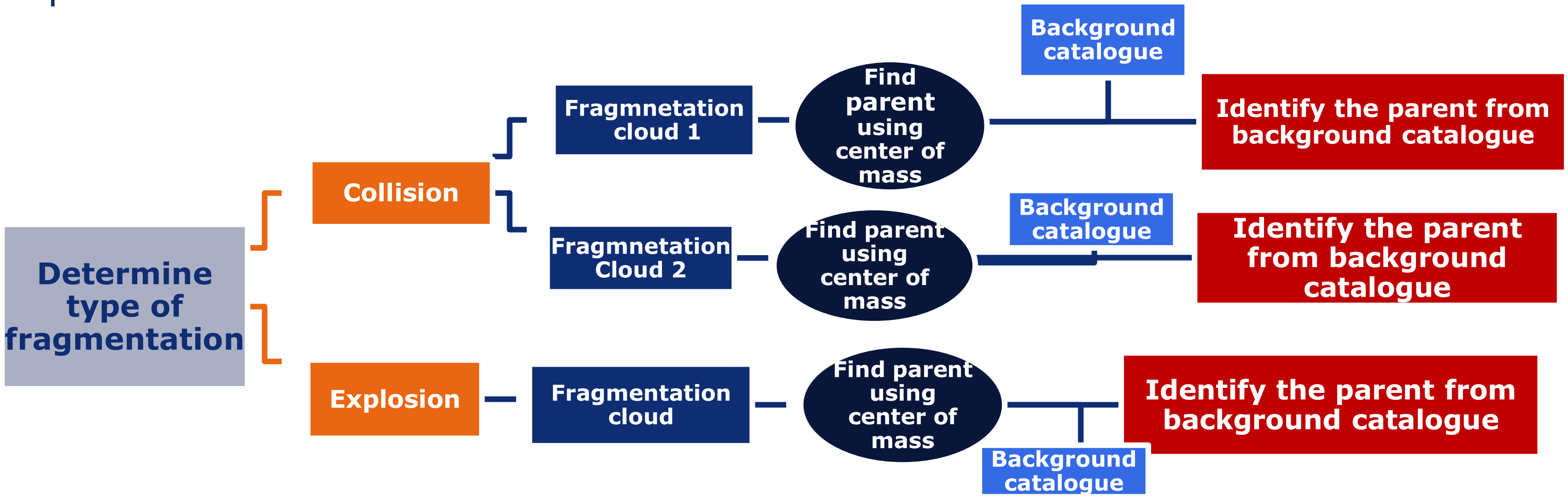

3. SIMULATIONS CASES

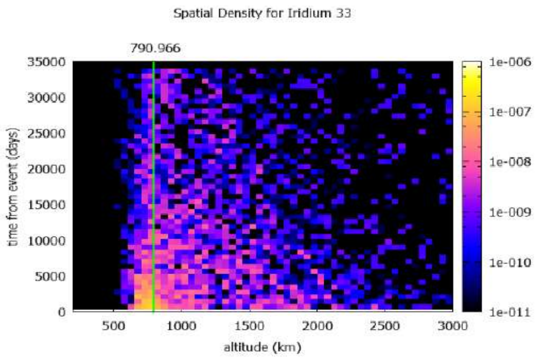

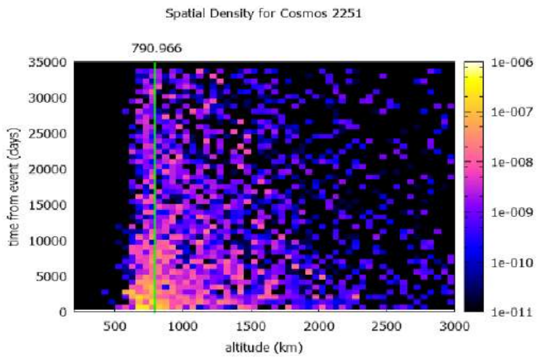

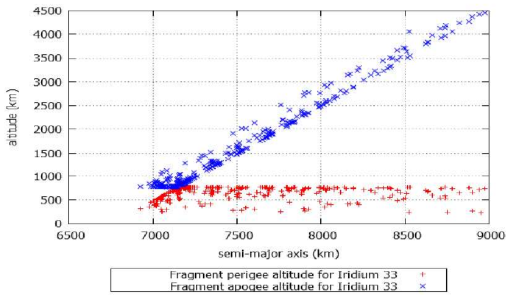

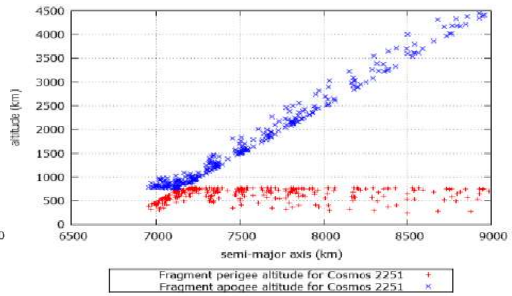

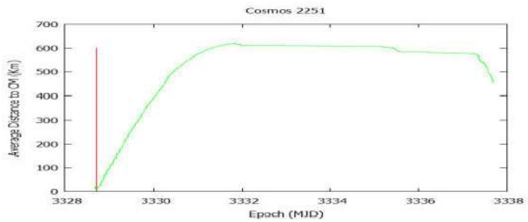

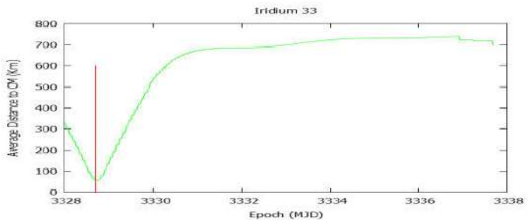

Page 498

3.1 Collsion Cosmos 2251-Iridum 33- FREG

- The collision between Cosmos 2251 and Iridium 33 is one of the most important fragmentation events of the last years.
- The 2009 satellite collision was the first accidental hypervelocity collision between two intact artificial satellites in low Earth orbit (LEO).

Event type	Object type	Simulation epoch	Mass (kg)
Collision (Impact velocity = 11.625 km/s)	Spacecraft	2009-02-10 T16:56:0.000	556
	Spacecraft		900

Type of event	Num. of fragments > 1 cm	Num.of fragments > 10 cm	Total num. of fragments	Num. of Representativ e fragments
Iridium 33	35378	608	208356039523	484 (>1cm)
Cosmos 2251	[illegible]	[illegible]	29900736244[illegible]	[illegible]>1cm)

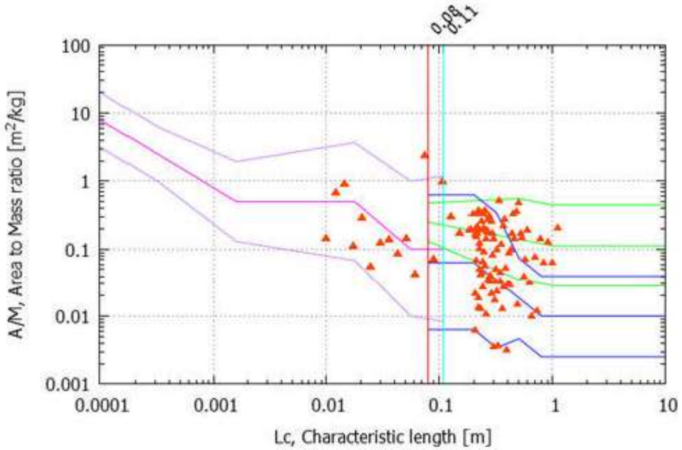

Figure 2: Mean value and $\pm 2\,\sigma$ *confidence interval for the bi-*modal normal distribution used for area-to-mass

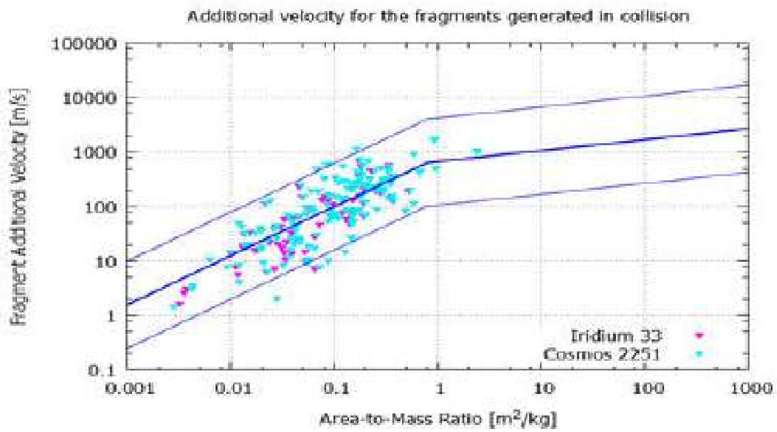

Figure 3: Delta-V vs. A-to-M of fragments for Cosmos-Iridium (mean value and $\pm 2\,\sigma$ *of the distribution*

Page 499

3. Simulation cases

3.1 Collsion Cosmos 2251-Iridum 33-IFEST

- The cloud of representative fragmnts (greater than 1 cm) are fed into IFEST and evaluated
- The Gabbard plot and the plotting script for creating them is automatically generated in IFEST
- Many of the generated fragments concentrate around the altitude of the collision (790.966 km) after the breakup.

Gabbard diagrams from FREG for collision at the event epoch, left plot corresponds to the Iridium 33 fragments, where right plot is associated to the Cosmos 2251 pieces:

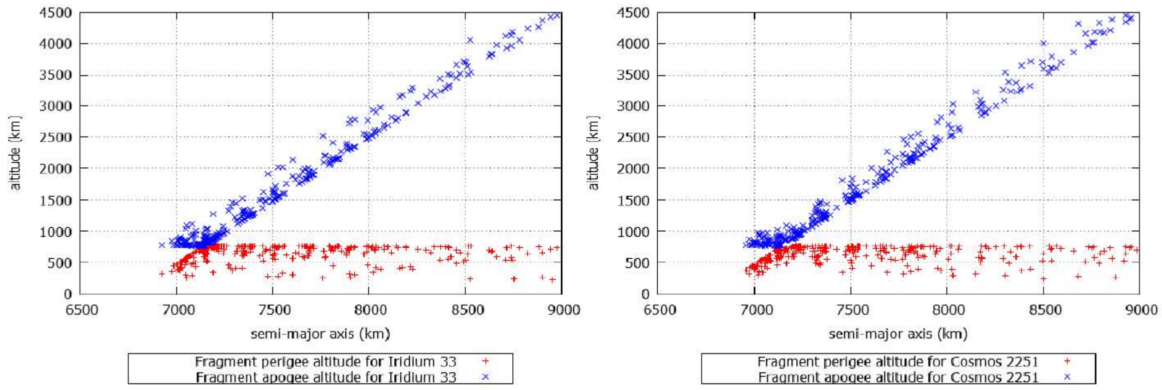

Gabbard diagram for the collision between Cosmos 2251 and Iridium 33 (provided by ESA):

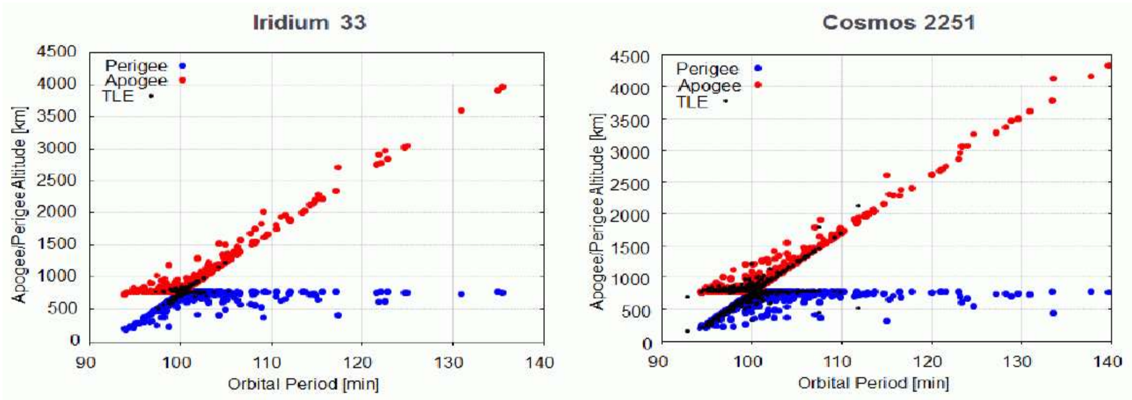

3. Simulation cases

3.1 Collsion Cosmos 2251-Iridum 33-IFEST

Evolution of the fragmentation clouds from Cosmos 2251-Iridium 33 collision. From left to right and from top to bottom, the : 1 day, 50 days, 200 days, 1000 days, 20 years and 96 years.

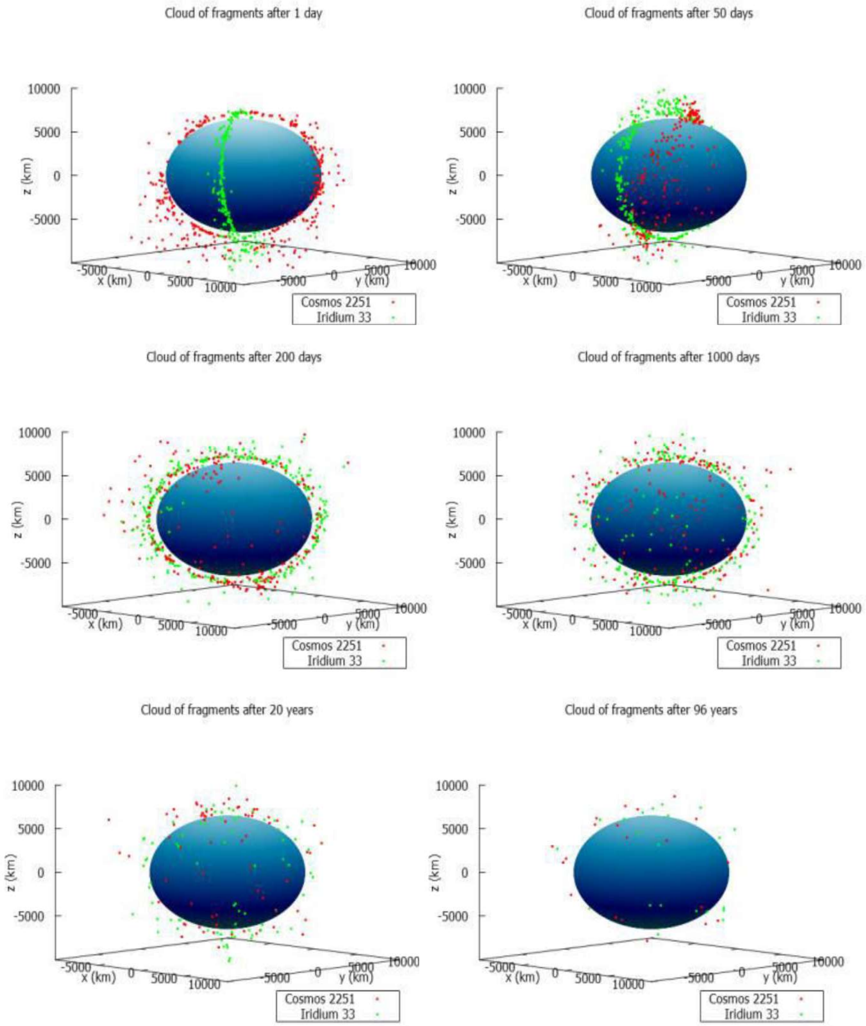

Spatial density for Cosmos-Iridium as a function of altitude over 1year, 10 years and over 100 years (bottom)

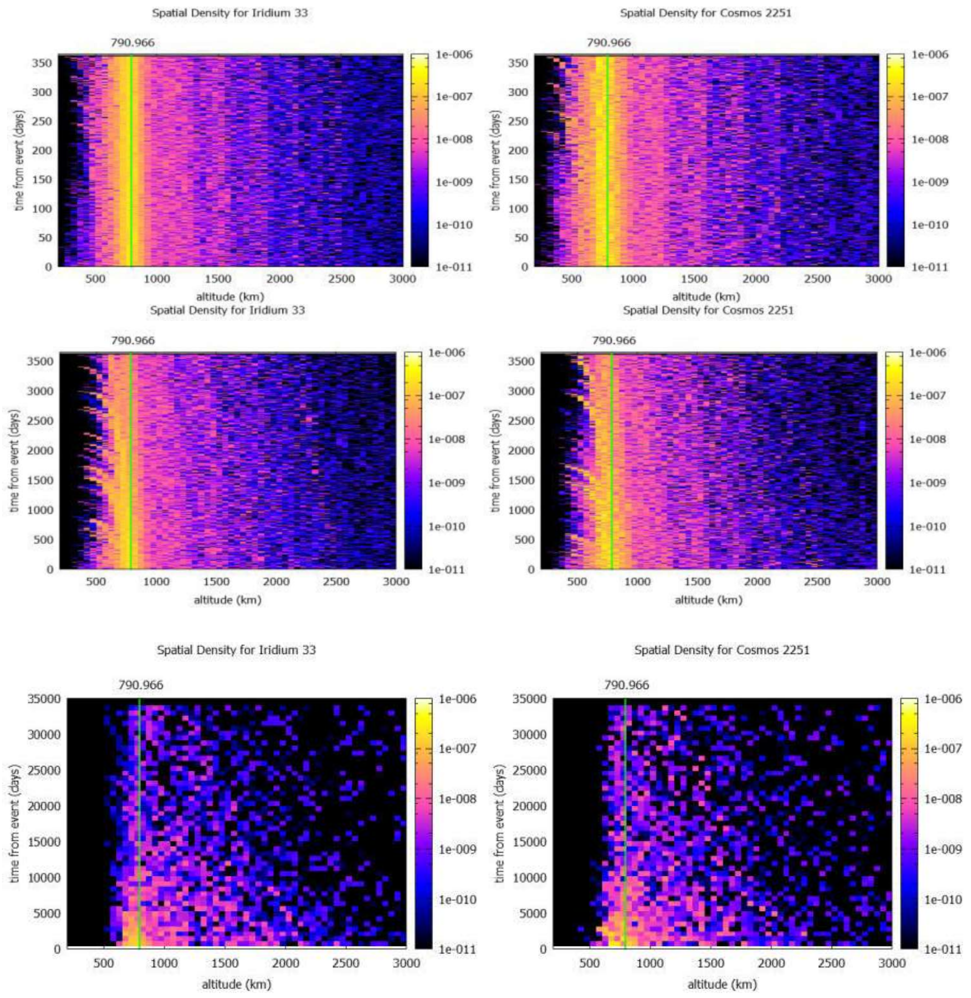

Page 501

3.1 Collsion Cosmos 2251-Iridum 33-SOFT

- The released collision pieces started to be catalogued by the JSpOC (Joint Space Operations Center) and added to the TLE catalogue starting with 18 February 2009.
- The identification of the fragmentation event was simulated with SOFT using as input a TLE catalogue from 19 February 2009 containing the catalogued fragments.
- As background catalogue, we used another TLE catalogue that contained the space population as of 09 February 2009.
- According to SOFT the fragmentation happened on 2009-02-10 16:55:40.038 for Cosmos 2251 and on 2009-02-10 16:47:30.038 for Iridium 33.
- The difference between the two results could be explained by different accuracy of the clouds observation and also because TLEs do not provide information about mass and diameter and random values are associated to them for propagation.

3. Simulation cases

3.1 Collsion Cosmos 2251-Iridum 33-SOFT

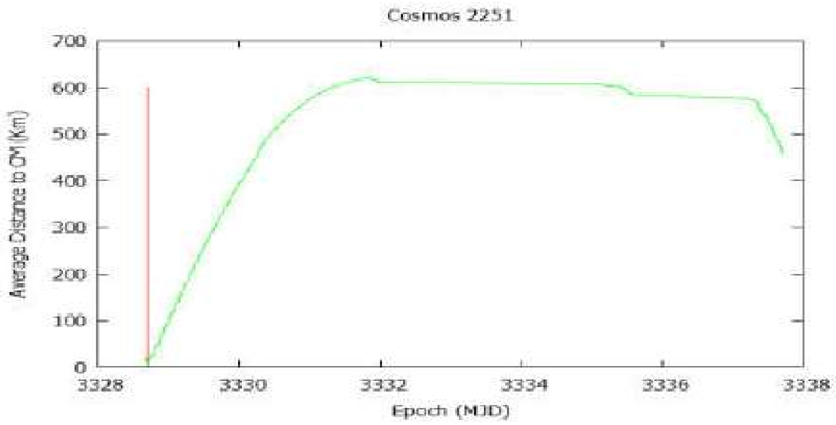

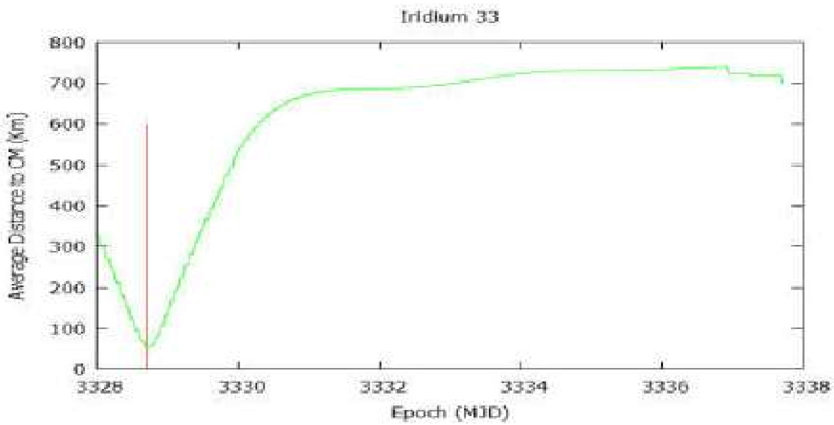

	SMA [km]	Ecc	Inc [deg]	raan [deg]	Ident. time of event
Comp. Parent 1	7135.31	0.0048	74.05	17.12	3328.71
Orbital elements of candidate parents					
Cosmos 2251	**7155.37**	**0.0012**	**74.04**	**17.16**	**3328.71**
Comp. Parent 2	7089.52	0.007	86.42	121.11	3328.7
Orbital elements of candidate parents					
Cosmos 1470	6939.41	0.0015	82.55	119.19	3328.7
Iridium 33	**7153.58**	**0.0014**	**86.45**	**121.20**	**3328.7**

Objects identified by the SOFT tool as objects involved in the fragmentation (time in MJD2000)

Page 503

Backwards propagation of clouds Cosmos 2251 and Iridium 33

3.2 Explosion of Breeze-M R/B-FREG/IFEST

- On 20 January 2016, at approximately 19:00 UTC, the JSpOC (Joint Space Operations Center) identified a possible breakup of a Breeze-M R/B (NORAD id 41122) in GEO.

Event type	Object type	Simulation epoch	Mass (kg)
Explosion (Scaling factor= 1.0)	Rocket Body	2016-01-19 T19:05:16.107	1600

Type of event	Num. of fragments > 1 cm	Num. of fragments > 10 cm	Total num. of fragments	Num. of representative fragments
Breeze-M R/B	11056	248	23886430 232	136 (> 10 cm) and 595 (>1 cm)

1 day, 10 days, 30 years, 50 years.

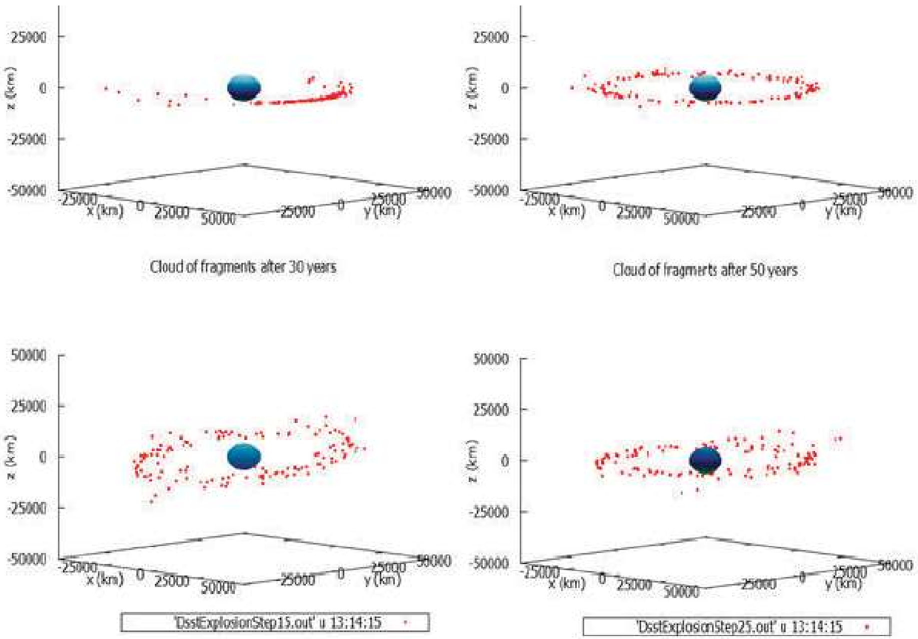

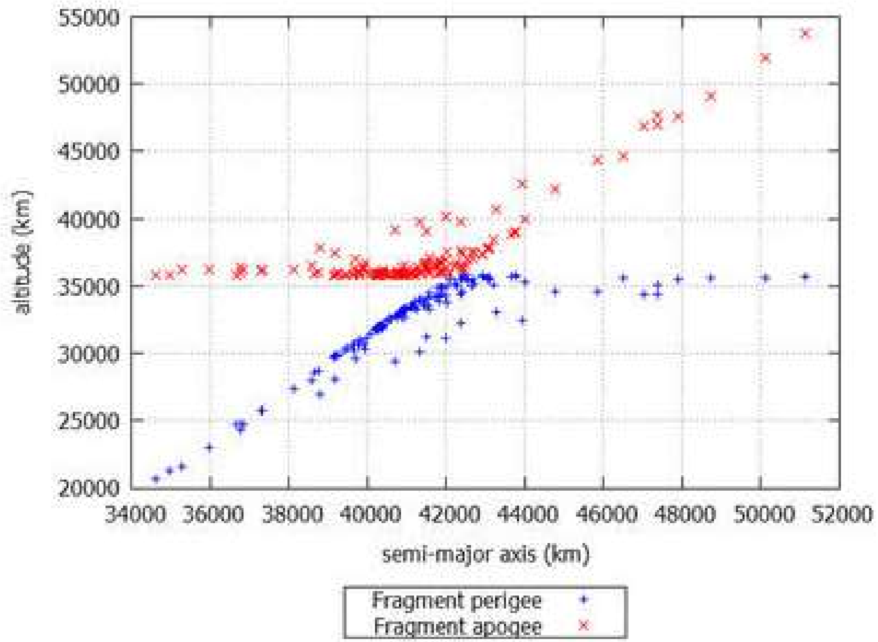

Page 504

3.2 Explosion of Breeze-M R/B-IFEST

- Spatial density as a function of longitude over 2000 days
  - libration effect visible: part of the fragments that are oscillating around the stable point located at -105° .

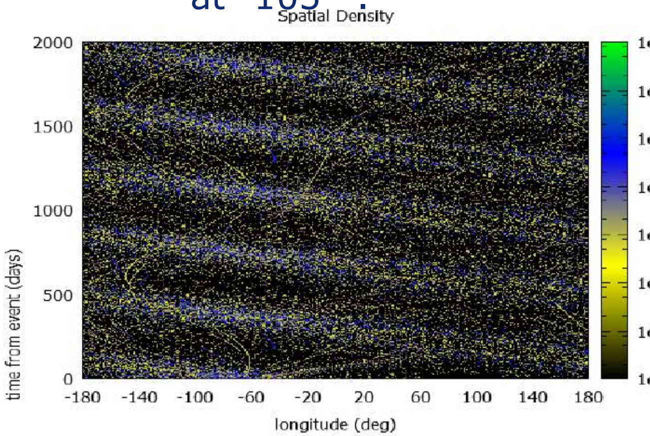

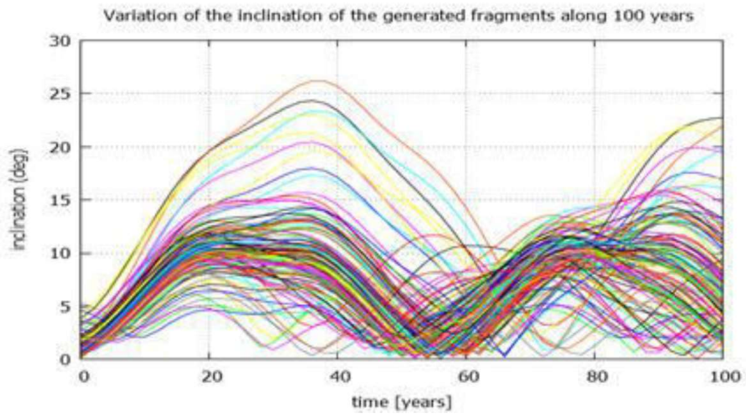

Spatial density and percent increases in background spatial density in the proximity of GEO altitude

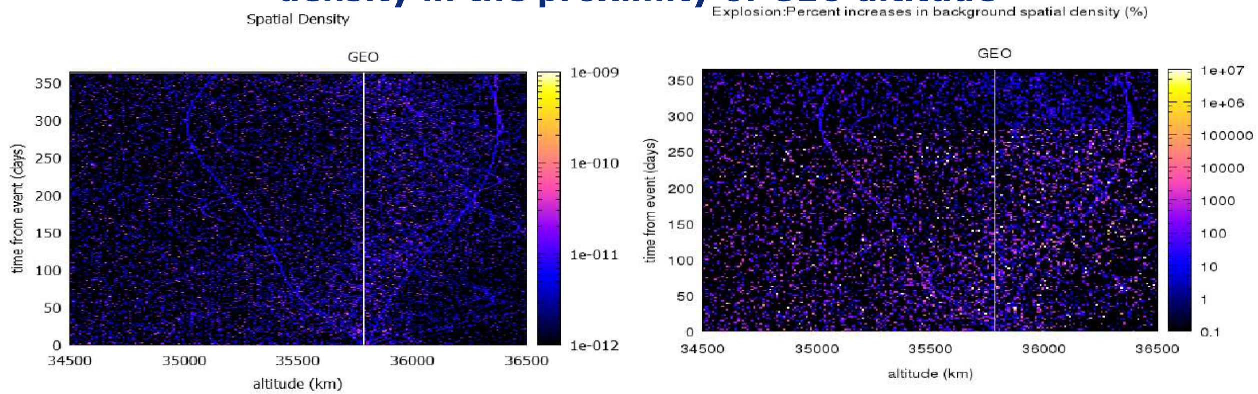

Spatial Density over 10 (right) and 100 years (left)

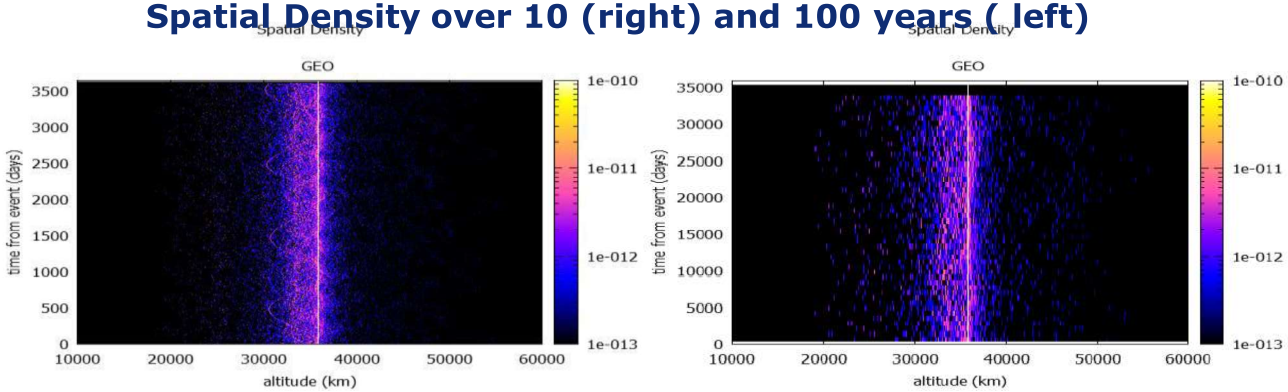

- Variation of inclination for the fragments obtained from the explosion :

- typical secular trend is produced by third-body perturbations: variation of inclination up to ±15° with a period of approximately 30 years.

Page 505

3.2 Explosion of Breeze-M R/B-SOFT

- For the simulation of Breeze-M R/B explosion, the SOFT tool used as input the cloud of fragments obtained from FREG (fragments greater than 1 cm)
- As background catalogue was used a TLE catalogue that contained the space population of 19 January 2016.
- The computed time was 18:57 .

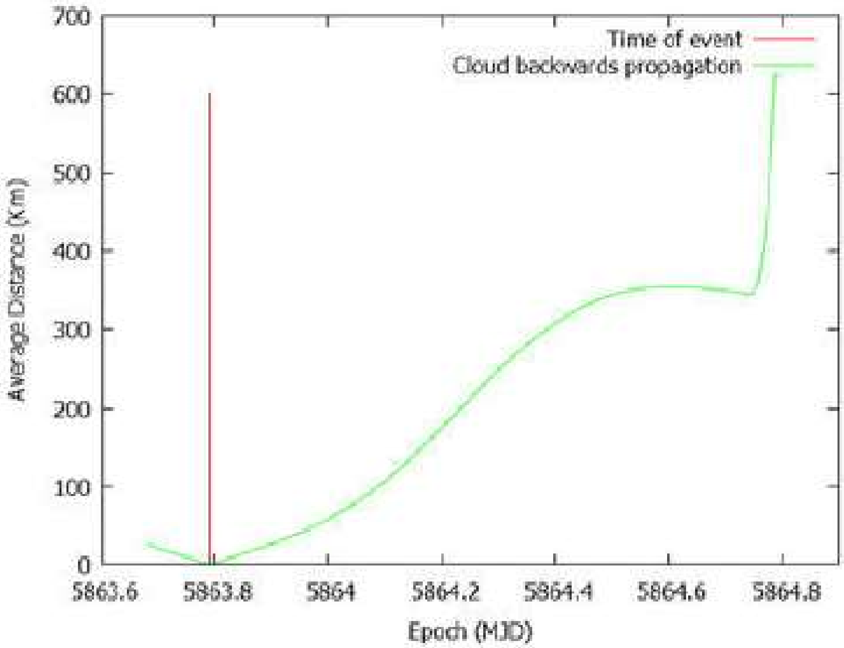

	SMA [km]	Ecc	Inc [deg]	Raan [deg]	Ident. Time of event
Computed Parent	41064.59	0.0294	0.25	109.28	5863.79
Orbital elements of candidate parents					
SL-12 R/B(2)	41929.15	0.0021	14.51	357.27	5863.79
Breeze-M R/B	40979.09	0.0302	0.26	111.11	5863.79

3.2 Explosion of Breeze-M R/B-SOFT

- The situations when the fragmentation clouds are incomplete (not all objects created in an event are detected) and inaccurate (the orbits of the fragments are known with a certain error) lead to considerable errors in the identification of the fragmentation event.

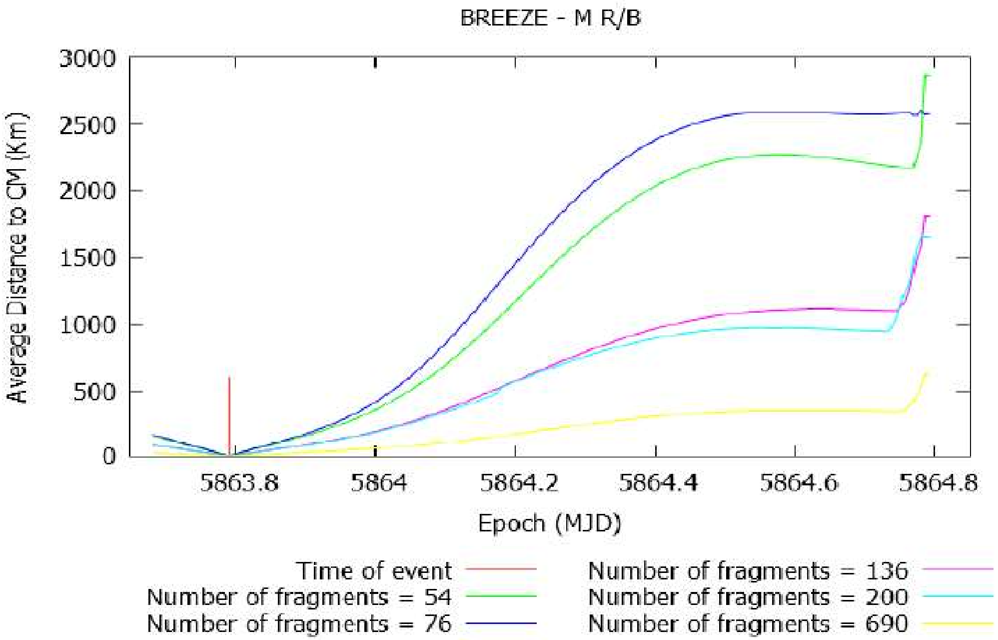

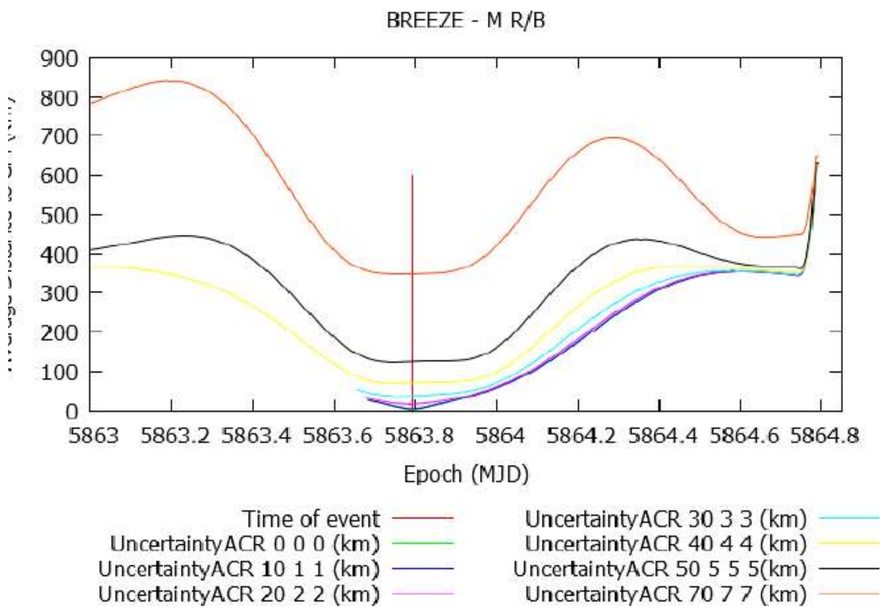

Page 507

3. CONCLUSIONS

- The tools presented support the study of fragmentation events, either by simulating them or by using real orbital data obtained from a sensors network and also from TLE information.
- It is possible to study the long term effect of these events by means of the resulting spatial density, allowing comparison with the ESA MASTER tool.
- It is also possible to attempt to locate the position and orbit of the object(s) involved in the event in spite of having not complete clouds and poor accuracy.
- These tools can be used independently (in order to support studies such as the examples presented in this paper), or as part of a longer processing toolchain

Thank you for you attention

Questions ???

www.elecnor-deimos.com

Presentation 2518

Big Data SW framework for EGSE products

Big Data SW framework for EGSE products

Project overview

Aerospace Europe CEAS 2017 Conference, Bucharest, 19 October 2017

The problem

- Electrical Ground Support Equipment (EGSE) is essential at all levels of pre-launching testing of satellite and spacecraft, namely AIT / AIV.

- Systems under test are continuously evolving and becoming more complex, using communication networks with significantly higher data rates (e.g. AFDX in Airbus or SpaceWire in the space domain) and also employ significantly more interfaces (e.g. I/O analog/digital discrete interfaces) connecting the different sub-systems, with increased sampling rates.

- This trend imposes also a major challenge in the design of the EGSEs, since they need to store, process and analyze a continuously increasing volume of test-data, usually in very accurate time-series format, in real-time or in near real-time in order to satisfy the demanding requirements of air/space-craft AIT activities.

- The main problem with the current EGSE SW architectures is that they do not scale well with the increased volume of test-data. The data volume imposes a major bottleneck, even with the use of modern multi-processing PC systems, fast SSD disks and advanced RDBMS systems.

The challenge

- Big Data processing has gained particular attention in the ICT domain due to the significant challenges it imposes and it has increased the demand of information management architectures and specialists.

- Big Data uses exceptional technologies to efficiently process large quantities of data within tolerable elapsed times and several frameworks are currently available (Apache Hadoop and related projects).

- The required flexibility in Test Benches in order to fulfil the AIT requirements can be provided by spinning-in existing Big Data technologies and architectures to the EGSE domain.

- Currently in the market, there is no Big Data solution adapted for the EGSE domain available, although Big Data related products are already a stated requirement of the Space Industry.

Objective of the study

- **The main vision: Spinning-in existing Big Data technologies and architectures into the EGSE domain.**

- **The objective of the activity is to design, develop and validate a proof-of-concept prototype of a Big Data SW framework for EGSEs, with particular focus on high data rate DFEs based on SpaceWire interfaces.**

- **The overall activity includes the following main work elements:**
  - Big Data SW framework tuning and optimisation for EGSEs.
  - Big Data models design, definition and retrieval and analysis tools development.
  - Test Consoles and user MMI design and development.
  - Integration with of the Big Data SW framework with DFE interfaces supporting SpaceWire.
  - Validation of the developed the Big Data SW framework at a representative testbed in order to reach TRL5.

Participants and main roles

- **TELETEL Space Srl (Romania) as prime-contractor, bringing its experience in EGSEs and SpaceWire technology, through its mother company TELETEL SA, and having incorporated Big Data among the main strategic components in its business plan. Its main role includes:**
  - Requirements consolidation and system top-level partitioning.
  - Fine-tuning and optimization of Big Data SW framework.
  - Design and development of the required Big Data SW sub-systems, services and tools.
  - Integration and verification of the Big Data SW Framework.
  - Design and development of the test cases for the demonstrator.

- **Thales Alenia Space France (Cannes), as sub-contractor, will provide requirements to TELETEL Space Srl and will also validate the project results in a representative EGSE demonstrator. Its main role includes:**
  - Provision of system and validation requirements for a Big Data SW framework for EGSEs.
  - Validation of the integrated Big Data SW Framework with the iSAFT DFE in a representative demonstrator.

Main Work Areas

- **WP1 - Requirements definition and validation plan**
- **WP2 - Design and development of the Big Data SW framework for EGSEs**
- **WP3 - Integration and verification of the Big Data SW Framework**
- **WP4 - Validation and demonstration of the Big Data SW Framework in TAS-F facilities**

Big Data SW Framework

- **Candidate Technologies**
  - Apache Hadoop and related projects.

- **Activities & Functionalities**
  - Big Data SW framework configuration and tuning.
  - HW infrastructure selection and tuning.
  - Development of automated installation, configuration and system monitoring tools.
  - Definition of data models and their schema.
  - Integration of Big Data analytics tools and frameworks.
  - Development of queries and parallel MapReduce programs for data processing and querying.
  - Development of a data management and transfer SW layer at the DFE interfaces.
  - Development of a set of services and tools to provide data retrieval and processing capabilities to the test users.

Integration with DFEs – iSAFT SpaceWire Simulator/Recorder

- **The iSAFT SpaceWire Simulator / Recorder is an advanced EGSE platform with traffic generation capabilities that simulates SpaceWire devices or instruments, enabling S/C integration tests before the availability of Flight Models.**
  - Site Rackmount System (3U) HW platform.
  - Octal SpaceWire PCIe NIC.
  - SpW simulation/recording support for eight (8) ports.
  - iSAFT client API (C++ or Python) for interfacing/integration with 3rd party SW.
  - Configuration & Control Application (GUI for complete local operation).

iSAFT SpaceWire Simulator / Recorder by TELETEL SA

- Support for transmission triggers, filters for the captured data and statistics.
- Time synchronisation with other components in a testbed through IRIG.
- Protection of flight equipment against internal failures (FMEA).
- Interfaces with EGSE Central Checkout Systems (C&C CCSDS or EDEN).

- **Activities**
  - Provision of the iSAFT SpaceWire Simulator / Recorder SW API .
  - Design and development of the DFE API abstraction layer.
  - Integration with the Big Data SW framework.

Validation testing in a representative AIT Test Bench

- **Validation will be performed in accordance with a defined Test Plan for the Big Data SW framework integrated with the iSAFT DFE.**

- **A set of functional and performance tests will be executed in representative spacecraft AIT Test Benches at TAS-F premises in Cannes.**

- **The following test beds have been identified:**
  - The Elite Step 2 test bench procured and manufactured to test the new TAS-F avionics dedicated to Science and Observation mission.
  - The SpaceBus 4000Mk2 test bench assembled to test the new generation of TAS-F avionics dedicated to Telecommunication missions.

- **The final environment for TAS-F will be selected during the initial phase of the project.**

Project Main Outcomes – Timeplan

- **System Top-Level Partitioning**
  - Milestone: SRR
  - Planned date: January 2018
- **Big Data SW framework installed and fine-tuned – Design available**
  - Milestone: PDR
  - Planned date: April 2018
- **Big Data SW framework integrated with SpaceWire DFE**
  - Milestone: CDR/TRR
  - Planned date: October 2018
- **Demonstrator and Test Results Synthesis**
  - Milestone: FAR
  - Planned date: December 2018

Foreseen follow-up activities

- Addressing additional DFE technologies and interfaces (such as MIL-STD-1553, CAN, TTEthernet, SpaceFibre etc.), provided by various suppliers.

- Integration with SCOE components addressing various I/O analog/digital discrete interfaces including HPC, BSM, ASM, RSA, TSM etc., provided by various suppliers.

- Harmonisation with EGS-CC architecture and interfaces (http://www.egscc.esa.int/).

- Design and development of a Time Synchronisation module for accurate time stamping across EGSE components, enabling timely accurate analysis of Big Datasets in EGSEs.

- Product qualification in integrated EGSEs and Primes’ Test Benches.

Contact Information

- **TELETEL Space Srl**

  Mr. Christoforos KAVADIAS

  Email: c.kavadias@teletelspace.ro

  Tel: +40 21 313 2840

  Web: www.teletelspace.ro

- **Thales Alenia Space France (Cannes)**

  Mr. Adrien CHARLET

  Email: adrien.charlet@thalesaleniaspace.com

  Tel: +33 4.92.92.79.82

  Web: www.thalesaleniaspace.com

Presentation 2519

ESACCS

New European Operational Tool for Satellite Constellation Management

ESACCS

New European Operational Tool for Satellite Constellation Management

INNOVATING SOLUTIONS

CONTENT

Two Parts:

- ESACCS up to date
- Future work

ESACCS Tool

ESACCS – EUROPEAN CONTEXT

esa

Sign In

ESACCS main objective is to provide a web based portal system that securely facilitates the exchange of information between constellations flying in a convoy or those which are operated by different control centres.
The ESACCS aims at providing a centralized information flow between different missions within a constellation. It receives information from the different MOCs regarding the current satellites status and their current and predicted orbits. Based on this information, it performs a set of flight dynamics analyses to assess the safety of the constellation as a whole and the safety of the individual satellites. If any issue is detected (e.g. control box exit, conjunctions), it automatically informs the affected MOCs by generating alarms or warning status for each satellite of the constellation. The ESACCS should support information and configuration of multiple constellations containing different missions operated through separate Mission Operations Centres (MOCs).

The exchange of MOCs operational relevant information between ESACCS and each MOC should be made through the CCSDS Mission Operations (MO) services. Reports generated by ESACCS should be able to be exchanged with MOCs. Taking into account that not all the MOCs are offering and accessing MO services or planning to integrate them in the near future, ESACCS has been designed to be flexible enough so to adopt other existing protocols/services additionally to MO ones.

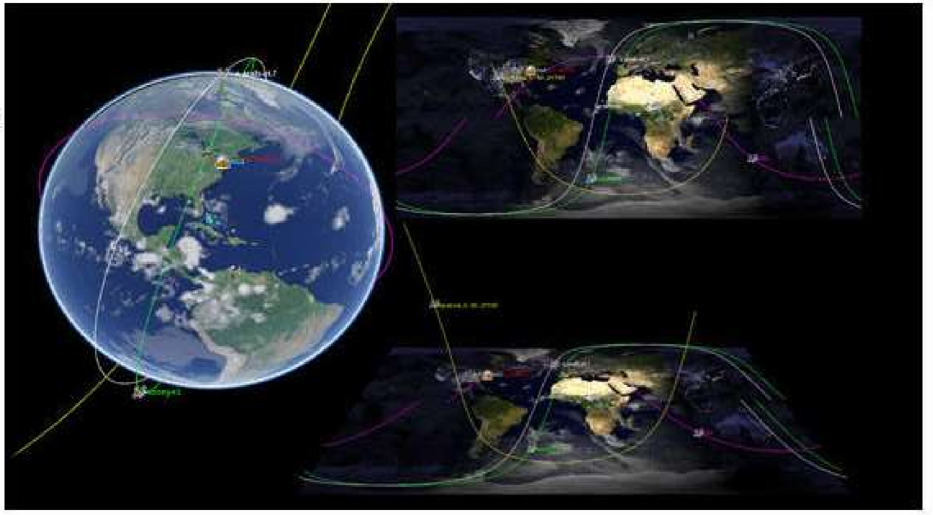

What it is?

Why it is needed?

Where can it be used?

When it will be ready?

Page 527

ESACCS – PROTOTYPE PHASE

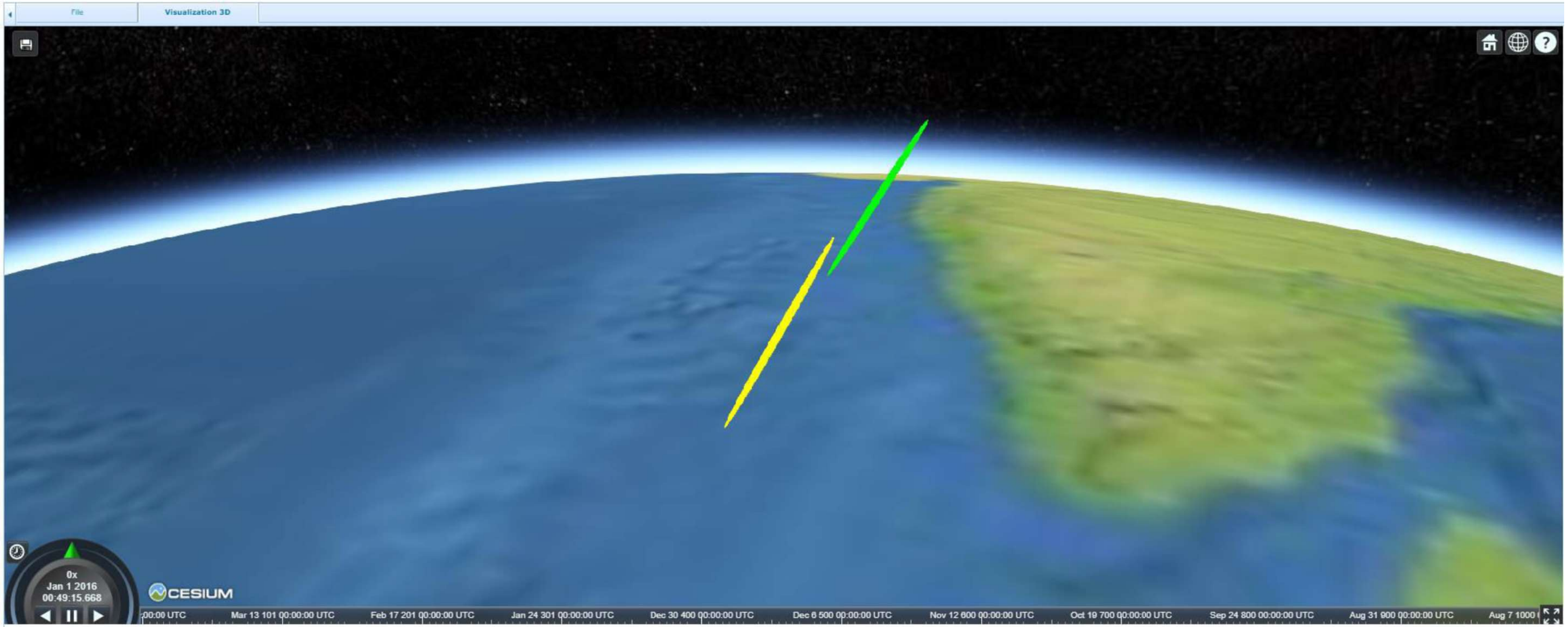

Features:

- Automatizing
- Interoperability
- Modularity
- Technology independence

ESACCS operational tool will maintain these previous features providing a better stability, scalability, security and configurability.

ESACCS – COMPONENTS

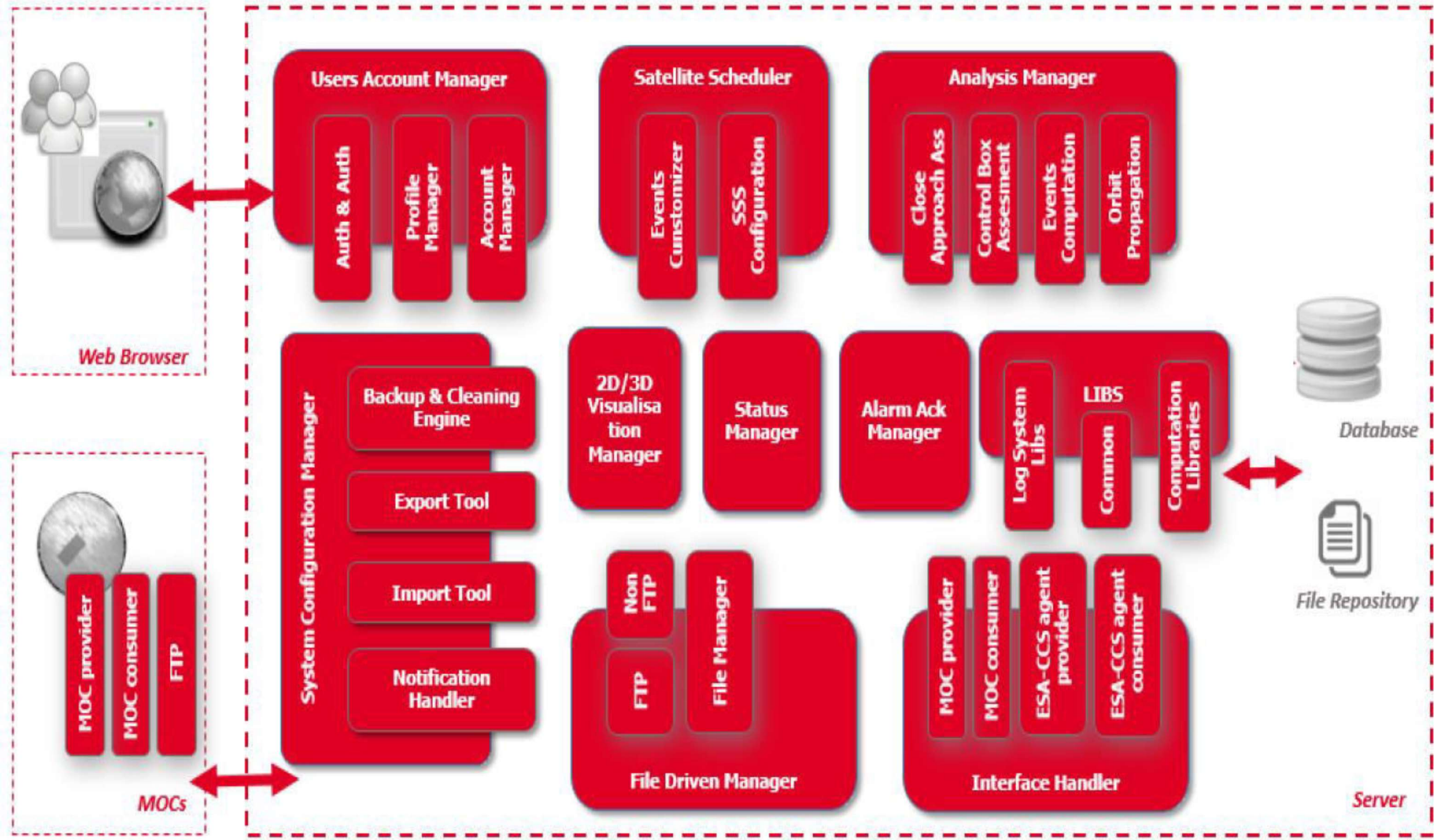

Page 529

ESACCS – ARCHITECTURAL MODEL

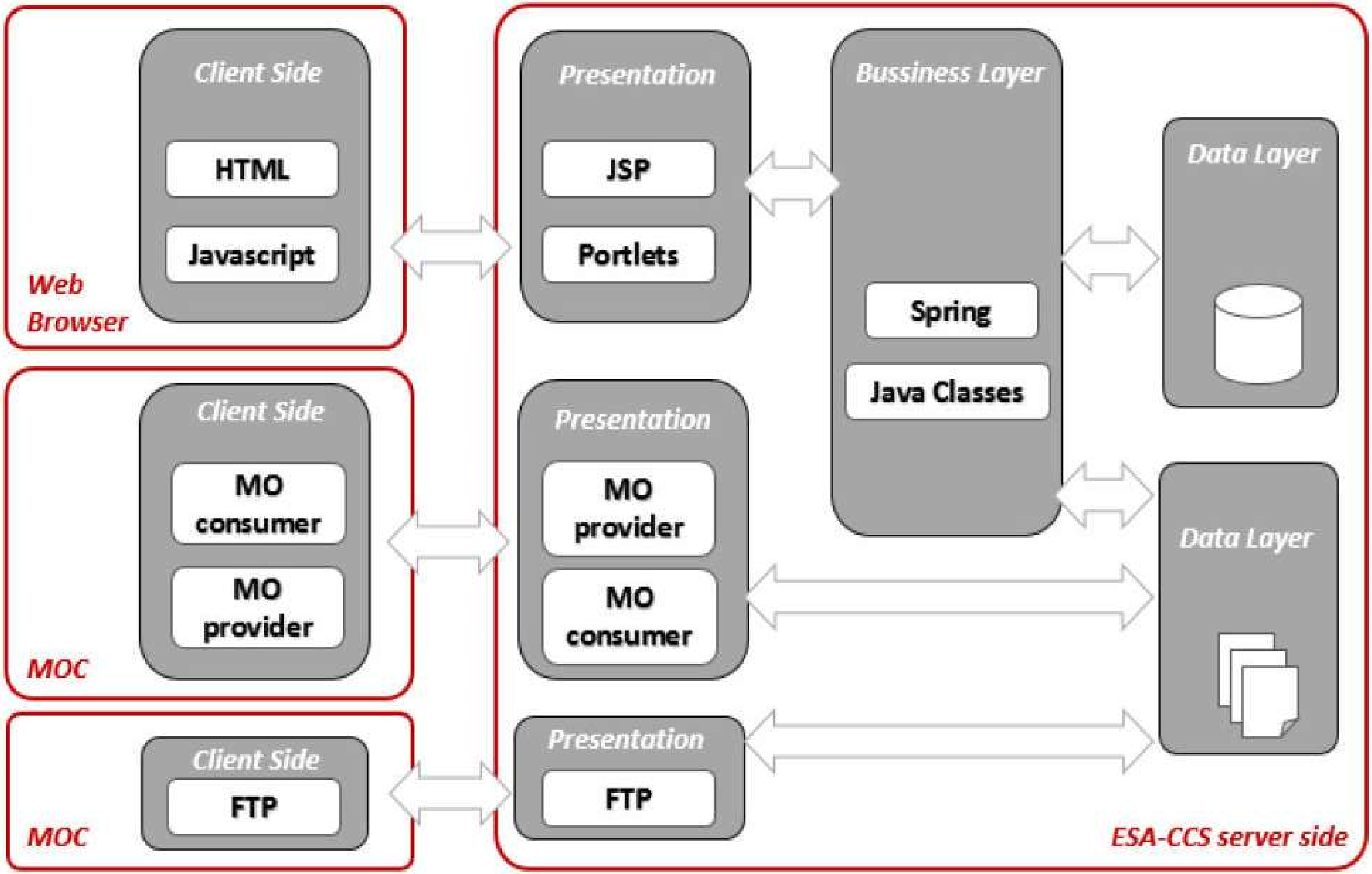

ESACCS – THE WEB APP(1)

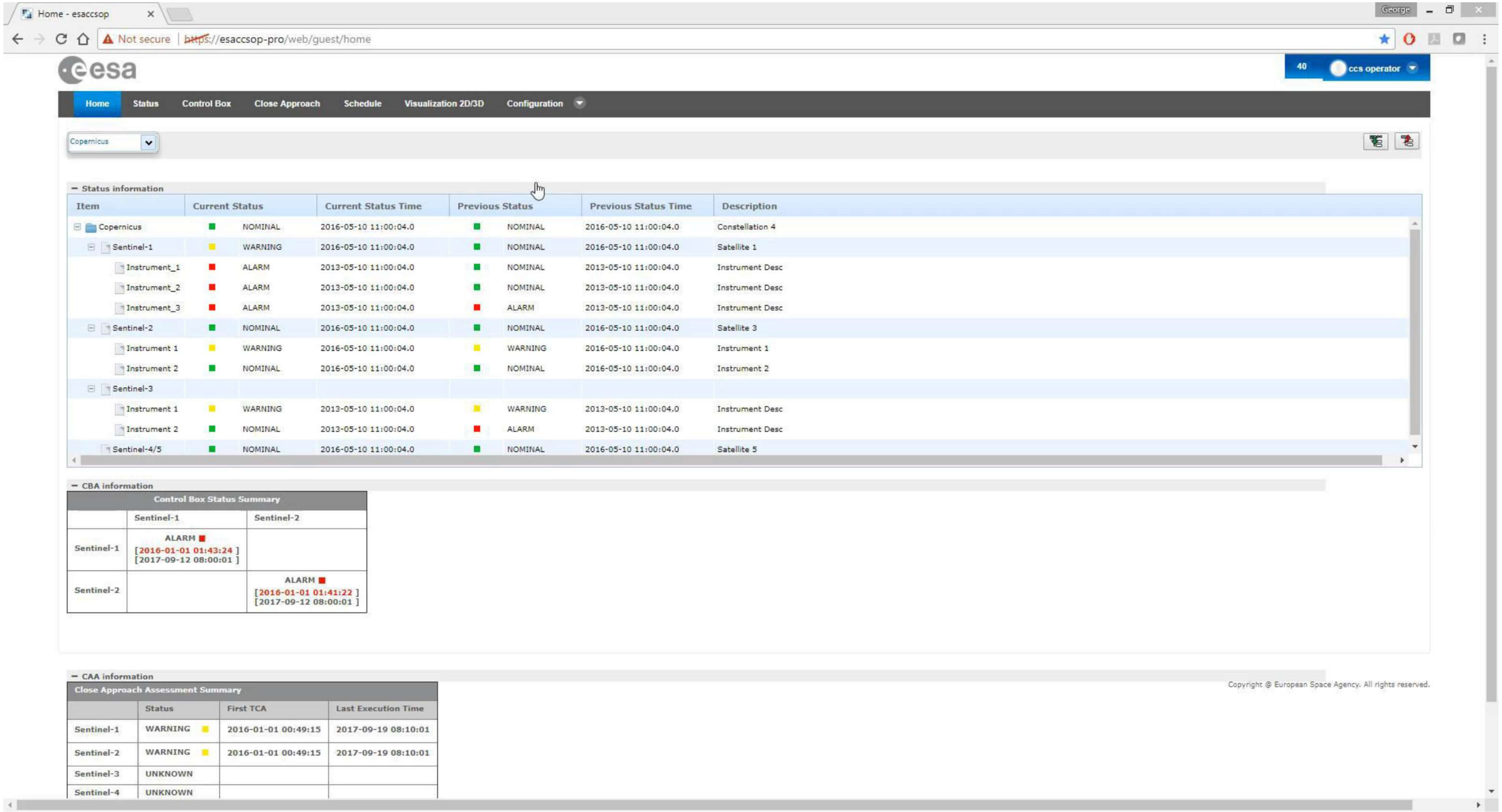

Page 531

ESACCS – THE WEB APP(2)

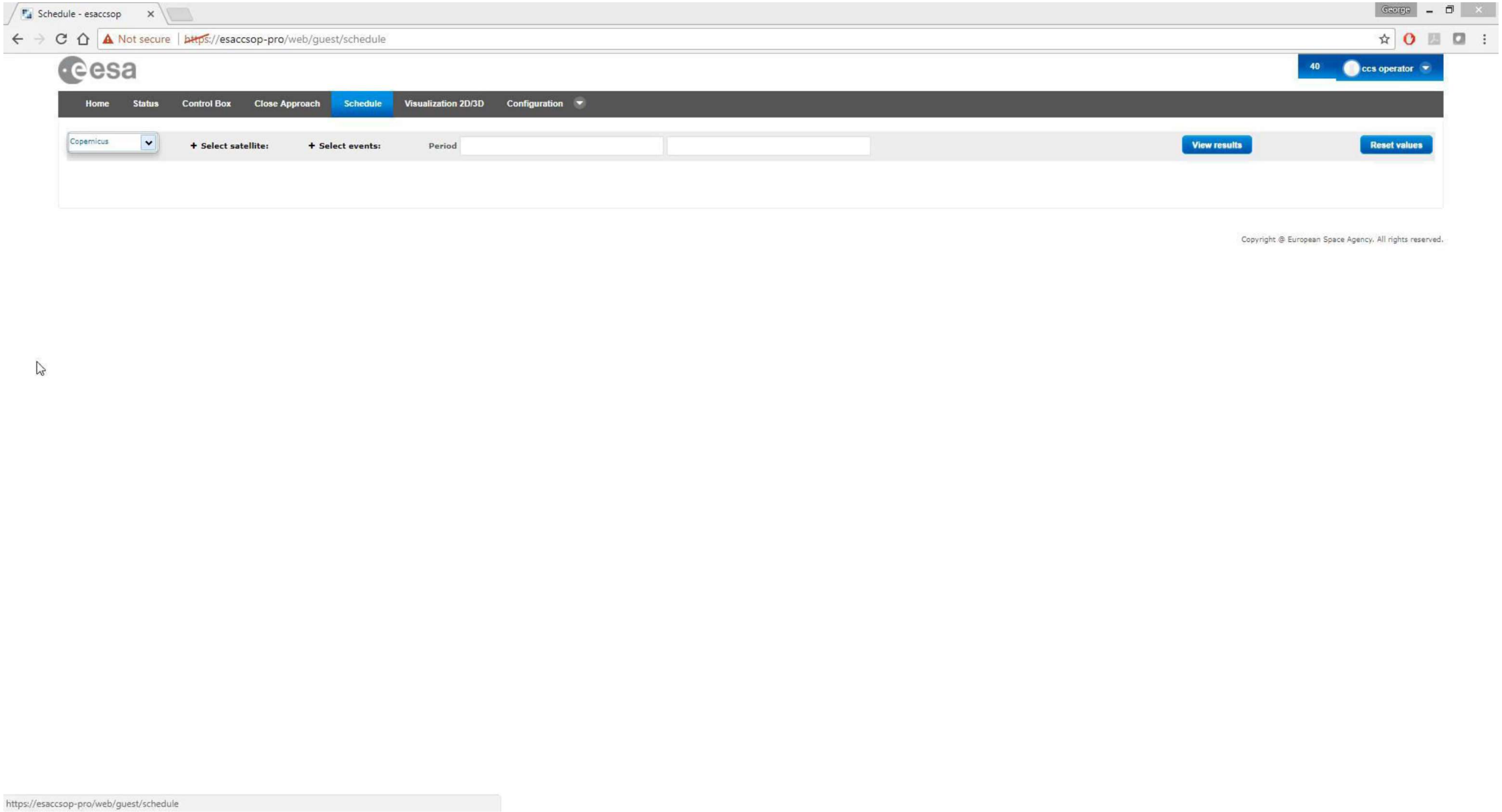

Page 532

FUTURE WORK

ESACCS – TO BE UPDATED/CREATED

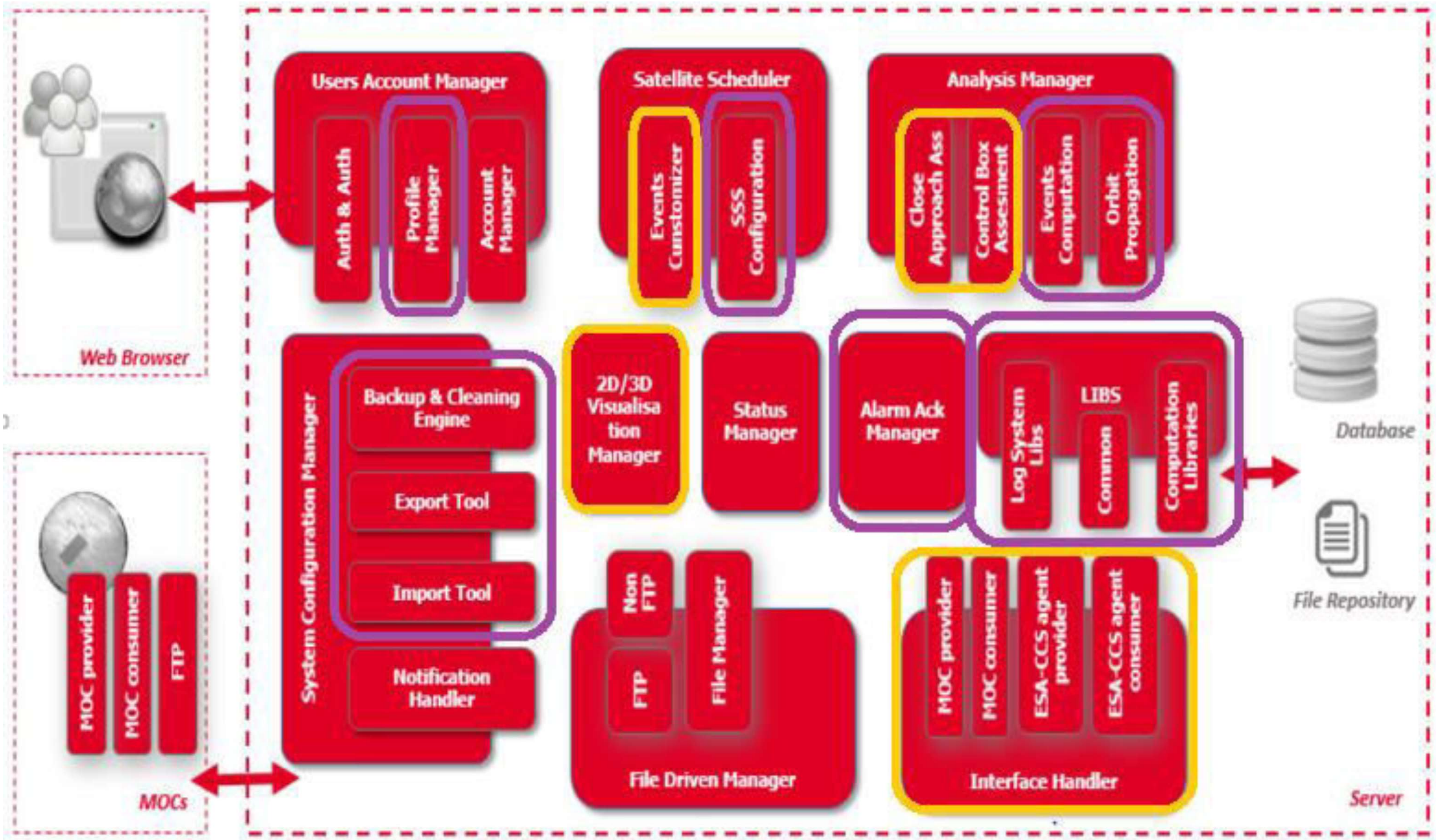

ESACCS - ROADMAP

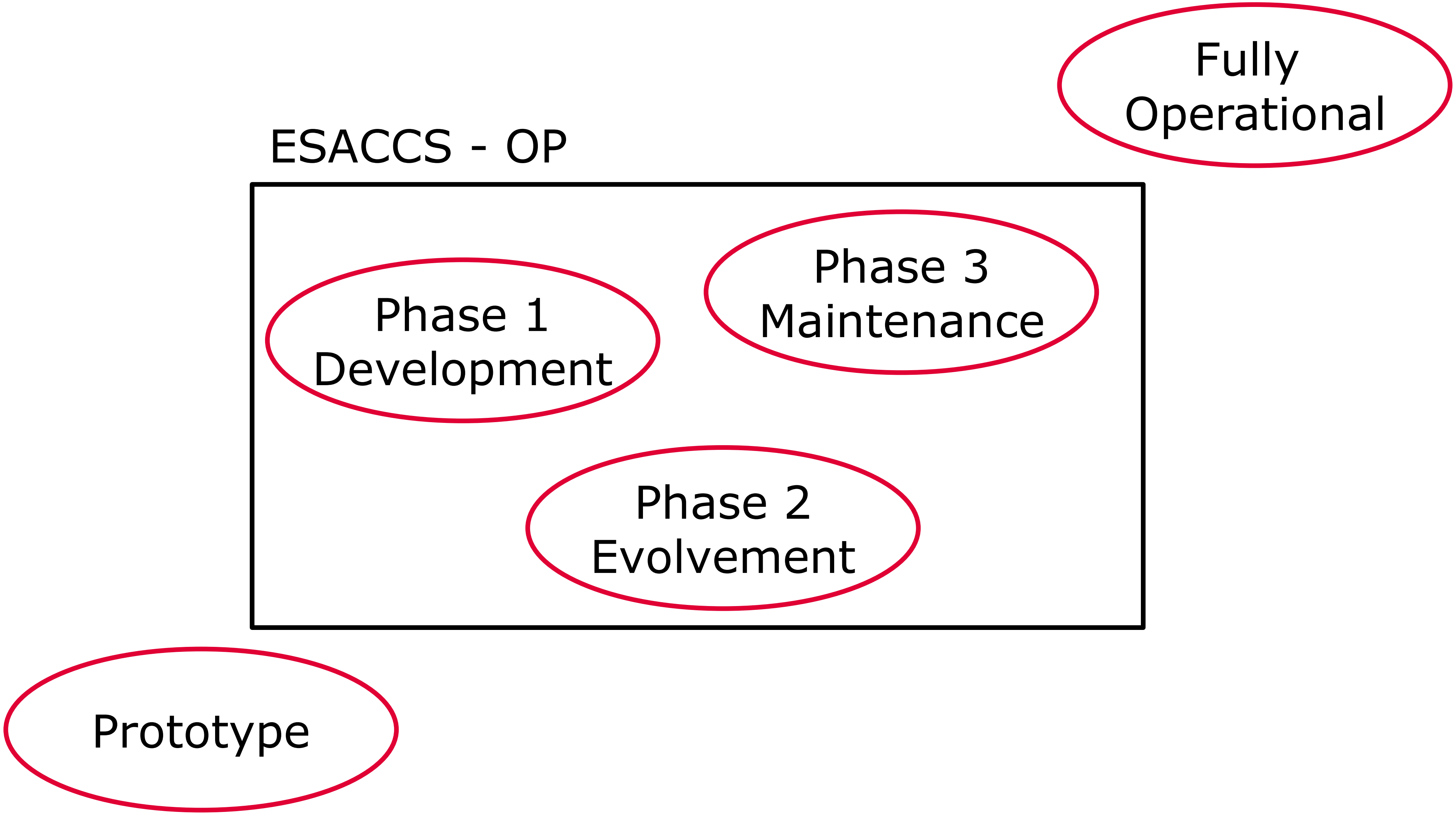

Page 535

ESACCS – FULLY OPERATIONAL

- More stable
- More suitable to the user’s needs.
- More flexible in terms of configuration.
- More reliable in terms of validation for computations results and different configuration schemas.

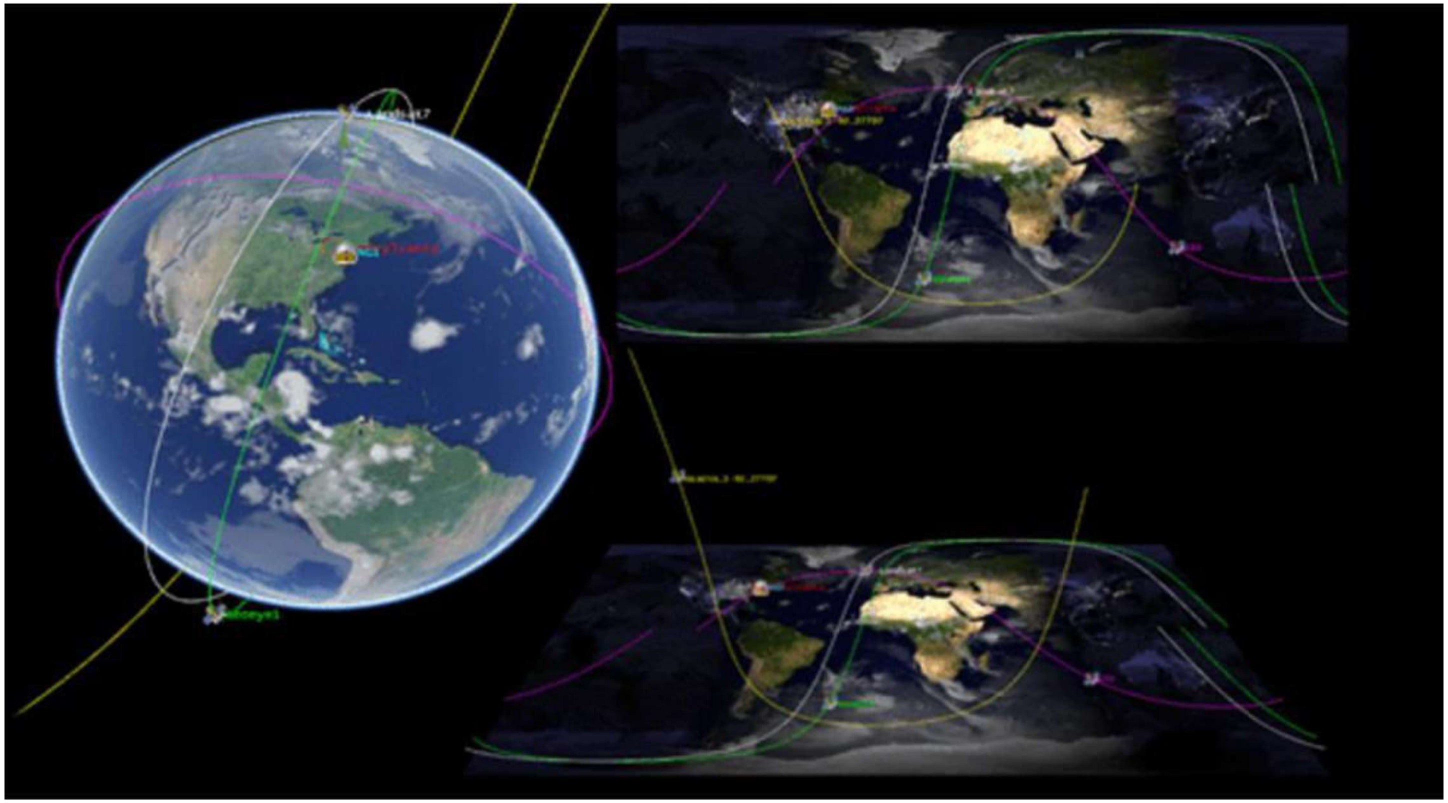

Thank you!

ESACCS team, GMV-ROM

Presentation 2520

MULCOBA

MULTICONSTELLATION GNSS OPERATIONAL BENEFITS FOR AVIATION

MULCOBA

MULTI-CONSTELLATION GNSS OPERATIONAL BENEFITS FOR AVIATION

CONTENTS

- **Main Objectives**
- **Methodology**
- **Integrity Results**
- **Conclusions**

MULCOBA

Main Objectives

Main Objectives

- Identify horizontal RAIM algorithms part of aircraft avionics
  - ARAIM-H & classic horizontal RAIM for multi-constellation/frequency
- Describe in detail the selected algorithms
  - identify explicit or implicit assumptions and required input flows
- Assess GPS SPS ground segment
  - Focus on the underlying failure concept and the monitors it implements to prevent it from happening
- Statistical analysis of a large data set of historical GPS
  - determination of the probabilities of narrow and wide failures
  - characterisation of fault-free errors in terms of URE/SISE and biases
  - assess the validity of the assumptions made
  - identify shortfalls of current GPS infrastructure
- Assess the validity of the assumptions made by the different user algorithms under consideration
  - ARAIM-H & those implicit to the GPS SPS ground segment

MULCOBA

Methodology

Methodology

Main inputs:

1. Historical data covering 2008-2014:
   - Navigation data (BRDC RINEX files)
   - Clock/orbit reference data (IGS SP3 products)
   - Antenna offset data (ANTEX files)

Main outputs:

1. Maximum projected error (maxPE)
2. maxPE/URA
3. Statistics for maxPE and for maxPE/URA
4. Satellite failure probability

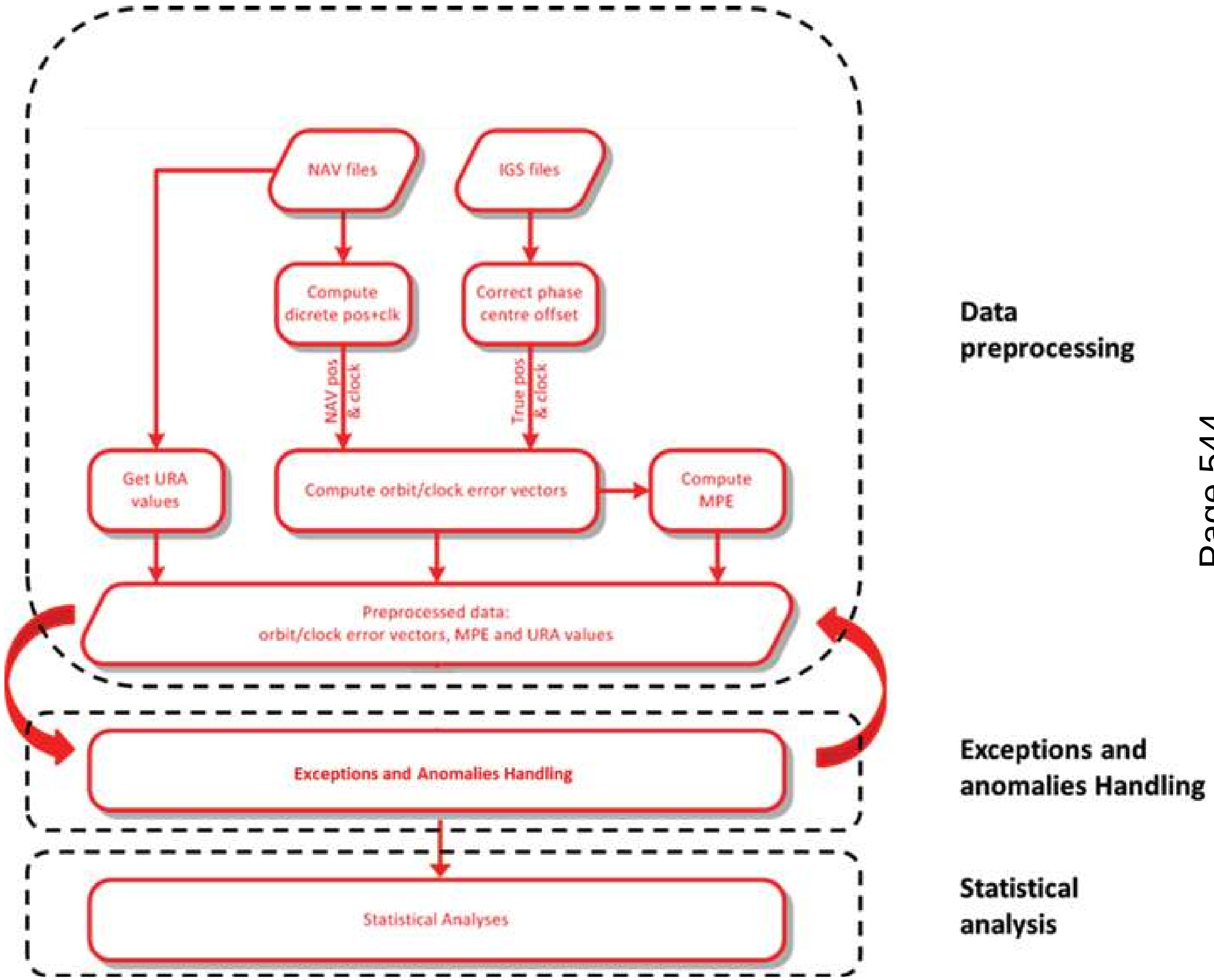

Methodology

MAIN STEPS:

1. Data Preprocessing
   - Orbit/Clock errors
     - maxPE
     - URA
2. Exceptions and anomalies handling
   - BRDC anomalies detection
   - NANU exceptions (if applicable)
3. Statistical analysis

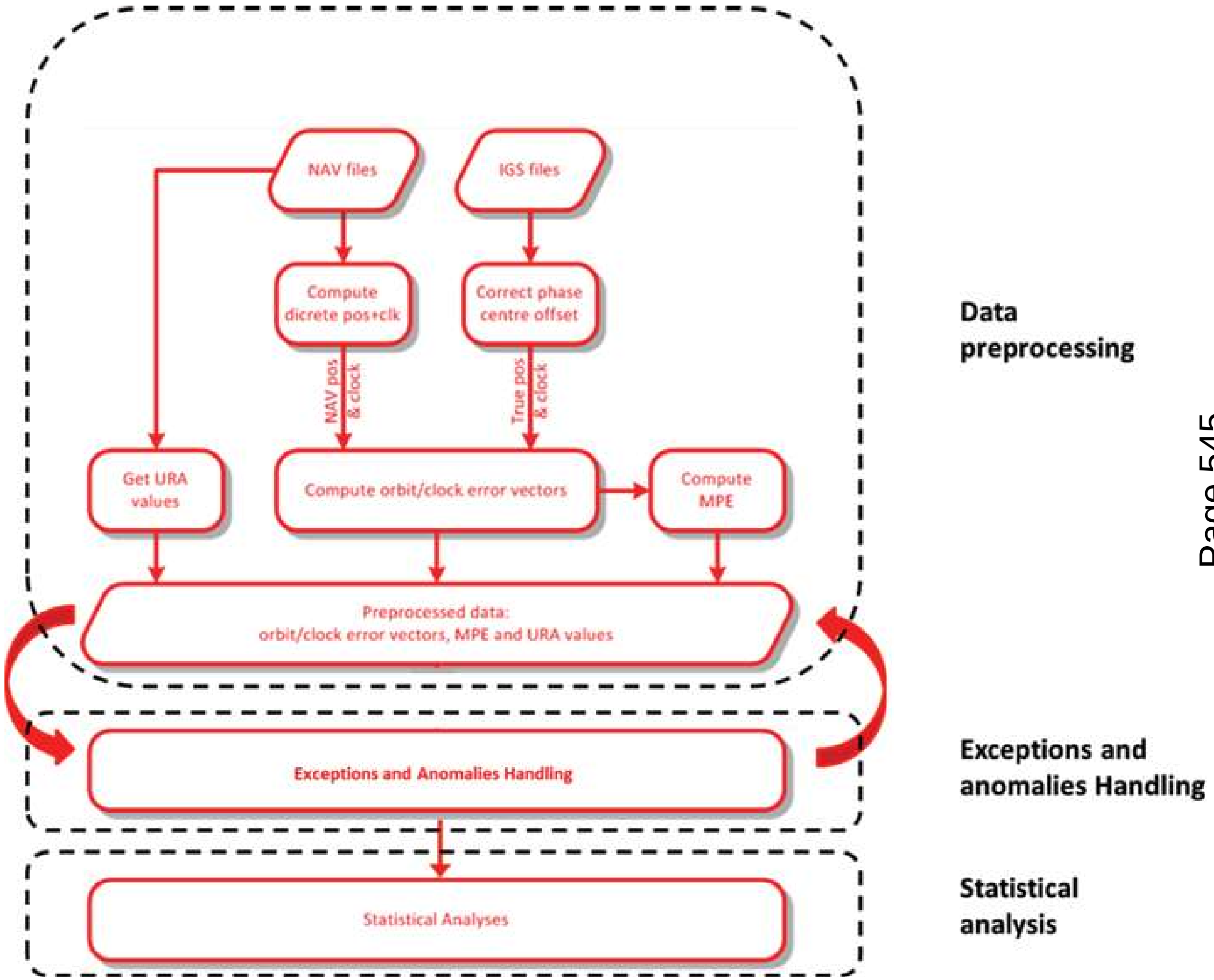

MULCOBA

Integrity results

Integrity Results

Taking into account NANUs:

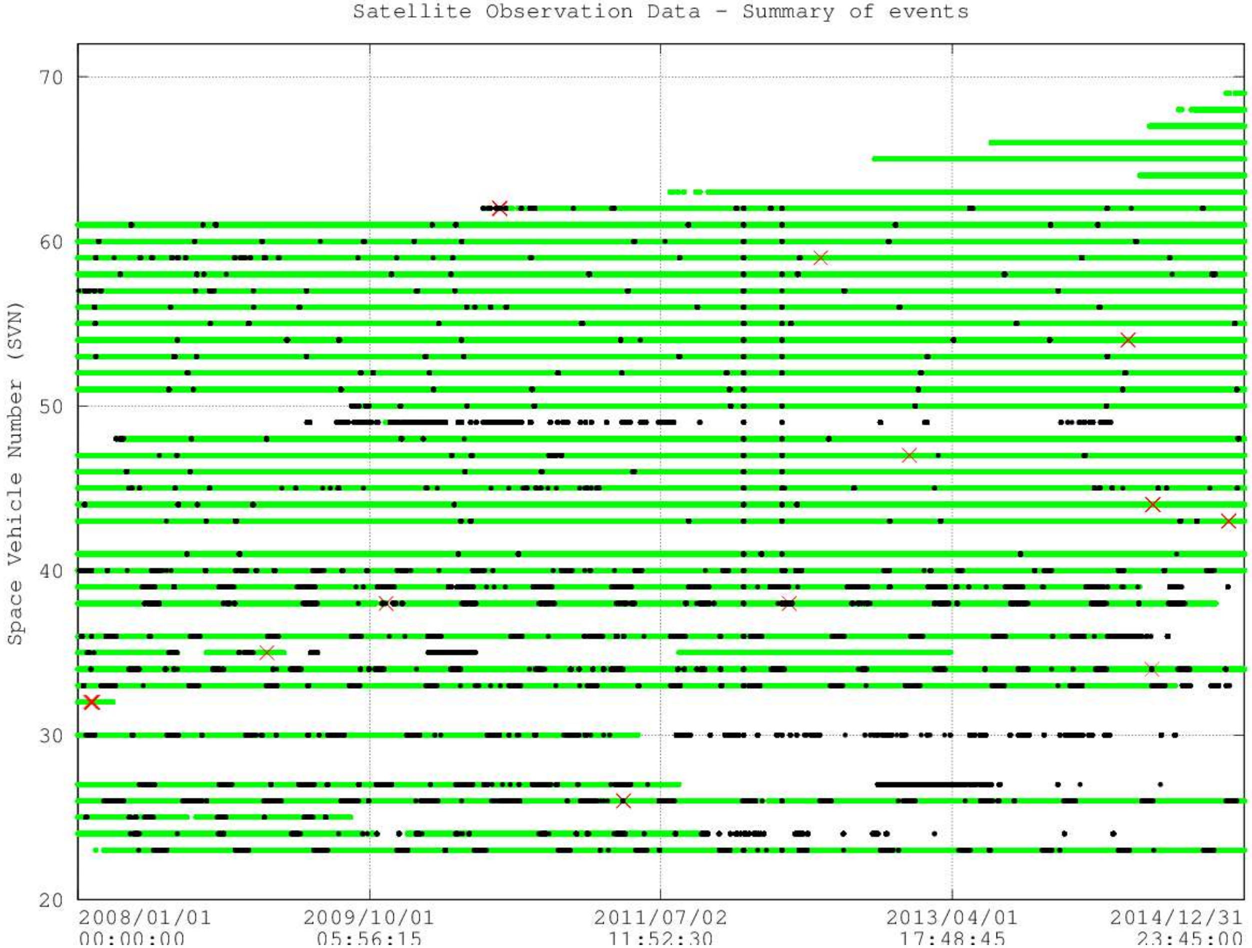

Summary of events for all satellites

Integrity Results

Integrity events taking into account NANUs:

SVN	PRN	IODE	Start date	Start time	End date	End time	Approx Duration [HH:MM]
32	1	108	27.01.2008	00:00	27.01.2008	00:00	-
32	1	104	30.01.2008	22:00	31.01.2008	00:00	02:00
32	1	190	01.02.2008	22:00	01.02.2008	23:30	01:30
35	5	94	17.02.2009	17:15	17.02.2009	17:30	00:15
38	8	67	05.11.2009	18:45	05.11.2009	19:00	00:15
62	25	62	15.07.2010	00:00	15.07.2010	04:00	04:00
26	26	8	12.04.2011	01:00	12.04.2011	01:45	00:45
38	8	7	08.04.2012	20:30	08.04.2012	20:45	00:15
59	19	0	17.06.2012	00:15	17.06.2012	00:30	00:15
47	22	23	28.12.2012	21:30	28.12.2012	21:45	00:15
54	18	47	21.04.2014	22:45	21.04.2012	23:30	00”45
34	4	64	13.06.2014	00:00	13.06.2014	00:00	-
44	28	9	14.06.2014	20:15	14.06.2014	23:15	01:00
43	13	43	28.11.2014	08:30	28.11.2014	10:00	01:30

Integrity results

Taking into account NANUs:

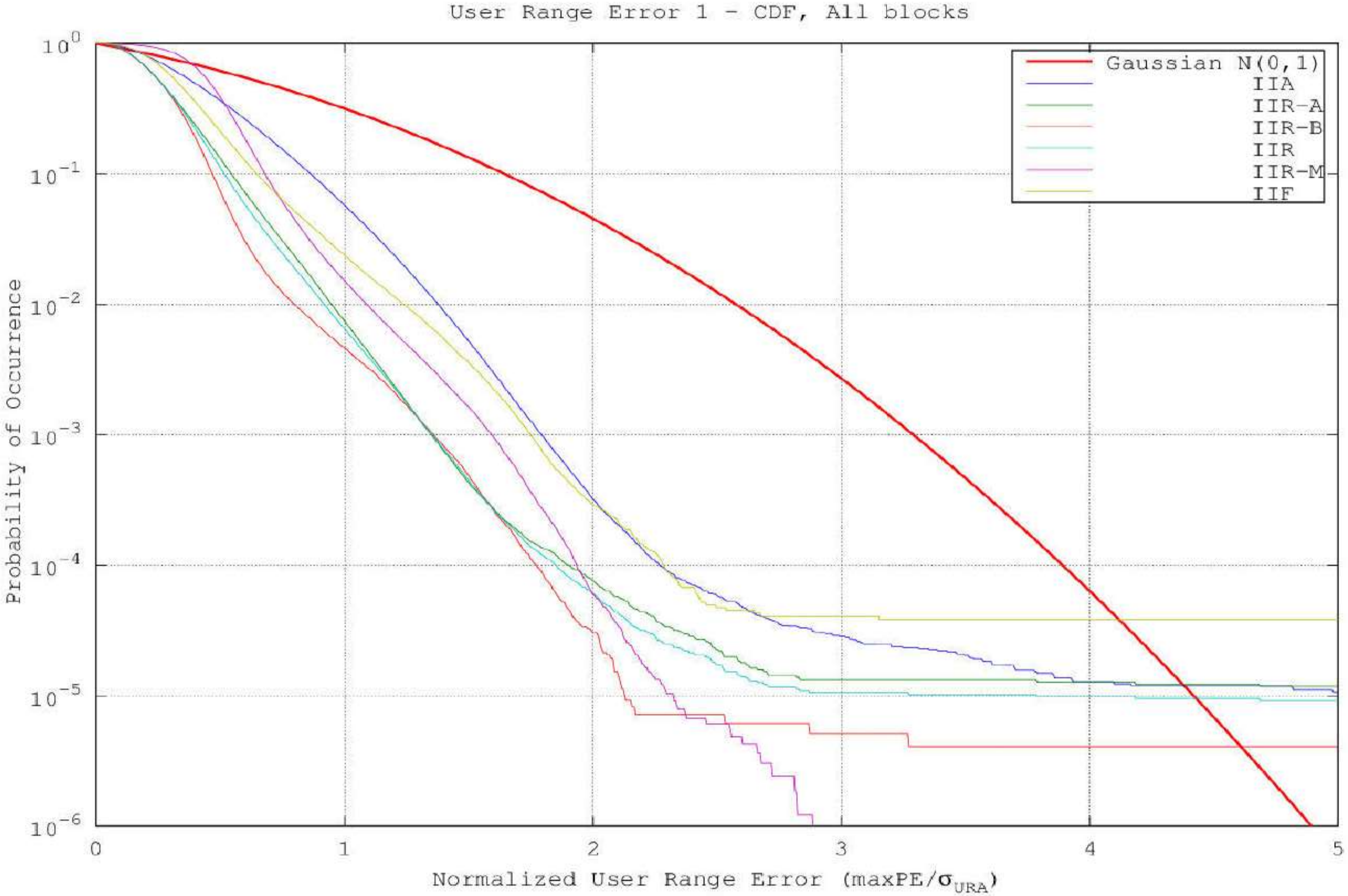

maxPE/URA CDF per all satellite blocks

Integrity results

Taking into account NANUs:

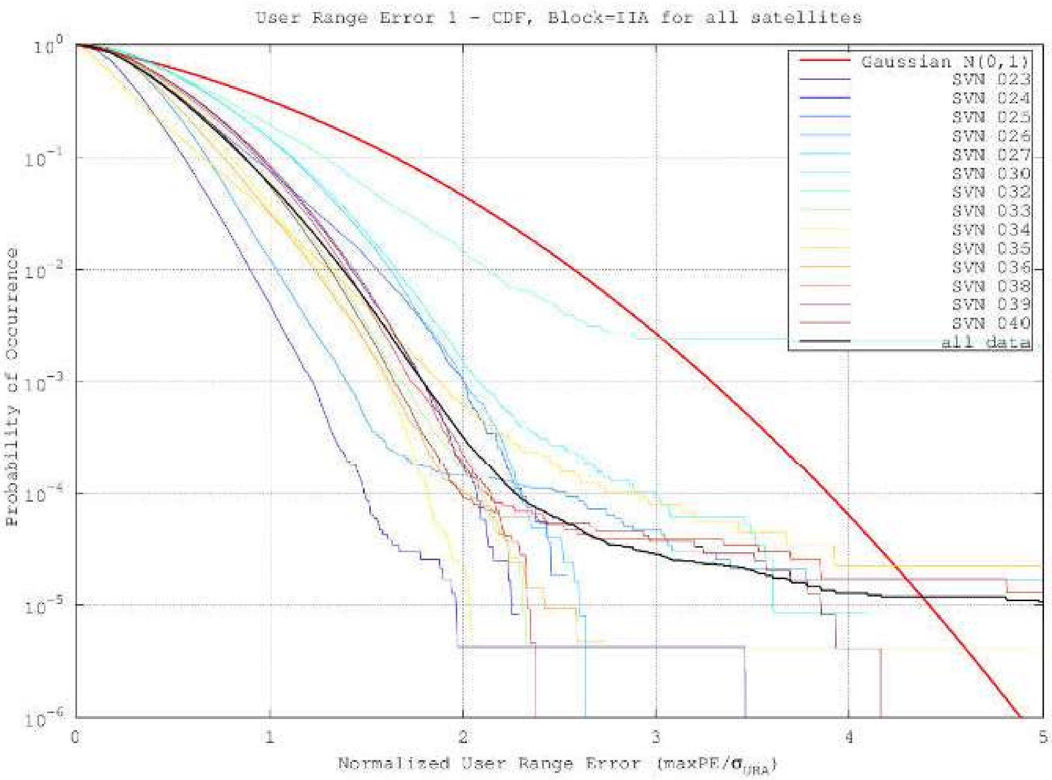

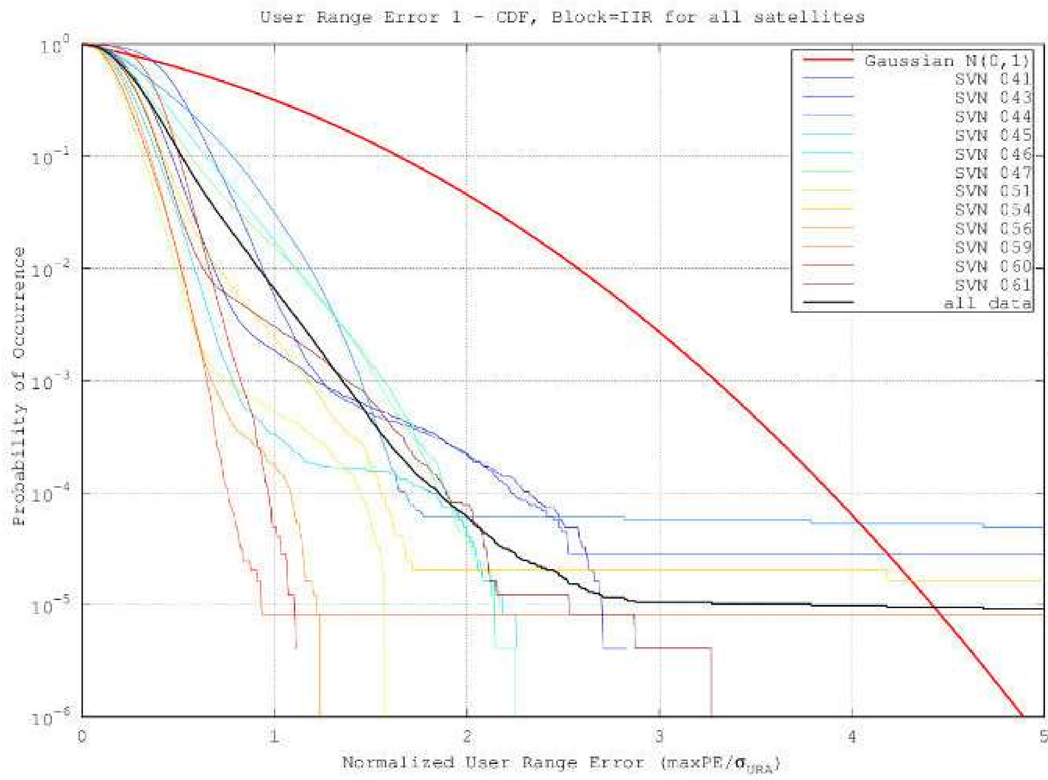

Block IIA **Block IIR**

maxPE/URA CDF for each satellite per block

Integrity results

Taking into account NANUs:

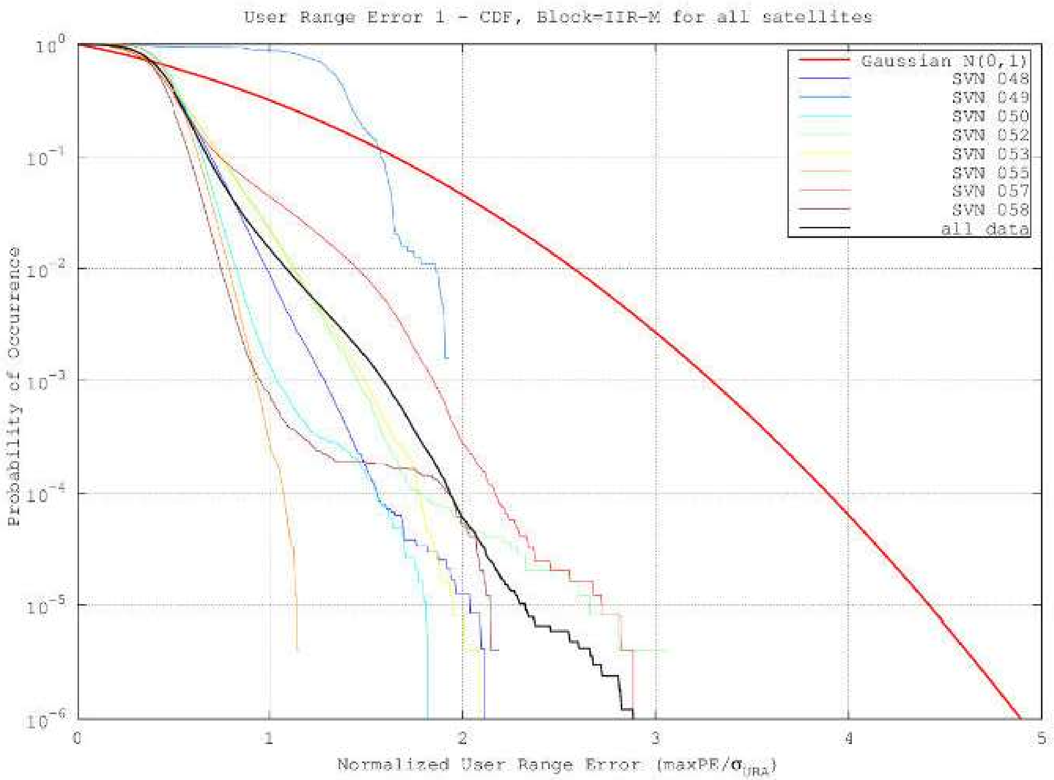

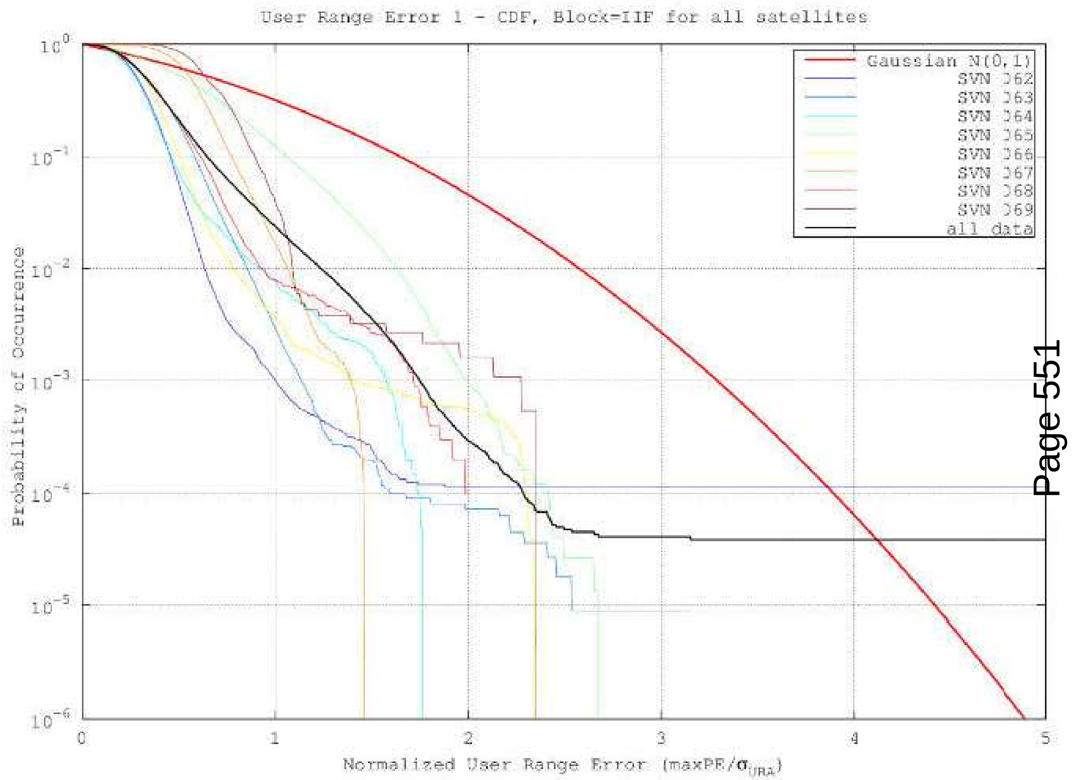

Block IIR-M **Block IIF**

maxPE/URA CDF for each satellite per block

Integrity Results

NOT taking into account NANUs (only BRDC anomalies):

Summary of events for all satellites

NOT taking into account NANUs (only BRDC anomalies):

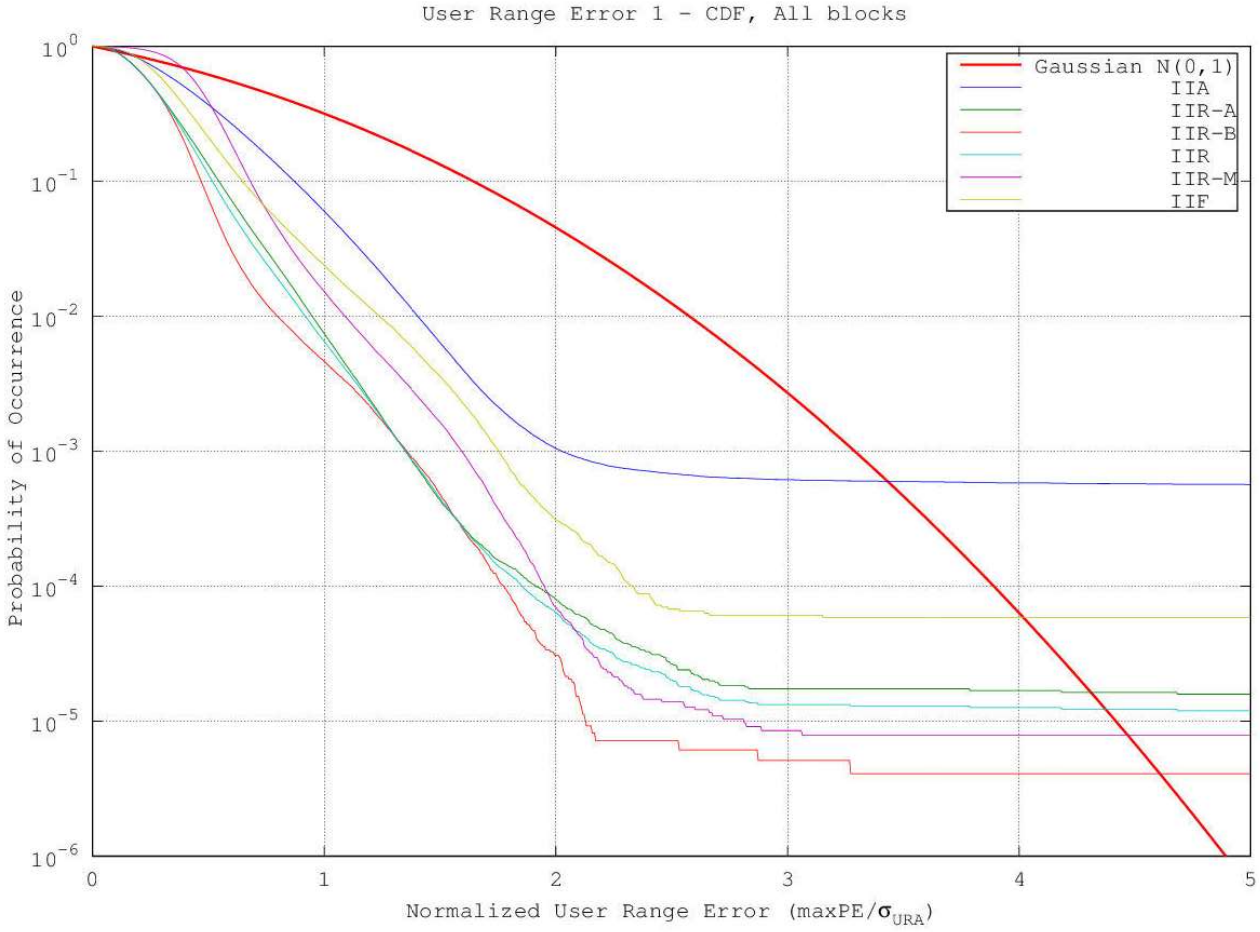

maxPE/URA CDF per all satellite blocks

Integrity results

NOT taking into account NANUs (only BRDC anomalies):

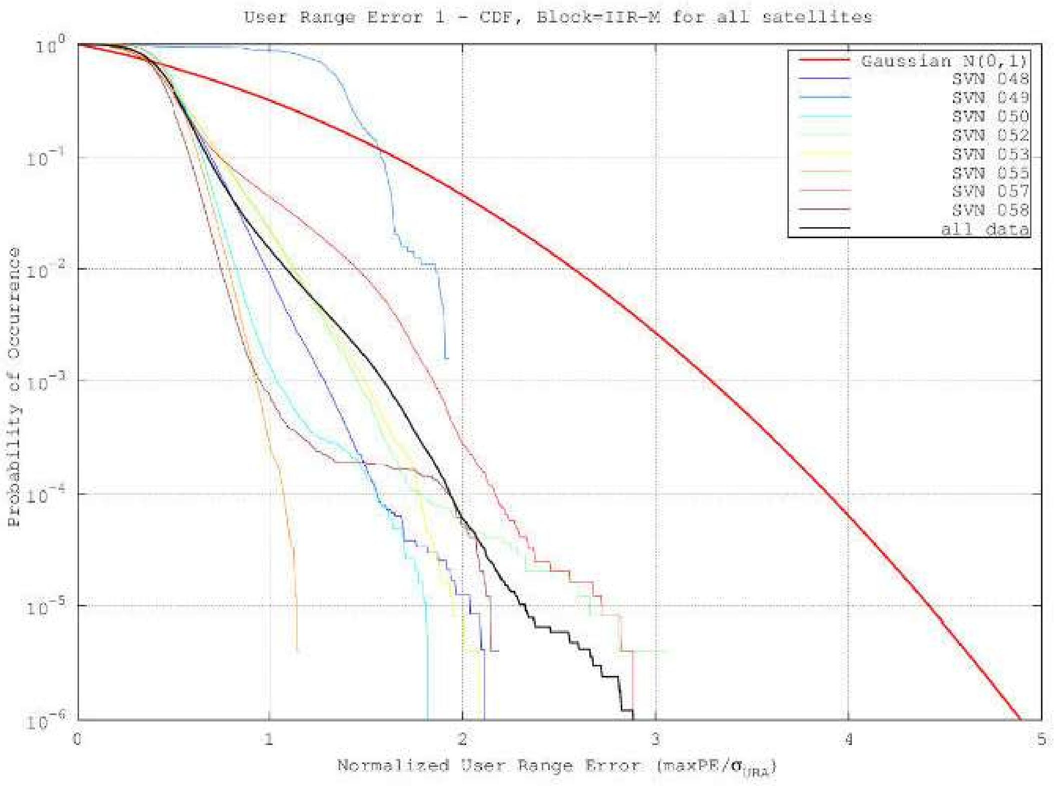

Block IIA

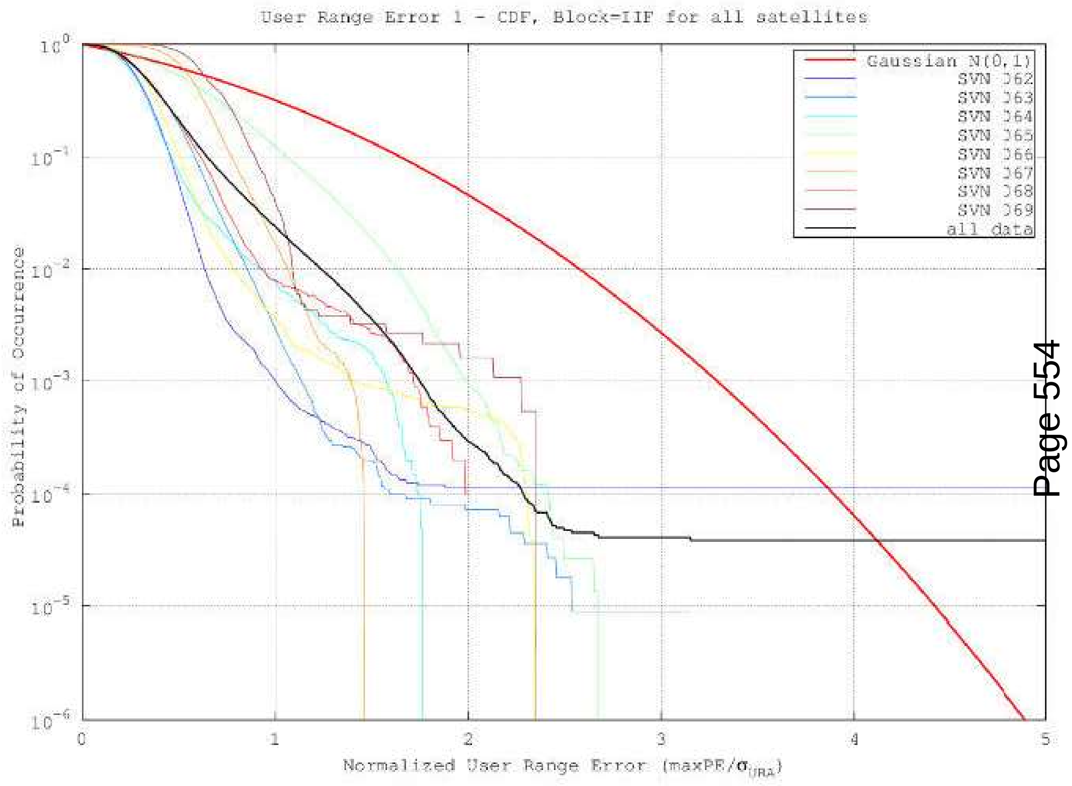

Block IIR

maxPE/URA CDF for each satellite per block

Integrity results

NOT taking into account NANUs (only BRDC anomalies):

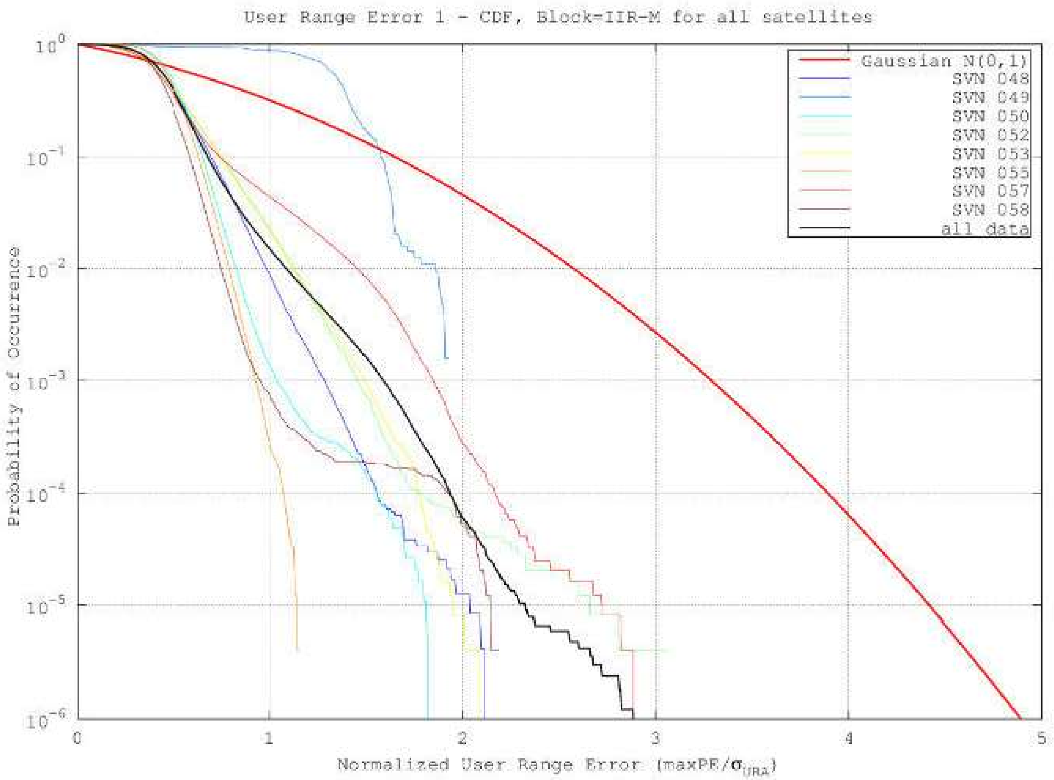

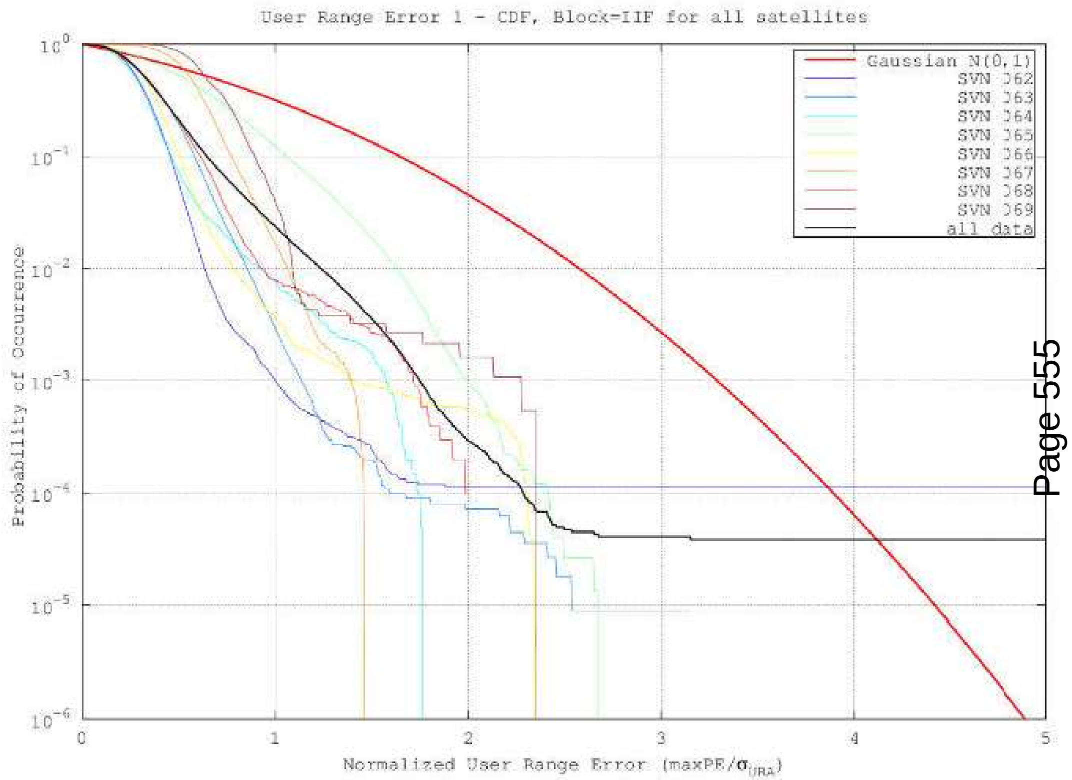

Block IIR-M **Block IIF**

maxPE/URA CDF for each satellite per block

Fault Probabilities

Taking into account NANUs:

SV N	Availability percentage [%]	Fault percentage [%]	Fault probability [Faults/hour]	SV Total Time [years]
23	97.97438	0	0	6.693350
24	98.14861	0	0	3.437414
25	98.92616	0	0	1.548545
26	96.76789	0.00169	1.6963e-05	6.729566
27	94.51372	0	0	3.531992
30	95.98972	0	0	3.294606
32	100	0.23082	1.6293e-03	0.210188
33	96.80793	0	0	6.435987
34	98.47463	0.00041	1.6576e-05	6.886929
35	92.50360	0.00224	4.4860e-05	2.544720
36	96.22766	0	0	6.019749
37	0	-	-	-
38	98.28750	0.00172	3.4442e-05	6.628853
39	97.18911	0	0	6.153425
40	98.77937	0	0	6.896176
41	99.84178	0	0	6.987814
43	99.73734	0.00286	1.6357e-05	6.978881
44	99.85968	0.00531	1.6338e-05	6.986929
45	99.76346	0	0	6.981221
46	99.84993	0	0	6.987871
47	99.68331	0.00081	1.6376e-05	6.971005
48	99.72509	0	0	6.750086
49	12.68537	0	0	0.018065

SV N	Availability percentage [%]	Fault percentage [%]	Fault probability [Faults/hour]	SV Total Time [years]
50	99.55862	0	0	5.317237
51	99.75235	0	0	6.966324
52	99.73447	0	0	6.978396
53	99.72226	0	0	6.978196
54	99.79598	0.00163	1.6355e-05	6.979966
55	99.73123	0	0	6.978910
56	99.77033	0	0	6.979937
57	99.63421	0	0	6.965097
58	99.69895	0	0	6.975228
59	99.74838	0.00081	1.6354e-05	6.980422
60	99.76468	0	0	6.981279
61	99.73078	0	0	6.967009
62	99.49791	0.01121	2.6385e-05	4.326513
63	100	0	0	3.187785
64	100	0	0	0.585303
65	100	0	0	2.139755
66	100	0	0	1.513527
67	100	0	0	0.557334
68	100	0	0	0.289526
69	100	0	0	0.052911

Fault Probabilities

NOT taking into account NANUs (only BRDC anomalies):

SV N	Availability percentage [%]	Fault percentage [%]	Fault probability [Faults/hour]	SV Total Time [years]
23	97.97438	0	0	6.693350
24	98.14861	0	0	3.437414
25	98.82068	0.07518	2.5595e-04	1.783990
26	96.74955	0.04277	2.5413e-04	6.737900
27	94.94978	0.13848	5.2753e-04	4.327911
30	95.76759	0.07010	3.7620e-04	3.337900
32	97.08737	0.55405	2.7027e-03	0.211187
33	96.61549	0	0	6.435987
34	98.46350	0.00165	4.9723e-05	6.887500
35	92.61281	0.61815	3.0908e-03	2.585388
36	96.21164	0.00663	9.4800e-05	6.020833
37	0	-	-	-
38	98.20656	0.01893	1.2048e-04	6.632334
39	96.66210	0.11837	5.3638e-04	6.171975
40	98.77588	0.00620	3.3103e-05	6.897003
41	99.84178	0	0	6.987814
43	99.73734	0.00286	1.6357e-05	6.978881
44	99.85968	0.005300	1.6338e-05	6.986929
45	99.76346	0	0	6.981221
46	99.84993	0	0	6.987871
47	99.68331	0.00081	1.6376e-05	6.971005
48	99.72509	0	0	6.750086
49	12.76469	1.86046	1.8605e-02	0.018408

SV N	Availability percentage [%]	Fault percentage [%]	Fault probability [Faults/hour]	SV Total Time [years]
50	99.55862	0	0	5.317237
51	99.74667	0.00327	1.6385e-05	6.966924
52	99.73245	0.00040	1.6358e-05	6.978653
53	99.72226	0	0	6.978196
54	99.79598	0.00163	1.6355e-05	6.979966
55	99.73123	0	0	6.978910
56	99.77033	0	0	6.979937
57	99.63421	0	0	6.965097
58	99.69895	0	0	6.975228
59	99.74838	0.00081	1.6354e-05	6.980422
60	99.76468	0	0	6.981279
61	99.73078	0	0	6.967009
62	99.49467	0.01187	5.2768e-05	4.326684
63	100	0.00716	7.1606e-05	3.188442
64	100	0	0	0.585303
65	100	0	0	2.139755
66	100	0	0	1.513527
67	100	0	0	0.557334
68	100	0	0	0.289526
69	100	0	0	0.052911

Fault probabilities

- Considering NANUs:
  - Most satellites have <2% of unavailability due to invalid IGS reference data.
  - In the period analyzed, fault probability in the order of 10^-5 in most satellites.
- Not considering NANUs:
  - Availability of IGS reference data and the SV total is slightly modified.
  - Big impact on fault probabilities.
  - Fault probability ranges from 10^-3 to 10^-5
  - More satellites present integrity failures.
- Note that SVN 49 was a test satellite for L5, presents strange behaviour.
- SVN 32 also presents high fault probability. It was decommissioned at the beginning of 2008.
- 1 Failure in 7 years (2008-2014) equals to 1.631*10^5 failures/hour

Comparative results

Taking vs. NOT taking into account NANUs:

Summary of events for all satellites

Taking into account NANUs

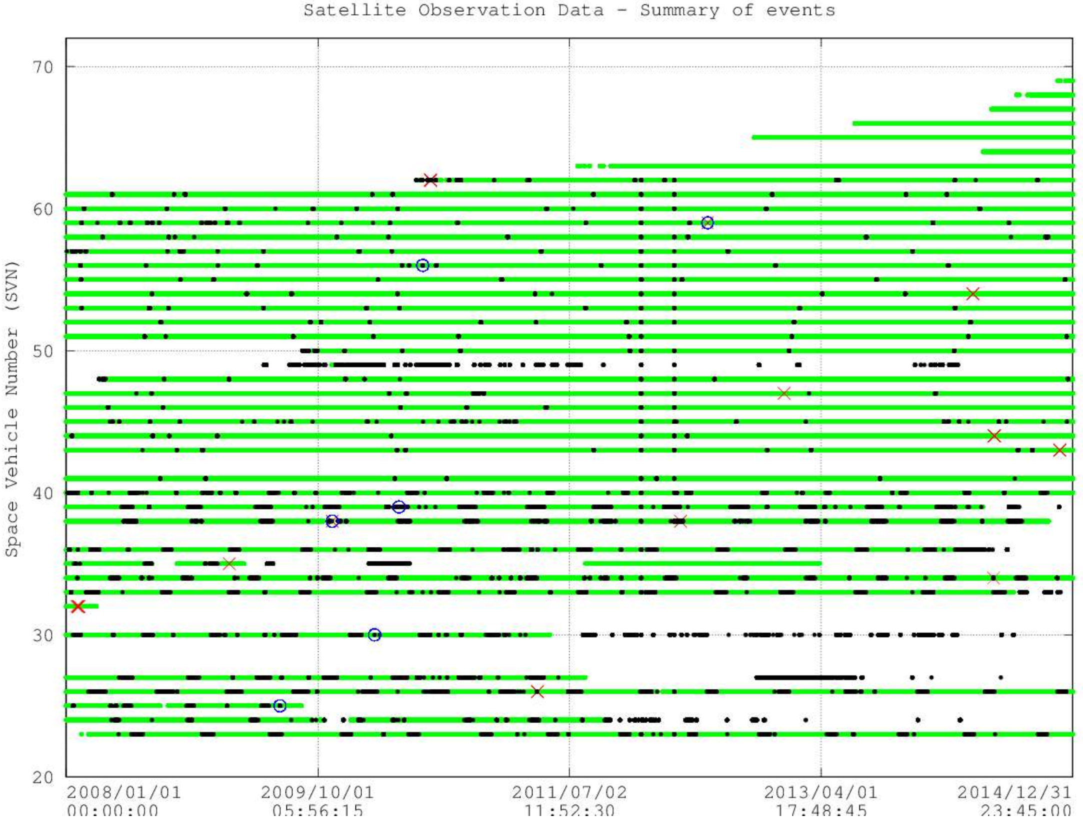

NOT taking into account NANUs

MULCOBA

Conclusions

Conclusions

- The use of NANUs has been analyzed and its impact on the fault rate explored
- Considering NANUs leads to better results
  - Satellite fault probability in the order of 10^-5 faults/hour
- Not considering NANUs
  - Satellite fault probability in ranges from 10^-3 to 10^-5 faults/hour

Conclusions

- Wrong BRDC data may lead to high errors
  - Navigation data reported by only one reference station is ignored
  - It could be argued that more than one station reported wrong data (i.e. wrong healthy bit).
  - Besides, NANUs reported some of the failures in advance.
- Reported integrity events have been compared to similar studies. Events missing in MULCOBA's study are related to the availability of valid IGS reference data.
- This fact supports the possibility that IGS missing references may be associated to real integrity events.

www.gmv.com

THANK YOU

gmv BLOG

MULCOBA

Auxiliary Materials

Page 27

Integrity Results

Taking into account NANUs:

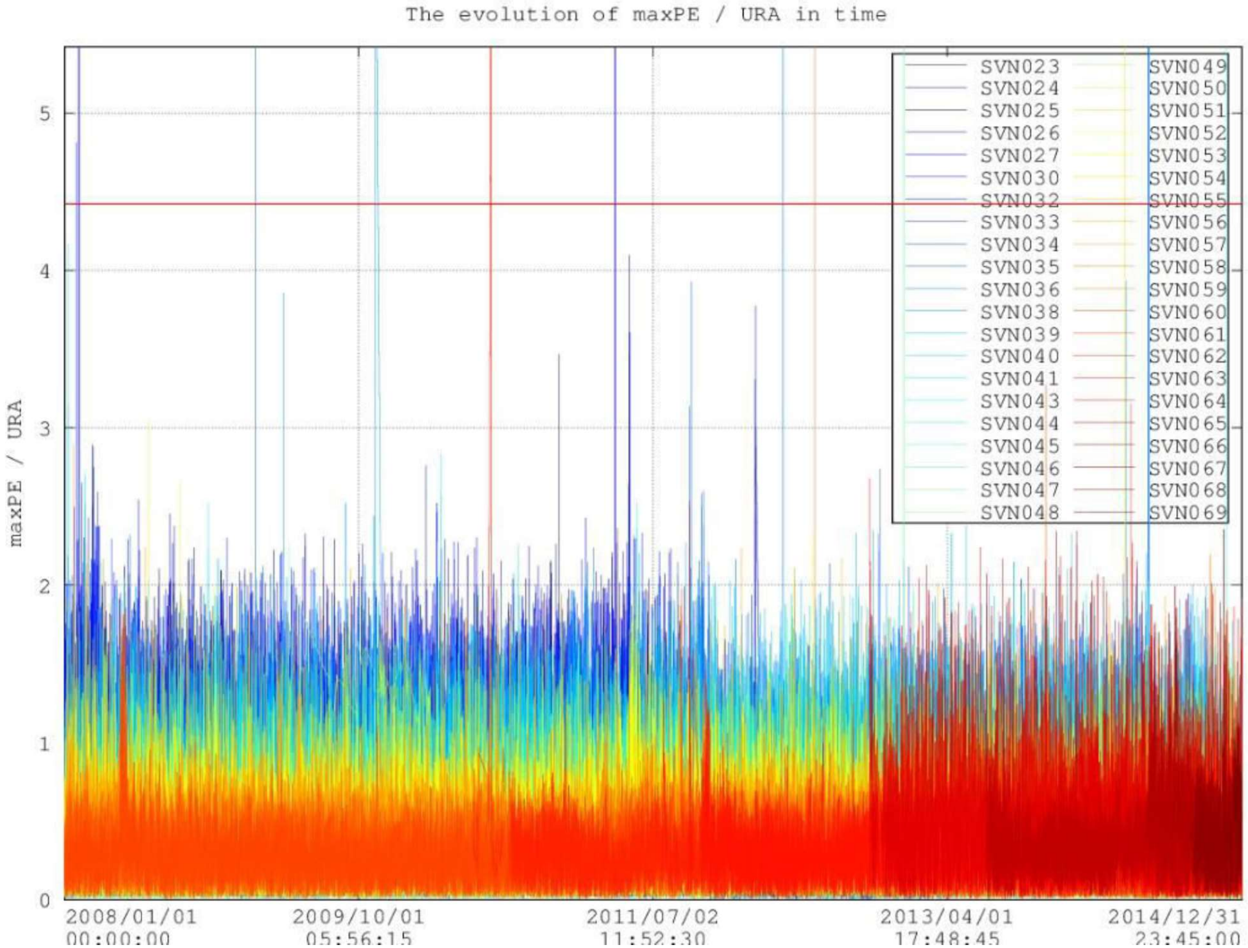

Evolution of maxPE/URA in time for all satellites

Integrity Results

NOT taking into account NANUs (only BRDC anomalies):

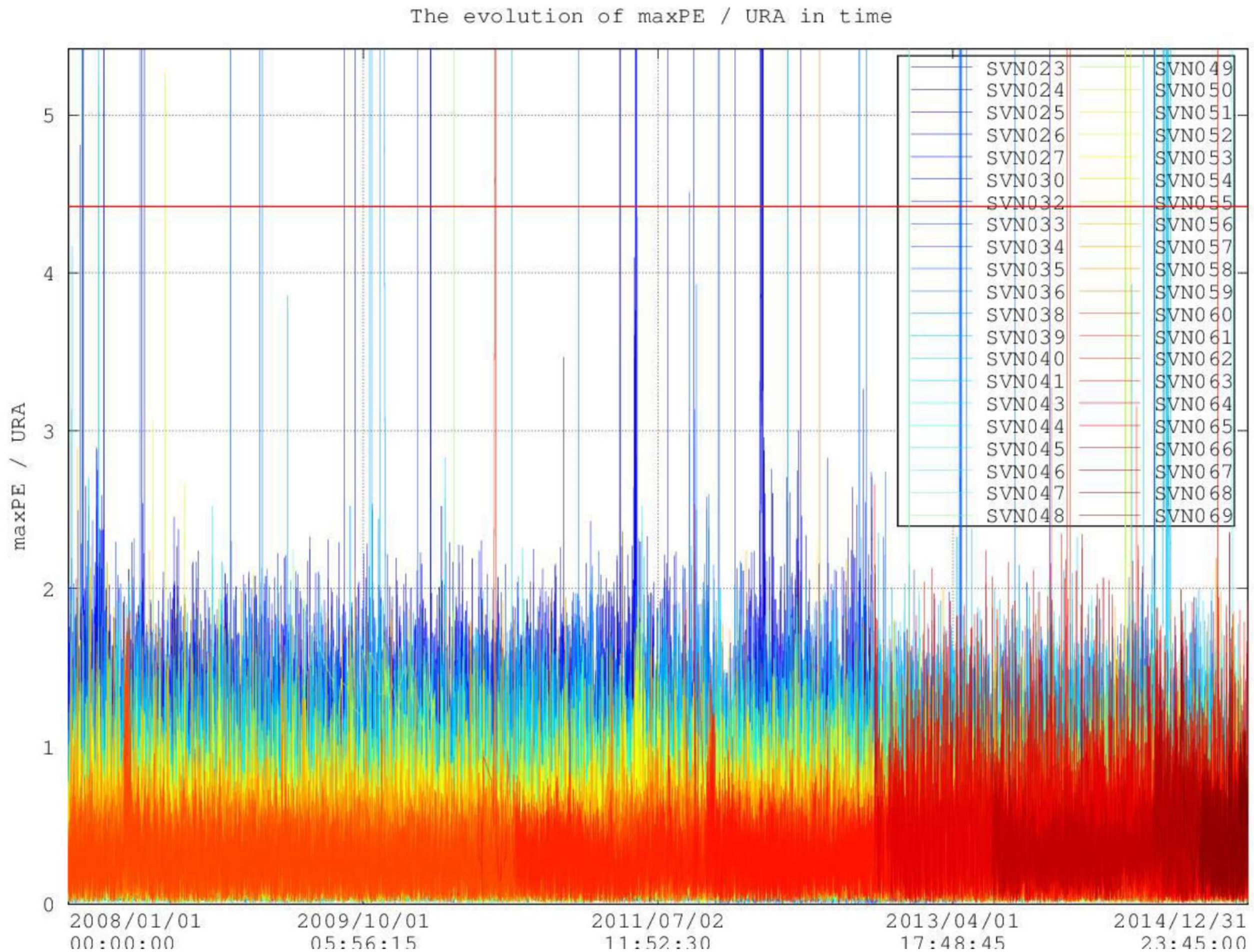

Evolution of maxPE/URA in time for all satellites

Integrity results

Taking into account NANUs:

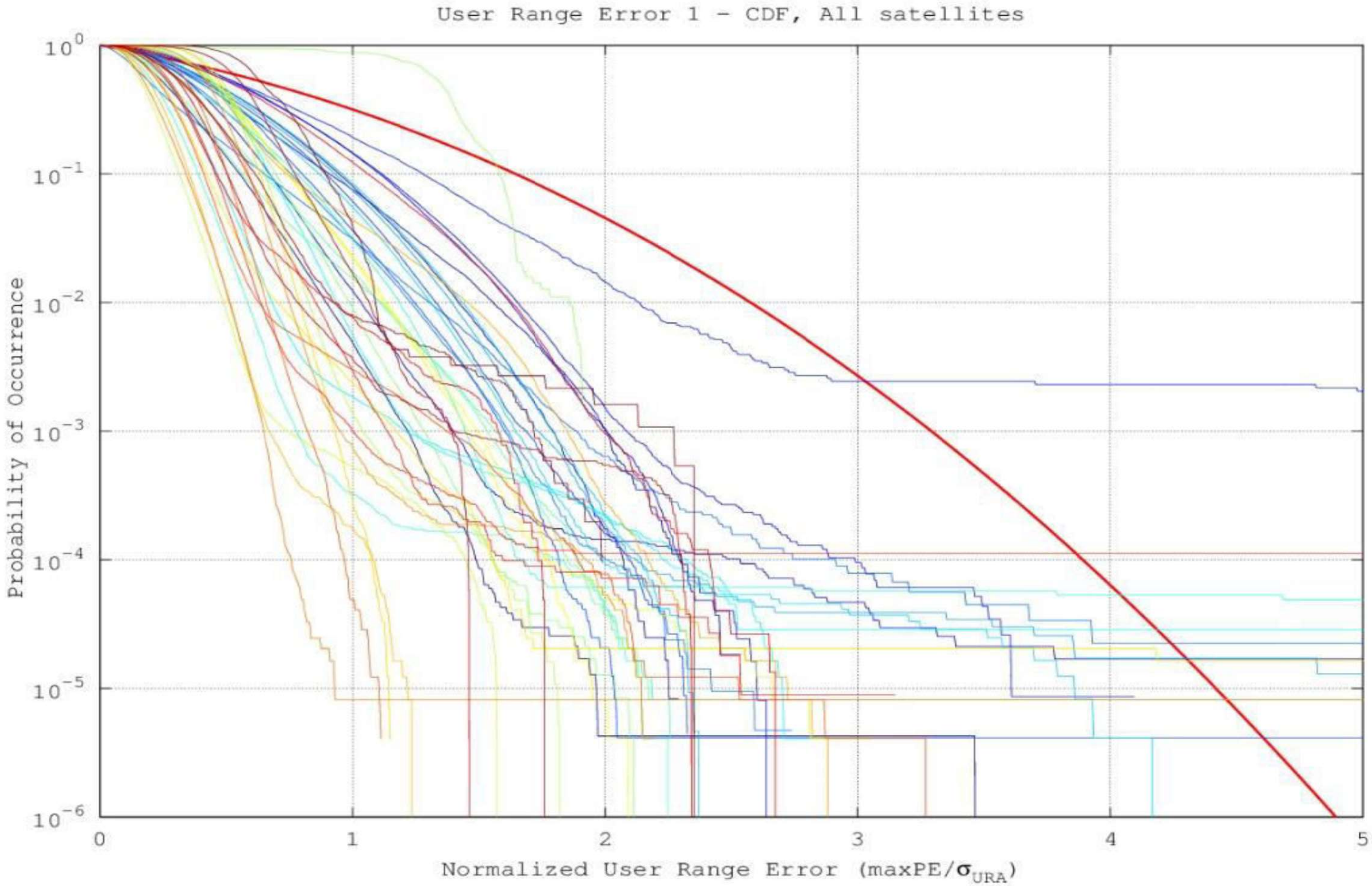

maxPE/URA CDF per all satellites

Integrity results

NOT taking into account NANUs (only BRDC anomalies):

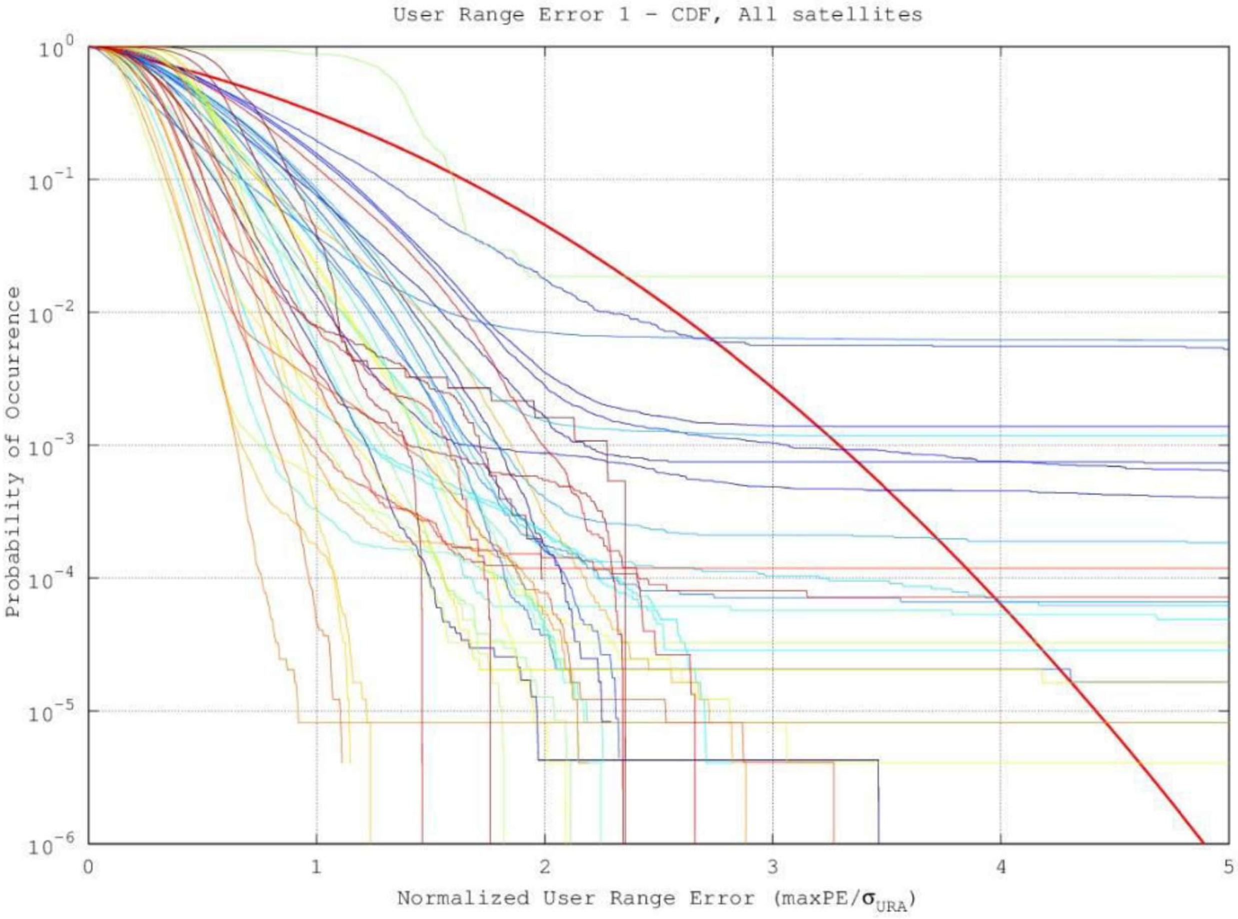

maxPE/URE CDF per all satellites

Comparative results

Taking vs. NOT taking into account NANUs:

URE CDF per all blocks

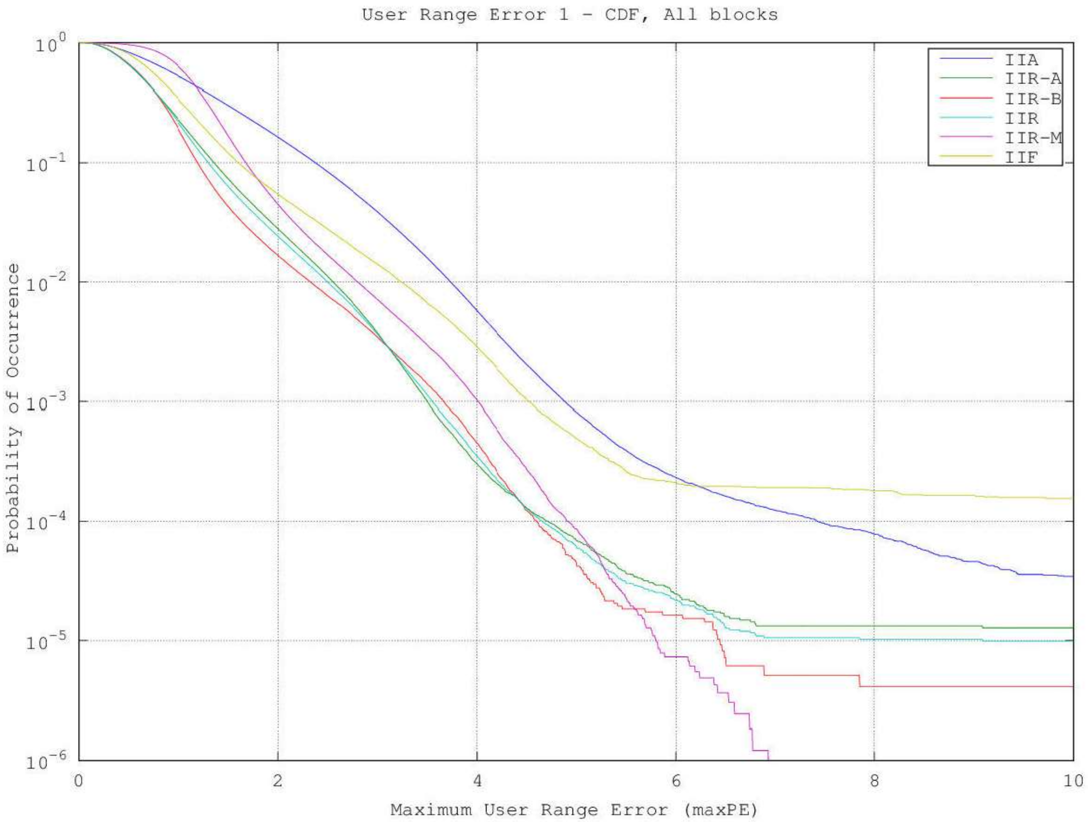

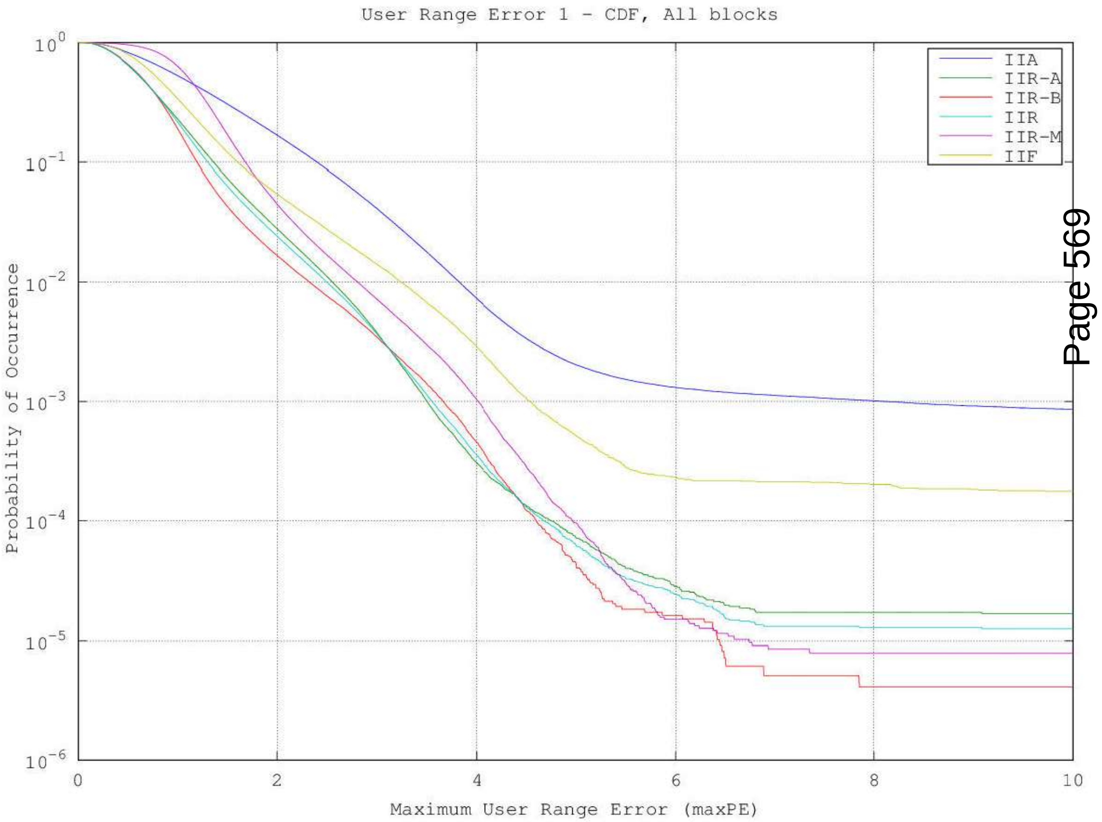

Presentation 2521

A-E Electronics

A-E Electronics

Location

A-E Electronics

12 Condorilor Street,
Bacau, 600302

Tel +40 234 585800

Fax +40 234 585900

E-mail: office@aee.ro

Website: www.aee.ro

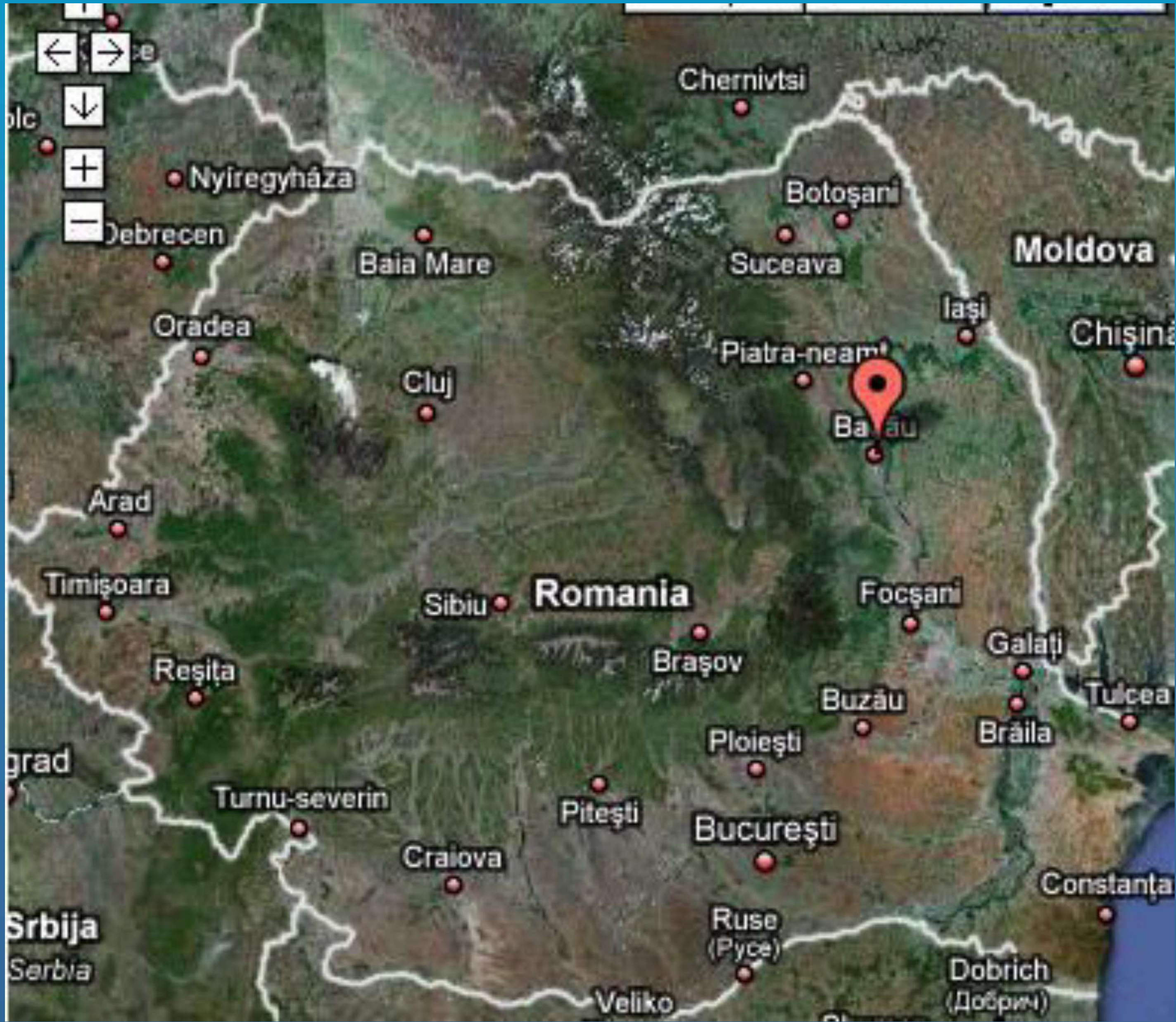

Background

- Founded in 1998
- Shareholder ELBIT SYSTEMS Ltd. (Israel)
- Over 5,000 sq.m. of modern facility
- Production equipment and technology for PWAs, cables & optical assemblies
- ESD and RH controls over the whole production area
- 240 highly skilled and motivated employees

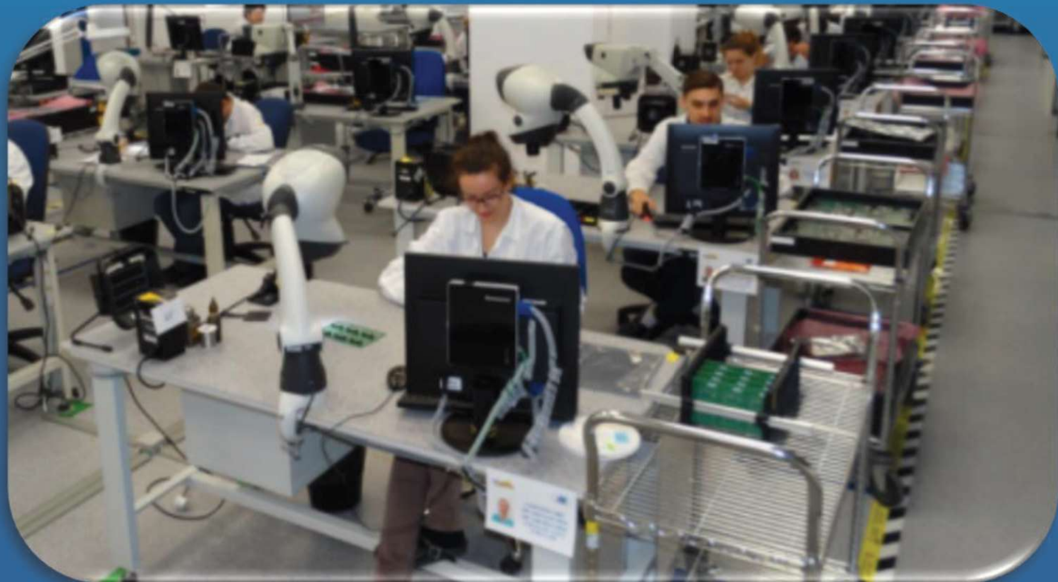

Test Engineering

Complete Test Solutions for SRU / LRU

Design & manufacture, software, hardware and mechanics

All in one

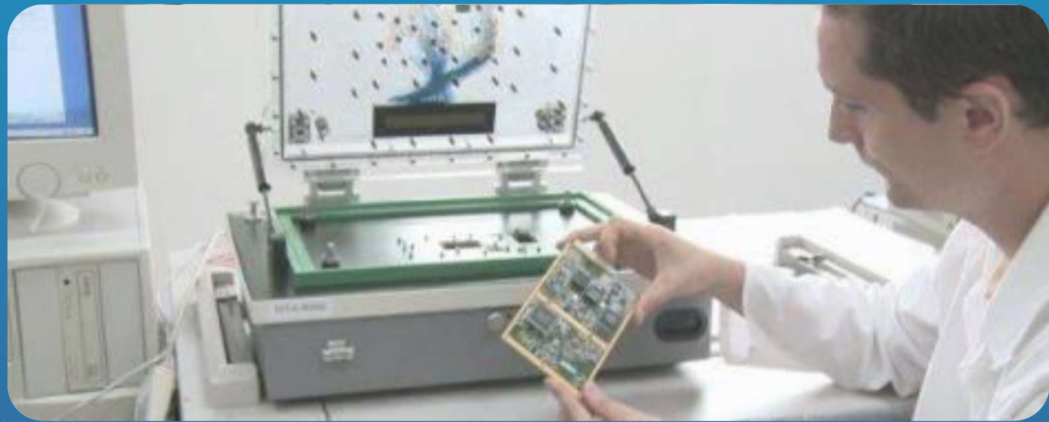

Main activities

- In Circuit Test (ICT)
- Boundary-scan (JTAG)
- Functional Test (FCT)
- Electrical & Mechanical design for Space (PROBA3 satellite)
- Technical assistance for delivered test solutions

Operations Department

- Over 4,000 sq.m. of production area, with further options for development
- Work environment complying with:
  - ANSI/J-STD-001;
  - ANSI/ESD S20.20 / MIL-STD-1686;
  - IPC-J_STD033 B .

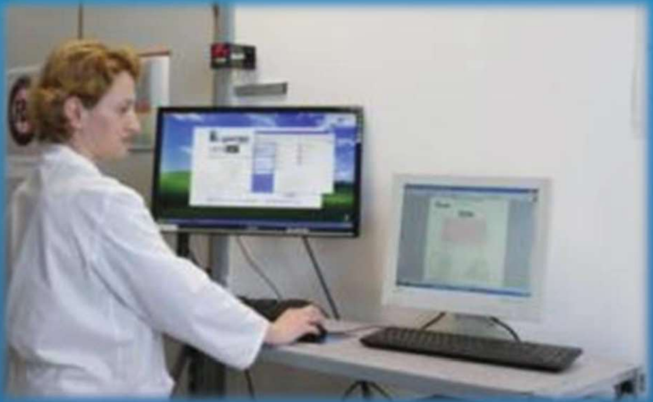

Operations Department

Electronic Assemblies Main Manufacturing Processes

SMT Assembly

AOI

X-Ray

Selective Soldering

Manual assembling

Testing

Operations Department

BGA reballing & SMT/BGA rework

ESS test

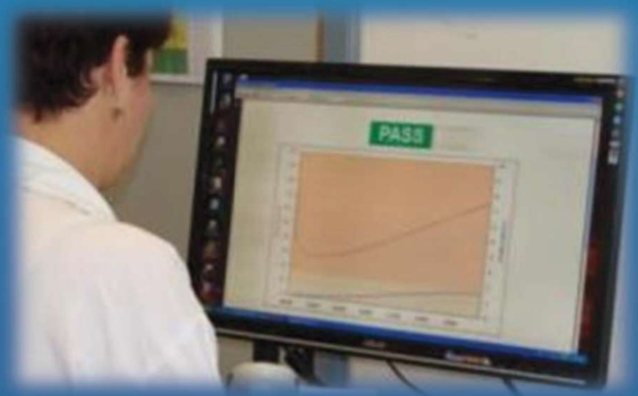

Cleaning

Coating

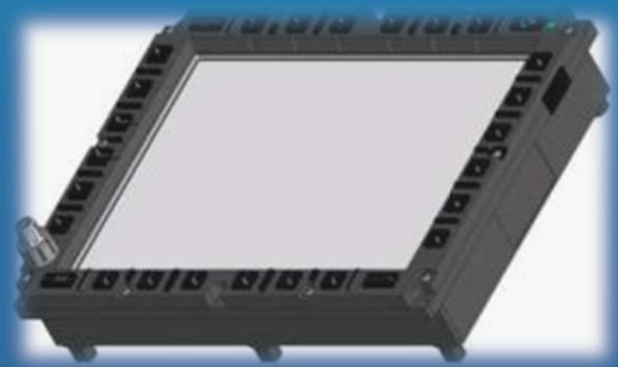

LCD assembling
(clean room ISO7 & ISO5)

Operations Department

Military Cables & Harnesses Main Manufacturing Processes

Laying

Protection cover

Connecting & assembling

Automatic testing

QMS Certifications

- AS 9100C-Requirements for Aviation, Space and Defense
- ISO-9001:2008-Requirements for Quality Management Systems
- Certified employees for ESA
- Boeing production approval per projects
- EASA production approval for commercial projects

Space Projects

In 2013 AEE was invited by OIP Belgium to join their efforts in a space project for ESA

PROBA3

ESA's PROBA3 mission

- Two spacecrafts flying in a close proximity, forming a giant Coronagraph.
- The Coronagraph is implemented by one satellite occulting the sun and the other satellite flying a telescope.

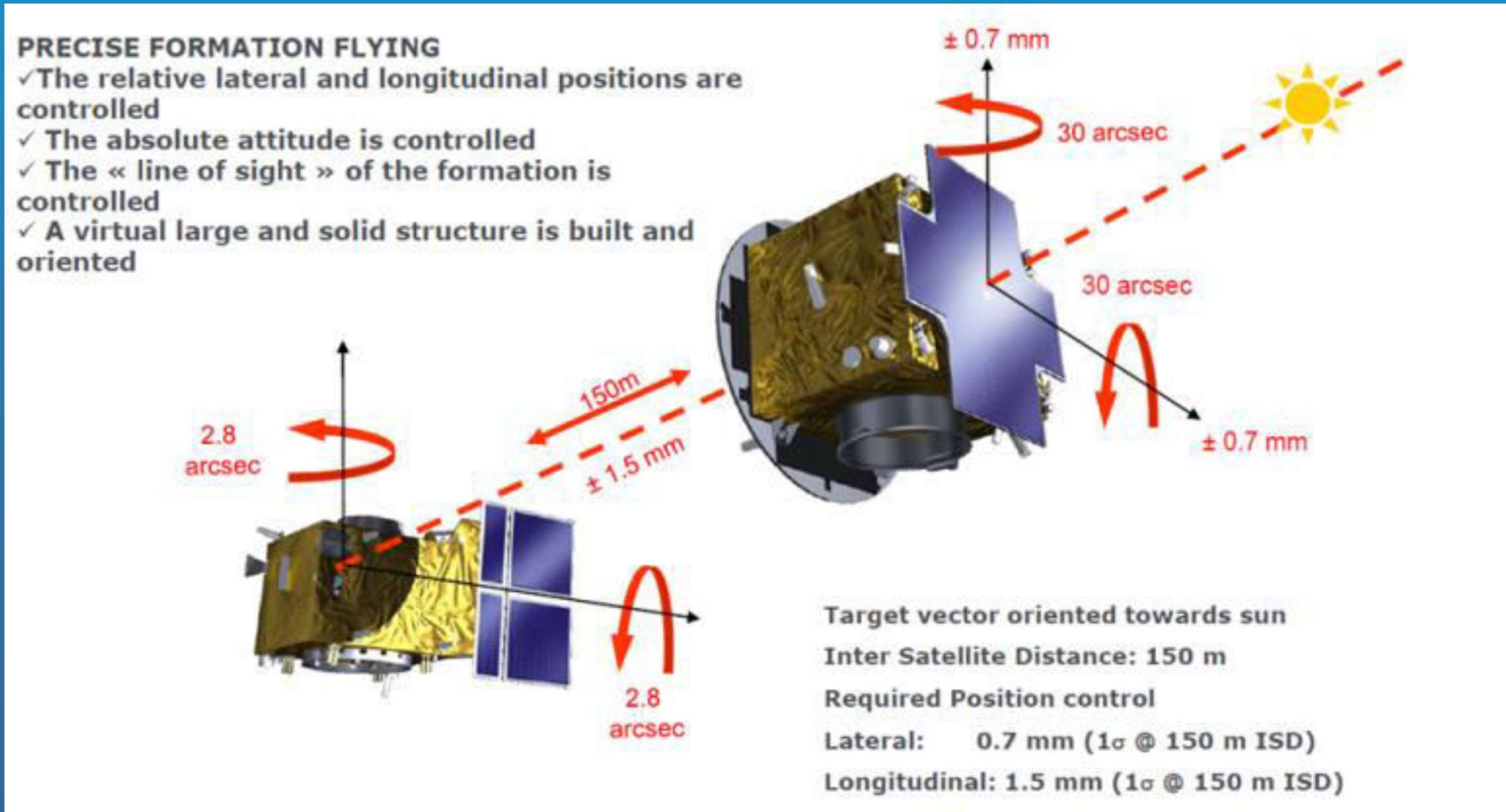

AEE's contribution in Proba3

- The Coronagraph is equiped with an electronic camera.
- AEE in collaboration with OIP Belgium, designed the two main boards of the electronic camera:
    - FPA (focal plane assembly) – captures the image using an image sensor;
    - CEB (camera electronic box) – processes the signals from the image sensor;
- AEE manufactured the boards, designed the electrical test solution and performed the electrical tests of these boards.
- Currently, the project is in EQM phase.

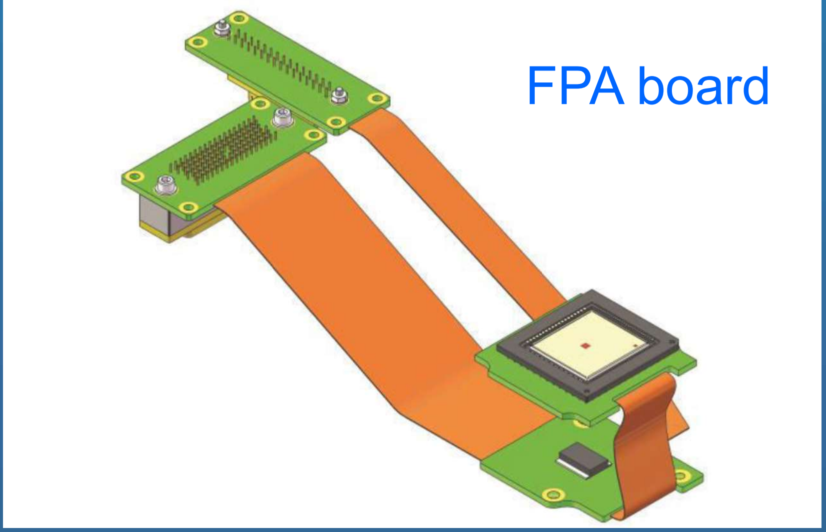
FPA board

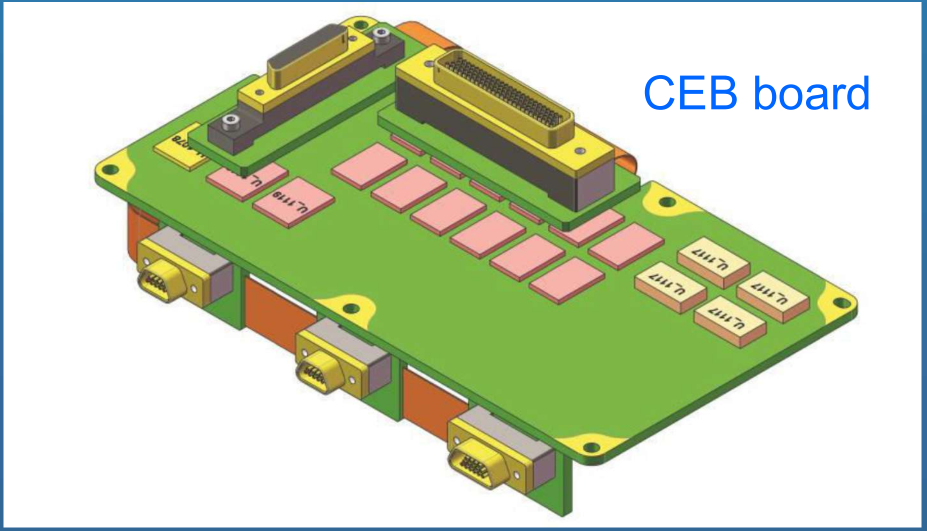
CEB board

A-E Electronics with the support of

European Space Agency

is carrying out:

"Preparatory Activities for the Design, Manufacturing and Testing of Electrical Harnesses and Electronics for Space Instruments"

Preparatory activities for Space projects (cont.)

- Issuance of the compliance matrix between AEE’s work procedures and ESA’s standards
- Certification of operators and inspectors according to some specific ESA’s standards:
  - ECSS-Q-ST-70-08 – manual soldering of high-reliability electrical connections;
  - ECSS-Q-ST-70-38 – high-reliability soldering for surface mount and mixed technology ;
  - ECSS-Q-ST-70-28 – repair and modifications of PCB assemblies for space use;
  - ECSS-Q-ST-10-09 – non-comformance control system.

Preparatory activities for Space projects (cont.)

Preparation and submitting of **Verification Programme**

- Issuance of the PID (Process Identification Document)
- Preparation of the working area (environmental & technological)
- Acquire of specific equipment and tools
- Design of the Test Vehicles according to PCB design rules agreed by ESA
- Procurement of materials for Test Vehicles
- Performance of the environmental tests (vibration and thermal cycles) and microsesctions on the Test Vehicles

Preparatory activities for Space projects (cont.)

SMT line specially asigned for space projects with following features:

- Enclosed area with restricted human traffic;
- Controlled air temperature and humidity;
- Slight suprapressure of air;
- Easy to clean surfaces – all equipment is raised from the floor.

SMT line: paste printer -> pick&place-> reflow oven

drying oven

dry cabinet

Preparatory activities for Space projects (cont.)

Acquire specific tools , equipment and PCB design software, including:

- ECAD software license
- Soldering bath
- Tinning robot
- Ultrasonic cleaning bath

ECAD software for PCB design

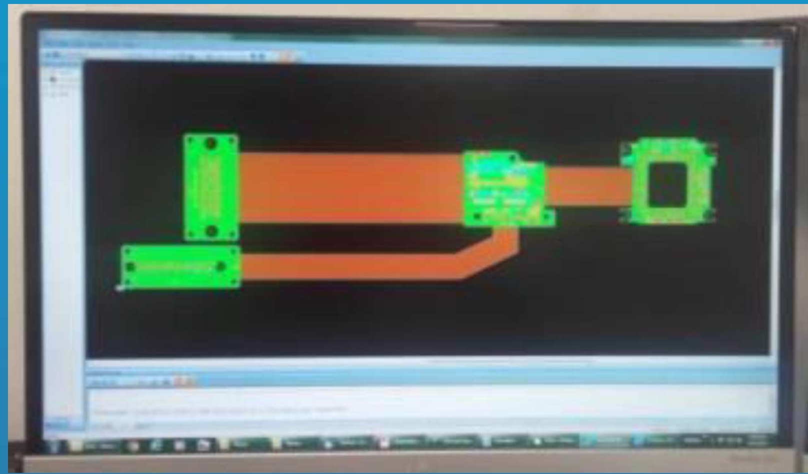

Soldering bath & tinning robot

Ultrasonic cleaning baths

Company Overview

Full turn-key facility:

- Logistic support and Purchasing
- Complete production – including final assembly , final tests & ESS
- Quality Assurance
- Production Engineering
- Design electrical testing (at SRU and LRU level)
- After Sales Support
- Future ESA certification for electronic boards design and production

Continous improvements

Excellence

Moving to lean Management

A-E Electronics

Your reliable partner!

Section V

Innovation in Aero - Engines

Paper 2701

Combining Data Science and Physical Simulations:

New Data-Driven Methods for Aerospace Engineering

R. Ahlfeld and F. Montomoli
Imperial College London and UQuant Ltd.
Kensington, London SW7 2AZ
r.ahlfeld14@imperial.ac.uk

Combining Data Science and Physical Simulations: New Data-Driven Methods for Aerospace Engineering

R. Ahlfeld and F. Montomoli
Imperial College London and UQuant Ltd.
Kensington, London SW7 2AZ
r.ahlfeld14@imperial.ac.uk

1 Introduction

Aerospace engineers are constantly challenged to increase the life expectancy and overall efficiency of their machines. However, as the complexity of machines increases so does the complexity of the computer simulations used to study their structure, aerodynamic flow, or heat transfer. This complexity makes it increasingly challenging for engineers to evaluate and estimate the effect of manufacturing errors and operational variability on their products. In our research, we develop efficient mathematical and computational methods to interface most recent advances in data science with complex computer simulations.

2 Uncertainty Quantification

The term **Uncertainty Quantification (UQ)** has become an umbrella term for all methods that complement deterministic, purely physical engineering simulations with statistical methods (like random sampling, Bayesian inference or machine learning) to predict the real-life variability of Aerospace engineering products based on simulations. Such UQ methods can be used to efficiently integrate manufacturing, experimental or operational data into design simulations. This is attractive for the engineering industry, because it helps to improve product efficiency, reliability, and safety. However, current methods still have various limitations, which have prevented a wider industrial application so far.

3 Research Contribution

This research analyses the existing problems in industry and contributes new solutions to five major problems: data scarcity, the curse of dimensionality, rare events, discontinuous models and modelling errors (epistemic uncertainty).

The major contribution of this work is a new **data-driven Polynomial Chaos** algorithm called SAMBA that can be used to improve engineering designs by efficiently and accurately accounting for manufacturing or in-service uncertainties in industrial physics simulations. SAMBA allows to address many problems in uncertainty quantification with a single method. It is particularly useful for applications where only **scarce statistical data** is available, and to efficiently quantify the likelihood of **rare events** with disastrous consequences, the so-called **Black Swan**. Other benefits are the simple reconstruction of adaptive and anisotropic sparse grid quadrature rules to alleviate the so-called curse of dimensionality (increase of computational effort with increasing number of variables), a simpler combination of different data types like arbitrary distributions or raw random data, and improved convergence for large data-sets that do not follow any prescribed distribution. To deal with special cases, two extensions have been added to SAMBA's algorithmic framework: first, a more generic form of Padé approximation to extend it to **models containing discontinuities** (for example caused by shock waves) problems and second, a multi-fidelity framework to counteract modelling errors, also referred to s **epistemic model-form uncertainty**.

The newly developed methods have been applied to a range of engineering case studies carried out with industrial partners in Formula 1, turbomachinery design, and space launch systems.

References

Ahlfeld, R., Belkouchi, B., & Montomoli, F. (March 2016)."SAMBA: Sparse Approximation of Moment-Based Arbitrary Polynomial Chaos." *Journal of Computational Physics*

Ahlfeld, R., & Montomoli, F. (June 2016)."A Single Formulation for Uncertainty Propagation in Turbomachinery: SAMBA PC." *Journal of Turbomachinery*

Ahlfeld, R., Montomoli, F., Scalas, E., & Shahpar, S. (January 2017)."Uncertainty Quantification for Fat-Tailed Probability Distributions in Aircraft Engine Simulations." *Journal of Propulsion and Power*

Ahlfeld, R., Carnevale, M., Salvadori, S. & Montomoli, F. (July 2017)."Autonomous Uncertainty Quantification for Discontinuous Models Using Multivariate Padé Approximations." *Journal of Turbomachinery*

Mazzoni, C. M., Ahlfeld, R., Rosic, B., & Montomoli, F. (January 2017)."Uncertainty Quantification of Leakages in a Multistage Simulation and Comparison with Experiments." *Journal of Fluids Engineering*

Paper 2702

Explicit parametric solutions for Stokes flow and saddle-point problems with PGD

P. Díez, S. Zlotnik, A. Huerta
Laboratori de Cŕlcul Numčric (LaCŕN),
ETS de Ingenieros de Caminos, Canales y Puertos,
Universitat Politčcnica de Catalunya, BarcelonaTech, Spain
pedro.diez@upc.edu

Explicit parametric solutions for Stokes flow and saddle-point problems with PGD

P. Díez, S. Zlotnik, A. Huerta

Laboratori de Càlcul Numèric (LaCàN),
ETS de Ingenieros de Caminos, Canales y Puertos,
Universitat Politècnica de Catalunya, BarcelonaTech, Spain
pedro.diez@upc.edu

Design optimization and uncertainty quantification, among other applications of industrial interest, require fast or multiple queries of some parametric model. The Proper Generalized Decomposition (PGD) provides a separable solution, a computational vademecum explicitly dependent on the parameters, efficiently computed with a greedy algorithm combined with an alternated directions scheme and compactly stored. This strategy has been successfully employed in many problems in computational mechanics. The application to problems with saddle point structure raises some difficulties requiring further attention.

Separable approximations efficiently deal with high-dimensional data. In particular, the PGD provides separable functions as solutions of boundary value problems. The general PGD framework contains a large family of methodologies, all of them providing solutions in for of separable objects, that is a sum of terms, being each term a product of 1D functions (or arrays). Some of the PGD methodologies have been conceived to tackle nonlinear problems.

We present a general methodology use the PGD in the context of Stokes and other saddle-point problems. Various possibilities of the separated forms of the PGD solutions are discussed and analyzed, selecting the more viable option. The efficacy of the proposed methodology is demonstrated in numerical examples for both Stokes and Brinkman models.

Paper 2703

A Numerical Method for the Analysis of Component Interaction in Aero-Engines

Simone Salvadori1, Massimiliano Insinna
Department of Industrial Engineering, University of Florence
Via di Santa Marta, 3 – 50139 Firenze, Italia

A Numerical Method for the Analysis of Component Interaction in Aero-Engines

Simone Salvadori[1], Massimiliano Insinna
Department of Industrial Engineering, University of Florence
Via di Santa Marta, 3 – 50139 Firenze, Italia

The selling point of next-generation aero-engines concerns improvement of cycle efficiency and increased operability, maintaining low weight and reducing pollutant emissions. These are often conflicting goals that require an accurate evaluation of the mutual interaction between gas turbine components, with special interest in combustor/turbine interaction. In fact, lean-burn combustors operate with strong swirl motions, generating a complex flow field characterized by high turbulence level and non-uniform temperature profiles [1] that affect performance and reliability of the high-pressure turbine stage [2][3][4][5][6]. The fully-coupled numerical analysis of combustor and turbine at engine scale is the only affordable way to predict engine reliability. From a numerical point of view the simulation of a single domain characterized by a reactive flow with very different Mach number regimes (from low-Mach flow in combustion chamber to transonic flow in turbine) is problematic due to the different numerical requirements needed, especially concerning stability and accuracy. These problems could be overcome using coupled methods to simultaneously simulate combustor and turbine in separated domains which are managed by different solvers that communicate with each other.

The aim of our activity is to demonstrate the operation and the accuracy of the Multi-Domain Coupling Interface (MDCI) approach, which is a loosely coupled method developed at the Department of Industrial Engineering (DIEF) of the University of Florence [7][8]. The model is based on the separation of the computational domain into two overlapping subdomains that communicate with each other though the exchange of boundary conditions. Three different test cases have been simulated to validate the methodology: the first consists in the study of a supersonic nozzle (steady non-reactive), the second in the simulation of a vortex shedding behind a high-pressure vane trailing edge (unsteady, non-reactive), the third in the investigation of the reacting aero-thermal field generated by a triangular flame-holder (unsteady, reactive, see Figure 1). The simulations have been performed using the in-house HybFlow code developed at DIEF and the commercial code Ansys® FLUENT®.

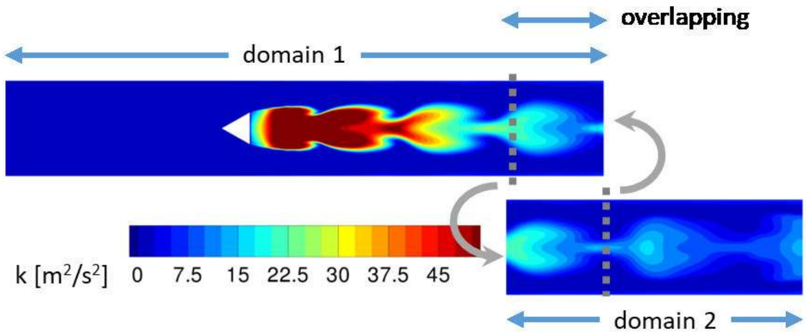

Figure 1 Time-resolved simulation of a bluff body stabilized flame.
Contours of instantaneous turbulent kinetic energy across two coupled subdomains.

[1] Andreini A., Facchini B., Insinna M., Mazzei L., Salvadori S., 2017. *Hybrid RANS-LES Modeling of the Aerothermal Field in an Annular Hot Streak Generator for the Study of Combustor–Turbine Interaction.* J Eng Gas Turb Power, doi: 10.1115/1.4034358

[2] Adami P., Salvadori S., Chana K.S., 2006. *Unsteady Heat Transfer Topics in Gas Turbine Stages Simulations.* ASME Turbo Expo, doi: 10.1115/GT2006-90298

[3] Salvadori S., Montomoli F., Martelli F., Adami P., Chana K.S., Castillon L., 2011. *Aerothermal Study of the Unsteady Flow Field in a Transonic Gas Turbine with Inlet Temperature Distortions.* J Turbomach, doi: 10.1115/1.4002421

[4] Salvadori S., Montomoli F., Martelli F., Chana K.S., Qureshi I., Povey T., 2012. *Analysis on the Effect of a Nonuniform Inlet Profile on Heat Transfer and Fluid Flow in Turbine Stages.* J Turbomach, doi: 10.1115/1.4003233

[5] Salvadori S., Ottanelli L., Jonsson M., Ott P., Martelli F., 2012. *Investigation of High Pressure Turbine Endwall Film Cooling Performance under Realistic Inlet Conditions.* J Propul Power, doi: 10.2514/1.59225

[6] Griffini D., Insinna M., Salvadori S., Martelli F., 2015. *Clocking Effects of Inlet Non-Uniformities in a Fully Cooled High-Pressure Vane: A Conjugate Heat Transfer Analysis.* J Turbomach, doi: 10.1115/1.4031864

[7] Salvadori S., Riccio G., Insinna M., Martelli F., 2012. *Analysis of Combustor/Vane Interaction with Decoupled and Loosely Coupled Approaches.* ASME Turbo Expo, doi: 10.1115/GT2012-69038

[8] Insinna M., Salvadori S., Martelli F., 2014. *Simulation of Combustor/NGV Interaction Using Coupled RANS Solvers: Validation and Application to a Realistic Test Case.* ASME Turbo Expo, doi: 10.1115/GT2014-25433

[1] Contact Author, simone.salvadori@unifi.it

Paper 2704

Multi-physics modeling of detonation engines

Bayindir H. Saracoglu
Aeronautics and Aerospace Department, von Karman Institute for Fluid Dynamics
Rhode-Saint-Genese, Belgium

Multi-physics modeling of detonation engines

Bayindir H. Saracoglu, Aeronautics and Aerospace Department, von Karman Institute for Fluid Dynamics, Rhode-Saint-Genese, Belgium

Majority of the modern aero engines are powered by constant pressure combustion process based on deflagration. Thermal efficiencies realizable with such engines reach to the attainable limits as the combustion temperatures approach to the adiabatic flame temperature. Hence, a radical change in the engine architecture is required to realize a step change towards highly efficient propulsion systems. In this regard, detonation engines based on pressure gain combustion opens a new paradigm for the future propulsion and energy production systems. Pressure gain combustion is defined as an unsteady process whereby gas expansion by heat release is constrained, causing a rise in stagnation pressure and allowing work extraction by expansion to the initial pressure. The process allows reaching higher outlet pressures for the same exit temperatures thanks to near-constant volume combustion allowing an elevation in theoretical cycle efficiency compared to the Joule-Brayton cycle.

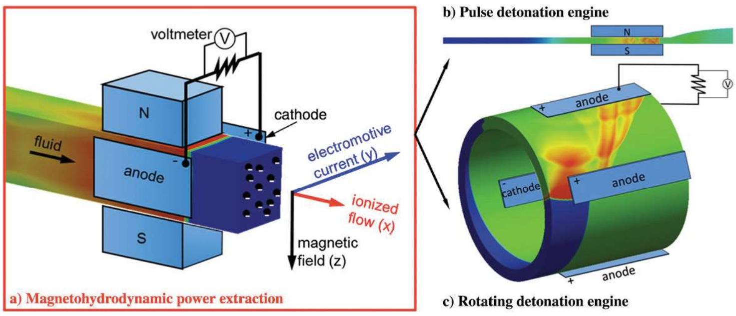

Figure 1. MHD principle applied on a detonation tube: a) current passing through a load resistance induced by the magnetic field with application to both b) a PDE and a c) RDE[1]

Multi-physics phenomena occurring within the pressure gain combustors are modeled through numerical simulations performed in open-source flow solver OpenFoam. The main features of the detonation process are investigated in both pulsed detonation engine (PDE) and rotation detonation engines (RDE) architectures. The effects of the incoming flow conditions on the reacting fluid and outlet field are analyzed through ddtFoam solver which models deflagration-to-detonation transition process with URANS simulations. Now, ddtFoam module is also augmented with an in-house developed conjugate heat transfer solver in order accurately to calculate the thermal loads on the structural components of the engine, which is exposed to cyclic flame temperatures well over 3000 K. Consequently, an adequate cooling system can be developed to prevent deterioration of the engines, especially RDEs, under long operation due to high temperatures. On the other hand, benefits of having such high temperatures in the flow field may also be exploited through magnetohydrodynamic (MHD) energy extraction through an induced magnetic field around the engine. The unsteady simulations performed with coupled OpenFoam and Mutation++ (an in house thermo-chemical library) suite showed that a considerable amount of energy can be harnessed owing to MHD effect observable in alkali metal seeded reacting flow through combustor.

[1] James Braun, Bayindir H. Saracoglu, Thierry E. Magin, and Guillermo Paniagua. "One-Dimensional Analysis of the Magnetohydrodynamic Effect in Rotating Detonation Combustors", AIAA Journal, Vol. 54, No. 12 (2016), pp. 3761-3767. DOI: 10.2514/1.J054989

Paper 2706

Multiscale Virtual Structural Testing

Towards simulation-based design and certification of aircraft structures

Cláudio S. Lopes, PhD
Design and Simulation of Composite Structures
IMDEA Materials Institute
Parque Científico y Tecnológico-Tecnogetafe
c/Eric Kandel, 2 – 28906 Getafe (Madrid), Spain

Multiscale Virtual Structural Testing

Towards simulation-based design and certification of aircraft structures

Cláudio S. Lopes, PhD
Design and Simulation of Composite Structures
IMDEA Materials Institute
Parque Científico y Tecnológico-Tecnogetafe
c/Eric Kandel, 2 – 28906 Getafe (Madrid), Spain

A virtual analysis strategy that physically describes the material behaviour at different length scales from ply to laminate, and to composite structure is being developed and validated at IMDEA Materials. The foundations of this multiscale approach lie in the in-situ characterization of the three elementary composite constituents (fibre, matrix and fibre/matrix interface) by means of experimental micromechanics. Then, the numerical simulation of the micromechanical behaviour of the composite plies is achieved by means of *Representative Volume Element* and *Embedded Cell Element* techniques that describe the elastic, plastic and fracture behaviour of the different phases by means of appropriate constitutive equations. At mesoscale level, laminates are simulated by means of continuum models for plies and ply-interfaces that take into account the mechanisms of deformation and failure as predicted by computational micromechanics and observed experimentally. At structural level, the composite is modelled by means of single shells that implicitly describe the behaviour of the plies in the laminate.

This multiscale computational environment constitutes a robust simulation framework for structural design and certification of composite structures in the aeronautical sector and others alike. This Virtual Test Lab enables the effective reduction of time-consuming and costly physical test campaigns. Moreover, this approach can be easily applied to design and optimize novel microstructures, non-conventional laminates, and next-generation structural composites that take full advantage of the potential design space and manufacturing possibilities in composites, such as steered-fibre composites. Hence, the exploration of the full range of possibilities allowed by composites becomes within reach, accelerating the design of the next-generation of aeronautical structures.

Table of content

Edited by the Romanian Research and Development Institute for Gas Turbines COMOTI